DOE/ER-0237

December 1985

United States Department of Energy

Office of Energy Research
Office of Basic Energy Sciences
Carbon Dioxide Research Division

PROJECTING THE CLIMATIC EFFECTS OF INCREASING CARBON DIOXIDE

CO2

DISCLAIMER

United States Department of Energy

Office of Energy Research
Office of Basic Energy Sciences
Carbon Dioxide Research Division
Washington, D.C. 20545

DOE/ER-0237
December 1985
Dist. Category UC-11

DOE/ER--0237

DE86 008810

PROJECTING THE CLIMATIC EFFECTS OF INCREASING CARBON DIOXIDE

Edited by:

Michael C. MacCracken and
Frederick M. Luther

Lawrence Livermore National Laboratory
Livermore, CA 94550

CONTRIBUTORS

ROBERT D. CESS
Laboratory for Planetary Atmospheric Research
State University of New York
Stony Brook, New York

ROBERT G. ELLINGSON
Department of Meteorology
University of Maryland
College Park, Maryland

BRIAN P. FLANNERY
Corporate Research Science Laboratories
EXXON Research and Engineering Co.
Linden, New Jersey

W. LAWRENCE GATES
Climatic Research Institute
Oregon State University
Corvallis, Oregon

MATTHEW C. G. HALL
Engineering Physics & Mathematics Division
Oak Ridge National Laboratory
Oak Ridge, Tennessee

MARTIN I. HOFFERT
Department of Applied Science
New York University
New York, New York

FREDERICK M. LUTHER
Atmospheric and Geophysical Sciences Division
Lawrence Livermore National Laboratory
Livermore, California

MICHAEL C. MacCRACKEN
Atmospheric and Geophysical Sciences Division
Lawrence Livermore National Laboratory
Livermore, California

JOHN F. B. MITCHELL
United Kingdom Meteorological Office
Bracknell, Berkshire
United Kingdom

MICHAEL E. SCHLESINGER
Department of Atmospheric Sciences
Oregon State University
Corvallis, Oregon

WEI-CHYUNG WANG
Atmospheric and Environmental Research, Inc.
Cambridge, Massachusetts

WARREN M. WASHINGTON
National Center for Atmospheric Research
Boulder, Colorado

THOMPSON WEBB, III
Department of Geological Sciences
Brown University
Providence, Rhode Island

T. M. L. WIGLEY
Climatic Research Unit
University of East Anglia
Norwich, United Kingdom

DONALD J. WUEBBLES
Atmospheric and Geophysical Sciences Division
Lawrence Livermore National Laboratory
Livermore, California

FOREWORD

Over the ages, human communities have had little or no effect on the Earth's global climate. Humans have accounted for only a small part of all of the species on the planet, and their activities have been essentially benign relative to the global atmosphere. Historically, communities were small and distant from each other and transportation was slow and difficult. Very little energy was consumed, with the burden of work being carried by humans and their domesticated animals with the assistance of elementary machinery.

Science and technology paved the way for the rapid societal changes of the 20th century. With the development of transportation and communication systems plus the machinery for industrial and agricultural production, global energy consumption grew by more than 10-fold from 770 million metric tons (10^{15} grams) of coal equivalent (mmtce) in 1900 to more than 9000 mmtce in 1984. Most of this energy was produced by burning fossil fuels. The world's population increased by threefold during the same period from 1.6 billion to 4.8 billion. (The American billion, 10^9, is the same as the British milliard, 10^9.) Urbanization, which resulted in a major increase in demand for energy, recorded an almost 20-fold increase in 84 years, as measured by the number of urban areas with populations greater than 1 million, expanding from 13 to 247 worldwide.

This immense increase in energy use is changing the layer of gases that constitutes the Earth's atmosphere, which in turn controls global climate. So, for the first time in the planet's history, humans are truly involved in a change of their environment.

Carbon dioxide (CO_2), a naturally occurring constituent of the atmosphere, is also the product of human activities—the burning of fossil fuels for energy and the clearing of land for agriculture and urbanization. Toward the end of the 19th century, Arrhenius calculated that a doubling of the CO_2 concentration would raise the average temperature by 5 or 6°C. Chamberlain later developed a hypothesis that related causes of glacial periods and the depletion of the atmospheric CO_2 concentration. Tolman, a student of Chamberlain, described the basic roles of the ocean in absorbing atmospheric CO_2 and moving and storing it globally.

Another important role of CO_2 was also recognized more than a century ago. Von Liebig demonstrated that plants get their carbon for photosynthesis and growth from the air. By this process, a relative atmospheric constancy is maintained where assimilation by plants is roughly balanced by CO_2 exhalation by animals. This notion of constancy became dogma until modern measurements clearly showed a change in the atmospheric concentration of CO_2 due to human intervention.

It is now known that the atmospheric CO_2 concentration in 1900 was approximately 300 parts per million by volume (ppm) (indicated by recent

measurements of glacial ice cores by Oeschger). However, it wasn't until 1938 that Callendar presented the first substantive data showing that the concentration of CO_2 in the atmosphere was increasing and suggested that the increase might affect the Earth's climate. After another 20 years Keeling began to monitor the atmospheric CO_2 concentration at the Mauna Loa Observatory in Hawaii. The measurements of atmospheric CO_2 in 1958 showed the annual average concentration was 316 ppm; it was approximately 345 ppm in 1985. Plass outlined theories to explain the relationship between atmospheric CO_2 and climate in 1956, and, soon after, Revelle and Suess described the relationship between CO_2 in the atmosphere and in the oceans, and Kaplan enlarged upon the role of CO_2 in the atmosphere in terms of the global heat balance.

In 1977 leading scientists assembled in Miami Beach, Florida, to discuss the current understanding of the carbon cycle, that is, the dynamics of carbon exchanges within the Earth's atmosphere, land, and oceans that determine the atmospheric CO_2 concentration. They also reviewed possible consequences of increases in atmospheric CO_2. In addition, they identified significant gaps in the knowledge base and made recommendations for research.

Since then, significant research has been carried out by the international scientific community. The Department of Energy (DOE), the lead United States agency in the study of CO_2, and other agencies including the National Science Foundation, National Oceanic and Atmospheric Administration, National Aeronautics and Space Administration, United States Geological Survey, United State Department of Agriculture, and Environmental Protection Agency, following the recommendations of the science community, have conducted and supported research activities in universities, national laboratories, industry, and other institutions.

Looking forward to the 21st century, the DOE believed it was important to "take an accounting" to see how far this considerable effort had come in 8 years in answering the questions that were previously posed and in determining future research directions. Accordingly, the Carbon Dioxide Research Division, Office of Basic Energy Sciences, of the DOE is publishing this series of four State-of-the-Art (SOA) volumes:

- *Projecting the Climatic Effects of Increasing Carbon Dioxide*—to project the magnitude and rate of the potential climate changes that could result from the increasing atmospheric CO_2 concentration.
- *Detecting the Climatic Effects of Increasing Carbon Dioxide*—to detect the changes in climate resulting from the increasing atmospheric CO_2 concentration and to isolate the climate changes from those caused by other contributing factors (natural or anthropogenic).
- *Atmospheric Carbon Dioxide and the Global Carbon Cycle*—to understand the mechanics of and quantify the sources, sinks, and exchanges of carbon between all elements of the global carbon system—the atmosphere, the biosphere, the oceans—including anthropogenic effects.
- *Direct Effects of Increasing Carbon Dioxide on Vegetation*—to determine the plant response to increased atmospheric CO_2 and develop the capability to predict crop and ecosystem responses to CO_2 enrichment.

An index and cross-reference volume accompanies the set of volumes. Two companion reports are also being published:

- *Characterization of Information Requirements for Studies of CO_2 Effects: Water Resources, Agriculture, Fisheries, Forests, and Human Health.*

- *Glaciers, Ice Sheets, and Sea Level: Effects of a CO_2-Induced Climatic Change,* from the National Research Council's (NRC) Committee on Glaciology of the Polar Research Board.

These complementary reports aid in ensuring that "the accounting" of CO_2 research activities for the past years encompasses the entire spectrum of research.

The SOAs document what is known, unknown, and uncertain about CO_2 data, analyses, and modeling capabilities. They outline potential avenues of research for reducing critical unknowns and uncertainties. More than 70 scientists from five nations have participated in the preparation of these volumes. Each chapter and each complete SOA volume has gone through extensive peer review by the American Association for the Advancement of Science (AAAS); this review, however, does not imply that AAAS endorses the statements or recommendations presented in these volumes.

These technical reports provide the basis for a Statement-of-Findings (SOF) report. While studies over the last several years have clearly shown that increasing CO_2 concentrations have the potential for significant impacts on our physical environment, these studies have not yet provided an adequate basis for addressing questions about the fundamental relationships between the benefits and impacts of various energy systems on society's activities. The SOF will summarize what we know and do not know and the degree of certainty of our knowledge. It will also present the rationale for further studies. These studies will be needed to provide an accurate scientific basis for assessments of the potential impacts of energy-related activities.

The citizens of today's nations have the responsibility for the stewardship of all the Earth, including their actions which may affect its climate. Exercising this responsibility requires an understanding of atmospheric CO_2 and its effects. Once understood, stewardship then becomes nurturing rather than unrecognized neglect.

Scientists have created the building blocks for this understanding, and the scientific community has recognized its responsibility to more fully understand CO_2-induced effects on our global environment. Through research, as we look towards the 21st century, the application of science will ensure that the additional understanding required for nurturing our planet Earth will be developed.

Sincere thanks go to everyone who has participated in developing the SOAs and companion reports. Special thanks go to the coordinator/editors, Jennifer D. Cure, Frederick M. Luther, Michael C. MacCracken, Boyd R. Strain, John R. Trabalka, Margaret R. White, and the NRC Committee Chairman Mark Meier; their respective chapter authors; and to the AAAS, Roger Revelle, Chairman of the Climate Committee, and David M. Burns of the AAAS staff.

We hope these definitive, scientific statements will motivate scientists to recommend explicit approaches for reducing the critical uncertainties that now exist in order to permit decision making within the next decade that is based on data, learning, understanding, and wisdom.

Frederick A. Koomanoff, Director
Carbon Dioxide Research Division
Office of Basic Energy Sciences
U.S. Department of Energy

PREFACE

There is little doubt that the increasing concentration of atmospheric carbon dioxide (CO_2) has the potential to modify the Earth's climate. Increased global surface temperatures, altered precipitation patterns, and changes in other climatic variables could have substantial economic and social consequences. The final goal of the CO_2 research program of the U.S. Department of Energy is to identify possible policy options for government action in response to these potential effects of increased atmospheric CO_2. Some of the basic information needed is the rate and magnitude of a potential climate change, the weather conditions that might be associated with such a change, and how such a climate change would differ from region to region.

The objective of this State-of-the-Art volume is to present the current knowns, unknowns, and uncertainties regarding the projected climate changes that might occur as a result of an increasing atmospheric CO_2 concentration. Further, the volume describes what research is required to estimate the magnitude and rate of a CO_2-induced climate change with regional and seasonal resolution.

Important progress has been made in the last decade. Theoretical projections of potential climate changes are now made with increasingly complex models that incorporate more realistic representations of oceans, geography, and the seasonal cycle. There also has been substantial expansion of the data base that is needed to verify climate projections and to improve climate modeling methodology.

Virtually all studies suggest that the increasing CO_2 concentration will significantly increase the global average temperature, but the projected regional and seasonal details vary considerably between models. Although the representation of oceans, geography, and the seasonal cycle have improved, additional research is required to further detail these features and other smaller scale processes not explicitly treated in the current models. As an example, a more thorough study is needed of the influences of changes in cloud distribution and characteristics and the associated feedbacks to the radiative balance. Future modeling efforts must concentrate on understanding why the model results differ, what data and new methodologies are required to improve the models, and how and whether model results can provide the regional information needed for formulating policy options.

Sincere thanks are due Michael C. MacCracken and Frederick M. Luther, Lawrence Livermore National Laboratory, for their contributions to this document as editors, authors, and researchers. They have participated in making this volume possible from its inception to its final production. The contributing authors are to be commended for the dedication and extensive work involved in the writing of this volume.

Michael R. Riches, Program Manager
Carbon Dioxide Research Division
Office of Basic Energy Sciences
U. S. Department of Energy

EDITORS' PREFACE

The State-of-the-Art (SOA) reports represent the culmination of a major effort to review the state of scientific understanding concerning the potential effects and impacts of the increasing carbon dioxide (CO_2) concentration. Preparation of the chapters included in these SOA reports has taken several years and would not have been possible without the cooperation and substantial effort provided by many participants, both within and beyond the research program funded by the Department of Energy (DOE).

The outline for this SOA was initially proposed in the fall of 1982, where suggestions were offered by those attending a DOE-sponsored CO_2 research conference at Berkeley Springs, West Virginia. After considerable revision, chapter authors were selected in late 1983 and outlines and early drafts of chapters were prepared for most chapters by mid-1984. These initial materials were reviewed at a meeting in Washington, D.C. attended by authors and other scientists active in studying this area.

To assure the authoritativeness of the reviews, the DOE contracted with the American Association for the Advancement of Science (AAAS) to arrange for external peer review of the individual chapters. This extensive review started during the second half of 1984 and continued for more than a year. The reviewers selected by AAAS provided many important comments and suggestions that have led to significant improvement of the chapters. Their assistance has been greatly appreciated.

After receiving the reviewers' comments, chapter authors modified and updated their chapters to assure that the SOA report adequately covers the many advances being made in understanding the potential effects of the increasing CO_2 concentration. Final versions of the chapters were submitted for editorial review and a final AAAS review throughout 1985.

The editors gratefully acknowledge the dedicated efforts of all of the chapter authors. They responded with patience and persistence to up to twelve AAAS-sponsored reviews for each chapter, to many comments from fellow authors, to extensive editorial suggestions intended to help better integrate the various chapters, and to requests to aid in review and preparation of summary and recommendation chapters. This has been greatly appreciated.

While these chapters have undergone extensive review, the views finally expressed are those of the authors of each chapter. As in all areas where active research is under way, there are differences of interpretation and emphasis. In reviewing these issues, the editors have attempted to assure thorough presentation and well-reasoned statements, not to coerce uniformity of view. Where differences are evident or uncertainties are presented, further study is recommended.

We want to express special gratitude to the many secretaries who have labored on these chapters at the various institutions. At LLNL, particular and special thanks go to Floy Worden, who has done everything from typing chapters from handwritten scribbles to communicating with authors and preparing camera-ready copy. She has been aided extensively by Nancy Badal, Pam Drumtra, Sandra Eyre, Lonnette Robinson, and Doris Swan, each of whom has willingly helped with each succeeding updating of texts.

Editorial and graphical support and handling of the manuscripts for the AAAS review process have been directed by Jon Findley, Nancy Brown, and co-workers of the MAXIMA Corporation in Rockville, Maryland. The index was prepared quickly and efficiently by Fred O'Hara through a contract with the Oak Ridge National Laboratory.

Michael C. MacCracken
Frederick M. Luther
Editors

This volume was prepared under the auspices of the Carbon Dioxide Research Division of the Office of Basic Energy Sciences, U.S. Department of Energy by the Lawrence Livermore National Laboratory under contract W-7405-ENG-48. Mr. Michael R. Riches served as DOE Project Manager.

AAAS REVIEW

In commissioning and publishing a summary of the state of current knowledge about the secular increase of atmospheric carbon dioxide and its effects, the Department of Energy has performed a valuable service. These volumes may prove to be the most comprehensive assembly to date of scientific results about this issue.

The Committee on Climate of the American Association for the Advancement of Science was asked to organize peer reviews of the component chapters of the books. These reviews were conducted in the traditional manner of refereeing scientific papers. We identified experts whom we knew to be well qualified, and we invited them to review anonymously an individual chapter in their field. In transmitting draft manuscripts to the reviewers, we alerted them to the ambitious nature of the "state-of-the-art" project, and particularly to the difficulties of adequately treating the many uncertainties.

The careful attention reviewers devoted to their tasks was gratifying and indicates the importance of this issue to the world scientific community. More than 300 specialists from 23 countries gave the draft papers a careful and thorough reading and offered detailed suggestions for revision and improvement. The authors and editors thus had available a significant input from their professional colleagues as they sought to improve their drafts. But the decision as to how to use the reviewers' suggestions was the responsibility of the author(s) of the paper and the editor(s) of the books.

These volumes make clear that investigating the causes and effects of alterations to the atmosphere is an exceedingly complex undertaking, touching a wide gamut of scientific disciplines. It hardly is surprising that there were (and are) differences of interpretation.

I am grateful to the many anonymous reviewers and to my colleagues on the Committee. I hope that we have been helpful to the authors and editors in their very challenging task.

Roger Revelle, Chairman
Committee on Climate
American Association for the
Advancement of Science (AAAS)

AAAS COMMITTEE ON CLIMATE

Roger Revelle, Chairman
Lester B. Lave
Estella Leopold
Sharon E. Nicholson
Norman J. Rosenberg
Stephen H. Schneider
Warren M. Washington
George M. Woodwell
David M. Burns, Staff Officer

AAAS SOA SUB-COMMITTEE

Wolfgang H. Berger
Kirk Bryan, Jr.
Charles F. Cooper
Robert Kates
J. Murray Mitchell
Dean F. Peterson
David Pimentel
David J. Rose (deceased)
Charles Stockton

CONTENTS

EXECUTIVE SUMMARY

Concern about the potential climatic effects of the increasing concentration of atmospheric carbon dioxide (CO_2) was first expressed over a century ago, but it was not until the advent of the computer that convincing quantitative projections of the possible effects could be made. Although making up only about 0.03% of the atmosphere's volume, CO_2 plays an important role in maintaining the Earth's moderate climate. Mankind's activities have inadvertently increased the atmospheric concentrations of CO_2 and other gases present in trace amounts (e.g., the CO_2 concentration has increased by about 25% over about the past 100 years), and further substantial increases are projected for the future. Experiments with numerical climate models indicate that increases in the atmospheric concentrations of CO_2 and trace gases, by altering the Earth's heat balance, will produce potentially significant changes in the climate.

The objective of this volume in the State-of-the-Art series of reports is to document what is known about projections of the climatic effects of the increasing CO_2 concentration and to describe the uncertainties and unknowns associated with such projections. This summary follows the same order in which material is presented in the rest of this volume. The changes in the radiation balance caused by the increasing CO_2 concentration (the radiative forcing) are described. The scientific basis for the theoretical models used to make climate projections is discussed, and the latest model results are reviewed. Consideration also is given to the potential climatic effects of perturbations other than increasing CO_2 and to the lessons that past climate changes can teach about what lies ahead. Recommendations are made for research tasks that would contribute toward reducing the uncertainties and improving the projections.

An increase in the atmospheric CO_2 concentration in the absence of an atmospheric response affects the radiation balance of the Earth by reducing the amount of longwave (infrared) radiation that is emitted to space. The CO_2 absorbs radiation that is emitted upward by the Earth's surface and by gases lower and higher in the atmosphere; CO_2 also emits energy upward and downward at a rate that depends on the temperature at the altitude of emission. This trapping of radiation creates temperature profiles that force precipitation-inducing convection and large-scale vertical overturning in order to transport upward a substantial fraction of the solar energy absorbed at the surface. When the concentration of CO_2 increases, the atmosphere absorbs more of the longwave radiation that is emitted upward by the Earth's surface and emits more longwave radiation downward to the surface. Because of the temperature structure of the atmosphere (i.e., temperature decreases with altitude through the troposphere), there is a decrease in the

upward emitted radiation that escapes to space when the CO_2 concentration increases. The trapped longwave radiation forces increased convection and acts to warm the atmosphere and surface until the longwave emission to space balances the net incoming solar radiation. This radiation-trapping mechanism is called the *greenhouse* effect. It is a capability implicit in the make-up of all gases that are radiatively active in the longwave regime.

Perturbations other than CO_2 may also affect the climate system. Such climate-perturbing influences include changes in the concentrations of water vapor, trace gases, volcanic aerosols, and other natural and anthropogenic aerosols as well as changes in the solar flux incident at the top of the atmosphere. All of these forcing mechanisms can affect the climate by initially perturbing the Earth's radiation budget. The climate system then tends to respond in such a way as to restore a balance in the net energy budget and in the mass budgets of the various atmospheric constituents. Coupling between physical, chemical, radiative, and dynamical processes distributes the effects of the perturbation throughout the climate system. These perturbations can then result in changes in temperature, precipitation, wind patterns, extent of sea ice, cloudiness, and atmospheric chemical composition.

Because of the complex coupling between physical, chemical, radiative, and dynamical processes in the climate system, it is not possible to derive any simple relationship describing how the climate parameters will change as the composition of the atmosphere is changed. Rather, the system of nonlinear equations that describes the climate system must be solved numerically. The resulting system of equations and solution techniques is called a climate model. Models vary greatly in complexity, depending on their intended application and the level of detail included in describing the various processes and mechanisms. Observational data play an important role in the verification of the climate models and as input to the model calculations. Study of past climates is useful in illustrating the natural variability of the climate on several temporal and spatial scales.

In making projections into the future, it is essential to recognize the distinction between climate and weather. *Weather* describes the state of the global atmosphere-ocean-ice-land system (i.e., the climate system) at one instant in time. Weather can be forecast only a few days in advance. Not only are observations of present conditions inadequate for making accurate, longer term forecasts, but there are also important theoretical limits to how far in advance specific weather conditions can be accurately predicted. The models described in this report cannot forecast changes in the weather, although such models in the future may be able to predict possible changes in the frequency of various weather events.

Climate is the aggregation of the weather, usually expressed in terms of the mean (or average) conditions and variations about this mean, including such statistics as the frequency of rainfall and of such extreme conditions as flood and drought. The normal climate is the collective result of interactions between the atmosphere, oceans, sea and land ice, and the land surface, including, especially, the biosphere. Projecting climate into the future requires predicting the evolution of the mean behavior of the atmosphere, for example, the average winter temperature. Thus, while the weather on a particular January day cannot be forecast, we may be able to predict that a typical January day in the 21st century will be warmer than a typical January day this century or that a typical January 100 years from now will have more mild days than a present January. To some extent, other forcing factors (e.g., a change in solar flux or in the composition of the atmosphere) also determine

how future climate will evolve. If the influences of these external factors were to become large, accurate climate projections for the next century would also require better estimates of their influence.

RADIATIVE EFFECTS OF CARBON DIOXIDE AND TRACE GASES

Because convective mixing leads to strong coupling between the upper troposphere (about 5–10 km) and the near surface layer as well as between the atmosphere and the Earth's surface, the change in the net radiative flux at the top of the troposphere (the tropopause) is the appropriate measure to use in calculating changes in temperatures throughout the troposphere and at the surface. A doubling of the CO_2 concentration with no change in atmospheric temperature or water vapor amount would increase the net downward radiative flux at the tropopause by about 4 W m^{-2} averaged hemispherically. These changes would range from nearly 5 W m^{-2} at low latitudes to about 2 W m^{-2} at high latitudes because of the different temperatures and water vapor mixing ratios in these regions. For comparison, the global average net incoming solar radiation at the top of the atmosphere is about 240 W m^{-2}. The maximum change in flux due to a doubled CO_2 concentration would occur in summer and the minimum in winter. Various model calculations of these quantities agree to within about $\pm$10–15%.

Changes in ozone (O_3), water vapor, and trace gas amounts also can have significant effects on the radiation balance and temperature structure of the atmosphere. Absorption of solar radiation by O_3 balances the emission of infrared radiation by CO_2 and creates the relatively warm and stable stratosphere extending upward from the tropopause to about 55 km. The atmospheric water vapor concentrated in the lower troposphere, together with the clouds that form, play the most important greenhouse role of all atmospheric constituents. The atmospheric trace gases that currently have the largest radiative effects (although still relatively small) are methane (CH_4), nitrous oxide (N_2O), and two chlorocarbons ($CFCl_3$ and CF_2Cl_2). Many of the trace gases have band strengths that are greater than the band strength of the 15-μm CO_2 band, but because of their small concentrations, these gases do not have radiative effects as large as that of CO_2. Although the radiative effect of trace gases is currently small, it could increase significantly in the future because the concentrations of many of the gases are projected to increase at relatively high rates as a result of anthropogenic activity. Within the next 50 years, the radiative effect of the trace gases may exceed that of the increasing CO_2 concentration.

Projections of the radiative effects of CO_2 and trace gases into the future are most uncertain because of uncertainties in the projected concentrations of these gases.

Accurate methods exist for computing the radiative effects of CO_2 and other radiatively active gases. Some uncertainty is introduced because of limitations in knowledge of the radiative characteristics of the atmospheric gases, namely the spectral line data and their pressure and temperature dependence. Lack of understanding about the radiative properties of water vapor (especially the absorption continuum and line shape) and simplifications in implementing radiative algorithms in climate models also contribute to the uncertainty in the overall calculations.

PROJECTING THE CLIMATIC RESPONSE TO INCREASING CARBON DIOXIDE

Methods for determining the climatic response to the increasing CO_2 concentration may be either empirical (based on observations) or theoretical (based on numerical models). It is not yet possible to uniquely identify the roles that various causal factors (such as volcanoes, CO_2, and solar variations) have had in affecting climatic variations that have occurred in the past. Consequently, it is not possible to predict the future climate by simply extrapolating trends from the recent past. Attempts have been made to determine the sensitivity of the climate system empirically by examining the changes in radiative fluxes and temperatures that occur during the normal cycle of seasonal change and as a result of small-scale perturbations. These approaches have not proven successful because the time and space domains of these analyses have not been comparable to those of the CO_2 problem.

The only applicable method for projecting future climates is the construction of mathematical models based on the full set of fundamental physical principles governing the climate system. The basic physical laws governing the behavior of many of the components of the climate system are relatively well known, although some aspects of the physics of the various interactive mechanisms and processes serving to link the components together are still uncertain. Some of these interactive processes, including especially changes in the amounts of atmospheric water vapor, cloud cover, and sea ice, have been identified as important feedback processes that can amplify or regulate the responsiveness of the climate system to perturbing influences such as increasing CO_2 and trace gas concentrations. In climate sensitivity studies, lack of knowledge about potential changes of cirrus clouds in low latitudes and stratus clouds in high latitudes contributes most to widening the range of estimates from different models.

Climate models of many types have proven useful in developing an improved understanding of the climate system. The most complex climate models are three-dimensional general circulation models, which represent the global atmosphere, land surface, and oceans. Atmospheric general circulation models are capable of simulating almost all of the observed large-scale features of the climate, and they reproduce the general character of day-to-day variations as well as seasonal changes of the circulation from winter to summer. However, these models do not yet adequately represent the observed regional features that are needed for making the detailed climate projections and assessments of ecological, agricultural, and societal impacts.

The CO_2 concentration is actually increasing slowly; however, it is easier to calculate what might happen if a large increase in the CO_2 concentration were to occur. With climatic feedback processes turned off, different climate models are in close agreement in their prediction of the change in global average surface air temperature for the radiative perturbation caused by a doubling of the CO_2 concentration; the projected temperature increase is in the range of 1.2 to 1.3°C. Global climate models that include feedback processes, however, are not in close agreement; at equilibrium, such models indicate that a doubling of the CO_2 concentration would increase the global average surface air temperature by approximately 1.5 to 4.5°C. The three most recent general circulation model results, which include realistic geography and seasonal dependence, show a CO_2-induced warming of the global average surface air temperature of about 3.5 to 4.2°C and an increase in the global average precipitation rate of about 7 to 11%. The better agreement of

the models on the projected global sensitivity is encouraging, but their projections of the regional patterns of such changes vary substantially depending on location.

Model results suggest that equilibrium changes in surface air temperature are likely to be larger in high-latitude regions, near the snow and ice boundaries, than in low-latitude regions. As a result of reductions in the extent of sea ice and snow cover, the predicted zonal mean warming is a maximum in winter and a minimum in summer in the high-latitude regions. This would indicate a significant reduction of the amplitude of the annual cycle of surface air temperature at these latitudes. Regions of positive and negative changes in precipitation rate are simulated, with the largest changes generally occurring between 30°S and 30°N. The change in zonal mean precipitation rate is calculated to be positive in the equatorial region throughout the year and negative in adjacent latitudes for at least part of the year. There are qualitative and quantitative differences among the simulations of the change in precipitation rate, reflecting the uncertainty in these results.

Because society is continually adapting to the current climate, albeit more or less slowly depending on the activity, knowing the expected rate of climate change can be at least as important as knowing what the ultimate change may be. Determining the rate of climate change requires taking proper account not only of the rate at which the atmospheric CO_2 concentration is changing and will change, but also in considering the various climate system mechanisms controlling the rate at which the climate can (and will) change. When perturbations are gradual and persistent, consideration must include the oceans (with their very large heat capacity and slow transport of heat to greater depths), the ice sheets (with their very large heat requirement to be melted), and, in some cases, the biosphere (with its potential to alter surface characteristics and atmospheric composition). The interactive damping factors act to slow the rate of climate change, but they do not change the eventual climatic equilibrium.

In the long term, well-tested, coupled atmosphere-ocean general circulation models may be able to serve as operational tools for simulating the transient climate changes, but these are not now available. A hierarchy of climate models is under development to predict the transient climate response resulting from increases in the CO_2 concentration. Comparison of model results with observed temperature changes in various parts of the globe currently must rely on relatively simplified and approximate approaches in comparison to the models now being developed.

Estimates of the rise in surface air temperature between 1850 and the present due to the increased CO_2 concentration alone range from about 0.5°C to more than 1.0°C, reflecting differences in the sensitivity of the models and differences in the lag time of the ocean response as depicted in the models. As a result, the observed Northern Hemisphere temperature change of about 0.5°C since 1850 cannot yet be used to provide more than approximate guidance on the actual equilibrium sensitivity of the climate to the increasing CO_2 concentration. Time-dependent climate model calculations using standard scenarios of fossil fuel CO_2 emissions indicate that a global warming of approximately 1°C may occur by the year 2000 relative to the year 1850, and an additional warming of a few degrees Celsius may occur over the next century if CO_2 and trace gas emissions continue as projected.

Important uncertainties in model calculations arise from limitations in our understanding of climatic mechanisms and in our ability to represent

the various processes in computer models. Representations of clouds, the planetary boundary layer, precipitation, and surface hydrology and of the sensitivity of these processes to changes in climatic parameters contribute most significantly to the uncertainties in the calculations of the potential change in the equilibrium climate.

Uncertainties concerning the climatic sensitivity and the response time of the oceans contribute most significantly to the uncertainties in the calculations of the transient climate change due to the increasing CO_2 concentration.

Uncertainty about the causes of the climatic variations that have been observed over the past 100 years means that the climate record can only provide approximate guidance about the actual equilibrium sensitivity of the climate to the increasing CO_2 concentration.

CLIMATIC EFFECTS OF OTHER PERTURBING FACTORS

The ongoing increase in the CO_2 concentration is not the only factor that scientists believe has already affected or will alter the climate. Geological evidence clearly demonstrates that climate has varied substantially in the past and that natural causes of climate change must be present. On multi-millennia time scales, changes in the eccentricity of the Earth's orbit, the seasonal variation of perihelion, and the tilt of its axis are believed to be very important. Some observations also indicate that large natural variations in the CO_2 concentration may have occurred during glacial cycling. On the time scale of centuries, small variations in solar output may play a role; on annual to decadal scales, injections of volcanic aerosols and solar flux variations have probably induced measurable climatic perturbations. In addition, climate variations may arise as a result of nonsteady interactions of the various components of the climate system, for example, as a result of aperiodic overturning of the oceans or long-term instabilities in ice sheet thickness and extent. Such oscillations internal to the climate system add to the background natural variability that may be perturbed by CO_2 and other factors treated as external to the system. Model studies estimate that variations in solar forcing (measured to be about 0.2%) may account for fluctuations in surface air temperature of a few tenths of a degree Celsius. Stratospheric aerosol loadings from major volcanic eruptions may cause a surface cooling of as much as a few tenths of a degree Celsius for periods of one to a few years. These estimates indicate that the climatic effects of solar variations and volcanic aerosols are considerably smaller in magnitude and shorter in duration than the warming projected to result from the increasing CO_2 concentration.

Many gases being injected into the atmosphere as a result of various societal activities can act like CO_2 to trap outgoing infrared radiation and to warm the climate. For example, CH_4 releases that occur as land is cleared, more cattle are raised, and more rice is grown are raising atmospheric concentrations by about 10 to 15% per decade, and emissions of $CFCl_3$ and CF_2Cl_2, which can chemically react to reduce stratospheric ozone, are projected to rise by about 40 to 50% per decade. Trace gases may affect the climate directly by their own radiative perturbation or indirectly by interacting chemically or climatically with species that are radiatively important. Conversely, changes in climate can affect chemical species concentrations by changing temperature-dependent chemical reaction rates. Climate model calculations suggest that,

on the time scale of decades, the combined climatic effects of concentration increases of atmospheric N_2O, CH_4, $CFCl_3$, and CF_2Cl_2 and their induced changes in O_3 from climate-chemistry interactions could be as large as those estimated from the expected increase in the CO_2 concentration alone.

Model assessments are affected by uncertainties concerning the feedback processes that involve coupling between atmospheric chemistry, dynamics, and radiation transfer.

Estimates of the future contribution of trace gases to the total projected change depend critically on the projected changes in species concentrations that are used in the calculations. In this regard, a better understanding of the source and sink processes affecting trace gas concentrations and their global budgets is needed to reduce uncertainties in the climate change projections.

THE STUDY OF PAST CLIMATES

The study of climates of the last hundred thousand years can contribute information that may be used to refine scenarios for possible future climates and that can provide independent data for testing the results of global climate models. In addition, such analyses can investigate the causes of past climate change and possibly provide indications of the nature of future climate change. For example, comparisons of warm and cold years in long-term instrumental records have indicated that temperature changes are larger in high latitudes than in low latitudes. This pattern is in general agreement with model simulations of the increasing CO_2 concentration.

Data from the mid-Holocene (about 5000–7000 years ago) indicate that the global mean temperature may have been 1°C warmer than at present, but limited data coverage makes precise determination of the global mean temperature change difficult. The climate during this period was significantly different from today; maps of July temperatures show regions of higher as well as lower temperature in the middle to high latitudes of the Northern Hemisphere. Patterns of precipitation show larger changes than do the temperature patterns, with more precipitation in the tropics and subtropics and less in the midwestern United States.

The analyses show that for most areas, the mean annual surface temperature has been remarkably stable during the past 10,000 years, with variations not exceeding 1 or 2°C. This stability did not extend to precipitation fields, which have exhibited large and extended fluctuations. If increased concentrations of CO_2 and trace gases raise the global mean surface temperature by 1.5°C or more, the resultant average global climatic conditions will be beyond the range of climates that have existed during the historical past and during recent geological times.

The usefulness of past climates for projecting the character of potential CO_2-induced perturbations is affected by uncertainties concerning the causes of past climate variations and the extent to which past warm climates represent the climate conditions that would exist because of a CO_2-induced warming.

SUMMARY OF CLIMATE PROJECTION STUDIES

The atmospheric CO_2 concentration has increased by about 25% since preindustrial times, and continued use of fossil fuels is projected to lead to substantial further increases in the future. Concentrations of trace gases having radiative properties similar to those of CO_2 are also rising. The increasing concentrations of these greenhouse gases will alter atmospheric radiative fluxes and warm the Earth by the very same interactions and processes that enable current concentrations of these gases to make our climate different than that of the Moon. Theoretical projections of the potential future climate changes using computer models whose results have been verified by comparison with the seasonal evolution of the natural atmosphere indicate that a global warming by a few degrees Celsius is possible during the next century. Uncertainties in these theoretical estimates arise in part as a result of the range of CO_2 and trace gas projections, but primarily at this stage they are due to limitations in our understanding and representation of cloud, ocean, cryospheric, and other processes and interactions. As a consequence, different models do not now agree on many of the important regional and seasonal details of expected temperature and precipitation changes, thereby contributing to the difficulty of preparing assessments of ecological, agricultural, and other societal impacts.

Progress in improving the ability to make climatic projections will require continued efforts to improve understanding through computer modeling and analysis and through laboratory observational studies. Detailed model comparisons should help to identify and resolve the causes of differences among models and thereby lead to more accurate projections. By more closely coupling these research efforts with diagnostic studies attempting to reconcile the climatic record of the past 100 years with possible causes of the observed changes and fluctuations, the rate of advance of our knowledge should increase.

Theoretical understanding provides a firm basis for projecting that continuing emissions of CO_2 and trace gases will warm the global climate by a few degrees Celsius during the next century. We are already committed to some of this warming as a result of emissions over the last several decades.

Important uncertainties concerning the regional and seasonal patterns of the temperature and precipitation changes can only be resolved by a broad-based improvement in understanding of climatic processes and mechanisms and in our ability to simulate the climate system.

TASKS FOR THE FUTURE

The overall goal of the CO_2 research program of the U.S. Department of Energy is to provide a stronger scientific and technical basis for projecting the climatic effects of increasing CO_2 concentrations and other perturbations. Such information is essential so that useful assessments of the potential ecological, agricultural, and societal impacts can be made. To achieve the goal of improved climatic projections, improvements need to be made in the models used to estimate the equilibrium climate sensitivity and the time-dependent climate response. Much can be accomplished during the next 10 years. The research needed to improve capabilities for projecting potential

future climatic conditions falls into the following five most important areas of activity:

1. *The ability of climate models to simulate observed climate behavior must be more thoroughly investigated.*
   - The results of climate models must be more exhaustively compared with observations of the present climate. Improvement of the ability of climate models to simulate the regional variations of climatic parameters is of special importance.
   - Where possible, climate models should be tested to determine if they can accurately simulate past variations in climate. This requires that the causes of past climate changes be investigated.
2. *Determination of the time rate of climate change requires that oceans and ocean-atmosphere coupling be more accurately treated in climate models.*
   - The dynamics of the upper ocean must be included in climate models so that potential changes in currents, mixed layer depths, and upwelling and bottom water formation rates can be represented.
   - The transport of heat from the mixed layer to deeper levels in the ocean must be included explicitly and realistically in climate models. Field observations will be required to gather the data needed to achieve better understanding of this process.
3. *The adequacy of representations of important atmospheric feedback processes in climate models must be evaluated and improvements added.*
   - The potential for clouds to amplify or moderate climate perturbations must be exhaustively investigated.
   - More accurate treatments of the growth and melting of sea ice and snow cover are required in models so that the high-latitude temperature changes can be accurately projected.
4. *The potential climatic effects of increasing trace gas concentrations require that they be considered as an integral part of the CO_2 climate effects research program.*
   - Atmospheric models capable of treating the radiative, chemical, and climatic interactions of the many trace gases must be developed and tested.
   - Monitoring and laboratory programs are required to provide the data needed to determine the global fluxes, balances, and trends of many trace gases.
5. *Increased effort must be devoted to including consideration of potential changes in climatic variability and the frequency of extreme events in model and analog projections of future climate.*
   - The ability of improved ocean-atmosphere climate models to represent the natural variability of the present climate on regional and larger scales must be documented.
   - Consideration must be given to developing alternative methods for projecting changes in the frequency of rare events. Statistical or analog methods may prove useful.

1. CARBON DIOXIDE AND CLIMATE CHANGE: BACKGROUND AND OVERVIEW

Michael C. MacCracken
Lawrence Livermore National Laboratory

CONTENTS

1.1 INTRODUCTION

The Earth's relatively equable climate (as opposed to the stark day-night contrasts of Mars and the Moon or the intense heat of Venus) is made possible by the beneficial interactions of the oceans, the biosphere, and the atmosphere. This thermal stability is achieved by a balance of the shortwave (solar) radiation reaching the Earth from the Sun, and the longwave (infrared) reradiation from the surface and atmosphere to space. Some of the species in the atmosphere play a particularly important role in maintaining this balance, especially water vapor, carbon dioxide (CO_2), ozone (O_3), and numerous other gases present in small amounts (referred to as trace gases) that have radiative characteristics similar to CO_2. Water vapor, CO_2, O_3, and other trace gases reduce the rate of loss to space of the thermal energy emitted by the surface and lower atmosphere, thereby increasing the global average surface temperature by more than 30°C above the nominal temperature that would occur in the absence of an atmosphere. As a consequence, the climatic effects of the increasing concentrations of these trace gases are of as much interest as those of CO_2, and much of what is said about CO_2 in this volume also applies to changes in concentration of these other trace gases.

Although there have been natural fluctuations and a long-term evolution of the atmosphere's composition, not until the 19th century were the activities of civilization sufficient to start playing a noticeable role. Mechanization of agriculture and the increased use of fossil fuel energy for industrialization, however, have released to the atmosphere large amounts of CO_2 that nature had previously held trapped in the soils, biota, and as fossil fuels. Our society has combined and transformed chemical substances into trace gases that, when released into the atmosphere, can significantly alter its chemical and radiative characteristics. Such alterations have the potential to perturb the behavior of the coupled atmosphere-ocean-land-ice-biosphere climate system, thereby upsetting society's adaptation to the present global environment.

Study of the potential effects of alterations in the atmospheric composition is especially important because these alterations may already be subtly influencing societal activities and they are likely to do so more visibly within the next few generations. The induced effects will be worldwide and are likely to persist for centuries and to be practically irreversible, therefore requiring long-term societal adaptation if not prevented. Trabalka (1985) reviews evidence indicating that the atmospheric concentration of CO_2, the best understood of the various trace gases, has risen by about 25% in the past 150 years and may more than double its preindustrial level in the next 120 years or less. The studies described in this volume suggest that a doubling of the atmospheric CO_2 concentration may raise the global average temperature to a level warmer than during any period in the last 100,000 years or more.

This State-of-the-Art (SOA) volume describes the potential climatic effects of the increasing atmospheric CO_2 concentration and briefly discusses the even less well understood effects of the release to the atmosphere of other trace gases. This chapter is designed to introduce the chapters in this SOA by presenting a framework of definitions and background information. In developing this background, the definitions will be related to the CO_2 and trace gas issue via examples intended to provide an overview of the potential climatic effects. The subsections will consider, respectively, the nature of climate. the means of predicting climate change, and an outline of the remaining chapters of this volume.

1.2 THE NATURE OF CLIMATE

1.2.1 Weather and Climate

The weather and climate of a region are important determinants of its character. What is happening at a particular instant can determine our health, how we dress, the rate and type of energy use, the growth rate of plants, our sense of safety and well-being, and much more. The combination of such long-term indices as temperature range and moisture availability determines whether the natural vegetation is forest, prairie, desert, or tundra and the ease with which society can adapt to nature's stresses. The frequency of such extreme events as tornadoes and drought as well as the durations and intensities of winter and summer affect the investment in resources required to moderate economic and physical stresses created by the weather and climate.

These many societal and ecological complexities make extremely difficult the development of satisfactory definitions of terms that relate our perception of the world to a mathematical or physical description. Two common terms used to describe our atmospheric environment are weather and climate (see National Research Council 1975; World Meteorological Organization 1979).

Weather is associated with the complete state of the atmosphere at a particular instant and location and with the change of this state through the generation, growth, and decay of individual atmospheric disturbances.

Climate is the average of weather over a specified period of time long enough to establish its statistical properties (averages, variances, probabilities of extreme events, etc.). Such a description may be conveniently called a *climatic state.* Thus, we experience and are affected by the weather, but future expectations and our cultures and civilizations have adapted to the climate.

Weather and, more so, climate also refer to the interactions of the atmosphere with the oceans and land. For example, the amount of rainfall from a thunderstorm, the snowfall accumulation during a blizzard, and the wintertime growth of sea ice are all encompassed in the perceptions raised by the terms weather and climate. Any attempt to project the future climate, therefore, requires consideration of not just the potential state of the atmosphere, but that of the oceans, the land, and the ice on sea and land.

Weather and climate must also be understood in terms of a spatial domain, the size of which, in some senses, determines the temporal separation to be used to distinguish between weather and climate. Atmospheric disturbances occur on many time and space scales, from dust devils and rain showers, which are weather, to planetary-scale circulations, including the Southern Oscillation (a several year fluctuation of pressure, wind, and rainfall patterns), which have aspects of both weather and climate. This wide range of phenomena makes the demarcation of appropriate space scales very difficult. Acknowledging implicitly the bounds of present scientific understanding and the limited abilities to predict a region's climate, those studying changes in climatic conditions usually refer to regions with scales of tens to hundreds of kilometers, with each region assumed to have relatively homogeneous conditions (often in terms of some parameter or parameters relevant to important societal activities). Examples might include the corn or winter wheat regions of the Midwest, major river basins, or forests in the southeastern United States.

Over these regional scales, likely values for temperature can be determined with reasonable confidence in some regions from measurements lasting for only a decade, whereas in other regions, especially near margins of climatic zones, long-term fluctuations may occur. For the latter type of region, very long records are required to determine a stable estimate for the "average" climate. Longer periods also are usually required to determine a useful estimate of mean precipitation; this is a result of the larger temporal and spatial variability of precipitation than of temperature. For all regions, it takes many decades to establish the higher moments of the statistical distribution (e.g., hurricane or drought frequency, number of days per month with temperatures higher than some value). Although these values are difficult to acquire, such knowledge is needed to properly establish the possible extreme situations that typically cause the most severe impacts on societal activities and structures.

Convention has arbitrarily chosen a moving time period of 30 years to define the *normal climate.* This special choice represents an attempt to balance the practical limitations of data accumulation and analysis with the statistical requirements for a record to be kept over periods long enough to develop stable statistical measures. Because most societal activities are well adapted to the normal climate, most interest focuses on deviations from the normal mean conditions. Differences between climatic states of the same kind over monthly, seasonal, annual, or decadal time scales are referred to as a *climatic variation.* A climatic variation will also include, in general, a change in the statistics, as well as a change of the time means. In some cases, a change in the variance may in fact be a more important aspect of a climatic variation than a change of the average. We may also introduce the concept of a *climatic anomaly* (defined as the departure of a particular climatic state from the average of a number of climatic states, such as the climatic anomaly of a particular January) and the concept of *climatic*

variability (defined as the variance among a number of climatic states of the same kind, such as the variability of January climates) [National Research Council 1975]. Climatic variability is usually considered to occur as a result of causes that are not yet completely understood. *Climate change,* however, refers to shifts in the normal climate, usually a consequence of perturbations of some known (or potentially knowable) factor, lasting over many years. Thus, year-to-year events, such as several years of extremely wet or dry conditions, are climatic variations if they are within the expected statistical deviations around the normal climate, whereas the gradual melting of sea ice due to hemispheric warming may result from a climate change.

Within rather broad limits, we can develop numerical models that can simulate the normal climate assuming a given atmospheric composition, solar irradiance, land-sea distribution, topography, and so forth. The capability does not yet exist to predict a specific sequence within such a normal climate, and the capability is only now developing to simulate the level of climatic variability expected within such a normal climatic state. Thus, we can attempt to simulate the climate for different concentrations of CO_2, but we cannot yet accurately predict the climatic anomalies that would be expected over a period of, say, the next few months.

Being certain that an emerging anomaly is actually a climate change instead of simply a variation within the normal climate may require a relatively long period—even well after a change has started and the potential impacts have begun to be felt. The essential point to recognize is the need, in every projection that is made, to express any potential climate change in terms of knowledge of the past behavior of the climatic parameter that is being examined. Unfortunately, as will be seen, a conflict exists that is not easily resolved, that is, it has been easiest to observe accurately the climate statistics of relatively small regions, whereas scientific attempts to make projections of climate change are most valid on large global scales over long periods of time. This mismatch has also carried over to the study of the impacts of CO_2-induced climate changes; biologists and ecologists seek detailed information on the projected changes of the local climate, whereas climatologists can most confidently provide large-scale integrals. This report is a review of the efforts being made to resolve this difficult problem of projecting potential climate changes in ways and with an accuracy suitable for use in conducting impact studies.

1.2.2 The Climate System

The climate of a region is a consequence of its latitude (which determines the annual cycle of the amount of solar radiation reaching the top of the atmosphere); the region's location with respect to nearby water masses, mountains, and land areas; and the weather systems that cross the region. The complex of weather systems a region experiences, however, is controlled not just by local factors, but by the totality of the global system. A recent example of such interactions has been the worldwide anomalous weather attributed to the few-degree rise in ocean temperatures in the tropical Pacific Ocean (the El Niño). In this case the interactions apparently were associated with an unusually warm 1982–1983 winter in the eastern United States and an unusually strong interaction of warm and cold air over the southeastern United States, resulting in extensive storm damage.

1.2.2.1 Climate System Components and Processes

Figure 1.1 is a schematic diagram of the components of the *climate system,* including the atmosphere, ocean, ice, biosphere, and land elements. The time- and space-dependent behavior of these elements is influenced by the collective behavior of a variety of phenomena, each dependent on a number of more fundamental processes. Thus, for example, atmospheric behavior is influenced by radiative processes, which are in turn dependent on the amount of solar radiation and cloudiness, the surface albedo (reflectivity), and the concentrations of radiatively active gases (water vapor, CO_2, O_3, and other trace gases such as methane and chlorocarbons). Ocean temperature is dependent, for example, both on interactions with the atmosphere and on internal oceanic factors (e.g., ocean circulation and composition). The interactions of these components and processes are governed by fundamental physical laws that drive the system toward a global and local equilibrium (or balance) of energy and momentum. Equilibrium, however, is never

quite achieved, because the daily, seasonal, annual, and longer term changes of solar insolation and factors such as atmospheric composition are constantly forcing the atmosphere to seek an equilibrium different from that which it was seeking earlier.

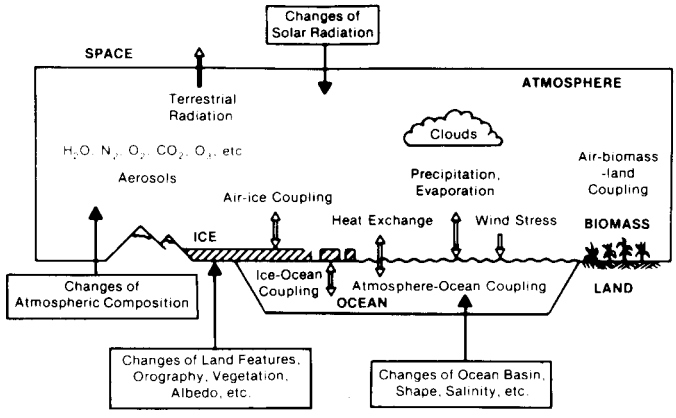

Figure 1.1. The principal interactions among the components of the atmosphere-ocean-ice-land surface climate system and some examples of external changes that may cause climatic variations. Source: Gates (1979).

In attempting to estimate the potential climatic effects of increasing CO_2 and other trace gas concentrations through the 21st century, it is essential to consider the effects of all of those elements of the climate system that may interact and be changed during the period over which the CO_2 concentration changes and over longer times as well (see further discussion in Chapter 3 of this volume). Because this time scale may be thousands of years, the climatic aspects of the CO_2 issue require consideration of all but the geological elements of the climate system. (Interestingly, however, study of the geological elements may provide indications of past atmospheric conditions that may help us to understand how the climate system has responded in the past.)

The heat capacity of the atmosphere is relatively small, equivalent to only about a 2.5 m depth of water; thus, its thermal inertia, or resistance to temperature change, is relatively small compared with that of the ocean, which is 4.5 km deep. Response times of processes in the atmosphere can, therefore, be quite short. Individual clouds typically exist for less than an hour; storm systems typically dissipate in several days, unless they are sustained by nonatmospheric forcing factors (e.g., ocean-land temperature contrasts).

The lower atmosphere, in which rapid vertical mixing by convection can occur and in which there are many radiatively active gaseous constituents, is called the *troposphere*, and it extends from the surface up to 8 to 12 km, depending on latitude. The capability to predict future atmospheric states is limited, because the troposphere requires only a few weeks to approach a new thermodynamic and dynamic equilibrium in response to a forcing. Above the troposphere is the *stratosphere*, where the approach to equilibrium is controlled to a greater extent by radiative and chemical processes (Blake and Lindzen 1973).

The fluxes of energy within the atmosphere-surface system can be illustrated using an energy balance diagram. Although many measurements have been made at the surface and from satellites, there are still uncertainties of 10–20% in the values of some of the fluxes because of the difficulty of making representative global measurements. In some cases model calculations have been used to generate estimates. The values shown in the diagram in Figure 1.2 are derived from consideration of energy balances prepared by Gates (1979), Liou (1980), and MacCracken (1984), and are only an approximation. The atmosphere absorbs approximately 23% of the incoming solar radiation, mostly in the troposphere. The atmosphere is driven primarily by the energy transferred to it from the land and ocean via infrared radiation (equivalent, somewhat surprisingly, to about 115% of incoming solar radiation), heat released when evaporated water vapor condenses (about 24% of incoming solar radiation), and the direct transfer of heat, often called sensible heat (about 7% of incoming solar radiation). The atmosphere loses heat almost exclusively by infrared emission to space and to the surface (about 60% and 100% of incoming solar radiation at the top of the atmosphere, respectively).

It might seem that significantly altering the climate would require substantial changes in these fluxes. This turns out not to be the case. For example, doubling the CO_2 concentration without allowing the climate system to readjust leads to reduction of the loss of infrared energy to space by less than 1% of the incoming solar radiation (see discussion in Chapter 2 of this volume). That small amount of heat, and an additional increment as a result of a vertical readjustment of the infrared flux, causes

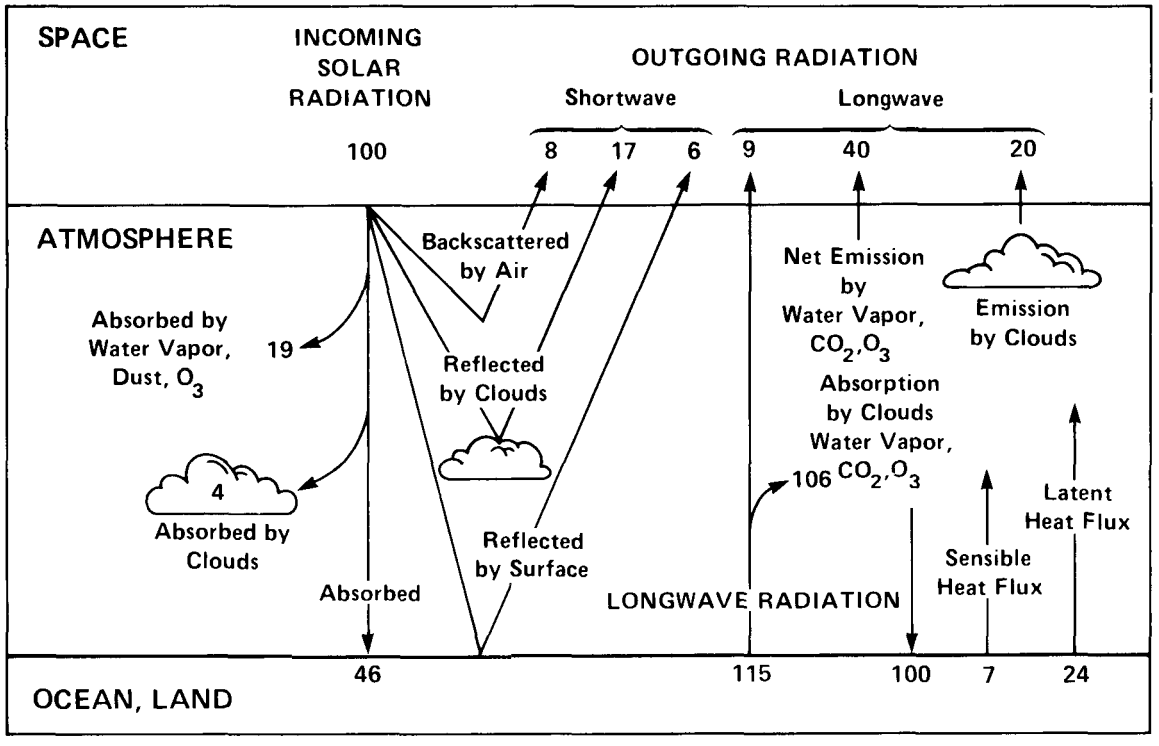

Figure 1.2. Schematic diagram of the global average components of the Earth's energy balance.

the atmosphere to warm enough to again radiate to space as much energy as was being radiated before the CO_2 concentration was increased (assuming no change in planetary reflectivity). Because the infrared radiation emitted from the atmosphere to the surface is a very large fraction of the infrared radiation emitted by the surface, a doubling of the CO_2 concentration can significantly raise the global average surface temperature. As discussed later in this chapter and particularly in Chapters 3 through 6 in this volume, calculating how much this warming will be, however, requires interactive consideration of many processes (e.g., clouds, sea ice, water vapor.)

The heat capacity of the land surface and its vegetation also introduces a variety of time scales. For short-term perturbations, the heat capacity of the land surface is smaller than that of the atmosphere, involving only the equivalent of a few tens of centimeters, depending on the particular characteristics of the surface. For bare, dry land, a thin layer of the surface responds within a few hours to variations in the incident solar radiation so that the temperature increases or decreases until losses that are due to the emission of infrared radiation and the convective heating of the atmosphere (and relatively small subsurface heat conduction) are equal to the absorbed solar radiation. For moist land, solar energy is used more for evaporation than for warming, especially in the presence of vegetation which can increase the effectiveness of moisture transport from the ground to the atmosphere. The evaporation of water transports energy from the surface to the atmosphere (the energy having been used for vaporization), where the condensation process releases the energy and heats the atmosphere. On an annual time scale, land surface temperatures may change to depths of 1 m or more as a result of accumulated subsurface heat conduction; the total energy stored, however, is relatively small. The effect of changes in the characteristics of the vegetation cover throughout the year, however, may cause more substantial changes in the fluxes of energy. The amount of solar radiation absorbed by the surface depends on its reflectivity (or albedo), which is partially controlled by vegetation. Vegetation depends on available moisture, and moisture loss (evaporation) depends on vegetation, precipitation, and the temperature; temperature and precipitation in turn depend on surface and atmospheric moisture and surface albedo. As a result, interactions can be complex and involve many time scales.

The average depth of the oceans is about 4 km, and if there were processes that closely coupled its various parts, the oceans would have a heat capacity (and thereby provide a *thermal inertia* or buffer) about a thousand times that of the atmosphere and the land. Because the density of sea water is a function of temperature and salinity, however, the ocean is usually stratified and is not rapidly or deeply mixed. The ocean water near the surface that is warmed by the Sun is mixed by the wind only to depths of 20 to 200 m, depending on season, temperature, latitude, and other factors. This well-mixed surface layer is, under most conditions, virtually disconnected from the deep ocean (depths greater than 1 km), except in near polar latitudes in winter (where cold surface water can sink), in highly saline oceanic regions (e.g., the Mediterranean), and in equatorial and a few coastal regions (where winds create a divergence of the warm surface waters, allowing upwelling of colder deep water). Because of this layering of the oceans, the well-mixed surface layer can change temperature within a few years whereas the deeper ocean takes centuries. The effects of these different ocean time constants on CO_2-induced climate changes are discussed in Chapter 5.

The cryospheric components of the climate system also introduce a variety of time constants. The altitude of polar continents and the large oceanic heat capacity below sea ice, for example, make the behavior of polar continents and an ice-covered polar sea quite different. The layer of snow on land is usually shallow, but, despite its low heat capacity, its heat of fusion gives it a larger thermal capacity than bare land. Because of its high reflectivity, snow can dramatically alter the amount of solar radiation absorbed at the surface. Sea ice is typically a few meters thick; the energy required to melt sea ice is about equal to that necessary to warm a 200-m-deep, well-mixed layer of water under it by 1°C. Because sea ice is highly reflective and does not allow significant heat transport from the underlying ocean to the atmosphere, it can have an important effect on energy fluxes. The Greenland and Antarctic ice caps are a few thousand meters thick, thereby introducing thermal inertias (when their volumes relative to the deep ocean are considered) that are approximately equivalent to that of the deep oceans were they to undergo a 10°C temperature change.

1.2.2.2 Climate System Behavior

Although Figures 1.1 and 1.2 portray the global climate system as a relatively simple system not far from equilibrium, the system is continually driven out of equilibrium by changing thermal gradients. Energy (in the form of both heat and water vapor) is transported from low latitudes, where incoming solar radiation is relatively intense, to high latitudes where it is relatively low or absent in winter. As ocean currents move from the equator to the poles, they transport absorbed solar energy from warm to cold regions. In winter, energy is transported from the oceans, which are slow to cool, to the atmosphere and then over the continents, thereby helping prevent even more extreme wintertime cooling of the continents. These transports and motions are the weather systems that, when accumulated over time, make up the climate.

The longitudinally averaged north-south (meridional) temperature distributions that result from these interactions are shown in Figure 1.3 for winter, summer, and annual periods. Changes as a function of both season and latitude are evident, resulting from the changing solar insolation with season. At each latitude, the temperature varies with longitude, depending primarily on the land-ocean distribution and the season (Figure 1.4). Temperature patterns vary even more on scales finer than those shown. with societally important variations occurring on scales as small as a few kilometers. By considering temperature patterns in even greater temporal detail, the difference between summer and winter average temperatures also can be seen to vary considerably, as do such additional measurements as daily temperature range, frequency of very hot days, and so forth.

Figure 1.5 shows the complexities of the seasonal precipitation patterns. Because precipitation is an intermittent rather than a continuous phenomenon, particularly important consequences can arise when extreme conditions occur. Similar results could be shown for soil moisture, snowfall, and other variables.

The atmospheric wind fields that carry heat and moisture are determined by the interaction of the Earth's rotation and gradients of pressure created by the variable patterns of temperature and moisture, which in turn have been determined by the

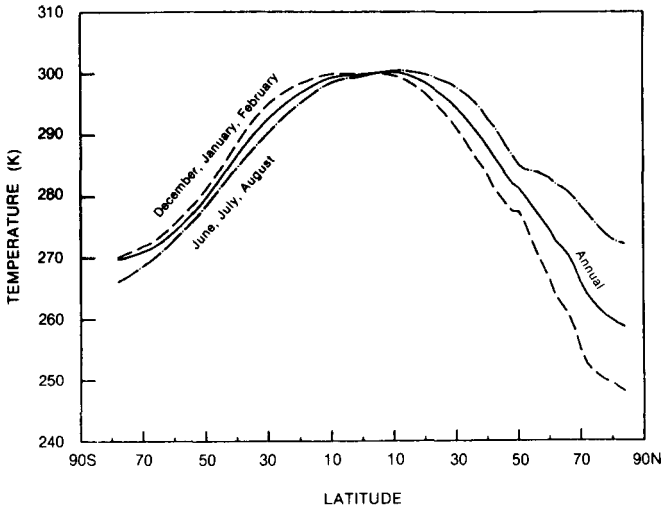

Figure 1.3. Zonal average 1000 mb air temperatures for June-July-August, for December-January-February, and for the yearly average, based on data from Oort (1983) (1000 mb = 100 kPa).

wind fields. In low latitudes there is, on the average, rising motion near the equator where meridional winds converge (the intertropical convergence zone) and descending motion in the subtropics (extending from about 10° to 30° latitude). This low-latitude circulation is known as the *Hadley circulation* (or Hadley cell). Rising air occurs primarily in individual convective cells (e.g., thunderstorms) that release large amounts of rainfall. The heat released from this condensation further lifts the air, leading to warming in the descending air of the subtropics as the air is compressed, thereby drying the air (i.e., reducing relative humidity) and reducing precipitation.

In middle latitudes, the surface pressure pattern is more complicated. At these latitudes, energy is most efficiently transported toward the poles via large-scale waves and cyclones that move warm air toward the pole and cold air toward the equator. The resulting air mass contrasts, particularly in winter and spring in the Northern Hemisphere when the equator to pole temperature contrasts are large, create the large- and small-scale storms that tend to move from west to east around the middle latitudes, often dramatically changing local weather every few days. In summer, there is less need to transport energy poleward because of the day-long solar input at high latitudes. At these times of year, the middle latitude waves are less intense, and temperatures depend more on local conditions than on global gradients.

1.2.3 The Climate Record

Despite the day-to-day variations of weather, the time-averaged conditions are, in most cases, remarkably stable from year to year over the normal human lifetime. One way this is indicated is by the relative stability of the ecosystems that have evolved in response to local climates. There have, however, been significant shifts and changes over long time scales (see discussion in Chapter 7 of this volume). During glacial times ice covered much of Canada and the northern United States; beginning about 12,000 years ago and especially from 5000 to 9000 years ago, the region of the present Sahara Desert was quite moist. It is not now clear whether large changes such as these occur gradually (and so could be adapted to) or in intermittent jumps over shorter periods (which could be very disruptive of societal activities). Developed societies tend to devote significant resources to building a resiliency to the climatic variations that they expect to experience. One of the most important but most difficult questions is whether the frequency of climatic extremes may change (or even whether it has changed) as a result of the varying CO_2 concentration. For example, determination of whether the frequency of drought might change would be especially important in planning for water resource development in the western United States; changes in the expected dates of first and last frosts could alter planting schedules.

One measure of the behavior of recent climate is the record of near-surface air temperature. A Northern Hemisphere record from land stations for which data are available over long periods of time and records of Northern and Southern Hemisphere nighttime marine air temperature assembled from ship observations are shown in Figure 1.6. These records and those of several other climatic indicators are discussed extensively in Chapters 3 to 7 of the accompanying SOA report (MacCracken and Luther 1985).

Over the last 100 years the large-scale *hemispheric-average* near-surface air temperature has varied over a range of about 0.5°C, with year-to-year fluctuations that are usually less than this amount. If the increasing CO_2 concentration were to raise global average temperatures by about 3°C, as suggested by Charney (1979) and the National

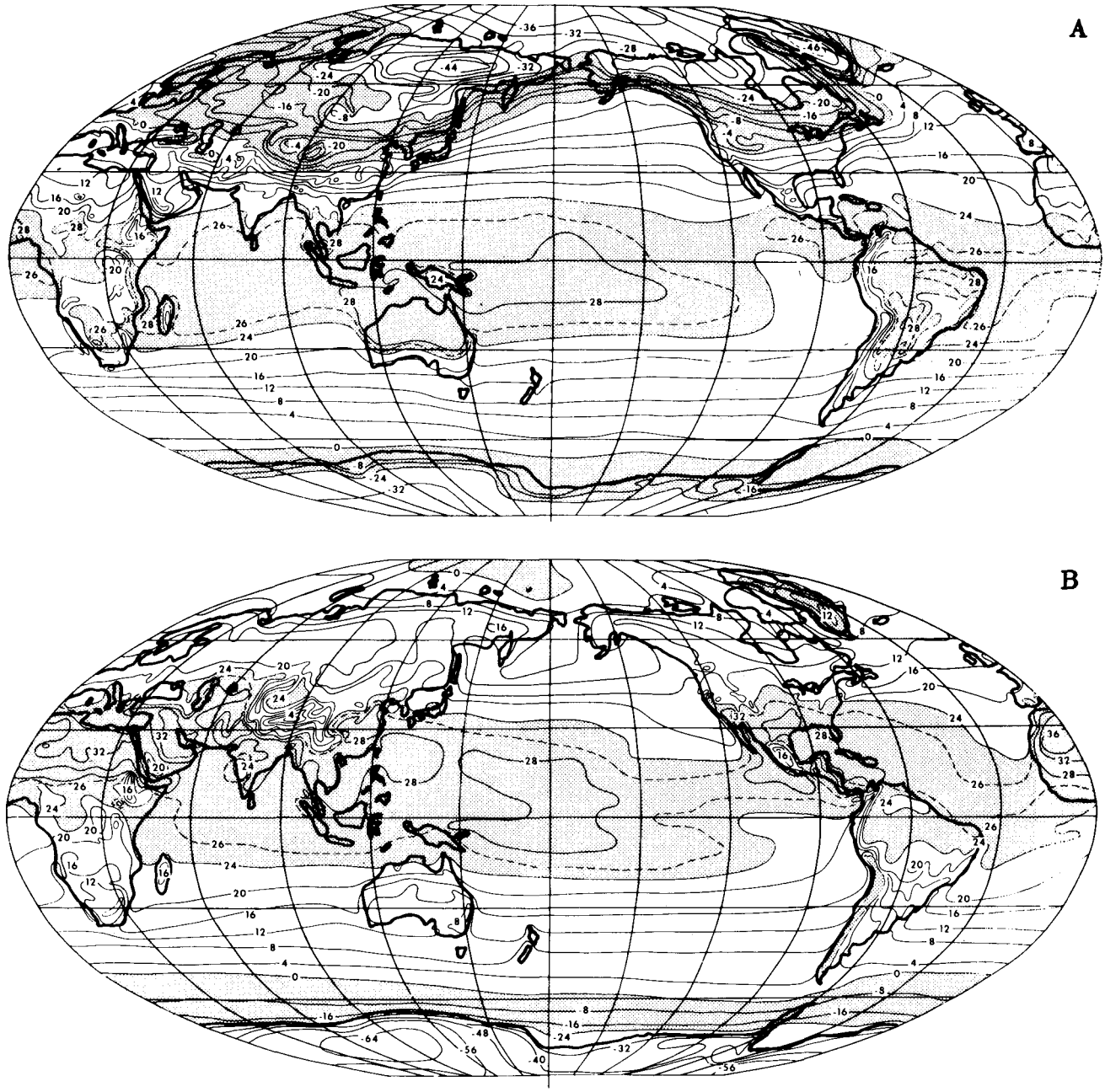

Figure 1.4. Global distribution of mean observed surface temperatures (°C) for January (A) and July (B), as presented by Manabe and Holloway (1975), based on data by Crutcher and Meserve (1970) and Taljaard et al. (1969). Areas having temperatures above 24°C or between 0 and −24°C are shaded.

Research Council (1983), the change would be evident on the hemispheric scale, causing average temperatures to reach levels not experienced over anomalous periods longer than about a month in the past 100 years, nor, based on other indicators, in as much as 100,000 years.

Although global average temperature fluctuations are only tenths of degrees, month-long and annual variations on smaller scales, particularly in middle latitude, midcontinental regions, can be larger, and annual average variations can be several degrees in either direction. We can expect that as the global average temperature rises, such strong local variations will likely continue to occur. Because of these large local fluctuations, it will continue to be difficult to identify temperature changes in local records. Such large variations, however,

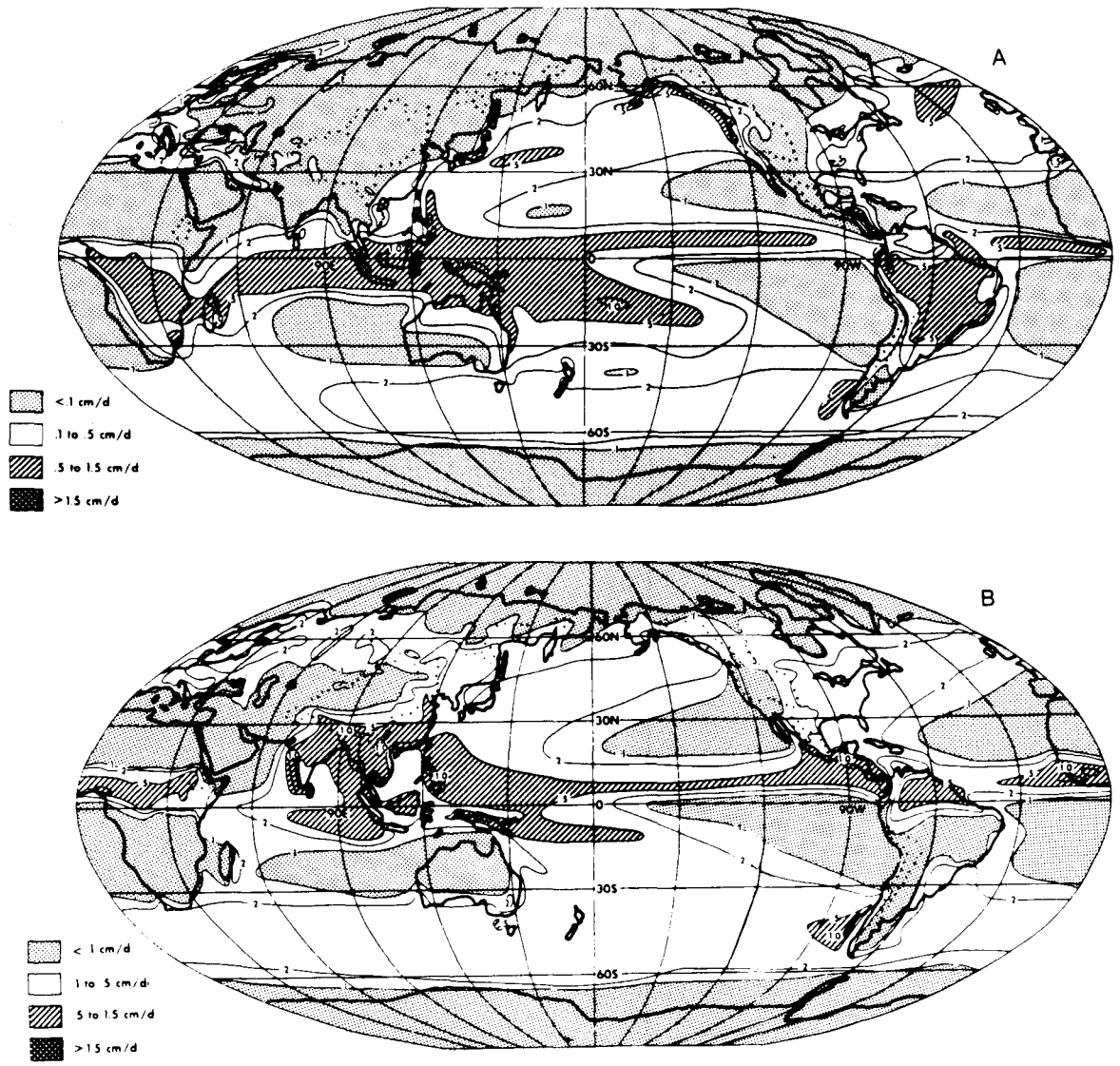

Figure 1.5. Global distribution of mean rate of precipitation for December, January, and February (A) and for June, July, and August (B), as presented by Manabe and Holloway (1975) based on estimated data from Möller (1951).

also mean that some local regions (mainly in middle rather than high or low latitudes) have experienced individual months probably not unlike the average conditions to be expected if the NRC projections are correct. In addition, when people move from place to place, as Schelling (1983) points out, they may experience conditions as different as might be expected to occur in the next 100 years. It is important to recognize, however, that the cultural and physical environment to which they are accustomed does not move with them, thereby introducing adaptive stresses.

For several reasons, however, such experiences should not be viewed as completely reassuring. Because animals, trees, plants, farms, soils, dams and flood control projects, and other structures are not as easily movable as people, the normal climate for them may become more like conditions that are now viewed as being relatively extreme. The continuing impacts of such a situation also can be expected to be more stressful than if the extreme is only short lived. In addition, although not indicated by present calculations, what are now considered to be extreme conditions could be more frequent than they are at present, further amplifying the impacts of any climatic stresses created by changes in the

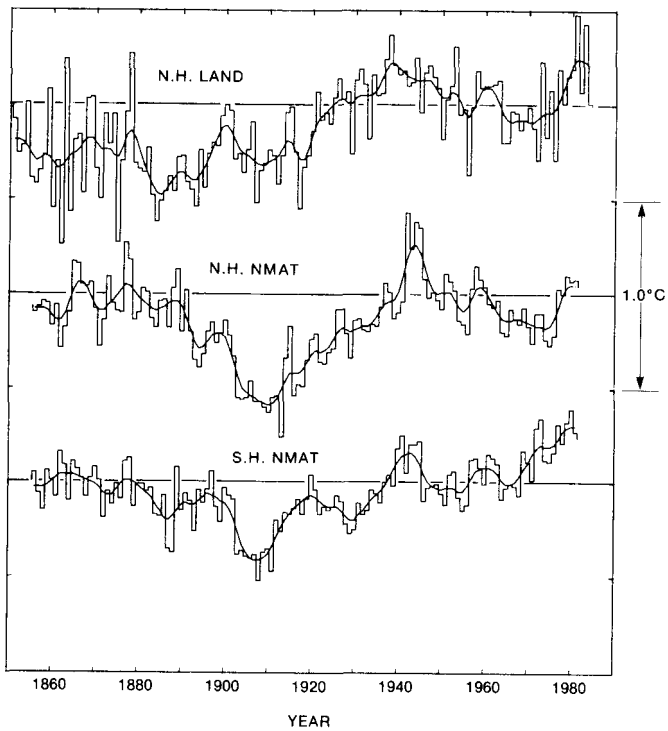

Figure 1.6. Comparison of Northern and Southern Hemisphere surface air temperature fluctuations. Data are from Jones et al. (1986) for the Northern Hemishere land areas and from Folland et al. (1984) for Northern and Southern Hemisphere nighttime marine air temperatures. The unpublished Southern Hemisphere data were supplied by D. E. Parker (personal communication). Smooth curves were obtained by using a 10-year Gaussian filter. Source: Wigley et al. (1985).

average climate. Of as much, and perhaps more, importance will be the rate at which these changes may occur; if the changes are slow, the adaptive stress will likely be more tempered and tolerable than if the changes are rapid.

It is the potential for significant societal stresses from the warming projected to result from increasing CO_2 and trace gas concentrations that accentuates the need for better scientific estimates and that has, to a large extent, prompted the organization of national and international CO_2 research programs. The following sections of this chapter and the rest of this report describe recent efforts that have been made to improve the understanding of this issue and summarize current estimates and uncertainties.

1.3 MEANS FOR PROJECTING THE FUTURE CLIMATE

Given the relative stability of the climate, one means for estimating future climatic conditions, if climatic system characteristics were being steadily perturbed over a long period of time, would be to extrapolate forward from past conditions. In the case of the increasing CO_2 and trace gas concentrations, however, the basic radiative characteristics change nonlinearly, and concentrations of some species are changing at an accelerating rate. To make climatic projections, therefore, it would be necessary either to find a past situation during which time similar changes were taking place (referred to hereafter as *climatic analogs*), or to develop theoretically based estimates, usually by means of mathematical models. Because of limitations in data bases, incomplete understanding of the causes of past climate changes, and an unprecedented rate of change of atmospheric CO_2 and trace gas concentrations, no perfectly suitable analog is available, and theoretically based estimates will have to be the primary means for looking ahead, even though the theoretical approach is also imperfect.

1.3.1 Mathematical Models of the Climate System

The climate system is exceedingly complex. When examined on a very fine scale (e.g., meters or less), nearly every process and alteration can be explained in terms of well-defined physical laws or statistically derived relationships governing stochastic occurrences on even finer spatial scales. The conservation laws for mass (of air, water, trace gases, etc.), energy, and momentum are the most important laws for the study of climate. Some of the important processes representing transfer for these quantities can be examined by laboratory and field experiments, and the applicability of representations of the processes can be confirmed. Limitations imposed by mathematical solution techniques and by the capacity and speed of computers prevent consideration of the global atmosphere in enough detail for these laws to be applied directly without making simplifying approximations. To make the set of equations more tractable, a variety of often interdependent assumptions and approximations (often referred to as *parameterizations*) must be made. This is one source of imperfection in the theoretical approach.

The choice of assumptions selected is usually tailored to the type of problem and the resources available for solution and analysis, as discussed more completely in Chapters 3 and 4 and in Appendix A of this volume. The resultant set of simplified equations and parameterizations is referred to as a *climate model.*

One class of assumptions concerns the components of the climate system included explicitly in the model. In some cases only the atmosphere is treated, with the ocean and land temperatures parameterized in terms of the atmospheric temperature (or vice versa); in other cases, the atmosphere, ocean, land, sea ice, and continental snow are all treated explicitly. The biosphere and glacial ice are rarely treated explicitly in present climate models, although on the time scales important for studying the potential effects of the increasing CO_2 concentration on climate, these domains may need to be treated.

Another class of assumptions concerns the set of equations treated by the model. *Energy balance models* (EBMs) usually base their calculations only on the conservation of energy, with the simplest EBMs treating the entire Earth as having a single temperature. More complex EBMs represent the land-ocean latitudinal differences and parameterize the transport of energy by atmospheric motions. *Radiative-convective models* (RCMs) treat the vertical structure of the global average atmosphere, assuming buoyantly stable stratification. These models are particularly well suited to detailed study of the radiative effects of CO_2, trace gases, and aerosols and of chemical interactions among species. *General circulation models* (GCMs) are three-dimensional models that explicitly include the conservation laws for mass of air (expressed in terms of surface pressure), mass of water vapor, energy, and the *zonal* and *meridional* components of momentum (west to east and south to north winds, respectively). There is a hierarchy of models between EBMs and GCMs, each making different assumptions about climate system components and parameterizations needed to represent aspects of the global system that are of particular interest.

Each model also makes choices concerning spatial resolution. EBMs and other simple models tend to treat the Earth as a single entity or to divide it into latitudinal bands, but do not treat vertical variations. RCMs divide the atmosphere vertically into several layers but do not treat horizontal variations or gradients, and are usually used for equilibrium calculations. The GCMs necessarily treat all three dimensions of the atmosphere or oceans, typically with a resolution of a few degrees latitude and longitude and with, in the models discussed in this report, two to nine layers in the vertical. These models are also time dependent.

Furthermore, approximations must be developed by each model for each of the many processes taking place, approximations that are valid on the space scales and over the time scales for which the model will be applied. An example is the need to represent clouds and cloud systems, which typically have dimensions of one to tens of kilometers, much less than the 500-km grid size typical of GCMs. Major difficulties arise in parameterizing cloud amounts and heights in different atmospheric layers, because these quantities are below the resolution of the model; they must, therefore, be expressed in terms of the large-scale GCM variables that can be calculated using the conservation equations. Because clouds are important in calculating the distribution of radiative energy, the manner in which this approximation is made may be critical. Other such difficulties arise in dealing with vertical convective mixing, sea ice, topographic effects, and other processes. In each case, an attempt has been made to test the accuracy and adequacy of the representation of each process against field experiment and laboratory data, but this is not always easy or even possible.

The number of conservation equations, the spatial resolution of the model, and the complexity of the approximations determine the size of the system of equations to be solved. For a simple EBM, there may be only one equation and one spatial box; for atmospheric GCMs and oceanic GCMs (OGCMs), or even for coupled atmosphere-ocean GCMs, there may be five or more conservation equations and 20,000 or more node points for the atmosphere and an equal number for the ocean, making a system of up to perhaps 200,000 equations, with each equation having terms that require extensive calculations. The set of equations for an EBM can be solved more rapidly (often by hand) than can the set for an atmosphere-ocean GCM, which requires advanced numerical techniques and

the largest available computers (hence the terms *numerical model* and *computer model*). As desirable as it is to develop GCMs with finer resolution, computer requirements increase roughly by a factor of 8 each time the horizontal grid size is halved, so one cannot, in practice, develop a model representing all of the scales of interest.

One might imagine that GCMs, which add together all of these physical laws, assumptions, and approximations, would be able to explain all future climatic behavior. Richardson (1922) attempted a small-scale weather calculation in this way before 1920 and eventually envisioned a large theater with the galleries filled with interactive computers (actually manually operated calculators) calculating the weather throughout the world. Even if at some instant, however, we knew the value of every important variable in every equation for every location, the numerous intercouplings of the equations and the limitations in computer and observational accuracy would make it impossible to carry out an exact projection. Theoretical analyses and numerical calculations have shown that for nonlinearly coupled systems such as the atmosphere, even very small differences (or errors) will grow and propagate over days and weeks until they noticeably affect the solution throughout the entire domain. Thus, in making weather forecasts, in which inherent differences in initial conditions exist because of uncertainties in the observed data (e.g., spatially unrepresentative measurements, biases in the instrument), it has been shown that the *theoretical* limit for locally accurate forecasts is a few days, and for the prediction of major global features it is only a few weeks. The day-to-day (or stochastic) variability of the weather makes prediction of the conditions very difficult.

If the weather cannot be predicted more than a few weeks into the future, even with perfect GCMs, much less with EBMs and other models that do not even attempt to calculate winds or precipitation, what is it that can be predicted? Although the "weather" that GCMs predict may not be identical to the manner in which the atmosphere would evolve from the initial conditions used in the model, many aspects of the space and time statistics of the model's atmosphere compare well with observed statistics, if the model is properly constructed and suitably complete. This comparison process is called *verification* and can involve the interactive (and sometimes arbitrary) adjustment of parameterizations to optimize the agreement with observed climate statistics. Once adjusted, the GCMs can produce both a sequence of atmospheric states that might be called *synthetic weather* and, over time, a set of model climate statistics that are representative of the longer term average modeled climate. If the model is accurate and working well, the results will be quite similar to the comparable observed quantities. Note, however, that EBMs and other climate models parameterize transport processes as well as other processes and simply project only the longer term, lowest moments of the climate statistics. They are, therefore, largely limited to studies designed to better understand the relative importance of various processes and to development of approximate estimates of potential climate changes.

In studies to project the climatic effects of CO_2 and trace gas emissions, for example, the model simulations of the present climate are referred to as the *control* simulations. The initial approach to studying climatic effects is to change a parameter by an arbitrary amount, for example to double the atmospheric CO_2 concentration, and then to determine the new *equilibrium* climate. This is referred to as the *perturbed state*. The difference between the perturbed and control simulations is a measure of the *climate sensitivity* to the chosen perturbation. These arbitrary perturbations are usually chosen to be large enough so that a statistically significant difference (*signal*) can be seen in the model's results, particularly in GCMs, which have an *internal* or *natural* climatic variability (*noise*) introduced by the weather that is approximately equivalent to that of the real atmosphere. (If a GCM truly represented the real world in all its complexity, the variability of the model and the observed climate would be equal. Because models necessarily simplify the climate system—for example, by leaving out the effects of changing ocean temperatures and volcanic aerosol injections—model variability is usually less than that of the real atmosphere.) An important advantage of simpler models is that because they do not attempt to predict the weather, their *signal-to-noise ratio* is substantially higher than for studies with GCMs, and hence it is somewhat easier to

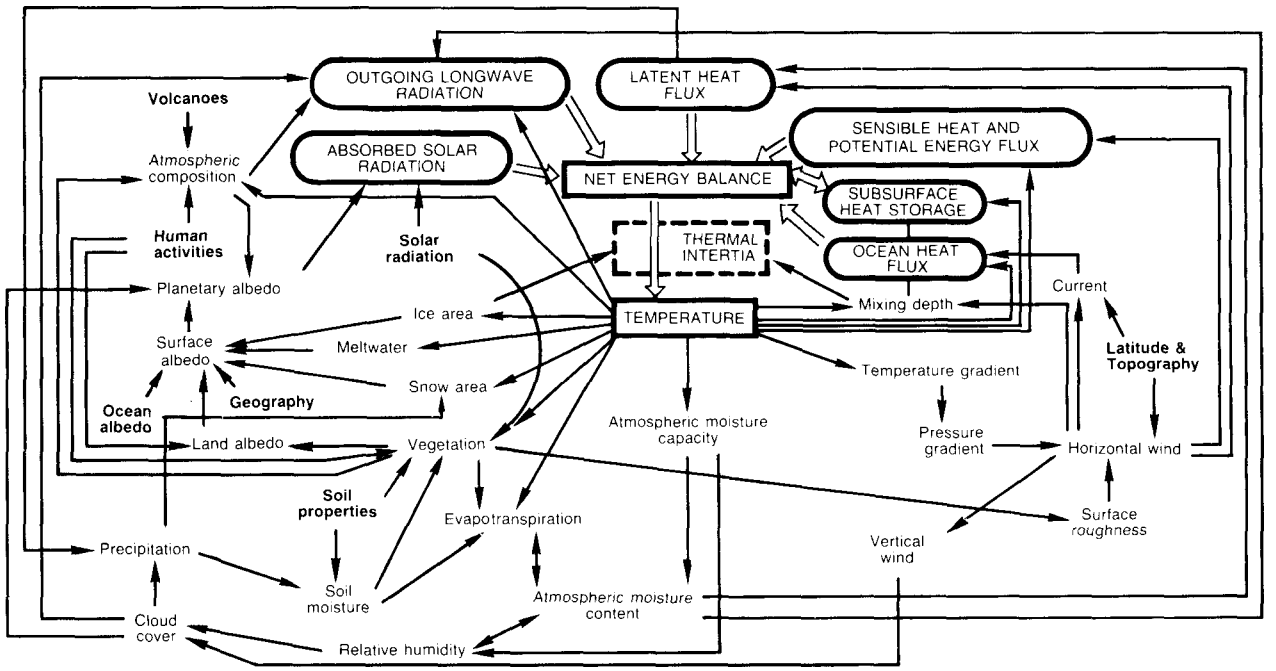

Figure 1.7. Schematic illustration of climatic cause and effect (feedback) linkages and variables that are often included in numerical models of the climate system. Source: Robock (1985).

identify the effects of smaller or shorter term perturbations in simpler models, even though climatic processes may not be as accurately represented.

Because GCMs require extensive computer time (typically tens of hours of time on the largest computers for each year of simulated time), they have been used primarily for sensitivity studies involving arbitrary, step function changes (i.e., discontinuous in time) in various parameters. In making these simulations, the GCMs calculate the transient changes in response to *step function forcing*. Unless a succession of very small increments is treated, however, this transient response does not necessarily represent the manner in which the real atmosphere would respond to a continuously changing concentration because different climate system components are responding at different rates than they normally would, and adjustments (or approximations) are often made in the models to achieve a more rapid approach to climatic equilibrium than would actually be the case. However, some EBMs, which require only seconds or minutes of computer time for each year simulated, have been used to study the evolution of the model climate to realistic, *time-dependent* (or *secular*) forcing induced by changes in radiative parameters. For example, such models have attempted to simulate the climatic response as the atmospheric CO_2 concentration has gradually increased over the last 100 years (Chapter 5). In lieu of such calculations with GCMs, interpolations of various types (typically logarithmic when dealing with CO_2 concentration) are usually made. The difficulty with such interpolations, however, is that the climate system has many time constants, and simple interpolations, especially of seasonally dependent effects, may result in misleading estimates.

Analyses of the results of sensitivity studies, particularly with EBMs and other simple models, have improved the understanding of many climatic interrelationships and interactions. Figure 1.7 is a schematic diagram of some of the interactions that need to be treated in climate models; no models now treat all of these process in sufficient detail. One of the interesting results of model studies has been the identification of important feedbacks, in which a change in one variable changes another (or a chain of other) variables, which in turn either amplifies or moderates the change in the first parameter, thereby causing either a *positive* or *negative feedback*.

Two of the most important positive feedback processes are the temperature-water vapor feedback

and the snow and sea ice albedo feedback. In the temperature-water vapor feedback, because the amount of water vapor in the atmosphere is approximately exponentially related to temperature, a temperature increase will allow the air to hold more water if the relative humidity remains constant. This added water will absorb and reemit more infrared radiation, thereby providing more radiation back to the surface, which in turn can cause more warming and further enhance the atmospheric moisture content. In the case of snow and sea ice albedo feedback, because snow and sea ice both have high reflectivities, a decrease in snow cover or sea ice extent will allow additional solar radiation to be absorbed at those latitudes and melt additional snow and sea ice, allowing even more absorption of solar radiation. Such amplifying feedbacks can also work in reverse. Without these two positive feedbacks to amplify the relatively small direct radiative effect of CO_2, there would be much less concern with the rise in the CO_2 concentration.

At least two other feedback processes may also be very important, but are much less well understood. Cloud feedbacks are extremely complex, involving possible changes in cloud height (top and bottom), amount, type, and optical properties. Increased low cloud amount, for example, can cool the Earth during the day (by reflecting more solar energy) and warm at night (by trapping more infrared energy). The net effect of clouds is not yet certain, nor is our knowledge of how cloud extent and properties may change. Convective feedback and, to a lesser extent, the seasonal cycle can serve as negative feedbacks because warming (cooling) leads to additional (lessened) transmission of energy to space. If these feedbacks are large and cloud feedbacks are negative, then the climate would change very little as the CO_2 concentration increases. Such a combination, however, seems unlikely.

Although researchers have made progress in understanding how well models represent the present climate, improving understanding of the degree to which models are capable of accurately projecting perturbed climates poses more difficult questions and makes model verification both important and difficult. To a limited extent, comparison of model simulations of the evolution of the seasons provides a test in which climate changes are far in excess of any expected from an increase in the CO_2 concentration. Such tests do indeed calibrate model representation of processes having certain time scales, but such tests do not adequately indicate whether processes with longer time scales are properly represented or whether changes in climatic variability (e.g., the frequency of drought) and the variability and extremes of the weather (e.g., the frequency of very hot days in summer) can be represented as the average climatic state changes.

To address the first of these difficulties, research is in progress to determine how well the models represent a variety of past climatic conditions, including a period that occurred 8000 to 4000 years B.P. (often referred to as the *Hypsithermal*), which some have viewed as a possible warm-period analog to a CO_2-warmed world, and the cold ice age conditions of 18,000 years B.P., which may be an inverse analog. Such different climatic conditions can be helpful in verifying that models work properly only if the causes of such changes are understood; recent efforts to link such paleoclimatic changes to variations in the Earth's orbit (the Milankovitch hypothesis) are particularly important (Berger et al. 1984). As will be discussed in the next section, information on past climates may also be helpful in other ways in projecting future climatic conditions.

For the purpose of verifying that the models can properly represent changes in the frequency of weather extremes and climatic variability, our present understanding of the causes for such fluctuations and present model development and verification techniques are deficient. An important future focus for research will be to better verify these aspects of models and to develop alternative approaches for estimating such changes.

In summary, because the climate system is so complex and the situation is unprecedented in historical records, carefully verified climate models provide the only opportunity to project the potential climatic effects of increasing CO_2 and trace gas concentrations into the future. Because such models can never be completely verified, however, it is essential to use our experience with the observed climate to provide a framework for the evaluation of the results of present climate models.

1.3.2 Learning from Past Climatic Behavior

Information on past climates offers two opportunities for improving our understanding of present and future climate: (1) to verify that climate models can accurately represent the present climate and possible climate changes; (2) to develop, if possible, analogs of what conditions could be like in a warmer world.

The combustion of large amounts of fossil fuel and emission of CO_2 into the atmosphere is an unprecedented geophysical event. We cannot expect the past record to provide an exact replication of the recent and projected climate change. We can, however, still learn about what may happen from what has happened in the past (see further discussion in Chapter 7). Climate change has played an important role in human migrations, creating an Asian-Alaskan land bridge during glacial periods and permitting the Norse to cross the North Atlantic during a warm period almost 1000 years B.P. During the Little Ice Age, a relatively cool period in Europe, extending roughly from the 15th to early 19th century, there was speculation that the Sun was emitting less energy as its fuel sources ran down and that further cooling was inevitable. Such speculation, however, prompted geologists to carefully examine past evidence of many types; they found evidence of both warmer and colder periods back into the distant past. More than 65,000,000 years ago, the dinosaurs apparently enjoyed a relatively warm tropical world that apparently had virtually no year-round snow or ice. Only 18,000 years B.P., however, ice a few kilometers thick covered much of Canada, the northern United States, and Europe and this ice lasted in some areas until the Hypsithermal.

With such a variety of past conditions, it would seem to be a straightforward task to develop analogs for a warmer world. There are, however, a number of problems (see, e.g., Bryson 1985). The first is that, in general, the farther one goes back in time, the less specific and less adequate are the data. The instrumental record for temperature goes back only a little more than 100 years; temperatures before that time must be inferred from such information as the length of the growing season, extent of sea ice, type of vegetation or fauna, and other alternative indicators. In addition, information is available only for particular regions, so it becomes difficult to distinguish a regional from a global anomaly. As we go back in time, we also lose temporal resolution, and so we have little information on the extremes and variances of temperature or any other climatic parameter.

A second difficulty is that we do not yet completely understand the cause or causes of past climate changes, nor do we have any evidence that a climatic warming due, for example, to increased solar insolation or altered orbital elements would be similar in pattern to a warming that may occur because of an increasing CO_2 concentration. An exciting new finding is that the CO_2 concentration may have varied during the past 100,000 years and that perhaps some of the past climatic fluctuations may have been due to these natural variations in the CO_2 concentration. If this is true, we may be better able to develop an analog to a CO_2-induced warming.

Until a complete CO_2-related analog is developed, however, the data on the characteristics of past warm climates can only provide a qualitative indication of whether the model results are plausible. In those cases in which the causes of past climate changes can be identified, such records can also provide test cases to be used in model verification studies. In pursuit of these objectives, two periods seem most likely to be able to provide helpful information.

1.3.2.1 The Hypsithermal (8000 to 4000 B.P.)

Interest in both the early development of civilization and the causes of the warming that terminated the ice age conditions of 18,000 B.P. have, over the past 100 years, prompted extensive efforts to reconstruct the evolving climatic conditions of the past 15,000 years. A variety of evidence has been developed that indicates that the last 10,000 years, known as the *Holocene*, has been relatively warm, although its conditions have not been constant. The *Viking period* of about 1000 B.P. was recognized as being warmer than the Little Ice Age conditions of 150 to 400 B.P., at least in the North Atlantic sector. Such preinstrumental determinations are based on what have become known as *proxy data*. Proxy data are indirect measures of the climate that sense its

effect on extant biological or environmental conditions rather than the climatic variables themselves. Mathematical relations that are based on observations of present-day relationships, known as transfer functions, are then used to transform such biological or environmental records into climate records.

A wide variety of proxy data techniques have been developed, much as a detective develops techniques to carefully search for and analyze evidence. The date of flowering of particular plant species, the pollen counts in annual sediment layers in lakes (varves), and the time of year of the breakup of drifting sea ice near Iceland, for example, provide evidence of year-to-year climatic fluctuations. The mixture of pollen grains and macro-fossils from various plants, as preserved in the middens of various animals (e.g., the pack rat) or in lake or swamp sediments, can indicate the type and mixture of vegetation present, which can in turn be related to multi-year average measurements of temperature and precipitation. Although the relationships are not perfect, taken together, they do provide a consistent picture of the climate of the Holocene period.

Proxy data, together with geological evidence (e.g., indications of past lake levels, extent of deserts), seem to indicate that the period from 8000 to 4000 B.P. was significantly different from the present, as it was apparently warmer in summers and the precipitation zones were shifted poleward. This period, referred to variously as the Hypsithermal, the *Altithermal*, or the *Climatic Optimum*, has been thought to have had an average hemispheric temperature as much as 2°C warmer than the present, but, as indicated in Chapter 7, this value is likely too large. If this warmth were proven, this period could provide important clues to what a warmer world might be like, the extent of warm belts, the sensitivity of sea ice to warming, and so forth.

An important problem, however, is that we are not yet certain about why past summer were apparently warmer than present summers. There are some indications that a natural variation in CO_2 concentration may have been at least a contributing cause (Trabalka, 1985), and cyclic variations in the Earth's orbital parameters may also have played a role. We are beginning to understand the extent and timing of the changes, but because the period is so far in the past, it may be difficult to develop information about the natural variability of climate during this period. This latter difficulty is disappointing because the extent of natural variability is one of the societally significant unknowns in present projections of potential CO_2 effects on the climate.

1.3.2.2 The Past 100 Years

Compilations of Northern Hemisphere land temperature observations over the past 100 to 150 years indicate that there have been variations on the order of 0.5°C in annual average surface temperature and of larger amounts in the records for particular months. It seems natural to ask whether we can learn about potential CO_2-induced warming by contrasting warm and cold periods during this time. An important advantage of such studies is that relatively large amounts of data are available, although before 1900 the data cover only relatively limited areas. It is also important to recognize that temperature is not an easily determined quantity, being quite different in the sunshine and in the shade, in the wind or in the calm, over grass or over a parking lot. Conventions have been developed on how to calculate the average temperature, with the most popular one at present being to average the maximum and minimum temperatures at a station over a 24-h period, often ending at a more convenient hour than midnight. Other problems include the sparsity of stations over the ocean, the effect of urbanization, and so forth. Despite these difficulties, several groups have struggled to develop homogeneous data sets as free of biases and pitfalls as possible. Although these efforts are not entirely independent, there is general agreement about the variations that have occurred (Figure 1.6).

To develop an insight into the potential patterns of CO_2-induced warming, a number of approaches have been pursued. All involve the contrasting of warm and cold periods; the difference between approaches is the manner in which each of these periods is developed. One approach, for example, is to compare the average of the several warmest and coldest years of the entire period; another approach is to contrast the warmest sequence of years with the coldest sequence. The problem with the former approach is that the short time constant of year-to-year variability (which the observational record

represents) does not allow for long time period adjustments (e.g., of sea ice and ocean temperatures) that would develop with the continued presence of an increased CO_2 concentration. The problem with contrasting warm and cold sequences is that the temperature changes are usually rather small because, for example, a warm decade often includes at least one cold year (and vice versa). For neither method do we understand whether the temperature differences were the result of natural fluctuations or whether they were caused by specific events such as injections of volcanic aerosols or variations in solar irradiance.

Despite these many difficulties, and therefore the limited applicability of such analogs, difference patterns in the observations, although much smaller than those expected from a doubling of the CO_2 concentration, have some resemblance to the climate changes projected by models. Thus, analysis of observations may be helpful in projecting future changes, as well as being essential in determining whether CO_2-induced changes are taking place.

1.4 OVERVIEW OF REMAINING CHAPTERS

When increased amounts of CO_2 are introduced into mathematical models of the climate, the infrared radiation balance is perturbed and the temperature increases. Although the projected warming associated with a given increase in the CO_2 concentration is not the same in all of the simulations made over the last 30 years, all of the simulations that have been based on the laws governing atmospheric physics and have been applied to study this question do project such a warming. Study of planetary atmospheres indicates that the concentrations of CO_2 and water vapor are critical determinants of the Earth's average temperature. For example, the very warm climate of Venus arises because its atmosphere contains about 200,000 times as much CO_2 per unit area as in the Earth's atmosphere, and the cold climate of Mars occurs because its atmosphere has only one thirty-thousandth as much water vapor as the Earth, although having about 40 times as much CO_2.

Chapter 2 of this SOA report describes in detail the role of CO_2 and other gases in the solar and terrestrial radiation balance. The theoretical aspects are largely understood, although there are still shortcomings in being able to estimate with sufficient accuracy the combined radiative effects of mixtures of gases, particularly water vapor and CO_2. Results of detailed mathematical models can be compared with laboratory measurements, and agreement has been quite good. An international intercomparison is now under way to ensure that the relatively simplified models that must be used in studying climatic effects are sufficiently accurate and in good agreement with observations and detailed radiation transport models.

Chapter 3 and Appendix A present a more detailed description of how climate models are constructed and the processes that determine climate sensitivity. Because the ranges of atmospheric and oceanic scales of motion and response time are so great, present climate models can only approximately represent the important processes. A wide variety of simplifications are made, resulting in a hierarchy of climate models, with the choice of assumptions depending on factors such as problem type (i.e., time and spatial period of interest), computer and personnel resource requirements, level of understanding and relative importance of the process, and so on. The best three-dimensional GCMs now available are able to represent the existence of major features of the global circulation patterns and the seasonal shifts in average temperatures and precipitation zones. These models are not, however, able to adequately represent climatic features at particular grid points and the intensities of some of the major dynamical features of climate, and can only begin to be helpful to those studying changes in subcontinental-scale climatic patterns. To provide the necessary details for CO_2 impact studies, some additional model improvements must be made and more extensive comparison of model results with observations must be performed, including comparison on subcontinental scales.

An additional approach to estimating climate change has been to develop empirical approaches by calibrating relatively simple theoretical models against real or conceptual experiments. Appendix B describes and analyzes this approach, which has led to some rather highly publicized, but very misleading, results because of assumptions and limitations in the interpretation of the experimental results.

Chapter 4 describes the results of major modeling studies designed to investigate the equilibrium sensitivity of the climate to relatively large changes in the CO_2 concentration (see also Appendix A). These calculations do not directly tell us what the change in climate has been over the last 100 years or more. The study of arbitrarily large step-function changes in CO_2 concentration (e.g., doubling or quadrupling of current or preindustrial levels) does, however, identify the potential differences in average climatic conditions that may exist between some time a century or more in the future and the climate of the recent past and help us to identify the most important physical processes. Such studies also provide a useful benchmark for comparing the results of models developed by different research groups. Investigating the causes of differences between models and of the uncertainty of model results is a very difficult but essential task. Appendix C discusses some of the difficulties in pursuing such analyses.

To date, computer resource requirements and limitations in our ability to fully represent interactive processes important on the multiyear scale have limited the use of GCMs to the study of the climate's sensitivity to large changes in the CO_2 concentration. It is important to recognize that these studies are thus examining relatively large changes between two near-equilibrium climatic states, an assumption that may not be valid for either the recent past or the future, because the CO_2 concentration continues to change. Even so, in these GCM sensitivity studies, statistically significant identification can usually be made of changes in global and hemispheric parameters, although not usually in regional- and continental-scale parameters. Because the real climate will be slowly changing rather than remaining in equilibrium, and because the time constants of the various climate system components are different, conclusions drawn from such sensitivity simulations will contain an inherent, but unquantifiable, uncertainty if used to interpolate the time dependent response.

Chapter 5 reviews the efforts that have been carried out to study directly the climatic response to the slowly increasing CO_2 concentration. The major difficulties in this type of study arise from three factors. The first is that the CO_2 concentration is increasing slowly (about 0.3% per year), so that the climate changes tend to be small, and long simulations (50 to 75 years) are required for the response to be adequately detectable in model results, especially in GCM simulations. Second, this slow response is accentuated by the thermal inertia provided by the large heat capacity of the oceans. Although the representation of the oceans can be greatly simplified in equilibrium sensitivity calculations (as described in Chapter 4), calculations with time-dependent forcing require an accurate treatment of the oceans, sea ice, and the atmosphere. Our knowledge about oceanic response mechanisms and our ability to simulate the ocean are, however, only now developing to the necessary level. The third difficulty is that if, indeed, we want to attempt to verify the accuracy of the response of the model to the time-dependent forcing that occurred over the past 100 years (a seemingly sensible task to undertake before projecting the climate into the future), we must consider the forcings caused by several factors in addition to the increasing CO_2 concentration. These include changes in volcanic aerosol loading, trace gas concentrations, solar irradiance, and the natural fluctuations of the climate system (the Southern Oscillation, etc.). Although these processes are important, their effects are not well understood, and the data bases available are only barely adequate. These difficulties are only now starting to be tackled in a comprehensive way. As an alternative to actually modeling the response to time-dependent forcing, simple interpolations (e.g., logarithmic in CO_2 concentration) of results from equilibrium sensitivity studies have been used to estimate the change in temperature that may have occurred over the last 100 years. For parameters other than temperature (e.g., the date of the melting of sea ice), such interpolations are likely to fail. In recognition of these numerous difficulties and the importance of improving our capabilities, study of the climatic response to time-dependent forcing is now a major thrust of research.

The CO_2 concentration is not the only potentially perturbing influence on the climate. There is recent recognition that increases in the concentrations of other trace gases will also be important. Because the concentrations of these gases are now so low, their absorption lines are not yet saturated, so that on a molecule-for-molecule basis these gases could have a much greater effect than CO_2. Only because emissions of the trace gases are much lower

than those of CO_2 are the potential climatic effects comparable. Chapter 6 describes studies of the sensitivity of the climate to both trace gases and to variations in volcanic aerosol loading and solar irradiance. Verifying that models can accurately simulate the present and past climate and assessing the potential for future climate change will require consideration of changes in CO_2 concentration, as well as these other factors. This formidable task is now starting to receive increased attention.

Chapters 2 through 6 describe the theoretical basis for climate calculations and the resultant estimates of climate change. The perspective of past climate changes as a means for evaluating the probable validity of the theoretical models, and in a limited sense of the projected climate changes, is covered in Chapter 7. By looking at the differences in climate between warmer and colder periods in the past, similarities can be sought in a comparison of modeled and observed anomalies. As indicated in Section 1.3.2, deductions concerning the significance or absence of similarities are limited by a lack of knowledge about the similarity of causes of past and present changes, problems of differing time scales, and so forth. Nonetheless, the past climatic state was real, and if dramatic differences between modeled and observed states were to be identified, there would be serious cause for concern. Fortunately, there appear to be some similarities in the responses found by the two approaches, which adds a measure of confidence to model results.

In the context of our ability to understand and represent the climate, Chapter 8 attempts to summarize the results of the various approaches (equilibrium sensitivity studies, studies with time-dependent forcing, observation-based analogs) to identify the points of agreement and disagreement and the degree of certainty and uncertainty and to highlight the unresolved issues. Although there appears to be rather widespread agreement that a doubling of the CO_2 concentration could induce a global average surface air temperature warming of a few degrees Celsius, and that increases in trace gas concentrations could substantially augment this warming, there is no agreement yet on many fundamental aspects of the issue that seemingly should be resolvable. For example, although numerical models developed by different groups are in approximate agreement (within 25 to 50%) on the projected global average temperature change to be expected from a doubling of the CO_2 concentration, their results differ significantly (by greater than a factor of 2) on expected changes in both low and high latitudes; that is, although there is some agreement that polar amplification of the temperature increase will occur, its magnitude is not well defined. There is also substantial disagreement on the relative importance of different processes in amplifying the warming, with primary attribution given to cloud feedback (a highly uncertain area) by one group, to sea ice feedback by another, and to water vapor feedback by another. As described more fully in Wigley et al. (1985), there is also an indication that model-derived climate changes of the last 100 years (based on logarithmic interpolation techniques) may be larger than the observed change and may exhibit a different time history, even when some rather uncertain adjustments are made to account for possible volcanic and solar variations. This apparent disagreement depends to a large extent on how the models treat the heat capacity and circulation of the oceans, which may delay the expected equilibrium warming by several decades or more.

In a variety of direct and indirect ways, increases in CO_2 and trace gas concentrations could significantly affect the environment in which we exist. For the climate research community to provide the reasonably definitive information necessary for the assessment of the importance of projected climate changes, considerably more research will be required, an overview of which is presented in Chapter 9. The major research thrusts identified in that chapter are not unique to the CO_2 issue but apply across the spectrum of issues involving global climate studies. These include further model development (particularly the development of coupled atmosphere-ocean models), more extensive evaluation of the adequacy of various parameterizations (particularly cloud processes), improved and more extensive model verification (especially of regional, subcontinental, and seasonal patterns), more thorough analysis of CO_2 sensitivity studies (particularly to understand disagreements among results from different models), and careful planning of studies with time-dependent forcing, which must

be done with coupled ocean-atmosphere GCMs (focusing on the verification and determination of appropriate time constants). Such a list presents a significant challenge for the next ten years and more.

1.5 SUMMARY

The study of the Earth's climate is being undertaken by many groups throughout the world, each looking at a variety of aspects of the issue, and progress is continuous. It is difficult to summarize all of these efforts and integrate them into a single volume. The chapters in this SOA report have been prepared by leading researchers in their fields, each attempting to portray a particular aspect of the CO_2 issue in the context of all of the other aspects, many, but not all, of which are treated in this volume.

Carbon dioxide is essential to life on Earth, and changes in its concentration will set off a chain of responses involving many interacting processes. The climate will surely respond in important ways. This SOA report attempts to define our current understanding of how this will happen, balancing what we know (and think we know) with what we do not yet know (and what we cannot know).

Certainly, the climatic aspects of the potential increase in the CO_2 concentration must be studied further so that better resolved and more accurate estimates of the future climate can be made available for assessment studies. At what stage these results will be certain enough to draw firm conclusions cannot be defined by scientists alone; such questions necessarily involve the importance of the decisions faced by public representatives. This volume attempts to present where we are and where we are going, leaving judgments of societal significance to other forums.

ACKNOWLEDGMENTS

I am indebted to the helpful comments of many reviewers and the authors of this volume, particularly to W. L. Gates for helping to tighten the definitions of the various terms.

REFERENCES

Berger, A., Imbrie, J., Hays, J., Kukla, G., and Saltzman, B. (eds.). 1984. *Milankovitch and Climate.* D. Reidel Publishing Co., Dordrecht, The Netherlands.

Blake, D., and Lindzen, R. S. 1973. "Effect of Photochemical Models on Calculated Equilibria and Cooling Rates in the Stratosphere." *Monthly Weather Review 101:*783–802.

Bryson, R. A. 1985. "On Climatic Analogs in Paleoclimatic Reconstruction." *Quarternary Research 23:*275–286.

Charney, J. 1979. *Carbon Dioxide and Climate: A Scientific Assessment.* Report of the Ad Hoc Study Group on Carbon Dioxide and Climate, National Research Council. National Academy Press, Washington, D.C.

Crutcher, H. L., and Meserve, J. M. 1970. "Selected Level Heights, Temperatures and Dew Points for the Northern Hemisphere." NAVAIR 50-1C-52. U.S. Naval Weather Service Command, Washington, D.C.

Folland, C. K., Parker, D. E., and Kates, F. E. 1984. "Worldwide Marine Temperature Fluctuations 1856–1981." *Nature 310:*670–673.

Gates, W. L., 1979. "The Physical Basis of Climate." 112–131. In *Proceedings of the World Climate Conference* (WMO No. 537), World Meteorological Organization, Geneva, Switzerland.

Jones, P. D., Raper, S. C. B., Bradley, R. S., Diaz, H. F., Kelly, P. M., and Wigley, T. M. L. 1986. "Northern Hemisphere Surface Air Temperature Variations 1851–1984." *Journal of Climate and Applied Meteorology.* In press.

Liou, K.-N. 1980. *An Introduction to Atmospheric Radiation.* Academic Press, New York, New York.

MacCracken, M. C. 1984. "Climatic Warming and Carbon Dioxide." *Energy and Technology Review.* (Report UCRL-52000-84-9). Lawrence Livermore National Laboratory, Livermore, California.

MacCracken, M. C., and Luther, F. M. (eds.). 1985. *Detecting the Climatic Effects of Increasing Carbon Dioxide* (DOE/ER-0235). U.S. Department of Energy, Washington, D.C. Available from NTIS, Springfield, Virginia.

Manabe, S., and Holloway, J. L., Jr. 1975. "The Seasonal Variation of the Hydrologic Cycle as Simulated by a Global Model of the Atmosphere." *Journal of Geophysical Research 80:*1617–1649.

Möller, F. 1951. "Quarterly Charts of Rainfall for the Whole Earth." *Petermanns Geographische Mitteilungen 95:*1–7 (in German).

National Research Council (NRC). 1975. *Understanding Climatic Change.* Report of the U.S. Committee for the Global Atmospheric Research Program, National Academy of Sciences, Washington, D.C.

National Research Council (NRC) 1983. *Changing Climate.* Report of the Carbon Dioxide Assessment Committee, National Academy Press, Washington, D.C.

Oort, A. H. 1983. *Global Atmospheric Circulation Statistics, 1958–1973* (NOAA Professional Paper 14). U.S. Government Printing Office, Washington, D.C.

Richardson, L. F. 1922. *Weather Prediction by Numerical Process.* Cambridge University Press, London; republished in 1965 by Dover Publications, New York, New York.

Robock, A. 1985. "An Updated Climate Feedback Diagram." *Bulletin of the American Meteorological Society 66*:786–787.

Schelling, T. C. 1983. "Climate Change: Implications for Welfare and Policy." In *Changing Climate: Report of the Carbon Dioxide Assessment Committee,* Board on Atmospheric Sciences and Climate, National Research Council, National Academy Press, Washington, D.C.

Taljaard, J. J., van Loon, H., Crutcher, H. L., and Jenne, R. L. 1969. "Climate of the Upper Air, 1, Southern Hemisphere, Vol. 1, Temperatures, Dew Points, and Heights at Selected Pressure Levels" (NAVAIR 50-1C-55). U.S. Naval Weather Service, Washington, D.C.

Trabalka, J. R. (ed.). 1985. *Atmospheric Carbon Dioxide and the Global Carbon Cycle* (DOE/ER-0239). U.S. Department of Energy, Washington, D.C. Available from NTIS, Springfield, Virginia.

Wigley, T.M.L., Angell, J. K., and Jones, P. D. 1985. "Analysis of the Temperature Record." In M. C. MacCracken and F. M. Luther (eds.). *Detecting the Climatic Effects of Increasing Carbon Dioxide* (DOE/ER-0235). U.S. Department of Energy, Washington, D.C. Available from NTIS, Springfield, Virginia.

World Meteorological Organization. 1979. *Proceedings of the World Climate Conference.* 12–23 February 1979, Geneva, Switzerland (WMO Report 537). World Meteorological Organization, Geneva, Switzerland.

2. CARBON DIOXIDE AND THE RADIATION BUDGET

Frederick M. Luther
Lawrence Livermore National Laboratory

Robert G. Ellingson
University of Maryland

CONTENTS

2.1 INTRODUCTION

This chapter addresses the radiative forcing of the Earth-atmosphere system caused by an increase in carbon dioxide (CO_2) levels that can lead to climate change. The importance of the Earth's radiation budget is described, and the radiative properties of CO_2 and other radiatively important gases are presented. Methods of computing gaseous absorption and their accuracy are discussed. Components of the radiation budget (solar and longwave) are described along with the effect of variations in CO_2 concentration. Because aerosols and clouds also have important radiative properties, the effects of changes in aerosol and cloud amounts are also discussed. The purpose of this chapter is to provide an overview of the radiative effects of CO_2 and other atmospheric constituents that are important in determining the potential climatic effects of changes in atmospheric composition (discussed in the following chapters).

The global energy balance provides a physical basis for relating energy transfer processes to the climatic state of the Earth-atmosphere system. Perturbations to the climate system originate as perturbations to energy transfer processes within the climate system. In the case of increasing CO_2 levels, the change in radiative energy transfer becomes the forcing mechanism leading to climate change.

The moisture budget for the atmosphere is intimately related to the energy budget because evaporation at the surface depends on available energy and moisture. The release of latent heat in the atmosphere is also an important component of the energy budget. Perturbations to the energy balance can affect components of the moisture budget, thereby leading to changes in the H_2O content of the atmosphere, cloud amounts, and precipitation rates, in addition to changing the temperature.

The process by which changes in species composition affect tropospheric temperatures can be understood by considering the energy balance at the top of the atmosphere. When the atmosphere is in radiative balance (which is essentially the case on an annual-average basis), the outgoing longwave radiation at the top of the atmosphere balances the net incoming solar radiation (downward minus upward). Figure 2.1 shows the spectral upward radiance at the top of the atmosphere as a function of wave number, which is the inverse of wavelength. The area under the spectral radiance curve in Figure 2.1 equals the outgoing longwave radiation. About 90% of the outgoing longwave radiation originates from the atmosphere; the rest originates from the Earth's surface. When the atmospheric concentration of a radiatively active gas such as CO_2 is increased, the outgoing radiation in the spectral region where that gas absorbs longwave radiation is reduced. To maintain a balance with the net incoming solar radiation, which is only slightly affected by an increase in CO_2, this decrease must be made up in some other part of the spectrum so that the area under the radiance curve remains unchanged. Through radiative exchange with the Earth's surface,[1] the surface temperature increases, leading to a larger emission to space in the 800–1200 cm^{-1} region where the atmosphere is highly transparent. As atmospheric temperatures increase, the radiance is increased at other wave numbers as well. The warming in response to the initial increase in atmospheric opacity because of CO_2 occurs until the radiation balance with incoming solar radiation at the top of the atmosphere is restored. Warming at the Earth's surface is expected to lead to increased H_2O abundance, which would further enhance the warming at the surface and in the lower atmosphere.

From the alternative perspective of considering the energy balance at the Earth's surface rather than at the top of the atmosphere, increasing the atmospheric opacity leads to increased downward emission from the atmosphere to the surface, which tends to warm the surface. As the surface warms, more energy is transferred from the surface to the atmosphere, resulting in higher atmospheric temperature and increased back radiation to the surface. The increase in atmospheric opacity reduces the amount of energy transmitted from the Earth's surface to space. The perturbation to the surface energy balance also changes the fluxes of sensible and latent heat from the surface. As the Earth's surface warms and absolute humidity increases, more and more of the absorbed solar and back radiation to the surface is used to evaporate

[1] The radiative exchange with the Earth's surface provides the initial forcing that leads to an increase in surface temperature. Changes also occur in the fluxes of sensible and latent heat from the surface in response to this forcing.

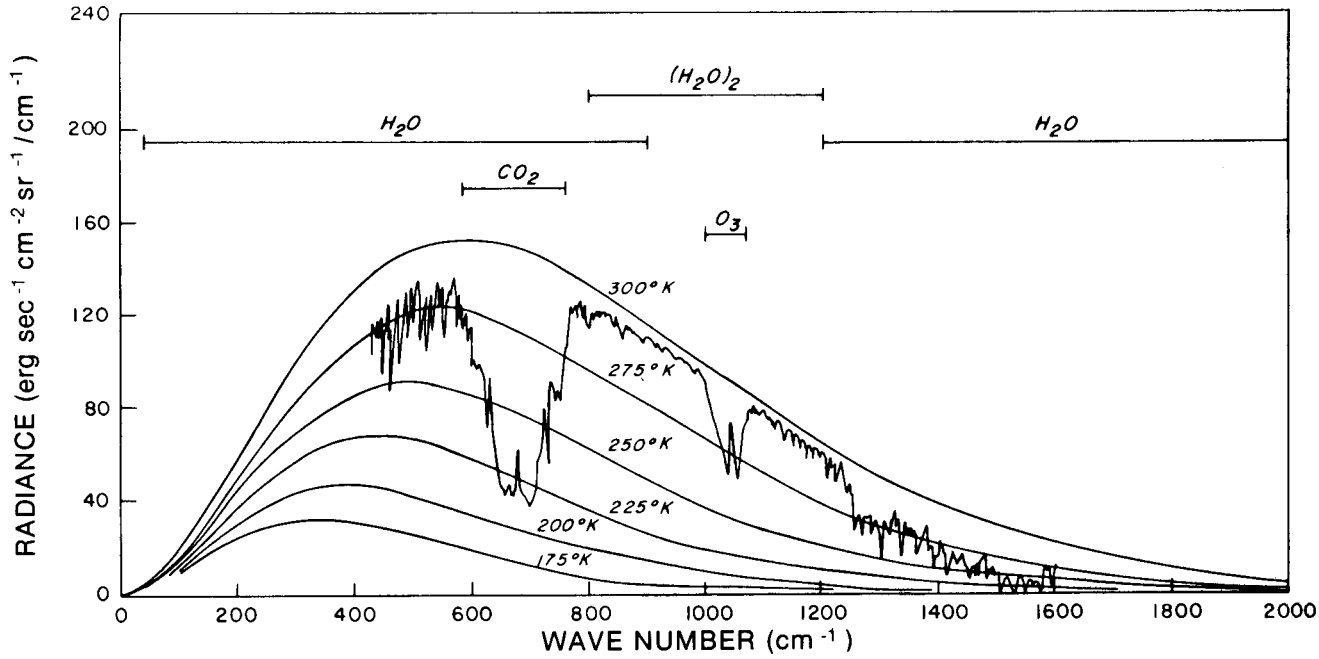

Figure 2.1. The terrestrial infrared spectra and various absorption bands. Also shown is an actual atmospheric emission spectrum taken by the Nimbus IV IRIS instrument near Guam at 15.1°N and 215.3°W on April 27, 1970. Source: Liou (1980).

water from the surface rather than increasing surface temperatures.

Both of these perspectives describe the process by which increases in the atmospheric abundance of *greenhouse gases* lead to warming at the Earth's surface. The term *greenhouse gases* refers to gases that are highly transparent to solar radiation but are relatively opaque to longwave radiation, similar to glass in a greenhouse. The process by which warming occurs in a greenhouse is different from that described above. In this regard the terms *greenhouse gas* and *greenhouse effect* are misnomers.

2.2 RADIATIVELY IMPORTANT ATMOSPHERIC CONSTITUENTS

CO_2 is one of many radiatively active atmospheric constituents. Although we consider here that increases in CO_2 would provide the initial radiative forcing, the resulting change in climate depends on the radiative properties of all the radiatively active atmospheric constituents. The various atmospheric constituents are listed in Table 2.1 along with their volume mixing ratios.[2] Many constituents have volume mixing ratios that vary slowly in space and time. The constituents CO_2, methane (CH_4), and nitrous oxide (N_2O) are examples of species in this category. The CH_4 and N_2O mixing ratios are nearly constant with altitude through the troposphere, declining in the upper stratosphere as photolysis becomes more effective at high altitude. Other species are highly variable in both space and time. In addition to the species listed in Table 2.1, clouds and aerosols also are important radiatively active atmospheric constituents.

Table 2.1
Atmospheric Constituents with Small Spatial and Temporal Variation

Constituent	Percent by Volume
Nitrogen (N_2)	78.084
Oxygen (O_2)	20.984
Argon (Ar)	0.934
Carbon Dioxide (CO_2)	0.033
Neon (Ne)	18.18×10^{-4}
Helium (He)	5.24×10^{-4}
Krypton (Kr)	1.14×10^{-4}
Hydrogen (H_2)	0.5×10^{-4}
Xenon (Xe)	0.089×10^{-4}
Methane (CH_4) (at surface)	1.7×10^{-4}
Nitrous Oxide (N_2O) (at surface)	0.3×10^{-4}

Source: Liou (1980).

[2] Volume mixing ratio is the number of molecules of the constituent in a unit volume divided by the number of molecules of air in that volume.

All of the gases as well as solid and liquid particles scatter sunlight. Gas molecules are very much smaller than the wavelength of light (i.e., the Rayleigh limit), so their scattering cross section varies inversely with wavelength to the fourth power (Chandrasekhar 1960; Liou 1980). The scattering of light by spherical particles is much more complex, depending on the particle size distribution and the wavelength-dependent complex index of refraction (Mie 1908; van de Hulst 1957).

The atmospheric constituents differ greatly in their absorptive properties. The general characteristics of atmospheric absorption are shown in Figure 2.2. The two curves show the energy distribution characteristic of blackbody emission at 6000 K (the solar temperature) and at 255 K (the average terrestrial emission temperature). The fractional absorption between the top of the atmosphere and ground level also is indicated as a function of wavelength in the lower part of the figure.

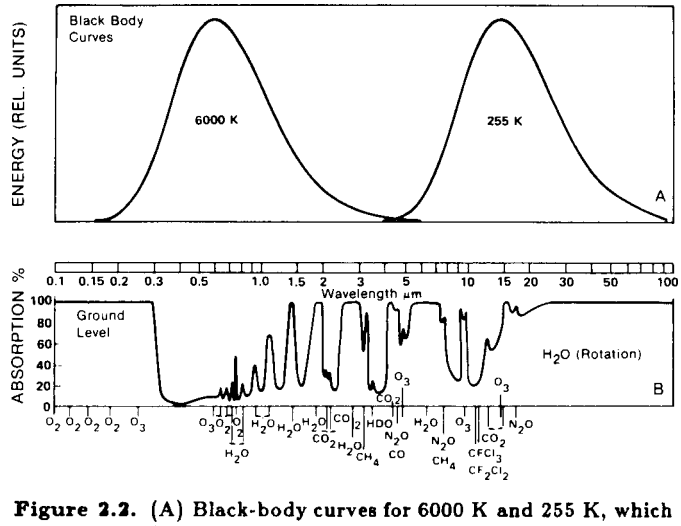

Figure 2.2. (A) Black-body curves for 6000 K and 255 K, which approximate the mean emitting temperatures of the sun and the Earth. (B) Atmospheric gaseous absorption for radiation passing from the top of the atmosphere to ground level.

There is very little gaseous absorption in the visible region (0.4–0.7 μm), although weak absorption bands of ozone (O_3) (the Chappuis bands) and NO_2 occur in this region. Ozone is the primary absorber of solar radiation at ultraviolet (UV) wavelengths between 0.20 and 0.36 μm. In the solar near-infrared (IR) region (0.7–4 μm), water vapor (H_2O) is the most important absorber. Carbon dioxide has several absorption bands between 1.4 and 5.2 μm, with the two strongest bands centered at 2.7 and 4.3 μm.

The main gases of the atmosphere, nitrogen and oxygen, contribute only slightly to solar absorption. Monatomic and diatomic gases where both atoms are the same element (e.g., N_2, O_2, and H_2) do not have a permanent dipole moment, which makes them ineffective absorbers of radiation at most solar and IR wavelengths. The absorption bands for these constituents are primarily due to transitions in electron energy levels, and this leads to absorption in the UV region. There are three weak oxygen absorption bands in the visible solar spectrum, centered at wavelengths of 0.63, 0.69, and 0.76, μm respectively. Oxygen also has several systems of absorption bands in the far IR where there is little solar energy. In the UV region the strong Schumann-Runge bands are located in the region 0.175 to 0.203 μm and the Herzberg bands are in the region from 0.20 to 0.26 μm. Triatomic molecules, such as CO_2, H_2O, and O_3, have vibrational and rotational energy transitions that lead to absorption in the IR region.

Many gases have absorption bands in the longwave region (wavelength > 4 μm). Among these, CO_2, H_2O, and O_3 are the most important absorbers. CO_2 has strong absorption bands in the 15-μm region (600 to 800 cm^{-1} in Figure 2.1). In addition, CO_2 has weak absorption bands near 10 μm (1000 cm^{-1}), which are not indicated in Figure 2.1. The 15-μm band coincides with the peak in the thermal emission from the Earth's surface, which has an emitting temperature of about 288 K. CO_2 absorbs upward radiation from below and replaces it with radiation emitted at the atmospheric temperature. The temperature corresponding to the spectral radiance shown in Figure 2.1 is the effective emitting temperature of the radiation being emitted to space. Because temperature decreases with altitude in the troposphere, the lower the radiation temperature, relative to the surface temperature, the higher the altitude in the atmosphere from which the radiation is emitted. Thus, the region of low radiation temperature in Figure 2.1 shows that the radiation emitted near the center of the 15-μm band of CO_2 originates from the stratosphere. As absorption becomes weaker farther from the center of the 15-μm band, the altitude from which the radiation is emitted moves lower. At 900 cm^{-1}, for example, the

atmosphere is relatively transparent and the radiation emitted to space is characteristic of the surface temperature.

Water vapor absorption bands span most of the longwave region. The 6.3 μm band (resulting from transitions in molecular vibrational energy) covers the region from about 1200 to 2000 cm^{-1}. Two other vibrational bands are located near 2.7 μm. The band resulting from transitions in rotational energy covers the region from 0 to 900 cm^{-1}. Between 800 and 1200 cm^{-1}, there is weak continuous absorption which is important in regions of high H_2O concentration.

Ozone has two narrow vibrational bands centered near 9.6 μm (1042 and 1103 cm^{-1}) and a weak vibrational band centered at 14.27 μm that overlaps the strong 15-μm absorption band of CO_2. A strong absorption band at 4.7 μm is in a portion of the blackbody emission curve where there is little energy, so it does not contribute significantly to the longwave energy budget.

There is relatively little atmospheric absorption in the region between 800 and 1200 cm^{-1} except for continuum H_2O absorption in the lower tropical troposphere. Because the atmosphere is essentially transparent in this portion of the longwave regime, this region (centered at 10 μm) is called the *atmospheric window.*

Other radiatively active trace gases are listed in Table 2.2 and the locations of the most effective absorption bands are indicated in Figure 2.2. Many of these gases have absorption bands that lie within the atmospheric window. By not overlapping strong absorption bands of other constituents, absorption bands in the window region can be very effective in decreasing the longwave radiation emitted to space. Many of these gases have very strong absorption bands. For example, $CFCl_3$ has a band strength[3] of 1700 cm^{-2} atm^{-1} at standard temperature and pressure (STP), whereas the 15-μm band of CO_2 has a band strength of 213 cm^{-2} atm^{-1} at STP. Because the concentration of $CFCl_3$ is several orders of magnitude less than that of CO_2, the radiative effect of $CFCl_3$ is less than that of CO_2. Although the radiative effects of trace gases are currently small, they could increase significantly in the future because the concentrations of many of the gases are projected to increase because of anthropogenic emissions (see Chapter 6 of this volume).

Table 2.2
Band Centers and Volume Mixing Ratios of Trace Gases Other Than CO_2

Trace Gas	Band Center (cm^{-1})	Mixing Ratio in Lower Troposphere (ppm)
N_2O	589, 1168, 1285	0.3
CH_4	1306, 1534	1.7
O_3	1041, 1103	0.02–0.1
$CFCl_3$ (CFC-11)	846, 1085, 2144	2.0×10^{-4}
CF_2Cl_2 (CFC-12)	915, 1095, 1152	3.5×10^{-4}
CF_4	632, 1241, 1261	6.0×10^{-5}
CF_2HCl (CFC-22)	1117, 1311	6.0×10^{-5}
CCl_4	776	1.5×10^{-4}
$CHCl_3$	774, 1220	1.0×10^{-5}
CH_2Cl_2	714, 736, 1236	4.0×10^{-5}
CH_3Cl	732, 1015, 1400	6.5×10^{-4}
CH_3CCl_3	707, 1084	1.3×10^{-4}
C_2H_4	949	$1.0–20.0 \times 10^{-4}$
SO_2	518, 1151, 1361	1.0×10^{-4}
NH_3	950	1.0×10^{-3}
HNO_3	1695, 1333, 850	$1.0–10.0 \times 10^{-4}$

Trace gases that are radiatively active predominantly in the longwave region, such as CH_4, N_2O, $CFCl_3$, and CF_2Cl_2, have behaviors similar to that of CO_2. These gases are essentially transparent to solar radiation but are opaque to longwave radiation in specific spectral bands, and they behave similarly to CO_2 in that they initially reduce the outgoing longwave radiation to space, which leads to a warming of the surface and troposphere until the radiation balance is restored. Trace gases that are radiatively active in both the solar and longwave regions, such as O_3 and NO_2, can lead to either warming or cooling at the surface depending on how they are distributed vertically (see Chapter 6) and on the relative strengths of the bands in the solar and longwave spectral regions.

Water vapor, CO_2, and O_3 are the most important radiatively active gases in terms of their contribution to the temperature structure of the atmosphere. Figure 2.3 shows the contribution of each of these gases to the net radiative heating rate as a function of altitude, as computed by Manabe and Strickler (1964). This figure applies to global annual-mean conditions. LH_2O, LCO_2, and LO_3

[3] Band strength is the sum of the strengths of all lines in a band and is an indicator of the potential absorption due to that band. For two gases, each with the same column amount at standard temperature and pressure, the gas with the larger band strength would have more absorption. Except for small absorber amounts, the absorption would not be directly proportional to band strength.

refer to the individual contributions to the rate of temperature change that is due to longwave radiation absorption and emission. The curve marked $SH_2O + SCO_2 + SO_3$ gives the rate of temperature change due to absorption of solar radiation by H_2O, CO_2, and O_3. Solar absorption by O_3 accounts for nearly all the solar absorption in the stratosphere (the region above ~13 km), and H_2O is the major source of solar absorption by gases in the troposphere (<13 km). CO_2 is a very weak absorber of solar radiation, but it is very important in terms of the longwave cooling rates, particularly in the stratosphere.

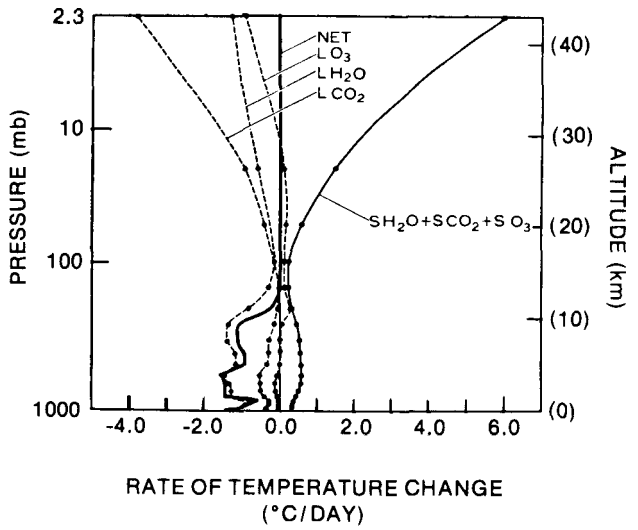

Figure 2.3. Radiative-convective model results for the longwave cooling and solar heating rates. The letters L and S denote longwave and solar, respectively. The model results are taken from Manabe and Strickler (1964).

In the stratosphere, temperature increases with altitude reflecting the heating due to absorption of solar radiation by O_3. On an annual-average basis, the solar heating is compensated primarily by longwave cooling due to CO_2. The temperature profile in the troposphere, with temperature decreasing with altitude, is a result of interactions between convection, large-scale dynamics and radiation. Radiative processes in the troposphere contribute to the net energy balance of the troposphere-surface system. The troposphere must radiate to space not only the solar energy absorbed there but also the bulk of that absorbed at the surface.

2.3 RADIATIVE TRANSFER THEORY

This section provides somewhat simplified descriptions of the radiatively important quantities that must be calculated or parameterized in a climate model. Because nearly 99% of the radiation incident from the sun falls at wavelengths <4 μm and approximately 99% of the energy thermally emitted by the Earth-atmosphere system is at wavelengths >4 μm (see Figure 2.2), and because the physical mechanisms dominating the transfer of radiation differ in these two portions of the spectrum, it is convenient then to discuss atmospheric radiation as either solar shortwave (wavelengths <4 μm) or as terrestrial longwave radiation. The theory of the transfer of electromagnetic radiation is well understood for horizontally homogeneous stratified atmospheres; the details concerning the basic equations can be found in several different texts (e.g., Goody 1964; Paltridge and Platt 1976; Houghton 1977; Liou 1980).

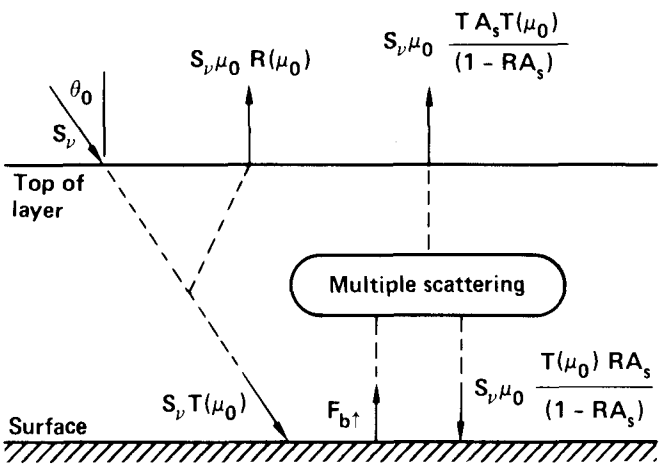

Figure 2.4. Diagram of solar flux components for a one-layer model.

For the sake of illustration, consider a one-layer atmosphere illuminated at the top by a monochromatic solar irradiance S_ν at local zenith angle θ_0 as shown in Figure 2.4. The monochromatic upward $F_\uparrow$ and downward $F_\downarrow$ flux densities at the top and bottom of the atmosphere (subscript t and b, respectively) may be written as

$$F_{t\uparrow} = S_\nu\mu_0\left[R(\mu_0) + \frac{TA_sT(\mu_0)}{(1-RA_s)}\right], \quad (2.1)$$

$$F_{b\downarrow} = S_\nu \mu_0 \frac{T(\mu_0)}{(1 - RA_s)} , \qquad (2.2)$$

and

$$F_{b\uparrow} = F_{b\downarrow} \cdot A_s , \qquad (2.3)$$

where ν is the frequency or wave number, A_s is the surface albedo, assumed to be Lambertian,[4] $\mu_0 = \cos\theta_0$, and R, T, $R(\mu_0)$, and $T(\mu_0)$ are the spherical and planar reflectivities and transmissivities, respectively. With the exception of μ_0, all the quantities are functions of ν but this subscript has been dropped for convenience.

Physically, Equation (2.1) states that the solar radiation reflected to space consists of a part coming from the atmosphere alone $[R(\mu_0)]$, including the effects of absorption and multiple scattering within the atmosphere, plus a part resulting from reflection from the surface that has been enhanced by multiple reflections between the surface and atmosphere [the $(1 - RA_s)^{-1}$ term]. Similarly, the radiation reaching the surface (Equation 2.2) is due to that portion transmitted, $T(\mu_0)$(direct + diffuse), which has been enhanced by multiple reflections between the surface and atmosphere.

The Rs and Ts are functions of the absorption and scattering properties of the radiatively active gases and particulate matter in a given spectral interval (i.e., the shape, sizes, number distribution, and complex index of refraction of the particulate matter, and the density and absorption and scattering coefficients of the gases). Detailed and approximate techniques for calculating the Rs and Ts for horizontally homogeneous conditions are described in the previously mentioned texts and in numerous papers (e.g., Lacis and Hansen 1974; Joseph et al. 1979; Meador and Weaver 1980). The techniques used to account for multiple scattering in climate models cover a wide range of sophistication, and the uncertainties in these techniques may be important as the radiative properties of the atmosphere vary. Although this is a potentially important problem, this chapter focuses on the atmospheric radiation budget and the effect of changes in CO_2.

Of particular concern to the CO_2 problem is the manner by which absorption by the atmospheric gases is calculated. When absorption alone is considered, the equation for the total downward solar flux density $f_\downarrow$ at altitude z may be written as

$$f_\downarrow(z;\mu_0) = \mu_0 \int_0^\infty S_\nu T_\nu(z, z_\infty; \mu_0) d\nu , \qquad (2.4)$$

where T_ν is the monochromatic transmissivity for the slant path from the top of the atmosphere z_∞ to z along μ_0. T_ν, for one absorbing gas with density ρ_a, is related to the monochromatic absorption coefficient k_ν for a plane parallel atmosphere as

$$T_\nu(z, z_\infty; \mu) = \exp\left(-\int_z^{z_\infty} k_\nu \rho_a \frac{dz''}{\mu_0}\right) . \qquad (2.5)$$

The downward longwave flux for a plane parallel axisymmetric atmosphere in thermodynamic equilibrium with no scattering is related to T_ν as

$$F_\downarrow(z) = -\int_0^\infty d\nu \int_z^{z_\infty} \pi B_\nu(z') \frac{\partial T_{F\nu}(z, z')}{\partial z'} dz' , \qquad (2.6)$$

where B_ν is the Planck function for the temperature at z' and $T_{F\nu}$ is the *flux* transmissivity defined as

$$T_{F\nu}(z, z') = 2\int_0^1 T_\nu(z, z'; \mu)\mu \, d\mu . \qquad (2.7)$$

Physically, Equation (2.4) states that the downward flux at z is equal to that portion of the solar flux incident on the top of the atmosphere transmitted to z, whereas the longwave flux at z is due to the sum of the contributions of each emitting element between z and the top of the atmosphere, each attenuated by the appropriate optical path. The equations for the upward short- and longwave fluxes have terms similar to those in Equations (2.4) and (2.6).

Because of the nearly discontinuous variation of the absorption coefficient k_ν with ν, only the integration over ν poses significant practical problems in the computation of clear-sky-radiation quantities. The next section summarizes the techniques commonly used to approximate the frequency integration.

[4] Radiation scattered by the Earth's surface is assumed to be uniform in all directions (that is, isotropic).

2.4 COMPUTATIONAL METHODS FOR GASEOUS ABSORPTION

2.4.1 Transmissivities for Individual Gases

2.4.1.1 Line-by-Line Technique

The most straightforward technique for the integration over ν is to perform a numerical integration after having specified k_ν at sufficiently small intervals (10^{-4} to 10^{-2} cm^{-1}). This is no small task because k_ν depends on the locations, strengths, and shapes of the spectral lines throughout the spectrum. Specifically, k_ν can be written as

$$k_\nu(T,p) = \sum_J S_J(T)\ f_J(T,p,\nu_{0J},\nu)\ , \qquad (2.8)$$

where S_J is the integrated line intensity for the Jth line, f_J is the line shape factor for the line centered at ν_{0J} for temperature T and pressure p. Because this technique involves summing the contribution of each line, it is usually called the line-by-line (LBL) technique. Details concerning variations of this technique may be found in Drayson (1967), Fels and Schwarzkopf (1981), and Scott and Chedin (1981).

Use of the LBL technique has become more widespread with the availability of documented spectral line data (e.g., McClatchey et al. 1973) and with the availability of high-speed computers. Comparisons of laboratory-observed transmittances with LBL-calculated transmittances have generally shown agreement to within 5–10% transmittance over narrow spectral intervals (e.g., McClatchey 1976) and to within several tenths of a percent for total band absorption for CO_2 (e.g., Fels and Schwarzkopf 1981). Because the principal uncertainties of this technique involve basic spectroscopic quantities (S_J and f_J) common to all techniques, rather than the integrations, many investigators use LBL calculations as a reference to check more approximate techniques. However, because of the large number of lines in the spectrum ($\sim 10^5$), the LBL technique consumes copious amounts of computer time on the fastest computers when applied to flux and heating rate calculations. As a result, it is not a technique useful for routine calculations in climate models.

2.4.1.2 Narrow Band Models

A common approximation for performing the frequency integration consists of dividing the spectrum into a finite number of spectral intervals that are small enough to regard B_ν or S_ν as constant across the interval, yet wide enough to smooth out the detailed spectral features. This technique, usually called the narrow band model (NBM) technique, requires the calculation of the frequency-averaged transmissivity T_i which, for a homogeneous path with absorber amount u, may be written as

$$T_i(u,p,T) = \frac{1}{\Delta\nu_i}\int_\nu^{\nu+\Delta\nu_i} e^{-k_\nu(T,p)u}\ d\nu\ , \qquad (2.9)$$

where typically $\Delta\nu < 50$ cm^{-1} and i is an index for the frequency or wave number interval.

In practice, two different approaches are used to determine the functional dependence of T_i on u, p, and T. One approach involves making assumptions concerning the distributions of the line parameters S_J and f_J, which will allow T_i to be expressed in terms of analytical functions with adjustable parameters. The parameters for a given spectral interval are specified from laboratory observations or by forcing agreement with spectroscopic theory in asymptotic limits. The resulting function is applied to atmospheric problems with the use of the Curtis-Godson approximation (Goody 1964), which defines a temperature-scaled amount of absorber at a definable mean pressure. Several different band models are discussed in Goody (1964) and applications to flux calculations have been numerous (e.g., Rodgers and Walshaw 1966; Haurwitz and Kuhn 1974; Ellingson and Gille 1978).

A somewhat different NBM approach transforms Equation (2.9) to an integral over k_ν in $\Delta\nu$, and the distribution of k_ν is determined from LBL calculations (e.g., Chou and Arking 1980). This so-called k-distribution technique is applied to atmospheric problems with the use of a one-parameter scaling approximation. Closely related to this technique is the sum of exponentials technique as discussed by Lacis and Hansen (1974) among others. The advantages of the k-distribution technique over the analytical band models are that the actual distributions of k_ν are employed, the frequency integration is accurately performed for homogeneous paths,

and the form of the expression for T_i allows a radiation model to be extended to include multiple scattering.

Another type of NBM uses empirical functions fit to a small range of observations or calculations (e.g., LOWTRAN, Selby et al. 1976). Although useful to some applications, this type of approach leaves large uncertainties when the empirical functions are used beyond the range of variables for which they were intended.

The analytical models suffer from the fact that one function cannot even reasonably be applied to one gas, let alone all gases in all spectral intervals. However, the associated errors may be reduced by a judicious calculation of the adjustable parameters, and the application of the analytical models to atmospheric calculations has firmer theoretical foundations than do the one-parameter scaling approximations. In either case, the NBM calculations overcome the computer time limitations of the LBL technique when applied to some climate model applications (e.g., frequent one-dimensional calculations). However, the NBMs generally still require too much computer time for practical applications in two- and three-dimensional climate models.

2.4.1.3 Wide Band Models

The third general approach to the transmission-absorption problem is the use of observations, LBL calculations or NBM calculations to construct models of the absorption over large band widths, or even the entire spectrum. These approaches are denoted here as wide band models (WBM). One example of this approach is the so-called emissivity approximation, which is an attempt to perform the entire spectral integration separately for each absorber. An historical account of emissivities is given by Hottel and Sarofim (1967), who point out that Schack (1924) was perhaps the first to show how data could be used to predict the emissivity. Atmospheric applications of this approach date at least to Elsasser (1942), and modifications and improvements are discussed by Ramanathan (1976). This approach is appealing to climate studies because the integrated absorption for the active gases may be measured over a wide range of variables in the laboratory, and because the calculations may be performed very rapidly on the computer. For example, Ramanathan (1976) and Kiehl and Ramanathan (1983) show good agreement of model-predicted and laboratory-observed integrated CO_2 absorptivities for the 15-μm band system. The primary difficulties with this approach are accurately accounting for the nonhomogeneous path and for overlap with other active gases.

A more recent WBM approach might be called the perturbation technique. As pointed out by Curtis (1956) and applied by Rodgers (1967), it is useful to precompute the transmissivity for those constituents that do not change and that are weakly dependent on temperature variations along the atmospheric path. Recently, Fels and Schwarzkopf (1981) extended this idea by computing the integrated absorptivities for the 15-μm band of CO_2 with an LBL integration for a standard pressure grid. Furthermore, they give the necessary matrices for extending the calculations to other pressures and temperatures. The major limitations of this approach include the necessity of large computer storage, as compared with the emissivity approach, the difficulty in accurately accounting for overlap with other absorbers, and the difficulty in accounting for a varying absorber concentration.

A technique related to the perturbation technique is the table look-up technique. In this approach, the pressure increments of atmospheric layers are fixed, except for the bottom layer. The H_2O, CO_2, and O_3 transmissivities are precomputed for a wide range of temperature and absorber amounts in each layer. When an actual sounding is used, the data are interpolated to the model grid, the necessary absorber amounts are calculated, and the integrals are calculated through interpolation of the precomputed data. This is very similar to a computerized version of the various radiation charts. Chou and Arking[5] have developed such a technique from the data presented in Chou and Arking (1980).

2.4.2 Treatment of Overlapping Absorption

Perhaps the most overlooked problem in atmospheric absorption is that of simultaneous absorption by two or more constituents across the same spectral interval (i.e., overlapping absorption). This is a particularly important problem for H_2O and

[5] M.-D. Chou and A. Arking, personal communication, 1982.

CO_2 absorption in the 2.7-, 10-, and 15-μm regions; for H_2O and O_3 absorption in the 9.6-μm region; and for H_2O, CH_4, and N_2O in the 7-μm region. In general, the frequency-averaged transmissivity for two gases absorbing in $\Delta\nu$, T_{i12}, may be written as

$$T_{i12} = \frac{1}{\Delta\nu_i} \int_{\Delta\nu_i} T_\nu(u_1) \times T_\nu(u_2)\, d\nu \ , \qquad (2.10)$$

where u_1 and u_2 are the absorber amounts for the two gases. For a narrow spectral interval for which there is little correlation between the individual lines or for which there is no wave number variation in either or both gases, Equation (2.10) may be written as

$$T_{i12} = T_i(u_1) \times T_i(u_2) \ . \qquad (2.11)$$

Experimental studies of the appropriateness of Equation (2.11) have been reported by Burch et al. (1956), Hoover et al. (1967), and Tubbs et al. (1967) for overlapping bands of several different gases. These studies have shown that if a spectral interval is broad enough to contain several lines, if the line centers are not commensurate and if the partial pressure of the broadening gas is much greater than the partial pressures of the absorbing gases, then the average error of Equation (2.10) is of the order of a few percent.

When the integration in Equation (2.10) extends over an entire band area, the multiplication property expressed by Equation (2.11) holds only if the correlation between the absorption features of the two gases is small. The WBM calculations generally express their versions of Equation (2.10) in terms of the absorptivities of the individual gases and an overlap term in the form of Equation (2.11) for a large band area. Burch et al. (1956) have shown experimental results that verify this type of approach for some overlapping, atmospherically active bands. However, the overlap correction term is not necessarily linear in the band absorptance as is assumed in climate model calculations. Overall, little evidence has been shown concerning the accuracy of these overlap approximations for all of the active atmospheric gases for either homogeneous path or atmospheric calculations.

The issue of overlapping absorption is important to climate assessments, particularly when one or both of the overlapping bands have strong absorption lines. Consider the two extreme cases where (1) there is nearly complete alignment of line positions for the bands of the two gases, and (2) the lines of one gas fall between the lines of the other gas. With alignment the absorption is minimized because once most of the energy near line centers is depleted by the one gas, there is little energy left to be absorbed by the second gas, and the transmission at wavelengths between the lines is not significantly reduced. Consequently, there may be significant transmission even though there is saturation near line centers.

On the other hand, absorption is maximized when the lines of the second band fall between the line positions of the first band. In this case, the absorption by the two bands is nearly additive (i.e., the sum of the two absorptions evaluated separately). The band models must make some assumption regarding the degree of randomness of the line positions in the two bands over spectral intervals. These assumptions are being evaluated at this time.

As an illustration of the effect of overlap, consider the overlap between the 15-μm bands of CO_2 and the rotational band of H_2O in the 12–18 μm spectral region. Kiehl and Ramanathan (1982) studied the effect of this overlap on the radiative heating resulting from increased CO_2, and their results are shown in Figure 2.5. The change in downward longwave flux at the surface because of a doubling of CO_2 is calculated as a function of latitude for annual-average conditions. The flux change is that resulting from a doubling of CO_2 before the atmosphere and surface respond to this forcing. Curve 1 is the case with no overlap between the CO_2 and H_2O absorption bands, and curve 2 is the case with overlap. There is a substantial reduction in the magnitude of the increase in downward flux to the surface when the overlap is included. The greatest difference occurs at tropical latitudes where there is a larger amount of H_2O. When the overlap with the H_2O continuum in the 12–18 μm region is added, there is very little increase in downward flux to the surface from doubled CO_2 because the lower tropical atmosphere is already essentially opaque.

When band overlap is included, there is a substantial increase in the tropospheric heating rates, which tends to compensate for the reduction in the downward flux at the surface. As a consequence, there is not a large change in the radiative forcing of the surface-troposphere system. The change in net

flux at the tropopause represents the radiative forcing of the surface-troposphere system. For a doubling of CO_2, the change in hemispheric-average net upward flux calculated by Kiehl and Ramanathan (1982) was -4.69 W m^{-2} with no overlap, was -4.18 W m^{-2} with rotational band overlap, and was -3.99 W m^{-2} when overlap with the continuum was included. Thus, the degree of overlap affects the way the net warming is partitioned between the surface and the troposphere, but it has only a weak effect on the total heating. As emphasized by several authors (Ramanathan et al. 1979; Manabe and Wetherald 1980; Kiehl and Ramanathan 1982), it is the surface-troposphere heating rather than surface heating that dominates the surface temperature response.

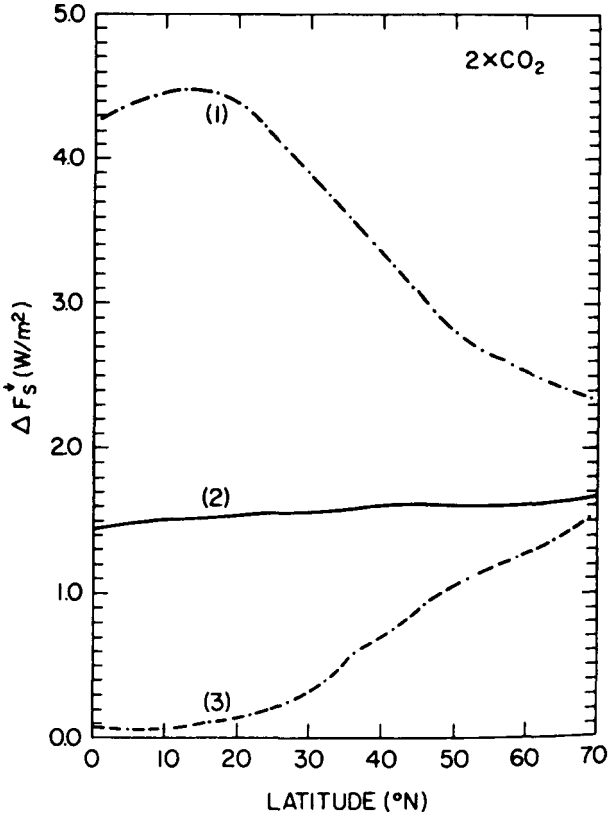

Figure 2.5. Increase in surface radiative heating because of doubled CO_2 for annual average case with average cloudiness: (1) without H_2O overlap; (2) rotational band overlap; (3) same as (2) but with the continuum band overlap. Source: Kiehl and Ramanathan (1982).

2.4.3 Summary of Model Approaches

Each of the approaches (line-by-line, narrow band, and WBMs) has some usefulness to climate modeling. The LBL calculations are very useful for checking the accuracy of NBM and WBM frequency integrations for homogeneous paths relative to the basic spectroscopic data. In addition, they allow for checks on the approximations made for the integrations over atmospheric paths. The NBM calculations are particularly useful for one-dimensional studies requiring high relative accuracy. Furthermore, the absolute accuracy of these calculations may be checked by comparing calculations with observations in narrow spectral intervals such as those that are available from space platforms or instrumented aircraft. Also, the NBM calculations may be used to calibrate the WBM calculations over a larger range of variables than might easily be checked with LBL calculations. The WBM calculations are best suited for the rapid calculations necessary for many climate studies, particularly those involving general circulation models.

2.5 ACCURACY OF LONGWAVE RADIATIVE TRANSFER MODELS

To determine the accuracy of radiative transfer models, a reference is needed with which to compare the model results. Laboratory and atmospheric measurements serve as an absolute reference for determining model accuracy. The LBL model calculations also provide a point of reference for evaluating the effects of simplifying assumptions used in less detailed models. The intercomparison of radiative transfer models and the comparison of model calculations with observations have both proven valuable in assessing the accuracy of radiative transfer models. Each of these two approaches has its advantages and disadvantages.

2.5.1 Intercomparison of Radiation Transfer Models

Intercomparison of radiative transfer models has been used many times to demonstrate the accuracy of a new modeling approach or to evaluate the effects of assumptions or numerical methods used in the models. The effects of using different spectral

or vertical resolution, using different band model assumptions, or using different spectral line data are examples of situations where the intercomparison of model results can be very valuable.

Walshaw and Rodgers (1963) compared cooling rates calculated with and without the Curtis-Godson approximation. They concluded that no significant error would be introduced by using the Curtis-Godson approximation for the 15-μm band of CO_2, but considerable errors could arise in the 9.6-μm O_3 band in the stratosphere.

Rodgers and Walshaw (1966) presented a number of model intercomparisons. Cases included comparison of calculations of the 15-μm CO_2 cooling to space with and without Doppler broadening, calculations with different numbers of spectral intervals, different methods of computing the diffuse transmission function, different vertical resolution, calculations with and without temperature dependence of absorption, and comparison of different methods of calculating cooling rates developed by various authors.

Stone and Manabe (1968) reported the results of a comparison among several numerical models used to compute longwave cooling rates. The comparison included the Rodgers and Walshaw (1966) model, the Manabe and Strickler (1964) model, the Plass (1956a, 1956b) CO_2 and O_3 models, the Hitchfeld and Houghton (1961) O_3 model, and the Kaplan (1959) model. The models were shown to agree reasonably well for CO_2 cooling rates, but there were some discrepancies for O_3 cooling rates.

Kiehl and Ramanathan (1983) contrasted a WBM for CO_2 with two NBMs and with laboratory data. They showed that using spectral intervals greater than 10 cm^{-1} for CO_2 in NBMs can lead to significant errors.

LBL model calculations are considered to be the best reference for model comparisons, so these calculations should be included wherever possible. For example, Liou and Ou (1983) compared H_2O cooling rates from two band models with LBL calculations obtained using a scheme developed by Chou and Arking (1980).

Recently, an international model intercomparison study was organized that incorporates many longwave models. The study is termed Intercomparison of Radiation Codes used in Climate Models (ICRCCM), and it is cosponsored by the World Meteorological Organization (WMO), the U.S. Department of Energy (DOE), and the International Radiation Commission of IAMAP (WMO 1985). A total of 39 sets of longwave calculations have been compared, including LBL models, NBMs, WBMs, and general circulation model algorithms. The ICRCCM study incorporates comparison with observations as well as model intercomparison. Initial sets of calculations were compared at a workshop held in August 1984 (WMO 1985), which led to the following findings.

The LBL models were in very good agreement with each other (to within a few W m^{-2} or usually within 1%). Differences in spectral intervals covered by each model can lead to differences greater than 1%, however. The radiative treatment of CO_2 seems satisfactory. Uncertainties in the H_2O line shape cause the fluxes to be more uncertain for H_2O, although the agreement is very good when the same line shape assumptions are made. The e-type continuum, the p-type continuum, and the temperature dependence of H_2O line widths are still sources of significant uncertainty in these calculations.

The NBMs showed a spread of 10–15% in the calculations of the downward flux at the surface for five reference atmospheres. For example, the range was 35 W m^{-2} for a midlatitude summer atmosphere without clouds. Calculations of the change in net flux at the tropopause when CO_2 is doubled ranged from -4.3 to -7.4 W m^{-2} for cloud-free conditions. The results for H_2O alone showed large variations between models for calculations of the surface flux and the change in flux when H_2O is varied.

The WBM results were very similar to the NBM results despite the fact that the WBMs are designed to achieve high computational efficiency. The reason for the general similarity between the two groups is probably due to the fact that the WBMs have been validated against NBM and LBL model results.

The major variation between model results was attributed to using different widths of the spectral intervals, different treatments of the H_2O continuum, errors in calculating the temperature dependence of spectral lines, errors in the numerical techniques used for the integration over altitude, different sources of spectral line data, and differences in the way band parameters are derived from the

spectral data. Differences in the treatment of individual gases can lead to significant variation in model results for one gas alone, but when all gases are included the effect of overlap reduces the range of variation. For example, whether or not the 10 μm band of CO_2 is included affects the results for CO_2 alone, but it does not make a significant difference compared with other sources of uncertainty for all gases together.

The intercomparison of models can be very useful for addressing a wide range of questions and issues, but it has the disadvantage that it does not provide an absolute assessment of accuracy (only a relative assessment). Observations or laboratory measurements are needed as absolute references for assessing model accuracy.

2.5.2 Comparison of Models with Observations

Comparisons of vertical profiles of observed flux densities and heating rates with calculations have been performed for cloudless and for homogeneous cloud conditions by many different investigators. Most of these comparisons, however, have involved the use of NBMs rather than the WBMs used in climate studies. The comparisons are often difficult to make and to interpret because of uncertainties in the observations and because of the lack of simultaneous measurements of all of the quantities necessary for the calculations. Cloudy conditions present the largest difficulties because the theory requires the measurement of more parameters than for clear sky conditions and it is more difficult to find quasi-horizontally homogeneous cloudy conditions. Because of the more uncertain nature of the cloudy sky comparisons, this section will attempt to summarize what comparisons with observations in cloudless sky conditions have concluded about the accuracy of the calculations.

The greatest quantity of clear sky flux data measured from within the atmosphere has been obtained during large-scale experiments designed to investigate the effects of aerosols on radiation. These studies include the Complex Atmospheric Energetics Experiment (CAENEX) discussed by Kondratyev et al. (1974), the Global Atmospheric Aerosol and Radiation Study (GAARS) described by DeLuisi et al. (1976), a study of Saharan aerosol advected over the tropical Atlantic Ocean described by Carlson and Caverly (1977), and studies of aerosol effects over Saudia Arabia and the adjacent Arabian Sea as part of the Monsoon Experiment (MONEX) discussed by Ackerman and Cox (1982) and Ellingson and Serafino (1984). In each of these studies, calculations based on the gaseous constituents agreed with pyranometer observations in the 0.3–2.8 μm region to within or to near the measurement uncertainty when the aerosol content was low (i.e., of the order of $\pm 5\%$ for the downward flux). The observed and calculated downward flux divergences generally agree to order $\pm 10\%$ for thick (150 mb) tropospheric layers in low aerosol conditions (Ackerman and Cox 1982). Although these differences are greater than the assumed relative accuracy of the observations ($\pm 5\%$ or better), these differences are usually attributed to aerosols or to uncertainties in the measured H_2O.

Several studies have shown comparisons of radiometersonde or pyrgeometer observations with model-calculated longwave fluxes that are in agreement to within $\pm 5\%$ or better, particularly for the upward fluxes (e.g., see Kuhn and Johnson 1966; Pilipowskij et al. 1968; Ackerman and Cox 1982; Ellingson and Serafino 1984). However, much larger observed than calculated downward fluxes have been noted in the lower stratosphere and upper troposphere in many studies employing radiometersondes (e.g., Pilipowskij et al. 1968; Ellingson and Gille 1978). These discrepancies have been attributed to invisible cirrus, stratospheric aerosols, H_2O uncertainties, or measurement errors. Recent downward flux comparisons employing pyrgeometer data have had mixed results at middle and high tropospheric levels (e.g., Ackerman and Cox 1982; Ellingson and Serafino 1984). In short, the downward flux differences have not been adequately explained.

Despite the differences between the observed and calculated downward fluxes, most comparisons between observed and calculated longwave heating rates have agreed to the order of $\pm 10\%$ for 100-mb layers. The best agreement usually occurs below 500 mb where the H_2O content is measured most accurately. It should be noted, however, that the number of cases studied is small, and there is little information concerning the geographical distribution of agreement between observations and calculations.

Most of the published longwave comparisons have involved only a few different wide and NBMs. As part of the ICRCCM, all of the participants were requested to perform calculations of the upward and downward fluxes for clear and cloudy soundings for which observations were available (see WMO 1985). Of the eight respondents, all of the model calculations agreed with the flux observations below 400 mb for both the clear and cloudy case to within the assumed ±5% measurement accuracy. Also, the models all reproduced the flux divergence below 500 mb to within the ±10% range of accuracy of the observations.

There is some literature concerning comparisons of satellite observations with model-calculated radiances for the longwave spectrum between 7 and 25 μm (e.g., LBL calculations—Kunde et al. 1974; NBM calculations—Ellingson and Gille 1978). For the few comparisons shown, the model-calculated radiances agree with those observed to near or to within the known errors of the observations and calculations. Ellingson and Gille (1978) used these comparisons to estimate the uncertainty of the calculation of the flux leaving the tropical atmosphere to be ±3%. However, this estimate is based on only five comparisons, and there were compensating errors in different wavelength regions.

Many observations of spectral radiance have been measured from instrumented aircraft in narrow spectral intervals used for remote sensing purposes (e.g., Smith et al. 1977). Comparisons of these observations with model calculations have generally shown good agreement (±5% or better). Although these results give us confidence, this type of agreement cannot be assumed for all narrow spectral intervals (say 5 cm^{-1}), because the accuracy of the radiance calculations across the spectrum and within the atmosphere has not been determined.

Comparisons of observed with calculated fluxes and radiances have generally been restricted to the troposphere except for relatively few high altitude balloon observations. Of possible importance for CO_2 studies are the results of experiments by McClatchey (1976) and McClatchey and D'Agati (1979). Comparisons of LBL calculations with radiometer observations of downward radiance in 20-cm^{-1} intervals across the 15-μm CO_2 band showed systematically lower observed than calculated radiance (10% less) from 250 to 10 mb. These comparisons indicate greater atmospheric opacity than is calculated. However, McClatchey and D'Agati (1979) tentatively identified the problem as being due to the assumption of the Planck function[6] as the source function. However, this problem appears to be unresolved, and the importance of these differences to estimates of stratospheric heating rates and to planetary radiation budgets has not been studied.

In summary, the comparisons of calculations with flux observations from within the atmosphere have generally shown agreement of the order of ±5% for cloudless, low aerosol content conditions. Although this sounds encouraging, in reality the uncertainty in the flux observations is so large that neither the reasons for the differences nor the significance of the intermodel differences can be established from the atmospheric observations alone. Although the comparisons of satellite- and aircraft-measured radiances with LBL and NBM calculations have given us confidence in the various approximations made in the calculations, the validation of the flux calculations remains incomplete.

2.6 THE RADIATIVE ENERGY BUDGET OF THE UNPERTURBED ATMOSPHERE

To better understand how increases in CO_2 perturb the radiation balance of the atmosphere, it is important to understand the radiative energy budget of the unperturbed atmosphere. In considering the solar and longwave components of the radiative energy budget, there are three regions of interest: the stratosphere, the troposphere, and the Earth's surface. Components of the solar and longwave radiative budgets are shown in Figures 2.6–2.8 for the stratosphere, the troposphere, and the Earth's surface, respectively.

The longwave radiative budget was computed using Ellingson and Gille's (1978) longwave radiative transfer model. The global annual mean values of the flux components were calculated by performing a calculation at each 10° of latitude and area

[6] The Planck function describes the emissive power of a blackbody as a function of wavelength at a given temperature. The function describes the shape of the curves shown in Figure 2.1.

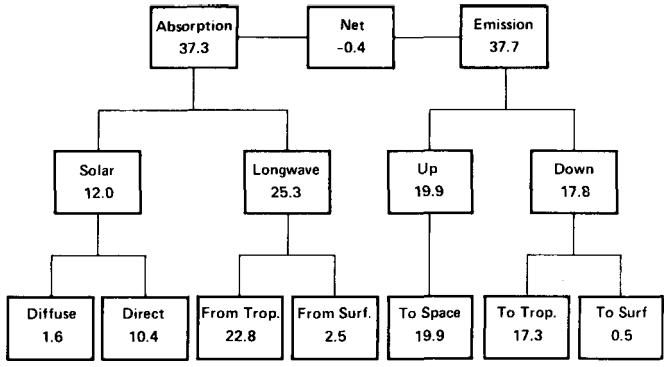

Figure 2.6. The annual-mean radiative budget for the stratosphere. Energy components have units of W m^{-2}.

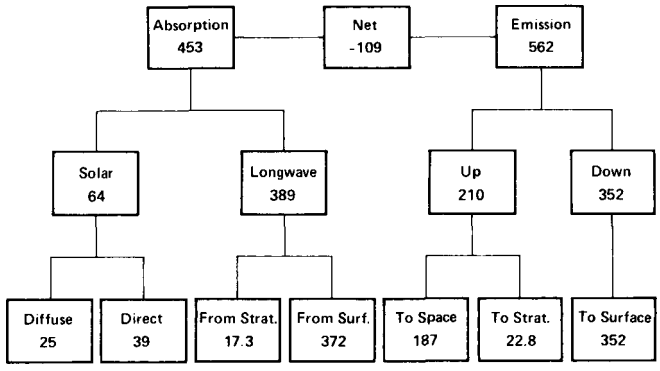

Figure 2.7. The annual-mean radiative budget for the troposphere. Energy components have units of W m^{-2}.

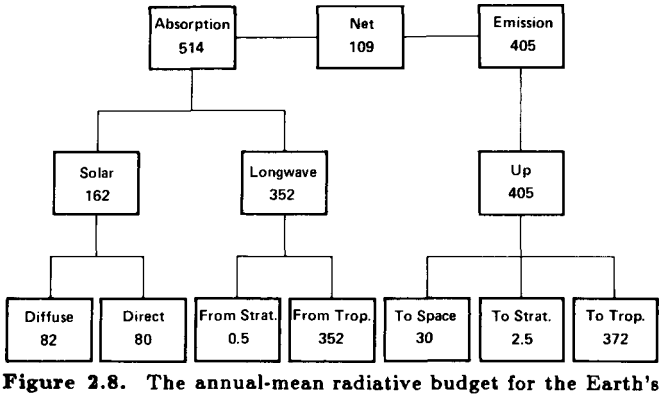

Figure 2.8. The annual-mean radiative budget for the Earth's surface. Energy components have units of W m^{-2}.

weighting the result. The atmospheric profiles of temperature, H_2O, and O_3 at each latitude were taken from Oort and Rasmusson (1971). The components of the solar radiative budget were based on calculations using a two-dimensional climate model (Potter et al. 1979; Ellingson and MacCracken 1981) with the same input conditions as the longwave model.

Figure 2.6 shows the components of the annual-mean radiative energy budget for the stratosphere. The values of the components of the stratospheric radiative budget are in good agreement with those of Ramanathan and Dickinson (1979). Solar and longwave absorption almost exactly balance longwave emission, the difference resulting from net dynamical transport of energy from the troposphere to the stratosphere. Because radiative absorption and emission are nearly equal, the stratosphere is very nearly in radiative equilibrium.

Solar absorption by O_3 contributes about 94% of the total solar absorption in the stratosphere, with H_2O and CO_2 contributing the remaining 6%. Longwave absorption is more than twice the total solar absorption. Because the temperature increases with altitude in the stratosphere, the longwave emission from the stratosphere to space is slightly greater than the downward emission to the troposphere and Earth's surface. The troposphere is highly opaque to longwave radiation, so only about 3% of the downward emission reaches the Earth's surface. Similarly, most of the absorbed longwave radiation in the stratosphere comes from tropospheric emission rather than from the Earth's surface.

The radiative budget for the troposphere is shown in Figure 2.7. Solar absorption in the troposphere equals about 18% of the solar radiation incident at the top of the atmosphere (which is 342 W m^{-2}). Longwave absorption (primarily resulting from emission from the surface) amounts to more than 100% of the solar flux incident at the top of the atmosphere. Longwave emission is significantly greater than the total absorption. The net excess of absorption over emission of 109 W m^{-2} is balanced by the convective flux of latent heat and sensible heat from the Earth's surface to the troposphere.

The radiative budget for the Earth's surface is shown in Figure 2.8. Longwave absorption is approximately twice the solar absorption. Longwave emission from the surface is approximately 118% of the incoming solar flux at the top of the atmosphere. The net longwave exchange between the surface and the atmosphere is a cooling of about 53 W m^{-2}. The solar absorption is significantly greater than the net longwave emission, with the excess energy being transported to the troposphere as sensible and latent heat.

The calculated global annual-mean solar and longwave flux components are shown in Figure 2.9. Because convective mixing leads to strong coupling

between the upper and lower troposphere, as well as between the troposphere and Earth's surface, changes in the net flux at the tropopause affect temperatures throughout the troposphere and at the surface. A frequent basis for estimating the climate change resulting from a perturbation to the atmospheric composition is the effect the perturbation has on the net flux at the tropopause.

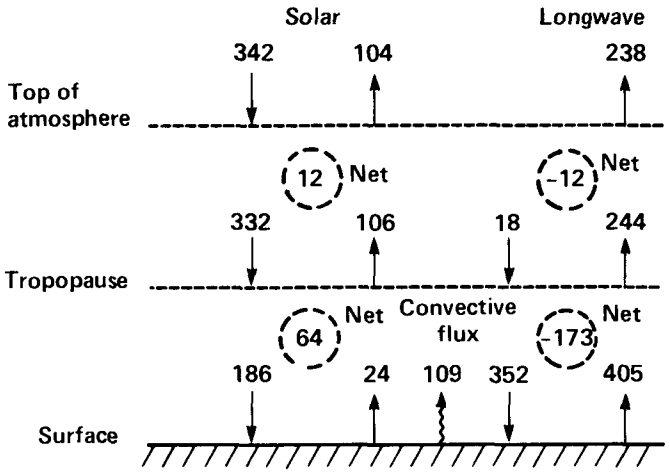

Figure 2.9. Solar and longwave radiative fluxes (W m^{-2}) calculated for the global annual-mean energy balance of the atmosphere and Earth's surface.

2.7 THE RADIATIVE EFFECT OF VARIATIONS IN CARBON DIOXIDE CONCENTRATION

The absorption bands of CO_2 near 15 μm consist of a combination of strong and weak lines. The effect of a change in absorber amount (in this case CO_2) depends on the strength of the line. The absorption versus wave number is shown in Figure 2.10 for weak, intermediate, and strong absorption. The curve labeled $u = 0.1$ refers to the case of weak absorption. In the limiting case of very weak absorption, the absorption by a single isolated line is proportional to the absorber amount. As the absorber amount increases (or equivalently as the line strength increases), the largest increase in absorptivity occurs at the line center with smaller absolute increases in the line wings. Eventually, there is complete absorption near the line center (referred to as saturation) after which the increased absorption occurs in the line wings. In the strong line limit, the absorption by a single line is proportional to the square root of the absorber amount. Intermediate absorption cases fall somewhere between the linear and square-root limits.

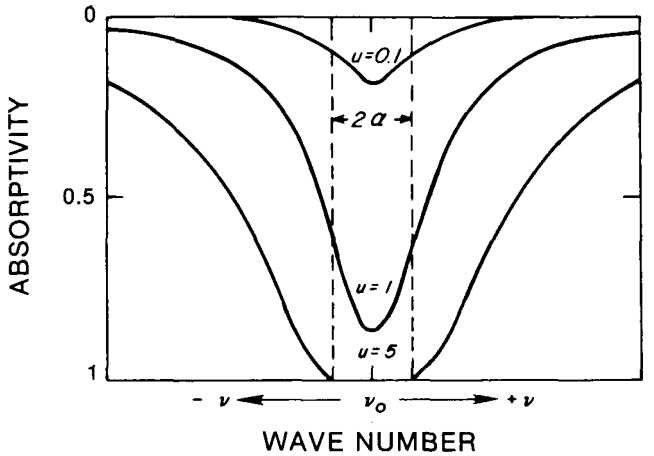

Figure 2.10. Single line absorption for various absorber path lengths. Source: Liou (1980).

Trace gases have small absorber amounts. Thus, they fall within the weak line limit. Their radiative effect is, therefore, proportional to the amount of the trace gas. Several studies have shown that the climatic effect of several minor trace gases, when combined, can be comparable to that resulting from a CO_2 increase (Flohn 1978; Ramanathan 1980; Lacis et al. 1981).

There are many strong lines near the center of the 15-μm CO_2 band. Consequently, there is almost complete absorption in this portion of the band, with radiation emitted from the surface being absorbed within the lowest few kilometers of the atmosphere in the 15-μm wavelength region. Likewise, most of the downward emission by CO_2 to the surface comes from the central portion of the 15-μm band. Because of saturation of strong lines, most of the *change* in longwave absorption and emission resulting from an increase in CO_2 occurs in the weak lines and wings of strong lines. Consequently, the spectral regions of the CO_2 band contributing most to the change in longwave fluxes are the weaker absorption regions on either side of the 15-μm band center.

The contribution of the weak absorption bands to the change in surface temperature resulting from increased CO_2 is significant, even though their contribution to ambient absolute longwave fluxes is small. The contribution to the increase in surface temperature by the stronger 15-μm bands and by the weak bands of CO_2 have been calculated by Augustsson and Ramanathan (1977) and is shown in

Figure 2.11. The 15-μm bands include the fundamental bands of $C^{12}O_2^{16}$ and three other isotopes of CO_2 plus the six strongest hot bands of $C^{12}O_2^{16}$ with band centers in the 15-μm region (see Ramanathan 1976 for a list of band centers and band strengths). Hot bands are those bands that have excited vibrational levels for their lower level. The weak bands include four hot bands in the 12–18 μm region, two hot bands in the 10-μm region, and a weak pressure-induced fundamental band in the 7.6-μm region.

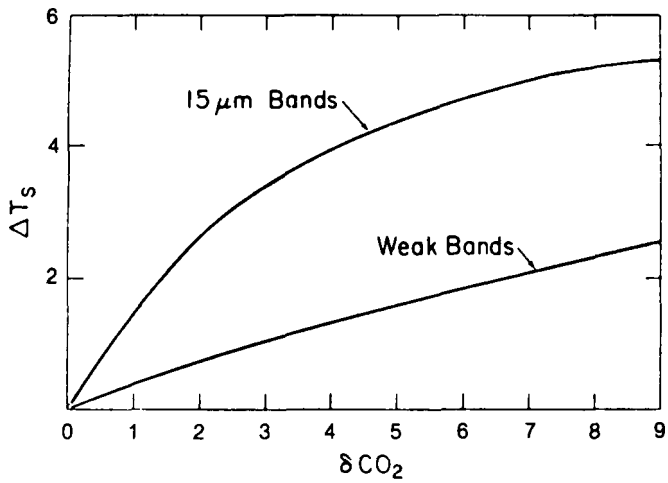

Figure 2.11. Individual contribution to the increase in surface temperature by the 15-μm bands and the weak bands. The results are for the constant cloud top altitude model. δCO_2 = [CO_2 (perturbed)–CO_2 (ambient)]/CO_2 (ambient). Ambient CO_2 = 320 ppm (by volume); T_s = surface temperature. The number of bands and their band centers included in the category of the weak bands is given in the text. Source: Augustsson and Ramanathan (1977).

Figure 2.11 shows that the change in surface temperature that is due to the weak bands increases almost linearly with the increase in CO_2. On the other hand, although the 15-μm bands make a larger contribution to the change in temperature, the change in temperature is much less than linear with the CO_2 increase. Because the 15-μm bands are optically thick, the temperature change due to those bands increases logarithmically with CO_2. The change in temperature due to the weak bands is a significant fraction of that due to the 15-μm bands, even though the total band strength for the weak bands is more than an order of magnitude less than the total band strength for the 15-μm bands.

The contribution of the fundamental band and the hot bands of CO_2 in the 15-μm region to longwave cooling rates is shown in Figure 2.12. The first hot bands refer to transitions that have the first excited vibrational state as the lowest energy level. The strengths of the fundamental and first hot bands are considerably greater than the other bands, so the fundamental and first hot bands make the greatest contribution to the cooling rate. The 15-μm bands referred to in Figure 2.11 include the fundamental bands, the isotope bands, the first hot bands, and two of the second hot bands shown in Figure 2.12.

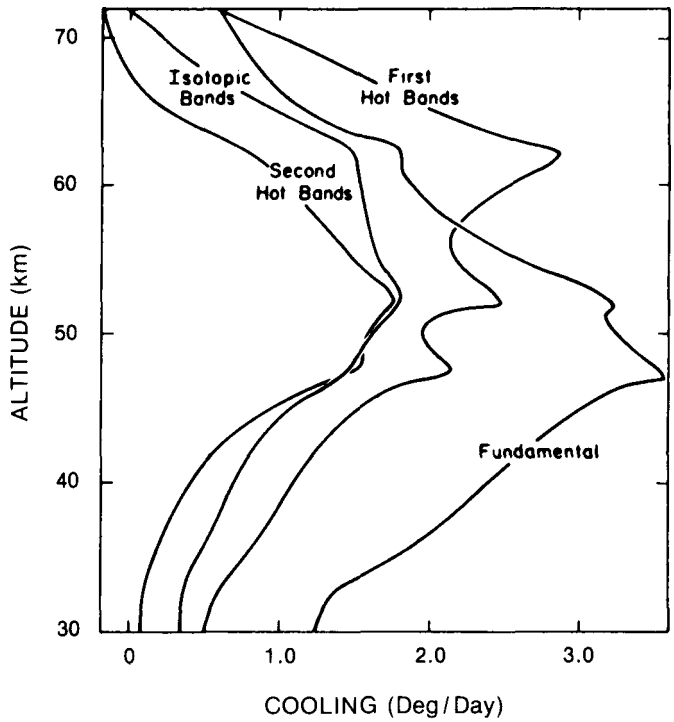

Figure 2.12. Longwave CO_2 cooling rates showing the contributions from fundamental, hot, and isotopic bands. Source: Dickinson (1973).

The temperature dependence of the band absorptance of the 15-μm band has an important effect on the radiative forcing because of a change in CO_2. Augustsson and Ramanathan (1977) showed that neglecting the temperature dependence of the band absorptance could result in an underestimate of about 25% in the value of the change in surface temperature resulting from a doubling of CO_2.

There have been several recent model studies of the effect of increased CO_2 concentrations on the atmospheric radiation budget (Augustsson and Ramanathan 1977; Ramanathan et al. 1979; Hansen et al. 1981; Ramanathan 1981; Kiehl and Ramanathan

1982; Wang and Ryan 1983). All these model studies show that increased CO_2 would reduce the longwave radiative loss by the troposphere-surface system, which would result in an increase in temperature.

The direct radiative forcing due to a doubling of CO_2 is the change in radiative flux densities that would occur while holding all other parameters fixed (no change in atmospheric temperature, moisture content, etc.). The increase in downward longwave flux at the surface when CO_2 is doubled has been calculated to be 1.1–1.8 W m^{-2} (Ramanathan et al. 1979; Hansen et al. 1981; Ramanathan 1981). The magnitude varies with latitude, being smallest at low latitudes and largest at high latitudes. This latitude variation results from the variation in water vapor abundance. The overlap of H_2O and CO_2 bands within the 12–18 μm region diminishes the effect of an increase of CO_2 where H_2O is most abundant. These ranges of values were calculated without including the effect of overlap of the H_2O continuum absorption in the 12–18 μm region. When this overlap was included in calculations by Kiehl and Ramanathan (1983), the hemispherically averaged increase in downward longwave flux at the surface that is due to CO_2 changed from 1.56 W m^{-2} without the overlap to 0.55 W m^{-2} with the overlap. Consequently, the direct longwave forcing due to increased CO_2 varies significantly, depending on the degree of overlap assumed between the rotational lines and continuum of H_2O and the 15-μm band of CO_2. This overlap is not sufficiently understood at present to determine which values are correct.

The direct radiative heating of the surface-troposphere system because of doubled CO_2 with no change in atmospheric temperatures or H_2O amounts is about 4 W m^{-2} averaged hemispherically, ranging from nearly 5 W m^{-2} at low latitudes to about 2 W m^{-2} at high latitudes. This forcing also has a seasonal dependence (Ramanathan et al. 1979), with little seasonal variation at low latitudes and a range (maximum to minimum) of about 1 W m^{-2} at high latitudes. The maximum heating occurs in summer and the minimum in winter. These seasonal variations are caused by the temperature dependence of the opacity of the CO_2 hot bands and the Planck function in the 15-μm region.

In the stratosphere, increased CO_2 concentrations result in enhanced longwave emission to space and an increase in downward emission to the troposphere. The downward emission to the troposphere increases by 1–2 W m^{-2}, the smallest value occurring at low latitudes and the largest at high latitudes. The increased emission to the troposphere is included in the calculated change in net flux at the tropopause given above. The increased emission to space compensates in part for the reduced upward emission at the tropopause. The calculated decrease in the upward longwave flux at the top of the atmosphere ranges from 1.6 to 2.4 W m^{-2} (Ramanathan and Coakley 1978; Hansen et al. 1981).

An increase in CO_2 concentration also affects solar absorption in the atmosphere. The increased solar absorption by CO_2 is about 0.4 W m^{-2} for a doubling of CO_2 levels. By absorbing more solar radiation, CO_2 allows less radiation to reach the Earth's surface. The reduction in solar radiation absorbed by the Earth's surface is about 0.3 W m^{-2}, thus the net change for the atmosphere-surface system is an increase of only about 0.1 W m^{-2} in solar absorption. Consequently, increased CO_2 does not have a significant direct effect on the net solar heating of the atmosphere, but it does affect the partitioning between atmospheric and surface absorption.

Following the initial radiative forcing when CO_2 is doubled, there is an increase in downward flux to the surface as the atmosphere warms. The increased tropospheric temperatures lead to enhanced longwave emission by all of the radiatively active constituents, namely CO_2, H_2O, O_3, clouds, and trace gases. As the surface and troposphere warm, increased evaporation leads to increases in absolute humidity which acts to reduce longwave emission from the surface to space (leading to further heating of the troposphere) and enhances longwave emission from the atmosphere to the surface. Ramanathan (1981) has evaluated the effect of each of these processes on the downward flux at the surface. In his study these processes were evaluated in sequence to illustrate the importance of each process. In the real environment they would occur simultaneously as CO_2 increases gradually.

When CO_2 was doubled with temperatures remaining fixed, the increase in net downward radiative flux at the surface was 1.2 W m^{-2}. When tropospheric temperatures (but not surface temperature) were allowed to respond to the enhanced radiative heating, the downward flux at the surface increased by an additional 2.3 W m^{-2}. Finally, when the system was allowed to come to a new equilibrium state, including increased H_2O, there was an additional increase of 12.0 W m^{-2} in the net downward flux at the surface. Thus, the initial increase of 1.2 W m^{-2} grew to 15.5 W m^{-2} as the various feedback processes were added. A similar calculation by Hansen et al. (1981) showed an initial radiative forcing at the surface of 0.8 W m^{-2} which increased to 15.3 W m^{-2} at equilibrium.

2.8 RADIATIVE EFFECT OF AEROSOLS

Aerosols affect the climate directly by modifying the solar and longwave radiation budgets of the atmosphere and indirectly by their effect on clouds. Aerosols directly inhibit the transmission of solar radiation to the surface and can scatter a fraction of the incident radiation back to space. The solar radiative effect depends not only on the local concentration and optical properties of the aerosols but also on the surface albedo and solar zenith angle. Aerosols suspended over a darker underlying surface (such as the ocean) tend to increase planetary albedo, whereas the same aerosols suspended over land with a higher surface albedo (such as snow or deserts) generally tend to decrease planetary albedo.

The longwave effects of aerosols are similar to those of the greenhouse gases in that they reduce the upward longwave flux at the top of the atmosphere and increase the downward longwave flux at the Earth's surface. The aerosols differ from gases, however, in that they can absorb and emit radiation over the entire longwave spectrum, including the 8–12 μm window region, with the optical properties depending primarily on composition, particle shape, and particle size distribution.

Aerosols affect the optical properties of clouds by acting as condensation and freezing nuclei. Thus, aerosols affect the number and size of cloud droplets and ice crystals, which determine the cloud optical properties. The presence of aerosols within and between cloud droplets also affects the albedo of the cloud. Changes in solar and longwave heating rates caused by aerosols can induce changes in atmospheric stability, which in turn can affect the amount of clouds formed. Twomey (1977) showed that an increase in the number of condensation nuclei tends to increase the optical thickness and the backward scattering of clouds, thus increasing the cloud albedo. Imbedding absorbing aerosols inside and between cloud droplets tends to decrease the cloud albedo. The indirect effects of aerosols are poorly understood, and much more theoretical and experimental research is needed in order to quantify these effects.

The composition, size, and spatial and temporal distributions of aerosols vary according to the source of the aerosols. The basic aerosol components include soot, dust, maritime, sulfate, and volcanic ash aerosols. Soot is found primarily in urban and industrial settings, and it has also been shown to be present in Arctic haze. Unlike the other components, soot is highly absorbing at visible wavelengths. The presence of carbonaceous material in aerosol samples accounts for most of the absorptive property of the aerosols (Ackerman and Toon 1981). Dust consists of wind-blown soil and sand. Maritime aerosols consist generally of water soluble sulfates and larger sea salt particles originating from sea spray. Stratospheric aerosols consist primarily of 75% H_2SO_4 droplets and volcanic ash. The background stratospheric aerosol layer consists of H_2SO_4 droplets. Energetic volcanic injections of sulfur-containing gases (such as Agung in 1963 and El Chichón in 1982) can significantly enhance the amount of H_2SO_4 in the stratosphere in addition to injecting volcanic ash. More detail about each of these aerosol components is contained in Chapter 6.

The aerosol size distribution is typically represented by either a log-normal distribution

$$\frac{dN(r)}{d(\log r)} = \frac{n}{\sqrt{2\pi}\log\sigma}\exp\left[-\frac{(\log r - \log R)^2}{2(\log\sigma)^2}\right] \tag{2.12}$$

or the modified gamma function

$$\frac{dN(r)}{dr} = Ar^{\alpha}\exp\left(-br^{\gamma}\right) , \tag{2.13}$$

where $N(r)$ is the number of particles having radii less than r; n is the total number of particles; R

is the geometric mean radius; σ is the geometric standard deviation; and A, α, b, and γ are constants. In some cases, the size distribution may be the combination of two or more separate aerosol distributions, in which case the total size distribution may be described by superposition of the individual components (e.g., see Shettle and Fenn 1979).

Assuming that the particle size distribution can be characterized by a log-normal distribution, values of R and σ have been obtained for the various aerosol components (WMO 1983). The results are shown in Table 2.3. The geometric mean radius varies greatly, depending on the aerosol component. Desert dust storm and sea salt aerosols have the largest mean radii. Soot, water soluble, and H_2SO_4 aerosols have very small mean radii. The geometric mean standard deviation is usually in the range 1.8–2.2.

Table 2.3
Particle Size Distribution Parameters for Log-Normal Size Distribution

	Parameter	
Aerosol Type	R (μm)	σ
Soot	0.012	2.00
Oceanic		
1	0.05	2.03
2	0.40	2.03
3	3.3	2.03
Dustlike	0.47	2.51
H_2SO_4 (75%)	0.070	1.86
Volcanic Ash	0.22	1.77

Source: WMO (1983).

The aerosol optical properties are characterized by the volume extinction coefficient σ_e, the volumn scattering coefficient σ_s, and the asymmetry factor g, which is the average cosine of the scattering angle. For isotropic scattering where half of the scattered energy goes in the forward-scattering hemisphere and half in the backward-scattering hemisphere, the value of g is zero. Values of g greater than zero imply larger forward scattering than backward scattering.

Other optical properties include the volume absorption coefficient and single-scattering albedo. The absorption coefficient is the difference between the extinction and scattering coefficients ($\sigma_a = \sigma_e - \sigma_s$), and the single-scattering albedo is the ratio $\omega_0 = \sigma_s/\sigma_e$.

Optical properties for various aerosol components are shown in Table 2.4. The single scattering albedo indicates the absorptive nature of the aerosols; a small value indicating a highly absorbing aerosol. Soot is a very strong absorber of visible radiation, and dust and urban aerosols are also effective absorbers. The other aerosols primarily scatter rather than absorb visible radiation. When the aerosol particles are large, the extinction coefficient in the longwave region $\sigma_e(10\ \mu m)$ may be as large as the extinction coefficient in the visible region $\sigma_e(0.55\ \mu m)$. Normally, however, the ratio of longwave extinction to visible extinction is in the range 0.03–0.1.

Table 2.4
Mean Aerosol Radiative Properties

	Radiative Properties			
Aerosol Type	ω_0 (0.55 μm)	g	ω_0 (10 μm)	$\frac{\sigma_e\ (10\ \mu m)}{\sigma_e\ (0.55\ \mu m)}$
Soot	0.209	0.34	0.	0.038
Oceanic	1.0	0.78	0.692	0.250
Dustlike	0.653	0.88	0.558	1.08
H_2SO_4 (75%)	1.0	0.73	0.010	0.050
Volcanic Ash	0.947	0.70	0.130	0.035
Water Soluble	0.957	0.63	0.209	0.109

Note: ω_0 is single-scattering albedo, g is asymmetry factor, and σ_e is extinction coefficient.
Source: WMO (1983).

Optical depth τ is a unitless measure of the vertical loading and radiative effectiveness of aerosol material. The optical depth is defined by

$$\tau(\lambda, z) = \int_z^\infty \sigma_e(\lambda) u(z)\, dz\ , \qquad (2.14)$$

where u is the aerosol number density and σ_e is the monochromatic extinction cross section. The visible optical depth usually refers to the optical depth at 0.55 μm, which corresponds to the peak in the solar irradiance.

The visible optical depth of stratospheric aerosols is about 0.005 for unperturbed conditions (Toon and Pollack 1976). The stratospheric optical depth is variable, and values of 0.02–0.03 occur frequently. Stratospheric optical depths greater than 0.1 are possible after large volcanic injections (Pollack et al. 1976).

Tropospheric aerosol optical depths vary greatly with season and geographical location. On particularly clear days, the aerosol optical depth is about 0.05. Annual mean continental aerosol optical depths vary from about 0.25 at low latitudes to about 0.1 at high latitudes (Toon and Pollack 1976). Seasonal variations are a significant fraction of the annual mean value (e.g., they can be ±50%) with the largest optical depths usually occurring in summer. In urban areas the annual mean optical depth can range from 0.125 to 0.75. Because of the large temporal and spatial variations of aerosol composition and mass loading, it is difficult to characterize typical tropospheric aerosol optical properties. Models that are often used to characterize stratospheric and tropospheric aerosols have been developed by Elterman (1968), Toon and Pollack (1976), and Shettle and Fenn (1979).

There have been many studies of the effect of tropospheric and stratospheric aerosols on the solar and longwave radiation budgets. Such assessments are a necessary step in the process of estimating the effect of aerosols on climate. In this section, the discussion is limited to the effect of aerosols on the radiation budget. The climatic effect of aerosols is discussed in Chapter 6.

McCormick and Ludwig (1967) were the first to suggest that increased aerosol loading resulting from pollution would increase the fraction of incoming solar radiation scattered back to space, thus tending to cool the surface. Charlson and Pilat (1969) showed that an aerosol layer could lead to either warming or cooling, depending on the relative magnitudes of the absorption and backscatter coefficients.

Atwater (1970) calculated the change in planetary albedo as a function of surface albedo and the ratio of absorption to backscattering. He developed an expression for the critical ratio of scattering to backscatter for which there is no net change in solar heating of the Earth-atmosphere system. Mitchell (1971) did a more detailed analysis of the effect of aerosols on the energy budget of the atmosphere, and he included terms that were neglected by Atwater (1970) in deriving an expression for the critical ratio of absorption to backscatter for optically thin aerosol layers:

$$\frac{b_{abs}}{b_{bs}} = \frac{(1-a)^2}{2a}, \qquad (2.15)$$

where b_{abs} is the absorption coefficient, b_{bs} is the backscattering coefficient, and a is the albedo of the underlying surface.

Chýlek and Coakley (1974) used a two-stream model to study the effect of aerosols on planetary albedo, and they showed that the expression derived by Mitchell (1971) for optically thin aeosol layers also applies to optically thick layers. Chýlek and Coakley (1974) showed how the planetary albedo may either increase or decrease, depending on the optical properties of the aerosols, their optical depth, and the albedo of the underlying surface.

Rasool and Schneider (1971) considered the effect of aerosols on both the longwave and solar radiative fluxes at the top of the atmosphere. An increase in tropospheric aerosol amount decreases the amount of longwave radiation emitted to space (holding temperatures fixed), which tends to warm the Earth-atmosphere system, but the longwave effect was found to be much smaller than the solar effect.

Following these early studies, there have been many more assessments of the effects of tropospheric and stratospheric aerosols on solar and longwave radiative fluxes. Solar radiation calculations included more detailed treatment of multiple scattering (Yamamoto and Tanaka 1972; Braslau and Dave 1973a, 1973b, 1975; Reck 1974a, 1974b, 1975; Wang and Domoto 1974; Yamamoto et al. 1974; Herman and Browning 1975; Liou and Sasamori 1975; Konyukh et al. 1979; Blanchet and Leighton 1981). These studies showed the effect of aerosols on planetary albedo and solar heating rates as a function of solar zenith angle, surface albedo, and aerosol radiative properties. Solar absorption within the aerosol layer typically leads to heating rates in the range 1–9°C per day.

Studies of the longwave effects of aerosols indicate that these effects can be important in terms of their effect on cooling rates and surface temperature. Increased upward emission of longwave radiation by the aerosols tends to cool the layer (Grassl 1973; Wang and Domoto 1974; Ackerman et al. 1976; Harshvardhan and Cess 1978). The longwave cooling rate can be enhanced due to the aerosols by up to several degrees Celsius per day. The magnitude of the change in upward longwave flux at the top of the atmosphere depends on the

temperature contrast between the surface and the aerosol layer; the greater the temperature difference, the greater is the reduction in outgoing longwave radiation. Because aerosols in the upper troposphere and lower stratosphere have a large temperature difference compared with the surface, they are very effective in reducing longwave emission to space.

Many studies have focused on the solar and longwave effects of stratospheric aerosols (Remsberg 1973; Cess 1976; Coakley and Grams 1976; Harshvardhan and Cess 1976; Herman et al. 1976; Luther 1976; Pollack et al. 1976; Harshvardhan 1979; Lenoble et al. 1982). These studies have shown that enhanced backscattering of solar radiation is the dominant effect except in the case of high surface albedo. Longwave effects can be significant, but generally are not dominant.

Figure 2.13 shows the change in spherical (or globally averaged) albedo, $\Delta\alpha_p$, because of the addition of tropospheric aerosols as calculated by Coakley et al. (1983) for the three aerosol models of Shettle and Fenn (1979) using a visible optical depth of 0.1. There is an increase in spherical albedo for small surface albedos, resulting in a decrease in net solar heating (i.e., cooling) of the Earth-atmosphere system. There is a reversal to heating at high surface albedos. Although the impact of aerosols over high albedo surfaces such as snow and ice is an increase in solar heating, this does not necessarily mean that surface temperature will increase. Regions of high surface albedo occur mostly at high latitudes where solar zenith angles are large. Large solar zenith angles lead to increased backscattering, which tends to increase planetary albedo, partially compensating for the increased aerosol absorption over a high albedo surface.

Coakley et al. (1983) have calculated the annual-mean change in planetary albedo due to the presence of a tropospheric aerosol with a real refractive index of 1.5 and imaginary refractive index of 0.005. Their results are shown as a function of latitude in Table 2.5. The aerosol optical depth is 0.16 at low latitudes (0–30°N), 0.12 at middle latitudes (30–60°N), and 0.07 at high latitudes (>60°N).

The aerosol produces cooling (i.e., increase in planetary albedo) at all latitudes except near the pole where there is slight heating. The temperature change calculated for this radiative forcing showed

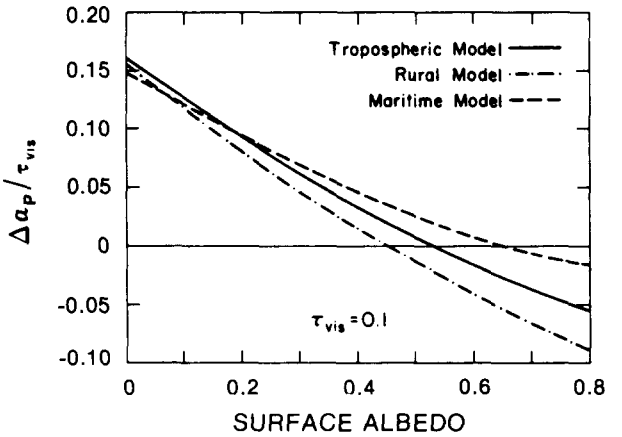

Figure 2.13. Change in spherical albedo $\Delta\alpha_p$ calculated for the three aerosol models of Shettle and Fenn (1979) and for $\tau_{vis} = 0.1$. Source: Coakley et al. (1983).

Table 2.5
Aerosol-Induced Changes in Albedo, $\Delta\alpha$, Because of the Presence of an Aerosol With Real Refractive Index of 1.5 and Imaginary Refractive Index of 0.005

Latitude	$\Delta\alpha$ (clear)	$\Delta\alpha$ (overcast)
5	0.0073	0.0028
15	0.0083	0.0023
25	0.0091	0.0021
35	0.0072	0.0018
45	0.0065	0.0019
55	0.0062	0.0018
65	0.0062	0.0007
75	0.0033	-0.0001
85	-0.0007	-0.0006
Average	0.0073	0.0021

Source: Coakley et al. (1983).

a cooling at all latitudes, with the maximum cooling occurring at high latitudes. Because of feedback processes and coupling between latitudes, the change in temperature is not directly proportional to the initial radiative forcing from the presence of aerosols at that latitude.

The longwave effect of tropospheric aerosols tends to compensate partially for the solar effect. Estimates of the magnitude of the longwave effect range from negligible (Coakley et al. 1983) to about 25% of the solar effect (Hansen et al. 1980; Charlock and Sellers 1980) depending on the radiative properties chosen for the aerosol.

The effect of a stratospheric aerosol layer on the Earth's radiation budget is shown in Figure 2.14. The change in net outgoing radiation (solar plus longwave) at the top of the atmosphere has been calculated for 75% H_2SO_4 aerosol with an optical

depth of 0.1 in the visible (Harshvardhan 1979). The stratospheric aerosol layer leads to a net energy loss for the Earth-atmosphere system at all latitudes and seasons except the polar winter. The energy gain in the polar winter occurs due to the greenhouse effect of the aerosols with no solar radiation present. The largest perturbation to the radiation balance (8–9 W m^{-2}) occurs at high latitudes in the spring and fall. Equatorward of 60° latitude, the perturbation is in the range 2.5–5.0 W m^{-2}.

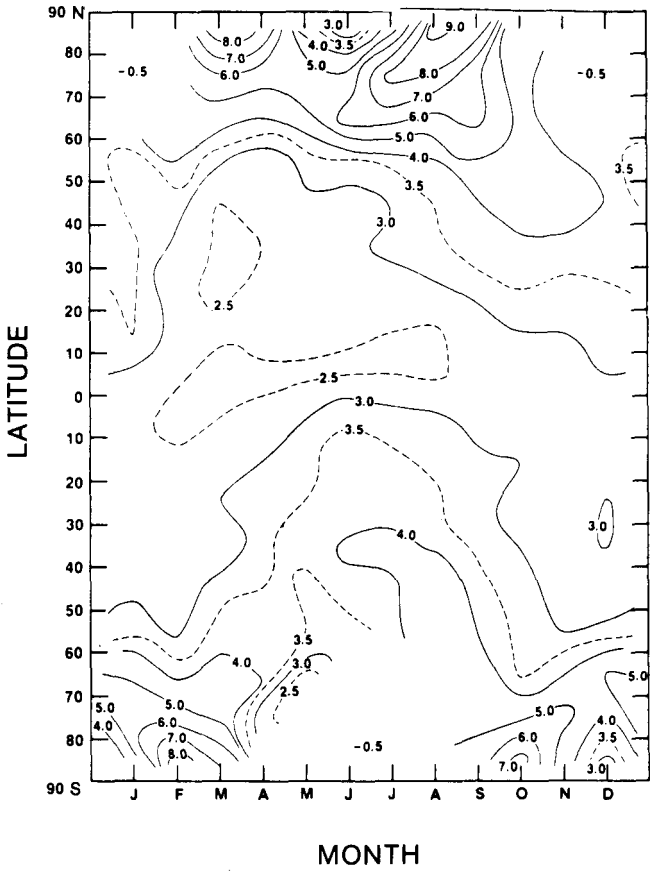

Figure 2.14. Reduction in the zonal radiation balance (W m^{-2}) with addition of aerosol layer of $\tau_{vis} = 0.1$. Source: Harshvardhan (1979).

It has been shown, therefore, that the perturbations to the Earth's radiation budget because of increased aerosol loading can be comparable in magnitude to that due to a doubling of CO_2. The radiative effects of aerosols depend on their composition and spatial distribution as well as the albedo of the underlying surface. It is not known whether or how aerosol amounts would change in response to a CO_2-induced climate change. Changes to the hydrologic cycle might affect the amount of dust contained in the atmosphere, and changes in soil moisture and wind speeds might alter the amount of wind-blown dust on a regional basis, but such changes are only speculative.

2.9 RADIATIVE EFFECTS OF CLOUDS

Covering about half the Earth's area, clouds have a major impact on the solar and longwave radiative budgets of the atmosphere. Cloud albedo varies with cloud type and solar zenith angle, with the average albedo being 0.45–0.50 (Ramanathan and Coakley 1978). The average cloud albedo is considerably greater than the albedo in the portion of the atmosphere that is cloud free (albedo typically in the range 0.14–0.18). Consequently, clouds reduce the solar energy that would be absorbed by the atmosphere and surface if clouds were not present.

Clouds are generally opaque to longwave radiation; thus, they reduce the outgoing radiation to space by absorbing radiation emitted by the warmer surface and atmosphere below and replacing it with radiation that is emitted at the colder cloud-top temperature. The downward longwave emission by clouds increases the flux incident at the Earth's surface. Because the longwave effect of clouds on outgoing longwave radiation at the top of the atmosphere depends on the temperature contrast between the cloud-top temperature and the temperature of the underlying atmosphere and Earth's surface, the longwave effect depends strongly on cloud altitude and thickness.

Of course, cloud elements have finite sizes and they are distributed nonuniformly in the horizontal and in the vertical. Because the cloud particles scatter radiation within and among the cloud elements, because the finite cloud elements shade each other, and because the cloud elements have no fixed shape, the calculation of the transfer of radiation in a real cloud field is complicated, and this constitutes the largest unsolved problem in atmospheric radiation. As a result of these complications, most of our knowledge of the radiative effects of clouds has arisen from calculations based on relatively simple models of clouds. The effects of cloud cover are usually estimated for a single cloud layer by taking the cloud amount weighted average of calculations for clear and complete cloud cover conditions. The effects of overlapping of cloud layers are usually accounted for by assuming maximum, minimum, or

random overlap of the individual layers (e.g., Kuhn 1978).

The calculations for complete horizontally homogeneous cloud cover may be readily performed by a variety of techniques (e.g., two-stream—Lacis and Hansen 1974; Monte-Carlo—Davies et al. 1984) if the cloud particles are assumed to be pure water spheres. If the phase of the particles and the vertical distribution of the particle size distribution are known, the Mie (1908) theory may be used to calculate the parameters necessary for the model calculations (for details, see Liou 1980; Paltridge and Platt 1976). It should be noted, however, that the radiative transfer theory is not as advanced for nonspherical particles, such as cirrus particles, and dissolved nuclei may change the absorption properties of the droplets.

In recent years there has been a significant improvement in the understanding of the effects of the finite sizes of clouds as a result of better theoretical and computer models (e.g., McKee and Cox 1974; Davies 1978; Harshvardhan and Weinman 1982; Ellingson 1982). These studies have shown that, in addition to the cloud fraction and optical depth of the cloud elements, it is important to know at least the geometrical thickness, the aspect ratio, and the manner by which the cloud elements are distributed in the horizontal. Although some simplifications of the detailed calculations have been developed for including the effects of the finite sizes in routine calculations (e.g., Harshvardhan 1982; Ellingson 1982), these parameterizations have not been adapted to climate calculations because the geographical distribution of the required cloud parameters is largely unknown, and because the various climate models are generally incapable of estimating more than the cloud fraction of different cloud types (if those).

Theoretical and empirical studies have shown, however, that the solar and longwave effects of clouds have opposing influences on the surface temperature. Studies by Manabe and Wetherald (1967), Schneider (1972), and Ellis (1977) indicate that clouds have a net cooling effect on the surface temperature. Manabe and Wetherald (1967) showed that the strongest cooling effect of clouds occurs with low clouds. The magnitude of the cooling effect decreases with increasing cloud altitude and can reverse sign (leading to warming) for high clouds. They obtained the following results using a radiative convective model (with a constant cloud albedo for each cloud type):

$$\text{Low clouds} \quad \frac{dT_s}{dA_c} = -82 \text{ K}$$

$$\text{Middle clouds} \quad \frac{dT_s}{dA_c} = -39 \text{ K}$$

$$\text{High clouds} \quad \frac{dT_s}{dA_s} = 38 \text{ K (black)}$$

$$= 4 \text{ K (half - black)} ,$$

where T_s is the surface temperature and A_c is the cloud fraction.

Stephens and Webster (1981) reexamined and corroborated many aspects of the study of Manabe and Wetherald (1967). Most importantly, however, this study established the water path of a cloud at a given height to be the critical parameter in determining the magnitude of dT_s/dA_c in addition to the cloud amount and altitude. This parameter is important because it determines both the longwave and shortwave radiative properties of the cloud (i.e., albedo and emissivity). Because of the sensitivity of the surface temperature to the cloud fraction, Stephens and Webster (1981) urge care in the radiation parameterization of the cloud amount.

One measure of the relative magnitudes of the competing cloud feedback process is the cloud sensitivity parameter, δ, defined by Schneider (1972) as

$$\delta = \frac{\partial Q_{abs}}{\partial A_c} - \frac{\partial F}{\partial A_s} , \qquad (2.16)$$

where Q_{abs} is the solar flux absorbed by the Earth-atmosphere system, and F is the outgoing longwave radiation. Q_{abs} may be written as

$$Q_{abs} = Q_0(1 - \alpha) , \qquad (2.17)$$

where Q_0 is the available solar radiation, and α is the planetary albedo. If $\delta < 0$, the albedo effects dominate, whereas the albedo and longwave effects compensate when $\delta = 0$. Many different model studies have found negative values of δ. However, Cess and Ramanathan (1978) point out that δ may not be evaluated by a model unless the model can predict the cloud amounts of the individual layers in relation to changes of the total cloud amount.

Recently, Cess et al. (1982) compared four different empirical studies which have attempted to

determine the relative magnitude of the albedo versus the longwave effects of the cloud amount feedback (e.g., Cess 1976; Ohring and Clapp 1980; Hartmann and Short 1980). Cess et al. (1982) discuss a number of uncertainties associated with the various data sets, and they caution about making conclusions concerning the relative roles of the albedo and longwave components of the cloudiness feedback. Harshvardhan (1982), in a theoretical study using finite-sized cloud elements, has solidified this conclusion by showing that satellite measurements of the outgoing longwave and reflected solar radiation alone cannot be used to deduce the cloud feedback term accurately. Instead, it is necessary to also know the cloud fraction, the degree of brokenness of the cloud field, and the aspect ratio of the broken cloud elements.

In addition to the uncertainties in the cloud radiation calculations, the manner by which clouds are assumed to respond to a climate perturbation can have a significant impact on the resultant temperature change. In one-dimensional climate models, cloud fraction and cloud-top and cloud-bottom altitudes are specified as well as cloud optical properties. The initial cloud temperature is determined by the temperature profile. As the model responds to the perturbation, the cloud-top altitude must be assumed. It is commonly assumed either that the cloud-top altitude remains constant (and the cloud temperature is varied) or that the cloud temperature remains constant (and the cloud altitude varies). Assuming that the cloud fraction remains constant, the assumption of fixed cloud-top temperature results in a change in surface temperature that is 60–85% greater than that calculated assuming constant cloud-top altitude (Cess 1974; Ramanathan 1976).

In general circulation models cloud amounts are generally calculated at each pressure level rather than being specified. These calculations are based on one or more independent variables, usually relative humidity, altitude, and vertical wind speed. However, the verification of the forecast cloud amounts and the proper inclusion of the cloudiness in the radiative parameterizations constitute major challenges to atmospheric scientists. The International Satellite Cloud Climatology Project (ISCCP) (see WMO 1984) should provide the data necessary to check many of the outstanding uncertainties.

2.10 FUTURE RESEARCH

The radiative properties of CO_2 have been studied extensively and are well understood. Differences between model calculations involving absorption or emission by CO_2 alone can be traced to modeling approach (i.e., model assumptions and numerical methods). LBL models, which require the least number of assumptions, are in good agreement with each other and with laboratory measurements. The major area of uncertainty concerning CO_2 is the line shape, which is known to have weaker absorption in the line wings than that of Lorentzian lines, but an accurate model for the line wings has yet to be developed.

A great deal of work is needed on water vapor to resolve the rather large discrepancies between various model results, particularly in the 8–12 μm window region. The H_2O continuum is an important factor affecting transmission in this spectral region, and a theoretical model needs to be developed for this continuum. In the absence of such a model, an empirically derived treatment of the continuum would be an acceptable approach. Much of the difficulty lies in trying to distinguish between absorption in the window region from the tails of strong lines outside this region and absorption from the continuum itself (assuming that water dimers or clusters are responsible for some of the absorption).

Because much of the radiative feedback process leading to enhanced longwave radiation from the atmosphere to the surface when CO_2 is doubled involves emission by H_2O, the radiative properties of H_2O must be better understood. More laboratory measurements of H_2O absorptance over the range of temperature and pressure in the atmosphere where the bulk of the H_2O is contained would help to evaluate the model results. Because H_2O increases, along with CO_2 doubling, add a major portion to the estimates of the temperature change, understanding the hydrologic cycle is critical for future estimates of CO_2 impact.

Most laboratory measurements involve measuring the absorptance of one gas at a time. More measurements are needed of mixtures of gases over ranges of temperature, pressure, and gas mixing ratios. These measurements would enable the accuracy of the treatment of overlap between the bands of different gases in band models to be evaluated.

Normally, one would expect that LBL models could provide a reference in lieu of laboratory measurements, but the uncertainty about line shape and the H_2O continuum makes it premature and unreliable to perform these calculations without first developing a better understanding of the H_2O continuum absorption and line shape.

Model results for the longwave radiative effects of O_3 are in good agreement. Understanding of the temperature and pressure dependence of O_3 absorption is not complete, but O_3 makes such a small contribution to total longwave fluxes in the troposphere and to changes in these fluxes when temperatures are perturbed that these shortcomings do not have a significant impact on CO_2 assessment calculations.

Model estimates of the radiative effects of increases in CH_4 concentrations differ by as much as 30%, and the disagreement is worse for N_2O. Work is progressing to determine the cause of these differences. A better understanding of most of the radiatively important trace gases will be needed if the radiative and climatic effects of these gases are to be identified and isolated from those of CO_2 and H_2O. Because of the importance of H_2O, the higher priority should be placed on improving the understanding for H_2O rather than trace gases. Ultimately, both sets of issues should and will be addressed.

Most of our knowledge on the accuracy of the clear-sky radiation calculations is based on comparisons of calculations with homogeneous path laboratory observations. However, to verify the atmospheric calculations spectrally, as well as for total fluxes, it is necessary to compare the calculations with observations when all of the radiatively active constituents are measured simultaneously. Such a comprehensive atmospheric radiation experiment has not been performed. However, data from such an experiment are necessary to place more precise estimates on the errors in the radiation calculations applicable to approximately 50% of the atmosphere, the clear-sky regions.

The main question of concern is what impact the differences in radiative transfer model approaches have on climate model sensitivity and accuracy. As more atmospheric constituents are added to the longwave models (e.g., starting with CO_2 only, then adding H_2O and O_3), the discrepancy between model results is reduced. The models do well in the limits of strong or weak absorption; the greatest potential for error occurs at the intermediate levels of absorption. With more atmospheric constituents, the effect is to move more toward the strong absorption limit in many spectral intervals. Interpretation of model results in terms of accuracy and sensitivity would be improved if we had a better understanding of the impact of simplifying assumptions used in the modeling approach; work is progressing in this area.

In terms of overall climate model performance, there is less discrepancy between calculated radiation budgets and flux perturbations than there is between elements of the hydrologic cycle, including the flux of latent heat from the Earth's surface, calculated humidity fields and cloud amounts, and spatial distribution. Improvements to climate model performance will require that attention be given to coupled processes, not just to the radiative transfer calculations.

REFERENCES

Ackerman, S. H., and Cox, S. K. 1982. "The Saudi Arabian Heat Low: Aerosol Distributions and Thermodynamic Structure." *Journal of Geophysical Research 87*:8991–9002.

Ackerman, T. P., and Toon, O. B. 1981. "The Absorption of Visible Radiation in Atmospheres Containing Mixtures of Absorbing and Nonabsorbing Particles." *Applied Optics 20*:3661–3667.

Ackerman, T. P., Liou, K. N., and Leovy, C. B. 1976. "Infrared Radiative Transfer in Polluted Atmospheres." *Journal of Applied Meteorology 16*:1372–1373.

Atwater, M. A. 1970. "Planetary Albedo Changes Due to Aerosols." *Science 170*:64–66.

Augustsson, T., and Ramanathan, V. 1977. "A Radiative-Convective Model Study of the CO_2 Climate Problem." *Journal of the Atmospheric Sciences 34*:448–451.

Blanchet, J. P., and Leighton, H. G. 1981. "The Influence of the Refractive Index and Size Spectrum on Atmospheric Heating Due to Aerosols." *Beitrage zur Physik der Atmosphare 54*:143–158.

Braslau, N., and Dave, J. V. 1973a. "Effect of Aerosols on the Transfer of Solar Energy through Realistic Model Atmospheres, Part I: Nonabsorbing Aerosols." *Journal of Applied Meteorology 12*:601–615.

Braslau, N., and Dave, J. V. 1973b. "Effect of Aerosols on the Transfer of Solar Energy Through Realistic Model Atmospheres. Part II: Partly-Absorbing Aerosols." *Journal of Applied Meteorology 12*:616–619.

Braslau, N., and Dave, J. V. 1975. "Atmospheric Heating Rates Due to Solar Radiation for Several Aerosol-Laden Cloudy and Cloud-Free Models." *Journal of Applied Meteorology 14*:396–399.

Burch, D. E., Howard, J. N., and Williams, D. 1956. "Infrared Transmission in Synthetic Atmospheres V. Absorption Laws for Overlapping Bands." *Journal of the Optical Society of America 46:*452–455.

Carlson, T. N., and Caverly, R. S. 1977. "Radiative Characteristics of Saharan Dust at Solar Wavelengths." *Journal of Geophysical Research 82:*3141–3152.

Cess, R. D. 1974. "Radiative Transfer Due to Atmospheric H_2O: Global Considerations of the Earth's Energy Balance." *Journal of Quantitative Spectroscopy and Radiative Transfer 14:*861–871.

Cess, R. D. 1976. "Climate Change: An Appraisal of Atmospheric Feedback Mechanisms Employing Zonal Climatology." *Journal of the Atmospheric Sciences 33:*1831–1843.

Cess, R. D., and Ramanathan, V. 1978. "Averaging of Infrared Cloud Opacities for Climate Modeling." *Journal of the Atmospheric Sciences 35:*919–922.

Cess, R. D., Briegleb, B. P., and Lian, M. S. 1982. "Low-Latitude Cloudiness and Climate Feedback: Comparative Estimates from Satellite Data." *Journal of the Atmospheric Sciences 39:*53–59.

Chandrasekhar, S. 1960. *Radiative Transfer.* Dover Publications, New York, New York.

Charlock, T. P., and Sellers, W. D. 1980. "Aerosol Effects on Climate: Calculations with Time-Dependent and Steady-State Radiative Convective Models." *Journal of the Atmospheric Sciences 37:*1327–1341.

Charlson, R. J., and Pilat, M. J. 1969. "Climate: The Influence of Aerosols." *Journal of Applied Meteorology 8:*1001–1002.

Chou, M.-D., and Arking, A. 1980. "Computation of Infrared Cooling Rates in the H_2O Bands." *Journal of the Atmospheric Sciences 37:*855–867.

Chýlek, P., and Coakley, J. A. 1974. "Aerosols and Science." *Science 183:*75–77.

Coakley, J. A., and Grams, G. W. 1976. "Relative Influence of Visible and Infrared Optical Properties of a Stratospheric Aerosol Layer on the Global Climate." *Journal of Applied Meteorology 15:*679–691.

Coakley, J. A., Jr., Cess, R. D., and Yurevich, F. B. 1983. "The Effect of Tropospheric Aerosols on the Earth's Radiation Budget: A Parameterization for Climate Models." *Journal of the Atmospheric Sciences 40:*116–138.

Curtis, A. R. 1956. "The Computation of Radiative Heating Rates in the Atmosphere." *Proceedings of the Royal Society of London A236:*156–159.

Davies, R. 1978. "The Effect of Finite Geometry on the Three-Dimensional Transfer of Solar Irradiance in Clouds." *Journal of the Atmospheric Sciences 35:*1712–1725.

Davies, R., Ridgway, W. L., and Kim, K. E. 1984. "Spectral Absorption of Solar Radiation in Cloudy Atmospheres: A 20 cm^{-1} Model." *Journal of the Atmospheric Sciences 41:*2126–2137.

DeLuisi, J. J., Furakawa, P. N., Gillette, D. A., Schuster, B. G., Carlson, R. J., Porch, W. M., Fegley, R. W., Herman, B. M., Rabinoff, R. A., Twitty, J. T., and Weinman, J. A. 1976. "Results of a Comprehensive Atmospheric Aerosol-Radiation Experiment in the Southwestern United States. Parts I and II." *Journal of Applied Meteorology 15:*441–463.

Dickinson, R. E. 1973. "Method of Parameterization for Infrared Cooling Between Altitudes of 30 and 70 Kilometers." *Journal of Geophysical Research 78:*4451–4457.

Drayson, S. R. 1967. "Atmospheric Transmission in the CO_2 Bands Between 12 μ and 18 μ." *Applied Optics 5:*385–391.

Ellingson, R. G. 1982. "On the Effects of Cumulus Dimensions on Longwave Irradiance and Heating Rate Calculations." *Journal of the Atmospheric Sciences 39:*886–896.

Ellingson, R. G., and Gille, J. C. 1978. "An Infrared Radiative Transfer Model. Part 1: Model Description and Comparison of Observations with Calculations." *Journal of the Atmospheric Sciences 35:*523–545.

Ellingson, R. G., and MacCracken, M. C. 1981. "A Study of the Global Energy Balance." 136–138. In *Proceedings of the Fourth Conference on Atmospheric Radiation.* American Meteorological Society, Washington, D.C.

Ellingson, R. G., and Serafino, G. N. 1984. "Observations and Calculations of Aerosol Heating Over the Arabian Sea During MONEX." *Journal of the Atmospheric Sciences 41:*575–589.

Ellis, J. S. 1977. *The Planetary Radiation Budget and Climate* (Doctoral Dissertation, Department of Atmospheric Sciences). Colorado State University, Fort Collins, Colorado.

Elsasser, W. M. 1942. "Heat Transfer by Infrared Radiation in the Atmosphere." *Harvard Meteorological Studies No. 6,* Harvard University Press, Cambridge, Massachusetts.

Elterman, L. 1968. "UV, Visible, and IR Attenuation for Altitudes to 50 km, 1968" (AFCRL Environmental Research Paper No. 285). Air Force Cambridge Research Laboratories, Bedford, Massachusetts.

Fels, S. B., and Schwarzkopf, M. D. 1981. "An Efficient, Accurate Algorithm for Calculating CO_2 15μm Band Cooling Rates." *Journal of Geophysical Research 86:*1205–1232.

Flohn, H. 1978. "Estimates of a Combined Greenhouse Effect as Background for a Climate Scenario During Global Warming." 227–237. In J. Williams (ed.), *Carbon Dioxide, Climate, and Society* (IIASA Proceedings Series, Environment, Vol. 1). International Institute for Applied Systems Analysis, Laxenburg, Austria.

Goody, R. M. 1964. *Atmospheric Radiation I: Theoretical Basis.* Oxford University Press (Clarendon), London, United Kingdom.

Grassl, H. 1973. "Aerosol Influence on Radiative Cooling." *Tellus 25:*386–395.

Hansen, J. E., Lacis, A. A., Lee, P., and Wang, W. C. 1980. "Climatic Effects of Atmospheric Aerosols." *Annals of the New York Academy of Sciences 338:*575–587.

Hansen, J. E., Lee, P., Rind, D., and Russell, G. 1981. "Climate Impact of Increasing Atmospheric CO_2." *Science 213*:957–966.

Harshvardhan. 1979. "Perturbation of the Zonal Radiation Balance by a Stratospheric Aerosol Layer." *Journal of the Atmospheric Sciences 36*:1274–1285.

Harshvardhan. 1982. "The Effect of Brokenness on Cloud-Climate Sensitivity." *Journal of the Atmospheric Sciences 39*:1853–1861.

Harshvardhan, and Cess, R. D. 1976. "Stratospheric Aerosols: Effect Upon Atmospheric Temperature and Global Climate." *Tellus 28*:1–10.

Harshvardhan, and Cess, R. D. 1978. "Effect of Tropospheric Aerosols Upon Atmospheric Infrared Cooling Rates." *Journal of Quantitative Spectroscopy and Radiation Transfer 19*:621–632.

Harshvardhan, and Weinman, J. A. 1982. "Infrared Radiative Transfer Through a Regular Array of Cuboidal Clouds." *Journal of the Atmospheric Sciences 39*:431–439.

Hartmann, D. L., and Short, D. A. 1980. "On the Use of Earth Radiation Budget Statistics for Studies of Clouds and Climate." *Journal of the Atmospheric Sciences 37*:1233–1250.

Haurwitz, F., and Kuhn, W. R. 1974. "The Distribution of Tropospheric Planetary Radiation in the Southern Hemisphere." *Journal of Applied Meteorology 13*:417–429.

Herman, B. M., and Browning, S. R. 1975. "The Effect of Aerosols on the Earth-Atmosphere Albedo." *Journal of the Atmospheric Sciences 32*:1430–1445.

Herman, B. M., Browning, S. R., and Rabinoff, R. 1976. "The Change in Earth-Atmosphere Albedo and Radiational Equilibrium Temperatures Due to Stratospheric Pollution." *Journal of Applied Meteorology 15*:1057–1067.

Hitchfeld, W., and Houghton, J. T. 1961. "Radiative Transfer in the Lower Stratosphere Due to the 9.6 Micron Band of O_3." *Quarterly Journal of the Royal Meteorological Society 87*:562–577.

Hoover, G. M., Hathaway, C. E., and Williams, D. 1967. "Infrared Absorption of Overlapping Bands of Atmospheric Gases." *Applied Optics 6*:481–487.

Hottel, H. C., and Sarofim, A. F. 1967. *Radiative Transfer*. McGraw-Hill, New York, New York.

Houghton, J. T. 1977. *The Physics of Atmospheres*. Cambridge University Press, Cambridge, United Kingdom.

Joseph, J. H., Wiscombe, W. J., and Weinman, J. A. 1979. "The Delta-Eddington Approximation for Radiative Flux Transfer." *Journal of the Atmospheric Sciences 33*:2452–2459.

Kaplan, L. D. 1959. "A Method for Calculation of Infrared Flux for Use in Numerical Models of Atmospheric Motion." 170–177. *The Atmosphere and the Sea in Motion—Scientific Contributions to the Rossby Memorial Volume*. The Rockefeller Institute Press, New York, New York.

Kiehl, J. T., and Ramanathan, V. 1982. "Radiative Heating Due to Increased CO_2: The Role of H_2O Continuum Absorption in the 12–18 μm Region." *Journal of the Atmospheric Sciences 39*:2923–2926.

Kiehl, J. T., and Ramanathan, V. 1983. "CO_2 Radiative Parameterization Used in Climate Models: Comparison with Narrow Band Models and with Laboratory Data." *Journal of Geophysical Research 88*:5191–5202.

Kondratyev, K. Ya., Vassilyev, O. B., Grishechkin, V. W., and Ivlev, L. S. 1974. "Spectral Radiative Flux Divergence and Its Variability in the Troposphere in the 0.2–0.4 μ Region." *Journal of Applied Optics 13*:478–486.

Konyukh, L. A., Yurevich, F. B., Cess, R. D., and Harshvardhan. 1979. "Tropospheric Aerosols: Effects Upon the Surface and Surface-Atmosphere Radiation Budgets." *Journal of Quantitative Spectroscopy and Radiation Transfer 22*:483–488.

Kuhn, P. M., and Johnson, D. R. 1966. "Improved Radiometersonde Observations of Atmospheric Infrared Irradiance." *Journal of Geophysical Research 71*:367–373.

Kuhn, W. R. 1978. "The Effects of Cloud Height, Thickness and Overlap on Tropospheric Terrestrial Radiation." *Journal of Geophysical Research 83*:1337–1346.

Kunde, V. G., Conrath, B. J., Hanel, R. A., Maguire, W. C., Prabhakara, C., and Solomonson, U. V. 1974. "The Nimbus 4 Infrared Spectroscopy Experiment 2. Comparisons of Observed and Theoretical Radiances from 425–1450 cm^{-1}." *Journal of Geophysical Research 79*:777–784.

Lacis, A. A., and Hansen, J. E. 1974. "A Parameterization for the Absorption of Solar Radiation in the Earth's Atmosphere." *Journal of the Atmospheric Sciences 31*:118–133.

Lacis, A., Hansen, J., Lee, P., Mitchell, T., and Lebedeff, S. 1981. "Greenhouse Effect of Trace Gases, 1970–1980." *Geophysical Research Letters 8*:1035–1038.

Lenoble, J., Tanre, D., Deschamps, P. Y., and Herman, M. 1982. "A Simple Method to Compute the Change in the Earth-Atmosphere Radiative Balance Due to a Stratospheric Aerosol Layer." *Journal of the Atmospheric Sciences 39*:2565–2576.

Liou, K.-N. 1980. *An Introduction to Atmospheric Radiation*. Academic Press, New York, New York.

Liou, K.-N., and Ou, S.-C. 1983. "Theory of Equilibrium Temperatures in Radiative-Turbulent Atmospheres." *Journal of the Atmospheric Sciences 40*:214–229.

Liou, K.-N., and Sasamori, T. 1975. "On the Transfer of Solar Radiation in Aerosol Atmospheres." *Journal of the Atmospheric Sciences 32*:2166–2177.

Luther, F. M. 1976. "Relative Influence of Stratospheric Aerosols on Solar and Longwave Radiative Fluxes for a Tropical Atmosphere." *Journal of Applied Meteorology 15*:951–955.

Manabe, S., and Strickler, R. F. 1964. "Thermal Equilibrium of the Atmosphere with a Convective Adjustment." *Journal of the Atmospheric Sciences 21*:361–385.

Manabe, S., and Wetherald, R. T. 1967. "Thermal Equilibrium of the Atmosphere with a Given Distribution of Relative Humidity." *Journal of the Atmospheric Sciences 24*:241–259.

Manabe, S., and Wetherald, R. T. 1980. "On the Distribution of Climatic Change Resulting from an Increase in CO_2 Content of the Atmosphere." *Journal of the Atmospheric Sciences 37*:99–118.

McClatchey, R. A. 1976. "Satellite Temperature Sounding of the Atmosphere: Ground Truth Analysis." In *Air Force Surveys in Geophysics, No. 356* (AFGL-RT-76-0279). Air Force Cambridge Research Laboratory, Bedford, Massachusetts.

McClatchey, R. A., Benedict, W. S., Clough, S. A., Burch, D. E., Calfee, R. F., Fox, K., Rothman, L. S., and Garing, J. S. 1973. "AFCRL Atmospheric Absorption Line Parameters Compilation" (AFCRL-TR-73-0096). Air Force Cambridge Research Laboratory, Bedford, Massachusetts.

McClatchey, R. A., and D'Agati, A. P. 1979. "An Atmospheric Temperature Profile Measured with an In-Situ Radiometer." In *Environmental Research Papers No. 661* (AFGL-TR-79-0100). Air Force Cambridge Research Laboratory, Bedford, Massachusetts.

McCormick, R. A., and Ludwig, J. H. 1967. "Climate Modification by Atmospheric Aerosols." *Science 156:*1358–1359.

McKee, T. B., and Cox, S. K. 1974. "Scattering of Visible Radiation by Finite Clouds." *Journal of Geophysical Research 83:*1337–1346.

Meador, W. E., and Weaver, W. R. 1980. "Two-Stream Approximations to Radiative Transfer in Planetary Atmospheres: A Unified Description of Existing Methods and a New Improvement." *Journal of the Atmospheric Sciences 37:*630–643.

Mie, G. 1908. "Beigrad Zur Optik Trüber Medien." *Speziell Kolloidaler Metallösungen Ann. Physik 25:*377–445.

Mitchell, J. M., Jr. 1971. "The Effect of Atmospheric Aerosols on Climate With Special Reference to Temperature Near the Earth's Surface." *Journal of Applied Meteorology 10:*703–714.

Ohring, G., and Clapp, P. 1980. "The Effect of Changes in Cloud Amount on the Net Radiation at the Top of the Atmosphere." *Journal of the Atmospheric Sciences 37:*447–454.

Oort, A. H., and Rasmusson, E. M. 1971. "Atmospheric Circulation Statistics" (NOAA Professional Paper 5). U. S. Department of Commerce, Washington, D.C.

Paltridge, G. W., and Platt, C. M. R. 1976. *Radiative Processes in Meteorology and Climatology.* Elsevier Scientific Publishing, New York, New York.

Pilipowskij, S., Weinman, J. A., Clemesha, B.., Kent, G. S., and Wright, R. W. 1968. "Investigation of the Stratospheric Aerosol by Infrared and Lidar Techniques." *Journal of Geophysical Research 73:*7553–7560.

Plass, G. N. 1956a. "The Influence of the 9.6 Micron O_3 Band on the Atmospheric Infrared Cooling Rate." *Quarterly Journal of the Royal Meteorological Society 82:*30–44.

Plass, G. N. 1956b. "The Influence of the 15 μ Carbon-Dioxide Band on the Atmospheric Infrared Cooling Rate." *Quarterly Journal of the Royal Meteorological Society 82:*310–324.

Pollack, J. B., Toon, O. B., Sagan, C., Summers, A., Baldwin, B., and VanCamp, W. 1976. "Volcanic Explosions and Climatic Change: A Theoretical Assessment." *Journal of Geophysical Research 81:*1071–1093.

Potter, G. L., Ellsaesser, H. W., MacCracken, M. C., and Luther, F. M. 1979. "Performance of the Lawrence Livermore Laboratory Zonal Atmospheric Model." 852–871. In W. L. Gates (ed.), *Report of the JOC Study Conference on Climate Models: Performance, Intercomparison and Sensitivity Studies* (GARP Publications Series No. 22). World Meteorological Organization, Geneva, Switzerland.

Ramanathan, V. 1976. "Radiative Transfer within the Earth's Troposphere and StratosphereModel." *Journal of the Atmospheric Sciences 33: A Simplified Radiative-Convective:*1330–1346.

Ramanathan, V. 1980. "Climatic Effects of Anthropogenic Trace Gases." 269–280. In *Interactions of Energy and Climate.* D. Reidel Publishing, Dordrecht, Holland.

Ramanathan, V. 1981. "The Role of Ocean-Atmosphere Interactions in the CO_2 Climate Problem." *Journal of the Atmospheric Sciences 38:*918–930.

Ramanathan, V., and Coakley, J. A., Jr. 1978. "Climate Modeling Through Radiative-Convective Models." *Reviews of Geophysics and Space Physics 16:*465–489.

Ramanathan, V., and Dickinson, R. E. 1979. "The Role of Stratospheric O_3 in the Zonal and Seasonal Radiative Energy Balance of the Earth-Troposphere System." *Journal of the Atmospheric Sciences 36:*1084–1104.

Ramanathan, V., Lian, M. S., and Cess, R. D. 1979. "Increased Atmospheric CO_2: Zonal and Seasonal Estimates of the Effect on the Radiation Energy Balance and Surface Temperature." *Journal of Geophysical Research 84:*4949–4958.

Rasool, S. I., and Schneider, S. H. 1971. "Atmospheric CO_2 and Aerosols: Effects of Large Increases on Global Climate." *Science 173:*138–141.

Reck, R. A. 1974a. "Influence of Surface Albedo on the Change in the Atmospheric Radiation Balance Due to Aerosols." *Atmospheric Environment 8:*823–833.

Reck, R. A. 1974b. "Aerosols in the Atmosphere: Calculation of the Critical Absorption/Backscatter Ratio." *Science 186:*1034–1036.

Reck, R. A. 1975. "Influence of Aerosol Cloud Height on the Change in the Atmospheric Radiation Balance Due to Aerosols." *Atmospheric Environment 9:*89–99.

Remsberg, E. E. 1973. "Stratospheric Aerosol Properties and Their Effects on Infrared Radiation." *Journal of Geophysical Research 78:*1401–1408.

Rodgers, C. D. 1967. "The Radiative Heat Budget of the Troposphere and Lower Stratosphere" (Report No. A2). Massachusetts Institute of Technology, Cambridge, Massachusetts.

Rodgers, C. D., and Walshaw, C. D. 1966. "The Computation of Infrared Cooling Rates in Planetary Atmospheres." *Quarterly Journal of the Royal Meteorological Society 92:*67–92.

Schack, A. 1924. "The Radiation from Combustible Gases and its Practical Determination." *Zeitschrift fuer Technishe Physik 5:*267–278.

Schneider, S. H. 1972. "Cloudiness as a Global Climatic Feedback Mechanism: The Effects on the Radiation Balance

and Surface Temperature of Variations in Cloudiness." *Journal of the Atmospheric Sciences 29:*1413–1422.

Scott, N. A., and Chedin, A. 1981. "A Fast Line-by-Line Method for Atmospheric Absorption Computations: The Automatized Atmospheric Absorption Atlas." *Journal of Applied Meteorology 20:*801–812.

Selby, J. E. A., Shettle, E. P., and McClatchey, R. A. 1976. "Atmospheric Transmittance from 0.25 to 28.5 μm: Supplement LOWTRAN 3B" (AFGL-TR-76-0258). Air Force Geophysics Laboratory, Bedford, Massachusetts.

Shettle, E. P., and Fenn, R. W. 1979. "Models for the Aerosols of the Lower Atmosphere and the Effects of Humidity Variations on Their Optical Properties" (AFGL-TR-79-0214). Air Force Geophysical Laboratory, Bedford, MA. Available from NTIS (ADA 085951), Springfield, Virginia.

Smith, W. L., Shen, W. C., and Howel, H. B. 1977. "A Radiative Heating Model Derived from the GATE MSR Experiment." *Journal of Applied Meteorology 16:*384–392.

Stephens, G. L., and Webster, P. J. 1981. "Clouds and Climate: Sensitivity of Simple Systems." *Journal of the Atmospheric Sciences 38:*235–247.

Stone, H. M., and Manabe, S. 1968. "Comparison Among Various Numerical Models Designed for Computing Infrared Cooling." *Monthly Weather Review 96:*735–741.

Toon, O. B., and Pollack, J. B. 1976. "A Global Average Model of Atmospheric Aerosols for Radiative Transfer Calculations." *Journal of Applied Meteorology 15:*225–246.

Tubbs, L. D., Hathaway, C. E., and Williams, D. 1967. "Further Studies of Overlapping Absorption Bands." *Applied Optics 6:*1422–1423.

Twomey, S. 1977. "The Influence of Pollution on the Shortwave Albedo of Clouds." *Journal of the Atmospheric Sciences 34:*1149–1152.

van de Hulst, H. C. 1957. *Light Scattering by Small Particles.* John Wiley & Sons, New York, New York.

Walshaw, C. D., and Rodgers, C. D. 1963. "The Effect of the Curtis-Godson Approximation on the Accuracy of Radiative Heating-Rate Calculations." *Quarterly Journal of the Royal Meteorological Society 89:*122–130.

Wang, W. C., and Domoto, G. A. 1974. "The Radiative Effect of Aerosols in the Earth's Atmosphere." *Journal of Applied Meteorology 13:*521–534.

Wang, W. C., and Ryan, P. B. 1983. "Overlapping Effects of Atmospheric H_2O, CO_2 and O_3 on the CO_2 Radiative Effect." *Tellus 35B:*81–91.

World Meteorological Organization (WMO). 1983. "Report of the Experts Meeting on Aerosols and Their Climatic Effects." 28–30 March 1983, Williamsburg, Virginia. A. Deepak and H.E. Gerber (eds.). World Climate Research Programme Report WCP-55. WMO, Geneva, Switzerland.

World Meteorological Organization (WMO). 1984. "The International Satellite Cloud Climatology Project (ISCCP)." Report of the Third Session of the International Working Group on Data Management, March 6–8, 1984, Tokyo. World Climate Programme Report WCP-82, WMO, Geneva, Switzerland.

World Meteorological Organization (WMO). 1985. "The Intercomparison of Radiation Codes in Climate Models (ICRCCM), Longwave Clear-Sky Calculations." F. M. Luther (ed.), Report of a Meeting in Frascati, Italy, 15–18 August 1984. World Climate Research Programme Report WCP-93. WMO, Geneva, Switzerland.

Yamamoto, G., and Tanaka, M. 1972. "Increase of Global Albedo Due to Air Pollution." *Journal of the Atmospheric Sciences 29:*1405–1412.

Yamamoto, G., Tanaka, M. and Ohta, S. 1974. "Heating of the Lower Troposphere Due to Absorption of the Visible Solar Radiation by Aerosol." *Journal of the Meteorological Society of Japan 52:*61–68.

3. MODELING AS A MEANS OF STUDYING THE CLIMATE SYSTEM

W. Lawrence Gates
Climatic Research Institute, Oregon State University

CONTENTS

3.1 INTRODUCTION

The popular notion of climate is the average of weather in a particular location or region. The climate scientist also uses this concept, along with a variety of other statistics that describe the structure and variation of climate, but is required to be more precise about the period of averaging. In the scientific study of climate, it is useful to regard shorter term averages of the order of one month as particular examples of climate and to study their relationship to climate statistics over other time scales.

From the study of past climates, it is known that many regions of the Earth have witnessed a long and complex series of varied climates, but how this evidence fits together remains an unsolved puzzle. Both climate and climate change are presumably governed by basic physical laws; the form these laws take in specific application to the Earth's climate system is a goal of modern climate research. That this research is not yet complete is shown by the fact that there is no unifying general theory of climate, and it is therefore not surprising that there is uncertainty over the prediction of climate changes.

Climate presents the scientist with an extraordinarily complex problem. Attempts to understand the inner workings of climate have been made by the study of sequences of observed events and the examination of geological records. Both approaches have shown that the natural climate can undergo wide variations. Statistical analysis of geological records during the past few decades has identified a series of cyclic advances and retreats of the continental ice sheets over the past million years (the ice ages). Although the timing of these events sometimes points to a possible cause, the details and confirmation of the physical processes at work cannot come from diagnostic studies alone. As discussed by Wigley et al. (1985), similar diagnostic analyses of the climate of the past hundred years indicate the presence of both short-term variations and longer term trends. Unique identification of the possible role of various causal factors [e.g., volcanoes, carbon dioxide (CO_2), solar variations] cannot be made, however, by such analyses alone.

Just as we cannot completely understand the causes of past climate change by looking at what happened, diagnosis of past changes indicates that we cannot predict the future climate by simply extrapolating trends for the recent or distant past. As discussed in Chapter 7 of this volume, although we can learn a great deal from the past about the characteristics of a possible future warm climate, the increase in CO_2 concentration that is now occurring is quite likely unique in the Earth's history.

Attempts have also been made to determine the sensitivity of the climate system empirically by examining the changes in radiative fluxes and temperature that occur during the normal change of season and as the result of small-scale perturbations. While such empirical approaches have some merit, it is difficult to find observed situations that exhibit time and space domains comparable to those of the CO_2 problem. Moreover, the interpretation of observations in terms of climate sensitivity requires, at the least, the use of a conceptual model of how the climate system works. As explained more fully in Appendix B, these difficulties have led to misleading results in some attempts to develop empirical estimates of future climate change.

As a result, the only way known to study the details of the many physical processes responsible for the structure and variation of climate, and to develop a reliable capability for projecting future climates, is to construct mathematical models based on the full set of fundamental physical principles governing the climate system. Such models represent quantitatively the various interacting elements. In addition to the atmosphere, the scientific definition of climate also includes the average behavior of the world's oceans and ice masses and the condition of the land surface and its associated biomass. In comprehensive climate models these elements are linked together in a worldwide system, with changes in one part affecting the behavior of the others, setting in motion a chain of effects that may either reinforce or cancel each other.

There are a large number of possible mechanisms that cause climate changes, and the observed variations of past climate represent the attempts of the system to reach a balance. Because the oceans, however, change much more slowly than the atmosphere, and the ice masses and the land surface with its vegetation change even more slowly, the statistics of climate also undergo slow changes. The spectrum of climate change is made even broader by the influence of factors beyond the atmosphere and

ocean, such as changes in radiation from the Sun, composition of the atmosphere, and the distribution of the Earth's oceans and continents over geological time. Because climate is the result of such processes, it may change in different ways and at different rates in various parts of the world. Unravelling the course of these changes and organizing their characteristics in terms of physical causes and effects is the scientific goal of current climate research programs (Global Atmospheric Research Programme 1974; National Research Council 1983; Houghton 1984).

3.2 THE CLIMATE SYSTEM AND CLIMATE CHANGE

3.2.1 Components of the Climate System

Once it is noted that climate involves the Earth's oceans, other surface waters, ice masses, and surface soil and vegetation as well as the air, these physical entities may be conveniently grouped into the components of the climate system (Gates 1979a). This system consists of the atmosphere (comprising the Earth's gaseous envelope and its aerosols), the hydrosphere (comprising the liquid water distributed on or beneath the Earth's surface), the cryosphere (comprising the snow and ice on or beneath the surface), the surface lithosphere (comprising the rock, soil, and sediment of the Earth's surface), and the biomass (comprising the Earth's plant and animal life, including humans). Each of these components has different physical characteristics, and they are linked to each other and to conditions external to the system by a variety of physical processes (Figure 3.1).

The most important component of the climate system (as far as society is concerned) is the *atmosphere,* which displays a spectrum of conditions ranging from the microclimates of local sites to the climate of the entire planet. For many human activities, the most important elements of the atmospheric climate are the seasonal regimes of temperature and precipitation. It is on this basis that the climates of the world have traditionally been classified. The detailed geographical distribution of (atmospheric) climatic types reveals the moderating influence of the oceans on seasonal temperature

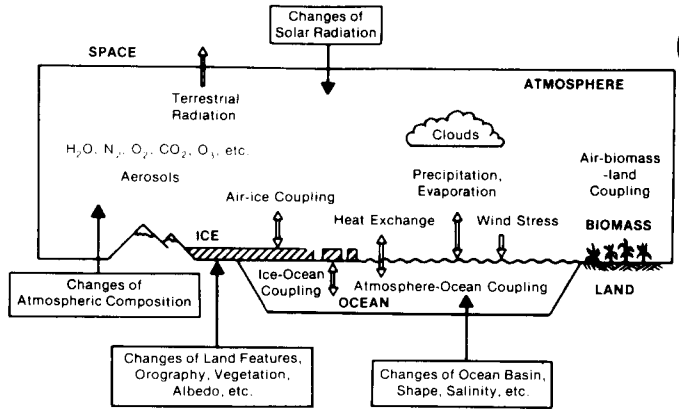

Figure 3.1. The principal interactions among the components of the atmosphere-ocean-ice-land surface climate system and some examples of external changes that may cause climatic variations. Source: Gates (1979a).

changes and shows the extremes of both temperature and precipitation introduced by the continents and their mountains. The statistics of other atmospheric variables, such as sunshine, cloudiness, humidity, and wind, are also part of the atmospheric climate and are important in such activities as energy generation and the management of water supplies.

The atmosphere may generally be expected to respond to an imposed change more rapidly than the other components of the climate system. This is due to the ease with which the atmosphere can be heated and set in motion. The time scales of the atmosphere's response range from a few minutes or hours for local convective motions, to a few days for large-scale transient cyclones of middle latitudes, to a few months for seasonal changes in solar radiation. Such phenomena play an important role in climate and are in turn regulated by the structure and circulation of the atmosphere on other scales. Because these phenomena display greater amplitude in the atmosphere than their counterparts in other components of the climate system, the atmosphere is characterized by relatively large diurnal, synoptic, and seasonal fluctuations. The atmosphere's response also may be characterized in terms of the time required to generate (or dissipate) atmospheric temperature and motion patterns in response to heating and frictional forces. This time is estimated to be about one month, which is longer than the lifetime of an individual atmospheric cyclone but shorter than a season.

The *hydrosphere* is a close second to the atmosphere in terms of overall importance in the climate system. The world's oceans supply the global hydrological cycle of evaporation, condensation, precipitation, and runoff. Once in the atmosphere, water substance, in either vapor, liquid, or solid form, plays an important role in climate through its selective absorption of radiation and its reflection of both solar and terrestrial radiation.

The climate of the hydrosphere consists of the statistical distribution of the temperature, salinity, and velocity of the oceans and the distribution and amount of land surface and water. In comparison with the atmosphere, the liquid portion of the climate system is relatively unexplored, although the oceans play a major (if not a dominant) role in many climate changes. Because the oceans cover approximately two-thirds of the Earth, most of the solar radiation reaching the surface strikes the oceans, where it is absorbed by the uppermost few meters of water. Because of the high specific heat of water, this absorbed radiation results in a relatively small change in ocean temperature as compared with that which would occur over land. The oceans, therefore, act as a heat reservoir and slowly transport their heat by ocean currents from the tropical regions toward the generally colder middle latitude and polar regions. This oceanic advection process is much slower than the corresponding heat transport brought about by the atmosphere, but the total amount of heat transported poleward by the oceans is comparable to the transport in the atmosphere.

Although a portion of the heat stored in the surface waters of the oceans is transferred to the atmosphere through conduction and convection in those regions in which the ocean is warmer than the overlying air, a larger portion is used to evaporate water into the atmosphere. This so-called latent heat or energy is later released upon the condensation of water vapor into clouds and precipitation and is a major heat source for the atmospheric circulation on both small and large scales. The oceans are also free to move in response to heating, but unlike the atmosphere, they are primarily heated or cooled at or near the surface. This surface heat exchange may initiate convective motions or vertical overturning in the oceans to a depth that depends on the magnitude of the surface cooling and the local vertical density stratification of the oceans. These factors determine the time scales on which ocean water at various depths is in effective communication with the surface. The surface mixed layer, which is present over most of the world's oceans in the top 50 m or so, responds to changes of surface heating on time scales of days and weeks, whereas the thermocline, which is found at several hundred meters below the surface, responds to seasonal changes in the surface heat budget. The deeper water, which comprises the bulk of the ocean, responds even more slowly because of its relatively large thermal and mechanical inertia and reacts to changes of surface conditions on time scales of decades and centuries (Figure 3.2).

The *cryosphere,* like the hydrosphere, consists of a portion that is closely associated with the sea (sea ice) and portions that are associated with the land (snow, glaciers, and ice sheets). The importance of the cryosphere to the climate system is related to the high reflectivity (or albedo) and the low thermal conductivity of snow and ice. The surface albedo is greatly increased when snow covers a land surface or when a layer of sea ice forms on the ocean; because snow and ice are good insulators, the exchange of heat with the underlying land or ocean is thereby reduced. These effects tend to lower the net surface heating and, therefore, favor a colder local climate in regions with snow or ice cover. In the Northern Hemisphere, a considerable portion of the land is covered by snow and ice each winter, whereas the ice pack surrounding Antarctica undergoes a dramatic wintertime expansion from the coast to nearly 60°S latitude.

Significant variations in the cryosphere also occur over much longer time periods. In response to gravity, the ice in a mountain glacier moves slowly downward and outward and, over the period of a century or so, may either greatly expand its area or disappear altogether, depending on the local snow accumulation and temperature. Glaciation also occurs on dimensions of continents in the form of ice sheets, and those ice sheets now covering much of Greenland and Antarctica (and those that have covered parts of Europe and North America in the past) have lifetimes of tens of thousands to millions of years, depending on whether the climate (which the ice sheets themselves help to determine) is favorable or unfavorable for their maintenance. Ice may also have an indirect influence on climate by lowering

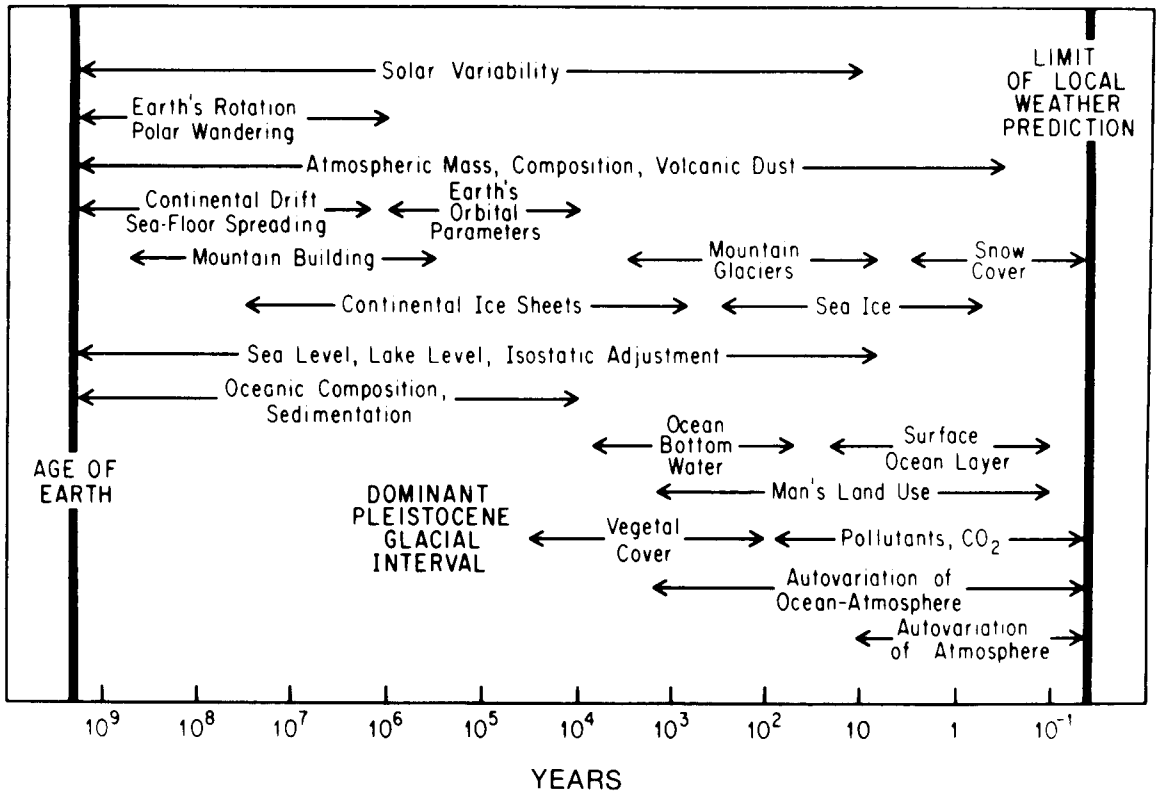

Figure 3.2. Characteristic time scales of climatic events and processes. Source: Gates (1979a).

the level (and thereby reducing the area) of the sea during periods of extensive glaciation.

The surface *lithosphere,* in contrast to the atmosphere, hydrosphere, and cryosphere, is a relatively passive component of the climate system. Even though the diurnal, synoptic, and seasonal variations of temperature over land are greater than those over water, the physical characteristics of surface soil and rock are usually taken as fixed elements in the determination of climate. One exception is the amount of moisture in the surface, which is closely related to the local surface and ground hydrology. Such soil moisture exerts a marked influence on the local surface balance of moisture and heat through its influence on the surface evaporation rate and on the albedo and thermal conductivity of the soil.

The remaining component of the climate system, the surface *biomass,* interacts with the other components on time scales that are characteristic of the life cycles of the Earth's vegetative cover. Most prominent among these is the seasonal cycle of plant growth in response to the variations of solar radiation, temperature, and rainfall. The trees, plants, and ground cover in turn modify the surface radiation balance and surface heat flux and play a major role in the seasonal variations of local surface hydrology. These biospheric effects are at a minimum in desert regions, although there is evidence that the stability and lateral extent of the deserts themselves are influenced by the vegetation in the surrounding areas. Over time scales of hundreds to thousands of years, the surface biomass is closely linked with the prevailing atmospheric and hydrospheric climate. The record of fossil species, as preserved in soils and sediments, and the record represented by the varying widths and composition of tree rings are important sources of biological evidence of the variation of ancient climates.

Although sometimes not considered to be a part of the climate system, many human activities have significantly altered the Earth's vegetative cover and, therefore, have interfered with the natural biospheric component of climate. Over time scales of hundreds to thousands of years, agricultural and grazing practices have changed the character of large portions of the Earth's surface and may have had a greater effect on local climates than have

the more recent (and more publicized) increases in urbanization and atmospheric CO_2 concentrations.

3.2.2 Physical Processes of Climate

The response time of each component of the climate system is the result of the physical processes that dominate the behavior of that component. In the case of the atmosphere and ocean—the more mobile components of the system—these physical processes include the transfer of fluid properties, such as momentum and temperature, by large-scale organized motions (advection), small-scale turbulent motions (diffusion), vertical overturning as a result of hydrostatic instability (convection), the selective absorption and emission of radiation, and (in the case of the atmosphere) the release of latent heat accompanying condensation. The occurrence of these processes is regulated by the various dynamical regimes characteristic of the atmosphere and ocean, such as local convective circulations, inertia-gravity waves, and large-scale synoptic and planetary waves. These motions are the natural responses of the Earth's fluids to the forcing represented by the sources and sinks of momentum and heat, the amplitudes of which are controlled by the dimensions and physical properties of the system. Together with the rotation of the Earth, these properties determine whether climate is dominated by convective circulations (as in lower latitudes) or by transient baroclinic disturbances (as in middle and higher latitudes). In this sense the distribution of the oceans and water sources (hydrosphere), land ice and sea ice (cryosphere), and surface vegetation (biomass) combines with the atmosphere to determine the general circulation or climate on continental and regional scales.

The physical processes that determine climate also may be viewed in terms of those that act among the various components of the climate system. Of particular importance among such coupling or feedback processes are those involving the exchange of heat and momentum between the atmosphere and oceans (Figure 3.3). As noted above, the surface layer of the oceans absorbs most of the solar radiation that reaches the Earth's surface, and much of this heat is, in turn, transferred to the atmosphere via evaporation. This moisture flux is effected by turbulent motions in the lower atmosphere and is dependent on the humidity of the surface air (or low-level vertical moisture gradient) and the surface wind speed. Depending on the temperature of the surface air relative to that of the surface itself (that is, the low-level vertical temperature gradient), these same turbulent motions also cause a transfer of sensible heat between the ocean surface and the overlying air. There are similar transfers of heat and moisture between the atmosphere and land surfaces as a function of the land surface character, roughness, and vegetative cover and between the atmosphere and snow- and ice-covered surfaces as well (Figure 3.1).

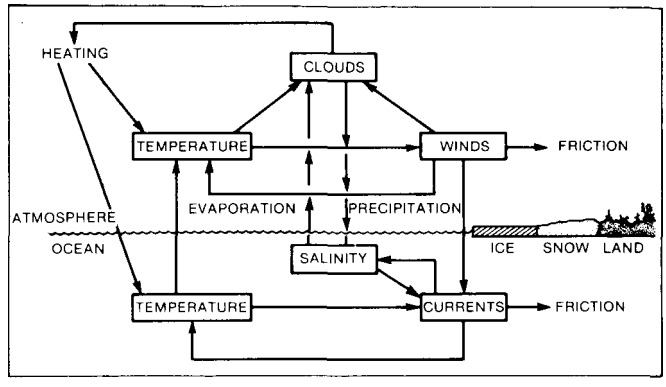

Figure 3.3. Major components of atmosphere-ocean feedback processes. Source: Gates (1979a).

The transfer of momentum between the atmosphere and oceans consists primarily of a turbulent flux from the more rapidly moving atmosphere to the underlying ocean. This surface drag represents a principal mechanism for the dissipation of atmospheric kinetic energy; for the ocean it represents the major driving force for the system of large-scale currents that are themselves regulated by frictional processes within the ocean. Ocean currents also may be produced by variations of temperature and salinity, which are in turn tied to atmospheric processes (Figure 3.3).

Because the atmosphere and ocean are the only components of the climate system that may move freely, their interaction is of fundamental importance to the dynamical behavior of the system. Although the oceans and atmosphere together accomplish the poleward transports of heat and momentum required for global balance, a significant portion of this transport is due to the oceans. From this point of view, the oceans may play a greater role than the atmosphere in determining climate

variation, and atmosphere-ocean interactions may produce climate changes over time scales of decades or centuries even when external conditions are unchanged.

3.2.3 External Influences and Climate History

The complete climate system may be regarded as a single physical system whose behavior is subject to a set of imposed geophysical conditions. From this viewpoint, the external or boundary conditions of the system are the variations of solar radiation at the top of the atmosphere; the chemical composition of the atmosphere and oceans; the size, mass, and rotation rate of the Earth; and the topography of the Earth's crust, including the distribution of mountains and the geometry of ocean basins (Figure 3.1). These external conditions themselves have changed markedly over the course of geological time and have had a profound influence on the evolution of climate during the history of the Earth (Figure 3.2). Without the Earth's oceans and biomass, the atmosphere would not have evolved into its present oxygen-rich state and would not contain the water vapor necessary to provide nourishing amounts of rainfall.

Because of the complexity of the climate system and the variety of time scales over which it changes, it has proven convenient to focus on one portion of the system at a time. This portion may then be regarded as the internal component, with all other components considered to be external with known behavior. Thus, over time scales of months and seasons, the atmosphere is commonly considered as the sole component of the (internal) climate system, with the ocean, ice, and land treated as boundary conditions. When the time scales of interest extend over years to decades, however, the atmosphere and oceans should be considered together as internal components, whereas for even longer periods of time, the ice, land surface, and biomass must also be treated as variable rather than fixed portions of the system. Aside from simplifying the mathematical description of climate, this procedure helps to identify the conditions or processes that influence the climate and, therefore, that may act as causes of climate change (Figure 3.2).

The climatic history of the Earth is revealed by a variety of chemical, biological, and geological records as preserved in natural layered deposits, the formation of which is sensitive to one or more elements of the climate. When calibrated against modern conditions, the marine fossil concentration in deep-sea sediments, the isotopic composition of ice layers, and the density and composition of ancient soil, for example, can be made to yield estimates of temperature and precipitation in the past. Such indirect or "proxy" sources of climate data combine to yield a picture of climate variation over the past million years that is dominated by the occurrence of ice ages about every 100,000 years.

3.2.4 Characteristics of Climate Change and Feedback Processes

The physical processes that are responsible for climate change are the same as those responsible for the maintenance of the climate itself. However, we have only a limited understanding of how or why these processes interact to produce a variation in climate. The empirical method of studying climate change through the assembly and analysis of observational data has provided a knowledge of the distribution of present and past climates of the Earth. These data also may be used to estimate the statistical likelihood or probability of future climate changes on the time scales of the data themselves. Such an actuarial approach to climate, however, assumes that the statistics of future climates will resemble those of the past.

The large number of interrelated physical processes acting at different rates within and between the components of the climate system makes the identification of the "cause" of climate change a difficult task. It seems likely that there is no single cause in most instances and that the relative importance of different effects strongly depends on the time and space scale of the climatic states being considered. For example, interannual differences in sea surface temperature may be related to the variations of local and regional atmospheric circulation, whereas interannual differences in the extent of mountain glaciers are probably not. On the other hand, changes of continental glaciation are related to variations in the Earth's orbital parameters over periods of tens to hundreds of thousands of years and are, therefore, probably related to changes of

global sea surface temperature over similar time periods. Climate variations, however, also may occur as the result of changes in the effective internal driving mechanisms (the "autovariations" shown in Figure 3.2), with no change in the external conditions. The inherent irregularity of weather is sufficient to ensure that these driving mechanisms will not operate in a perfectly smooth or cyclic way, and the result is the typical irregularity of the climate record seen on all time scales.

It is characteristic of climate change that two (or more) processes in the system compensate each other. Such interactions or feedback mechanisms may act either to amplify the value or anomaly of one of the interacting variables (positive feedback) or to damp it (negative feedback). For example, the snow cover albedo-temperature interaction is a positive feedback process, in which an increase in the extent of snow (or ice) increases the surface albedo, thereby contributing to a lowering of the surface temperature. In turn, with all else being equal, this may lead to a further increase in the extent of snow or ice, reinforcing the initial snow cover anomaly. Another familiar example of a positive feedback process is the water vapor-temperature feedback, in which an increase of the amount of water vapor (or absolute humidity) increases the absorption of longwave radiation, thereby contributing to a warming of the atmosphere. This warming in turn may result in increased evaporation and an augmentation of the initial humidity anomaly. This feedback operates virtually continuously in the atmosphere and (along with CO_2) is responsible for the greenhouse effect whereby the lower atmosphere is warmer than it would otherwise be.

While we know of many such feedbacks in the climate system, only a few are understood in a quantitative fashion. All such feedback processes, however, represent a considerable simplification of the actual sequences of events, and the key phrase in this description is "all else being equal." In a system as complex as climate, this is usually not the case, and an anomaly in one part of the system may be expected to set off a series of adjustments throughout the remainder of the climate system, depending on the nature, location, and size of the initial disturbance. The difficulty of tracing such adjustments makes the net effect of individual processes difficult to detect in most cases, although they can serve as the basis of diagnostic and modeling studies (Hansen et al. 1984). We should also recognize that any positive feedback must eventually be checked at some level by the intervention of other processes, or climate would exhibit a runaway behavior.

Climate change may therefore be viewed as the result of the adjustment among compensating feedback processes, each of which behaves in a characteristically nonlinear fashion. The fact that the climate of the Earth has historically varied between rather narrow limits is testimony to the efficiency and robustness of these feedbacks. This feature also permits the system to satisfy the global balances of heat, momentum, and moisture through the contributions of several, sometimes competing, processes. Diagnostic studies of the distribution or partitioning of these fluxes among the various modes and components of the system reveal much about how the climate is maintained in a near-equilibrium state, and when such studies are made for a succession of climatic states, they provide important clues to the mechanics of climate change.

One of the more basic physical processes of the climate system is the global balance of heat (see Figure 1.2). On the average, as much energy leaves the top of the atmosphere in the form of longwave radiation as enters it in the form of shorter wavelength solar radiation. If the absorbing or scattering properties of the atmosphere were to change (as, for example, by the addition of large amounts of volcanic dust or CO_2), the relative roles of these properties in the heat balance would change, with a consequent adjustment in other participating processes. This determination of the possible ways in which the enhancement (or removal) of one or more processes would change other processes, and therefore the climate, illustrates the need for climate models.

3.3 THE PHYSICAL BASIS OF CLIMATE MODELS

Knowledge of the physical basis of climate and climate variation is most usefully and comprehensively organized in terms of models, which are mathematical representations of the physical laws governing the behavior of the climate system. From such models, the structure of a climatic state may, in principle, be determined, and in this sense climate models represent a rational physical basis for studying the

climate. Climate models have shown considerable skill in reproducing the present climate of the Earth and the climate at selected times in the past, and their use in the prediction of future climate is the subject of intensive research (Gates 1979b). The most difficult problem in climate modeling is the proper representation of effects on unresolved scales, and progress in this and other areas of climate modeling has been periodically reviewed (Smagorinsky 1974; Schneider and Dickinson 1974; Gates 1975; Berger and Nicolis 1984; Peixoto and Oort 1984; Houghton 1984).

3.3.1 Basic Dynamical Equations and Boundary Conditions

The basic physical laws governing the time-dependent behavior of most of the components of the climate system, and on which a climate model may therefore be based, are relatively well known, as are the physics of the various interactive processes serving to link the components together. In the atmosphere these laws are expressed by the equations for the conservation of momentum, heat, and moisture, the so-called atmospheric primitive equations. Because some of the variables in these equations will be referred to later, it is useful to present them here in the isobaric (or constant pressure) coordinate system as follows:

wind change:

$$\frac{d\vec{v}_H}{dt} = -\underbrace{f\vec{k}\times\vec{v}_H}_{\substack{\text{Earth's}\\ \text{rotation force}}} - \underbrace{\nabla_p\Phi}_{\substack{\text{pressure}\\ \text{force}}} + \underbrace{\vec{F}_H}_{\text{friction}} ; \qquad (3.1)$$

temperature change:

$$\frac{dT}{dt} = \underbrace{\frac{\omega\alpha}{c_p}}_{\substack{\text{pressure}\\ \text{change}}} + \underbrace{\frac{\dot{Q}}{c_p}}_{\substack{\text{heating}\\ \text{rate}}} ; \qquad (3.2)$$

water vapor or moisture change:

$$\frac{dq}{dt} = \underbrace{E-C}_{\substack{\text{evaporation}-\\ \text{condensation}}} . \qquad (3.3)$$

Here $\vec{v}_H = u\vec{i} + v\vec{j}$ is the vector horizontal velocity, with u and v being the eastward and northward velocity components, respectively, and $\vec{i}$, $\vec{j}$, and $\vec{k}$ the corresponding eastward, northward, and vertical unit vectors; $f = 2\Omega\sin\phi$ is the Coriolis parameter, where Ω is the Earth's angular rotation rate and ϕ is the latitude; $\nabla_p\Phi$ is the isobaric gradient of the geopotential Φ, which is a measure of the potential energy; $\vec{F}_H$ is the horizontal frictional force per unit mass; T is the temperature; $\omega = dp/dt$ is the vertical velocity with p representing pressure; α is the specific volume; c_p is the specific heat at constant pressure; $\dot{Q}$ is the external heating rate per unit mass; q is the water vapor mixing ratio; and $E - C$ is the net rate of addition of water vapor by evaporation (E) and condensation (C).

When written in this form, Equations (3.1) to (3.3) serve to emphasize that horizontal velocity, temperature, and water vapor are the primary atmospheric variables, the time-dependent behavior of which is determined by the horizontal equation of motion (3.1), the thermodynamic energy equation (3.2), and the water vapor continuity equation (3.3). Here the effects of both horizontal and vertical advection are represented in the d/dt terms on the left-hand sides; the first and second terms on the right-hand side of Equation (3.1) represent the Coriolis and pressure-gradient forces, respectively; and the first term on the right-hand side term of Equation (3.2) represents the adiabatic effects of vertical motion whereby potential energy is converted into kinetic energy (and vice versa). But of equal (if not more) importance for climate are the last terms on the right-hand sides in Equations (3.1) to (3.3), which represent the sources (or sinks) of momentum, heat, and atmospheric water vapor, respectively. The energy equation that may readily be formed from Equations (3.1) and (3.2) shows that it is the frictional dissipation of kinetic energy and the net diabatic heating due to radiation, conduction, and latent heat release that are responsible for changes in the total atmospheric energy content, whereas the difference between the total evaporation and condensation is responsible for the atmosphere's net gain or loss of moisture in Equation (3.3).

Because these equations involve the six variables $\vec{v}_H$, T, q, ω, α, and Φ, it is necessary to have three additional independent equations to formally complete the dynamical system in terms of these quantities. These are provided by the equation of mass

continuity, the hydrostatic equation (which is a simplification of the vertical equation of motion that equates the pressure to the weight of overlying air), and the equation of state of the atmospheric gas. For the atmosphere these equations may be written in isobaric coordinates as:

$$\frac{\partial \omega}{\partial p} + \nabla_p \cdot \vec{v}_H = 0 \ , \tag{3.4}$$

$$\frac{\partial \Phi}{\partial p} + \alpha = 0 \ , \tag{3.5}$$

$$p\alpha - RT = 0 \ , \tag{3.6}$$

where p is the pressure (the independent vertical variable in the isobaric coordinate system), R is the gas constant for air, and $\nabla_p \cdot \vec{v}_H$ is the divergence of the wind. These equations are diagnostic in that they do not explicitly involve time derivatives, in contrast to the prognostic or predictive Equations (3.1) to (3.3). The Equations (3.4) to (3.6) describe the balances or equilibria that must exist among the variables at all times and serve to determine the distribution of ω, Φ, and α in terms of the prognostic variables $\vec{v}_H$, T, and q.

The problem remains of specifying the boundary conditions that are necessary to determine a unique solution of the system Equations (3.1) through (3.6). Because there are no lateral boundaries in the atmosphere, these conditions usually take the form of the specification of ω at the top of the atmosphere (usually the free-surface condition, $\omega = 0$), the kinematic boundary condition of zero motion normal to the surface of the Earth, and the specification of the geopotential at the Earth's surface. (The presence of mountainous terrain poses a difficulty in isobaric coordinates, in that at the surface ω is less easily determined than is the vertical velocity itself.) For atmospheric models, it is also necessary to specify the solar flux at the top of the atmosphere (i.e., the incoming solar radiation) and either the temperature or the heat flux at the Earth's surface. Over bare land and ice-covered surfaces the condition of zero net heat flux often is used, whereby the surface or ground temperature is determined by a balance of the heat fluxes; over water surfaces, the surface temperature itself may be specified, although in a coupled atmosphere-ocean model the sea-surface temperature is internally determined. When the surface soil layer is included in the modeled climate system, a thermal boundary condition is applied below the surface, with the land surface temperature given by an additional prognostic equation.

3.3.2 Parameterization of Subgrid-Scale Processes

The equations considered above are basically the same as those that are routinely used in numerical weather prediction, except that in their application to climate more attention must be given to the slowly varying sources and sinks of momentum, heat, and moisture ($\vec{F}_H$, $\dot{Q}$, and $E-C$, respectively), which are relatively unimportant on the time scales of weather. It is therefore necessary that there be no accumulating errors in the source or forcing terms on the right-hand sides of Equations (3.1) to (3.3), because these could lead to a spurious change of climate over an extended period of time. This requirement applies both to the large-scale processes which can be portrayed reasonably well by models and to the small-scale processes which cannot be explicitly resolved and which are, therefore, treated parametrically. Because an important fraction of the vertical fluxes of heat and moisture in the atmosphere is accomplished by smaller scale motions (such as the turbulent fluxes in the surface boundary layer and the convective fluxes associated with clouds), the parameterization of such processes in terms of the resolved larger scale behavior is perhaps the most important feature of a climate model.

The horizontal force $\vec{F}_H$ in Equation (3.1) represents the transfer of (horizontal) momentum from one part of the atmosphere to another and from the atmosphere to the underlying surface by the effects of viscosity. (The effects of vertical frictional forces are precluded in the present hydrostatic system.) Such transfer in the actual atmosphere occurs by means of small-scale turbulent eddies that also serve to dissipate the kinetic energy. In a climate model these effects must be represented in terms of the large-scale flow (i.e., that given by $\vec{v}_H$), and this parameterization usually takes the form of a proportionality to the local vertical shear of the horizontal wind, $\partial \vec{v}_H / \partial p$, with the proportionality factor depending on either an assumed background eddy viscosity or the intensity of atmospheric convection and diffusion or both. In the free atmosphere such processes represent an important mechanism for the exchange of momentum between levels and between

one region and another through the action of gravity waves.

The frictional force at the Earth's surface that transfers the momentum from the atmosphere to the underlying land, ice, or ocean surface is represented in terms of the surface wind, that is, the wind near the surface or at standard anemometer level. This parameterization usually follows the bulk aerodynamic formula, whereby the surface frictional force or drag is proportional to $\vec{v}_s|\vec{v}_s|$, where $\vec{v}_s$ is the surface wind. In this formulation the proportionality factor depends on a drag coefficient, the value of which is a function of the assigned surface character or roughness (and perhaps also a function of $|\vec{v}_s|$). This parameterization is therefore an important aspect of the surface (turbulent) boundary layer, through which the lowest layer of the atmosphere loses relative momentum to the slower moving surface at the same time as atmospheric kinetic energy is dissipated. [The transfer of absolute angular momentum, we may note, involves only the zonal or easterly component of Equation (3.1) and depends on the sign of u as well as on the torque that may be exerted by the pressure at the Earth's surface.]

The diabatic heating rate $\dot{Q}$ in Equation (3.2) represents the total or net atmospheric heating due to radiation and latent heating and the effects of conduction, convection, and diffusion. Because these processes characteristically occur on scales too small to be resolved by a climate model, they must be represented in terms of the large-scale distributions of temperature, pressure, and water vapor. Of these parameterizations, perhaps the most physically complex is that of radiation, because it involves the vertical flux of both longwave and solar radiation in the presence of atmospheric water vapor and clouds over surfaces with different radiative properties (as has been discussed more fully in Chapter 2 of this volume).

The parameterization of longwave radiation in a climate model is usually based on the equation for the flux of black-body radiation as a function of the temperature, pressure, and water vapor content of the atmosphere, neglecting scattering and angular dependence. The total or net flux of longwave radiation is usually found at the surface and at each level of the atmosphere by using empirical transmission functions for water vapor, CO_2, and other trace species. The effects of clouds at different levels are considered by treating them as black-body radiators in proportion to the fractional sky coverage of each cloud type represented in the model. The parameterization of solar radiation, on the other hand, begins with the radiation incident at the top of the atmosphere (usually considered to be a function of latitude, time of day, and season of the year) and uses empirical functions for scattering and absorption as a function of pressure, water vapor, and ozone and other trace gas concentrations. By assigning an albedo to the surface and to the atmosphere itself, the effects of multiple reflection and scattering may be considered, whereas the scattering, reflection, and absorption by clouds is usually parameterized as a function of the height and thickness of clouds and their assigned optical properties.

A second important source of atmospheric heating that must be parameterized is that due to the release of latent heat upon condensation of water vapor. This heating, and the simultaneous formation of clouds, is assumed to occur when the air becomes saturated as a result of vertical motion and resultant cooling associated with either large- or small-scale flow. In most climate models it is also assumed that the condensed water vapor falls toward the surface as precipitation, some of which may evaporate. The large-scale latent heating, and the accompanying large-scale cloudiness and precipitation, is that resolved by the large-scale vertical motion ω in the system of Equations (3.1) to (3.6) as a result of convergence in the large-scale horizontal flow $\vec{v}_H$, as frequently occurs in middle and high latitudes in association with synoptic-scale waves.

The larger part of the atmosphere's latent heating, however, occurs as a result of convective-scale motions that are not resolved explicitly. Vertical motions on these subgrid scales, and the accompanying convective-scale cloudiness and precipitation, are usually parameterized in terms of a convective adjustment mechanism. In this parameterization the temperature lapse rate is not allowed to exceed the appropriate adiabatic value, and any layer in which this limit is exceeded is instantaneously adjusted by the vertical movement of sufficient air to ensure a stable stratification. Such "convection" may be confined to a shallow layer or penetrate through a deep portion of the atmosphere, depending on local conditions, and may in turn result in the

formation of convective cloudiness and precipitation. This parameterization is especially important in portraying the convective systems that are prominent in the tropical and equatorial atmosphere.

The turbulent conduction of heat from (or to) the Earth's underlying surface is a third component of the atmosphere's diabatic heating that requires parameterization. As in the case of momentum, this heating usually is represented by the bulk aerodynamic method, whereby the conductive heat flux is proportional to the product of the wind speed and the vertical gradient of temperature in the lowest air layer. This gradient is commonly taken as the difference between the temperature of the air near the surface and the temperature of the surface itself, and the proportionality constant is the drag coefficient appropriate to the surface. Therefore, when the surface air is colder than the underlying surface as is often the case in winter over the oceans in higher latitudes, the atmosphere is heated by the parameterized conductive heat flux from the surface.

The term $E - C$ in Equation (3.3), representing the net rate of addition of water vapor to the atmosphere, usually is taken to be proportional to the difference between the net rates of evaporation and condensation. As noted previously, the rate of condensation consists of contributions from both large- and small-scale processes and usually is considered to be equal to the net rate of precipitation. When the possibility of the evaporation of some (or all) of falling precipitation is considered, it is only the net condensation in the air column and the surface evaporation that are effective in changing the net moisture content of the air. The rate of surface evaporation usually is parameterized, in a manner analogous to that of the surface fluxes of momentum and sensible heat, by the bulk aerodynamic method. In this method evaporation is considered to be proportional to the product of the surface wind speed and the vertical gradient of water vapor in the atmosphere near the surface, which usually is approximated by the difference between the mixing ratio in the air near the surface and that at the surface itself. At a water surface the mixing ratio is assumed to be the saturation value at the surface temperature; at a land surface the mixing ratio depends on the ground temperature and the ground wetness, which is itself determined from a ground water budget in which any excess of precipitation over evaporation is partitioned between ground water storage and surface runoff.

Most of the parameterizations described above depend either directly or indirectly on the representation of the air near the surface and are therefore dependent on a model's treatment of the atmospheric boundary layer (which lies above the surface or constant-flux layer considered in the bulk aerodynamic method). In some models the structure of the boundary layer is resolved with closely spaced levels in the lowest kilometer or so, whereas in other models the boundary layer is treated parametrically as a bulk property. A critical element in either treatment is the determination of the surface temperature, which in turn controls the vertical stability and therefore the degree of vertical turbulent mixing and convection. In most models the surface temperature of land, ice, or snow is found from the surface heat budget, in which the temperature-dependent surface fluxes of sensible heat, latent heat, and longwave radiation are balanced by the net surface flux of solar radiation. It is primarily through this calculation that the local radiative, thermal, hydrologic, and aerodynamic properties of the Earth's surface are effectively parameterized for use with the large-scale variables of a climate model. If the possible absorption and storage of heat in the surface itself is also considered, the surface temperature becomes a prognostic variable, as noted earlier.

3.3.3 Simplified Climate Models

Once the dynamical equations have been established, the domain of the model must be determined. This choice affects many characteristics of the climate model and determines the nature of the parameterizations that are needed. If the model is to describe only the climate as averaged, say, over one or more dimensions (such as latitude or height), the governing atmospheric equations of the model could formally be derived by appropriately averaging the system of Equations (3.1) to (3.6). In the extreme, such averaging could be performed over all dimensions to yield a model for the globally averaged climate, in which case the motion of the atmosphere would become implicit; the globally averaged

temperature and water vapor are then the dependent variables of the model, which are often parameterized in terms of the surface temperature (and humidity). The model is then developed around the budget equation for the flux of radiation, and sensible and latent heat at the surface, of which the prototype model is that described by Budyko (1969).

In other versions of "heat balance" models, averaging is performed only in the vertical and longitudinal directions, with each term in the surface heat budget now parameterized in terms of the surface temperature as a function of latitude. Such models, of which that of Sellers (1973) is a well-known example, are able to portray the basic latitudinal dependence of the Earth's heat and hydrologic balances when the meridional transports of heat and moisture are parameterized. Because in actuality this transport is accomplished in middle and higher latitudes by the large-scale atmospheric motions, which are not present in the model, this parameterization in terms of the zonally averaged temperature is a critical element of such climate models.

Other important classes of simplified climate models are those that resolve only the variation of the temperature in the vertical, usually called "radiative-convective" models, and those that combine statistical representations with simplified or averaged dynamics, usually called "statistical-dynamical" models. Radiative-convective models combine the effects of vertical radiative heat transfer and of vertical convection. Such models were first introduced by Manabe and Wetherald (1967); their structure and application to the study of CO_2 effects are described briefly in Chapter 4 of this volume and more extensively in Appendix A. Statistical-dynamical models are usually constructed based on versions of the conservation equations that have been averaged over longitude, with the effects of the synoptic eddies parameterized statistically in the meridional plane. The structure of these and other simplified climate models has been reviewed by Saltzman (1978).

3.4 GENERAL CIRCULATION MODELS OF THE ATMOSPHERE

The most complex climate models are those in which no explicit spatial averaging is introduced. Such three-dimensional models require the more or less straightforward integration of the governing dynamical equations [Equations (3.1) to (3.6)] over the globe. With an effective horizontal resolution of several hundred kilometers, such models are able to resolve the large-scale transient cyclones, but not mesoscale features such as thunderstorms or fronts. General circulation models (GCMs) began with the pioneering calculations of Phillips (1956) and Smagorinsky (1963), and GCMs with global boundary conditions and subgrid-scale parameterizations similar to those discussed earlier are now widely used. Before reviewing the climate simulation capability of these models, however, it is useful to consider briefly their characteristic structure.

For the dynamical system represented by Equations (3.1) to (3.6), including the necessary boundary conditions and parameterizations, the first step in the construction of a GCM is the selection of the vertical levels at which the model will be applied. This choice of vertical resolution determines the pressure thickness or mass of the layers which the dependent variables of the model are assumed to represent and is therefore a determinant in the effective parameterization of the convective and turbulent subgrid-scale processes in terms of these variables. The vertical structure or pressure dependence of the system [Equations (3.1) to (3.6)] is such that it is usually convenient to determine the horizontal velocity, temperature, and mixing ratio at the midlevel of each layer of the model, with the vertical velocity determined at the levels between each layer. With the pressure, temperature, and moisture determined at the Earth's surface, this leads to a natural vertical staggering of the modeled variables as illustrated for the case of a two-level model in Figure 3.4. Depending on their intended use, GCMs may have several dozen levels in the atmosphere and may contain relatively elaborate parameterizations of the unresolved physical processes, especially those at or near the Earth's surface.

When the vertical structure of the GCM is chosen and the model equations are written in terms of the variables at appropriate levels, the next step is to design a numerical solution method for the global atmospheric domain. This normally takes the form of a finite-difference grid with a mesh size of several hundred kilometers, or a spectral representation with a maximum wave number of about 20 or 30. (These choices are a compromise between the

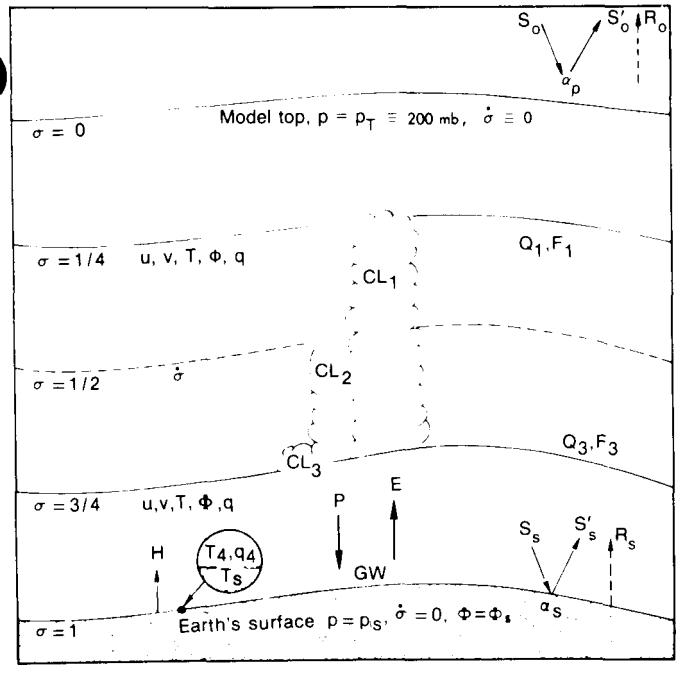

Figure 3.4. Schematic representation of the structure and principal variables of atmospheric GCMs as illustrated by a two-layer GCM (after Gates and Schlesinger 1977). Here $\sigma = (p - p_T)(p_s - p_T)^{-1}$ is a mass-weighted vertical coordinate with p representing pressure, p_T indicating pressure at the top of the model, and p_s indicating surface pressure; u and v are horizontal velocity components; T is temperature; Φ is geopotential; q is water vapor mixing ratio; H is surface flux of sensible heat; P is precipitation; E is evaporation; GW is ground wetness; S and S' are incident and reflected solar radiation, respectively; R is outgoing longwave radiation; α_p and α_s are planetary and surface albedo, respectively; Q is diabatic heating; F is friction; and CL is cloudiness. The subscripts 1 and 3 denote evaluation at the upper and lower tropospheric levels of the model, respectively, and 4 and s denote evaluation near the surface and at the surface, respectively.

need to accurately represent atmospheric processes, on the one hand, and the rapid increase of computing requirements with increased resolution on the other.) The equations of the model at each level must then be written in terms of the variables at discrete grid points or in terms of discrete wave numbers, with care taken to minimize the truncation error in the approximation of spatial derivatives. In the case of finite-difference operators, particular attention also must be given to their compatibility with integral invariants such as the global conservation of kinetic energy in the absence of sources and sinks; when these constraints are violated by the spatial finite differences of the model, nonlinear numerical instability may result from the accumulation of energy in selected computational modes.

The stability of a model's numerical integration also is affected by the size of the finite time increment Δt used in the approximation of the time derivatives of the prognostic variables. Depending on the particular numerical method used to advance the solutions in time, a condition of the form $\Delta t \leq \Delta s/U$ is usually required to avoid computational instability, where Δs is the (minimum) size of the horizontal grid's mesh length and U is the (maximum) wave speed resolved in the model. This criterion limits Δt to a fraction of an hour in GCMs that typically employ horizontal mesh lengths of a few hundred kilometers.

Once all of the numerical approximations, constants, and boundary conditions required for the solution of a model have been assembled, the time integration can, in principle, be carried out for an indefinite period starting with given initial conditions. Sometimes an initial state of rest, isothermalcy, and dryness is chosen for simulations on climatic time scales, although initial conditions that more closely resemble typical large-scale atmospheric conditions are also often used. In either case, however, the location and intensity of any individual feature cannot, even theoretically, be predicted accurately beyond a few weeks because of the inevitable growth of errors. In the case of climate simulation with a GCM, the numerical solution is extended beyond this predictability limit and undergoes an adjustment over a period of a few weeks or few months, during which the various large-scale and parameterized physical processes in the model adjust to each other and to the imposed boundary conditions in accordance with the model's equations. After this spin-up period, the statistics of the model's solution (i.e., the climate) may then be determined by averaging over time scales that are appropriate for the climatic state being studied. Because GCMs resolve large-scale synoptic eddies (the familiar moving cyclones and anticyclones of daily weather), it is necessary to take averages over sufficient time to acquire representative and stable climatic statistics in the presence of these essentially unpredictable fluctuations; this makes the detection of a simulated climate change (i.e., a change in the average conditions) a formidable statistical task, especially in view of the climate variability that may be induced by fluctuations outside the atmosphere.

3.5 MODELS OF THE OCEAN, ICE, AND LAND SURFACE

Although our attention has been focused on models of the atmosphere, models also have been constructed for the oceanic, cryospheric, and land surface components of the climate system. These models are generally not as highly developed as their atmospheric counterparts, partly because they represent more slowly acting processes that may be either prescribed or neglected altogether in atmospheric models, and partly because there are fewer observations on which to develop and test the necessary model parameterizations. On the longer climatic time scales, however, the interactions of the atmosphere with the underlying ocean, ice, and land surface are critical elements in the behavior of the climate and must be addressed.

For the purposes of climate modeling, the ocean has usually been treated in a basin-sized "box" or in a global domain as a GCM. In the latter case, the oceans are described by a system of equations similar to Equations (3.1) to (3.6), but modified by the ocean's incompressibility, with a continuity equation for salinity replacing that for water vapor. Unlike the atmosphere, however, there is no internal latent heating in the ocean, and the heat and water exchanged with the overlying air determine the changes of the sea surface temperature and density and therefore the formation of sea ice. These exchanges are the forcing functions for the ocean's thermally driven circulation, the time scale of which depends on the efficiency of the vertical exchange processes within the ocean. The oceanic surface or mixed layer interacts with the atmosphere on time scales of weeks, whereas the deeper water responds more slowly because of the small vertical mixing and the large thermal capacity in the oceanic interior.

Another important source of oceanic forcing is that exerted by atmospheric wind stress at the surface; the atmosphere's loss of momentum by friction at the surface represents a gain by the oceans and serves to sustain the global system of wind-driven currents. The ocean's response to this forcing is relatively rapid and is generally confined to the near-surface water in which vertical mixing is strongest. Because global ocean models do not generally resolve the highly energetic mesoscale eddies (which are the dynamical counterpart of the transient synoptic-scale cyclones in the atmosphere), this parameterization must be made in terms of the relatively inviscid and stable gyral-scale oceanic circulation. By using solution methods similar to those used in atmospheric models, such oceanic GCMs (as typified by the models of Bryan et al. 1975 and Han 1984) successfully portray the average large-scale distribution of oceanic temperature, salinity, and current in response to realistic surface forcing and realistic basin geometry. The observed average seasonal distribution of sea ice also has been successfully simulated by oceanic GCMs, as well as by simplified models of the surface mixed layer of the ocean.

From the viewpoint of modeling the climate system, however, models in which the atmosphere and oceans are coupled are more interesting. Of the few GCMs of the coupled atmosphere-ocean system, that of Bryan et al. (1975) is perhaps the most well known. Aside from the possible long-term effects of the coupling method used, more recent research (e.g., Gates et al. 1985) shows that the simulated climate may be significantly affected by the presence of a coupled ocean. In lower latitudes, where the distribution of rainfall is determined largely by the sea surface temperature, the atmospheric solution of the coupled model is more realistic than that of a model with a fixed ocean, and in middle latitudes the oceanic circulation accounts for an appreciable fraction of the total poleward transport of heat. The climatic effects of oceanic heat transport and storage also are seen in the moderation of the temperature in middle and high latitudes and in the seasonal lag of the ocean's temperature relative to that of the continents. When the ocean is not permitted to store or transport heat, the long-term thermal response may be modeled by the assumption of a local balance of surface heat fluxes. Such ocean models have been used in a variety of climate simulations in which the transient response of the oceans (and therefore the atmosphere) is not of primary concern.

Although those portions of the cryosphere represented by sea ice and surface snow are usually modeled as components of the ocean and atmosphere, respectively, the world's large-scale ice sheets and larger mountain glaciers must also be considered in

a comprehensive climate model designed for long-term integration. The dynamical basis of ice sheet models is provided by the equations for momentum, heat, and mass conservation, along with appropriate equations of state and vertical pressure forces. Such models have successfully simulated the Antarctic ice sheet in response to a prescribed surface climate (Budd and Smith 1982); when coupled with the atmosphere and ocean, the ice sheet responds to the evolving global climate while providing an updated ice boundary. Of particular concern in such models are conditions at the bottom of the ice which significantly influence the movement, lateral stability, and basal melting of the ice mass; these conditions, along with the effects of nonuniformities in the ice density, are the principal processes that require parameterization. Because the response time of large-scale ice sheets is on the order of thousands of years, their inclusion as parts of a coupled global climate model will require an effective method for treating their interaction with the much more rapidly varying oceans and atmosphere.

In a similar fashion, a truly comprehensive climate model also should include an interactive treatment of the Earth's land surface. Although the surface heat and water budgets are used in atmospheric models to determine the ground surface temperature and surface soil moisture as described previously, these have not generally been used to calculate the changes of surface properties such as the surface albedo, transpiration, and surface roughness. Such changes are dependent upon the properties of the surface soil and vegetative cover (Mintz et al. 1983), but have generally not been considered in an interactive fashion. In addition to such coupling, a land surface model must parameterize the highly complex pattern of local surface properties in terms of large-scale variables and must portray the characteristic seasonal variations of surface vegetation.

3.6 CLIMATE SIMULATION WITH ATMOSPHERIC GENERAL CIRCULATION MODELS

Although it is instructive to think of the problem of climate from the viewpoint of the complete climate system, only the performance of atmospheric GCMs will be considered, as it is only for such models that enough solutions have been made to permit a meaningful assessment.

When used with observed boundary conditions (which includes specification of the sea surface temperature), typical atmospheric GCMs are capable of simulating almost all of the large-scale regional features of the climate as now observed, including the average distribution of the pressure, temperature, and wind both near the surface and aloft. An example of this performance is shown in Figure 3.5, in which the distribution of the average February surface air temperature, simulated by the GFDL GCM with a coupled mixed-layer ocean, is shown. Despite the errors of both amplitude and structure that are apparent (and which are in general not unlike those found with virtually every GCM [Gates 1979b]), it is of particular interest that such models are able to reproduce the seasonal changes of the circulation from winter to summer. This annual display of the atmosphere's sensitivity to the Sun's radiation (and to the heating implicit in the seasonally prescribed sea surface temperature) is the best documented climate change and provides a useful model calibration. In general, atmospheric GCMs simulate the observed patterns of those variables associated with small-scale processes, such as cloudiness and precipitation, with less accuracy than is the case for other variables.

The characteristic performance of climate models also may be judged from the growing number of atmospheric GCM integrations now available over monthly (and in some cases seasonal) time scales. As a preliminary comparison, the results of selected global atmospheric GCMs are shown in Figures 3.6 and 3.7 in terms of their simulations of the zonally averaged January sea level pressure and zonally averaged January precipitation rate. These models have approximately the same horizontal resolution, and each has made use of the observed global topography and observed January sea surface temperature distribution as lower boundary conditions. Otherwise, the various models differ considerably with respect to the number of vertical levels used and in their parameterizations of subgrid-scale processes. A summary of the features of some current atmospheric GCMs is given in Chapter 4.

In comparison with the observed January averages, also shown in Figures 3.6 and 3.7, the models collectively bear some resemblance to reality,

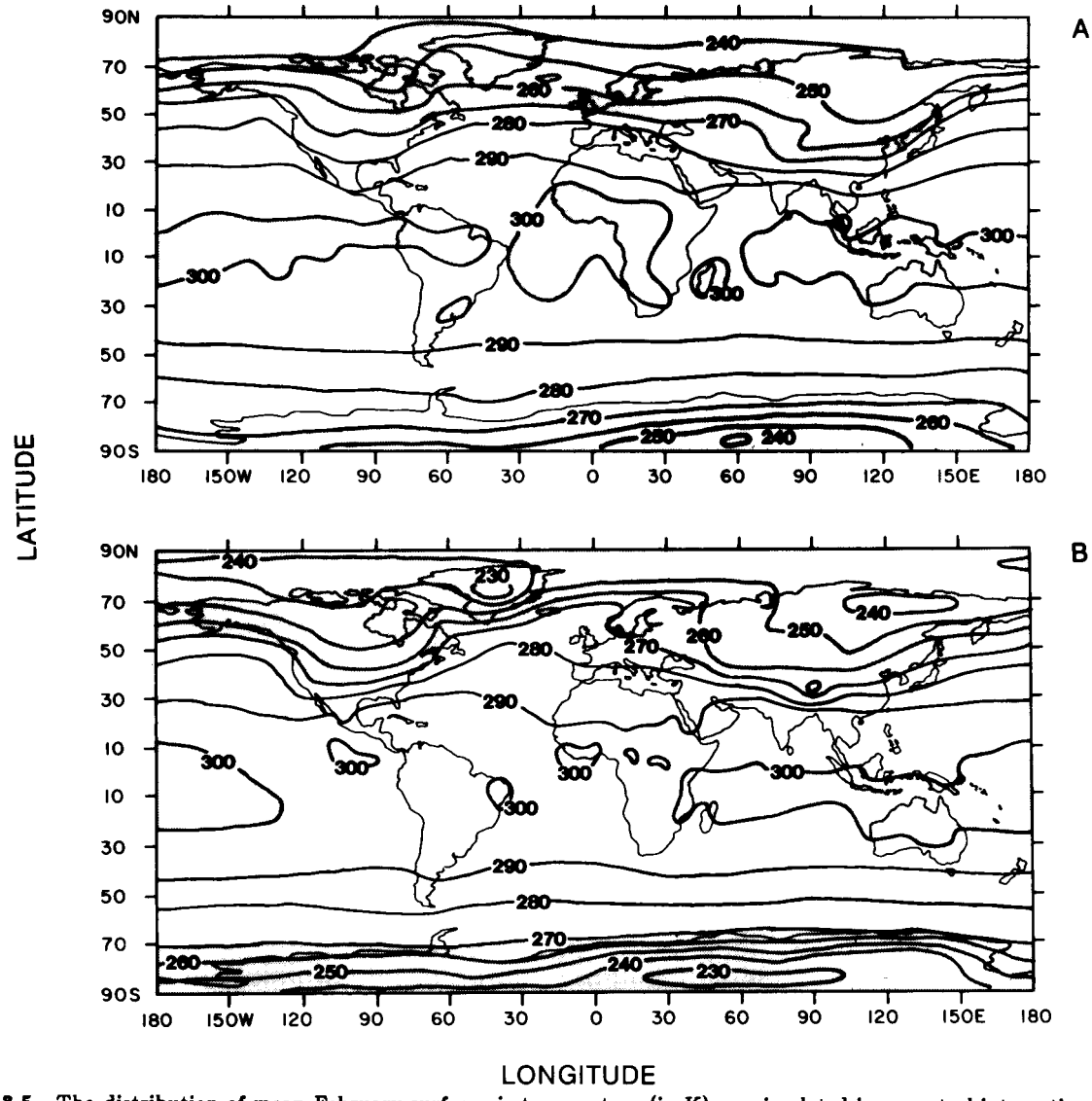

Figure 3.5. The distribution of mean February surface air temperature (in K), as simulated in a control integration of the GFDL atmospheric GCM with (A) a coupled mixed-layer ocean, and (B) as observed. The regions above 300 K and below 270 K are shaded. Source: Gates (1984), as redrawn from Manabe and Stouffer (1980).

although no model has a clear superiority in all respects. Some models accurately portray the January sea level pressure profile at all but middle northern latitudes, whereas others systematically simulate sea level pressures that are too low in low and middle latitudes and too high in higher latitudes. Some models also systematically overestimate the January precipitation rate, especially in lower latitudes, whereas others tend to underestimate it at almost all latitudes. Although other (and possibly more accurate) versions of these and other models exist, the scatter among the models shown here is perhaps greater than would have been expected and serves to illustrate, albeit in an incomplete fashion, the sensitivity of the simulated climate to differences in model structure and the approximations used.

The utility of GCMs as climate models, however, should not be judged solely, or even most importantly, on the basis of such comparisons. In addition to their prediction of many other variables such as temperature, wind, and cloudiness, the models also yield simulations of the various components of the global heat, momentum, and hydrologic balances. Most models portray these processes with

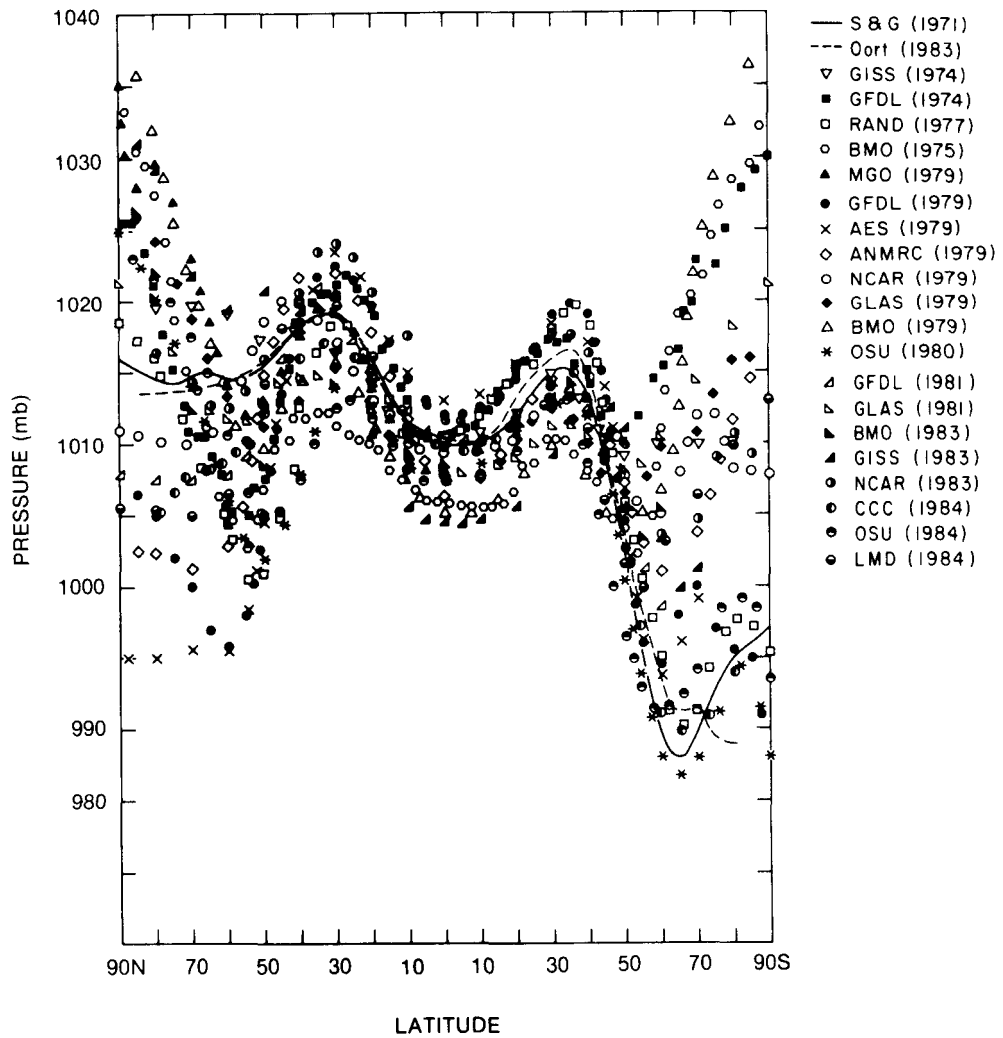

Figure 3.6. Zonally averaged mean January sea-level pressure as simulated by various atmospheric GCMs (symbols) and as observed (solid and dashed lines). Source: Gates (1985), where full references to models are given.

reasonable accuracy, although some tend to overestimate the strength of the zonal wind systems and underestimate the observed total cloudiness. Although they differ in vertical resolution and in subgrid-scale parameterization (see Chapter 4), atmospheric GCMs simulate the fluxes of heat, momentum, and moisture over the oceans with only modest accuracy. When coupled with an ocean model, large-scale systematic errors can result in the simulated sea surface temperature (Gates et al. 1985).

In addition to their simulation of the mean distribution of climatic variables, an important part of the performance of climate models is their portrayal of the variability which surrounds the climatic mean. In many instances this variability, and the associated likelihood of the occurrence of extreme events, is of more practical importance than the average conditions, yet this aspect of GCMs has not received the attention it deserves. In general, atmospheric GCMs exhibit reasonable synoptic variability on synoptic, monthly, and seasonal time scales but show less longer term variability than does the observed atmosphere; an adequate simulation of interannual variability evidently requires coupling with the ocean (Manabe and Hahn 1981).

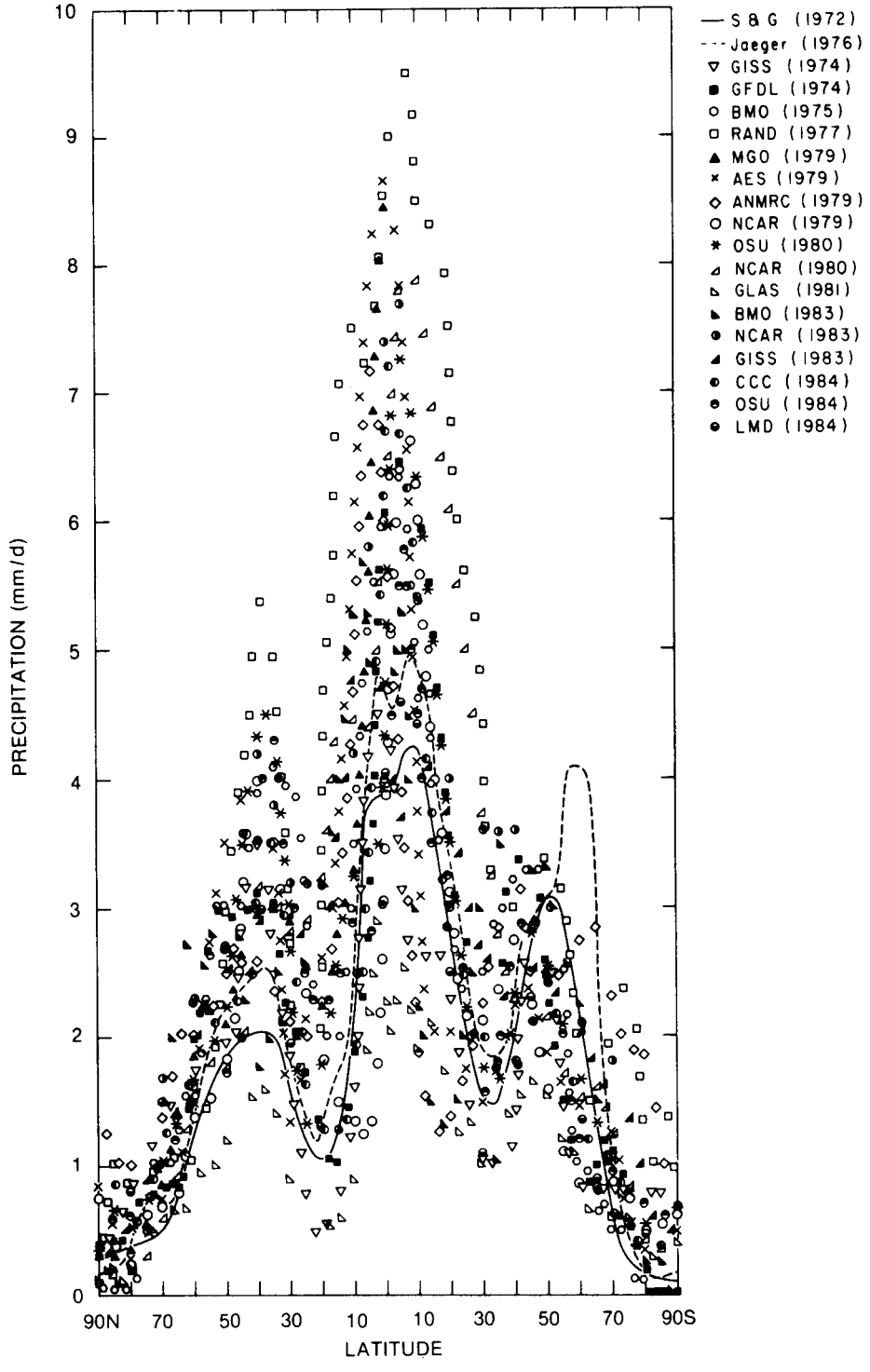

Figure 3.7. Zonally averaged mean January precipitation rate as simulated by various atmospheric GCMs (symbols) and as observed (solid and dashed lines). Source: Gates (1985), where full references to models are given.

3.7 CRITICAL MODELING PROBLEMS AND RECOMMENDED RESEARCH

Although a number of remarks have already been made on the design and analysis of climate models, several problems should be addressed that are of particular importance for future climate modeling and for the simulation of CO_2-induced climate changes in particular.

Research should be undertaken to determine the optimal model structure and resolution for the study of potential CO_2 effects. In general, the vertical and horizontal resolution of a model may be expected to have an effect on its ability to simulate the detailed structure and behavior of the atmosphere (or ocean), and for short-range prediction, a model of the highest practicable resolution should be used. For climate purposes, however, it is not clear how much resolution is required, and it is possible that much of the output of GCMs may be climatically redundant. The problem is to determine those processes that are critical for the maintenance and variation of climate and the precision with which they need to be represented. It seems that at least several tropospheric model levels are required if even a marginally satisfactory portrayal of baroclinic eddies is to be achieved, and it is possible that several levels in the lower stratosphere will ultimately prove to be necessary. For many climatic purposes, however, the highest possible horizontal resolution may not be required, and in some cases higher resolution has actually worsened the climatic performance of GCMs. It seems likely that with suitable parameterizations (which might themselves be drawn from models of higher resolution), at least the large-scale climatic regions of the world could be satisfactorily simulated with less resolution than is now commonly used, although resolution of the large-scale distribution of continents and oceans is probably required. In view of the computational burden imposed by GCMs of high resolution, more precise information on the sensitivity of climate simulations to resolution is needed. This question is also related to the problem of the representativeness of model simulations, that is, the areas or scales to which the model solutions are most applicable. The translation of model-generated climate into information on the fine-grained structure of local climates is also important in connection with impact studies (Gates 1984).

A second major problem of climate modeling, and the one most directly concerned with the model's physics, is improvement of the representation of important climatic processes. Better treatments of clouds, convection, the surface boundary layer, and dissipative processes are required. In general, present models simulate the observed cloudiness rather poorly, especially the occurrence of nonprecipitating stratiform and cirrus clouds and the diurnal variation of low-level clouds, and, at present, take no account of the advection of cloud or of cloud microphysics. The parameterization of clouds and convection is also closely related to the behavior of the planetary boundary layer, the treatment of which also needs to be improved in nearly all climate models.

A third critical problem in climate modeling is the need to use models that actively couple the world's oceans with the atmosphere. Although a number of oceanic GCMs have been provisionally coupled with atmospheric models, none of these models has taken into proper account the oceanic surface mixed layer that controls the all-important variations of sea surface temperature. Compared with the atmosphere, the oceans are relatively resistant to large decreases of surface temperature because of the downward vertical mixing that occurs as a result of unstable stratification. Surface heating, on the other hand, tends to stabilize the surface water, and heat is mixed downward largely through the action of wind-induced turbulence. The local surface salinity increase that occurs when evaporation exceeds precipitation is also an important destabilizing process, especially in the lower latitudes. Recent theories of the mixed layer take these processes into account, and their successful parameterization in an oceanic GCM, and thereafter in a coupled GCM, is a matter of high priority in climate modeling.

The use of GCMs for climate simulation requires exceedingly large amounts of computer time; present atmospheric GCMs, with horizontal resolution of a few hundred kilometers, run at speeds several hundred times as fast as nature on machines of the class of the CRAY-1. Decreasing the horizontal grid size and requiring the execution of several runs

to increase confidence in the significance of the results usually limits climate simulations to periods of only a few decades. In view of the large number of important climate experiments that should be performed and analyzed, a substantial increase in the computing power available for climate modeling and climate diagnosis is required. For at least the next few years, climate modelers will have to accept out of necessity the challenge of developing significantly faster models by somehow merging the key elements of GCMs and statistical-dynamical models and will have to devote greater attention to the analysis of all available climate simulations.

More systematic comparison of model results with observations (to the extent that they are available) and more insightful analysis of simulations in terms of the basic physical processes of the model are also required. Although several GCMs and a variety of simpler models have been used to determine the climatic effects of deliberate changes in the boundary conditions, such as changes in the solar constant, atmospheric CO_2 concentration, or sea surface temperature, the analysis of such experiments has not revealed clearly the mechanisms responsible for the response of the model. It is particularly important that such analyses be carried out with the more sophisticated GCMs, because they presumably introduce the least distortion into the physics of the climate system and have the best chance of representing all of the interacting processes simultaneously. The response characteristics of climate models also should be determined as a function of the magnitude, scale, and location of deliberate changes in the model and in the boundary conditions; from such a model response matrix, the quantitative diagnosis of the modeled feedback processes may then be made in a systematic fashion. Beyond this, the determination of the model-dependent portion of the simulated climate changes looms as a critical and almost unrecognized problem in studying the climatic effects of the increasing CO_2 concentration.

REFERENCES

Berger, A. L., and Nicolis, C. (eds.). 1984. *New Perspectives in Climate Modeling.* Elsevier, Amsterdam, The Netherlands.

Bryan, K., Manabe, S., and Pacanowski, R. C. 1975. "A Global Ocean-Atmosphere Climate Model. Part II. The Oceanic Circulation." *Journal of Physical Oceanography 5:*30–46.

Budd, W. F., and Smith, I. N. 1982. "Large-Scale Numerical Modelling of the Antarctic Ice Sheet." *Annals of Glaciology 3:*42–49.

Budyko, M. I. 1969. "The Effect of Solar Radiation Variations on the Climate of the Earth." *Tellus 21:*611–619.

Gates, W. L. 1975. "Numerical Modelling of Climate Change: A Review of Problems and Prospects." In *Proceedings WMO/IAMAP Symposium on Long-term Climatic Fluctuations* (WMO No. 421). World Meteorological Organization, Geneva, Switzerland.

Gates, W. L. 1979a. "The Physical Basis of Climate." 112–131. In *Proceedings of the World Climate Conference* (WMO No. 537). World Meteorological Organization, Geneva, Switzerland.

Gates, W. L. (ed.). 1979b. *Report of the JOC Study Conference on Climate Models: Performance, Intercomparison and Sensitivity Studies, Vol. I and II* (GARP Publication Series 22). World Meteorological Organization, Geneva, Switzerland.

Gates, W. L. 1984. "The Use of General Circulation Models in the Analysis of the Ecosystem Impacts of Climatic Change" (Report No. 52). Climatic Research Institute, Oregon State University, Corvallis, Oregon.

Gates, W. L. 1985. "Problems and Prospects in Climate Modeling." In U. Radok (ed.), *Problems and Prospects in Climate Analysis and Forecasting.* Westview Press, Boulder, Colorado.

Gates, W. L., Han, Y.-J., and Schlesinger, M. E. 1985. "The Global Climate Simulated by a Coupled Atmosphere-Ocean General Circulation Model: Preliminary Results." 131–151. In J. Nihoul (ed.), *Coupled Atmosphere-Ocean Models.* Proceedings of the 16th International Liege Colloquium on Ocean Hydrodynamics). Elsevier, Amsterdam, The Netherlands.

Gates, W. L., and Schlesinger, M. E. 1977. "Numerical Simulation of the January and July Global Climate with a Two-Level Atmospheric Model." *Journal of Atmospheric Sciences 34:*36–76.

Global Atmospheric Research Programme. 1974. *The Physical Basis of Climate and Climate Modelling* (GARP Publication Series 16). World Meteorological Organization, Geneva, Switzerland.

Han, Y.-J. 1984. "A Numerical World Ocean General Circulation Model. Part II. A Baroclinic Experiment." *Dynamics of Atmospheres and Oceans 8:*141–172.

Hansen, J., Lacis, A., Rind, D., Russell, G., Stone, P., Fung, I., Ruedy, R., and Lerner, J. 1984. "Climate Sensitivity: Analysis of Feedback Mechanisms." 130–163. In *Climate Processes and Climate Sensitivity* (Geophysical Monograph 29), American Geophysical Union, Washington, D.C.

Houghton, J. T. (ed.). 1984. *The Global Climate.* Cambridge University Press, Cambridge, United Kingdom.

Manabe, S., and Hahn, D. G. 1981. "Simulation of Atmospheric Variability." *Monthly Weather Review 109:*2260–2286.

Manabe, S., and Stouffer, R. J. 1980. "Sensitivity of a Global Climate Model to an Increase of CO_2 Concentration in the Atmosphere." *Journal of Geophysical Research 85:*5529–5554.

Manabe, S., and Wetherald, R. T. 1967. "Thermal Equilibrium of the Atmosphere with a Given Distribution of Relative Humidity." *Journal of Atmospheric Sciences 24:*241–259.

Mintz, Y., Sellers, P. J., and Willmott, C. J. 1983. "On the Design of an Interactive Biosphere for the GLAS General Circulation Model" (NASA Technical Memorandum 84973). Goddard Space Flight Center/NASA, Greenbelt, Maryland.

National Research Council. 1983. *Changing Climate.* Report of the Carbon Dioxide Assessment Committee, Board on Atmospheric Sciences and Climate, National Academy of Sciences. National Academy Press, Washington, D.C.

Peixoto, J. P., and Oort, A. H. 1984. "Physics of Climate." *Reviews of Modern Physics 56:*365–429.

Phillips, N. A. 1956. "The General Circulation of the Atmosphere: A Numerical Experiment." *Quarterly Journal of the Royal Meteorological Society 82:*123–164.

Saltzman, B. 1978. "A Survey of Statistical-Dynamical Models of the Terrestrial Climate." *Advances in Geophysics 20:*183–304.

Schneider, S. H., and Dickinson, R. E. 1974. "Climate Modeling." *Reviews of Geophysics and Space Physics 12:*447–493.

Sellers, W. D. 1973. "A New Global Climatic Model." *Journal of Atmospheric Sciences 12:*241–254.

Smagorinsky, J. 1963. "General Circulation Experiments with the Primitive Equations. I. The Basic Experiment." *Monthly Weather Review 93:*99–164.

Smagorinsky, J. 1974. "Global Atmospheric Modelling and the Numerical Simulation of Climate." In W. N. Hess (ed.), *Weather Modification.* Wiley Interscience, New York, New York.

Wigley, T. M. L., Angell, J. K., and Jones, P. D. 1985. "Analysis of the Temperature Record." In M. C. MacCracken and F. M. Luther (eds.). *Detecting the Climatic Effects of Increasing Carbon Dioxide* (DOE/ER-0235). U.S. Department of Energy, Washington, D.C. Available from NTIS, Springfield, Virginia.

4. MODEL PROJECTIONS OF THE EQUILIBRIUM CLIMATIC RESPONSE TO INCREASED CARBON DIOXIDE

Michael E. Schlesinger
Oregon State University

John F. B. Mitchell
United Kingdom Meteorological Office

CONTENTS

Note: Full page copies of the illustrations in this chapter, showing latitude-longitude comparisons of general circulation model results not published elsewhere, are available from the editors of this volume.

4.1 INTRODUCTION

If the Earth's atmosphere were composed of only two major constituents, nitrogen (N_2, 78% by volume) and oxygen (O_2, 21%), the Earth's surface temperature would be close to the −18°C radiative-equilibrium value necessary to balance the approximately 240 W m^{-2} of solar radiation absorbed by the surface-atmosphere system (see Section B.6 of Appendix B). The fact that the Earth's surface temperature is a life-supporting 15°C is a consequence of the greenhouse effect of the atmosphere's minor constituents, mainly water vapor (H_2O, 0.2%) and carbon dioxide (CO_2, 0.03%). Measurements taken at Mauna Loa, Hawaii show that the CO_2 concentration has increased from 316 parts per million by volume (ppm) in 1959 to 342 ppm in 1983 (Elliott et al. 1985), an 8% increase in 24 years. A variety of direct CO_2 measurements and indirect reconstructions indicate that the preindustrial CO_2 concentration during the period from 1800 to 1850 was 270 ± 10 ppm (World Meteorological Organization [WMO] 1983). A study by Rotty (1983) reports that the CO_2 emission from the combustion of fossil fuels (gas, oil, coal) increased at a nearly constant rate of 4.6% per year from 1860 to 1973 and has continued to increase since 1973 at the diminished growth rate of 2.3% per year. Projections of future usage of fossil fuels, discussed by Trabalka (1985), indicate that the CO_2 concentration could reach twice the preindustrial values sometime during the 21st century. This chapter addresses the question of the extent to which a doubling of the CO_2 concentration would alter the Earth's climate.

To address this question, a hierarchy of mathematical climate models has been used to simulate the change in the equilibrium climate resulting from a doubling of the CO_2 concentration, such as from 300 to 600 ppm. In these equilibrium climate change studies, the climate model calculation proceeds forward in time from some initial condition until the equilibrium is attained after the transient adjustments are completed. A separate simulation is performed for the lower CO_2 concentration (control run) and for the higher CO_2 concentration (experiment run). The differences between the experimental and control climates represent the CO_2-induced changes in the equilibrium climate. Although these simulations of CO_2-induced equilibrium climate change are usually time dependent, they generally have been performed in a manner that minimizes the time required to reach equilibrium in order to economize on computer time. Moreover, equilibrium climate change simulations are made with fixed CO_2 concentrations for both the control and experimental climates, not with the reconstructed, observed or projected CO_2 evolutions. Therefore, most equilibrium climate change simulations cannot be used to estimate the actual temporal response of the climate system to either an abrupt or realistic CO_2 increase. The transient response aspect of CO_2-induced climate change is the subject of Chapter 5 of this volume (henceforth chapters referenced will be from this volume only). In this chapter we present and critique the results obtained from the simulations of CO_2-induced equilibrium climate change by energy balance models (EBMs), radiative-convective models (RCMs), and atmospheric general circulation models (GCMs).

4.2 STUDIES USING SIMPLIFIED CLIMATE MODELS

Historically, the first assessments of the potential climatic effects of a doubling of the CO_2 concentration were performed using simplified climate models. As understanding of the various components and feedback processes in the climate system has progressed, and as computer capabilities have improved, the modeling approaches have become increasingly more complex and computationally intensive. The simplified climate models continue to have a very useful role in climate research related to the potential effects of increased CO_2 concentrations in that they are particularly well suited for sensitivity studies that would be computationally prohibitive and exceedingly difficult to analyze if GCMs alone were used.

The purpose of this section is to show the historical progression of assessment studies. This discussion is not intended to be complete in describing all models that have been used for these studies. The emphasis is on EBMs and RCMs, because studies using these models have been particularly useful in investigating the impact of feedback processes on model sensitivity. This section is a summary of the detailed discussion of EBM and RCM studies that is presented in Appendix A. The technically oriented

reader is encouraged to read Appendix A to gain a deeper appreciation of the analysis upon which the conclusions presented in Section 4.2 are based.

4.2.1 Energy Balance Models

Energy balance models predict the change in temperature at the Earth's surface that results from a change in heating based on the requirement that the net flux of energy does not change. The earliest estimates of the CO_2-induced temperature change were obtained from surface energy balance models (SEBMs) wherein the energy balance condition was applied at the Earth's surface. Later, planetary energy balance models (PEBMs) were used to determine the CO_2-induced temperature change from the balance condition applied at the top of the atmosphere. In this section we review these EBM studies of CO_2-induced temperature change, beginning with the first SEBMs and concluding with PEBMs.

First, however, we introduce a formulation for EBMs that is generalized to encompass both SEBMs and PEBMS. This formulation also facilitates the quantitative evaluation of feedback, thus enabling comparison of EBMs among themselves and with the other models presented in the following sections.

Energy balance models predict the change in temperature at the Earth's surface (ΔT_*) from the requirement that the change in the net energy flux (ΔN) is zero. The net energy flux depends on quantities, E_i, that can be regarded as external to the climate system, that is, quantities whose change can lead to a change in climate, but that are independent of climate. The net energy flux also depends on quantities, I_j, that are internal to the climate system, that is, quantities that can change as the climate changes, and, in so doing, feed back to modify the climate change. The external quantities include, for example, the solar constant, the optically active ejecta from volcanic eruptions, trace gas concentrations, and, for purposes of this report, the CO_2 concentration (although eventually the CO_2 concentration also may change in response to climate change). The climatic effects of the first three external factors are discussed further in Chapter 6; the climatic effects of CO_2 are discussed here and in Chapter 5.

The internal quantities include all the variables of the climate system other than T_*. Because T_* is the only dependent variable in an EBM, the internal quantities must be represented as functions of T_*. The change in N due to a change in one or more external quantities, ΔE_i, can be expressed as

$$\Delta Q = \sum_i \frac{\partial N}{\partial E_i} \Delta E_i \ . \tag{4.1}$$

The resultant change in surface temperature can be related to the perturbation ΔQ by

$$\Delta T_* = G_f \ \Delta Q \ , \tag{4.2}$$

where G_f is the gain (output/input) of the system. If N is independent of the internal quantities, or if the internal quantities are independent of T_*, then the input ΔQ to the system is transferred directly to the output, and

$$\Delta T_* = (\Delta T_*)_0 \equiv G_0 \Delta Q \ , \tag{4.3}$$

where G_0 is the gain without feedback.

The effect of the feedback can be characterized on the basis of the ratio of the ΔT_* with feedback to that without feedback. Thus, by Equations (4.2) and (4.3) we define the feedback gain ratio

$$R_f \equiv \frac{\Delta T_*}{(\Delta T_*)_0} = \frac{G_f}{G_0} = \frac{1}{1-f} \ , \tag{4.4}$$

where f is the feedback factor (Bode 1975, p. 32) or, here, simply the feedback.[1] For $f = 0$, $R_f = 1$; hence $(\Delta T_*)_0$ represents the zero feedback temperature change.

From Equations (4.3), (4.4), and the relationships described in Appendix A, we can write

$$\Delta T_* = \frac{G_0}{1-f} \ \Delta Q \quad , \tag{4.5}$$

where

$$f = G_0 \sum_j \frac{\partial N}{\partial I_j} \frac{dI_j}{dT_*} \ , \tag{4.6}$$

and

$$G_0 = \left(\frac{\partial N}{\partial T_*} \right)^{-1} \ . \tag{4.7}$$

Thus, the determination of ΔT_* induced by an increase in the CO_2 concentration requires knowledge

[1] Hansen et al. (1984) call f (their g) the system gain and R_f (their f) the net feedback factor.

of the associated thermal forcing ΔQ, the zero-feedback gain of the system G_0, and the feedback f. These in turn require knowledge of the partial derivatives of N with respect to the CO_2 concentration, the temperature, and the internal quantities, as well as the total derivative of the internal quantities with respect to the temperature.

In EBMs, Equation (4.5) may be applied either at the Earth's surface (SEBMs) or at the top of the atmosphere (PEBMs). Consequently, ΔQ is the perturbation at the Earth's surface in the SEMB, and it is the perturbation at the top of the atmosphere in the PEMB.

As discussed in greater detail in Appendices A and B of this volume, a wide range of values for G_f has been obtained for SEBMs depending on modeling assumptions. The wide range in the values of G_f obtained from SEBMs is, in part, a consequence of the nonlinear dependence of G_f on f. From Equation (4.4)

$$\frac{\partial G_f}{\partial f} = \frac{G_0}{(1-f)^2}\,, \tag{4.8}$$

hence the change in G_f resulting from a given change in f rapidly increases as $f \to 1$. This sensitivity of G_f to f means that f must be determined with both high accuracy and precision. The difficulty of achieving this has been due to the neglect of certain fluxes in the earlier SEBMs, and to the inability of SEBMs in general to determine the behavior of the climate system away from the surface energy balance level.

The surface and the troposphere are strongly coupled, hence, neither the surface nor the atmosphere can be considered in isolation. Because of the inherent difficulty of specifying the behavior of the atmosphere in terms of the surface temperature in SEBMs and the large sensitivity of ΔT_s in SEBMs to this specification, it is preferable to use models that calculate the atmosphere's behavior based on the fundamental laws of physics.

As shown in Appendix A, the feedback in PEBMs depends on the specification of the behavior of the atmosphere and the Earth's surface. Thus, PEBMs have the same problem as SEBMs; namely, they need to treat the behavior of the climate system away from the energy balance level. In PEBMs this has been done semi-empirically following the initial studies by Budyko (1969) and Sellers (1969). The equilibrium surface temperature change for a CO_2 doubling ranges in PEBMs from 0.6°C (Rasool and Schneider 1971) to 3.3°C (Ramanathan et al. 1979).

In addition to the EBMs mentioned above, there are also one-dimensional (latitude) and two-dimensional (latitude and altitude) EBMs that have played important roles in illustrating the magnitude of several climate feedback processes. These EBMs are reviewed in North et al. (1981).

4.2.2 Radiative-Convective Models

The essential difficulty in using EBMs to determine climate change lies in their inability to accurately and precisely determine the feedbacks. This occurs because of the limited set of internal variables that can be selected in these models and because of the limited knowledge of the relationships of the chosen internal variables to the surface temperature. Simply stated, EBMs are limited because they do not include a physically based model of the atmosphere.

What physical processes must be included in such a model of the atmosphere if the objective is to simulate the change in the surface temperature ΔT_s induced by a change in the CO_2 concentration ΔC? If we knew ΔT_s observationally, as presumably we will in the future, then we could answer the question by sequentially inserting different processes into the model and retaining only those that significantly contribute to ΔT_s. Because we cannot do this yet, we can take the not unreasonable approach of determining which processes are required in the model to reproduce the present-day temperature profile of the atmosphere, $T(z)$. Proceeding in this way, however, does not guarantee that some physical processes essential to the determination of ΔT_s may not be important for the reproduction of $T(z)$, and, therefore, that some essential physical processes (and feedbacks) are not left out of the model.

The transfers of solar and longwave radiation are essential physical processes in establishing the atmospheric temperature profile. Accordingly, a thermodynamic climate model based solely on the thermodynamic energy equation can be developed that includes only the heating and cooling by solar and longwave radiation, respectively. The calculation of the radiative fluxes requires a radiative transfer model (see Chapter 2) and knowledge of

the vertical distributions of the gaseous absorbers—principally water vapor, carbon dioxide, ozone, and clouds—which may be prescribed along with the solar constant, the solar zenith angle, and the albedo of the Earth's surface. The atmosphere may then be subdivided vertically into layers, and the radiative-equilibrium temperature for each layer may be determined by integrating the thermodynamic energy equation in time from an arbitrary initial temperature until equilibrium is established.

Such a purely radiative thermodynamic climate model is successful in reproducing the observed vertical temperature distribution of the stratosphere, but it gives temperatures that are colder in the upper troposphere and warmer near the surface than those observed (Manabe and Strickler 1964). The resultant tropospheric temperature lapse rate, $\Gamma = -\partial T/\partial z$, is larger than the dry adiabatic lapse rate, $\Gamma_{da} \approx 10°C\ km^{-1}$, which defines the neutral stratification for the vertical displacement of unsaturated air. This superadiabatic stratification, $\Gamma > \Gamma_{da}$, is unstable and cannot persist in the actual atmosphere due to the ameliorating processes of convection (i.e., gravitational forces will induce vertical mixing and overturning).

For a vertical model of the atmosphere to calculate a realistic temperture profile, the thermodynamic energy equation must be modified to include the nonradiative transfer of energy from the surface to the atmosphere (Q_{sfc}) as well as the convective redistribution of energy within the atmosphere (Q_{conv}). The physical processes that comprise Q_{sfc} and Q_{conv} are complex because they involve the turbulent transfer of energy in both unsaturated and saturated conditions, and would, if explicitly treated, place an impractical computational burden on the model. Consequently, simplified (parameterized) treatments of these processes have been in use since the pioneering work of Manabe and Strickler (1964), in which Q_{sfc} was determined as an equivalent radiative energy exchange and Q_{conv} was determined by convective adjustment. In this convective adjustment, the temperatures of adjacent model layers are adjusted in an energetically conservative manner such that the lapse rate is restored to a prescribed value Γ_p whenever $\Gamma > \Gamma_p$. This type of model is called a radiative-convective model and, as first shown by Manabe and Strickler (1964), is capable of reproducing many of the observed features of the temperature profiles in both the stratosphere and troposphere.

Since the development of the first RCM by Manabe and Strickler (1964), a large number of RCMs have been constructed with different radiative transfer models, different parameterizations of Q_{sfc} and Q_{conv}, and additional physical processes and feedbacks of potential importance for CO_2-induced (and other) climate changes. The first study with an RCM of CO_2-induced temperature change was carried out by Manabe and Wetherald (1967). In their RCM, the cosine of the solar zenith angle and the length of the day were taken equal to their respective annual mean values for the globe. The surface energy flux was treated as an equivalent radiative exchange, convection was parameterized by convective adjustment with a fixed critical lapse rate, the atmospheric water vapor mixing ratio was calculated assuming a fixed profile of relative humidity, and three cloud layers with fixed pressure were prescribed along with a fixed surface albedo. The equilibrium vertical temperature profiles computed for prescribed CO_2 concentrations of 150, 300 and 600 ppm are shown in Figure 4.1. Each profile exhibits a troposphere between the surface and about 13 km with a lapse rate Γ equal to the prescribed critical value Γ_p, and a stratosphere from 13 to 42 km where the temperature is first isothermal and then increases with increasing altitude. The stable stratifiction in the stratosphere shows that it is in pure radiative equilibrum, whereas the critical lapse rate of the troposphere indicates that it is in radiative-convective equilibrium. Figure 4.1 shows that doubling the CO_2 concentration, either from 150 to 300 ppm or from 300 to 600 ppm, increases the temperature at the surface and in the troposphere, and decreases the temperature in the stratosphere above 20 km.

The surface temperature changes simulated by 17 RCMs for a doubled CO_2 concentration are presented in Table 4.1. The values are all positive and range from a minimum of 0.48°C to a maximum of 4.20°C. These tabulated results primarily depend on the processes included in the RCM. In Appendix A the physical processes are analyzed that result in this wide range of simulated surface temperature changes induced by a doubling of the CO_2 concentration.

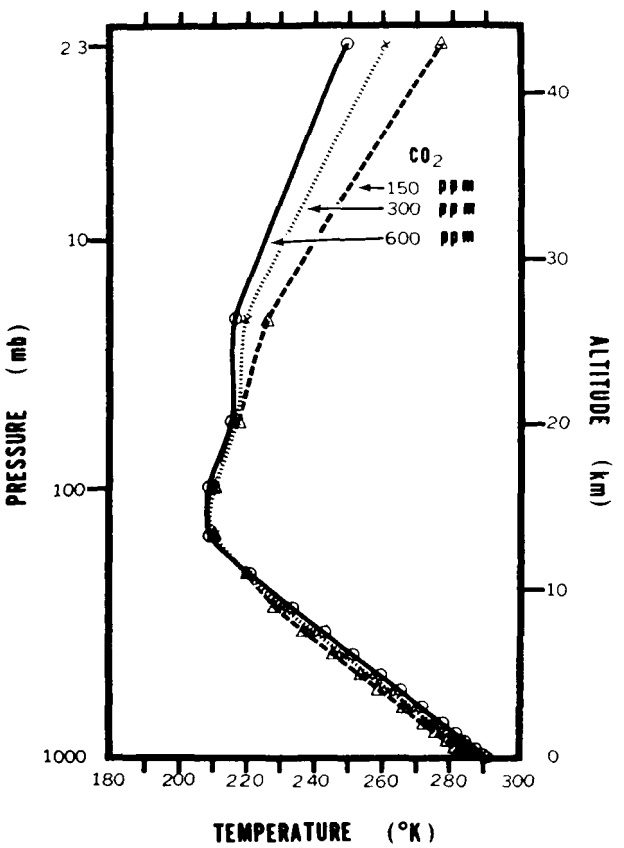

Figure 4.1. Vertical distributions of temperature in a radiative-convective model for fixed relative humidity (FRH) and fixed cloud cover (FCL). The surface temperature change is 2.88°C for a CO_2 doubling from 150 to 300 ppm and 2.36°C for 300 to 600 ppm. Source: Manabe and Wetherald (1967).

Table 4.1
Surface Temperature Change Induced by a Doubled CO_2 Concentration as Calculated by Selected Radiative-Convective Models

Study	ΔT_s (°C)
Manabe and Wetherald (1967)	1.33–2.92
Manabe (1971)	1.9
Augustsson and Ramanathan (1977)	1.98–3.2
Rowntree and Walker (1978)	0.78–2.76
Hunt and Wells (1979)	1.82–2.2
Wang and Stone (1980)	2.00–4.20
Charlock (1981)	1.58–2.25
Hansen et al. (1981)	1.22–3.5
Hummel and Kuhn (1981a)	0.79–1.94
Hummel and Kuhn (1981b)	0.8–1.2
Hummel and Reck (1981)	1.71–2.05
Hunt (1981)	0.69–1.82
Wang et al. (1981)	1.47–2.80
Hummel (1982)	1.29–1.83
Lindzen et al. (1982)	1.46–1.93
Lal and Ramanathan (1984)	1.8–2.4
Somerville and Remer (1984)	0.48–1.74

These CO_2-induced surface temperature changes can be understood in terms of the direct radiative forcing, the response to this forcing in the absence of feedbacks, and the amplification and damping of the response that results from positive and negative feedbacks, respectively. The direct radiative forcing occurs predominantly in the longwave radiation and is characterized by a decrease in the net upward flux at the surface and throughout the atmosphere. The decrease at the surface acts to warm the surface. In the troposphere the magnitude of the decrease in the net upward longwave flux increases with altitude, which acts to warm the troposphere. In the stratosphere the magnitude of the decrease in the net upward longwave flux decreases with altitude, which acts to cool the stratosphere. This cooling tendency occurs primarily because of the greater upward and downward emission from the stratosphere itself. The warming tendency of the troposphere is caused primarily by the increased downward flux from the stratosphere, and the warming tendency of the surface occurs primarily because of the greater downward emission from the troposphere.

The surface temperature response of the climate system without feedbacks to the radiative forcing caused by increased CO_2, ΔR_T, can be characterized by a zero-feedback surface temperature change $(\Delta T_s)_0 = G_0 \Delta R_T$, where G_0 is the climate system gain without feedbacks. The gain G_0 can be estimated from a PEBM as 0.3°C (W m^{-2})$^{-1}$. Thus, $(\Delta T_s)_0 = 1.2$°C for the nominal value of $\Delta R_T = 4$ W m^{-2}. This estimate of $(\Delta T_s)_0$ is in agreement with several RCM studies that were made without feedbacks.

The surface temperature response of the climate system with feedbacks can be characterized by

$$\Delta T_s = \frac{G_0}{1 - f} \Delta R_T \ , \qquad (4.9)$$

where f is the feedback, which varies from -1.5 to 0.7 in the RCM studies of CO_2-induced climate change. The physical mechanisms that contribute to this range include, as T_s increases: the increase in the amount of water vapor in the atmosphere as a consequence of the quasi-constancy of the relative humidity; the decrease in the lapse rate; the changes in cloud altitude, cloud cover, and cloud optical depth; and the decrease in surface albedo.

A study with the of Oregon State University (OSU) two-layer RCM was performed to determine the independence of the above feedbacks. This study shows that the individual feedbacks of water vapor, cloud altitude, and surface albedo are positive; the individual cloud cover and cloud optical depth feedbacks are essentially zero; and the individual moist adiabatic lapse rate (MALR) feedback is negative. This study also shows that the feedbacks of water vapor and either lapse rate, cloud altitude, or surface albedo are additive; hence, these feedbacks are independent. This is not the case for the water vapor feedback with either the cloud cover or cloud optical depth feedbacks. Both variable cloud cover and variable optical depth act as negative feedback mechanisms when they act in conjunction with the positive water vapor feedback.

A positive water vapor feedback occurs when the relative humidity is held fixed because then the absolute humidity increases nonlinearly with increasing temperature due to the Clausius-Clapeyron relation, and the increased water vapor reduces the atmospheric transmissivity, which enhances the CO_2 greenhouse effect. A positive feedback of $f_W = 0.340$ was obtained by the OSU RCM, and values from 0.371 to 0.533 were obtained by the other RCMs, with their actual values depending on the temperatures of the control simulation and whether the atmosphere was clear or cloudy. A reasonable estimate allowing for these dependencies is $f_W = 0.3$–0.4. The value of f_W would be larger (smaller) than this if the relative humidity were not constant and instead increased (decreased) with increasing temperature.

Radiative-convective model studies have shown that the CO_2-induced warming decreases by 12% as the prescribed temperature lapse rate is decreased from 6.5 to 5.0°C km^{-1}. When the lapse rate is allowed to vary, a lapse rate feedback is obtained. A positive feedback is found for the baroclinic adjustment lapse rate (BADJ), which should be applicable in middle and high latitudes where baroclinic adjustment is prevalent. We estimate $f_{BADJ} \sim 0.15$ if $f_W = 0.3$. A negative feedback is found for the MALR with values of –0.409 and –0.262 from the OSU and other RCMs, respectively. Because the former value is probably an overestimate by the two-layer RCM, a reasonable estimate of this feedback is $f_{MALR} \simeq -0.25$ to –0.4. A negative feedback is also found when the lapse rate is determined by penetrative convection with a value of $f_{PC} = -0.654$ given by one RCM. One or both of these negative feedbacks are likely to be found in the tropics where cumulus convection is prevalent.

Cloud feedback can occur from changes in cloud altitude, cloud cover, and cloud optical depth. Three treatments of cloud altitude have been used in RCMs: fixed cloud altitude (FCA), fixed cloud pressure (FCP), and fixed cloud temperature (FCT). Fixed cloud altitude and FCP have frequently been taken to be synonymous even though this strictly is not the case. For FCA the cloud temperature increases by the same amount as the surface temperature, and there is no feedback. For FCP the cloud temperature increases less than the surface temperature; hence, to achieve equilibrium the CO_2-induced surface temperature warming must be greater with FCP than with FCA. Therefore, FCP is a positive feedback process; however, there is insufficient information to evaluate this feedback quantitatively. For FCT, the cloud temperature does not change with a change in the surface temperature; hence, the CO_2-induced surface temperature warming for FCT must be even larger than that required for FCP to achieve equilibrium. The FCT feedback f_{CA} is 0.261 from the Oregon State University RCM and 0.168 to 0.203 from another RCM, the latter is in comparison with the FCP case. Thus, a reasonable range of f_{CA} is perhaps from 0.15 to 0.30.

The feedback caused by changes in cloud cover A_c depends in part on the quantity

$$\delta = -\frac{S_0}{4}\frac{\partial \alpha_p}{\partial A_c} - \frac{\partial R_0}{\partial A_c}, \qquad (4.10)$$

which itself depends on the competing effects of changes in the planetary albedo, α_p, and in the net upward longwave flux at the top of the atmosphere, R_0. An analysis of several RCM studies shows that $\delta \simeq -100$ W m^{-2} for low clouds, $\delta \simeq -50$ W m^{-2} for middle clouds, and $\delta \simeq 5$–80 W m^{-2} for high clouds, the latter generally increasing with cloud emissivity. Thus, for the case $dA_c/dT_s > 0$, low and middle clouds make a positive contribution to the cloud cover feedback, f_{CC}, and high clouds make a negative contribution, while the sign of these contributions reverses for $dA_c/dT_s < 0$. A single RCM study of cloud cover feedback gave a positive value of f_{CC} for doubled CO_2, but a negative value for a

2% solar constant increase. These seemingly contradictory findings can be understood on the basis of the changes in the vertical cloud cover profile, which demonstrates that it is the vertical integral of $\delta \Delta A_c$ that determines the sign and magnitude of the cloud cover feedback. Because of this, cloud altitude feedback is subsumed in cloud cover feedback.

The feedback due to changes in cloud optical depth, τ_c, depends in part on the quantity

$$\phi = -\frac{S_0}{4} \frac{\partial \alpha_p}{\partial \tau_c} - \frac{\partial R_0}{\partial \tau_c} , \qquad (4.11)$$

which also depends on the competing albedo and longwave effects. For black clouds, $\partial R_0/\partial \tau_c = 0$ and $\phi < 0$. For non-black clouds, $\partial R_0/\partial \tau_c < 0$ and ϕ may be positive or negative. Thus, for the case of $d\tau_c/dT_s > 0$, low and middle clouds make a negative contribution to the cloud optical depth feedback f_{OD} and high clouds can make either a positive or negative contribution, while the sign of these contributions reverses for $d\tau_c/dT_s > 0$. Two RCM studies, each with a single cloud layer, found that f_{OD} was negative with values of -0.427 and -1.05 to -1.32. Another study found that f_{OD} was essentially zero for doubled CO_2, but was negative for the case of a 2% solar constant increase. This latter study, as that above for the cloud cover feedback, showed that the cloud optical depth feedback depends on the vertical integral of $\phi d\tau_c/dT_s$ throughout the atmosphere.

Finally, the feedback due to changes in the extent of ice depends in part on

$$-\frac{S_0}{4} \frac{\partial \alpha_p}{\partial \alpha_s} \frac{d\alpha_s}{dT_s} .$$

Because the amount of ice decreases as the surface temperature increases, $d\alpha_s/dT_s < 0$. Consequently, because $\partial \alpha_p/\partial \alpha_s > 0$, the ice-albedo feedback f_{SA} is positive. A single RCM study gives values of f_{SA} from 0.141 to 0.193.

Based on the RCM studies reviewed in this section, we can summarize our knowledge of water vapor, lapse rate, cloud altitude, cloud cover, cloud optical depth, and surface albedo feedbacks as

$$f_W = 0.3 \text{ to } 0.4 ,$$

$$f_{BADJ} \simeq 0.15 ,$$

$$f_{MALR} = -0.25 \text{ to } -0.4 ,$$

$$f_{PC} \simeq -0.65 ,$$

$$f_{CA} \simeq 0.15 \text{ to } 0.30 ,$$

$$f_{CC} = \text{unknown} ,$$

$$f_{OD} \simeq 0 \text{ to } -1.32, \text{ and}$$

$$f_{SA} = 0.14 \text{ to } 0.19 .$$

However, we cannot be highly confident of these quantitative results because RCMs are not models of the global climate system and, more importantly, because RCMs must prescribe (or ignore) the behavior of much of that system. In particular, water vapor feedback is predicted assuming constant relative humidity, lapse rate feedback generally is predicted on the basis of baroclinic or moist adiabatic adjustment, cloud feedbacks are predicted on the basis of greatly simplified cloud models, and surface albedo is predicted on the basis of an assumed constant temperature for the equatorward position of the ice extent. However, the relative humidity may not be constant; the lapse rate may differ from those given by baroclinic or moist adiabatic adjustments; the altitude of clouds may not conform to FCA, FCP, or FCT; the cloud cover and cloud optical depth may vary vertically in a complex manner, and the change in surface albedo depends on snow and ice, the equatorward extent of which may not have a constant dependence on temperature. These changes can be predicted credibly only by a physically based global model that includes the essential dynamical and thermodynamical processes in addition to radiative transfer. Nevertheless, RCMs are extremely valuable because their comparative simplicity permits a more complete understanding of their feedbacks than the more comprehensive, and therefore more complex, models described in the next section.

4.3 STUDIES USING GENERAL CIRCULATION MODELS

Many aspects of climate, such as the horizontal transport of heat and land/sea contrasts, are omitted in RCMs and are inadequately treated in one- and two-dimensional EBMs. Consequently, considerable effort has been devoted to the development of atmospheric GCMs whose formulation and design

are presented in Chapter 3. In this section we review the studies of CO_2-induced equilibrium climate change that have been made using GCMs with several different treatments of the ocean and sea ice. These studies will be categorized in what follows according to whether or not they include the annual cycle of insolation.

4.3.1 Simulations Without the Annual Insolation Cycle

Several studies of CO_2-induced climate change have been made with GCMs coupled to a very simple model of the ocean in which both the oceanic heat storage and transport are ignored and the sea surface temperature is determined diagnostically such that the net energy exchange at the air-sea interface is zero. This type of ocean model is called a *swamp* model because of its similarity to perpetually wet land. In a swamp model the existence of sea ice is predicted whenever the sea surface temperature drops below the temperature at which sea water normally freezes. The studies shown in Table 4.2 have been conducted with GCM/swamp ocean models because of their relative computational economy. These models require about 300 days to attain their equilibrium climates, which is an order of magnitude less time than that required for GCMs that include the simplest ocean formulation with heat capacity. However, because of the absence of heat storage in the swamp model, the diurnal and annual solar cycles must be neglected, or else the ocean would freeze in the nighttime hemisphere and in the polar night latitudes.

It should be recognized that the climate simulated by models using annual mean insolation is markedly different from the observed annual mean climate of the Earth. The models are used to help our understanding of the mechanisms involved in the response of climate, not to produce predictions of changes in regional annual mean climate. In view of this, some studies using annual mean insolation assume a simplified distribution of the oceans and continents (Manabe and Wetherald 1975, 1980; Wetherald and Manabe 1981). In other studies (Hansen 1979; Schlesinger 1982; Washington and Meehl 1983) realistic geography has been used. These and other differences in the models (fixed or prescribed cloud cover and the parameterization of other physical processes) inevitably produce differences in the sensitivity of the models to an increased CO_2 concentration. Here, we attempt to identify the aspects of the response that are qualitatively similar.

Table 4.2
Model Characteristics and CO_2-Induced Changes in Global Mean Surface Air Temperature, ΔT_s, and Precipitation Rate, ΔP, Simulated by GCM/Swamp Ocean Models with Annual Mean Insolation

Study	CO_2 Multiplier	Geography	Clouds	ΔT_s (°C)	ΔP (%)
Manabe and Wetherald (1975)	2	Idealized	Fixed	2.9	7.8
Manabe and Wetherald (1980)	2	Idealized	Computed	3.0	7.0
	4	Idealized	Computed	5.9	11.6
Wetherald and Manabe (1981)	4	Idealized	Fixed	6.0	12.8
Hansen (1979)	2	Realistic	Computed	3.9	6.0
Schlesinger (1982)	2	Realistic	Computed	2.0	5.1
Washington and Meehl (1983)	2	Realistic	Fixed	1.3	2.7
	2	Realistic	Computed	1.3	3.3
	4	Realistic	Fixed	2.7	6.5
	4	Realistic	Computed	3.4	6.0

The changes in global mean surface air temperature simulated for a CO_2 doubling range from 1.3 to 3.9°C, and the accompanying changes in precipitation rate range from 2.7 to 7.8% (Table 4.2). Although the quantitative values vary significantly, the qualitative changes in the global and zonal mean distributions of these quantities show reasonable agreement. Results from a few of the studies listed in Table 4.2 are presented below as examples of the results obtained with GCM/swamp ocean models.

4.3.1.1 Changes in Zonal Mean Air Temperature

Latitude-altitude cross sections of the change in zonal mean air temperature simulated for a CO_2 doubling by Manabe and Wetherald (1975, 1980) with sector versions of the Geophysical Fluid Dynamics Laboratory (GFDL) model are presented in Figure 4.2. In panel (a) the clouds were fixed, and in panel (b) the clouds were computed. Each of the simulations in Table 4.2 shows that the stratospheric temperatures decrease and the tropospheric temperatures increase in response to the doubled

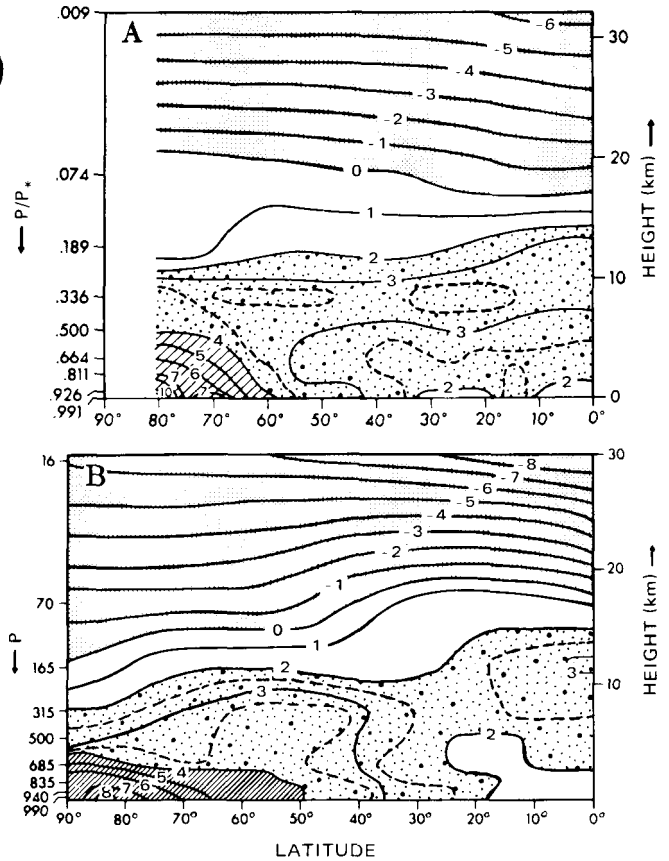

Figure 4.2. The zonal mean temperature differences (°C) for doubled CO_2: (A) the simulation by Manabe and Wetherald (1975); (B) the simulation by Manabe and Wetherald (1980). Dense stipple shows a temperature decrease, light stipple shows increases between 2 and 4°C, and hatching shows increases larger than 4°C. Pressure p is in millibars; surface pressure is p_*. Source: Schlesinger (1984a).

CO_2 concentration. The vertical distribution of CO_2-induced temperature change is similar to that obtained by the RCMs (see Figure 4.1).

The stratospheric cooling increases with increasing altitude in the simulations. In the Manabe and Wetherald (1975) simulation with fixed clouds, the cooling at any altitude in the stratosphere is a maximum in the tropics and approaches a smaller constant value in the poleward direction. In the Manabe and Wetherald (1980) simulation with computed clouds, the CO_2-induced stratospheric temperature decrease also becomes smaller from the tropics toward the poles above about 26 km. Below this altitude, however, the cooling decreases with latitude only to the subtropics and then increases toward the pole. This results in a minimum cooling in the subtropical stratosphere.

The tropospheric warming increases from the surface upward to a maximum value at about 10 km in tropical and subtropical latitudes in the Manabe and Wetherald (1975) simulation. This upward amplification of the tropospheric warming was attributed to the maintenance of the moist adiabatic temperature lapse rate by moist (cumulus) convection, a parameterized subgrid scale process, and the fact that this lapse rate decreases with increasing temperature. The upward amplification is also found in the Manabe and Wetherald (1980) simulation, although it is somewhat more confined to low latitudes. A similar upward amplification was obtained at almost all latitudes in the global model simulation by Schlesinger (1982). In contrast an upward amplification of the tropospheric temperature increase is either nonexistent or very weak in the simulations with the National Center for Atmospheric Research (NCAR) model, both for fixed and computed clouds (Washington and Meehl 1983).

The GFDL simulations also display a poleward amplification of the warming in the lower half of the troposphere, with maximum temperature increases at the surface near 80° latitude that are four to five times the minimum increases in the tropics. This poleward amplification is attributed to the ice-albedo feedback mechanism (whereby an initial warming in high latitudes is amplified by melting snow and/or sea ice which, in turn, results in a large decrease in surface albedo and an increase in the absorbed solar radiation) and to the vertical confinement of this surface warming by the low-level temperature inversion (Manabe and Wetherald 1975).

The contrasting response in low and high latitudes leads to a reduction in the meridional temperature gradient. This is most pronounced near the surface. Manabe and Wetherald (1980) argue that an increase in the poleward transport of energy, mainly in the form of latent heat, also contributes to the reduction in the meridional temperature gradient. This is discussed further below.

The observed meridional temperature gradient contributes to the occurrence of the midlatitude synoptic disturbances (depressions) found in nature. Manabe and Wetherald found a decrease in the transient kinetic energy in the lower atmosphere in midlatitudes, indicating that there are fewer and/or less-intense disturbances, and they suggest that the

reduction in the meridional temperature gradient is probably responsible for this.

Although the GFDL models used by Manabe and Wetherald (1975, 1980) differ in more ways than just their treatment of clouds (particularly, there is a difference in the parameterization of longwave radiative transfer), a comparison of the GFDL simulations with fixed and computed clouds suggests that the influence of clouds on CO_2-induced tropospheric temperature change is of secondary importance.

A comparison of the zonal mean surface air temperature changes simulated by several models is shown in Figure 4.3. The zonal means for the GFDL sector models of Manabe and Wetherald (1975, 1980) both show a minimum warming of about 1.5°C in the tropics followed by an increase toward the subtropics. The rise is more rapid in the 1975 simulation and reaches a maximum value of 2.5°C near 15° latitude. The warming then decreases to about 2°C between 20° and 30° latitude and increases virtually monotonically to a maximum value of nearly 11°C at the highest model latitude. On the other hand, the 1980 simulation does not display a secondary maximum in the tropics; rather, it increases monotonically to a maximum value of about 7.5°C at 83° latitude and then decreases to about 5°C near the pole.

The zonal mean of the simulation using the OSU model (Schlesinger 1982) is quite similar to that of the 1980 GFDL simulation between 30°S and 25°N, with a minimum warming of about 1.25°C in the tropics and an increase to about 3°C in the subtropics. However, in marked contrast to the almost 1°C increase in warming that occurs between 34° and 38° latitude in the 1980 GFDL simulation, there is a decrease in warming in the OSU simulation to about 1.5°C at 55°S and 40°N. This is similar to the result of the 1975 GFDL simulation, albeit there is about a 10° latitude difference in positions of the resultant low-latitude warming maxima. Poleward of these latitudes the warming in the OSU simulation again increases with latitude to a value that is larger in the Arctic than in the Antarctic, namely, 3.9°C at 86°N and 3.0°C at 86°S. If the OSU curve were shifted upward such that the midlatitude minimum warming in each hemisphere intersects the 1980 GFDL curve, the poleward amplification in the OSU simulation would be seen to be approximately half that of the 1980 GFDL simulation.

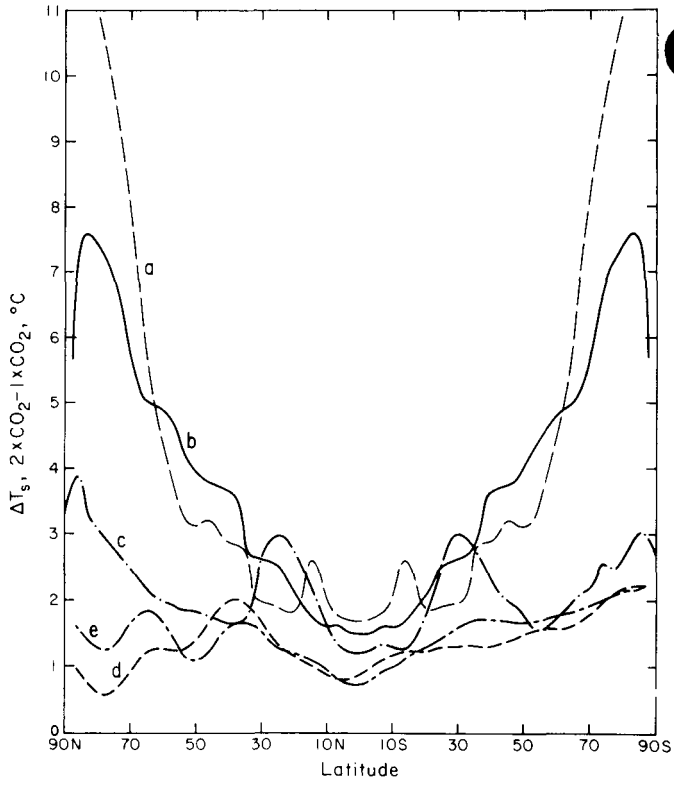

Figure 4.3. Changes in zonal mean surface air temperature (ΔT_s) simulated by five GCMs for doubled CO_2 concentration. Curve (a) from data by Manabe and Wetherald (1975) and curve (b) from data by Manabe and Wetherald (1980) are plotted symmetrically about the equator. Other curves: c, Schlesinger (1982); d, Washington and Meehl (1983); computed clouds; e, Washington and Meehl (1983), prescribed clouds. Source: Schlesinger (1984a).

The zonal mean of the NCAR simulation with computed clouds (Washington and Meehl 1983) shows a minimum warming of about 1°C in the tropics, a relatively uniform warming of about 1.5°C in the midlatitudes of the Southern and Northern Hemispheres, a poleward amplification from about 50°S to 70°S, and no poleward amplification in high northern latitudes. The zonal mean warming in this NCAR simulation is smaller than that obtained by the GFDL and OSU simulations, except near 70°S, where there is agreement with the OSU result.

Figure 4.3 also shows the zonal mean surface temperature change from the NCAR simulation with fixed clouds. This figure shows that inhibiting the response of clouds to increased CO_2 in this NCAR model leads to a larger surface warming almost everywhere. This contradicts the results of other investigators (see Section 4.3.2).

Analysis of the geographical distributions of changes in surface air temperature from the calculations of Manabe and Wetherald (1975, 1980) and Schlesinger (1982) shows that in general there is a negative correlation between changes in surface air temperature and changes in soil moisture. This negative correlation occurs presumably through the change in surface evaporation, with increased (decreased) soil moisture resulting in increased (decreased) evaporative cooling and smaller (larger) warming of the Earth's surface and surface air.

4.3.1.2 Changes in Precipitation and Soil Moisture

In all studies cited in Table 4.2, there is an increase in the areal mean precipitation and evaporation rates. The flux of longwave radiation reaching the surface is enhanced due to the increased CO_2 concentration (and the subsequent increase in atmospheric temperature and water vapor), making more energy available for evaporation. Manabe and Wetherald (1975) point out a further reason for the increase in evaporation. The radiative energy absorbed by the surface is transferred to the atmosphere as sensible and latent heat. The saturation water vapor pressure increases nonlinearly with an increase in temperature. As a result, when the surface temperature increases, a greater proportion of the radiative heating is converted to latent rather than sensible heat. Indeed, Manabe and Wetherald found a decrease in the flux of sensible heat from the surface, further enhancing the latent heat flux (evaporation). The increase in surface temperature increases the saturation vapor pressure at the surface so that the ratio of latent heat (and evaporation) to sensible heat increases. At equilibrium the increase in evaporation must be balanced by an increase in precipitation.

The latitudinal structure of the zonally averaged changes in precipitation is broadly similar in all the studies for which data are available, with a marked increase in precipitation in high latitudes and smaller changes of either sign near the equator (Figure 4.4) The changes in the zonal mean precipiation rate for doubled CO_2 simulated by the NCAR model (Washington and Meehl 1983) with both computed and fixed clouds are shown in Figure 4.4. Both of the NCAR simulations show an increase in the equatorial precipitation rate, with the maximum increase being smaller and shifting northward for fixed clouds compared to that for computed clouds. Both simulations show a maximum decrease near 10°N which agrees with both the 1975 and 1980 GFDL simulations. Both NCAR simulations also show a maximum increase between 40° and 50°N, as does the OSU model, and generally increased precipitation in high northern latitudes, in agreement with both the OSU and GFDL models. The two NCAR results show greater disagreement between each other in the Southern Hemisphere. The model with computed clouds simulates a decrease in the zonal mean precipitation rate near 30° and 65°S, whereas the model with fixed clouds simulates increased rates near these locations. However, both simulations generally show an increase in the precipitation rate poleward of about 40°S, which agree with both the GFDL and OSU simulations.

The differences in low latitudes are not only due to the diversity of models represented, but are also a reflection of the inherent variability of simulated precipitation in the tropics (Manabe et al. 1981). The warming accompanying the increase in CO_2 concentration increases the capacity of the atmosphere to hold moisture. There is a marked increase in the transport of warm moist air into high latitudes, which produces the increase in precipitation found there.

The increases in evaporation are relatively uniform with latitude, whereas there are large increases in precipitation in high latitudes and small increases, or even reductions near 35° to 50°, associated with a potential shift in the latitude of maximum precipitation. As a result there is a marked reduction in the supply of moisture from the atmosphere to the surface (precipitation minus evaporation), and the model soil moisture decreases in these regions. In high latitudes the increase in precipitation exceeds that in evaporation, and there is an increase in model runoff. The region of decreased precipitation near 35° to 50° latitude in Figure 4.4 coincides approximately with the main decrease in transient eddy kinetic energy, so it seems likely that the reduction in meridional temperature gradient and subsequent reduction in the number or intensity of atmospheric disturbances is responsible for the reduction in precipitation at these latitudes.

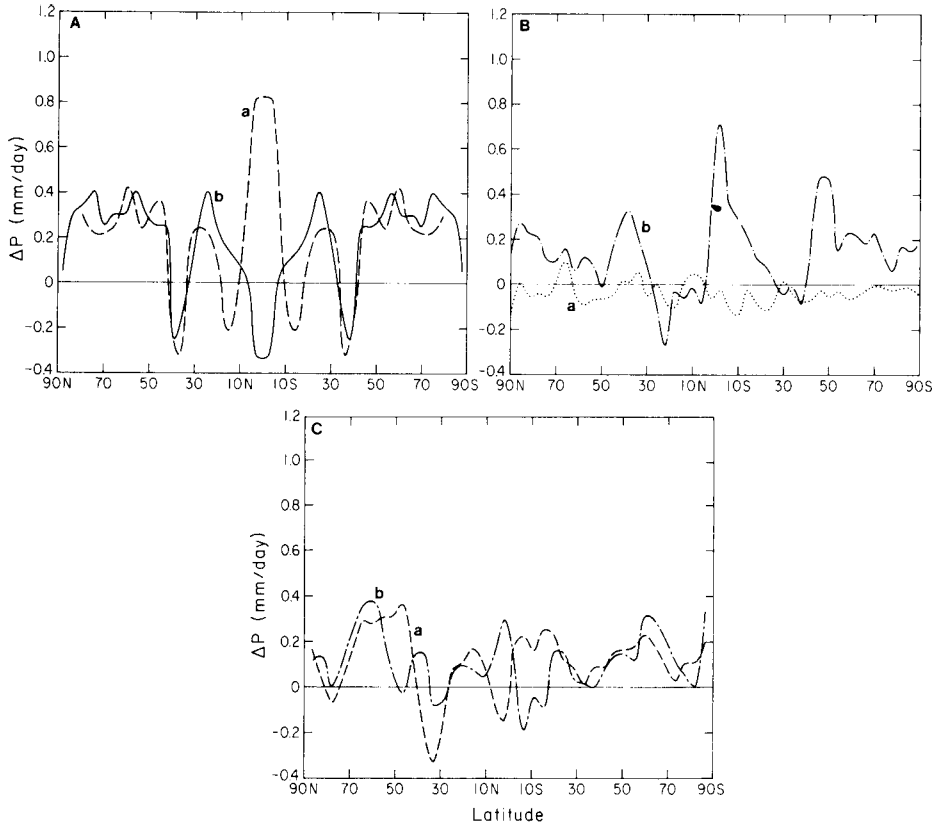

Figure 4.4. The change in zonal mean precipitation rate (ΔP) simulated by six GCMs for doubled CO_2. (A) Data from Manabe and Wetherald (1975, curve a; 1980, curve b) plotted symmetrically about the equator. (B) Data from Gates et al. (1981, curve a) and Schlesinger (1982, curve b). (C) Data from Washington and Meehl (1983; curve a, predicted clouds; curve b, prescribed clouds). Source: Schlesinger (1984a).

There is a tendency for the tropical and midlatitude regions of minimum and maximum warming to occur where the soil is moistened and dried, respectively. Similarly, there is a tendency for the tropical and midlatitude regions of increased and decreased soil moisture to occur where the precipitation rate increased and decreased, respectively.

Figure 4.4 also shows the changes simulated by the OSU model with prescribed sea surface temperature and sea ice (Gates et al. 1981). It is evident that generally, these changes are not only considerably smaller than those of the other models, they are negative almost everywhere.

The geographical distributions of the soil moisture change simulated by the sector models of Manabe and Wetherald (1975, 1980) are presented in Figure 4.5. This figure shows that in both simulations the soil moisture decreased almost everywhere poleward of 35° latitude and increased over most of the continent equatorward of this latitude. The maximum drying of the soil occurs in a band that stretches from coast to coast centered near 35° and 40° latitude in the 1975 and 1980 simulations, respectively. This drying band in each simulation is the most prominent feature of the zonal mean soil moisture change. These calculations raised concern about the potential effects of increased CO_2 concentration on agricultural production in middle latitudes.

4.3.1.3 Changes in Cloud Cover

The realistic representation of clouds in climate models is one of the main problems facing numerical modelers. Nevertheless, some studies have been made with models in which crude parameterizations of cloud cover have been included. Manabe and Wetherald (1980) and Washington and Meehl (1983) found that cloud cover decreased in most of the tropics and in the middle troposphere, but increased near the surface and in high latitudes near the tropopause when the CO_2 concentration

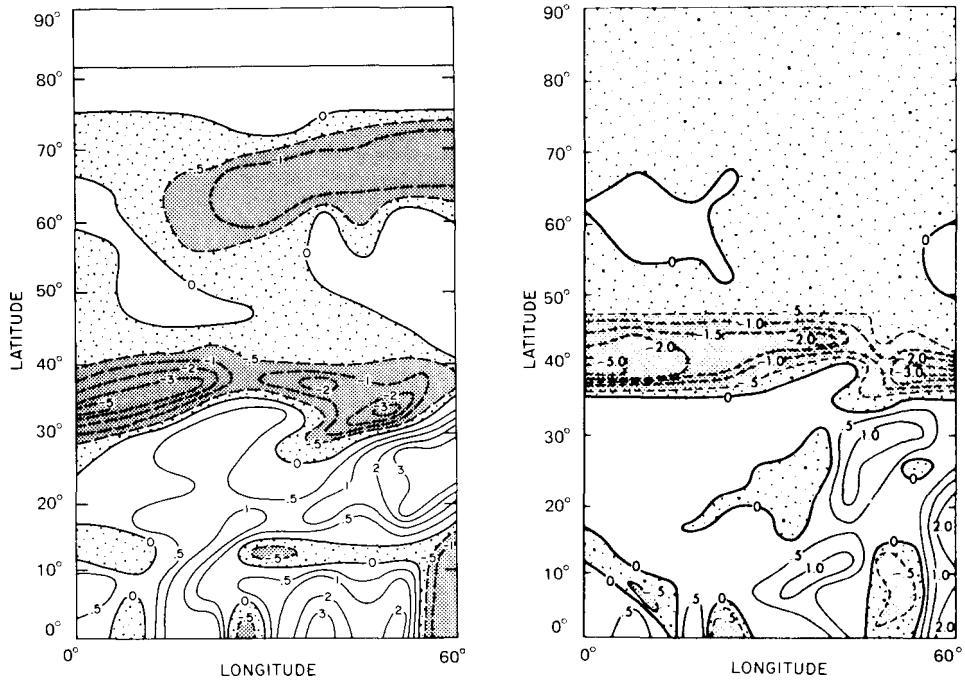

Figure 4.5. Manabe and Wetherald (1975, 1980) simulations of change in soil moisture (cm) for doubled CO_2. Sparse shading indicates decreases smaller than 0.5 cm; dense shading indicates decreases larger than 0.5 cm; Left, data from 1975; right, data from 1980. Source: Schlesinger (1984a).

was doubled. Hansen (1979) noted that the cloud cover parameterization in the Goddard Institute for Space Studies (GISS) GCM, in which cloud top height increased with increasing temperature, provided a positive feedback mechanism (see Appendix A). This may have contributed significantly to the large warming (3.9°C) obtained in his CO_2 doubling experiment.

Wetherald and Manabe (1980) have made a detailed analysis of the changes in cloudiness in their model caused by increasing the solar constant. They found the changes in cloudiness to be qualitatively similar to those caused by increased CO_2. As in the integration with increased CO_2, there is an increase in the cloudiness of the lowest model layer in high latitudes and in the subtropics. It was noted previously that evaporation increases at the expense of sensible heat. Thus, there is a marked increase in the transfer of moisture in the lowest layer, with little change in the transfer of heat. The stable stratification of the lower atmosphere in the subtropics and in high latitudes inhibits the transport of this extra moisture out of the lowest layer, producing an increase in relative humidity and cloudiness. In the middle and upper troposphere, cloudiness decreases. This change is most marked at those latitudes where the (zonally averaged) motion is upwards. The zonally averaged vertical circulation is weaker in the integration with the increased solar constant, so this pattern is to be expected. It is not obvious immediately why cloudiness should decrease where there is a reduction in zonally averaged descending motion. Wetherald and Manabe (1981) argue that the cloudiness decrease in this region is due to the increase in the variance of vertical velocity, which lowers the relative humidity there. Hence, the area mean precipitation increases, but the area mean cloudiness decreases. Further discussion of cloudiness is included in Section 4.3.4.

4.3.2 Early Simulations With the Annual Insolation Cycle

In the previous section results were presented from GCM/swamp ocean models in which, necessarily, the annual cycle of insolation was omitted. Although these models are relatively economical to run to equilibrium and provide some insight into the change in annual mean climate induced by increased CO_2, their projections of regional climate change must be viewed with caution because of their

neglect of the annual insolation cycle and, therefore, the seasonal variation of climate.

Two different approaches to the treatment of the ocean and sea ice have been used in calculations that include the annual insolation cycle. In the first and more usual approach, the sea surface temperature and sea ice extent are predicted by an ocean/sea ice model in which at least the heat capacity of the upper ocean must be included to permit the annual insolation cycle. In the second approach, the effect of CO_2 is regarded as a perturbation, because the changes in the global mean radiative and turbulent heat fluxes caused by doubled CO_2 are considerably less than 10% of their present day values (Manabe and Wetherald 1975). In the control integration, sea surface temperatures are prescribed from climatology, whereas in the increased CO_2 integration, the changes in sea surface temperature are prescribed from a succession of perturbation experiments that approximate equilibrium with increasing accuracy. The first (or predicted) approach has the advantage that the sea surface temperature and sea ice extent can interact with the atmosphere to establish the equilibrium climate. This approach has the disadvantage that deficiencies in the atmospheric and/or ocean models can produce errors in the sea surface temperatures and sea ice extent of the control ($1 \times CO_2$) integration, which can influence the CO_2-induced climate change. The second (or prescribed) approach has the advantage that, for contemporary GCMs, the simulated control climate is closer to the observed climate than that with predicted sea surface temperature and sea ice extent. The disadvantage of this method is the need to separately determine the CO_2-induced change in sea surface temperature and sea ice extent, and the strong influence of these prescribed changes on the CO_2-induced climate. Studies using both of these approaches are summarized in Table 4.3 and are described below.

4.3.2.1 Studies With Prescribed Sea Surface Temperatures and Sea Ice Extent

The changes in the surface and atmospheric heating rates caused by a CO_2 doubling or quadrupling are a small fraction of the ambient heating. Therefore, in the prescribed approach, these changes are assumed to be sufficiently small to be regarded as a perturbation. Mitchell and co-workers at the United Kingdom Meteorological Office (UKMO) performed a set of experiments in which the sea surface temperatures and sea ice extent were prescribed, and the response to increased CO_2 was determined sequentially. A high degree of accuracy can be attained in the simulation of present day climate using prescribed climatological sea surface temperatures and sea ice extent, and the transport of heat caused by ocean currents is included implicitly. In the first experiment (Mitchell 1983), the response of the ocean was ignored. In the second (Mitchell 1983), the ocean temperature increase was assumed to be the same everywhere. In the third (Mitchell and Lupton 1984), the ocean temperature changes were prescribed as a function of latitude on the basis of the previous two experiments.

The sensitivity of the model to an instantaneous increase in CO_2 in the absence of oceanic feedbacks was simulated by Gates et al. (1981) and also in the first experiment by Mitchell (1983), and the results are shown in Table 4.3. The rise in global mean surface temperature resulting from changes in temperature only over sea ice and the continents for a doubling of CO_2 concentration was about 0.2°C, whether cloudiness was predicted, as in the simulation with the OSU GCM by Gates et al. (1981), or cloudiness was fixed, as in the simulation with the GCM by Mitchell (1983). This value is an order of magnitude smaller than that obtained with the OSU GCM/swamp ocean model by Schlesinger (1982) (see Table 4.2). Furthermore, the global mean and zonal mean precipitation changes simulated by a GCM with prescribed sea surface temperature and sea ice extent are negative (Table 4.3 and Figure 4.4) in contrast to the results obtained by a GCM with predicted oceanic quantities (Tables 4.2 and 4.3).

The net surface heating in the above experiments with prescribed oceanic quantities increased by 3.0 to 3.5 W m^{-2} on doubling CO_2, indicating that had the ocean been free to respond, the surface temperature would have increased until the ocean was once more in equilibrium with the atmosphere. Mitchell (1983) repeated the $2 \times CO_2$ experiment, additionally enhancing sea surface temperatures everywhere by 2°C, and found that the magnitude of the change in net surface heating was only 0.8 W m^{-2}. Therefore, the ocean and atmosphere were

Table 4.3
Model Characteristics and CO_2-Induced Changes in the Global Mean Surface Air Temperature, ΔT_s, and Precipitation Rate, ΔP, Simulated by GCMs With the Annual Insolation Cycle

Study	CO_2 Multiplier	Sea Surface Temperature and Sea Ice	Geography	Clouds	ΔT_s^a (°C)	ΔP^a (%)
Gates et al. (1981)	2	Prescribed[b]	Realistic	Computed	0.20	−1.5
	4	Prescribed[b]	Realistic	Computed	0.46	−3.3
Mitchell (1983)	2	Prescribed[c]	Realistic	Fixed	0.16	−2.5
	2	Prescribed[d]	Realistic	Fixed	2.25	5.2
Mitchell and Lupton (1984)	4	Prescribed[e]	Realistic	Fixed	4.7	7.5
Manabe and Stouffer (1979, 1980) and Manabe et al. (1981)	4	Predicted[f]	Realistic	Fixed	4.1	6.7
Wetherald and Manabe (1981)	4[*]	Predicted[f]	Idealized	Fixed	4.8	10.0
Hansen et al. (1984)	2	Predicted[g]	Realistic	Computed	4.2	11.0
Washington and Meehl (1984)	2	Predicted[h]	Realistic	Computed	3.5	7.1
Wetherald and Manabe (1986)	2	Predicted[f]	Realistic	Computed	4.0	8.7

[a] Annual mean values.
[b] Prescribed sea surface temperatures and sea ice extents updated at 1-day intervals from monthly climatological values.
[c] Prescribed sea surface temperatures and sea ice extents updated at 5-day intervals from Fourier analyzed climatological values.
[d] As in footnote *c* except 2°C was added to the prescribed climatological sea surface temperatures in the 2 × CO_2 simulation.
[e] As in footnote *c* except a change in sea surface temperature that varied with latitude was added to the prescribed climatological sea surface temperatures in the 4 × CO_2 simulation. In low latitudes the change in sea surface temperature was estimated by requiring that there should be no net increase in surface heating on quadrupling CO_2, whereas in higher latitudes the changes were based on Figure 18 of Manabe and Stouffer (1980).
[f] Slab ocean model with depth of 68 m and no horizontal heat transport. Sea ice thickness predicted based on thermodynamic sea ice model.
[g] Slab ocean model with prescribed seasonally varying depth based on observations, but constrained not to excceed 65 m. Meridional heat transport in the ocean prescribed based on GCM simulation with prescribed observed sea surface temperatures. Sea ice thickness predicted based on thermodynamic sea ice model.
[h] As in footnote *f* except with depth of 50 m.

much closer to equilibrium than in the first experiment.

The changes in temperature in the second experiment were predetermined largely by the prescribed change in sea temperatures. There was, for example, no reduction in the meridional temperature gradient in the lower troposphere. The zonally averaged changes in the hydrological cycle, however, were qualitatively very similar to the models with an interactive ocean, as can be seen in Figure 4.6, which compares the time latitude variation of precipitation minus evaporation ($P-E$) with that from Manabe and Stouffer (1980). The unshaded and black areas indicate an increase and decrease in both experiments, respectively. An increase was simulated in low latitudes in summer and in high latitudes for all months. A decrease of $P-E$ was simulated in the subtropics, except in the Northern Hemisphere in summer when there was a decrease in middle latitudes. The fact that similar results were obtained under two very different sets of assumptions suggests that the mechanism causing the change is common to both experiments.

The following hypothesis may account for much of the similarity. In each approach the change in boundary conditions (increased CO_2 concentration, enhanced sea surface temperatures) produces a warmer, moister atmosphere. The meridional (north-south) moisture flux in the model is proportional to qv, where q is the specific humidity and v is the meridional wind. The zonally and vertically averaged meridional moisture fluxes from the control integration (Figure 4.7, dashed line) show the transport of moisture from the subtropics to high latitudes, and from the winter to the summer tropics. If changes in the circulation (v) are sufficiently small, the changes in moisture flux will be dominated by the increase in humidity (q), and the main troughs and peaks in Figure 4.7 will be enhanced as found in the anomaly simulation (solid line). There is then a greater flow of moisture into high latitudes, which must be balanced by an increase in the flux of moisture to the ground ($P-E$, see Figure 4.6). In the winter hemisphere, the increased flow of moisture out of the region between the equator and 40° is consistent with the local decrease in $P-E$. Hence,

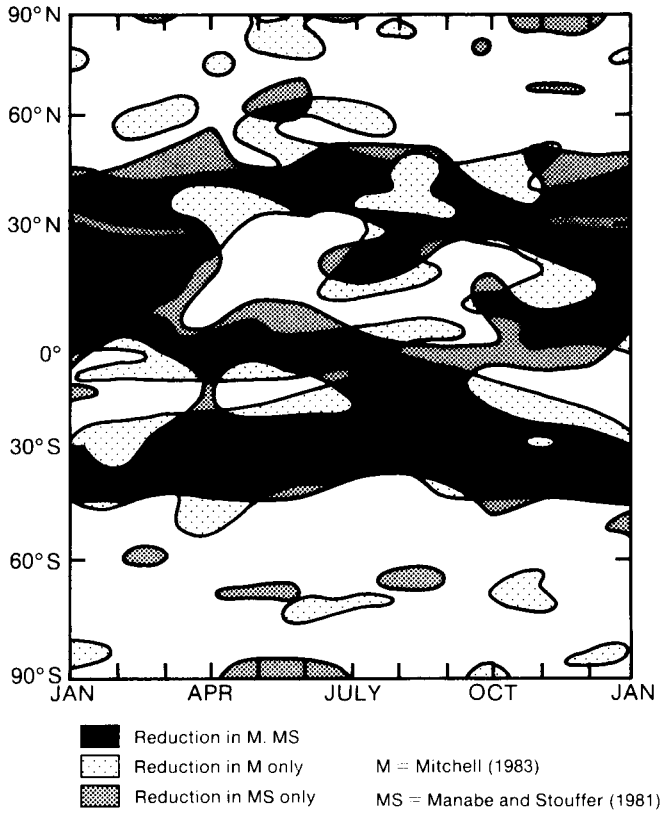

Figure 4.6. Latitude-time distribution of change of precipitation minus evaporation ($P - E$) in the experiments by Manabe and Stouffer (1980) and Mitchell (1983). Source: Gilchrist (1983).

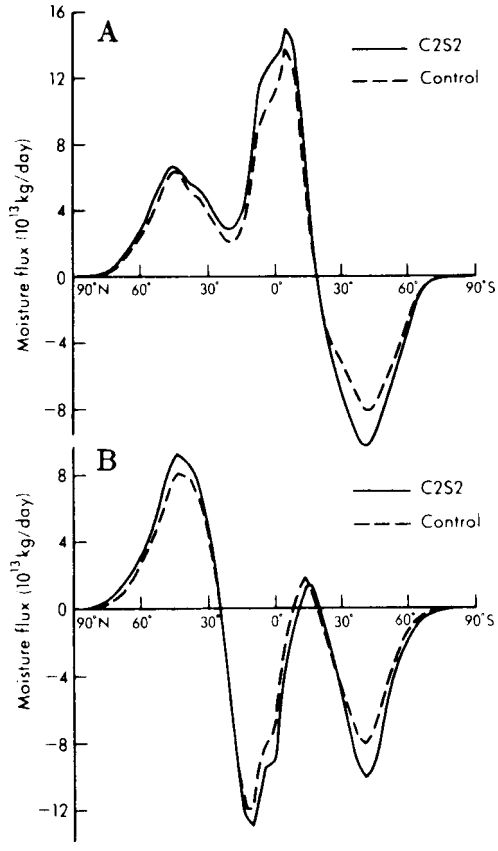

Figure 4.7. Seasonal mean meridional transport of moisture (10^{13} kg d^{-1}), averaged over 2 years. Solid line, doubled CO_2 integration with a change in sea surface temperature of 2°C prescribed everywhere (C2S2); dashed line, control. (A) June to August; (B) December to February. Source: Mitchell (1983).

much of the simulated change in the hydrological cycle may be explained in terms of the increase in moisture content of the atmosphere alone. However, changes in circulation modify this simple picture, especially in middle latitudes in summer.

Mitchell and Lupton (1984) have further refined the estimate of sea surface temperature changes to include a latitudinal variation. In low latitudes, sea surface temperature changes were estimated by not allowing the net surface heating to change for a quadrupling of CO_2. This is equivalent to requiring the meridional convergence of heat by the oceans to remain unchanged. In higher latitudes, the changes were based on Figure 18 of Manabe and Stouffer (1980). In the 4 × CO_2 integration, the global mean atmospheric humidity increased by 29%; and, as one might expect from the arguments advanced above, there were significant increases in precipitation in the main regions of convergence, including middle to high latitudes in winter, and the low latitudes in summer (over South America, South Africa and Northern Australia during December to February, and over the southern United States, northern Africa and southeast Asia during June to August, Figure 4.8). In the subtropics, there were statistically significant decreases in precipitation, including a region over southern Europe and extending into central Asia in summer. In general, the response of the model was very similar to that reported by GFDL. For example, the changes in model soil moisture during June to August shown in Figure 4.8 are broadly similar to those shown in Figure 4.12.

In one respect, however, there was a marked difference. In the UKMO experiment the warming in the tropical upper troposphere is two to three times that at the surface, in contrast to modest amplification with height evident in Figure 4.9. A similar contrast is found between the GISS and later GFDL results (see Figures 4.36, 4.37). This is probably because both the UKMO and GISS models use a penetrative convection scheme that is more efficient

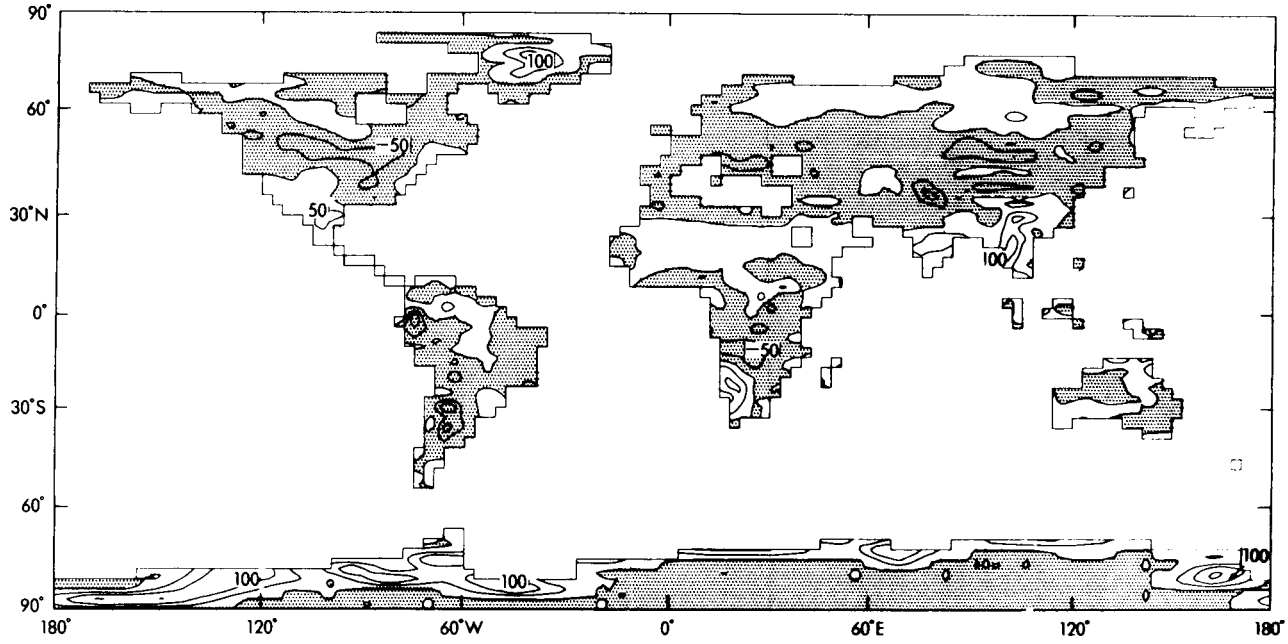

Figure 4.8. Changes in model soil moisture for the June to August period caused by quadrupling the CO_2 concentration and including prescribed increases in sea surface temperature that increase with latitude. Isopleths are shown every 50 mm. Areas of decrease are stippled. Source: Mitchell (1984).

in transporting heat and moisture into the upper troposphere than the moist convective adjustment scheme used by GFDL (and NCAR).

It should be noted that the UKMO model uses a higher resolution than is usual in CO_2 studies, and hence is more able to resolve synoptic disturbances. For example, in the control integration there is westerly flow as observed over western Europe in summer (Mitchell, 1983) rather than the strong northeasterly flow characteristic of low resolution models. Rowntree and Bolton (1983) found that soil moisture anomalies over Europe were more persistent when the horizontal resolution of the model was reduced, as the low level flow became easterly rather than westerly, and the frequency of moisture-bearing disturbances from the neighboring ocean areas was reduced. However, the UKMO results and those from GFDL (Manabe et al 1981) indicate that the drying in northern midlatitudes in summer (Figures 4.8 and 4.12) is not particularly sensitive to horizontal resolution.

Wilson and Mitchell[2] have investigated the CO_2-induced changes in variability over western Europe

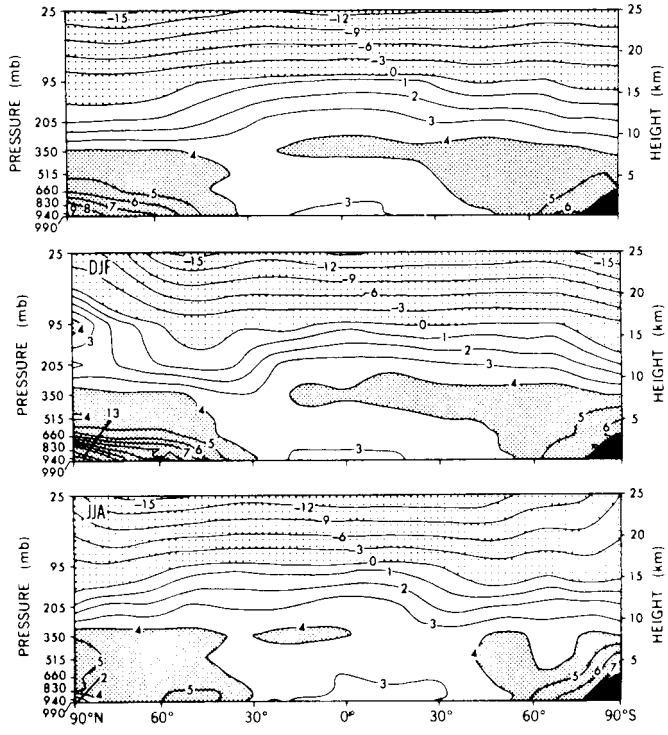

Figure 4.9. Latitude-altitude distribution of the change in zonal mean annual mean temperature (top), December-January-February (DJF) temperature (middle), and June-July-August (JJA) temperature (bottom) between the 4 × CO_2 and 1 × CO_2 simulations of Manabe and Stouffer (1980). Source: Manabe and Stouffer (1980).

[2] C. A. Wilson and J. F. B. Mitchell, "Simulated Climate and CO_2-Induced Climate Change over Western Europe," manuscript in preparation.

in the UKMO simulation. They find, for example, that the frequency of easterly winds over eastern England is halved, and that the frequency of precipitation and the mean amount on wet days are reduced over southern Italy. The statistical significance of the changes has been assessed using tests developed by Katz (1983). Wilson and Mitchell point out that although their work illustrates the potential of numerical models to produce data for impact studies, there is little consistency from model to model in the detailed regional changes simulated with increased CO_2.

The experiments carried out by Mitchell and coworkers at UKMO were intended to be complementary to those carried out elsewhere by using assumptions which, though reasonable, are substantially different. In spite of this, many of the results obtained are similar and reinforce each other. Moreover, by examining their differences, the sensitivity of the results to the variations in formulation can be assessed.

4.3.2.2 Studies With Predicted Sea Surface Temperatures and Sea Ice Extent

The first simulation of the seasonal variation of CO_2-induced climate change with a model in which sea surface temperatures and sea ice were predicted was carried out by Manabe and Stouffer (1979, 1980). In their study, the GFDL GCM was coupled to a fixed depth mixed-layer ocean model without horizontal and vertical heat transports. The 68 m mixed-layer depth was chosen to best fit the observed annual cycle of sea surface temperatures. To increase the statistical significance of their results, Manabe and Stouffer investigated the climatic changes induced by a quadrupling of the CO_2 concentration. Subsequently, a follow-up study was conducted by Wetherald and Manabe (1981) to elucidate the differences in the climatic changes with and without the annual insolation cycle. These early studies are summarized in Table 4.3 and are described below. More recently three simulations of the equilibrium climate change for doubled CO_2 have been performed by Hansen et al. (1984), Washington and Meehl (1984), and Wetherald and Manabe (1986) with the GISS, NCAR, and GFDL GCMs coupled to mixed-layer ocean models. These more recent studies also are summarized in Table 4.3 and are described in Section 4.3.4.

The latitude-altitude distributions of changes in zonal mean temperatures simulated by Manabe and Stouffer (1979, 1980) for a CO_2 quadrupling are presented in Figure 4.9 for the annual mean, December-January-February (DJF), and June-July-August (JJA) averages. The annual mean temperature changes for quadrupled CO_2 with the seasonal insolation cycle, realistic geography, and fixed clouds shown in Figure 4.9 (top) are qualitatively similar to those obtained for doubled CO_2 with idealized geography and fixed or predicted clouds and without the seasonal insolation cycle, as obtained by Manabe and Wetherald (1975, 1980) (see Figure 4.2). In particular, the stratosphere cools, with the cooling increasing with altitude, and the troposphere warms, with the warming increasing with altitude in the tropics and with latitude at the surface. The surface warming is larger in the Arctic than in the Antarctic, as was also found in the doubling simulation by Schlesinger (1982) (see Figure 4.3). Figure 4.9 shows, however, that the CO_2-induced temperature changes are not uniform throughout the year, particularly near the surface in the Arctic where there is a distinct winter maximum and summer minimum in the warming.

The geographical distribution of the change in the annual mean surface air temperature is shown in Figure 4.10 along with the corresponding maps for DJF and JJA. The annual mean temperature change shows warming everywhere with minimum values of about 2.5°C in the tropics, poleward amplification in both hemispheres, and warming in the Arctic that is about 4°C larger than that in the Antarctic. Figure 4.10 also shows a large seasonal variation of the CO_2-induced warming in the middle and high latitudes of both hemispheres with greater warming in winter and lesser warming in summer. The greatest warming occurs over sea ice in winter, leading to the pronounced east-west asymmetry evident in the annual mean changes. Conversely, the temperature rises over the Arctic in summer are much smaller than those over the surrounding continents. Over land, where the surface is dry or has become sufficiently dry to restrict evaporative cooling, the surface warming is likely to be enhanced as described previously. This mechanism undoubtedly contributes to some of the longitudinal asymmetries

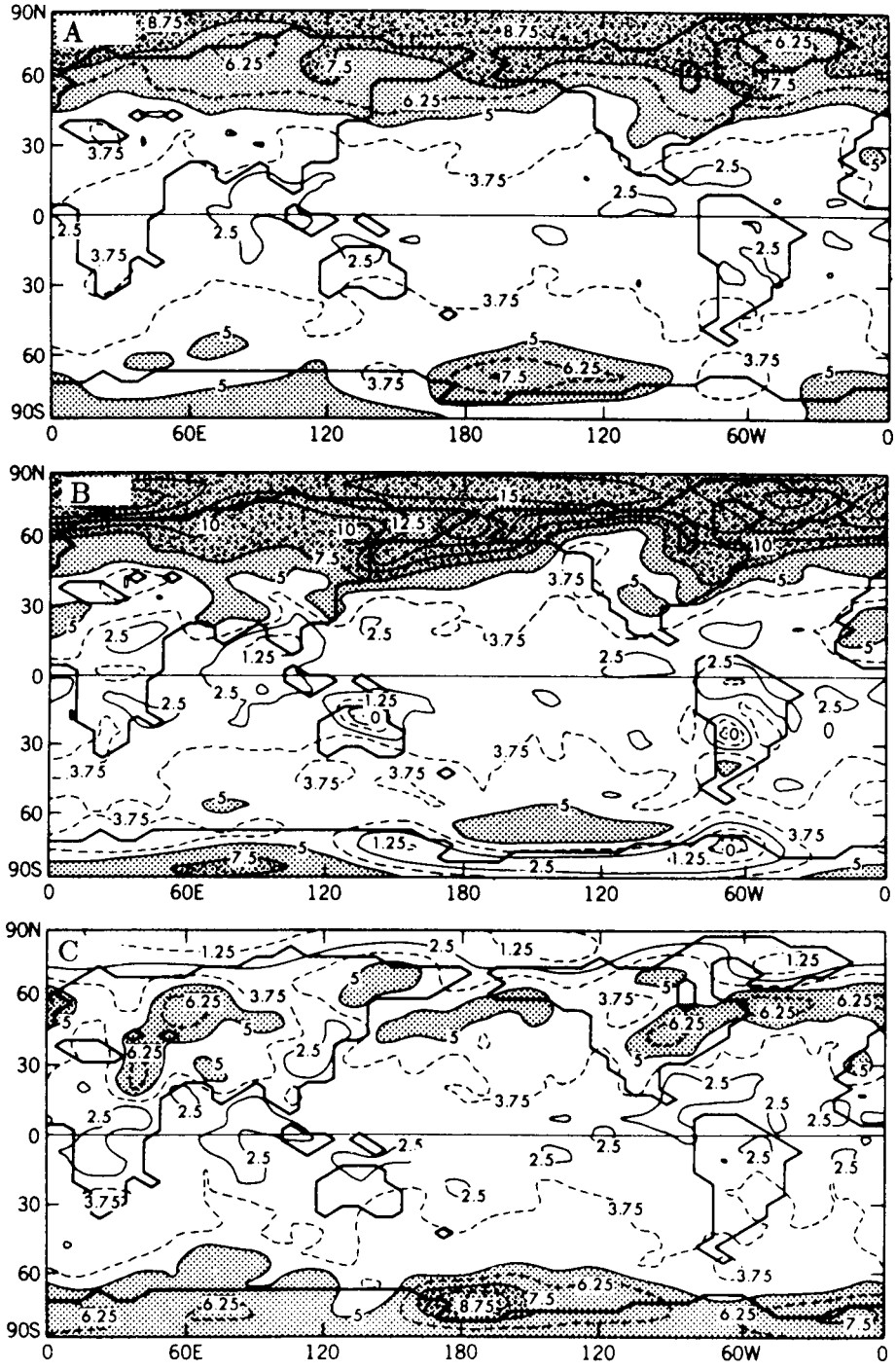

Figure 4.10. GFDL model simulation of the change in surface air temperature for quadrupled CO_2. (A) Annual mean; (B) DJF; (C) JJA. Sparse shading indicates increases between 5 and 7.5°C, dense shading indicates increases greater than 7.5°C. Source: Manabe and Stouffer (1980).

evident in summer. However, Manabe and Stouffer (1980) note that many of the small-scale variations may not be statistically significant given the year-to-year variability in seasonal mean temperatures.

The seasonal nonuniformity of the CO_2-induced temperature change is strikingly revealed in Figure 4.11, which shows the annual cycle of the change in the zonal mean surface air temperature. The zonal mean warming is a maximum in winter and minimum in summer over both the oceans and continents in the high latitudes of the Northern Hemisphere. This indicates a large reduction of the

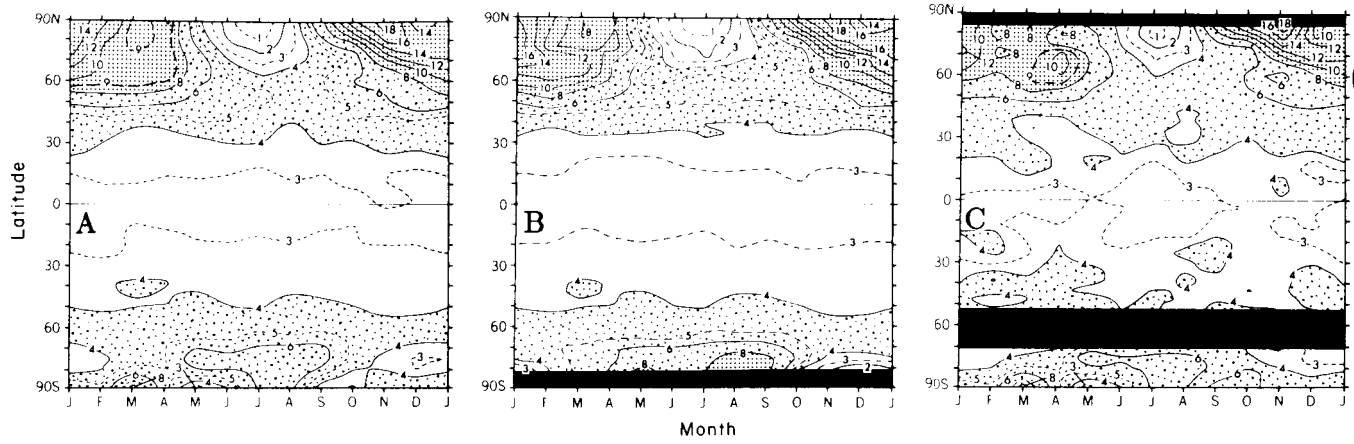

Figure 4.11. GFDL model simulation of the annual cycle of the change in zonal mean surface air temperature (°C) for quadrupled CO_2. (A) Oceans and continents; (B) oceans; (C) continents. Sparse shading indicates increases between 4 and 8°C, dense shading indicates increases larger than 8°C. Source: Manabe and Stouffer (1980).

amplitude of the annual temperature cycle in these latitudes.

In the summer Arctic, the surface temperature is constrained to remain at the freezing point until all the ice has melted, at which time the surface temperature changes little because of the thermal inertia of the mixed layer. Because this holds for both present day and increased CO_2 integrations, the changes in summer are small. Further, the temperature-albedo feedback over the continents is minimal because there is little snow cover in summer. In the winter half of the year, changes in high latitudes are large because the atmospheric warming is confined to a shallow stable layer, and snow and ice cover are sufficient to allow significant ice- and snow-albedo feedback. In the spring this effect is particularly marked over land when snow cover is still extensive and insolation is large. Over much of Antarctica the temperature remains below freezing throughout the year because of the elevation of the surface, and there is little amplification of the surface warming by ice- and snow-albedo feedback. However, the absorption of solar radiation over the high-latitude ocean is increased substantially in summer because the ocean has a much lower albedo than sea ice, but the surface temperature changes little because of the large thermal inertia of the mixed layer. This thermal lag also delays the onset of freezing in autumn. The ice is both thinner and less extensive throughout the rest of the year, allowing a considerable increase in the flux of heat from the ocean to the atmosphere and contributing to the increases in surface temperature, particularly in the autumn.

There is little seasonal variation in the surface temperature changes within the tropics. This is not surprising in view of the limited seasonal variation in present day climate and the large thermal inertia due to the predominance of oceans at these latitudes.

The geographical distribution of the change in the annual mean precipitation rate are discussed by Manabe and Stouffer (1980). There is a predominance of precipitation rate increases poleward of about 45° latitude in both hemispheres in this simulation. Regions of both increased and decreased precipitation rates are located between 45°N and 45°S, with the largest changes occurring between ±30° latitude, which agrees with the OSU global model and the GFDL sector models. The global mean precipitation rate increased by 6.7% (Table 4.3).

Manabe and Stouffer (1980) found that the latitudinal distribution of the supply of moisture to the surface, that is, $P - E$, was qualitatively similar to that without the annual insolation cycle, with marked increases in high latitudes and a reduction near the Equator. However, in the seasonal model the zone of reduced $P - E$ migrates latitudinally through the seasons, this variation being pronounced over the continents, which contributes to the seasonal variation of surface wetness. In the Northern Hemisphere during summer, two drier zones occur near 65° and 45°N in the integrations with quadrupled CO_2.

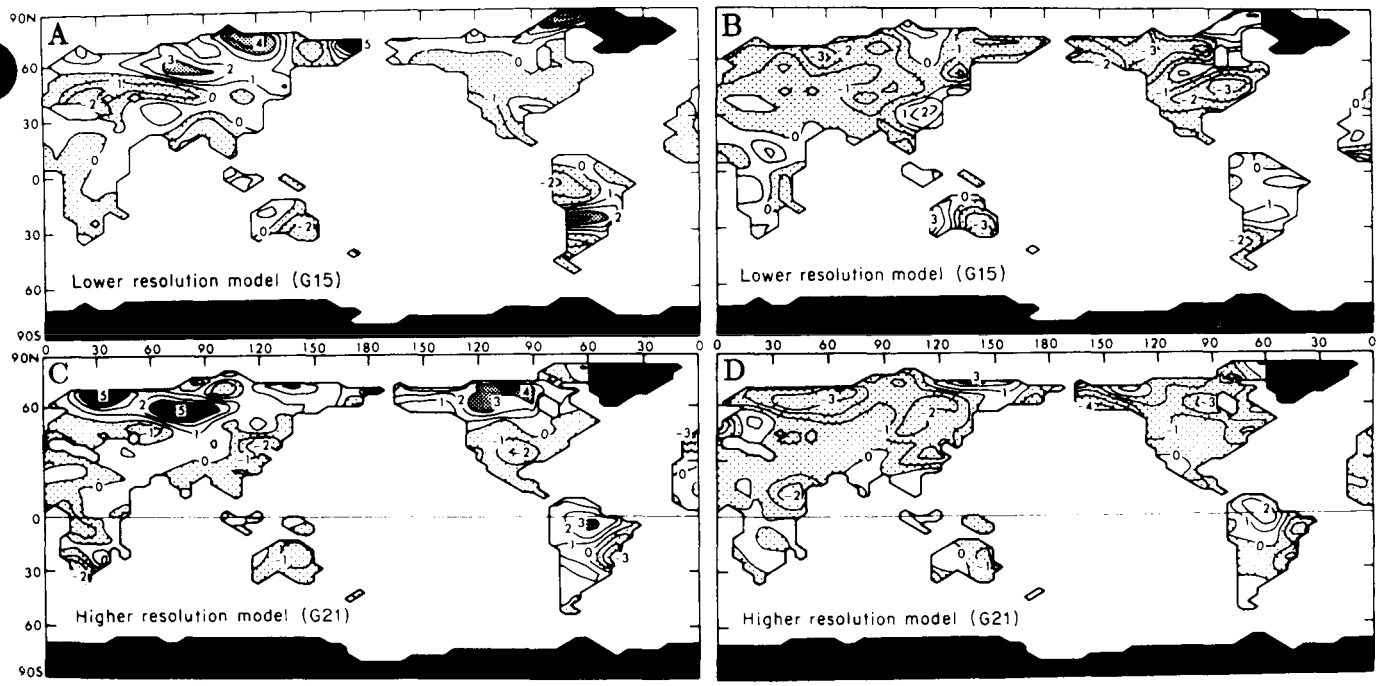

Figure 4.12. GFDL model simulation of the change in soil moisture (cm) for quadrupled CO_2. Upper and lower panels are simulations with 15 and 21 waves, respectively (for both longitude and latitude); left and right panels are for Northern Hemisphere spring and summer, respectively. Source: Manabe et al. (1981).

Manabe et al. (1981) discuss the geographical distribution of soil moisture changes in several GFDL studies. During March-April-May (MAM), the fourfold increase in CO_2 concentration produces increases in soil moisture in high northern latitudes, with small or reversed changes near the Equator (Figure 4.12A). During JJA, the surface is drier in middle and high latitudes (Figure 4.12B). The latitudinal changes are consistent with the zonally averaged changes in soil moisture in a higher resolution, but otherwise identical model from Manabe et al. (1981). However, some of the regional differences from the high-resolution model shown in Figure 4.12D for JJA are at variance with the results from the low resolution model (Figure 4.12B). This is particularly true in low latitudes, for example, over Africa and South America, where the year-to-year variability is large and changes are not statistically significant.

Manabe et al. (1981) also made a detailed analysis of the summer dryness caused by increased CO_2 in the various GFDL model studies and found that the following factors are responsible. The snowmelt ends earlier in the $4 \times CO_2$ integration so that normal summer drying caused by evaporation begins earlier and also is stronger. This is the dominant mechanism in high latitudes. In middle latitudes, reduced snow accumulation with accompanying reduced snowmelt and stronger evaporation in the enhanced CO_2 integrations produce a drier surface from late spring to autumn.

Using results from a model with idealized topography, Manabe et al. (1981) identified two dynamical mechanisms that further enhance the summer midlatitude drying. The simulated extratropical rainbelt, which migrates between 45°N in winter and 55°N in summer, is displaced to the north when CO_2 is quadrupled. Thus, near 50°N the wet season ends earlier and begins later in the CO_2 quadrupling experiment than in the control, and there is less precipitation from spring to autumn in the midlatitudes. In addition, Manabe et al. (1981) argued that the reduction in transient disturbances, which is particularly marked in spring and autumn, produces an earlier beginning and a later termination to the summer period of weak disturbances with a consequent reduction in precipitation.

An assessment of the effects of the annual insolation cycle on CO_2-induced climate change was conducted by Wetherald and Manabe (1981) by performing two simulations with the same (sector) model, one with the annual solar cycle (hereafter

called the seasonal model) and the other with annual mean insolation (hereafter called the annual model). In both models the ocean was treated as a 68-m slab mixed layer.

By comparing the zonal mean temperature differences of the annual and seasonal models in response to quadrupled CO_2, the principal effect of the annual insolation cycle is shown to be a reduction in the warming of the zonal mean surface air temperature at all latitudes, with the reduction increasing with latitude from about 0.5°C in the tropics to 4°C poleward of 70° latitude. A comparison of the annual mean temperature differences reveals that the longitudinal variation of the response of the seasonal model is smaller than that of the annual model, particularly equatorward of 45° latitude. Furthermore, the seasonal model is less sensitive to the CO_2 quadrupling than is the annual model, especially in high latitudes where the maximum warming is 4°C smaller. This reduced sensitivity of the seasonal model is attributable to the absence of the ice-albedo feedback mechanism in summer when there is no snow cover or sea ice in both the seasonal model experiment and control, while ice-albedo feedback apparently exists perpetually in the annual model (Wetherald and Manabe 1981). This comparison indicates that the influence of the seasons on the CO_2-induced annual mean temperature changes is not negligible.

The geographical distribution of the change in the annual mean precipitation rates simulated by the annual and seasonal models for the CO_2 quadrupling reveals several interesting similarities and differences. In both simulations there are only increases in the precipitation rate poleward of about 45° latitude, and there are both decreases and increases equatorward of this latitude. Both the annual and seasonal simulations display reduced precipitation rates in midlatitudes over the eastern ocean and western continent, as well as over the western part of the ocean in low latitudes. However, the seasonal model simulates increased precipitation rates everywhere over the continent in low latitudes, as well as over the eastern ocean, while the annual model does not. The results for the precipitation rate also indicate that there is a non-negligible influence of the seasons on the CO_2-induced annual mean precipitation changes.

The most significant differences between the two simulations occur for the comparison of changes in soil moisture. The changes in the annual mean soil moisture simulated by the annual and seasonal models are shown in Figure 4.13. Comparison of these results reveals several notable differences. First, the seasonal model simulates a very large moistening in high latitudes in contrast to the small drying simulated by the annual model. Second, the intense midlatitude drying belt in the annual model simulation is broader and much stronger than that in the seasonal model simulation. Finally, the extremes of drying and moistening simulated by the seasonal model in the tropics, particularly over the east coast, are weaker than those simulated by the annual model. The smoothing and weakening of the changes in soil moisture in low and middle latitudes that are simulated by the seasonal model in comparison with the annual model are also found for the changes in surface air temperature and precipitation rate. A more thorough discussion and analysis of the differences between the simulations with the annual and seasonal models is presented by Schlesinger (1984a).

4.3.3 The Dependence of Carbon Dioxide-Induced Climate Change on the Control Climate

The dependence of the CO_2-induced global mean climate change on the global mean control climate ($1 \times CO_2$) has been discussed by Schlesinger (1984a) and by Spelman and Manabe (1984). Schlesinger (1984a) related the CO_2-induced changes in the global mean surface air temperature and precipitation rate to the corresponding global means of the control for the simulations of Manabe and Wetherald (1975), Manabe and Stouffer (1979, 1980), Manabe and Wetherald (1980), Gates et al. (1981), Mitchell (1983), Wetherald and Manabe (1981), Schlesinger (1982), Washington and Meehl (1983). Tables 4.2 and 4.3 show that these simulations were made with models having differences in their prescribed insolation (annual mean vs. seasonally varying), ocean treatment (prescribed vs. predicted sea surface temperature and sea ice extent), geography (idealized sector vs. realistic distribution of continents and oceans), cloud treatment (fixed vs. computed) and CO_2 increase ($2 \times CO_2$ vs. $4 \times CO_2$).

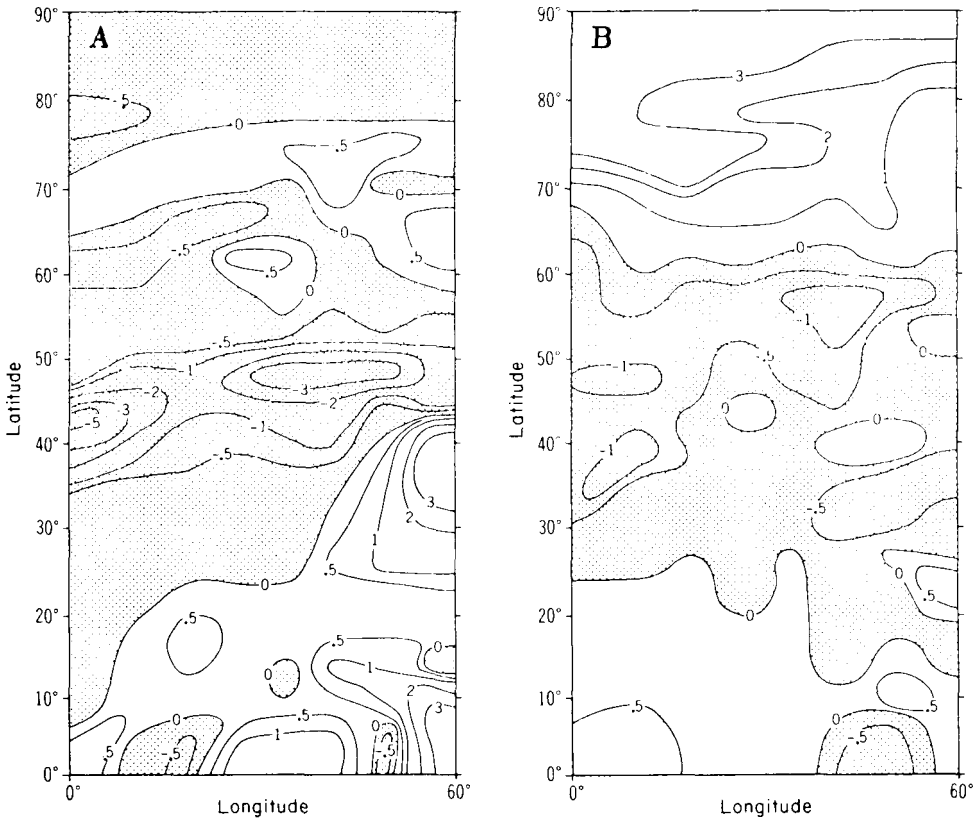

Figure 4.13. Wetherald and Manabe (1981) simulations of changes in soil moisture (cm) for quadrupled CO_2. (A) Annual model; (B) seasonal model. Stipple indicates decrease. Source: Schlesinger (1984a).

Nevertheless, the comparisons presented in Figures 4.14 and 4.15 provide a useful summary of the results of these models.

The precipitation rate, P, for each control simulation is shown plotted versus its corresponding surface air temperature, T_s, in the lower panel of Figure 4.14. The observed values of precipitation rate and surface air temperature are denoted in the figure. The seasonal simulations of the annual global mean temperature and precipitation with the GFDL model of Manabe and Stouffer (1980) and the OSU model of Gates et al. (1981) are closest to the observed values. This close agreement occurs even though the OSU model used prescribed sea surface temperature and sea ice whereas the GFDL model predicted the sea surface temperature from a 68-m mixed-layer ocean model and the sea ice from a thermodynamical model. The seasonal and annual simulations of Wetherald and Manabe (1981) employed the same ocean and sea ice models as did the simulations of Manabe and Stouffer, but Wetherald and Manabe's simulated T_s and P are warmer and smaller, respectively, than the observed values. This increased discrepancy of the results of Wetherald and Manabe (1981) compared with that of Manabe and Stouffer (1980) is likely, in part, the result of the former using a sector model in contrast to the latter using a global model. When the mixed-layer ocean and thermodynamic sea ice models are replaced with a swamp ocean in the sector model, as in Manabe and Wetherald (1980), the temperature error increases considerably whereas the precipitation error decreases. A more accurate portrayal with a swamp model, at least insofar as global mean temperature, is given by the OSU model (Schlesinger 1982). However, the NCAR simulations with a swamp model for both computed and fixed clouds (Washington and Meehl 1983) have relatively larger temperature and precipitation errors.

The change in the surface air temperature is shown plotted versus the corresponding surface air temperature in the upper panel of Figure 4.14. This

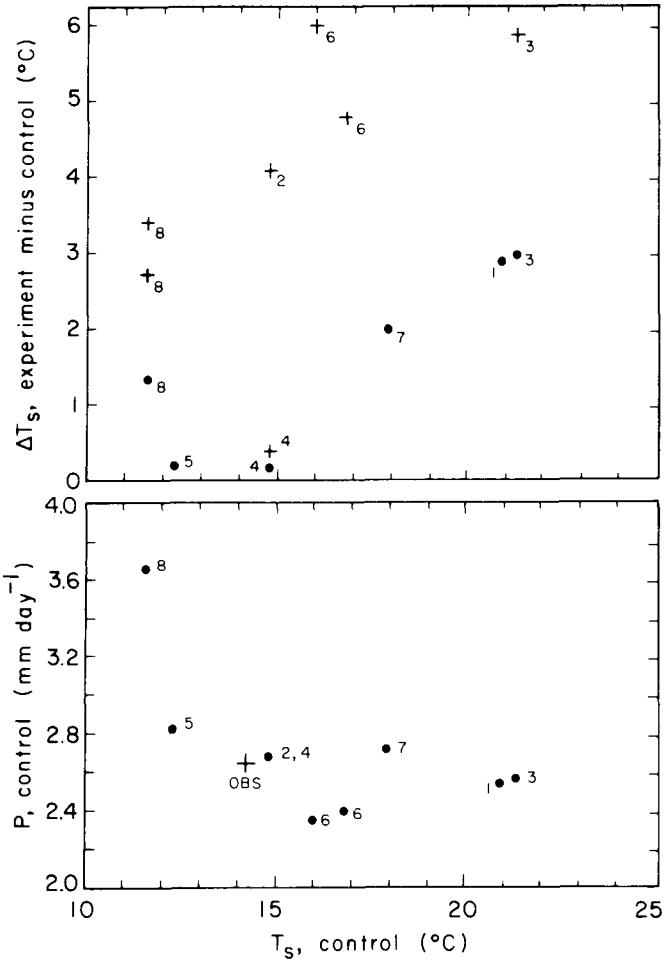

1. Manabe and Wetherald (1975)
2. Manabe and Stouffer (1979, 1980)
3. Manabe and Wetherald (1980)
4. Gates et al. (1981)
5. Mitchell (1983)
6. Wetherald and Manabe (1981)
7. Schlesinger (1982)
8. Washington and Meehl (1983)

Figure 4.14. Top: change in global mean surface air temperature ΔT_s induced by doubled (•) and quadrupled (+) CO_2 versus the global mean surface air temperature T_s of the control simulation for eight GCMs. Bottom: global mean precipitation rate P of the control simulation versus global mean surface air temperature of the control simulation for eight GCMs. Observed value, + OBS. Source: Schlesinger (1984a).

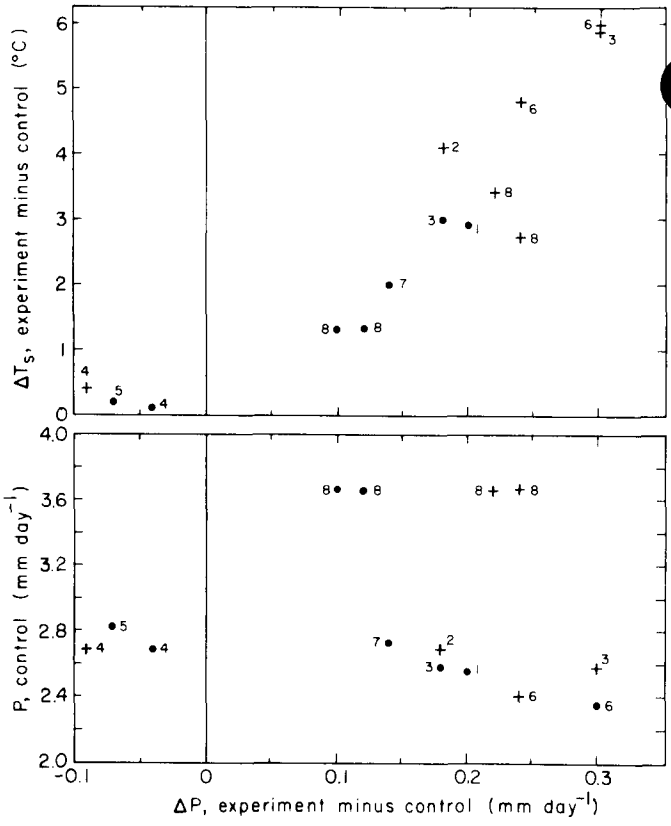

1. Manabe and Wetherald (1975)
2. Manabe and Stouffer (1979, 1980)
3. Manabe and Wetherald (1980)
4. Gates et al. (1981)
5. Mitchell (1983)
6. Wetherald and Manabe (1981)
7. Schlesinger (1982)
8. Washington and Meehl (1983)

Figure 4.15. Top: the change in global mean surface air temperature ΔT_s induced by doubled (•) and quadrupled (+) CO_2 versus the change in global mean precipitation rate ΔP for eight GCMs. Bottom: global mean precipitation rate of control simulation versus change in global mean precipitation rate induced by doubled (•) and quadrupled (+) CO_2 for eight GCMs. Source: Schlesinger (1984a).

panel indicates that, in the sense of intermodel comparison, the warmer the control, the larger the CO_2-induced warming. This relation could be due to the nonlinear increase of atmospheric water vapor with temperature and the water vapor greenhouse effect, that is, the water vapor feedback mechanism described in Appendix A.

The simulated precipitation rate changes for the CO_2 doubling and quadrupling are shown plotted versus their corresponding surface air temperature changes in the top panel of Figure 4.15. This figure indicates that, in the sense of intermodel comparison, the larger the simulated warming, the larger the increase in the simulated precipitation rate. Because the global mean evaporation rate must equal the global mean precipitation rate for an equilibrium simulation, the above relation implies an identical relation between the surface evaporation increase and the surface air temperature warming. Both relations are likely the result of the increase of the surface saturation mixing ratio with temperature caused by the Clausius-Clapeyron relation, described in Appendix A.

Because ΔP increases with ΔT_s, and ΔT_s increases with T_s of the control, ΔP must increase

with T_s. Again, in the sense of intermodel comparison, the warmer the control, the larger the CO_2-induced precipitation rate increase. For this reason the precipitation rate increase simulated by the seasonal model of Manabe and Stouffer (1980) is smaller than that of the annual model of Manabe and Wetherald (1980), and similarly for the seasonal and annual models of Wetherald and Manabe (1981).

Spelman and Manabe (1984) have investigated the effect of ocean dynamics on the sensitivity of climate to increased CO_2 by performing two experiments with the GFDL spectral GCM with idealized geography and annually averaged insolation. In the first experiment [SM1(A)] the ocean was represented by a 68-m deep mixed layer with no currents, and in the second experiment [SM2(A)] the GFDL finite difference ocean general circulation model was used. Figure 4.16 shows that the zonally averaged surface air temperature changes induced by quadrupling CO_2 were smaller in the simulation with ocean currents, particularly in the middle and high latitudes. This can be explained by the difference in the climates of the two control simulations. In the simulation with ocean currents [SM2(A)], the snow and ice cover were less extensive than in the simulation without ocean currents because of the poleward transport of heat by the oceans. Consequently, the snow- and ice-albedo feedback was smaller in the simulation with ocean currents because the snow and ice were confined to a smaller area and at higher latitudes where the insolation is smaller.

The global mean CO_2-induced warming of the surface air temperature of these simulations is shown plotted versus the corresponding global mean surface air temperature of the control in Figure 4.17. This figure shows that T_s of the SM2(A) simulation with ocean currents is close to the observed value and $\Delta T_s \simeq 5.5°C$ for the quadrupled CO_2. The value of T_s of the SM1(A) simulation without ocean currents is almost 10°C colder than that of SM2(A) and the observed T_s because of the absence of oceanic heat transport. The corresponding $\Delta T_s \simeq 13°C$ is larger than that with ocean currents, again because the more extensive sea ice cover in SM1(A) yields a larger ice-albedo feedback. Figure 4.17 also shows results from another $1 \times CO_2/4 \times CO_2$ simulation pair with this model. In SM3(A) the solar constant was reduced and the emissivity of

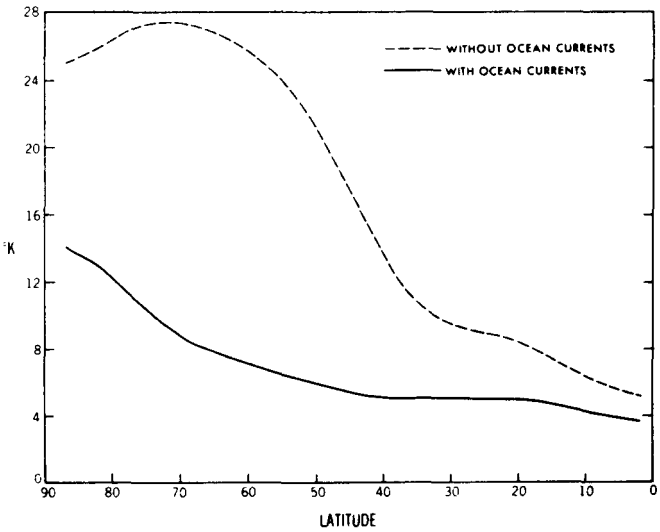

Figure 4.16. Latitudinal variation of the change of zonally averaged surface air temperature caused by quadrupling the atmospheric CO_2 content for both the model with ocean currents (solid line) and the model without ocean currents (dashed line.) Source: Spelman and Manabe (1984).

cirrus clouds increased in comparison with their values in the SM1(A) and SM2(A) simulations. These changes result in a control climate whose $(T_s, \Delta T_s)$ point lies on a straight line connecting the corresponding points of SM1(A) and SM2(A). Therefore, in the sense of intramodel comparison, the warmer the control, the smaller is the CO_2-induced warming. This relationship also is revealed by the solar constant sensitivity studies of Wetherald and Manabe (1975, 1980).

Figure 4.17 also shows the results from the studies by Manabe and Stouffer (1980) and Wetherald and Manabe (1981). Taken by themselves, they do not look unlike what is seen in the top panel of Figure 4.14. Consequently, temperature sensitivity to increased CO_2 apparently can either increase or decrease with the temperature of the $1 \times CO_2$ control, depending, respectively, on whether the water vapor feedback or the ice-albedo feedback is dominant. Because the CO_2-induced temperature change is dependent on the temperature of the control climate, it is necessary to simulate the latter correctly. Unfortunately, however, this is not a sufficient condition for simulating the CO_2-induced temperature change correctly.

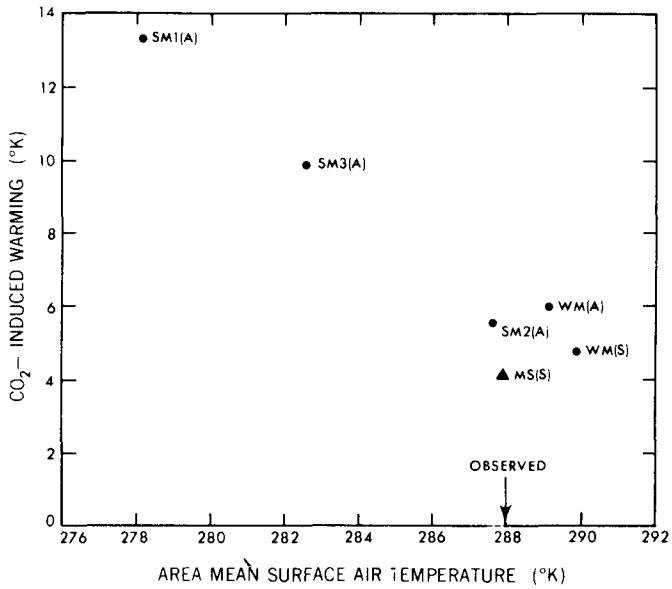

The Characteristics of Spectral Climate Models Used for Recent Studies of CO_2-Climate Sensitivity

Model	Insolation	Solar Constant (W m^{-2})	Cirrus Blackness	Computational Domain	Geography	Atmosphere	Ocean	Reference
SM1(A)	annual	1356	80%	1/6 globe	idealized	spectral GCM	mixed layer	Spelman and Manabe (1984)
SM2(A)	annual	1356	80%	1/6 globe	idealized	spectral GCM	full ocean	Spelman and Manabe (1984)
SM3(A)	annual	1349	100%	1/6 globe	idealized	spectral GCM	mixed layer	Spelman and Manabe (1984)
WM(A)	annual	1370	100%	1/6 globe	idealized	spectral GCM	mixed layer	Wetherald and Manabe (1981)
WM(S)	seasonal	1370	100%	1/6 globe	idealized	spectral GCM	mixed layer	Wetherald and Manabe (1981)
MS(S)	seasonal	1356	100%	global	realistic	spectral GCM	mixed layer	Manabe and Stouffer (1980)

Figure 4.17. Sensitivity of area mean surface air temperature to quadrupling the atmospheric CO_2 content for various climate models versus the area mean surface air temperature of the normal CO_2 case. Solid dots indicate models having limited computational domain with idealized geography; the triangle indicates that the model treats a global domain with realistic geography. The observed value of the area mean surface air temperature is indicated for reference. Source: Spelman and Manabe (1984).

4.3.4 Recent Simulations With the Annual Insolation Cycle

Three simulations of the changes in the equilibrium climate induced by a doubling of the CO_2 concentration have been performed using models in which sea surface temperatures were predicted by simple mixed-layer ocean models and the seasonal insolation cycle was included. These simulations were performed with the GISS GCM (Hansen et al. 1984), the NCAR GCM (Washington and Meehl 1984; Meehl and Washington 1985a, 1985b; Bates and Meehl 1985), and the GFDL GCM (Wetherald and Manabe, 1986; Manabe and Wetherald[3]). Since the CO_2-induced climate change depends on the control climate, as demonstrated in the preceding sections for the earlier studies, a comparison of the control climates of these most recent simulations with the observed climate will be made in Section 4.3.4.1. The simulations of the changes in the equilibrium climate induced by a doubling of the CO_2 concentration will be compared in Section 4.3.4.2.

The GISS GCM used by Hansen et al. (1984) has been described by Hansen et al. (1983), and the NCAR GCM employed by Washington and Meehl (1984) has been described by Pitcher et al. (1983) and Ramanathan et al. (1983). The GFDL GCMs used by MW86 and Wetherald and Manabe (1986) are the same as that of Manabe and Stouffer (1980), except that clouds are predicted based primarily on the formulation of Wetherald and Manabe (1980). The three GCMs that predict clouds are intercompared in Table 4.4 in terms of 21 model and simulation characteristics.

All three atmospheric GCMs integrate the primitive equations in spherical coordinates for the entire globe, and all three represent the vertical derivative

[3] S. Manabe and R. Wetherald, manuscript in preparation. This work will hereafter be referred to as MW86.

Table 4.4
Characteristics of the GCMs Used to Simulate Equilibrium Climate Change Induced by Doubling the CO_2 Concentration

	General Circulation Modeling Study		
Model Characteristic	GISS[a]	NCAR[b]	GFDL[c]
Horizontal domain; coordinates	Global; latitude-longitude	Global; latitude-longitude	Global; latitude-longitude
Vertical domain; coordinates	Surface to 10 mb; σ^d	Surface to 0 mb; σ^d	Surface to 0 mb; σ^d
Solution method	Finite difference in vertical, time, and horizontal	Finite difference in vertical and time; spectral transform in horizontal.	Finite difference in vertical and time; spectral transform in horizontal.
Horizontal resolution	8° latitude by 10° longitude	Rhomboidal 15 truncation, advection and physics computed on a ~4.5° latitude by 7.5° longitude grid.	Rhomboidal 15 truncation, advection and physics computed on a ~4.5° latitude by 7.5° longitude grid.
Vertical resolution	9 layers	9 layers	9 layers
Land/ocean distribution	Realistic	Realistic	Realistic
Topography	Realistic	Realistic	Realistic
Ocean	Mixed layer with seasonally varying depth is prescribed from climatology but with a maximum allowed depth of 65 m. No vertical heat flux to the thermocline. Horizontal heat transport is prescribed seasonally based on the transport implied in a simulation with prescribed seasonally varying sea surface temperatures.	Mixed layer is 50 m deep with no vertical heat transport to the thermocline and no horizontal heat transport.	Mixed layer is 50 m deep with no vertical heat transport to the thermocline and no horizontal heat transport.
Sea ice	Occurrence is predicted when ocean cools to −1.6°C. Initial thickness is 1 m. Grows horizontally at 1 m thickness until gridbox is covered up to the limit prescribed for leads, $0.1/Z_{ice}$, where Z_{ice} is ice thickness in meters. Further heat loss increases ice thickness. Two-layer sea ice model with conduction between ice and ocean. Ocean temperature beneath ice can change but is not allowed to exceed 0°C until all the ice within the gridbox is melted. No ice advection.	Occurrence is predicted when ocean cools to −1.9°C. Ice thickness horizontally uniform within a gridbox and no leads. One-layer sea ice model with no heat flux from ocean to ice. Ocean temperature beneath ice is kept at −1.9°C. Conduction heat flux within ice is balanced by latent heat of freezing or melting at ice bottom. No ice advection.	Occurrence is predicted when ocean cools to −1.9°C. Ice thickness horizontally uniform within a gridbox and no leads. One-layer sea ice model with heat flux from ocean to ice. Ocean temperature beneath ice is kept at −1.9°C. Conduction heat flux within ice balanced by latent heat of freezing or melting at ice bottom. No ice advection.
Snow	Precipitation falls as snow when lowest GCM layer temperature <0°C. Snow mass determined prognostically from mass budget.	Precipitation falls as snow when lowest GCM layer temtemperature <0°C. Snow mass determined prognostically from mass budget.	Precipitation falls as snow when air temperature at 300 m <0°C. Snow mass determined prognostically from mass budget.

[a] Hansen et al. (1984).
[b] Washington and Meehl (1984).
[c] Wetherald and Manabe (1986).
[d] $\sigma = (p - p_T)/(p_s - p_T)$ where p is pressure, p_T the pressure at the top of the model, and p_s the surface pressure.

Table 4.4
(continued)

	General Circulation Modeling Study		
Model Characteristic	GISS	NCAR	GFDL
Soil moisture	Determined prognostically from two-layer model with upper/lower layer field capacities in cm prescribed as 1/1 desert, 3/20 tundra, 3/20 grass, 3/30 shrub, 3/30 woodland, 3/45 deciduous forest, 3/45 evergreen forest, 20/45 rainforest.	Determined prognostically from one-layer model with 15 cm field capacity.	Determined prognostically from one-layer model with 15 cm field capacity.
Surface temperature	Determined prognostically from two-layer model with depths of about 10 cm and 4 m.	Determined diagnostically such such that the net surface heat flux is zero.	Determined diagnostically such that the net surface heat flux is zero.
Surface albedo/emissivity	Prescribed to vary with season (winter, spring, summer, autumn) for 8 prescribed vegetation types (desert, tundra, grass, shrub, woodland, deciduous forest, evergreen forest, rainforest) separately for visible (wavelength <0.7 μm) and near-IR (≥ 0.7 μm) solar radiation. Sea ice albedo in visible/ near-IR is 0.55/0.3. Snow albedo is a function of underlying vegetation type, snow depth, masking depth of vegetation type, and snow age. Land-ice albedo is the same as for aged snow. Ocean albedo is a specified function of surface wind speed and solar zenith angle. Ocean emissivity is a function of wave-length and wind speed. Land emissivity is a function of wave-length for desert, snow and ice, and unity for other surfaces.	Prescribed albedo of 0.25 for desert and 0.13 for other snow-free land. Sea ice albedo is 0.7. Snow albedo is 0.8 independent of depth. Ocean albedo is $0.05/(\cos\zeta + 0.15)$ where ζ is the solar zenith angle. In the 8–12 μm region the emissivity is 0.75 for deserts, 0.95 for other land surfaces and unity for ocean. Emissivity is unity for other spectral IR regions.	Prescribed for 6 prescribed vegetation types (woodland, grass, and cultivation; forest steppe and grassland; steppe desert; desert tundra, mountain and arctic flora) and land ice. Sea ice albedo is a function of latitude, underlying ocean albedo, ice thickness and surface melting. Snow albedo is a function of underlying vegetation type, snow depth, and a masking depth. Ocean albedo is a prescribed function of latitude. Surface emissivity is unity everywhere
Terrestrial (longwave) radiation	H_2O [6.25 μm vibration-rotation band, 10 and 20 μm continuum bands, >10 μm rotation band]; CO_2 [15 μm vibration rotation band], O_3 [9.6 μm vibration-rotation band], N_2O [4.5, 7.78, 17.0 μm vibration-rotation bands], CH_4 [7.66 μm vibration-rotation band].	H_2O [4–8 μm vibration-rotation band, 8–12 μm continuum, and ≥ 12 μm rotation band; no e-type absorption], CO_2 [fundamental, 1st and 2nd hot bands for four isotopes in 12–18 μm region], O_3 [9.6 μm vibration-rotation band].	H_2O [6.3 μm vibration-rotation band, 8–13 μm continuum band, >10 μm rotation band, with e-type absorption], CO_2 [15 μm vibration-rotation band], O_3 [9.6 μm vibration-rotation band].

Table 4.4
(continued)

Model Characteristic	General Circulation Modeling Study		
	GISS	NCAR	GFDL
Solar (shortwave) radiation	Scattering by molecules and aerosols. Absorption by H_2O, CO_2, O_3, and NO_2.	Scattering by molecules. Absorption by H_2O, CO_2, O_3, and O_2.	No scattering by molecules. Absorption by H_2O, CO_2, and O_3.
Insolation	$S_0 = 1367$ W m^{-2} with seasonal and diurnal cycles.	$S_0 = 1370$ W m^{-2} with seasonal cycle.	$S_0 = 1467$ W m^{-2} with seasonal cycle.
Large-scale condensation	Occurrence is predicted when relative humidity >100%. Large-scale precipitation is taken equal to condensation Saturation vapor pressure is determined with respect to ice for "unseeded" clouds colder than −40°C and for "seeded" clouds (ice falling into a layer from above) colder than 0°C.	Occurrence is predicted when relative humidity >100%. Large-scale precipitation is taken equal to condensation	Occurrence is predicted when relative humidity >100%. Large-scale precipitation is taken equal to condensation
Cumulus convection	Occurrence is predicted when $h_\ell > h^*_k$, $k = \ell - 1, \ldots, 1$ and $\ell = 9 \ldots, 2$ where h is the moist static energy, h^* is the saturated moist static energy, and ℓ is the vertical layer index with 1 representing the top layer. The fraction of layer ℓ which can rise to layer k is taken as 50%. The air from layer ℓ rises without entrainment and conserves its moist static energyuntil it encounters a layer with respect to which it is stable. Precipitation occurs during ascent if saturation occurs. After determination of the mass penetrating to all higher levels, mixing with the environment is performed starting at the highest layer and working downward; precipitation reevaporates to the extent that lower layers are unsaturated. The procedure is repeated with the second layer as the source of rising air, mixing with the environment, repetition with the third layer as source, etc. Vertical transport of horizontal momentum is included.	Occurrence is predicted when the equivalent potential temperature θ_e decreases with increasing altitude and the relative humidity $RH > RH_C = 80\%$. Parameterized as moist convective adjustment wherein θ_e becomes uniform and $RH = RH_C$ vertically within the convection region. Vertical transport of horizontal momentum and penetrative convection are not included.	Occurrence is predicted when the equivalent potential temperature θ_e decreases with increasing altitude and the relative humidity $RH > RH_C = 100\%$. Parameterized as moist convective adjustment wherein θ_e becomes uniform and $RH = RH_C$ vertically within the convection region. Vertical transport of horizontal momemtum and penetrative convection are not included.

Table 4.4
(continued)

Model Characteristic	General Circulation Modeling Study		
	GISS	NCAR	GFDL
Clouds	Clouds are allowed to form in each layer below 100 mb due to large-scale condensation and cumulus convection. A large-scale cloud can occur when $RH > 100\%$; cloud cover $C = 0$ if $f_s < N_r$ and $C = 1$ if $f_s > N_r$, where f_s is the saturated fraction of a gridbox obtained under the assumptions that the absolute humidity is uniform throughout the gridbox and the temperature has a prescribed Gaussian subgrid-scale form, and N_r is a generated random number between 0 and 1. A convective cloud can occur when there is cumulus convection; cloud cover $C = 0$ if $\gamma M < N_r$ and $C = 1$ if $\gamma M > N_r$, where M is the mass of saturated air rising through the base of a layer and $\gamma = 2.5$ m^2 s kg^{-1}. Optical depth for large-scale clouds $\tau = 1/3$ for $T < 258$ K and $\tau = 0.0133(p - 100)$ for $T > 258$ K, where T is the layer temperture and p is the level pressure in mb. For convective clouds $\tau = 0.08\Delta p$ where Δp is the cloud pressure thickness in mb. Cloud absorptivity and emissivity are derived from phase function and single-scattering albedo based on Mie computations with radii of 10 μm and 25 μm for water and ice clouds, respectively.	Clouds are allowed to form in each layer above the lowest layer and below 250 mb for $\mid \phi \mid < 45°$ and below 400 mb for $\mid \phi \mid > 45°$ latitude due to large-scale condensation and cumulus convection. A large-scale cloud occurs when $RH > 80\%$ with a cloud cover $C = 0.95$. Convective cloud occurs when $\partial\theta_e/\partial z < 0$ and $RH > 80\%$ with $C = 0.30/N$ in each of the N layers undergoing moist convective adjustment. Clouds in different layers are assumed to be randomly overlapped. Cloud albedo $\alpha = \beta\mu/(\beta + \cos\varsigma)$ where ς is the zenith angle, $\mu = \min(1, \sqrt{LWC/10})$ with LWC (g cm^{-2}) the column condensate during one hour of model time, $\beta = 0.6$, 0.3, 0.15 for low ($0.811 \leq \sigma \leq 0.991$), middle ($0.5 \leq \sigma \leq 0.811$) and high ($\sigma < 0.5$ and $p > 250$ mb for $\mid \phi \mid < 45°$ and $p > 400$ mb for $\mid \phi \mid > 45°$ latitude), respectively. For clouds occurring simultaneously in two or more layers, the albedo is taken equal to the maximum over all the layers. Cloud absorption only by water vapor and ozone. Emissivity $\epsilon = 1$ for high cloud and $\epsilon = \mu$ for middle and low clouds.	Clouds are allowed to form in each layer. Large-scale cloud occurs when $RH > 99\%$ with a cloud cover $C = 1.0$. Convective cloud occurs when $\partial\theta_e/\partial z < 0$ and $RH > 100\%$ with $C = 1.0$. For thin clouds (existing in one layer only), the albedo and absorptivity for $\lambda < 0.7$ μm ($\lambda > 0.7$ μm) are 0.21 (0.19) and 0.0 (0.04) for high cloud (>10.5 km), and 0.45 (0.35) and 0.0 (0.2) for middle cloud (~4.0 to 10.5 km), 0.65 (0.55) and 0.0 (0.30) for low cloud (0.0 to 4.0 km). For thick cloud (existing in two or more contiguous layers), the albedo and absorptivity are 0.57 (0.47) and 0.0(0.3). The emissivity is 0.6 for high cloud and unity for middle and low cloud.
Length of integration	45 unaccelerated solar cycles for 1 × CO_2, 35 unaccelerated solar cycles for 2 × CO_2.	For the 1 × CO_2 simulation, 12 solar cycles with calendar accelerated by 9 (40.6 days/solar cycle), then 4 solar cycles with acceleration of 3 (121.7 days per solar cycle), finally 11 unaccelerated solar cycles. For the 2 × CO_2 simulation, only the 4 accelerated (3x) and 11 unacclerated solar cycles.	49 unaccelerated solar cycles.
Averaging length for 1 × CO_2 and 2 × CO_2 results.	Last 10 years of simulations.	Last 3 years of simulations.	Last 10 years of simulations.

in these and other equations by finite differences with nine vertical layers between the surface and, essentially, the top of the atmosphere. The GISS model also represents the horizontal derivatives by finite differences with an 8° latitude by 10° longitude resolution. However, the NCAR and GFDL models employ the spectral method to evaluate the horizontal derivatives, but the advection terms are evaluated by the transform method on a 4.5° latitude by 7.5° longitude grid. In all three models the so-called physics terms such as diabatic heating also are computed on the grids of the models. The global distribution of land and ocean is realistic within the horizontal resolutions of the models, as is the Earth's topography, albeit the latter is smoothed.

Each of the atmospheric GCMs is coupled to a mixed-layer ocean. In the NCAR and GFDL models the depth of the mixed layer is constant, and there is no horizontal heat transport. In the GISS model the depth of the mixed layer is prescribed to vary seasonally based on observations, and the horizontal oceanic heat transport is prescribed geographically and seasonally. The oceanic heat transport used is that implied from a GCM simulation with sea surface temperatures prescribed according to observations. This prescribed horizontal oceanic heat transport strongly constrains the model with predicted sea surface temperatures to reproduce the observed values for the control ($1 \times CO_2$) simulation.

The calculations of large-scale condensation and snow are essentially the same in all three models. The calculations of sea ice, soil moisture, and surface temperature are essentially the same in the NCAR and GFDL model and different in the GISS model. Fractional sea ice cover can occur within a gridbox in the GISS model, but not in the NCAR and GFDL models; the GISS model has two layers within the ice, whereas the NCAR and GFDL models have a single layer. This also is true for the number of soil layers used for the soil moisture and surface temperature calculations; for the former, the NCAR and GFDL models have a prescribed field capacity of 15 cm everywhere, whereas the GISS model uses a geographical distribution with values that range from 2 to 65 cm for both layers together.

The parameterization of cumulus convection is similar in the NCAR and GFDL models and different in the GISS model. The NCAR and GFDL models employ moist convective adjustment, the former with a critical relative humidity for the existence of convection of 80%, and the latter with a value of 100%. The GISS model uses a parameterization of cumulus convection with similarities to that of Arakawa et al. (1969), which includes shallow, middle-level, and deep convection.

The treatment of terrestrial and solar radiation is similar in the three models in that they include the principal absorbers and emitters, H_2O, CO_2, and ozone (O_3). The NCAR and GISS models also include absorption of solar radiation by oxygen (O_2), and the GISS model also includes solar absorption by nitrogen dioxide (NO_2), and the effects of nitrous oxide (N_2O) and methane (CH_4) are included in the longwave radiation calculation. The solar calculation essentially follows the method of Lacis and Hansen (1974) in all three GCMs, although different band models are used in the longwave in each GCM. The prescriptions of the surface albedo and surface emissivity also are different in each model. Even the value of the solar constant differs among the models. The GISS and NCAR models use 1367 and 1370 W m^{-2}, respectively, which are within the current observational uncertainty, whereas the GFDL model uses 1467 W m^{-2}. Only the GISS model includes the diurnal cycle as well as the seasonal cycle.

All three models form clouds by both large-scale condensation and convection. Large-scale clouds occur when the relative humidity exceeds 80, 99, and 100% in the NCAR, GFDL, and GISS models, respectively; although the GISS model assigns cloud cover in a gridbox only a certain percentage of the time (based on an extrapolated subgrid-scale temperature variance, calculation of the fraction of the gridbox that is saturated, and comparison to a random number generated in the interval 0 to 1) to mimic the effect of partial cloud cover. Large-scale cloud cover is 100, 95, and 100% in the GFDL, NCAR, and GISS models, respectively. Convective clouds occur when there is moist convection in all three models, although the GISS model actually generates a convective cloud only if another contingency test based on a random number generator is satisfied. Convective cloud cover is 100% in the

GFDL and GISS models, and $0.30/N$ per layer in the NCAR model, where N is the number of layers undergoing convection. The optical properties of clouds depend on whether they are low, middle, or high clouds in the GFDL and NCAR models, as well as on the solar zenith angle in the NCAR model. In the GISS model the optical depth of clouds depends on their temperature, pressure, and pressure thickness.

From this description of the characteristics of the three models, it appears that the NCAR and GFDL models are quite similar, both in the fundamental numerical approaches and in the physical parameterizations. The GISS model differs from the NCAR and GFDL in both of these characteristics. Regarding the physics, the principal differences are found in the treatments of cumulus convection, sea ice, soil moisture, and surface temperature. The treatment of clouds is different in each of the models, again particularly in the GISS model.

Finally, Table 4.4 shows the length of the integration and the averaging period of the results for each of the model simulations. The NCAR simulation uses an acceleration method to attain equilibrium with a minimum of computer time, whereas the GISS and GFDL simulations are straightforward integrations of the model. The GISS and GFDL results are averages over the last 10 years of 35- and 49-year integrations, respectively, and the NCAR results are averages over the last 3 years obtained from 11 unaccelerated and 16 accelerated years (solar cycles).

4.3.4.1 Comparison of the Simulated and Observed 1 × CO_2 Climates

The 1 × CO_2 climates simulated by the GISS, NCAR, and GFDL models with predicted clouds are compared with the observed climate in Table 4.5 in terms of the annual global mean surface air temperature and precipitation rate. This table shows that both the NCAR and GFDL models slightly overestimate the temperature, whereas the GISS model matches the estimated value of 14.2°C. The largest temperature difference is displayed by the GFDL model, a result that perhaps is not surprising considering that the prescribed solar constant for this model exceeds the observed value by about 100 W m^{-2} (Table 4.4). Table 4.5 also shows that all three models overestimate the observed precipitation rate; however, the differences are probably within the uncertainty of the observed value. Comparing the results of Table 4.5 and Figure 4.14 shows that the temperatures simulated by these three most recent studies are more accurate than those simulated in the earlier studies, although the precipitation differences are generally larger. In the following sections, we present and discuss the latitude-altitude temperature cross sections and the geographical distributions of the surface air temperature and precipitation rate for the GISS, NCAR, and GFDL models.

Table 4.5
Annual Global Mean Surface Air Temperature and Precipitation Rates for Three GCM Simulations and Difference From the Corresponding Observed Values

Study	Temperature (°C)		Precipitation (mm d^{-1})	
	GCM	Diff.[a]	GCM	Diff.[b]
Hansen et al. (1984)	14.2	0.0	3.2	0.6
Washington and Meehl (1984)	14.4	0.2	3.3	0.7
Wetherald and Manabe (1986)	14.8	0.6	2.9	0.3

[a] Difference between model with 1 × CO_2 and observed value of 14.2°C, which is based on data of Crutcher and Meserve (1970) and Taljaard et al. (1969) as given by Jenne (1975).
[b] Difference between model with 1 × CO_2 and observed value of 2.6 mm d^{-1}, which is based on Jaeger (1976).

GISS Model (Hansen et al. 1984). The latitude-altitude cross sections of the zonal mean air temperature simulated by the GISS model for DJF and JJA are presented in Figures 4.18 and 4.19, respectively, together with the corresponding observed and simulated-minus-observed fields. These figures show that the model correctly simulates the decrease of temperature with increasing altitude in the troposphere, the low-level inversion in the Arctic winter, the cold tropical tropopause, and the nearly isothermal structure of the stratosphere. The largest errors occur in the stratosphere where the temperature is 5–10°C colder than is observed over the Arctic during both seasons, and 10–15°C warmer and colder than is observed over the Antarctic in winter and summer, respectively. Temperatures about 5°C warmer than those observed are

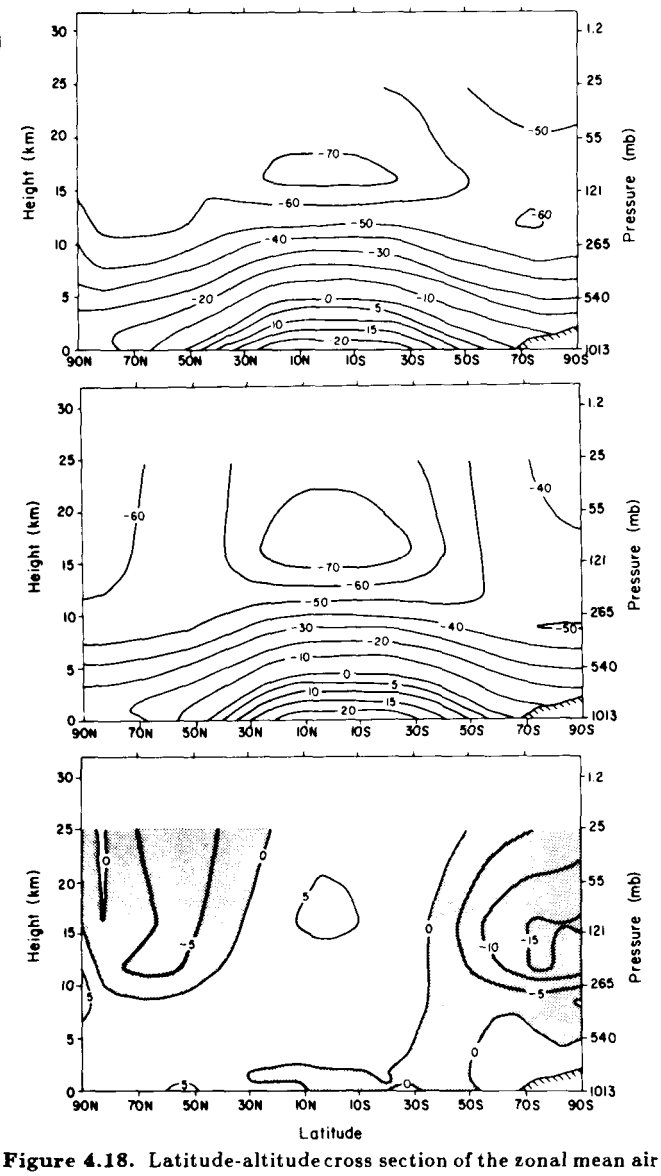

Figure 4.18. Latitude-altitude cross section of the zonal mean air temperature (°C) for DJF: (top) simulated with the GISS GCM by Hansen et al. (1984); (middle) observed based on Oort (1983); (bottom) simulated minus observed with negative values shaded.

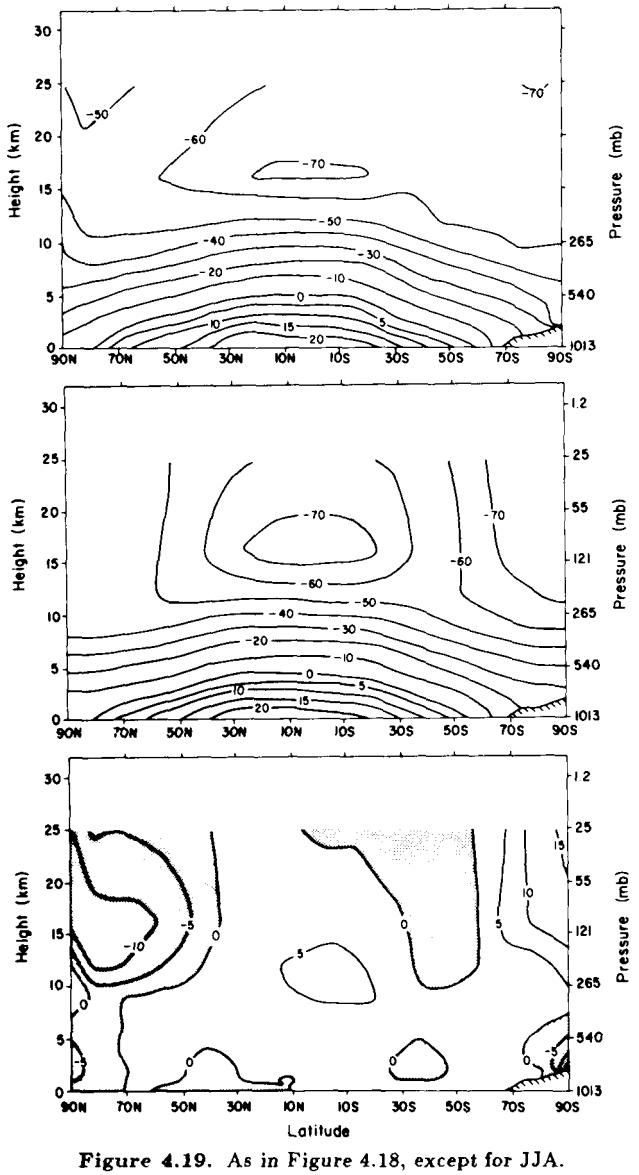

Figure 4.19. As in Figure 4.18, except for JJA.

simulated in the upper tropical troposphere during both seasons and at the surface near 50°N in winter.

The geographical distributions of the surface air temperature simulated by the GISS model for DJF and JJA are shown in Figures 4.20 and 4.21, respectively, together with the corresponding observed and simulated-minus-observed temperature distributions. These figures show that during both seasons the model simulates the observed general decrease of surface air temperature with latitude from the tropics toward both poles[4] and the land-ocean temperature contrasts. The errors in the simulated air temperature over the open ocean are less than 5°C virtually everywhere. Undoubtedly these small errors are partly the result of the geographical and seasonal prescription of the horizontal oceanic heat transport as described in the preceding section and in Table 4.4. The largest maritime surface air temperature errors are found over the Arctic and Antarctic sea ice, where the simulated

[4] It is of interest to note that if the Earth did not have an ocean, the maximum DJF and JJA temperatures would be located in the high latitudes of the summer hemisphere, not in the tropics (Schlesinger and Gates 1981).

temperatures are up to 5–10°C colder than the observed temperatures. However, the simulated temperatures are warmer than the observed temperatures near 100°W on the periphery of Antarctica. This may be related to the fact that the simulated sea ice extent is about 15% less than that shown by the climatologies of Walsh and Johnson (1979) and Alexander and Mobley (1976). Over land the simulated surface air temperatures generally agree with the observed values to within ±5°C. These relatively small errors probably are the result of the use of the two soil layers and geographically prescribed field capacities for storing soil moisture as described in the preceding section and Table 4.4. Exceptions are found over Greenland during both seasons, over northeastern Asia and North America during winter, over the North American plains in summer and over Antarctica, particularly during summer. This simulation of warmer-than-observed surface air temperatures over Antarctica is an error common to most GCMs (Schlesinger 1984b).

The geographical distributions of the precipitation rate simulated by the GISS model for DJF and JJA are shown in Figures 4.22 and 4.23, respectively, together with the corresponding observed and simulated-minus-observed precipitation distributions. These figures show that during both seasons the maximum precipitation is simulated in the equatorial region from the Indian Ocean to the central Pacific Ocean as observed, and precipitation maxima are simulated south of the Equator in DJF and north of the equator in JJA over Africa and South America as observed. A precipitation maximum is simulated in DJF, and a minimum in JJA, near the Gulf of Alaska as observed. Precipitation minima are simulated in the Southern Hemisphere subtropics off the west coasts of Africa, Australia, and South America during both seasons as observed, and precipitation minima are simulated over the Arctic and Antarctic during both seasons as observed. There are also errors in the simulated precipitation rate. For example, the model simulates an Asian monsoon in DJF as well as in JJA, the simulated precipitation over the tropical central Pacific Ocean and the tropical Atlantic Ocean is larger than the observed values in both seasons, and the model underestimates the precipitation rate observed between 60°E and the dateline off the coast of

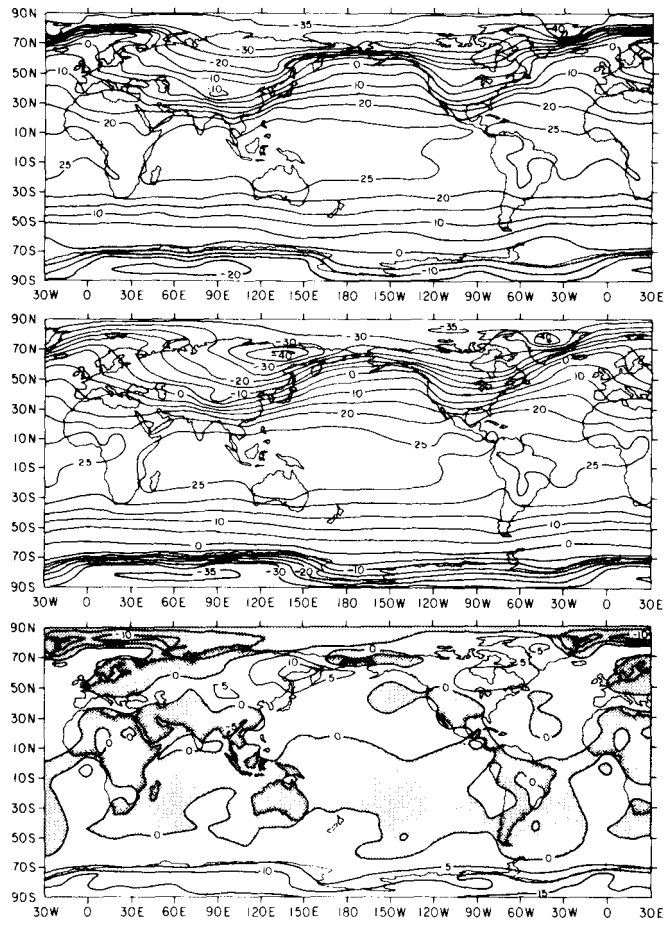

Figure 4.20. Geographical distribution of the surface air temperature (°C) for DJF: (top) simulated with the GISS GCM by Hansen et al. (1984); (middle) observed based on Crutcher and Meserve (1970) and Taljaard et al. (1969) as available from the National Center for Atmospheric Research archive (Jenne 1975); (bottom) simulated minus observed with negative values shaded.

Antarctica in DJF. This latter discrepancy is common to all GCMs (Schlesinger 1984b) and may actually represent an error in the precipitation observations. On balance, considering the uncertainty of the precipitation observations over the oceans, the simulated precipitation rates can be considered in reasonable agreement with the observations, particularly given the coarse horizontal resolution of the GISS model (Table 4.4).

NCAR Model (Washington and Meehl 1984). The latitude-altitude cross sections of the zonal mean air temperature simulated by the NCAR model for DJF and JJA are presented in Figures 4.24 and 4.25, respectively, along with the corresponding observed and simulated-minus-observed fields that were determined graphically by hand.

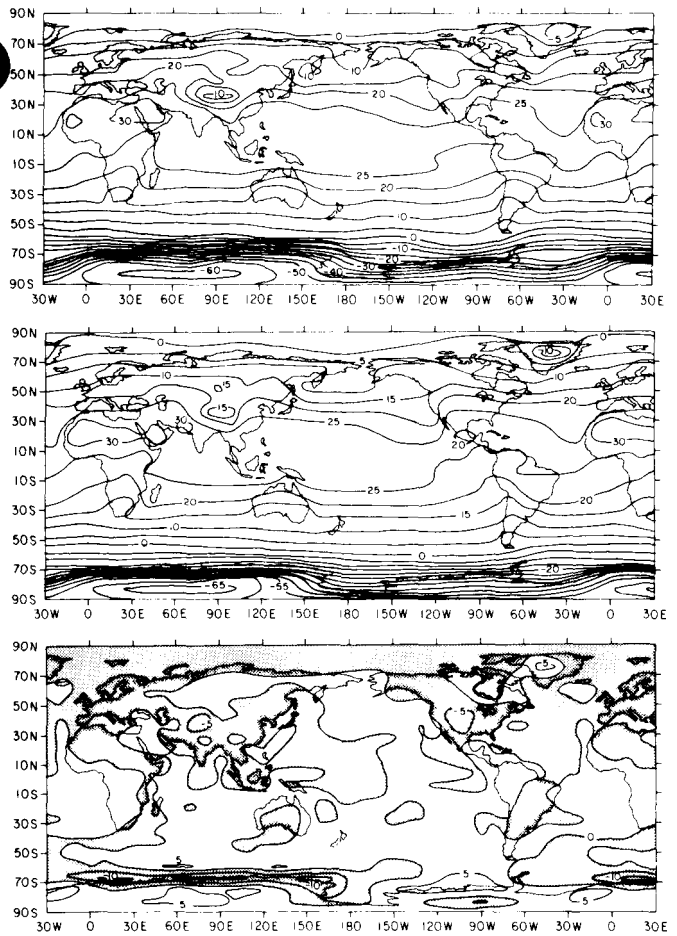

Figure 4.21. As in Figure 4.20, except for JJA.

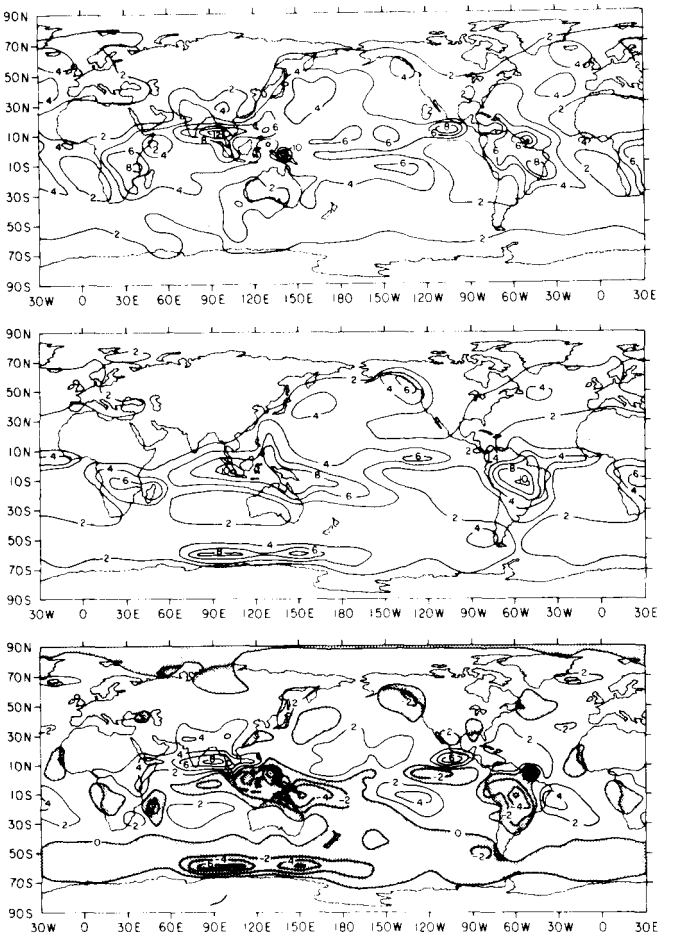

Figure 4.22. Geographical distribution of the precipitation rate (mm d^{-1}) for DJF: (top) simulated with the GISS GCM by Hansen et al. (1984); (middle) observed based on Jaeger (1976); (bottom) simulated minus observed with negative values shaded.

The observed temperature data set chosen by Washington and Meehl and shown in these figures is not the same as that shown in Figures 4.18 and 4.19. Figures 4.24 and 4.25 show that the model correctly reproduces the decrease of temperature with increasing altitude in the troposphere, with a low-level inversion in the Arctic winter and the cold tropical tropopause, the nearly isothermal structure of the stratosphere in the winter polar region, and the increase of temperature with latitude from the winter to summer poles in the middle stratosphere. The simulated temperatures in both seasons are colder than the observed temperatures everywhere except in the middle stratosphere, the tropical tropopause, and near the surface in the tropics, with errors in excess of $-10°C$ located in the lower stratosphere over the poles.

The geographical distributions of the surface air temperature simulated by the NCAR model for DJF and JJA are shown in Figures 4.26 and 4.27, respectively, together with the corresponding observed temperatures. These figures show that during both seasons the model simulates the general decrease of surface air temperature with latitude from the tropics toward the poles and the temperature contrasts between the land and ocean. However, the model generally overestimates the temperatures over the eastern tropical oceans, over land in the tropics where errors ranging from 5 to 15°C are found, over the continental interiors in summer and North America in winter, and over Antarctica in winter by as much as 20°C. As previously noted, the simulation of excessively warm surface air temperatures over Antarctica is common to most GCMs (Schlesinger 1984b). On the other hand, the NCAR model underestimates the maritime surface air temperatures in the high latitudes, particularly in the winter hemisphere. In association with

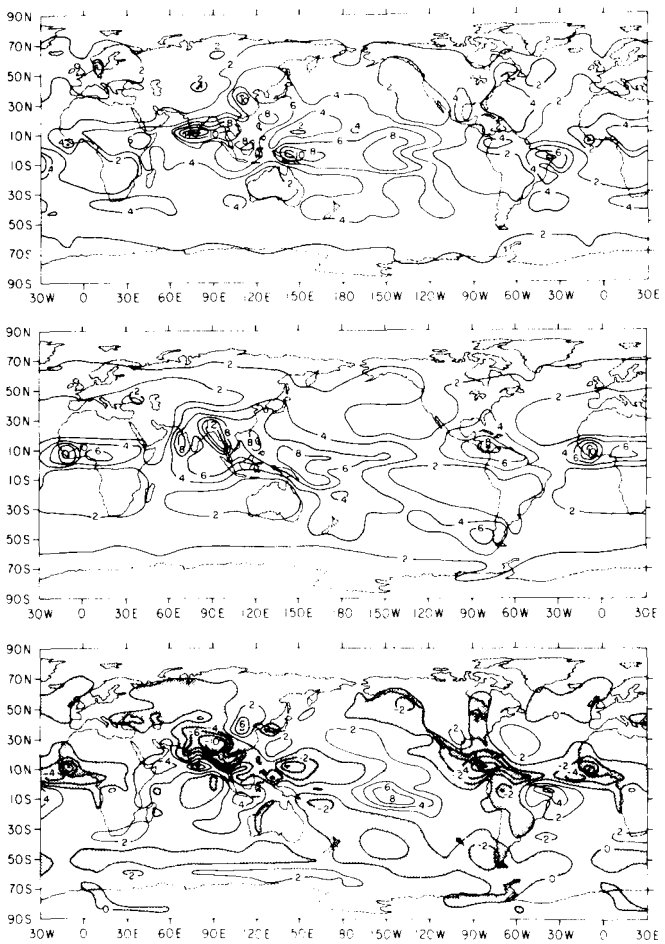

Figure 4.23. As in Figure 4.22, except for JJA.

these colder-than-observed high latitude temperatures, the model overestimates the observed equatorward extent of sea ice. These errors may be the result of the absence of horizontal heat transport in the mixed-layer ocean model.

The geographical distributions of the precipitation rate simulated by the NCAR model for DJF and JJA are shown in Figures 4.28 and 4.29, respectively, together with the corresponding observed distributions. These figures show that the model simulates many of the characteristics of the observed precipitation patterns. In particular, the model simulates the tropical maritime precipitation maximum that extends from the Indian Ocean across the Pacific Ocean, the precipitation maxima over South America in DJF and over Africa during both seasons, the Indian and Southeast Asian monsoons, the subtropical dry regions over the eastern oceans in both hemispheres, and the precipitation minima in the Arctic and Antarctic. However, the

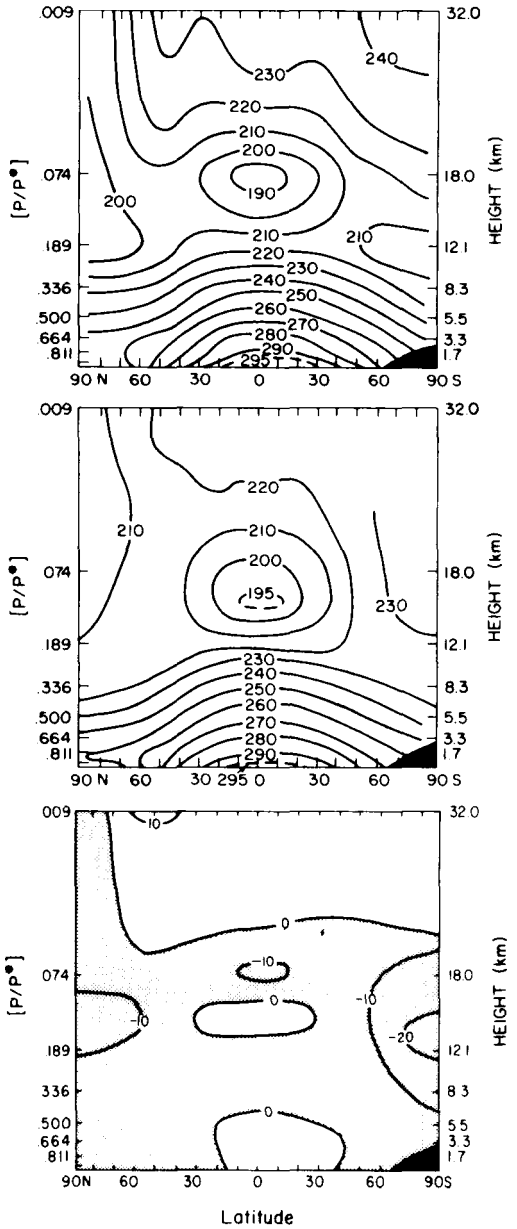

Figure 4.24. Latitude-altitude cross section of the zonal mean air temperature (°C) for DJF: (top) simulated with the NCAR GCM by Washington and Meehl (1984); (middle) observed based on Newell et al. (1972); (bottom) simulated minus observed, obtained by graphical subtraction of the top and middle panels; negative values are shaded.

model fails to simulate the precipitation maxima off the west coast of Chile in DJF and over Central America in JJA as well as the maxima located near the Antarctic coast in DJF. Furthermore, the precipitation simulated near 40°S exceeds the observed precipitation during both seasons, as does the simulated precipitation east of the Asian mainland.

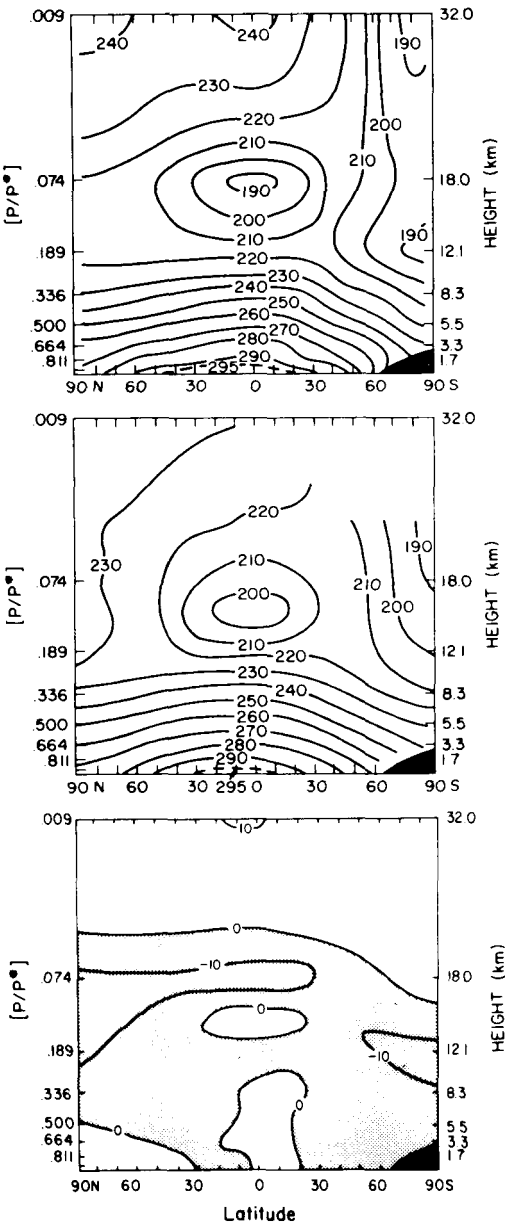

Figure 4.25. As in Figure 4.24, except for JJA.

GFDL Model (Wetherald and Manabe 1986). The latitude-altitude cross sections of the zonal mean air temperature simulated by the GFDL model for DJF and JJA are presented in Figures 4.30 and 4.31, respectively, along with the corresponding observed fields. The observations are the same as those shown for comparison with the GISS model simulations (Figures 4.18 and 4.19) and are therefore different from those presented with the NCAR model simulations (Figures 4.24 and 4.25). Figures 4.30 and 4.31 show that the GFDL model simulates the observed temperature structure of the troposphere and stratosphere in both seasons reasonably well, including the surface inversion in the high latitudes of the winter hemisphere, the cold tropical tropopause, and the stratospheric temperature minimum in the polar night region. However, a comparison of the simulated and observed temperatures also shows several quantitative errors. The model simulates temperatures at the surface that are warmer than observed by 5°C over Antarctica and 10°C over the circum-Antarctic ocean during both seasons, and by 5°C in the tropics during DJF. Furthermore, the temperatures simulated in the north polar region are 5°C too cold in winter and 5°C too warm in summer. The model also simulates the minimum tropical tropopause temperature to be warmer than observed by 5°C in JJA and 10°C in DJF, the polar-night minimum temperatures to be colder than observed by 5°C in JJA and 20°C in DJF, and the summer polar stratospheric temperatures to be 10°C too warm in JJA and 10°C too cold in DJF.

The geographical distributions of the surface air temperature simulated by the GFDL model for DJF and JJA are shown in Figures 4.32 and 4.33, respectively, together with the observed temperatures. These figures show that the GFDL model is successful in reproducing most of the features of the observed temperature distributions for both seasons. The most notable model errors are found over Greenland and Antarctica, where the simulated temperatures are 10°C to 20°C warmer than observed during both DJF and JJA, and over the low-latitude continental regions, where the simulated temperatures are 5°C warmer than observed during both seasons.

The geographical distributions of the precipitation rate simulated by the GFDL model for DJF and JJA are shown in Figures 4.34 and 4.35, respectively, together with the corresponding observations. Figure 4.34 shows that the model simulates the subtropical dry regions off the west coasts of Africa, Australia and South America reasonably well, but overestimates the precipitation over northern Africa, the Himalayas and most of Asia, the North Pacific and North Atlantic oceans, and the polar regions of both hemispheres. The model is successful in reproducing the precipitation maxima that extend from Africa to the central Pacific Ocean and the maximum precipitation over South America

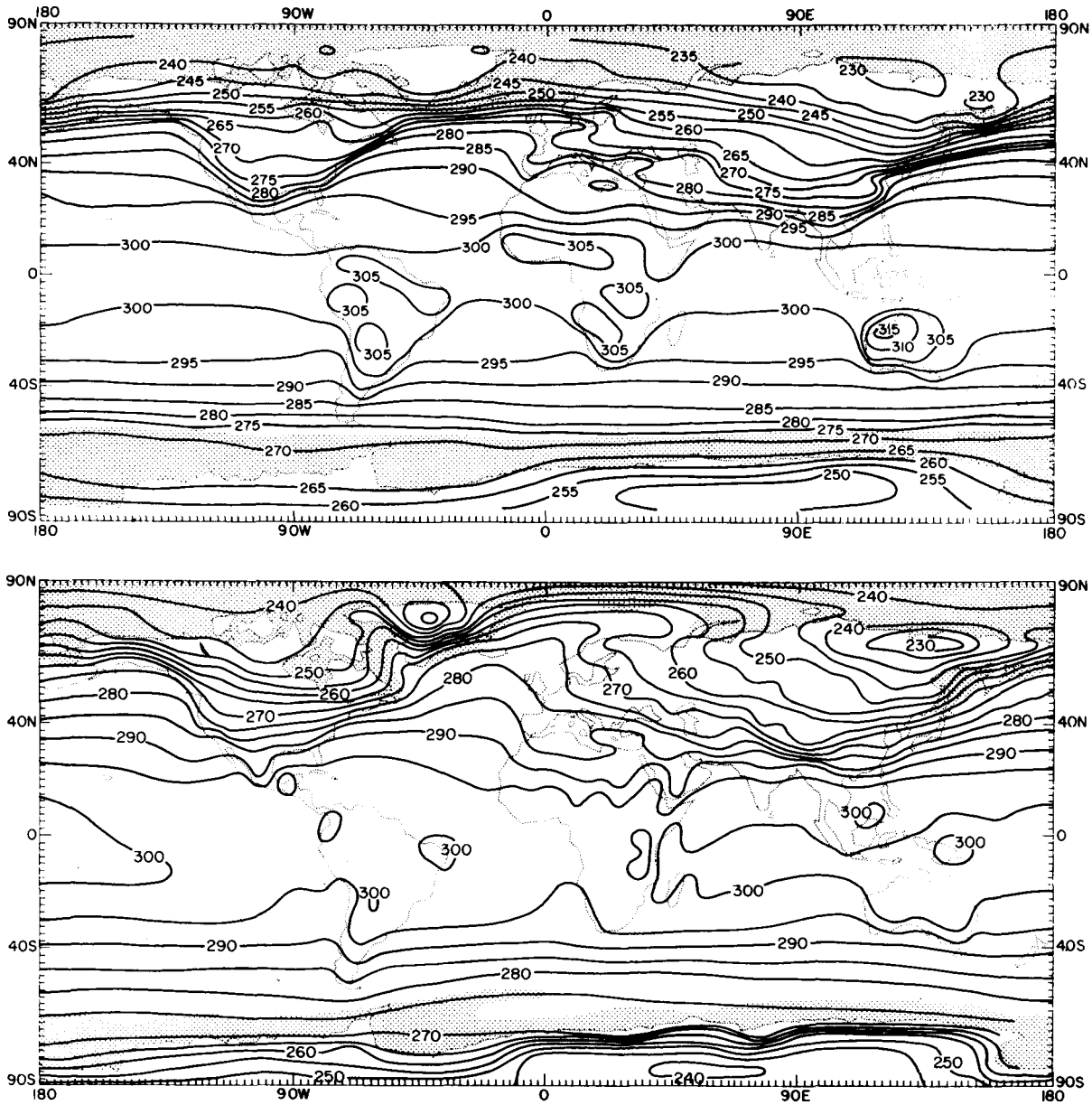

Figure 4.26. Geographical distribution of the surface air temperature (°C): (top) simulated for DJF with the NCAR GCM by Washington and Meehl (1984); (bottom) observed for January from Schutz and Gates (1971) based on Crutcher and Meserve (1970) and Taljaard et al. (1969). Simulated sea ice limits show the edge of sea ice 0.2 m thick. Observed sea ice limits from Alexander and Mobley (1976).

and the Gulf of Alaska, but fails to simulate the precipitation maxima west of Chile and near Antarctica between 70°E and 150°W longitude. However, as previously noted, the latter observed precipitation maximum is not found in other observed data sets and so may be spurious. Figure 4.35 shows that the model simulates the observed precipitation for JJA with greater accuracy than that for DJF, with dry regions over the subtropical eastern ocean basins, North Africa eastward to central Asia, and the Gulf of Alaska, and rainy regions in the intertropical convergence zones, the Asian monsoon, and off the west coast of Chile. The most prominant errors are the overestimates of precipitation in the subtropics of the Southern Hemisphere, the Asian monsoon, and the polar regions of both hemispheres.

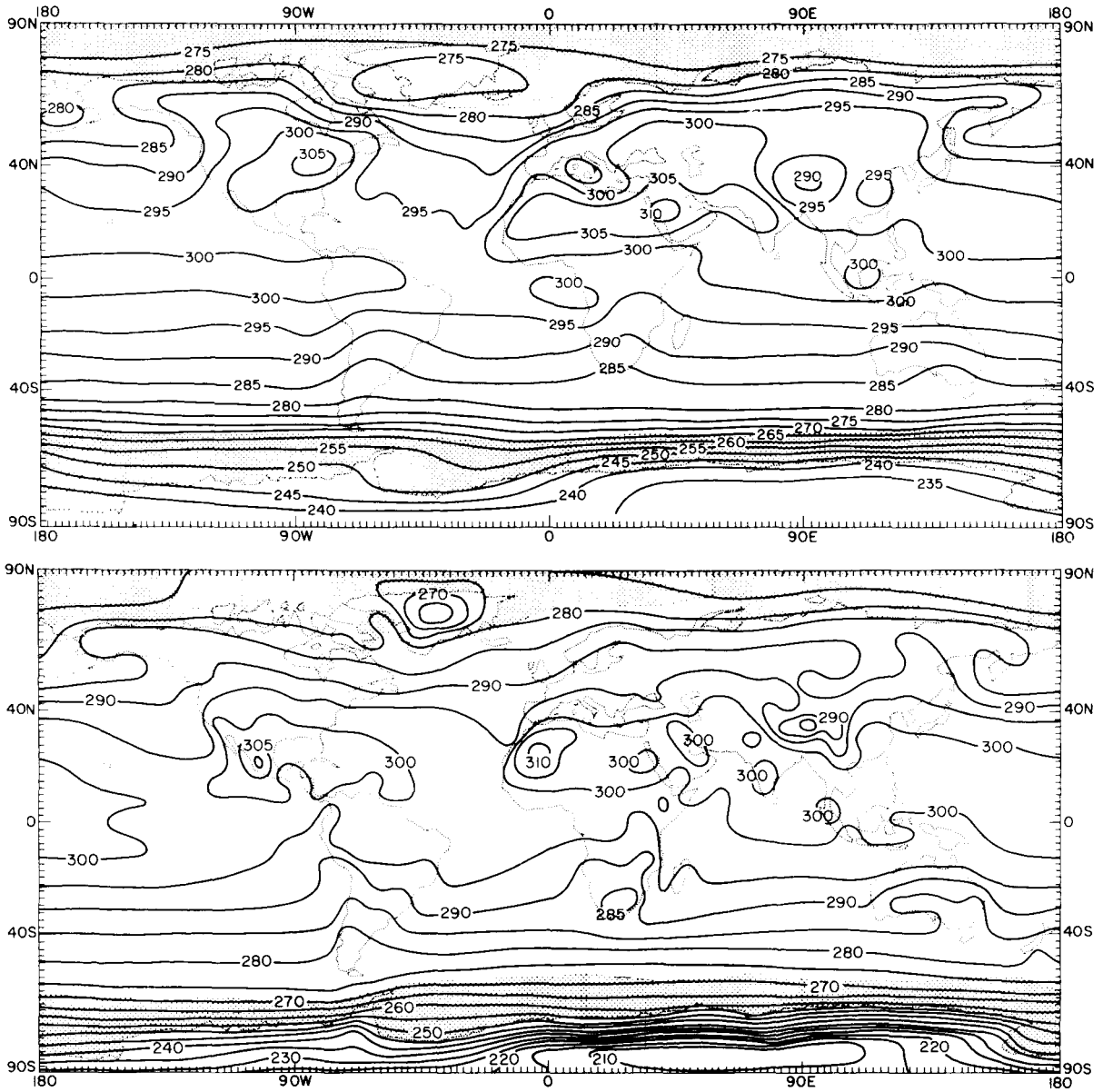

Figure 4.27. As in Figure 4.26, except: (top) simulated for JJA; (bottom) observed for July from Schutz and Gates (1972).

4.3.4.2 Comparison Of Recent Simulations Of $2 \times CO_2 - 1 \times CO_2$ Climate Changes

The $2 \times CO_2 - 1 \times CO_2$ climate changes simulated by the GISS model (Hansen et al. 1984), the NCAR model (Washington and Meehl 1984) and the GFDL model (Wetherald and Manabe, 1986) are shown in Table 4.3 for the annual global mean surface air temperature and precipitation rate. This table shows that these models simulate a CO_2-induced warming of the surface air temperature of 3.5 to 4.2°C and an increase in the precipitation rate of 7.1 to 11.0%.

It is of interest to contrast these results with those obtained from the earlier studies shown in Tables 4.2 and 4.3. An earlier version of the GISS model with computed clouds and annual mean insolation (Hansen 1979) obtained a 3.9°C warming and a 6.0% increase in precipitation rate, whereas the current GISS model with computed clouds and the annual insolation cycle obtained 4.2°C and 11%. The contemporary NCAR model with computed clouds and annual mean insolation (Washington and

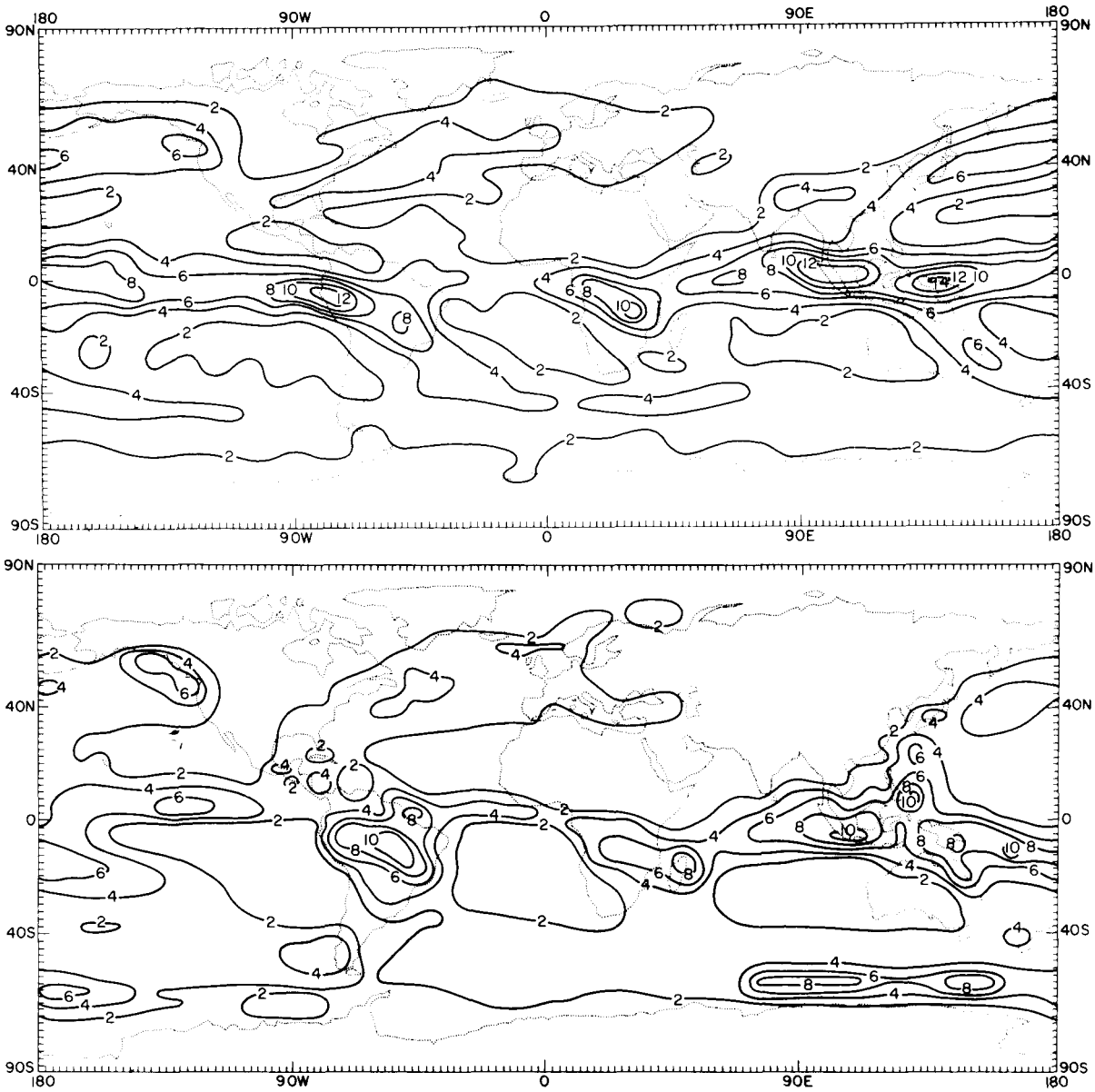

Figure 4.28. Geographical distribution of the precipitation rate (mm d^{-1}) for DJF: (top) simulated with the NCAR GCM by Washington and Meehl (1984); (bottom) observed based on Jaeger (1976).

Meehl 1983) obtained a 1.3°C warming and a 3.3% increase in precipitation rate, whereas the NCAR model with computed clouds and the annual insolation cycle obtained a 3.5°C warming and 7.1% increase in precipitation rate. Thus, both the GISS and NCAR models with the annual insolation cycle produce a larger 2 × CO_2-induced climate change than these models with annual mean insolation. These results are in contrast to what was found by Wetherald and Manabe (1981) from a model with idealized geography and fixed clouds, namely that the 4 × CO_2-induced climatic change with the annual insolation cycle was less than that with annual mean insolation (see Tables 4.2 and 4.3).

Regarding the GISS model, the result may be caused by the differences between the versions of the model used by Hansen (1979) and Hansen et al. (1984). Furthermore, the GISS models were global with realistic geography and predicted clouds, whereas the GFDL model used by Wetherald and Manabe (1981) was a sector of the Earth with idealized geography and fixed clouds. These differences may also contribute to the difference

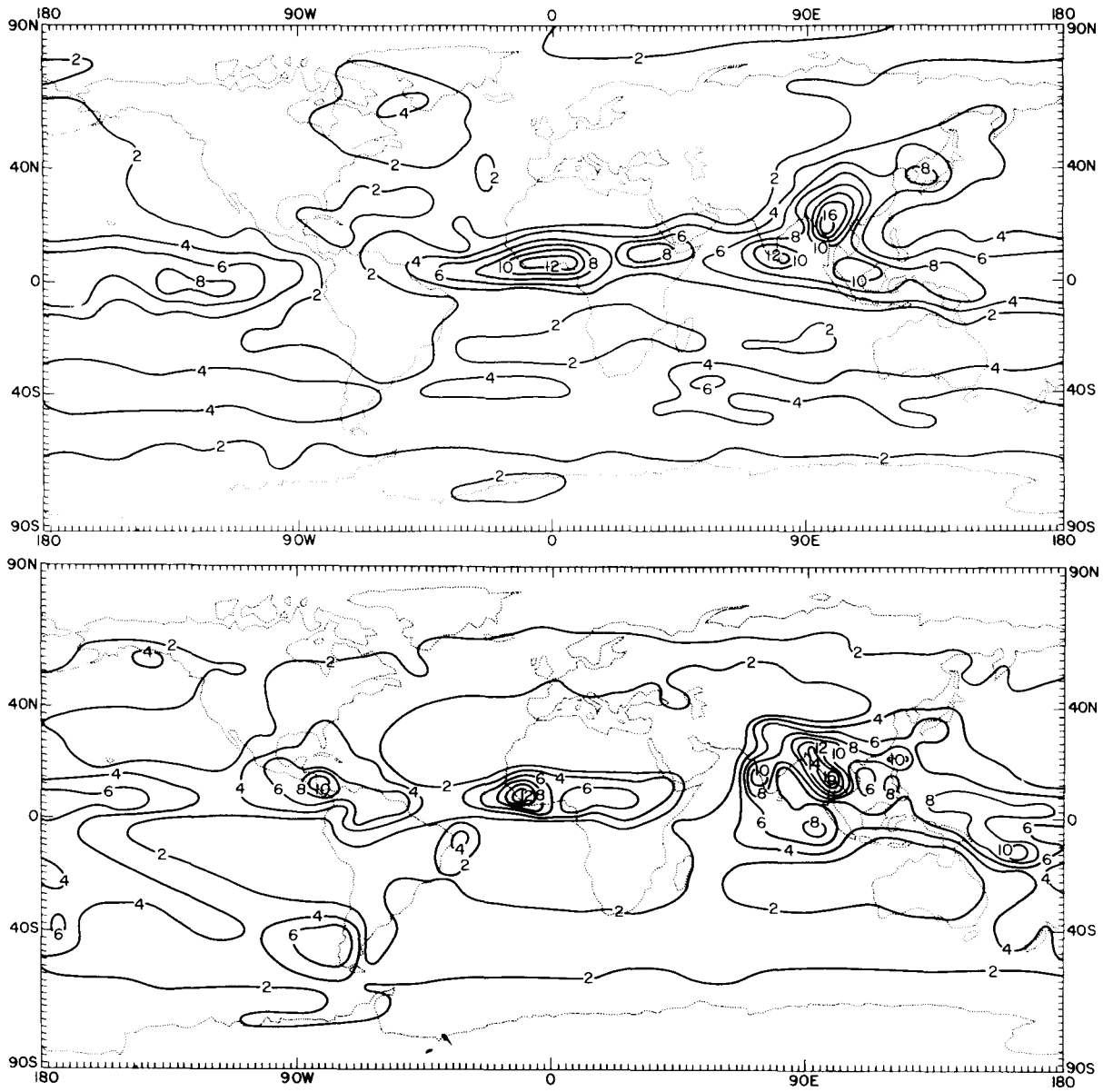

Figure 4.29. As in Figure 4.28, except for JJA.

with the NCAR model. However, a more likely explanation lies in the ice-albedo feedback mechanism and the fact that both GFDL simulations were performed with a mixed-layer ocean model, whereas a mixed-layer ocean model was used in the seasonal NCAR simulation and a swamp ocean model in the annual NCAR simulation. The 1 × CO_2 annual simulation with the GFDL model is colder than the 1 × CO_2 seasonal simulation (Figure 4.17) and likely has a larger sea ice extent; this would produce a larger CO_2-induced ice-albedo feedback and larger warming. The 1 × CO_2 annual simulation with the NCAR model is also colder than the 1 × CO_2 seasonal NCAR simulation (see Figure 4.14 and Table 4.5); therefore, it would also be expected to have a larger warming. The fact that it has a smaller warming may indicate that there is less sea ice in the 1 × CO_2 seasonal simulation with the mixed-layer ocean model. Perhaps less sea ice occurs in the swamp model because it is diagnostically determined and can thus change to open ocean (and vice versa) in a single time step, whereas the sea ice in the mixed-layer model is prognostically determined

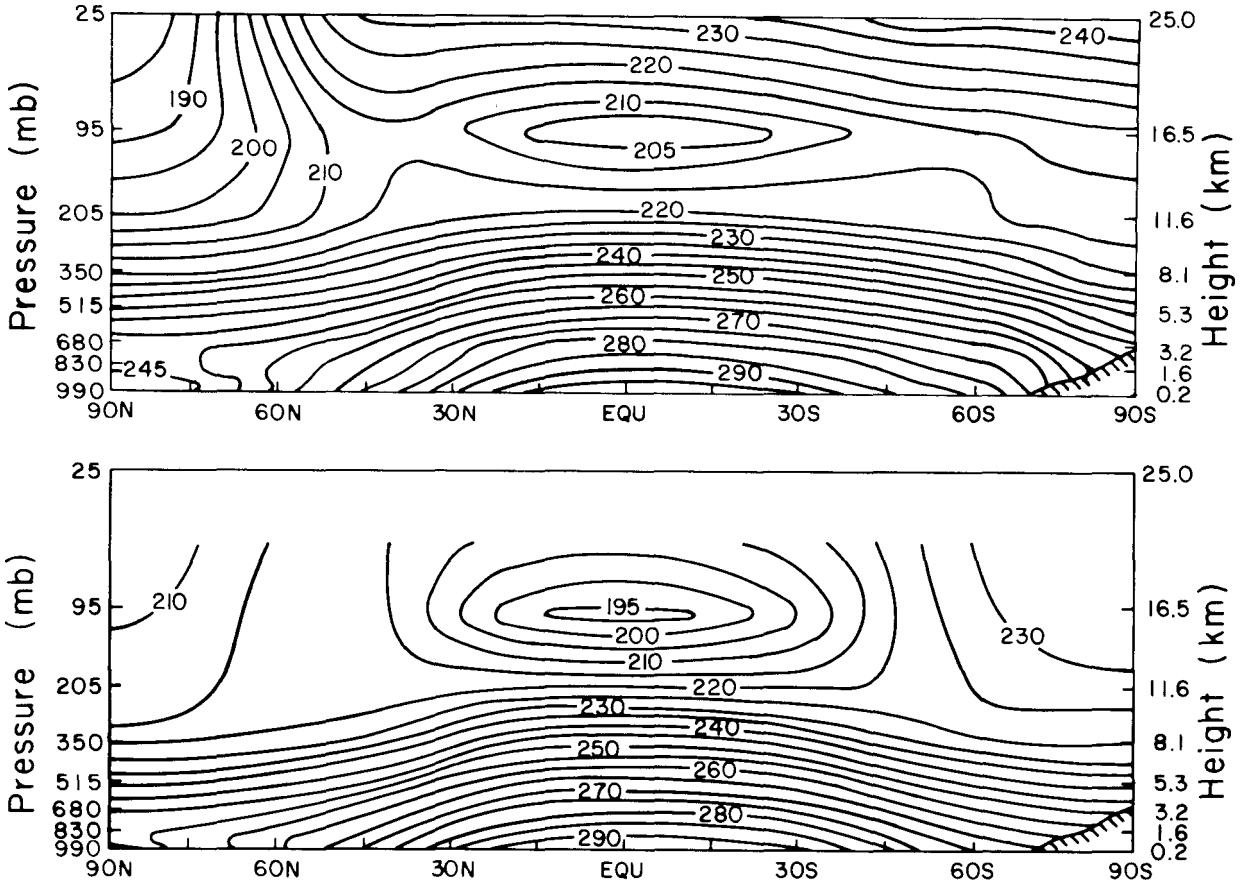

Figure 4.30. Latitude-altitude cross section of the zonal mean air temperature (°C) for DJF: (top) simulated with the GFDL GCM by Wetherald and Manabe (1986); (bottom) observed based on Oort (1983).

and, therefore, changes more slowly. Clearly, further analyses of the simulations are required to clarify the contradiction between the studies of Hansen (1979), Wetherald and Manabe (1981), Washington and Meehl (1983, 1984), and Hansen et al. (1984).

Comparing the results of the Wetherald and Manabe (1986) study with those of Manabe and Stouffer (1980) is also useful. Table 4.3 shows that the 4.0°C warming obtained by Wetherald and Manabe (1986) for a CO_2 doubling is virtually the same as the 4.1°C warming obtained by Manabe and Stouffer for a CO_2 quadrupling, with the percentage change in precipitation rate being larger for the CO_2 doubling than for the quadrupling. As described in Section 4.3.4 and shown in Table 4.4, the only difference between the models used by Manabe and Stouffer (1980) and Wetherald and Manabe (1986) is that clouds are prescribed in the former and predicted in the latter. Thus, these results indicate that clouds are of extreme importance in CO_2-induced climate change. But this contradicts the findings of Manabe and Wetherald (1975, 1980) and Washington and Meehl (1983) shown in Table 4.2, which indicate virtually no difference between the CO_2-induced temperature changes with prescribed and predicted clouds. The explanation for this contradiction remains to be determined.

In the following discussion we present the geographical and temporal distributions of the $2 \times CO_2 - 1 \times CO_2$ climate changes simulated by the GISS, NCAR, and GFDL models.

Temperature. In this subsection we present latitude-altitude cross sections, geographical distributions, and latitude-time cross sections of the equilibrium temperature changes induced by doubled CO_2 as simulated by the GFDL, GISS, and NCAR models.

The latitude-altitude cross sections of the zonal mean $2 \times CO_2 - 1 \times CO_2$ air temperature differences simulated by the GFDL, GISS, and NCAR models for DJF and JJA are presented in Figures

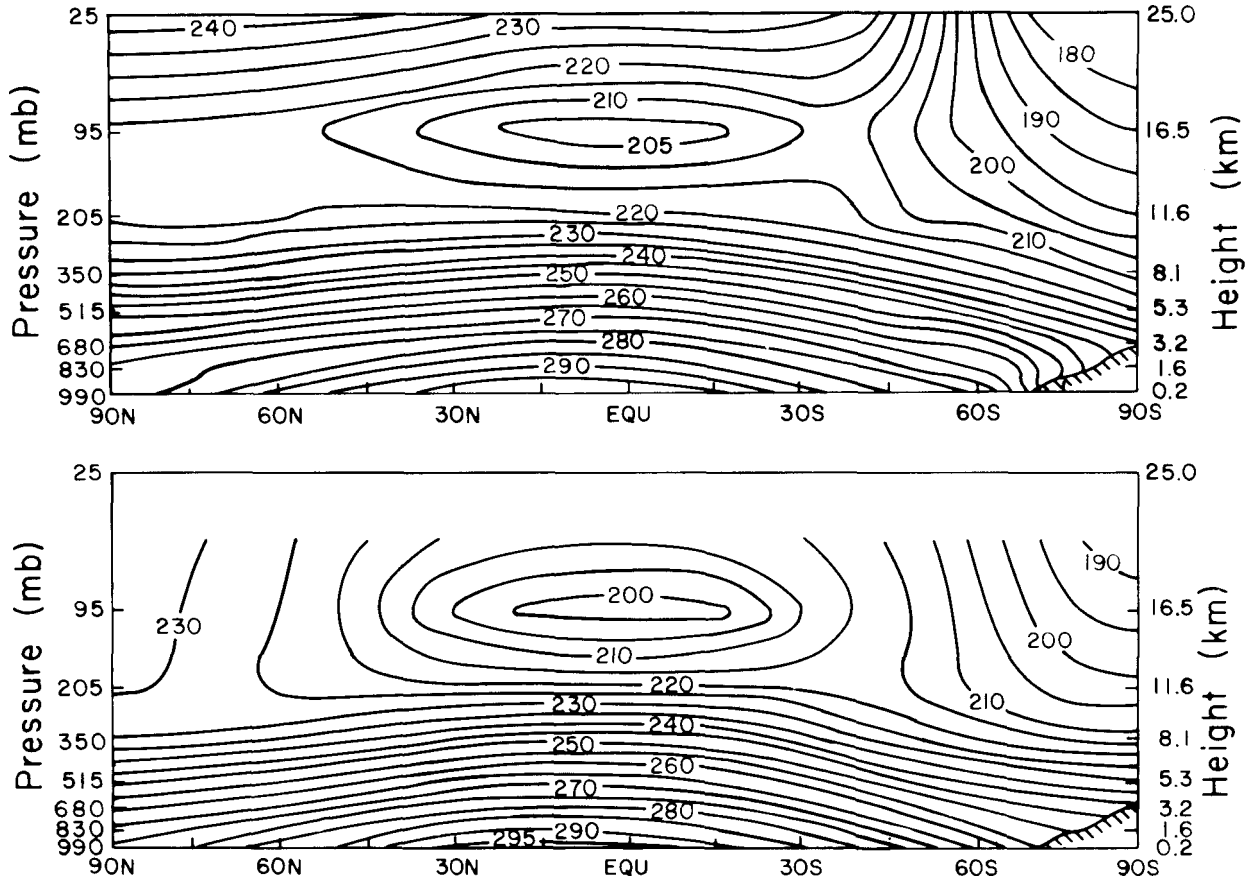

Figure 4.31. As in Figure 4.30, except for JJA.

4.36 and 4.37, respectively, from the surface to the middle of the uppermost layer of each model. These cross sections show the following qualitative similarities: (1) the CO_2-induced temperature changes during both seasons are negative in the stratosphere above 20 km and positive in the lower stratosphere, troposphere, and at the surface; (2) the stratospheric cooling increases with altitude everywhere during both seasons; (3) the tropospheric warming increases with altitude between about 30°S and 30°N in DJF and between about 40°S and 90°N in JJA; and (4) the surface warming increases from the tropics toward the higher latitudes in the winter hemisphere in both seasons and also in the summer (southern) hemisphere during DJF. The cross sections also show the following quantitative differences: (1) the magnitude of the maximum stratosphere cooling at 25 km ranges from −3°C in the GISS model to −8°C in the GFDL model during both seasons; (2) the altitude of the maximum tropical tropopause warming ranges from about 8 km in the NCAR model to about 10 km in the GFDL and GISS models during both seasons; (3) the stratospheric cooling begins at 15 km altitude in the NCAR model and 20 km in the GFDL and GISS models; (4) the magnitude of the tropical tropopause warming ranges from 3°C in the NCAR model to 7°C in the GISS model for both seasons; (5) the latitude of the maximum Northern Hemisphere surface warming in DJF ranges from 65°N in the NCAR model to 80°N in the GFDL model; and (6) the magnitude of the maximum surface warming in the winter hemisphere ranges from 7°C in the GISS and NCAR models to 14°C in the GFDL model during DJF and from 7°C in the GFDL and GISS models to 13°C in the NCAR model during JJA.

As previously noted, contrasting the GFDL model study of Wetherald and Manabe (1986) with that of Manabe and Stouffer (1980) is useful because these models differ only in their treatment of cloudiness, the former being predicted and the latter being prescribed. Comparing the top panel of Figure 4.36 with the middle panel of Figure 4.9

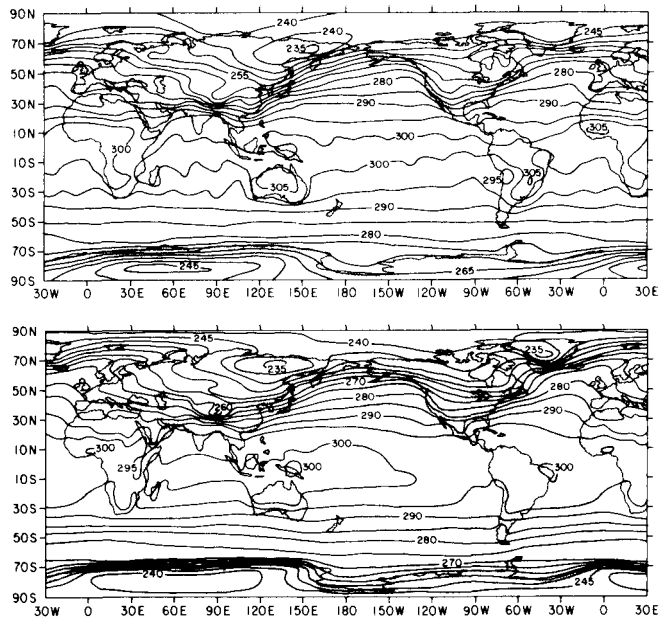

Figure 4.32. Geographical distribution of the surface air temperature (°C): (top) simulated for DJF with the GFDL GCM by Wetherald and Manabe (1986); (bottom) observed for January from Schutz and Gates (1971) based on Crutcher and Meserve (1970) and Taljaard et al. (1969).

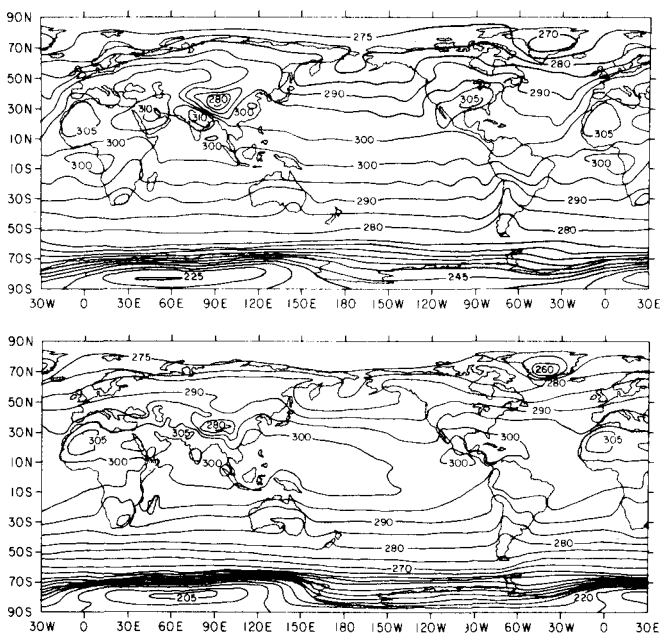

Figure 4.33. As in Figure 4.32, except: (top) for JJA; (bottom) for July from Schutz and Gates (1972).

and the top panel of Figure 4.37 with the bottom panel of Figure 4.9 shows that, as expected, the $2 \times CO_2 - 1 \times CO_2$ stratospheric cooling is about half the $4 \times CO_2 - 1 \times CO_2$ cooling, but the $2 \times CO_2 - 1 \times CO_2$ tropospheric and surface warming

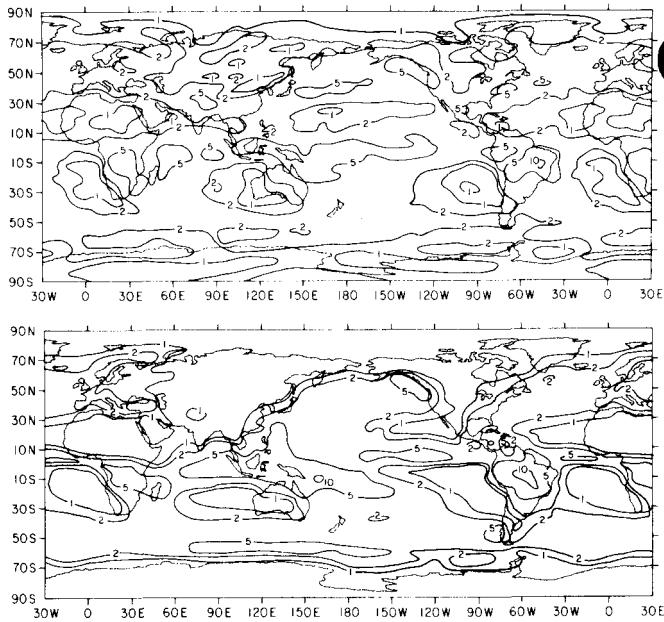

Figure 4.34. Geographical distribution of the precipitation rate (mm d^{-1}) for DJF: (top) simulated with the GFDL GCM by Wetherald and Manabe (1986); (bottom) observed based on Jaeger (1976).

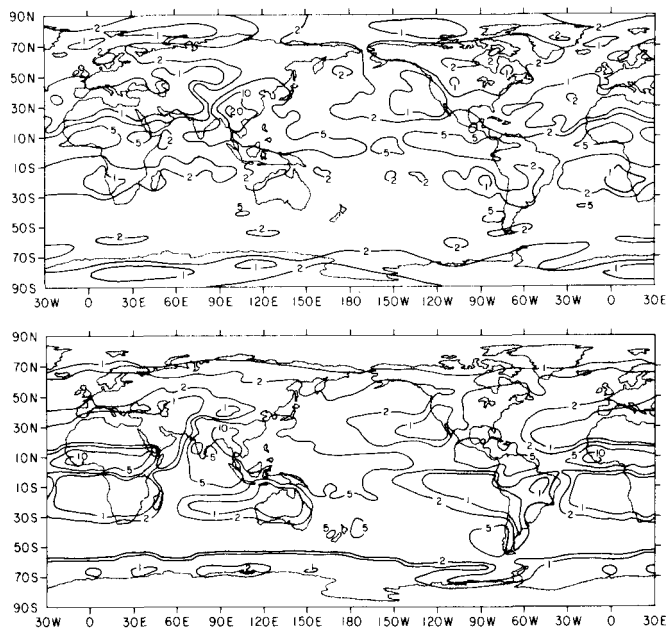

Figure 4.35. As in Figure 4.34, except for JJA.

is comparable to the $4 \times CO_2 - 1 \times CO_2$ warming and is even somewhat larger in the Arctic during DJF. Thus, the feedback of the predicted clouds in the Wetherald and Manabe (1986) study apparently almost doubles the sensitivity of the tropospheric and surface temperature changes to increased CO_2 concentrations.

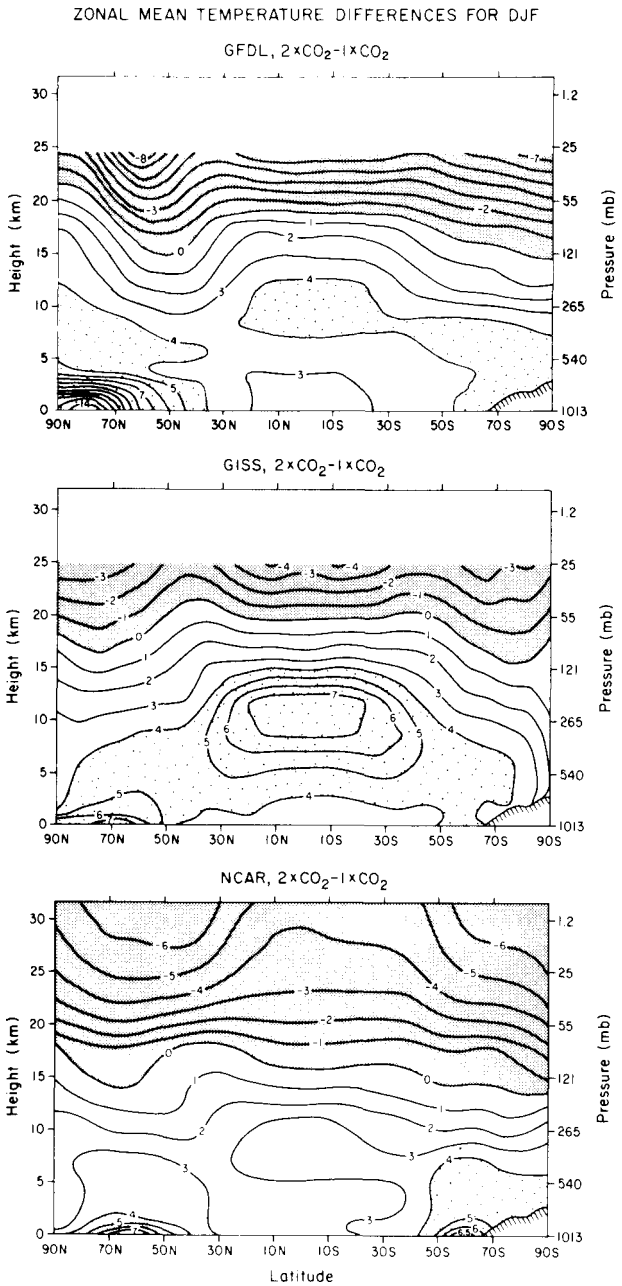

Figure 4.36. Latitude-altitude cross section of the change in zonal mean air temperature (°C), $2 \times CO_2 - 1 \times CO_2$, for DJF simulated with: (top) the GFDL GCM by Wetherald and Manabe (1986); (middle) the GISS GCM by Hansen et al. (1984); (bottom) the NCAR GCM by Washington and Meehl (1984). Heavy stipple indicates a temperature decrease and light stipple an increase larger than 4°C.

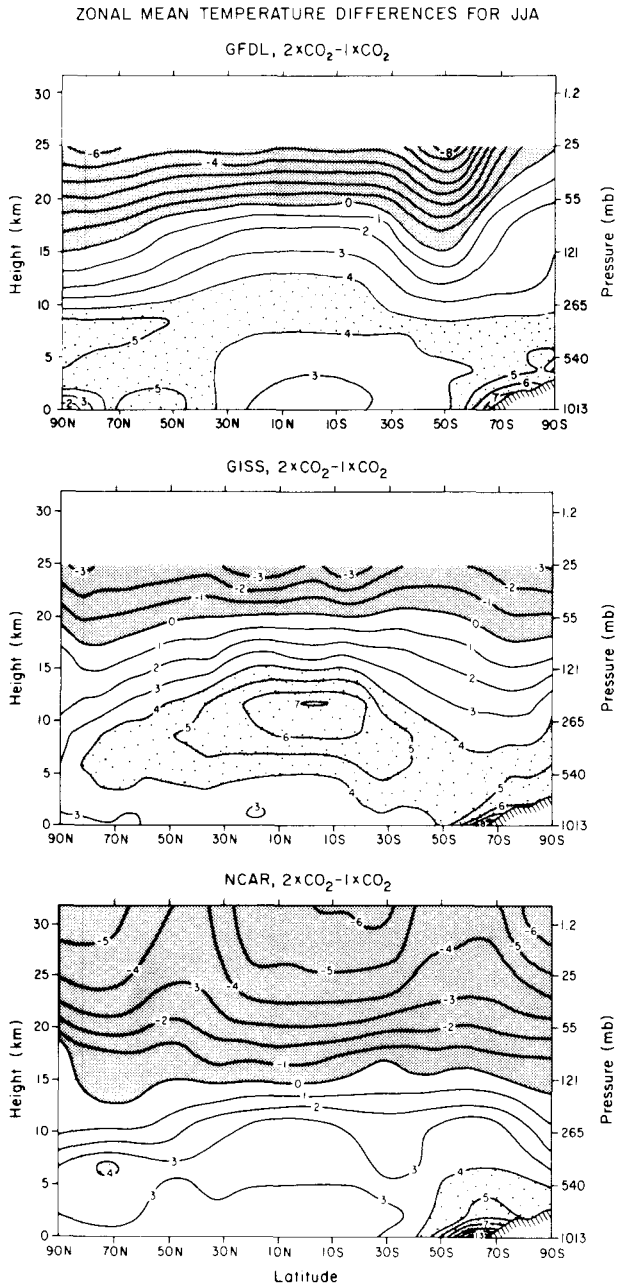

Figure 4.37. As in Figure 4.36, except for JJA.

The geographical distributions of the $2 \times CO_2 - 1 \times CO_2$ surface air temperature changes simulated by the GFDL, GISS, and NCAR models for DJF and JJA are presented in Figures 4.38 and 4.39, respectively. Hansen et al. (1984) analyzed the statistical significance of the annual mean surface air temperature changes for the last 10 years of the GISS simulations and found that the temperature change was larger than five times the standard deviation of the control simulation over most of the Earth. Washington and Meehl (1984) performed a similar analysis for the last 7 years of the NCAR simulations and found that the temperature differences were significant at or less than the 5% level almost everywhere. From the similarity of the 7-year mean results with the 3-year mean results shown in Figures 4.38 and 4.39, it is inferred that the latter

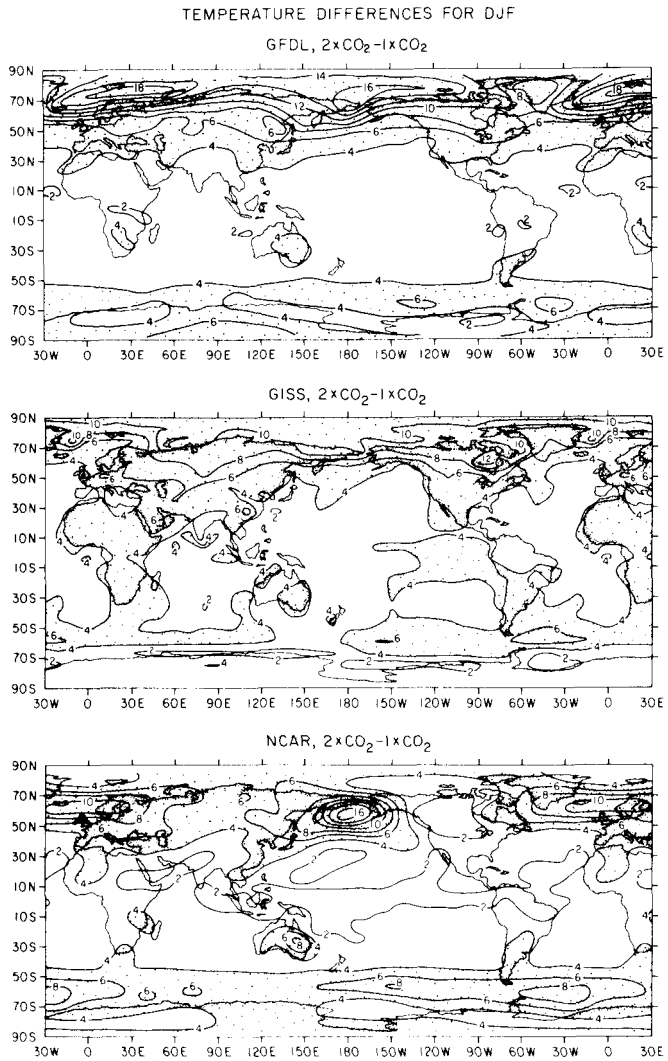

Figure 4.38. Geographical distribution of the surface air temperature change (°C), $2 \times CO_2 - 1 \times CO_2$, for DJF simulated with: (top) the GFDL GCM by Wetherald and Manabe (1986); (middle) the GISS GCM by Hansen et al. (1984); (bottom) the NCAR GCM by Washington and Meehl (1984). Stipple indicates temperature increases larger than 4°C.

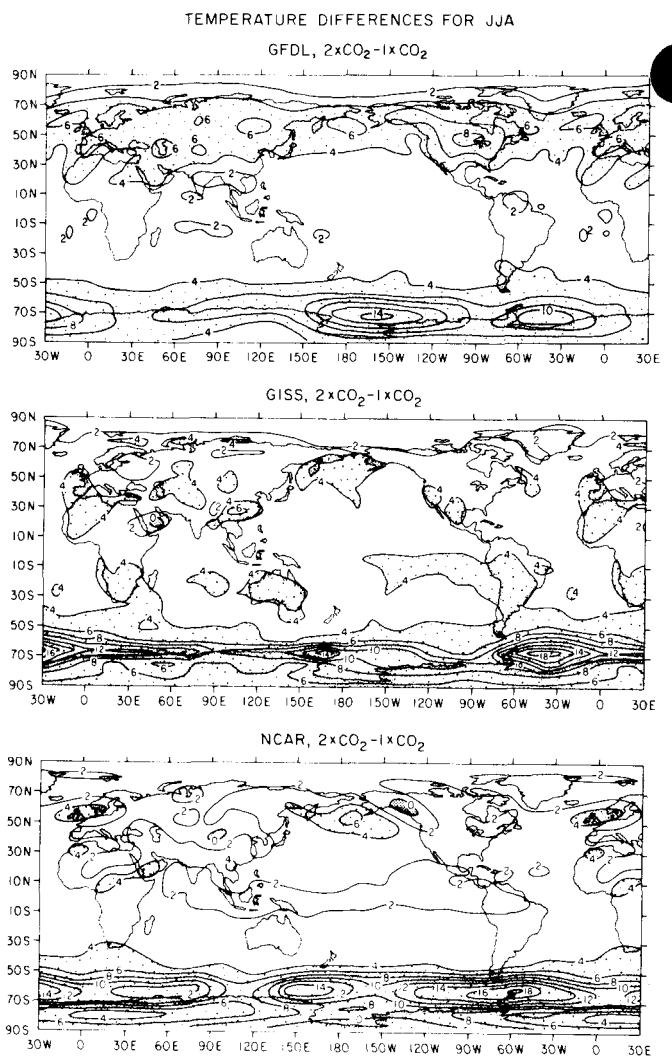

Figure 4.39. As in Figure 4.38, except for JJA.

also are significant at or below the 5% level almost everywhere.

Figures 4.38 and 4.39 show that all three models simulate a CO_2-induced surface air temperature warming virtually everywhere. In general, warming is minimum in the tropics during both seasons, at least over the ocean, and increases toward the winter pole. The tropical maritime warming minimum ranges from about 2°C in the NCAR simulation to about 4°C in the GFDL and GISS simulations. Maximum warming in DJF occurs in the Arctic in both the GFDL and GISS simulations and occurs near 65°N in the NCAR simulation. The maximum warming in JJA occurs around the Antarctic coast in all three simulations. The locations of the wintertime warming maxima in both hemispheres coincide with the locations where the $1 \times CO_2$ sea ice extent retreats poleward in the $2 \times CO_2$ simulation. The magnitude of the wintertime warming maxima in the Northern Hemisphere ranges from 10°C in the GISS simulation to 18°C in the GFDL simulation, and in the Southern Hemisphere it ranges from 14°C in the GFDL simulation to 18°C in both the GISS and NCAR simulations. In JJA there is a warming minimum in the Arctic of about 2°C in all three simulations. Next we will discuss the CO_2-induced warming for each of the continents.

In Africa the warming shows little seasonal dependence in the GFDL simulation with values generally less than 4°C. There is somewhat more

seasonal variation in the NCAR simulation with values also generally less than 4°C. The largest seasonal variation is shown by the GISS simulation, with warming in excess of 4°C everywhere in DJF, but occurring only in northern and southern Africa in JJA.

In the Arabian peninsula the warming is maximum in JJA in the GFDL and NCAR simulations, but is maximum in DJF in the GISS simulation. In India the warming is minimum in JJA in the GFDL simulation but shows little seasonal variation in the GISS and NCAR simulations. In Australia, warming in excess of 4°C is simulated by all three models in the southeastern region in DJF, whereas warming in excess of 4°C is simulated in JJA only by the GISS model.

All three models simulate only a small seasonal variation in the CO_2-induced warming in South America. The GFDL model simulates warming less than 4°C everywhere except in Chile and Argentina. The GISS model simulates a greater equatorward penetration of the 4°C warming than the GFDL model. The NCAR model simulates a warming of 2°C in the northern region during both seasons and warming of 4°C over Chile and Argentina only during DJF.

Large seasonal changes in the warming are simulated over Antarctica by all three models with the warming increasing from summer to winter. The summertime warming is about 4°C in the GFDL and NCAR simulations and is somewhat smaller in the GISS simulation. The wintertime warming varies with location from about 4 to 8°C in all three simulations.

In North America the wintertime warming generally increases with latitude in the GFDL and GISS simulations with values of 4°C in the south to about 10°C in the north. In contrast, the NCAR model simulates a warming less than 4°C everywhere with a minimum of 2°C centered over Canada. The summertime warming is simulated to be less than the wintertime warming virtually everywhere by the GISS model, and everywhere, except in the southwest, by the GFDL model. On the other hand, the summertime warming simulated by the NCAR model is larger than the simulated wintertime warming over most of Canada and the north-central United States.

In Eurasia all three models simulate a winter warming that is larger than the summer warming. The GFDL and GISS models simulate a wintertime warming that generally increases with latitude from about 4°C in the south to 10°C in the north. However, the NCAR model simulates a minimum wintertime warming in central Asia. This difference is likely caused by the maximum warming in the NCAR model being simulated at 65°N off the east and west coasts, whereas the maximum warming is simulated in the Arctic in the GFDL and GISS models. The summertime warming ranges from about 2°C in the NCAR model to 4°C in the GFDL model.

This presentation of the geographical distributions of the CO_2-induced surface air temperature changes for DJF and JJA shows that, although there are similarities in the simulations of the models, particularly the latitudinal variations, there are significant differences in both the magnitude and seasonality of the regional temperature changes.

The latitude-time cross sections of the zonal mean $2 \times CO_2 - 1 \times CO_2$ surface air temperature changes simulated by the GFDL, GISS, and NCAR models are presented in Figure 4.40. This figure shows little seasonal variation in the CO_2-induced temperature changes simulated by the three models between 50°S and 30°N, where the values range from about 2°C in the NCAR model to about 4°C in the GISS model. All three models simulate a large seasonal variation of the CO_2-induced temperature changes in the regions poleward of 50° latitude in both hemispheres. In the Northern Hemisphere a warming minimum of about 2°C is simulated near the pole by all three models in the summer. The three models also simulate a warming maximum in fall with values that range from 8°C in the NCAR model to 16°C in the GFDL model. This maximum extends into winter in the GFDL and GISS simulations, but not in the NCAR simulation, which exhibits a warming minimum near the pole. The NCAR model also simulates another polar warming minimum in spring that is not found in the GFDL and GISS simulations. In the Southern Hemisphere, all three models simulate a maximum warming in winter and a minimum warming in summer. The summer warming maximum occurs near the Antarctic coast in all three simulations, although about 5° more equatorward in the NCAR model simulation than in the GFDL and GISS model simulations, and

it ranges from 8°C in the GFDL simulation to 14°C in the NCAR simulation.

Generally speaking, Figure 4.40 shows more similarities among the zonal mean surface air temperature changes simulated by the three models than was evident in the comparison of their detailed geographical distributions (Figures 4.38 and 4.39). This indicates a partial cancellation of the differences among the longitudinal temperature changes of the models and suggests that we might place more confidence on the simulated zonal mean temperature changes than on the geographical distributions.

Hydrological Cycle. In this subsection, we present the DJF and JJA geographical distributions and latitude-time cross sections of the CO_2-induced changes in precipitation rate and soil moisture and the latitude-altitude cross section of the annual zonal mean change in cloudiness.

The geographical distributions of the $2 \times CO_2 - 1 \times CO_2$ precipitation rate changes simulated by the GFDL, GISS, and NCAR models for DJF and JJA are presented in Figures 4.41 and 4.42, respectively. Although the NCAR model results have been presented by Washington and Meehl (1984) and Meehl and Washington (1985b), and the GISS model results for the United States have been analyzed by Rind and Lebedeff (1984), the statistical significance of the simulated precipitation rate changes has not been analyzed for the results shown in Figures 4.41 and 4.42. However, an analysis of the statistical significance of precipitation rate changes for doubled CO_2 simulated by the OSU model with annual mean insolation (Schlesinger, 1982, 1984a), suggests that many of the small-scale features shown in these figures represent the natural variability of precipitation (noise) rather than a CO_2-induced change (signal).

Figures 4.41 and 4.42 show that both positive and negative changes in precipitation rate are simulated by all three models and that the largest changes generally occur between 30°S and 30°N. The precipitation changes poleward of these latitudes are generally positive in both seasons over both ocean and land. However, the GFDL model simulates a decreased precipitation rate in JJA over most of North America and Europe and over much of Asia. With this exception, the models generally simulate precipitation increases of less than 1 mm

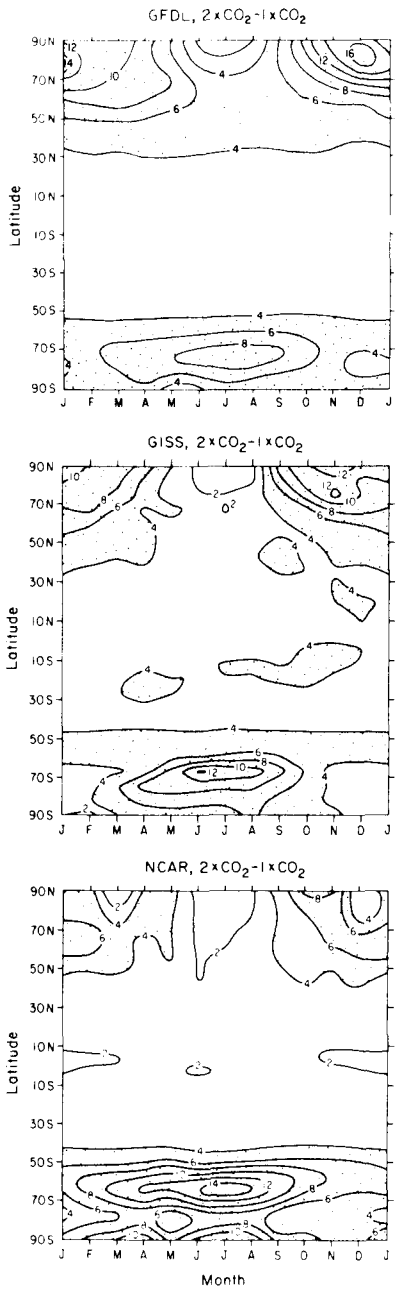

Figure 4.40. Latitude-time cross section of the zonal mean surface air temperature change (°C), $2 \times CO_2 - 1 \times CO_2$, simulated with: (top) the GFDL GCM by Wetherald and Manabe (1986); (middle) the GISS GCM by Hansen et al. (1984); (bottom) the NCAR GCM by Washington and Meehl (1984). Stipple indicates temperature increases larger than 4°C.

day^{-1} over the Northern Hemisphere continents and Antarctica during both seasons.

The precipitation changes between 30°S and 30°N simulated by the models show both qualitative and quantitative differences. For example, over the

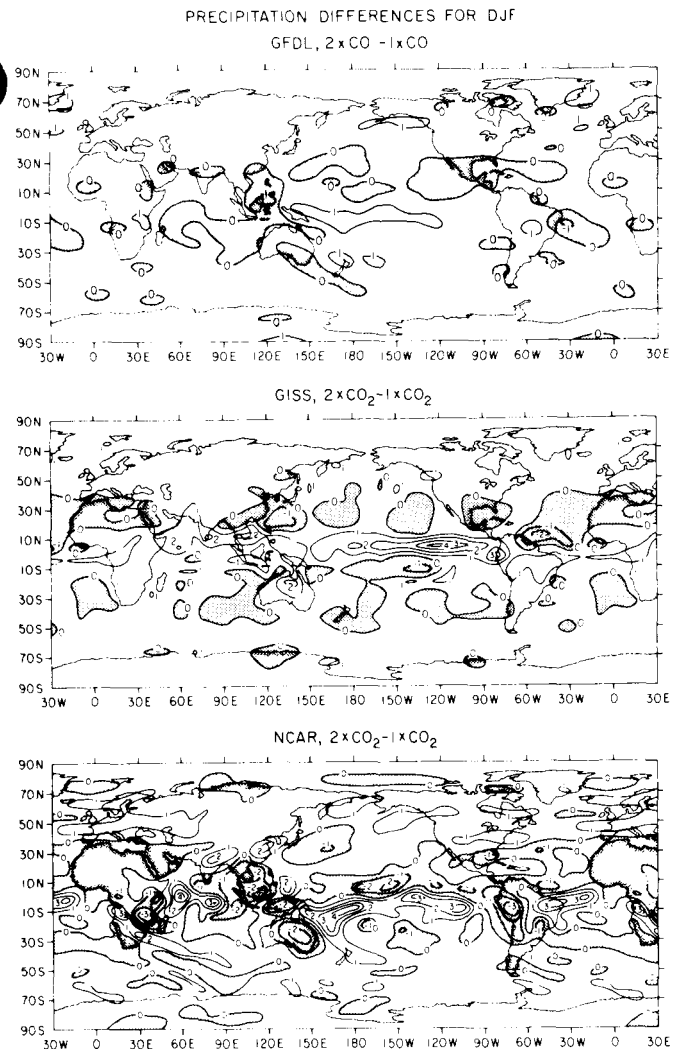

Figure 4.41. Geographical distribution of the precipitation rate change (mm d^{-1}), $2 \times CO_2 - 1 \times CO_2$, for DJF simulated with: (top) the GFDL GCM by Wetherald and Manabe (1986); (middle) the GISS GCM by Hansen et al. (1984); (bottom) the NCAR GCM by Washington and Meehl (1984). Stipple indicates a decrease in precipitation rate.

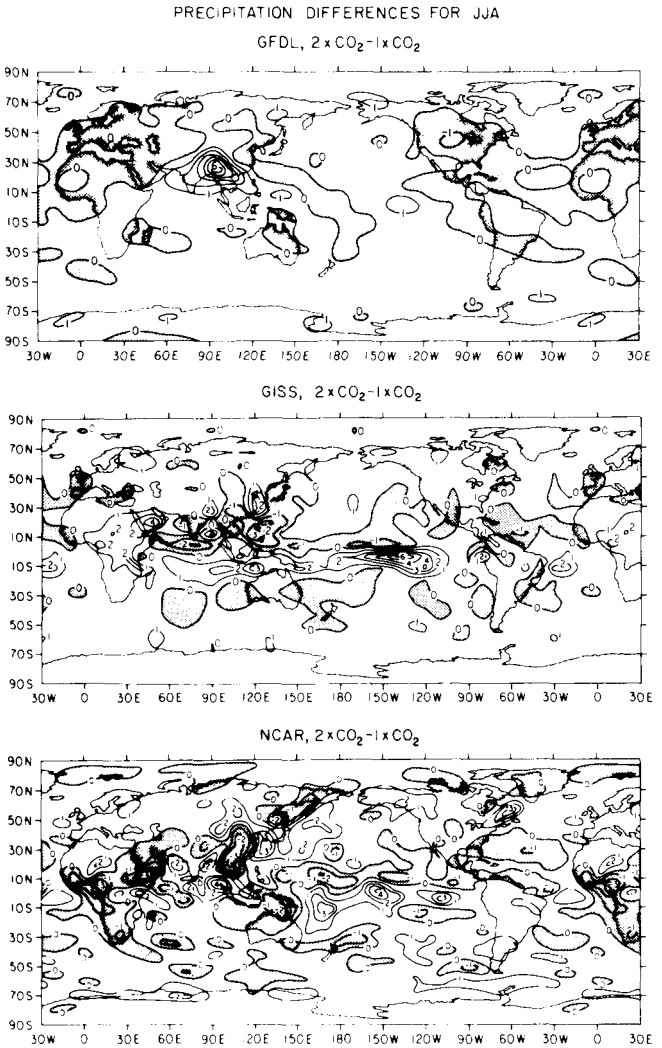

Figure 4.42. As in Figure 4.41, except for JJA.

Pacific Ocean in DJF, the GFDL and NCAR models simulate increases south of the equator and decreases to the north, whereas the GISS model simulates the reverse. Furthermore, in JJA the GFDL model simulates a large increase in the Indian monsoon precipitation whereas the GISS model simulates a small decrease. Perhaps, as suggested by Meehl and Washington (1985b) in their study of the NCAR model's tropical results, the differences in the statistically significant tropical precipitation changes (which have yet to be determined) reflect the modification of the models' Walker circulations induced by their different $2 \times CO_2 - 1 \times CO_2$ sea surface temperature changes superposed on their different $1 \times CO_2$ sea surface temperatures. On the other hand, as argued by Mitchell et al. (1985), if there is little change in circulation, then the pattern of CO_2-induced precipitation changes would be correlated with the $1 \times CO_2$ precipitation pattern.

The latitude-time cross sections of the zonal mean $2 \times CO_2 - 1 \times CO_2$ precipitation rate changes simulated by the GFDL, GISS, and NCAR models are presented in Figure 4.43. This figure shows that the precipitation rate changes simulated by all three models are positive in the equatorial region throughout the year and are negative in adjacent latitudes at least part of the year. Although the decreases in precipitation rate are similar in magnitude in the three simulations, the increases are not;

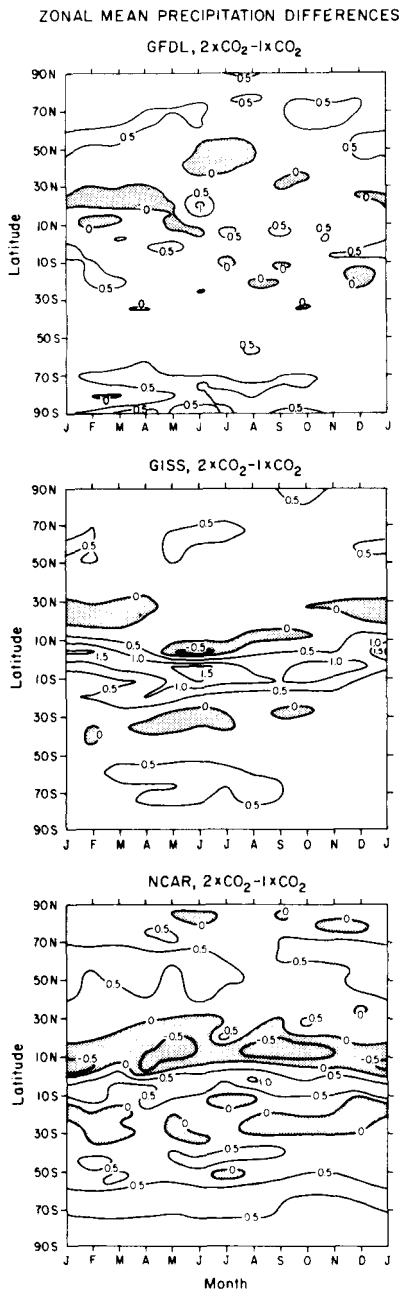

Figure 4.43. Latitude-time cross section of the zonal mean precipitation rate change (mm d^{-1}), $2 \times CO_2 - 1 \times CO_2$, simulated with: (top) the GFDL GCM by Wetherald and Manabe (1986); (middle) the GISS GCM by Hansen el al. (1984); (bottom) the NCAR GCM by Washington and Meehl (1984). Stipple indicates a decrease in precipitation rate.

the GISS and GFDL models produce the largest and the smallest increases, respectively. Elsewhere the precipitation changes are generally positive but small, except near 60°N and 70°S where increases of 0.5 mm day^{-1} are simulated.

The geographical distributions of the CO_2 induced changes in soil water over ice-free land simulated for DJF and JJA by the GFDL, GISS, and NCAR models are presented in Figures 4.44 and 4.45, respectively. The statistical significance of the soil moisture changes simulated by this GFDL model has been determined. Washington and Meehl (1984) analyzed the statistical significance of the soil moisture changes using the results for the last 7 years of the NCAR simulations and found statistically significant results that were at or less than the 5% level over most of the ice-free land. Again, the similarity between the 7-year mean results and the 3-year mean results shown in Figures 4.44 and 4.45 implies that both results are significant at or below the 5% level almost everywhere.

Figure 4.44 shows that there are many qualitative similarities among the simulated soil water changes for DJF. In particular, all three models produce a drying of the soil in most of Africa, the Arabian Peninsula, Central America, Mexico and the Gulf states, and a moistening of the soil in Europe, central Asia, western and central United States, and most of Canada. There also are qualitative differences; namely, moistening is simulated almost everywhere in Australia by the GFDL and GISS models, whereas the NCAR model produces a desiccation. The GFDL and GISS models also simulate an increased soil moisture in the Amazon Basin, whereas the NCAR model simulates a drying effect.

Figure 4.45 shows that there is less agreement among the simulated soil moisture changes for JJA. In Africa the GISS model simulates moistening everywhere except in North Africa; the NCAR model simulates drying everywhere except in North Africa; and the GFDL model produces drying in the east and moistening in the west. In Australia the GFDL and GISS models simulate drying in the south and moistening in the north, while the NCAR model simulates the reverse. The NCAR model simulates moistening virtually everywhere in South America, whereas both drying and moistening are simulated by the GFDL and GISS models. Of particular interest is the change in soil moisture in the Northern Hemisphere. The GFDL model simulates drying almost everywhere in Europe, Asia, and North America. This result is in accord with the summer drying simulated for quadrupled CO_2 by Manabe and

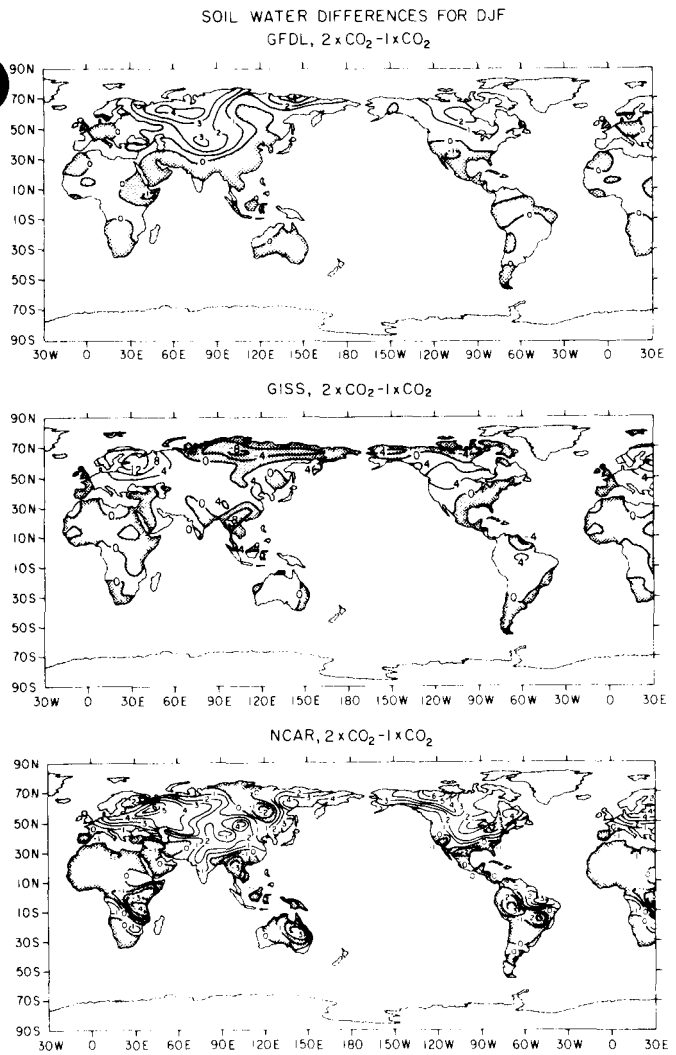

Figure 4.44. Geographical distribution of soil water change (cm), $2 \times CO_2 - 1 \times CO_2$, for DJF simulated with (top) the GFDL GCM by Manabe and Wetherald (1986); (middle) the GISS GCM by Hansen et al. (1984); (bottom) the NCAR GCM by Washington and Meehl (1984). Stipple indicates a decrease in soil water.

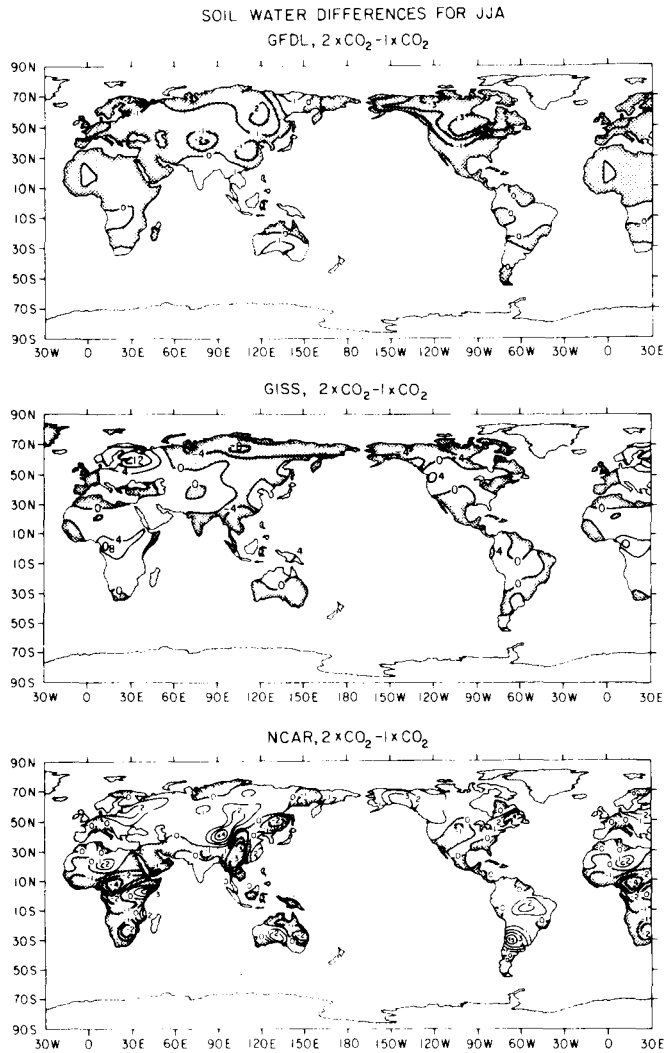

Figure 4.45. As in Figure 4.44, except for JJA.

Stouffer (1980) and Manabe et al. (1981) (Figure 4.12) and might be expected from the decreased JJA precipitation rates simulated over most of Europe, Asia, and North America (Figure 4.42). On the other hand, neither the GISS nor the NCAR models simulate such continent-scale desiccations. In fact, both the NCAR and GISS models produce an increased summer soil moisture over much of North America, Asia, and Europe, again in accord with what might be expected from the increased JJA precipitation rates simulated by these models (Figure 4.42). However, Washington and Meehl (1984) attribute the absence of a summer Northern Hemisphere drying in the NCAR simulation to an increased supply of moisture at the surface caused by an earlier snow melt in spring and a positive feedback among the soil moisture, precipitation, and clouds. In the NCAR model, the soil does not become saturated in spring in either the control or the $2 \times CO_2$ simulation, so one may speculate that all of the excess moisture accumulated in winter and spring is retained in the soil and hence decreases only slowly through the summer due to evaporation.[5] In any case, the differences among the Northern Hemisphere summer soil moisture changes simulated by the models are of particular importance

[5] G. A. Meehl, personal communication.

because these changes strongly determine the agricultural impact of CO_2-induced climate change.

The latitude-time cross sections of the zonal mean soil moisture changes over ice-free land are shown in Figure 4.46. Throughout most of the year all three models simulate a band of decreased soil moisture near 20°N and a band of increased soil moisture near 10°S. There is less agreement in the higher latitudes of both hemispheres, although in the Southern Hemisphere the differences represent only a few grid points. All three models show a moistening of the soil within 30–60°N from October to April. However, from April to September the GFDL model simulates a drying everywhere, the GISS model simulates a drying only during late summer equatorward of about 50°N, and the NCAR model simulates a moistening everywhere. Nevertheless, the moistening simulated by both the GISS and NCAR models reaches its minimum value in late summer.

The latitude-altitude cross sections of the annual zonal mean $2 \times CO_2 - 1 \times CO_2$ cloudiness differences simulated by the GFDL, GISS, and NCAR models are presented in Figure 4.47. This figure shows that both increases and decreases in cloudiness are simulated by all three models. The patterns of the simulated cloudiness changes display several qualitative similarities. In particular, the models simulate increased cloudiness in the stratosphere and near the surface in the high latitudes of both hemispheres, and they simulate decreased cloudiness throughout most of the troposphere in the tropics and middle latitudes of both hemispheres. Thus, dA_c/dT_s is both positive and negative, in agreement with the possibilities obtained from the simple cloud model of Wang et al. (1981) as shown in Appendix A. But, why does the cloudiness decrease in the moist and convectively active tropical and midlatitude regions, where precipitation increases, and decrease in the stable high-latitude surface regions and stratosphere?

Wetherald and Manabe (1980, 1986) have investigated the change in cloud cover in response to changes in thermal forcing caused by increases in either the solar constant or CO_2 concentration. These studies reveal a correlation between the cloud cover changes and changes in the relative humidity. This effect is illustrated in Figure 4.48 for the case of a 6% increase in the solar constant. The

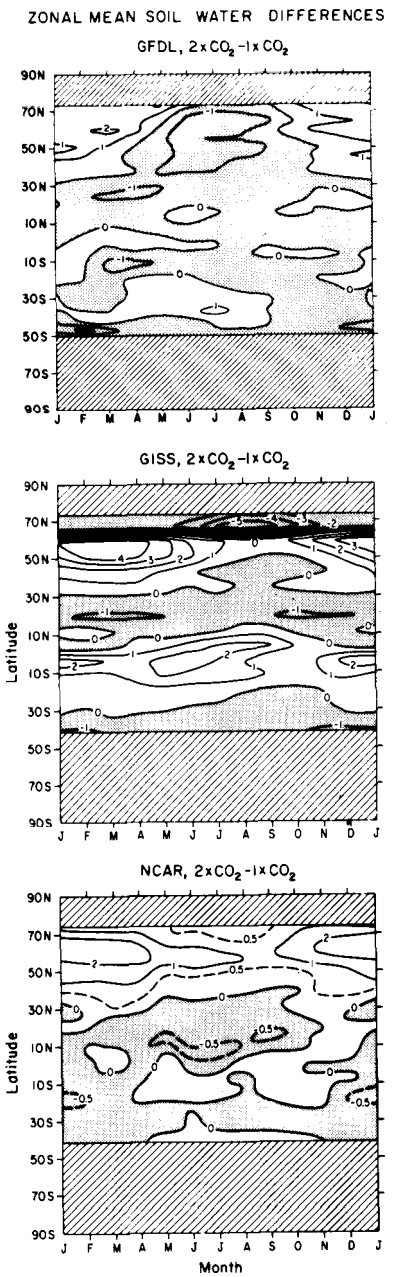

Figure 4.46. Latitude-time cross section of zonal mean soil water change (cm), $2 \times CO_2 - 1 \times CO_2$, only over ice-free land simulated with: (top) the GFDL GCM by Manabe and Wetherald (1986); (middle) the GISS GCM by Hansen et al. (1984); (bottom) the NCAR GCM by Washington and Meehl (1984). Stipple indicates a decrease in soil water, hatching indicates latitudes where there is no ice-free land.

increase in the relative humidity near the surface in both high latitudes and subtropics seen in Figure 4.48 was attributed by Wetherald and Manabe (1980) to the increase in evaporation from the surface, the stable stratification, and the decrease of the warming with height above the surface. These

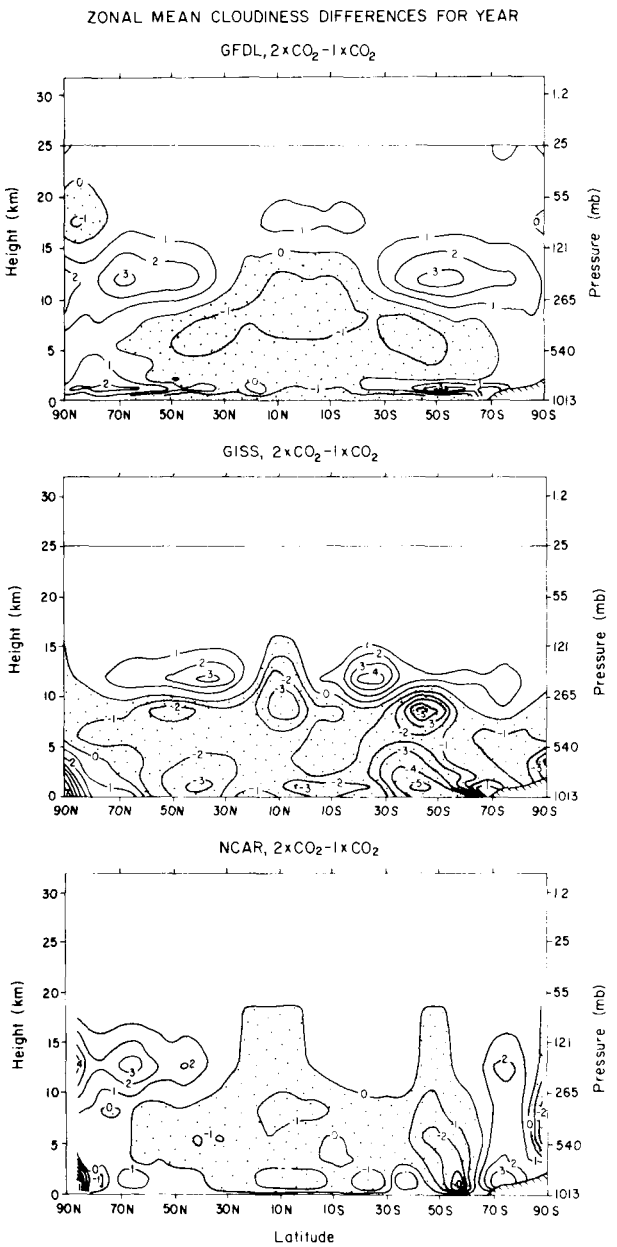

Figure 4.47. Latitude-altitude cross section of the annual zonal mean cloudiness change (percent coverage), $2 \times CO_2 - 1 \times CO_2$, simulated with (top) the GFDL GCM by Wetherald and Manabe (1986); (middle) the GISS GCM by Hansen et al. (1984); (bottom) the NCAR GCM by Washington and Meehl (1984). Stipple indicates a decrease in cloudiness.

factors, respectively, led to an increase in the moisture supplied from the surface to the atmosphere, the confinement of this additional moisture in the near-surface atmosphere, and a shift in the saturation vapor pressure profile, all of which tended to increase the low-level relative humidity. The increase in stratospheric relative humidity was attributed to an enhanced upward transport of moisture by large-scale eddies across the tropopause as a consequence of the reduced static stability there, the latter because the heating decreased with altitude in both the solar constant and CO_2 experiments. Following Wetherald and Manabe (1975), Wetherald and Manabe (1980) attributed the decrease in relative humidity throughout most of the tropical and midlatitude troposphere to an increase in the variance in the vertical velocity, as shown in Figure 4.49. This increase was caused by the enhanced condensational heating of the enhanced precipitation. The resultant intensification of the upward velocity maintained the increased precipitation, whereas the intensification of the compensating downward velocity tended to lower the humidity. The drying in the regions of subsidence tended to be larger than the moistening in the regions of ascent because the relative humidity cannot exceed 100% because of saturation. Consequently, the area-averaged relative humidity and clouds decreased, whereas the area-averaged precipitation increased.

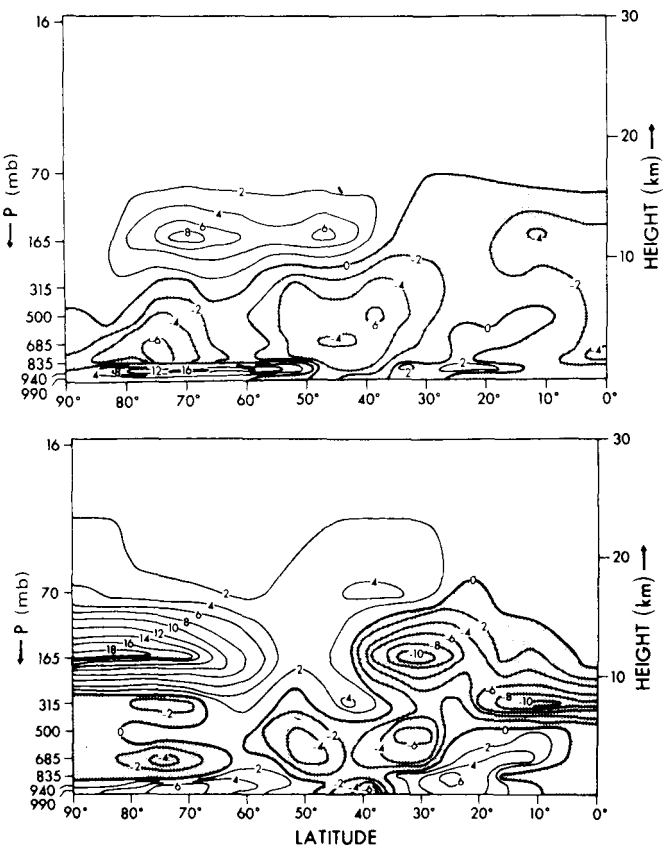

Figure 4.48. Latitude-height distribution of the difference in zonal mean cloud amount (top) and relative humidity (below) between the 6% solar constant increase experiment and control. Units are percent. Shaded areas indicate negative values. Source: Wetherald and Manabe (1980).

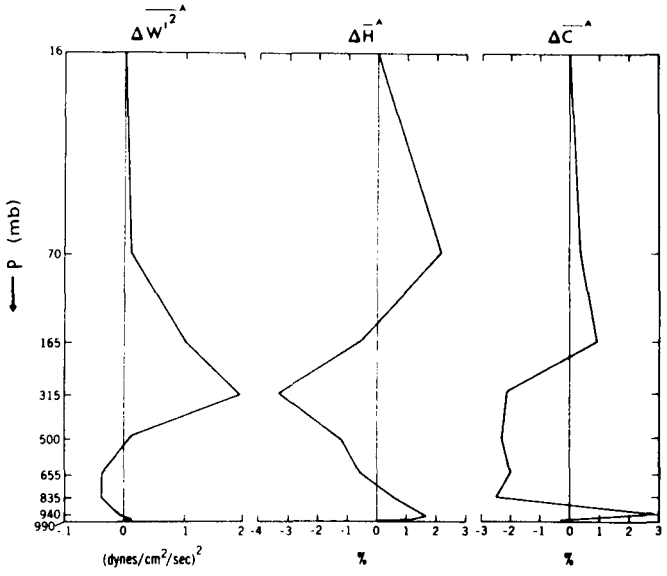

Figure 4.49. Vertical distributions of the area-mean differences in the variance of the deviation from the zonal mean of the vertical p-velocity, W' (left), relative humidity, H (middle); and cloudiness, C (right) between the 6% solar constant increase experiment and the control. Source: Wetherald and Manabe (1980).

This explanation for relating the change in cloudiness to changes in relative humidity may be applicable to large-scale condensation because this process is parameterized with an explicit dependence on a prescribed critical relative humidity (Table 4.4). Manabe and Wetherald's explanation may also be applicable for convective precipitation in the GFDL and NCAR models because these models use the moist adiabatic adjustment, which depends on a prescribed critical relative humidity (Table 4.4). But the tropical and midlatitude tropospheric cloudiness also decreased in the simulation with the GISS model (Figure 4.47), which employs a penetrative cumulus parameterization that does not explicitly depend on relative humidity (Table 4.4).

Mitchell and coworkers[6] at UKMO have investigated the effects of changes in tropospheric cloud cover in an idealized experiment using an 11-layer global GCM with realistic geography, seasonal variation and model-generated cloud amount. Calculations were made in which the present CO_2 concentration was assumed and in which the CO_2 concentration was doubled and sea surface temperatures were simultaneously increased by 2°C. An increase in the radiative cooling of the atmosphere was found that was particularly pronounced at the top of the troposphere. An analysis showed that the cooling in the upper troposphere was due mainly to the increase in tropospheric water vapor. Since H_2O rotational bands are not saturated in the upper troposphere, the increase in water vapor is particularly effective in increasing the divergence of infrared radiation through enhanced emission to the surface and space. The change in the vertical profile of heating encouraged deeper convection, so that relatively more moisture was detrained above the level of enhanced cooling and less moisture below. Thus, relative humidity and cloudiness increased at the top of the troposphere and decreased below. Although the change in relative humidity was small, the absolute humidity increased by 18%; this was substantially greater than the increase in precipitation. Therefore, the increase in precipitation may be attributed to the large increase in absolute humidity, whereas the reduction in cloud amount was due to a small change in relative humidity. Analyses of the GFDL, GISS, and NCAR simulations should be performed to determine whether this mechanism was responsible for the increase in precipitation and decrease in cloud cover simulated by these models.

Figure 4.47 shows that although there are qualitative similarities among the simulated CO_2 cloudiness changes, there are quantitative differences. In particular, the tropospheric changes simulated by the GISS model are generally larger in magnitude than those produced by the GFDL and NCAR models. Furthermore, a correlation between the magnitude of the cloudiness change and the magnitude of the temperature change seems apparent, particularly in the upper tropical troposphere, as can be seen by comparing Figure 4.47 with Figures 4.36 and 4.37. In this region the warming simulated by the GISS model is nearly double that simulated by the GFDL and NCAR models, and the decrease in cloudiness in the GISS model is also about twice that of the GFDL and NCAR models. The magnitude of the cloudiness change may determine the magnitude of the temperature change, but the converse appears to be the more likely relation. If this is so, then why is the temperature increase larger in the GISS model than in the GFDL and NCAR models? The answer may be that the GISS model has a parameterization for penetrative convection, whereas the NCAR and GFDL models use the moist

[6] J. F. B. Mitchell, C. A. Wilson, and W. M. Cunnington, personal communication.

adiabatic adjustment scheme, which ignores penetrative convection. It is likely that the penetrative cumulus convection parameterization produces a larger heating aloft than the moist adiabatic adjustment and thereby produces a larger upward enhancement of the surface warming. Although this in itself might tend to reduce the surface warming, the cloud modification aloft could mitigate this through cloud feedback to produce a warming throughout the tropical troposphere that is larger than in a model with only moist adiabatic adjustment. Such a difference in the vertical profile of temperature change is evident from Mitchell and Lupton (1984) and Manabe and Stouffer (1980), who used penetrative and convective adjustment schemes, respectively. As discussed in Appendix A, the actual feedback effect of a cloudiness change ΔA_c such as shown in Figure 4.47 depends on the vertical integral throughout the atmosphere of $\delta \Delta A_c$, where $\delta = \partial N_0 / \partial A_c$ and N_0 is the net radiation at the top of the atmosphere. A *post hoc* analysis of the cloud feedback has been performed for the GISS simulation as described below.

4.3.4.3 Feedback Analysis

Hansen et al. (1984) have used a RCM to analyze feedback processes in the GISS GCM simulation of the $2 \times CO_2 - 1 \times CO_2$ global mean surface air temperature difference. The basis for this analysis is a model of the climate system feedback that is essentially the same as that developed in Section 4.2 and Appendix A. From Equation (4.4) with ΔT_s replaced by ΔT_s,

$$f = 1 - \frac{(\Delta T_s)_0}{\Delta T_s} = \frac{\Delta T_s - (\Delta T_s)_0}{\Delta T_s}$$
$$= \frac{(\Delta T_s)_{\text{feedbacks}}}{\Delta T_s}$$
$$= \frac{\sum_{i=1}^{N} (\Delta T_s)_i}{\Delta T_s}$$
$$= \sum_{i=1}^{N} f_i \ , \qquad (4.12)$$

where

$$f_i = \frac{(\Delta T_s)_i}{\Delta T_s} \ , \qquad (4.13)$$

and

$$\Delta T_s = \sum_{j=0}^{N} (\Delta T_s)_j \ . \qquad (4.14)$$

This analysis assumes that the feedback mechanisms are independent so that the total temperature change ΔT_s is the sum of the zero-feedback change $(\Delta T_s)_0$, and the changes $(\Delta T_s)_i$ resulting from the feedbacks.

The validity of the above assumption is demonstrated by the results shown in Figure 4.50 and Table 4.6, which were obtained by making the indicated changes in the RCM. In the first column, the effect of doubling the CO_2 concentration without any feedbacks is shown to be $(\Delta T_s)_0 = 1.2°C$. In the second column the effect of the 33% increase in total water vapor simulated by the GCM was estimated by increasing the water vapor at each level of the RCM by 33%. In this RCM experiment, and those described below, the CO_2 concentration was not doubled, nor were any feedbacks permitted. The result then is $(\Delta T_s)_1 = 1.85°C$. To determine the effect of the change in the vertical distribution of water vapor simulated by the GCM, the water vapor profile from the GCM was inserted into the RCM and the resultant temperature change was decreased by $(\Delta T_s)_1$ to obtain $(\Delta T_s)_2 = 0.90°C$. To determine the effect of the change in lapse rate simulated by the GCM, the lapse rate from the GCM was inserted into the RCM and gave $(\Delta T_s)_3 = -1.1°C$. Similarly, for the GCM-simulated change in surface albedo, $(\Delta T_s)_4 = 0.38°C$. The total cloud effect on temperature was obtained by changing the cloud amounts at all levels in the RCM in proportion to the changes obtained in the GCM. The effect of changing only cloud cover, $(\Delta T_s)_6 = 0.42°C$, was obtained by inserting a uniform cloud change in the RCM equal to the total change in the GCM. The effect of the cloud altitude change, $(\Delta T_s)_5 = 0.51°C$, was obtained by subtracting $(\Delta T_s)_6$ from the total cloud effect. Summing these individual changes gives $\Delta T_s = 4.16°C$, which agrees with the GCM-simulated value.

The results of the feedback analysis using Equations (4.12) – (4.14) are presented in Table 4.6. The feedback resulting from the changes in water vapor amount and vertical distribution is $f_W = 0.661$. This is considerably larger than the $f_W = 0.3$ to 0.5 given by the RCMs reviewed in Section 4.2.2.

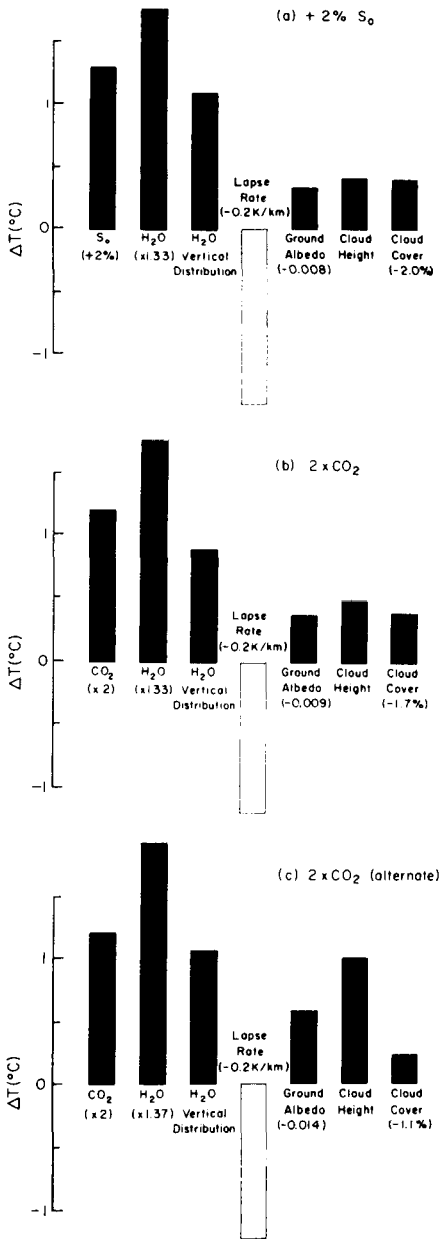

Figure 4.50. Contributions to global mean $2 \times CO_2 - 1 \times CO_2$ temperature rise as estimated by inserting changes obtained in GCM experiment into a radiative-convective model. Source: Hansen et al. (1984).

The much larger f_W estimated for the GISS GCM indicates that the relative humidity increased with doubled CO_2 in that model, unlike the constant relative humidity assumed by the RCMs; Hansen et al. (1984) state that the average relative humidity increased by 1.5% with a maximum of 6% at the 200 mb[7] level. The estimated lapse rate feedback, $f_{LR} = -0.264$, lies at the smaller limit given by the RCMs of Section 4.2.2 for the moist adiabatic lapse rate case, perhaps because the change in lapse rate of $-0.2°C\ km^{-1}$ is less than the change in the moist adiabatic value of $-0.5°C\ km^{-1}$. The cloud altitude feedback, $f_{CA} = 0.123$, also lies at the lower limit given by the RCMs in Section 4.2.2. The cloud cover feedback estimated for the GCM is positive, indicating the dominance of the albedo effect over the longwave effect. The surface albedo feedback caused largely by reduced sea ice is estimated as $f_{SA} = 0.091$, which is somewhat smaller than the estimates given by the RCMs in Section 4.2.2. The total feedback estimated for the GCM is $f = 0.712$, of which water vapor feedback, $f_W = 0.661$, is the single most important positive contributor, followed by cloud feedback, $f_C = 0.224$, and surface albedo feedback, $f_{SA} = 0.091$, with the lapse rate feedback, $f_{LR} = -0.264$, making a negative contribution.

Hansen et al. (1984) attribute the fact that the $2 \times CO_2$ warming implied from the $4 \times CO_2$ simulation of Manabe and Stouffer (1980) with the GFDL model, namely 2°C, is smaller than the 4.2°C warming simulated by the GISS model because there is no cloud feedback in the GFDL model (the clouds were prescribed), and the surface albedo feedback was presumably smaller because the extent of the $1 \times CO_2$ sea ice was underestimated. However, the feedback analysis shown in Table 4.6 suggests that perhaps the large water vapor feedback in the GISS model also contributes to the difference between the sensitivities of the GISS and GFDL models.

Table 4.6
RCM Analysis of the Feedbacks in the GISS GCM Simulation of $2 \times CO_2 - 1 \times CO_2$ Temperature Change.

Feedback Mechanism	Column in Figure 4.50 i	$(\Delta T_s)_{i-1}$ (°C)	f_i^a
None	1	1.20	0.000
Water Vapor Amount	2	1.85	0.445
Water Vapor Distribution	3	0.90	0.216
Lapse Rate	4	−1.10	−0264
Surface Albedo	5	0.38	0.091
Cloud Height	6	0.51	0.123
Cloud Cover	7	0.42	0.101
Total		4.16	0.712

Note: based on Hansen et al. (1984).

[a] $f_i = (\Delta T_s)_i / \sum_{j=1}^{7} (\Delta T_s)_{j-1}$ for $i = 2, \ldots, 7$.

[7] 100 mb equals 10 kPa.

4.4 SUMMARY

General circulation model studies of CO_2-induced changes in the Earth's equilibrium climate have been performed predominantly for a doubled or quadrupled CO_2 concentration, the former because of the projected doubling of the preindustrial CO_2 concentration sometime during the 21st century, and the latter simply to enhance the statistical significance of the simulated climate change. Atmospheric GCMs have been coupled to two types of simplified models of the ocean to allow these experiments to reach equilibrium more rapidly than would the actual climate system in an effort to minimize the required computer time. In the earliest and simplest ocean model, the swamp ocean model, the heat capacity of the ocean is neglected such that the ocean is perpetually in equilibrium with the atmosphere. This allows the climate system to equilibrate in about 300 days, but does not allow use of the annual cycle of insolation. Therefore, such atmospheric GCM/swamp ocean studies do not simulate the seasonal cycle of climate and its CO_2-induced change. Several simulations with this type of model have been conducted, beginning with models having idealized and restricted geography and topography, and extending to models that treat these aspects realistically. These simulations have provided some information about the mechanisms of climate change due to increased CO_2. Simulations with annual mean insolation produce a climate that is substantially different from the annually averaged climate simulated with seasonally varying insolation. To simulate seasonal effects, atmospheric GCMs have either been run with prescribed changes in sea surface temperature based on a series of perturbation experiments, or have been coupled to mixed-layer ocean models whose depth and horizontal heat transports are prescribed, most frequently as a constant or zero. These atmospheric GCM/mixed-layer ocean models require several decades to equilibrate, with the actual equilibration time dependent on the prescribed mixed-layer depth. Seasonal simulations with this type of climate model have most often been performed with realistic geography and topography and thus represent the most comprehensive projections of CO_2-induced equilibrium climate change.

The early studies of the changes in climate as portrayed by atmospheric GCM/swamp ocean models depict an Earth with a warmer global average surface air temperature and a greater global average precipitation rate. Increased zonally averaged temperatures were simulated for the entire troposphere, with warming near the surface increasing with latitude from the tropics toward both poles and increasing with altitude in tropical and subtropical latitudes. Decreased zonal mean temperatures were simulated for most of the stratosphere, with the stratospheric cooling increasing with altitude. Positive and negative changes in the zonal mean precipitaion rates were simulated by these climate models, with increased rates located in the middle and high latitudes and greater changes of both signs within the 30°S to 30°N latitude band. Changes of both signs were also simulated for the soil moisture, with these changes negatively correlated with the surface air temperature changes. The few simulations with predicted clouds, when compared with companion simulations with prescribed clouds, indicated virtually no effect of the simulated cloudiness changes and, therefore, a compensation between the albedo and longwave effects of the changed clouds.

The projections of CO_2-induced climate change provided by the atmospheric GCM/swamp ocean models described above show considerable qualitative agreement on changes in the global- and zonal-mean temperatures, precipitation rates, and cloudiness, but there is considerable disagreement concerning the quantitative changes in these mean quantities. For example, the change in global mean surface air temperature and precipitation rate simulated for a CO_2 doubling range from 1.3 to 3.9°C and from 2.7 to 7.8%, respectively. Furthermore, these simulations disagree qualitatively concerning the geographical distribution of the changes in all the climatic quantities. This lack of agreement is due, in part, to the differences among the atmospheric GCM/swamp ocean models, such as different geographical domains. They disagree also because the models have not run sufficiently long enough to attain equilibrium and statistically significant changes (Schlesinger 1982, 1984a).

The first study of the seasonal variation of CO_2-induced climate change with an atmospheric GCM/mixed-layer ocean model was performed by Manabe and Stouffer (1980) with the GFDL model

for a CO_2 quadrupling. A similar study with prescribed changes in sea surface temperature has been made by Mitchell and Lupton (1984). More recently, studies have been carried out for a CO_2 doubling by the following researchers: Hansen et al. (1984) with the GISS model; Washington and Meehl (1984) with the NCAR model; and Wetherald and Manabe (1986) with the GFDL model. In these studies clouds were predicted, whereas clouds were prescribed in the earlier studies.

In general the CO_2-induced changes in the zonal mean temperatures simulated by these atmospheric GCM/mixed-layer ocean models for DJF and JJA display features similar to those simulated by the atmospheric GCM/swamp ocean models for annual mean insolation. In particular, the temperature changes during both seasons are negative in the stratosphere above 20 km and are positive in the lower stratosphere, troposphere, and at the surface; the stratospheric cooling increases with altitude during both seasons; the tropospheric warming increases with altitude between about 30°S and 30°N in DJF and between about 40°S and 90°N in JJA; the surface warming increases from the tropics toward the higher latitudes in the winter hemisphere in both seasons, and it also increases in the Southern Hemisphere during summer. The changes in the annual cycle of zonal mean surface air temperatures simulated by the models show little seasonal variation between 50°S and 30°N, and a large seasonal variation poleward of 50° latitude in both hemispheres. The geographical distributions of the CO_2-induced surface air temperature changes also exhibit qualitative similarity in that maximum winter warming occurs in the high latitudes of both hemispheres where the sea ice in the $1 \times CO_2$ simulation retreats poleward in the enhanced CO_2 simulation. The location of maximum warming is thus dependent on the position of the sea-ice boundary in the control integration. The global mean surface air temperature change given by the three most recent simulations ranges from 3.5 to 4.2°C, which is considerably smaller than the 1.3 to 3.9°C range given by the earlier atmospheric GCM/swamp ocean models. However, the warming of these latest simulations is about twice that of the CO_2 doubling inferred from the quadrupling study of Manabe and Stouffer (1980). Although the latest studies show considerable quantitative agreement in their simulated global mean surface air temperature changes, they also show substantial disagreements in their simulated zonal mean temperature changes. For example, the tropical surface air temperature warming ranges from 2°C in the NCAR simulation to about 4°C in the GISS simulation, and the tropical tropopause warming ranges from 3°C in the NCAR simulation to 7°C in the GISS simulation. Furthermore, the simulated geographical distributions exhibit large differences in both the magnitude and the seasonality of the regional surface air temperature changes.

The three recent simulations of the climate change induced by a doubling of the CO_2 concentration exhibit an increase in the global mean precipitation rate with values that range from 7.1 to 11.0% of their respective $1 \times CO_2$ values. These changes give a narrower range than that produced by the atmospheric GCM/swamp ocean models with annual mean insolation, but are larger than the 6.7% increase obtained by the earliest seasonal study for a CO_2 quadrupling. Because this latter study also has a smaller inferred warming for a CO_2 doubling, there appears to be a relationship between the magnitude of the increases in global mean precipitation rates and surface air temperatures, which is likely the result of the temperature dependence of the water vapor saturation vapor pressure. The changes in precipitation rate simulated by the atmospheric GCM/mixed-layer ocean models show the same characteristic features simulated by the simpler swamp ocean models with annual mean insolation. In particular, both positive and negative changes in precipitation rate are exhibited, with the largest changes generally occurring between 30°S and 30°N. The precipitation changes poleward of these latitudes are generally positive during both DJF and JJA over both ocean and land, with increases less than 1 mm d^{-1} over the Northern Hemisphere continents and Antarctica during both seasons. However, despite these agreements, there are substantial regional differences among the portrayals of the CO_2-induced precipitation changes.

Somewhat surprisingly, considering the differences in the regional precipitation rate changes, the simulated changes in soil moisture display many qualitative similarities during DJF. However, there is less agreement among the simulated soil moisture changes for JJA. Summer soil moisture change

in the Northern Hemisphere is particularly important for the agricultural impact of a CO_2-induced climate change. The GFDL simulation for doubled CO_2, like its predecessor for quadrupled CO_2 and that of Mitchell and Lupton (1984), suggest a drying almost everywhere in Europe, Asia, and North America. However, both the NCAR and GISS models produce an increased summer soil moisture over much of these continents. There is some evidence that in the NCAR model this result is related to the unsaturated winter and spring soil moisture values in both the control and $2 \times CO_2$ integrations.

The changes in cloudiness simulated by the atmospheric GCM/mixed-layer ocean models are qualitatively similar to those produced by swamp ocean models with annual mean insolation, namely, increased cloudiness in the stratosphere and near the surface in the high latitudes of both hemispheres and decreased cloudiness throughout most of the troposphere in the tropics and middle latitudes. However, unlike the lack of sensitivity displayed by the atmospheric GCM/swamp ocean models to these cloudiness changes, the GCM/mixed-layer ocean models display great sensitivity. This is shown by: (1) the large increase in the global mean surface temperature warming for the GFDL model with predicted clouds (Wetherald and Manabe, 1986) compared to that of the GFDL model with prescribed clouds (Manabe and Stouffer (1980); (2) the negative correlation between the cloudiness changes near the tropical tropopause and the surface air temperature change (in all the recent simulations); and (3) an analysis of the GISS GCM sensitivity obtained by inserting the simulated changes sequentially into a RCM. This latter analysis shows that the feedback caused by changes in cloudiness contributes 0.224 to the GCM's total feedback of 0.712. However, the total water vapor feedback of 0.661 is of even greater importance. Because this estimated GCM value is about twice that obtained from RCM studies with fixed relative humidity, it appears that the documented relative humidity increase simulated by the GISS model for doubled CO_2 may have a dominant influence on the global mean surface air temperature sensitivity. This water vapor feedback far outweighs the surface albedo feedback of 0.091 and more than compensates the negative lapse rate feedback of –0.264. It is likely that the magnitudes of the dominant water vapor and cloudiness feedbacks depend critically on the parameterizations of cumulus convection and cloudiness in the GCMs.

4.5 DISCUSSION AND RECOMMENDATIONS

In this chapter we have reviewed the projections of equilibrium climatic response to increased CO_2 concentration that have been made with a hierarchy of climate models that includes surface and planetary EBMS, RCMs, and atmospheric GCMs. The EBMs compute only the surface temperature, and the RCMs compute only the vertical profile of temperature; both results are determined only at one point, which may, under some circumstances, be interpreted as the global average. Only the GCMs determine other climatic quantities such as precipitation, soil water, and clouds, and only the GCMs determine the global geographical distributions of these and other climatic quantities.

We have seen that each of the climate models (EBMs, RCMs, and GCMs) is limited by its treatment of the physical processes that are not explicitly resolved by the model. In EBMs these unresolved processes include all processes that do not occur at the energy balance level; that is, all the atmospheric processes for surface balance models and, in addition, all the surface processes in planetary energy balance models. Because of this, EBMs have given a wide range of projections of CO_2-induced surface temperature change and must, therefore, be used only in a qualitative sense and with great caution.

In RCMs, the unresolved physical processes include those having to do with the horizontal variations of the temperature, such as advection, and those having to do with any quantity other than temperature, such as water vapor, sea ice, and clouds. Nevertheless, these models are useful for preliminary hypothesis testing and for understanding some of the results simulated by the GCMs.

Although the GCMs include many climatic quantities other than temperature and resolve many of the physical processes that are not resolved by the RCMs and EBMs, they nevertheless do not resolve all of the physical processes that may be of importance to climate and climate change and which span

the fourteen orders of magnitude from the planetary scale (10^7 m) to the cloud microphysical scale (10^{-6} m). In fact, contemporary computers permit the resolution of physical processes over only two orders of magnitude, and even a thousand-fold increase in computer speed, which is not projected to occur within this century, would allow the resoluton of only one more order of magnitude! Clearly, even the GCMs are, and will continue to be, critically dependent on their treatments and parameterizations of the physical processes that occur on the unresolved subgrid scales.

Keeping these limitations and dependencies in mind, how can we be or become confident in the GCM projections of CO_2-induced equilibrium climate change? To have confidence in the GCM simulations of a potential future climate requires that these models correctly simulate at least one known equilibrium climate, with the present climate being the best choice because of the quantity, quality, and global distribution of contemporary instrumental observations. However, an evaluation of the fidelity of a GCM in simulating the present climate is not simple for a variety of reasons, including how well the simulated and observed climates represent their corresponding equilibrium climates and the poor quality of the observations of many climatic quantities such as precipitation over the ocean and soil moisture. However, forgetting these difficulties for the moment, suppose that a GCM simulates the present climate perfectly. How then can we gain confidence in its ability to simulate another climate different from that of the present? In the case of weather forecasting, this question can and has been answered by making thousands of forecasts and comparing them with the actual evolution of the weather. Unfortunately, this cannot be done for climate because only a few paleoclimatic reconstructions have been made, and these may or may not be of sufficient quality to provide a meaningful assessment of the GCM's capability. Thus, there is an inherent limitation in our ability to validate the accuracy of GCM perturbation simulations, which thereby affects our confidence in the accuracy of the GCM simulations of CO_2-induced climate change.

The state of the art is that GCMs simulate the present climate imperfectly, although some of the models do reasonably well, at least for the limited climatic quantities considered in this chapter and within our subjective assessment of the reliability of the observations. Yet these models frequently employ treatments of dubious merit, including prescribing the oceanic heat flux, ignoring the oceanic heat flux, and using incorrect values of the solar constant. Such approximations indicate that the models are physically incomplete and/or have errors in the included physics. Furthermore, the state of the art is that the CO_2-induced climate changes simulated by different GCMs show many quantitative and even qualitative differences; thus, we know that not all of these simulations can be correct, and perhaps all could be wrong. It is not productive now to dwell on the inherent limitation in establishing the confidence of the GCM simulations of equilibrium climate change. Rather we must concentrate on understanding the differences and similarities of the most recent simulations and develop more-comprehensive models of the climate system. The actions required to meet these two goals are elaborated below.

4.5.1 Goal I: Understanding the Contemporary General Circulation Model Simulations

Four simulations of CO_2-induced climate change using atmospheric GCM/mixed-layer ocean models that include the annual cycle have been performed, namely, the CO_2 quadrupling study by Manabe and Stouffer (1980) with the GFDL model and the CO_2 doubling studies by Hansen et al. (1984) with the GISS model, Washington and Meehl (1984) with the NCAR model, and Wetherald and Manabe (1986) with the GFDL model. Among these four simulations, there is a factor of two difference in the global mean surface air temperature warming, and among the latter three (which have predicted clouds) there is a factor of two difference in the tropical surface air temperature changes. To understand these differences, an estimate of the feedbacks in each GCM should be obtained with a compatible RCM following the feedback analysis performed by Hansen et al. (1984). An intercomparison of these feedback analyses for the GCMs will allow ranking of the feedbacks in terms of magnitude, and thereby illuminate the likely parameterized physical processes responsible for the differences.

GCM sensitivity studies should then be performed to verify the findings of the RCM feedback

analysis. For example, if it is indicated that cloudiness or ice albedo feedback is dominant, then a pair of 1 × CO_2 and 2 × CO_2 GCM simulations should be made with noninteractive clouds or sea ice and compared with the existing simulations with interactive clouds or sea ice. On the other hand, if water vapor feedback is dominant, then simulations with a different parameterization of cumulus convection may be warranted. Because these sensitivity studies may involve many reruns of the models, each for a period of several decades, it may be more economical to employ the adjoint sensitivity method described in Appendix C. Having established by RCM feedback analyses and GCM sensitivity studies which of the parameterized physical processes are most important for the CO_2-induced climate changes, how can we determine which of the contemporary parameterizations, if any, is correct? The answer is described below.

4.5.2 Goal II: Development of More-Comprehensive General Circulation Models

The development of more-comprehensive models is subdivided below into the validation of the parameterizations of subgrid scale processes, the development of physically based cloud parameterizations, and the development of coupled atmosphere/ocean GCMs.

4.5.2.1 Validation of Physical Process Parameterizations

In the past, simple parameterizations of the unresolved or subgrid scale physical processes have been developed. The simplicity of the parameterization has been justified because the processes are extremely complex, whereas our understanding of them is limited. This in fact was the justification for parameterizing cumulus convection by moist adiabatic adjustment (Manabe et al. 1965). Yet it is clear that this parameterization ignores penetrative convection and, therefore, produces a different vertical profile of heating from a parameterization that includes penetrative convection. Furthermore, there is circumstantial evidence that these differences in the convective vertical heating profile may be responsible for the differences in the tropical profiles of CO_2-induced temperature changes in the most recent GCM simulations.

Accordingly, it is now time to begin the very difficult task of systematically validating the GCM parameterizations of subgrid-scale processes. Fortunately, a prototype validation procedure has been developed and is currently being carried out, in this case for the parameterization of radiative transfer under the Intercomparison of Radiation Codes in Climate Models (ICRCCM, see Luther 1984). Following this prototypical program, scientists worldwide would be invited to intercompare results from their parameterizations for specifically agreed upon cases. However, to reduce the possibility that the parameterizations may all agree and yet be incorrect, it is essential to have corresponding results from highly detailed models that actually resolve the physical processes whose parameterizations are being compared and to have actual observations to validate these highly detailed models. Such a program, for example, the Intercomparison of Parameterizations in Climate Models (IPCM), should investigate all of the parameterized physical processes in the order of importance indicated by the previously described feedback analysis and sensitivity studies.

4.5.2.2 Development of Physically-Based Cloud Parameterizations

In Section 4.2, evidence was presented that cloud optical depth feedback may be large enough to potentially reduce the CO_2-induced global mean surface air temperature warming by 50%. Yet none of the GCM simulations of CO_2-induced climatic change has included cloud optical depth feedback. These facts suggest that the contemporary estimates of a global mean warming of 3.5 to 4.2°C could potentially be reduced to 1.7 to 2.1°C by cloud optical depth feedback. Furthermore, such a halving of the global mean temperature sensitivity would likely also give a corresponding reduction in the projected increase in global mean precipitation rate. Clearly, the uncertainty about cloud optical depth feedback must be considered to be one of the major uncertainties in our contemporary projections.

To rectify this deficiency, the development of physically based models of clouds and their radiative interactions is required. In particular, it is imperative that cloud liquid water and cloud ice amounts be predicted in GCMs, and that the effects of these variable cloud quantities on the optical depth of clouds be incorporated in the models. Such parameterizations should be validated, as described in Subsection 4.5.2.1, and then implemented in GCMs to ascertain the effects of cloud optical depth feedback on CO_2-induced climate change.

4.5.2.3 Development of Coupled Atmosphere/Ocean General Circulation Models

The earliest GCM simulations of CO_2-induced equilibrium climate change were performed using a swamp ocean model without heat capacity and without horizontal or vertical heat transport. These GCM/swamp ocean models permitted simulation of the CO_2-induced changes in what has been interpreted as the annual mean climate. The most recent GCM simulations have employed a mixed-layer ocean with prescribed depth, prescribed horizontal heat transport (usually zero), and no vertical heat transport. These GCM/mixed-layer ocean models permit simulation of the CO_2-induced changes in the annual cycle of climate. Yet these models do not allow any feedback caused by changes in the ocean's horizontal heat transport, nor do they allow thermal communication between the mixed layer and the underlying thermocline, intermediate, and bottom waters. The absence of oceanic horizontal heat transport forces the atmosphere to perform not only its own heat transport but that of the ocean as well. This probably produces errors in the atmospheric general circulation. The absence of vertical heat transport in the ocean probably produces errors in the simulated sea surface temperatures that also likely cause errors in the atmospheric general circulation (Meehl and Washington 1985a). Although it is possible to reduce these errors by prescribing the oceanic horizontal heat flux by the method of Hansen et al. (1984), this does not permit the feedback that changes in the ocean temperature structure and currents would produce. The neglect of this feedback in contemporary GCMs, and particularly its potential impact on the surface albedo feedback through changes in sea ice extent, must be regarded as a major uncertainty in contemporary projections.

To decrease this uncertainty requires the development of coupled atmosphere/ocean GCMs and their application to the CO_2-climate issue. Actually, prototypical calculations of CO_2-induced climate change with coupled atmosphere/ocean GCMs have been carried out by Bryan et al. (1982) and Bryan and Spelman (1985) with limited-domain versions of the GFDL model, and by Schlesinger et al. (1985) with the global OSU model. Whereas these simulations principally were carried out to determine the characteristic time scale for the transient climate change induced by increased CO_2 (see Chapter 5), they are also of interest for studying the equilibrium climate change. However, for the present discussion, it is the simulation of the $1 \times CO_2$ sea surface temperature that is of importance. The study by Han et al. (1985) of the OSU simulation described above, and the earlier coupled model studies by Manabe et al. (1979) and Washington et al. (1980) show systematic errors in the simulated sea surface temperatures in comparison with observations. These errors can be due to deficiencies in the individual ocean and atmospheric models and/or to the interaction between the atmosphere and ocean models. These errors can have a large impact on the extent of the simulated sea ice and, thereby, affect the surface albedo-feedback mechanism.

The analysis and correction of the simulation errors of coupled atmosphere/ocean GCMs are of fundamental importance in addressing our ability to simulate climate and climate change. These tasks and the enormous computational resources they require must be given high priority.

ACKNOWLEDGMENTS

We would like to thank Syukuro Manabe and Richard Wetherald of the Geophysical Fluid Dynamics Laboratory; James Hansen, Gary Russell, Andrew Lacis, and David Rind of the Goddard Institute for Space Studies, and Warren Washington and Gerald Meehl of the National Center for Atmospheric Research for making their results available to us and for their discussions of

these results. We express our gratitude to Jai-Ho Oh, Dean Vickers, and Mylynda Schlesinger for performing some of the calculations and graphics herein; to Larry Holcomb and John Stark for drafting; and to Monica Cox, Dee Dee Reynolds, Leah Riley, and especially Naomi Zielinski for typing the manuscript. We express appreciation to Fred Luther and Michael MacCracken for their editing, and to Robert Dickinson, James Hansen, Syukuro Manabe, Gerald Meehl, Stephen Schneider, Richard Wetherald, Warren Washington and several anonymous referees for their constructive reviews of this chapter. This study was supported by the Department of Energy under contract number DE-AC03-76SF00098, and by the National Science Foundation and the Department of Energy under grants ATM 82-05992 and ATM-8511889.

REFERENCES

Alexander, R. C., and Mobley, R. L. 1976. "Monthly Average Sea Surface Temperatures and Ice Pack Limits on a 1° Global Grid." *Monthly Weather Review 104*:143–148.

Arakawa, A., Katayama, A., and Mintz, Y. 1969. "Numerical Simulations of the General Circulation of the Atmosphere." IV-7 to IV-8-12. In *Proceedings of the WMO/IUGG Symposium on Numerical Weather Predication*. Japan Meteorological Agency, Tokyo, Japan.

Augustsson, T., and Ramanathan, V. 1977. "A Radiative-Convective Model Study of the CO_2 Climate Problem." *Journal of the Atmospheric Sciences 34*:448–451.

Bates, G. T., and Meehl, G. A. 1985. "The Effect of CO_2 Concentration on the Frequency of Blocking in a General Circulation Model Coupled to a Simple Mixed Layer Ocean Model." *Monthly Weather Review 113*:in press.

Bode, H. W. 1975. *Network Analysis and Feedback Amplifier Design*. Krieger, New York, New York.

Bryan, K., and Spelman, M. J. 1985. "The Ocean's Response to a CO_2-Induced Warming." *Journal of Geophysical Research 90*:11679–11688.

Bryan, K., Komro, F. G., Manabe, S., and Spelman, M. J. 1982. "Transient Climate Response to Increasing Atmospheric Carbon Dioxide." *Science 215*:56–58.

Budyko, M. I. 1969. "The Effect of Solar Radiation Variations on the Climate of the Earth." *Tellus 21*:611–619.

Charlock, T. P. 1981. "Cloud Optics as a Possible Stabilizing Factor in Climate Change." *Journal of the Atmospheric Sciences 38*:661–663.

Crutcher, H. L., and Meserve, J. M. 1970. *Selected Level Heights, Temperatures and Dew Points for the Northern Hemisphere* (NAVAIR-50-1C-52). Naval Weather Service Command, Washington, D.C.

Elliott, W. P., Machta, L., and Keeling, C. D. 1985. "An Estimate of the Biotic Contribution to the Atmospheric CO_2 Increase Based on Direct Measurements at Mauna Loa Observatory." *Journal of Geophysical Research 90*:3741–3746.

Gates, W. L., Cook, K. H., and Schlesinger, M. E. 1981. "Preliminary Analysis of Experiments on the Climatic Effects of Increased CO_2 with an Atmospheric General Circulation Model and a Climatological Ocean." *Journal of Geophysical Research 86*:6385–6393.

Gilchrist, A. 1983. "Increased Carbon Dioxide Concentrations and Climate: The Equilibrium Response." 219–258. In W. Bach, A. J. Crane, A. L. Berger, and A. Longhetto (eds.), *Carbon Dioxide: Current Views and Developments in Energy/Climate Research*, Reidel, Dordrecht, The Netherlands.

Han, Y.-J., Schlesinger, M. E., and Gates, W. L. 1985. "A Critical Evaluation of the Air-Sea-Ice Interaction Simulated by the OSU Coupled Atmosphere-Ocean GCM." 167–182. In J. C. J. Nihoul (ed.), *Coupled Ocean-Atmosphere Models*, Elsevier, Amsterdam, The Netherlands.

Hansen, J. 1979. Results presented in *Carbon Dioxide and Climate: A Scientific Assessment* (Report of an Ad Hoc Study Group on Carbon Dioxide and Climate). Climate Research Board, National Academy of Sciences, Washington, D.C.

Hansen, J., Johnson, D., Lacis, A., Lebedeff, S., Lee, P., Rind, D., and Russell, G. 1981. "Climate Impact of Increasing Atmospheric Carbon Dioxide." *Science 213*:957–966.

Hansen, J., Lacis, A., Rind, D., Russell, G., Stone, P., Fung, I., Ruedy, R., and Lerner, J. 1984. "Climate Sensitivity: Analysis of Feedback Mechanisms." 130–163. In J. E. Hansen and T. Takahashi (eds.), *Climate Processes and Climate Sensitivity* (Maurice Ewing Series, No. 5). American Geophysical Union, Washington, D.C.

Hansen, J., Russell, G., Rind, D., Stone, P., Lacis, A., Lebedeff, S., Ruedy, R., and Travis, L. 1983. "Efficient Three-Dimensional Global Models for Climate Studies: Models I and II." *Monthly Weather Review 111*:609–662.

Hummel, J. R., 1982. "Surface Temperature Sensitivities in a Multiple Cloud Radiative-Convective Model With a Constant and Pressure-Dependent Lapse Rate." *Tellus 34*:203–208.

Hummel, J. R., and Kuhn, W. R. 1981a. "Comparison of Radiative-Convective Models With Constant and Pressure-Dependent Lapse Rates." *Tellus 33*:254–261.

Hummel, J. R., and Kuhn, W. R. 1981b. "An Atmospheric Radiative-Convective Model With Interactive Water Vapor Transport and Cloud Development." *Tellus 33*:372–381.

Hummel, J. R., and Reck, R. A. 1981. "Carbon Dioxide and Climate: The Effects of Water Transport in Radiative-Convective Models." *Journal of Geophysical Research 86*:12035–12038.

Hunt, B. G., 1981. "An Examination of Some Feedback Mechanisms in the Carbon Dioxide Climate Problem." *Tellus 33*:78–88.

Hunt, B. G., and Wells, N. C. 1979. "An Assessment of the Possible Future Climatic Impact of Carbon Dioxide Increases Based on a Coupled One-Dimensional Atmospheric-Oceanic Model." *Journal of Geophysical Research 84:*787–791.

Jaeger, L. 1976. "Monatskarten des Niederschlags für die ganze Erde." *Berichte des Deutschen Wetterdienstes 139:* 1–38.

Jenne, R. L. 1975. "Data Sets for Meteorological Research" (NCAR-TN/IA-111). National Center for Atmospheric Research, Boulder, Colorado.

Katz, R. W. 1983. "Statistical Procedures for Making Inferences About Precipitation Changes Simulated by an Atmospheric General Circulation Model." *Journal of the Atmospheric Sciences 40:*2193–2201.

Lacis, A. A., and Hansen, J. E. 1974. "Parameterization for the Absorption of Solar Radiation in the Earth's Atmosphere." *Journal of the Atmospheric Sciences 31:*118–133.

Lal, M., and Ramanathan, V. 1984. "The Effects of Moist Convection and Water Vapor Radiative Processes on Climate Sensitivity." *Journal of the Atmospheric Sciences 41:*2238–2249.

Lindzen, R. S., Hou, A. Y., and Farrell, B. F. 1982. "The Role of Convective Model Choice in Calculating the Climate Impact of Doubling CO_2." *Journal of the Atmospheric Sciences 39:*1189–1205.

Luther, F. M. 1984. *The Intercomparison of Radiation Codes in Climatic Models (ICRCCM): Longwave Clear-Sky Calculations.* World Climate Research Programme, WCP-93, International Council of Scientific Unions and World Meteorological Organization, Geneva, Switzerland.

Manabe, S. 1971. "Estimate of Future Changes in Climate Due to Increase of Carbon Dioxide Concentration in the Air." 249–264. In W. H. Mathews, W. W. Kellogg, and G. D. Robinson (eds.), *Man's Impact on the Climate,* MIT Press, Cambridge, Massachusetts.

Manabe, S., and Stouffer, R. J. 1979. "A CO_2-Climate Sensitivity Study With a Mathematical Model of the Global Climate." *Nature 282:*491–493.

Manabe, S., and Stouffer, R. J. 1980. "Sensitivity of a Global Climate Model to an Increase of CO_2 Concentration in the Atmosphere." *Journal of Geophysical Research 85:*5529–5554.

Manabe, S., and Strickler, R. F. 1964. "Thermal Equilibrium of the Atmosphere With a Convective Adjustment." *Journal of the Atmospheric Sciences 21:*361–385.

Manabe, S., and Wetherald, R. T. 1967. "Thermal Equilibrium of the Atmosphere with a Given Distribution of Relative Humidity." *Journal of the Atmospheric Sciences 24:*241–259.

Manabe, S., and Wetherald, R. T. 1975. "The Effects of Doubling the CO_2 Concentration on the Climate of a General Circulation Model." *Journal of the Atmospheric Sciences 32:*3–15.

Manabe, S., and Wetherald, R. T. 1980. "On the Distribution of Climate Change Resulting From an Increase in CO_2-Content of the Atmosphere." *Journal of the the Atmospheric Sciences 37:*99–118.

Manabe, S., Bryan, K., and Spelman, M. J. 1979. "A Global Ocean-Atmosphere Climate Model With Seasonal Variation for Future Studies of Climate Sensitivity." *Dynamics of Atmospheres and Oceans 3:*393–426.

Manabe, S., Smagorinsky, J., and Strickler, R. F. 1965. "Simulated Climatology of a General Circulation Model With a Hydrological Cycle." *Monthly Weather Review 93:*769–798.

Manabe, S., Wetherald, R. T., and Stouffer, R. J. 1981. "Summer Dryness Due to an Increase of Atmospheric CO_2 Concentration." *Climatic Change 3:*347–386.

Meehl, G. A., and Washington, W. M. 1985a. "Sea Surface Temperatures Computed by a Simple Ocean Mixed Layer Coupled to an Atmospheric GCM." *Journal of Physical Oceanography 15:*92–104.

Meehl, G. A., and Washington, W. M. 1985b. "Tropical Response to Increased CO_2 in a GCM with a Simple Mixed Layer Ocean: Similarities to an Observed Pacific Warm Event." *Monthly Weather Review, 113:*in press.

Mitchell, J. F. B. 1983. "The Seasonal Response of a General Circulation Model to Changes in CO_2 and Sea Temperature." *Quarterly Journal of the Royal Meteorological Society 109:*113–152.

Mitchell, J. F. B. 1984. "The Effect of Global Pollutants on Climate." *Meteorological Magazine 113:*1–15.

Mitchell, J. F. B., and Lupton, G. 1984. "A 4 × CO_2 Integration With Prescribed Changes in Sea Surface Temperatures." *Progress in Biometeorology 3:*353–374.

Mitchell, J. F. B., Wilson, C. A., Ingram, W. J., and Lunnington, W. M. 1986. "Numerical Studies of the Effect of Increased Atmospheric Carbon Dioxide on Climate." Final report of Contract CL-114-UK(H) (unpublished). Available from the Meteorological Office, Bracknell, United Kingdom.

Newell, R. E., Kidson, J. W., Vincent, D. G., and Boer, G. J. 1972. *The General Circulation of the Tropical Atmosphere and Interactions with Extra-Tropical Latitudes,* Vol. 1, M.I.T. Press, Cambridge, Massachusetts.

North, G. R., Cahalan, R. F., and Coakley, J. A. 1981. "Energy-Balance Climate Models." *Reviews of Geophysics and Space Physics 19:*91–122.

Oort, A. H. 1983. *Global Atmospheric Circulation Statistics, 1958–1973.* (NOAA Professional Paper No. 14). U.S. Government Printing Office, Washington, D.C.

Pitcher, E. J., Malone, R. C., Ramanathan, V., Blackmon, M. L., Puri, K., and Bourke, W. 1983. "January and July Simulations With a Spectral General Circulation Model." *Journal of the Atmospheric Sciences 40:*580–604.

Ramanathan, V., Lian, M. S., and Cess, R. D. 1979. "Increased Atmospheric CO_2: Zonal and Seasonal Estimates of the Effects on the Radiation Energy Balance and Surface Temperature." *Journal of Geophysical Research 84:*4949–4958.

Ramanathan, V., Pitcher, E. J., Malone, R. C., and Blackmon, M. L. 1983. "The Response of a Spectral General Circulation Model to Refinements in Radiative Processes." *Journal of the Atmospheric Sciences 40:*605–630.

Rasool, S. I., and Schneider, S. H. 1971. "Atmospheric Carbon Dioxide and Aerosols: Effects of Large Increases on Global Climate." *Science 173:*138–141.

Rind, D., and Lebedeff, S. 1984. *Potential Climatic Impacts of Increasing Atmospheric CO_2 with Emphasis on Water Availability and Hydrology in the United States* (Report EPA 230-04-84-006). Environmental Protection Agency, Washington, D.C.

Rotty, R. M. 1983. "Distribution of and Changes in Industrial Carbon Dioxide Production." *Journal of Geophysical Research 88:*1301–1308.

Rowntree, P. R., and Bolton, J. A. 1983. "Simulation of the Atmospheric Response to Soil Moisture Anomalies Over Europe." *Quarterly Journal of the Royal Meteorological Society 109:*501–526.

Rowntree, P. R., and Walker, J. 1978. "The Effects of Doubling the CO_2 Concentration on Radiative-Convective Equilibrium." 181–191. In J. Williams (ed.), *Carbon Dioxide, Climate and Society,* Pergamon, Oxford, United Kingdom.

Schlesinger, M. E. 1982. "Simulating CO_2-Induced Climatic Change With Mathematical Climate Models: Capabilities, Limitations, and Prospects." *Proceedings: Carbon Dioxide Research Conference: Carbon Dioxide, Science and Consensus* (CONF-820970). U.S. Department of Energy, Washington, D.C. Available from NTIS, Springfield, Virginia.

Schlesinger, M. E. 1984a. "Climate Model Simulation of CO_2-Induced Climatic Change." 141–235. In B. Saltzman (ed.) *Advances in Geophysics, 26,* Academic Press, New York, New York.

Schlesinger, M. E. 1984b. "Atmospheric General Circulation Model Simulations of the Modern Antarctic Climate." 155–196. In *Environment of West Antarctica: Potential CO_2-Induced Change,* Committee on Glaciology, Polar Research Board, Commission on Physical Sciences, Mathematics and Resources, National Research Council, National Academy Press, Washington, D.C.

Schlesinger, M. E., and Gates, W. L. 1981. "Preliminary Analysis of Four General Circulation Model Experiments on the Role of the Ocean in Climate" (Report No. 25). Climatic Research Institute, Oregon State University, Corvallis, Oregon.

Schlesinger, M. E., Gates, W. L., and Y.-J. Han. 1985. "The Role of the Ocean in CO_2-Induced Climate Warming: Preliminary Results From the OSU Coupled Atmosphere-Ocean GCM." 447–478. In J. C. J. Nihoul (ed.), *Coupled Ocean-Atmosphere Models,* Elsevier, Amsterdam, The Netherlands.

Schutz, C., and Gates, W. L. 1971. *Global Climatic Data for Surface, 800 mb, 400 mb: January* (Report R-915-ARPA). Rand Corporation, Santa Monica, California. Available from NTIS (AD-736204), Springfield, Virginia.

Schutz, C., and Gates, W. L. 1972. *Global Climatic Data for Surface, 800 mb, 400 mb: July* (Report R-1029-ARPA). Rand Corporation, Santa Monica, California. Available from NTIS (AD-760283), Springfield, Virginia.

Sellers, W. D. 1969. "A Global Climate Model Based on the Energy Balance of the Earth-Atmosphere System." *Journal of Applied Meteorology 8:*392–400.

Somerville, R. C. J., and Remer, L. A. 1984. "Cloud Optical Thickness Feedbacks in the CO_2 Climate Problem." *Journal of Geophysical Research, 89:*9668–9672.

Spelman, M. J., and Manabe, S. 1984. "Influence of Oceanic Heat Transport Upon the Sensitivity of a Model Climate." *Journal of Geophysical Research 89:*571–586.

Taljaard, J. J., van Loon, H., Crutcher, H. L., and Jenne, R. L. 1969. *Climate of the Upper Air: Southern Hemisphere, Vol. 1. Temperatures, Dew Points and Heights at Selected Pressure Levels* (NAVAIR 50-1C-55). Naval Weather Service Command, Washington, D.C.

Trabalka, J. R. (ed.). 1985. *Atmospheric Carbon Dioxide and the Global Carbon Cycle* (DOE/ER-0239). U.S. Department of Energy, Washington, D.C. Available from NTIS, Springfield, Virginia.

Walsh, J., and Johnson, C. 1979. "An Analysis of Arctic Sea Ice Fluctuations." *Journal of Physical Oceanography 9:*580–591.

Wang, W.-C., Rossow, W. B., Yao, M. S., and Wolfson, M. 1981. "Climate Sensitivity of a One-Dimensional Radiative-Convective Model with Cloud Feedback." *Journal of the Atmospheric Sciences 38:*1167–1178.

Wang, W.-C., and Stone, P. H. 1980. "Effect of Ice-Albedo Feedback on Global Sensitivity in a One-Dimensional Radiative-Convective Climate Model." *Journal of the Atmospheric Sciences 37:*545–552.

Washington, W. M., and Meehl, G. A. 1983. "General Circulation Model Experiments on the Climatic Effects Due to a Doubling and Quadrupling of Carbon Dioxide Concentration." *Journal of Geophysical Research 88:*6600–6610.

Washington, W. M., and Meehl, G. A. 1984. "Seasonal Cycle Experiment on the Climate Sensitivity Due to a Doubling of CO_2 With an Atmospheric General Circulation Model Coupled to a Simple Mixed-Layer Ocean Model." *Journal of Geophysical Research 89:*9475–9503.

Washington, W. M., and Meehl, G. A. 1986. "General Circulation Model CO_2 Sensitivity Experiments: Snow-Sea Ice Albedo Parameterizations and Globally Averaged Surface Air Temperature." *Climatic Change 8:*in press.

Washington, W. M., Semtner, A. J. Jr., Meehl, G. A. Knight, D. J. and Mayer, T. A. 1980. "A General Circulation Experiment With a Coupled Atmosphere, Ocean, Sea Ice Model." *Journal of Physical Oceanography 10:*1887–1908.

Wetherald, R. T., and Manabe, S. 1975. "The Effects of Changing the Solar Constant on the Climate of a General Circulation Model." *Journal of the Atmospheric Sciences 32:*2044–2059.

Wetherald, R. T., and Manabe, S. 1980. "Cloud Cover and Climate Sensitivity." *Journal of the Atmospheric Sciences 37:*1485–1510.

Wetherald, R. T., and Manabe, S. 1981. "Influence of Seasonal Variation Upon the Sensitivity of a Model Climate." *Journal of Geophysical Research 86:*1194–1204.

World Meteorological Organization (WMO). 1983. "Report of the WMO (CAS) Meeting of Experts on the CO_2 Concentrations from Pre-Industrial Times to I.G.Y." World Climate Programme Report WCP-55. WMO, Geneva, Switzerland.

5. MODEL PROJECTIONS OF THE TIME-DEPENDENT RESPONSE TO INCREASING CARBON DIOXIDE

Martin I. Hoffert
New York University

Brian P. Flannery
Exxon Research and Engineering Company

CONTENTS

5.1 INTRODUCTION

Most climate models have been designed to further our understanding of the long-term equilibrium climate response that results from long-term and sustained changes in external forcing. Such models, therefore, are concerned mainly with hypothetical steady-state climates (see Chapter 4 of this volume). In the real world, however, climate is rarely, if ever, in a steady state; observed climatological properties almost always exhibit some variability from one averaging period to the next. Transient (time-varying) climatic behavior has occurred over a wide range of time scales in the course of the Earth's geological evolution (see Chapter 7). Such variations have been caused by a variety of external and internal factors (see Figure 3.2 in Chapter 3), some of which are not entirely understood at present. It is almost certain that changes in atmospheric composition, including the amount of carbon dioxide (CO_2) and perhaps other radiatively active trace gases in the atmosphere, have influenced and regulated the Earth's temperature and climate via the greenhouse effect.

The modeling of transient climate change driven by greenhouse heating from the increase in CO_2 concentration over the last 130 years is the subject of this chapter. This type of analysis requires treatment of all of the factors associated with modeling steady-state climates (see Chapter 4) plus the significant additional dimension of time. For example, the finite heat capacity of the oceans plays a critical role in damping climate fluctuations relative to values predicted by steady-state sensitivity models. In the case of increasing CO_2 concentrations in the atmosphere, the system may never reach the steady-state warming associated with the amount of CO_2 in the atmosphere at any given time (e.g., Wigley and Schlesinger 1985b). On the other hand, for some scenarios of fossil fuel use in which CO_2 emissions are drastically cut back early in the next century, it is possible for global warming to continue beyond the point of emission cutoff as a result of the nonequilibrium transient (Michael et al. 1981).

As an introduction to estimating the transient climatic effects over the period 1880–1980 (and earlier), when worldwide combustion of carbonaceous fossil fuel and other factors were increasing atmospheric CO_2 concentrations, consider the time series of surface air temperatures (Vinnikov et al. 1980; Jones et al. 1982) shown in Figure 5.1 and sea ice cover (Vinnikov et al. 1980; Zwally et al. 1983) shown in Figures 5.2 and 5.3. As described more fully in the accompanying state-of-the-art report on the *Detecting the Climatic Effects of Increasing Carbon Dioxide* (see Chapter 4 by Wigley et al. 1985), there is no clear indication of a monotonic warming over this period, as would be anticipated from the observed buildup of CO_2 in the atmosphere. Instead, these data sets indicate a complex picture including interannual variability and, perhaps, some systematic trends. Indeed, the global temperatures seem to have increased from 1885–1935, and the extent of Arctic sea ice decreased from 1925–1945. This was followed, however, by a leveling off and then a subsequent decrease in temperature. Although it is possible that the data sets are incomplete, these surface air temperatures do not appear to display the monotonic increase in global mean temperatures predicted by CO_2-driven climate models. This does not necessarily mean an absence of an effect thus far, because the superposition of climatic variability from other causes may obscure the signal. Among other things, therefore, transient climate models are needed to address whether historical records are consistent with predictions of past warming from increasing CO_2 concentrations, as well as where and when a climate change is likely to be observed in the future.

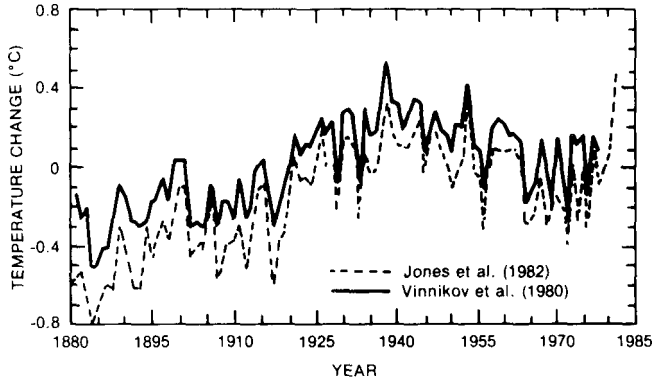

Figure 5.1. Annual mean surface air temperature anomalies from 1880–1981: (solid curve) Vinnikov et al. (1980); and (dashed curve) Jones et al. (1982). Figure from Weller et al. (1983), and includes points updated to 1981 by Jones.

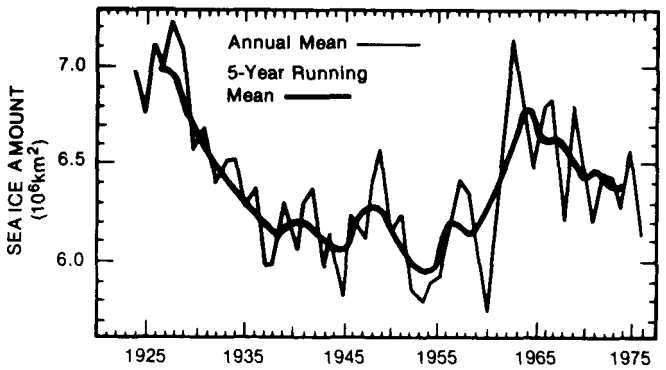

Figure 5.2. Annual mean and 5-year running mean sea ice amount in the Arctic Ocean from 1920–1975 (data from Vinnikov et al. [1980]).

To understand transient changes, it is necessary to understand how they are different from the equilibrium conditions considered in Chapter 4. Under steady-state conditions, the Earth's surface temperature is governed by the balance between solar heating and planetary cooling by longwave radiation to space. The main effect of greenhouse gases—water vapor, carbon dioxide, ozone, and certain trace gases—is to cause the spectrally averaged radiative cooling to occur from the atmosphere at higher, colder altitudes than if all the radiation came from the warmer surface of the planet, as would occur if there were no atmosphere. This greenhouse effect leads to the global mean surface temperature of the Earth being some 33°C warmer than it would be in the absence of the atmosphere.

If a sudden increase in atmospheric CO_2 concentration were to occur, the planet's radiative balance would be perturbed because the cooling rate would decrease. To restore the balance, the system would create a new climate by increasing the surface and tropospheric temperature until the longwave cooling from the higher tropospheric altitude associated with the increased CO_2 is large enough to balance solar heating. There are additional positive feedbacks from increasing water vapor, decreasing sea ice, and, perhaps, changes in cloud extent and distribution. The best estimates are that, together, these feedbacks amplify the CO_2-only warming by a factor of two to four (see Chapter 4). By itself, the atmosphere would come into a new steady state after a sudden change in the amount of CO_2 within a few months, but the high heat capacity of the surface ocean and underlying waters prevents such a rapid adjustment, resulting in a *transient lag.*

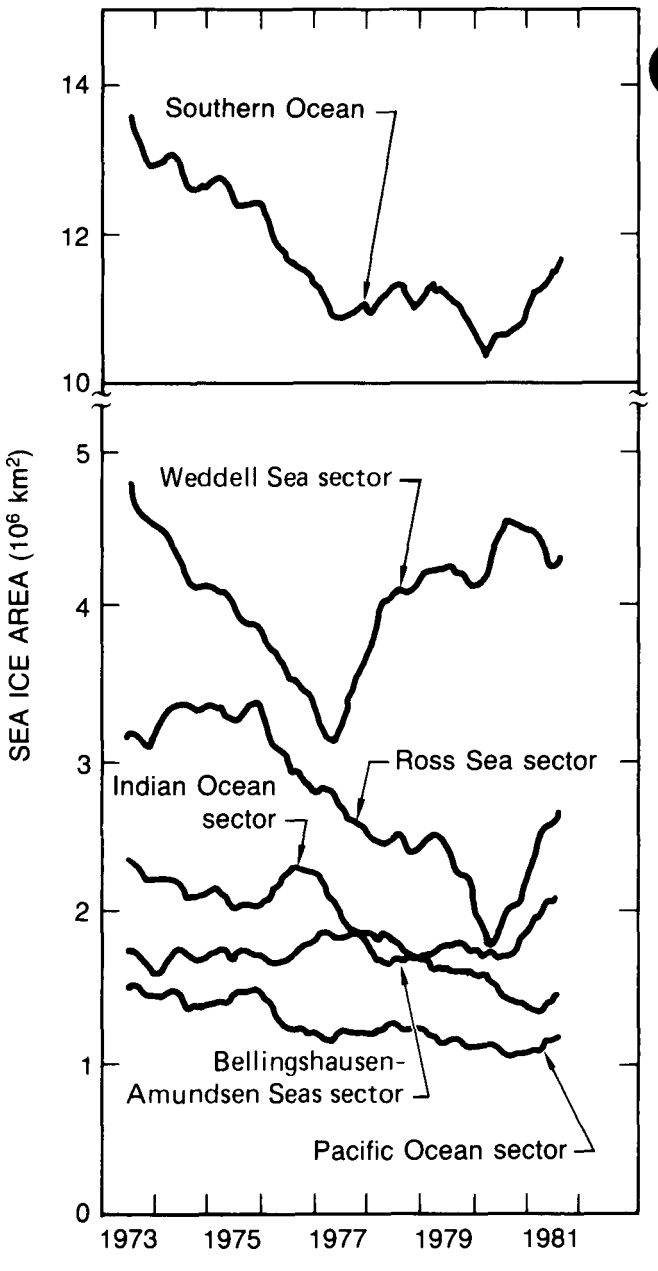

Figure 5.3. Annual (12-month running) mean of sea ice amount in the Southern Ocean off Antarctica from 1973–1981 (data from Zwally et al. [1983]). All series exhibit short-period (2–10 y) oscillations.

The coupling of the various thermal reservoirs of the climate system that can store heat is a central feature of the transient problem. So too is the relationship between climate sensitivity, including internal feedbacks, and the relaxation times of the heat-storing reservoirs. In the sections that follow, we begin with a description of a simple model for the transient response, analyze the time scales that come into play, and discuss the types of external

forcing and the time lags that can result. With the help of these ideas to put the problem in context, applications of climate models developed thus far for studies of the time-dependent climate response to increasing CO_2 concentrations will be reviewed, and areas of future research will be discussed.

5.2 A CONCEPTUAL MODEL FOR UNDERSTANDING THE TRANSIENT RESPONSE OF GLOBAL CLIMATE

To fully assess the impact of fossil fuel CO_2 on world climate, it is necessary to predict the transient response of a broad range of climatological variables (including temperatures, winds, precipitation, and hydrology) with sufficient spatial resolution to determine regional effects. The development of this capability requires use of coupled general circulation models (GCMs) of the Earth's atmosphere and oceans. However, certain essential features of the problem can be illustrated with simpler thermodynamic energy balance models (EBMs), which sacrifice detail for clarity of analysis by focusing on the principle of conservation of energy.

To put the results of more detailed models in context, consider the following conceptual model of the global energy balance. Let T be the global annually averaged surface temperature of the Earth, without, at this point, differentiating between air, water, or land temperatures. Also, let q be the surface atmospheric water vapor concentration, and let c be the concentration of CO_2 (well mixed in the troposphere). These constituents are of the order 1 and 0.03% by volume, respectively, at present. As in radiative-convective models of the troposphere, assume that the vertical temperature and water vapor profiles are defined by their surface values, and that $q(T)$ is given by the surface relative humidity and the (Clausius-Clapeyron) equation for water saturation vapor pressure.

The outgoing infrared (IR) energy radiated to space per unit surface area can be expressed by a relation of the form $Q_{IR} = Q_{IR}(T, q, c, \ldots)$, which includes the effect of integration over the entire IR spectrum and all path angles. Results of radiative-convective models suggest that Q_{IR} decreases approximately linearly with the logarithm of c (Augustsson and Ramanathan 1977). Such models, as well as direct observations by satellite radiometers (see, e.g., Warren and Schneider 1979), also indicate that Q_{IR} increases approximately linearly with T. Let S_0, a_0, c_0, and T_0 be the solar constant, planetary absorptance, atmospheric CO_2 concentration, and global mean surface temperature, respectively, at some reference state close to that of the current climate. The IR flux to space is then expressible approximately by a first-order Taylor series expansion in the vicinity of the reference state denoted by subscript zero:

$$Q_{IR}(T, c, q) \simeq Q_0 - A \ln\left(\frac{c}{c_0}\right) + B(T - T_0) \ , \quad (5.1)$$

where $Q_0 = a_0 S_0/4$ is the absorbed solar flux, which is equal to the outgoing IR flux at the reference state, and

$$A \equiv -\left\{\frac{\partial Q_{IR}}{\partial\left[\ln\left(\frac{c}{c_0}\right)\right]}\right\}_{q,T} ,$$

$$B \equiv \left\{\frac{\partial Q_{IR}}{\partial T}\right\}_{q,c} + \left\{\frac{\partial Q_{IR}}{\partial q}\right\}_{T,c}\left(\frac{\partial q}{\partial T}\right)$$

are coefficients that are essentially constant within the range of validity of the expansion. The second term on the right-hand side of the equation for B is the effect of water vapor-IR feedback and is negative because water vapor decreases the outgoing radiation, but this term is smaller than the first positive term. The flux Q_{IR} represents a distribution that peaks at a wavelength near 15 μm and is spectrally separated from the incoming solar flux, which peaks near 0.5 μm.

Without feedbacks, the incoming solar flux absorbed by the Earth is simply $Q_S = aS/4$, where S is the solar constant, a is the planetary absorptance, which is equal to incoming minus reflected solar energy, and 1/4 is the disk-to-surface-area ratio. In the presence of albedo-temperature feedback from sea ice and highly reflective snow cover on land, which is rapidly responding, absorbed solar radiation increases with increasing temperature as

$$Q_S(T, S, a) \simeq \frac{1}{4} S\left[a + \left(\frac{\partial a}{\partial T}\right)(T - T_0)\right] . \quad (5.2)$$

Additional feedback terms having a temperature dependence can enter the right-hand sides of Equations (5.1) and (5.2). A possibly important but uncertain feedback is associated with cloudiness

change during climate change. Suppose, for example, a warmer planet is cloudier. This decreases Q_S because more radiation is backscattered to space (clouds give the planet a higher albedo, or brightness); but clouds also decrease Q_{IR} by intercepting IR characteristic of high surface temperatures and radiating to space at a lower temperature. Cess (1976) and Cess et al. (1982) have argued from observational data that the effects tend to compensate in $Q_{NET} = Q_S - Q_{IR}$, which drives climate change (see also the discussion by Kandel 1983). Although we omit the cloudiness feedback from our simple model, it is worth mentioning that a number of GCMs include it through cloud and radiation parameterizations (see below).

It is useful to define the linear damping coefficient,

$$\lambda \equiv \left[\frac{\partial(Q_{IR} - Q_S)}{\partial T}\right]_c \simeq B - \frac{1}{4}S_0\frac{\partial a}{\partial T} . \qquad (5.3)$$

The approximation on the right-hand side includes water vapor-IR feedback (through B) and albedo-temperature feedback. More general expressions could be developed, in principle, to include cloudiness or other feedbacks, if their physics were better known from theory or observations. Neglecting higher order contributions from the perturbations $\Delta T = T - T_0$, $\Delta S = S - S_0$, $\Delta a = a - a_0$, and $\Delta c = c - c_0$, the net radiation (positive downward into the planet) for conditions in the vicinity of the reference state (where $Q_{NET} = 0$), from Equations (5.1)-(5.3), is:

$$Q_{NET}(T, S, a, c,) = Q_S - Q_{IR} \simeq \lambda\,[T_e(S, a, c) - T], \quad (5.4)$$

where

$$T_e(S, a, c) \equiv T_0 + \lambda^{-1}\left[\frac{1}{4}(Sa - S_0a_0) + A\ln\left(\frac{c}{c_0}\right)\right]$$

$$= T_0 + \lambda^{-1}\left\{Q_0\left[\frac{\Delta S}{S_0} + \frac{\Delta a}{a_0}\right] + A\ln\left(1 + \frac{\Delta c}{c_0}\right)\right\}$$

$$= T_0 + \lambda^{-1}\Delta Q_{NET} \qquad (5.5)$$

is the *equilibrium temperature*. This reference temperature was introduced by Hoffert et al. (1980) to express the shifting equilibrium tendency of the system in terms of factors forcing the climate system during transient climate change. As defined by Equation (5.5), T_e represents the temperature at any time toward which the system relaxes for values of S, a, or c that are different from those of the subscript zero reference climate. Note that $T_e(t)$ could itself be time dependent, being driven, for example, by time variations in solar, volcanic, and CO_2 greenhouse forcing through the time variations in $S(t)$, $a(t)$, and $c(t)$. This list of external causes is not exhaustive; Chapter 6 of this volume, for example, also estimates effects of potentially important anthropogenic greenhouse gases other than CO_2 (e.g., methane, nitrous oxide, and chlorofluorocarbons) on the equilibrium temperature.

In this simple model, we assume that the instantaneous imbalances in Q_{NET} are absorbed by only the well-mixed surface layer of the world oceans, which is taken to be of the order of 100 m thick. Heat capacities of the atmosphere and thermally interactive land surfaces are negligible by comparison, although the low heat capacity of land could affect the results if global air masses are not well mixed (see Thompson and Schneider 1979). Here we make the infinite wind assumption of Thompson and Schneider (1979) and assume that the planetary thermal inertia is dominated by the oceanic mixed layer. The heat capacity per unit area of ocean of such a layer is approximately 4×10^8 J m^{-2} K^{-1}. The global mean temperature $T(t)$ is then governed by the simple differential equation $C dT/dt = Q_{NET} \simeq \lambda\,[T_e(t) - T]$, or

$$\frac{dT}{dt} = \frac{[T_e(t) - T]}{\tau_{rm}} , \qquad (5.6)$$

where $\tau_{rm} \equiv C/\lambda$ is a characteristic radiative cooling time of the mixed layer. Note also from Equation (5.5) that the change in equilibrium temperature, $\Delta T_e \equiv T_e - T_0$, arising from changes in S, a, and c is expressible as

$$\Delta T_e \equiv \beta_T\left(\frac{\Delta S}{S_0} + \frac{\Delta a}{a_0}\right) + \beta_c\ln\left(1 + \frac{\Delta c}{c_0}\right), \quad (5.7)$$

where $\beta_T = Q/\lambda$ and $\beta_c = A/\lambda$ are climate sensitivity parameters. Typical values of the first two coefficients appearing in Equation (5.1) and above are (Hoffert et al. 1980): $Q_0 \simeq 238$ W m^{-2} and $A = 7.93$ W m^{-2}. Thus, both the relaxation time

of the mixed layer and the equilibrium temperature change scale inversely with the damping coefficient λ defined by Equation (5.3). These effects are in some sense compensatory, because a more sensitive climate (smaller λ) gives a larger temperature change in the final equilibrium, but it may take longer to get there. In any event, the numerical value of λ, a quantity associated with EBMs, GCMs, and the real climate, is obviously a key parameter in estimating both the equilibrium sensitivity and the transient response.

Warren and Schneider's (1979) analysis of atmospheric radiation data suggest $B = dQ_{IR}/dT$ is in the range of 1.0 – 3.5 W m^{-2} K^{-1}, which includes the direct temperature effect on radiation plus water vapor feedback. Values in a comparable range are generated by radiative-convective climate models. However, the linear damping coefficient $\lambda = B - (1/4)S_0 \partial a/\partial T$, which appears in Equations (5.4), (5.5), and (5.7), includes the effect of surface albedo-temperature feedback; in the classical case warmer (cooler) temperatures lead to less (more) extensive snow and sea ice, in turn leading to still warmer (cooler) global temperatures. Watts (1983) has estimated that $(1/4)S_0 \partial a/\partial T$ may be some 50% of B, thus decreasing λ by 50%. Such a value would decrease λ, relative to B. Although empirical seasonal and zonal relationships between temperature and planetary albedo have been used in simple climate models, the observed relationships depend on moisture variations as well as temperature, and it is not clear how moisture would change with long-term climate change. Some modelers (i.e., Källén et al. 1979) have even suggested that snow and ice cover at some latitudes and during some seasons might increase with a climate warming, thereby increasing λ relative to B. These uncertainties are lumped together in the linear damping coefficient and will be shown presently to have a major effect on both the steady-state and transient response. For purposes of estimation in this conceptual model, we assume a nominal value $\lambda \simeq 2.2$ W m^{-2} K^{-1}, although considerable variation exists in the literature derived from the output of general circulation models. Harvey and Schneider (1985b), for example, on the basis of numerical climate sensitivity studies, use a nominal λ of 1.8 W m^{-2} K^{-1}. Our nominal base case of $\lambda = 2.2$ W m^{-2} K^{-1} (Hoffert et al. 1980) corresponds to:

$$\tau_{rm} \simeq \left(\frac{2.8 \times 10^8 \text{ J m}^{-2} \text{ K}^{-1}}{2.2 \text{ W m}^{-2} \text{ K}^{-1}}\right) \times \left(\frac{1 \text{ y}}{3.15 \times 10^7 \text{ s}}\right) \simeq 4 \text{ y} , \quad (5.8a)$$

$$\beta_T \simeq \left(\frac{238 \text{ W m}^{-2}}{2.2 \text{ W m}^{-2} \text{ K}^{-1}}\right) \simeq 108 \text{ K} , \quad (5.8b)$$

$$\beta_c \simeq \left(\frac{7.93 \text{ W m}^{-2}}{2.2 \text{ W m}^{-2} \text{ K}^{-1}}\right) \simeq 3.6 \text{ K} . \quad (5.8c)$$

The sensitivities correspond to a ΔT_e of $\simeq 1$°C for a 1% solar constant increase. The value $A = 7.93$ W m^{-2} corresponds to an increase in net radiative forcing to the planet per unit area of $\Delta Q_{NET} = -\Delta Q_{IR} = +7.93 \ln 2 \simeq 5.5$ W m^{-2} for 2 × CO_2 doubling, which was calibrated to recover $\Delta T_e = \Delta Q_{NET}/\lambda \simeq 2.5$°C for a CO_2 doubling for the value $\lambda = 2.2$ W m^{-2} K^{-1} used here. This temperature change is consistent with the prior conclusions of the National Research Council (NRC 1982) that the equilibrium global surface warming from a doubling of CO_2 is "near 3°C, with a probable error of ±1.5°C." More recent studies with GCMs suggest comparable values for CO_2 sensitivity (see Chapter 4), although perhaps with a greater range of uncertainty (Schlesinger 1983). However, it is clear from our analysis that the equilibrium global warming depends on the ratio of the direct radiative forcing from the CO_2 greenhouse effect to the damping parameter. In assessing transient model results, it should be borne in mind that the forcing, ΔQ_{NET} for a CO_2 doubling, in addition to λ, is known to vary from model to model. For example, Bryan et al. (1982) have a forcing of 6.5 W m^{-2} for 4 × CO_2, which corresponds to 3.25 W m^{-2} for 2 × CO_2, whereas Hansen et al. (1984) have a direct forcing of 4.3 W m^{-2} for 2 × CO_2.

The main difficulty in making even so elementary a prediction as ΔT_e from a CO_2 doubling is the potentially important role of various poorly understood feedbacks: Watts (1983), for example, estimates an upper value of $\partial a/\partial T \simeq 0.0034$ K^{-1}. A value only half as large gives an albedo-temperature feedback contribution to λ of $-(1/4)S_0 \partial a/\partial T \simeq -0.6$ W m^{-2} K^{-1}, lowering λ by Equation (5.3) to 1.6 W m^{-2} K^{-1}. Cloudiness feedbacks may either increase or decrease λ, depending on whether the negative cloud-albedo feedback dominates the

positive cloud greenhouse feedback, or vice versa, with corresponding effects on τ_{rm} and ΔT_e. In their recent GCM simulation in which $\Delta T_e \simeq 4°C$ for a CO_2 doubling, Hansen et al. (1984) attribute $\simeq$35% of this warming to positive cloudiness feedback. But there are counterexamples, such as Washington and Meehl's CO_2-doubling experiment, cited by Schlesinger (1983), in which their GCM with interactive clouds gave a negative feedback, which is less warming than with fixed (no feedback) clouds. Other feedbacks can occur in climate models that incorporate coupled atmosphere-ocean GCMs, such as the idealized continental geometry model under development at the Geophysical Fluid Dynamics Laboratory in Princeton, New Jersey (Bryan et al. 1982). In summary, a nominal λ value of 2.2 W m^{-2} K^{-1} is within the range of uncertainty, but values greater or smaller than this by a factor of two associated with poorly understood feedbacks are possible and cannot be ruled out.

Finally, consider the solution to our simple mixed-layer model of Equation (5.6) for a step function change in forcing, ΔQ_{NET}, corresponding to $\Delta T_e = T_e - T_0 = \Delta Q_{NET}/\lambda =$ constant, applied at $t = 0$. Such a change can be thought of as arising from a sudden increase in the atmospheric CO_2 concentration maintained at a constant elevated level. This has become a standard diagnostic problem for transient climate models. The global temperature response is then a simple exponential approach to the new equilibrium temperature,

$$\Delta T(t) = T - T_0 = \Delta T_e \left[1 - exp\left(-\frac{t}{\tau_{rm}}\right)\right]. \quad (5.9)$$

The major results of this analysis are as follows: (1) A step increase in global heating rates, and hence in global equilibrium temperature, tends to be balanced by increased IR cooling until a new steady-state temperature is attained. This is a consequence of λ being positive, which implies that the climate is stable to small disturbances. (2) Positive (amplifying) feedbacks, such as water vapor-IR and ice-albedo, decrease λ, and negative feedbacks increase λ. (3) For a given forcing and system heat capacity, both the equilibrium (long-term) temperature change and the thermal relaxation time increase with decreasing λ; that is, the more positive the feedbacks, the greater the steady-state sensitivity, but it takes longer to approach a steady state.

5.3 TRANSIENT TIME SCALES OF MULTIRESERVOIR CLIMATE MODELS

The behavior of the transient climate response can be mathematically modeled by a system of coupled ordinary or partial differential equations based on the conservation of energy. The model equations described here are highly simplified. In particular, they neglect (or at best parameterize) dynamic effects that are responsible for energy transport. The solutions—typically obtained by numerical integration by a computer but available analytically under certain very idealized simplifying assumptions—define the time-dependent temperature distributions in a set of energy-exchanging thermal reservoirs in response to some specified external forcing. On the time scale of the CO_2 climate problem, these reservoirs should include at least the atmosphere, land, surface, upper mixed layer of the ocean (including sea ice), and the deep sea. On very long time scales, polar ice caps may need to be treated.

5.3.1 A Four-Reservoir Model

As a first step beyond the single-reservoir EBM of the last section, we now consider the transient response of a horizontally averaged (vertically resolved), coupled four-reservoir EBM, in which each layer represents one of the four global heat reservoirs cited above. This model is motivated by our intention to discuss the various time scales that can come into play during the transient response. Although the four-reservoir model discussed below is substantially less complex than coupled atmosphere-ocean GCMs, it has enough detail, at least schematically, to illustrate the various time scales involved in transient response and the role of coupling between reservoirs.

We will assume that the vertical heat flux within the layers occurs by radiative transport plus eddy thermal diffusivity in the atmosphere ($i = a$), thermal conduction of heat represented by molecular thermal diffusion to some penetration depth on land ($i = \ell$), turbulent eddy mixing in the surface ocean layer ($i = m$), and small-scale eddy diffusion plus upwelling of high-latitude bottom water (thermohaline overturning) in the deep sea ($i = d$). Both conduction and convective heat transfer are

modeled by Fourier heat conduction laws, $Q_{c,i} \simeq \rho_i C_i \kappa_i \partial T_i/\partial z$, where ρ_i, C_i, and κ_i are the density, specific heat per unit mass, and thermal diffusivity of the i-th reservoir, respectively.

The eddy thermal diffusivities κ_i used to represent turbulent motion in the fluid reservoirs ($i = a, m, d$) are orders of magnitude larger than the corresponding molecular values. Vertical eddy diffusivity in the atmosphere or ocean can be defined formally as $\kappa_i \equiv -\langle w_i' T' \rangle / (\partial T_i/\partial z)$, where the angular bracket denotes a Reynolds average over many fluctuation times and primes denote instantaneous fluctuations from the Reynolds average. In laboratory boundary layers and in atmospheric boundary layers using instrumented meteorological towers, it is often possible to make direct measurements of the eddy flux $\langle w'T' \rangle$ and of the mean temperature gradient $\partial \mathrm{T}/\partial \mathrm{z}$ simultaneously, by appropriate averaging of instantaneous values, and thereby to obtain a direct measurement of κ_i. In the atmosphere, the horizontal eddy diffusivity associated with atmospheric motions, $\kappa_{a,h} \equiv -\langle v' T_a' \rangle / [\partial T_a / \partial (R\phi)]$, can likewise be estimated from compilations of atmospheric circulation statistics (e.g., Oort 1983), where v' is a fluctuation in meridional (poleward) velocity, and $\mathrm{R}\phi$ is the distance from the equator along a meridian. Unfortunately, the vertical eddy diffusivity of the troposphere is difficult to measure directly owing to global sampling problems and the smallness of the w'-fluctuation. Moreover, in the oceans, it is difficult or impossible with present instrumentation technology to make either horizontal or vertical eddy diffusivity measurements directly by the flux-gradient method. Instead, eddy diffusivities are typically estimated by fitting observed distributions of transient and steady-state oceanic tracers (tritium, radiocarbon, total carbon, etc.) to solutions of simple mass-diffusion models of the oceans. This involves the additional assumption that heat and mass are transported analogously by oceanic eddies.

A consideration often cited in modeling heat transfer into the upper kilometer of the ocean (the thermocline) from oceanographic tracer distributions is the finding by chemical oceanographers that mass transport of tracers occurs predominantly along constant-density (isopycnal) surfaces that slant downward at shallow angles toward midlatitudes from high-latitude outcrops (see Trabalka 1985). This is partly a consequence of the stable density gradient in the thermocline damping the instabilities normal to isopycnals that lead to mixing. Hoffert et al. (1983) have found that eddy thermal diffusion across, rather than along, isopycnals is the dominant mode for downward heat transport because isopycnals are aligned very nearly with isotherms in the thermocline, and constant-temperature surfaces, by definition, have no gradient to provide a net transport of heat along them. The coincidence of isotherms and isopycnals in the thermocline is clearly illustrated in the two-dimensional ocean sections presented by Levitus (1982) and results from the relatively small contribution of salt to the density-temperature relationship in the thermocline. Accordingly, tracer data must be carefully interpreted in drawing analogies with thermal diffusion to the deep sea. The way ocean heat transport is modeled, and the values assumed for the coefficients, are important factors in predicting climatic transients because the heat diffusion rate into the deep sea significantly affects temperature evolution at the Earth's surface.

With these caveats, we write the upward heat flux in each of the four reservoirs in the form:

$$Q_a(z) = -Q_S(z) + Q_{IR}(z) - \rho_a c_a \kappa_a \left(\frac{\partial T_a}{\partial z} - \Gamma \right) , \tag{5.10a}$$

$$Q_\ell(z) = -\frac{\rho_\ell c_\ell \kappa_\ell \partial T_\ell}{\partial z} , \tag{5.10b}$$

$$Q_m(z) = -\frac{\rho_m c_m \kappa_m \partial T_m}{\partial z} , \tag{5.10c}$$

$$Q_d(d) = -\rho_d c_d \left[\frac{\kappa_d \partial T_d}{\partial z} + w\,(T_d - T_p) \right] . \tag{5.10d}$$

In the expression for atmospheric heat flux, $Q_s(z)$ and $Q_{IR}(z)$ are presumed to be known from a radiative transport model, and Γ is a specified atmospheric lapse rate introduced because the atmosphere's compressibility makes the potential, rather than the physical, temperature gradient appropriate in the Fourier heat conduction law. The use of a Fourier heat conduction law in the expression for Q_a is similar to the model of Liou and Ou (1983) for the vertical structure of radiative-turbulent atmospheres. (One-dimensional, radiative-convective models typically make a simpler convective-adjustment assumption in which the lapse rate equals Γ whenever the model computes an unstable profile $[-\partial T/\partial z > \Gamma]$.)

Figure 5.4 illustrates the major elements of an energy balance model for the thermal evolution of the deep ocean, and Table 5.1 provides a list of thermophysical properties that are important in the world climate system. The model includes thermal eddy diffusion, upwelling over most of the area of the global ocean and downwelling at temperature T_p in polar bottom-water-forming zones. Typically, $\kappa = 2000\ \mathrm{m^3\ y^{-1}}$, and $w \simeq 4\ \mathrm{m\ y^{-1}}$, with the downwelling flow rate balancing global upwelling. We refer to such a model as an upwelling-diffusion (UD) model, as opposed to a purely diffusive (PD) deep sea model with $w = 0$. A PD model was used by Oeschger et al. (1975) in deep sea radiocarbon calibration of κ_d. Although PD deep sea models have been used in some transient climate calculations (Hansen et al. 1981, 1984; Wigley and Schlesinger 1985a, 1985b), they inherently recover a uniform temperature profile versus depth in the steady state. The UD model recovers a more realistic exponential profile in the steady state, $Q_d = 0$ (Munk 1966; Hoffert et al. 1980, 1981; Cess and Goldenberg 1981; Harvey and Schneider 1985a, 1985b; Harvey 1985):

$$T_d(z) = T_p + (T_m - T_p)\, e^{-z/z^*}, \qquad (5.11)$$

where $z^* = \kappa_d / w \simeq 500$ m is a characteristic depth scale. Moreover, to re-equilibrate in response to a change in forcing, the PD model of Hansen et al. (1984) must adjust such that the temperature change at all depths ultimately equals the change at the surface (Harvey and Schneider, 1985a, 1985b). In UD models, the equilibrium temperature change can decrease with increasing depth. Thus, the total heat required to reach equilibrium is greater in PD models than in UD models with a cold polar bottom water source.

The transient energy balance in each reservoir requires that its time derivative of enthalpy per unit volume (the rate of increase of heat storage) be equal to the negative heat flux gradient (energy added per unit volume by heat transfer),

$$\frac{\partial (\rho_i c_i T_i)}{\partial t} = -\frac{\partial Q_i}{\partial z} \ . \qquad (5.12)$$

Substituting Equations (5.10a)-(5.10d) into (5.12) gives a system of four time-dependent partial differential equations governing the vertical temperature distribution in each reservoir. These equations

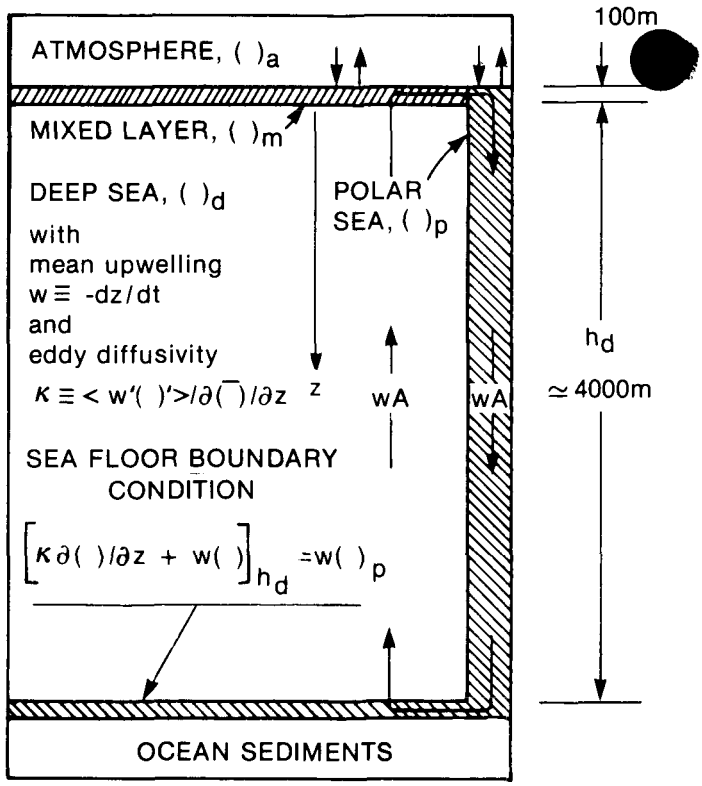

Figure 5.4. Schematic diagram of an idealized, one-dimensional box-advection-diffusion model for the world oceans showing coupling to other reservoirs. The sea floor boundary condition of this model equates the heat flux downwelled from the polar sea to the net (upwelling plus diffusion) upward heat flux at the ocean bottom.

are second-order in the z-variable, meaning that, in addition to initial profiles, two boundary values need to be specified per reservoir to get a solution. Because the reservoirs are coupled, we need boundary conditions at the top of the atmosphere and the bottom of the deep sea and two conditions at each interreservoir boundary.

In general, the surface temperature of the atmosphere and the surface temperature of land and sea are separated by an atmospheric boundary layer across which heat flux is continuous but temperature can jump; the transition is actually continuous, but rapid, in the thin surface layer on the order of 10–50 m thick. Taking into account the land/sea fractionation of heat flux, where $F_w \simeq 70\%$ is the global mean fraction of the Earth's surface covered by water, we express the surface heat flux boundary condition,

$$Q_a(0) = (1 - f_w) Q_\ell(0) + f_w Q_m(0) \ . \qquad (5.13)$$

Table 5.1
Thermophysical Properties and Relaxation Times of the Horizontally Averaged World Climate System

Property	Atmosphere[a] $i = a$	Land[b] $i = l$	World Ocean[c] Mixed Layer $i = m$	World Ocean[c] Deep Sea $i = d$
Horizontal Area, $A_i(m^2)$	5.10×10^{14}	1.76×10^{14}	3.34×10^{14}	3.34×10^{14}
Depth, $h_i(m)$	8400	2.3	100	4000
Density, ρ_i (kg m^{-3})	1.2	2800	1030	1030
Mass, $m_i=\rho_i h_i A_i$(kg)	5.10×10^{18}	1.13×10^{18}	3.44×10^{19}	1.38×10^{21}
Specific Heat, c_{pi}(J kg^{-1} K^{-1})	1000	750	4000	4000
Heat Capacity, $m_i c_{pi}$(J K^{-1})	5.10×10^{21}	8.48×10^{20}	1.37×10^{23}	5.52×10^{24}
Thermal Diffusivity, K_i(m^2 y^{-1})	3.2×10^{8}	16	3.0×10^{4}	2.0×10^{3}
Diffusion Time, $\tau_{diff} = h_i^2/K_i$(y)	0.2	0.3	0.3	8000
Internal Mixing Time, $\tau_{mix,i}$(y)	0.2	0.3	0.3	900
Radiative Relaxation Time[d], $(4\pi a^2 B)(y)$	0.1	0.02	3.9	156

[a] For this thermal response analysis, the atmospheric reservoir is reduced to sea level density $\rho_a=1.2$ kg m^{-3} so the effective depth is the scale height $h_a=m_a/(\rho_a A_a)$, where m_a is Verniani's (1966) value of atmospheric mass and $A_a=4\pi a^2$ is the Earth's surface area based on a planetary radius $a = 6.37\times10^6$ m. The values of c_{pa} and κ_a are typical values for specific heat and vertical eddy diffusivity in the troposphere.

[b] Whereas the Earth's crust is some 40 km deep under continental surfaces, the zone of thermal interaction with climatic forcing is confined to a thin skin depth (Sellers 1965), $h_l=(2\kappa_l/\Omega)^{1/2}$, where Ω is the circular frequency of the thermal wave applied at the surface. For consistency with the oceanic mixed layer, which is formed by forcing on an annual timescale, we set $\Omega=2\pi$ rad y^{-1}. The values of density, specific heat and molecular thermal diffusivity are typical of soil.

[c] The oceanic horizontal area is based on a 4100 m deep world ocean (mean depth of the Atlantic, Pacific and Indian Ocean basins excluding adjacent seas) and the Sverdrup et al. (1942) value of world ocean volume. This gives a fraction of the Earth covered by ocean of $f_o=A_{oc}/A_a=0.65$, somewhat less than the value based on the actual surface ocean area. This is compensated for to some extent by considering floating sea ice as part of the land surface. A typical mixed layer depth of 100 m is assigned (Kraus and Turner 1967). Eddy diffusivities of the mixed layer and deep sea are typical, but mixing time for the deep sea reservoir $\tau_{mix,d}=(K_d/h_d^2 + w/h_d)^{-1}$ includes the influence of a world ocean upwelling rate of $w \simeq 4$ m y^{-1} (see text).

[d] Based on a linear damping coefficient, $B \simeq 2.2$ W m^{-2} K^{-1} in the approximation for longwave radiation to space, i.e., $4\pi a^2 B = 3.54 \times 10^{22}$ J K^{-1} y^{-1}. Source: Hoffert et al. (1981).

We assume that both sensible and latent heat transfers across the turbulent surface boundary layer are proportional to the temperature jumps ΔT_{ma} and $\Delta T_{\ell a}$. Equating this surface heat loss to diffusive heat flux into the atmosphere gives

$$-\rho_a c_a \kappa_a \left(\frac{\partial T_a}{\partial z} - \Gamma\right) = \gamma_{ma}\Delta T_{ma} = \gamma_{\ell a}\Delta T_{\ell a}\ , \qquad (5.14)$$

where the γ_{ia}'s are heat transfer coefficients ($i = m, \ell$) that include the effect of both sensible and latent heat transfer and depend on surface windspeed. These considerations and Equation (5.8a) lead to *surface energy balances* for the land and water temperature differences

$$\Delta T_{ia} = \frac{[Q_a(0) + Q_S(0) - Q_{IR}(0)]}{\gamma_{ia}}\ ; \quad i = m, \ell \qquad (5.15)$$

between the atmosphere and land ($i = \ell$) or, ocean ($i = m$) reservoirs. Equations (5.13) and (5.15) are the interreservoir boundary conditions needed to couple the atmosphere and oceans. The climatological data presented by Oort (1983, p. 94) indicate that the ocean surface is a few degrees warmer on an annual mean basis at a given latitude belt than is the corresponding zonally averaged surface air temperature ($\Delta T_{ma} > 0$), with the largest values of ΔT_{ma} occurring at high latitudes.

It is also possible for the temperature difference between the surface and the atmosphere to change in the transition from one climate state to another, owing primarily to the different ratio of latent-sensible boundary layer heat transport. An example of differential warming of the air and sea is Harvey and Schneider's (1985a, 1985b) transient model, whose step function response has air and water temperatures asymptotic to different long-term values (see Figure 5.14). The coupled atmosphere-ocean GCM of Bryan et al. (1982), for example, also

shows sea surface temperatures responding differently than surface air temperatures to a step function forcing during the transient phase (see Figure 5.19b). Observations of global sea surface temperature changes from 1900–1970 by Paltridge and Woodruff (1981) indicate marked differences relative to the air temperature record, although these variations are less pronounced in a more recent sea surface temperature data analysis by Folland et al. (1984). In any event, it is important in transient model tests to track both surface-ocean and surface-air temperatures, and to compare model results against the appropriate data base.

5.3.2 Transient Relaxation Times

We will now discuss time scales of various processes that come into play during the transient response. If transfer to the deep ocean is negligible, then it is clear from the tabulations in Table 5.1 that most of the heat capacity of the system is in the oceanic mixed layer. Accordingly, atmospheric transients relax rapidly compared with those in the mixed layer, and the heat flux is approximately independent of altitude in annual mean models: $Q_{NET}(t) \simeq Q_a(\infty, t)$. Because the land heat capacity is also negligible compared with that of the mixed layer, we have $Q_\ell(0,t) \ll Q_m(0,t)$. From Equations (5.13) and (5.4),

$$Q_m(0,t) \simeq \frac{Q_a(0,t)}{f_w} \simeq \frac{Q_{NET}(t)}{f_w} \simeq \left(\frac{\lambda}{f_w}\right)[T_m(t) - T_e(t)], \quad (5.16)$$

where we have taken T_m to be approximately constant with depth in the mixed layer. For negligible heat transfer at the mixed layer-thermocline interface, $Q_m(h,t) = 0$, the vertical flux derivative in the mixed layer to first order is

$$\frac{\partial Q_m}{\partial z} \simeq \frac{Q_m(0,t) - Q_m(h,t)}{h} \simeq \frac{\lambda}{h f_w} \times (T_m - T_e), \quad (5.17)$$

where h is the mixed-layer thickness. Substituting this back into the mixed layer energy equation, Equation (5.9) for $i = m$, we recover our earlier simple model of Equation (5.6):

$$\frac{dT}{dt} = \frac{[T_e(t) - T]}{\tau_{rm}}, \quad (5.18)$$

where $\tau_{rm} = \rho_m c_m h f_w/\lambda \simeq m_m c_m (4\pi R^2 \lambda) \simeq 4$ y is the mixed layer radiative damping time, with m_m being the total mixed layer mass and $R \simeq 6.37 \times 10^6$ m is the Earth's radius.

More generally, we can define a radiative relaxation time of the i-th reservoir,

$$\tau_{ri} \equiv \frac{m_i c_i}{(4\pi R^2 \lambda)}. \quad (5.19a)$$

These time scales, based on the reservoir heat capacity and global thermal damping coefficient only, are the only relevant relaxation times for reservoirs that mix heat internally very rapidly compared with their cooling rates, that is, for reservoirs that can be treated as well-mixed boxes characterized by a single temperature. For reservoirs with finite internal vertical diffusivities κ_i, the diffusion times,

$$\tau_{diff} \equiv \frac{h_i^2}{\kappa_i}, \quad (5.19b)$$

come into play. Because both oceanic upwelling and diffusion operate in parallel in the UD model, its effective vertical mixing time is

$$\tau_{mix,d} \simeq \left(\frac{\kappa_d}{h_d^2} + \frac{w}{h_d}\right)^{-1} \quad (5.19c)$$

Typical values of the radiative, diffusive, and mixing times for the atmosphere, land, mixed layer, and deep ocean are given in Table 5.1.

The time scales listed in Table 5.1 indicate the following important characteristics of the climate system during transients: (1) the atmosphere and land both relax diffusively and radiatively in a fraction of a year; (2) the mixed layer "mixes" in a fraction of a year but takes of the order of 4 years to heat (or cool) to a new equilibrium in response to an applied forcing; and (3) the internal mixing time of the deep sea (taken to be 900 years) is longer than the thermal relaxation time of the deep sea as a well-mixed reservoir (160 years). This last result indicates that the deep ocean must be resolved in at least the vertical dimension for simulations of th

secular CO_2 transient response, which involve time scales of 50–200 years.

Additional time scales enter into the problem if horizontal resolution of the fluid reservoirs is included, associated with poleward transport of heat by atmospheric winds and oceanic currents. Because the meridional mixing time of the atmosphere ($\simeq$ 1.3 y, see below) is substantially greater than its vertical mixing time ($\simeq$ 0.2 y, see Table 5.1), there is some justification in developing a one-dimensional model resolved in latitude, with vertical adjustments in each atmospheric column assumed to take place instantly. Accordingly, a class of zonally averaged energy balance climate models have been designed to find the latitudinally resolved distributions $T_i = T_i(\phi, t)$, where ϕ is the latitude. Historically, a single temperature has been assigned to represent the atmosphere, land surface, and ocean mixed-layer in these formulations (Budyko 1969; Sellers 1969; North et al. 1981). Distinct temperatures for each reservoir can be modeled if boundary layer heat transfer is retained between the surface and atmosphere (Harvey and Schneider 1985a, 1985b; Hsieh 1984). These EBMs typically are driven by prescribed solar flux distributions: $\langle Q_S(\phi) \rangle$ for the annual mean models and $Q_S(\phi, t)$ for seasonal simulations. Seasonal variations of insolation in these calculations are essentially repetitive over time scales of hundreds of years of interest. Again, in such EBMs the poleward heat flux by atmospheric and ocean motions is often modeled by specifying an appropriate eddy diffusivity: $\kappa_{i,j} \equiv -\langle v' T_i' \rangle / \partial T_i / \partial (R\phi)$. The effect of meridional heat transfer by the atmosphere is then approximated by adding a term of the form

$$-\frac{\rho_i c_i \kappa_{i,h}}{2\pi R^2} \times \frac{\partial}{\partial x}\left[(1-x^2)\frac{\partial T_i}{\partial x}\right] \qquad (5.20)$$

to the right-hand side of Equation (5.12) (for $i = a$), where $x = \sin\phi$ and where the atmospheric horizontal eddy diffusivity is of the order of $\kappa_{a,h} \simeq 10^6$ m^2 s^{-1} $\simeq 3.2 \times 10^{13}$ m^2 y^{-1} (Oort 1983). More detailed analysis of atmospheric circulation statistics reveals that the poleward heat flux has sensible (temperature gradient) and latent (water vapor gradient) heat flux components of comparable magnitude. The corresponding meridional mixing time of the atmosphere,

$$\tau_{a,h} = \frac{R^2}{\kappa_{a,h}} \simeq 1.3 \text{ y} \qquad (5.21)$$

will therefore come into play in a latitude-resolved model. Also, at some latitudes, as much as 50% of the total poleward flux is carried by surface ocean currents. Again, the effect of poleward transport by the mixed layer can be approximated by adding a term of the form of Equation (5.12) to the right-hand side of Equation (5.9) (for $i = m$). The effective poleward heat diffusion coefficient of the atmosphere plus oceans is then $D = [(\rho ch)_a \kappa_a + (\rho ch)_m f_w \kappa_m] / (2\pi R^2)$; so their contributions are about equal when their horizontal diffusivities scale inversely with their total heat capacities. Because the mixed layer/atmosphere heat capacity ratio is $\simeq$27 (Table 5.1), $\kappa_{m,h} \simeq 1.2 \times 10^{12}$ m^2 y^{-1}, and

$$\tau_{m,h} = \frac{R^2}{\kappa_{m,h}} \simeq 35 \text{ y}. \qquad (5.22)$$

The interplay of the meridional transport, air-surface heat exchange, and radiative cooling times of the air, land, and water reservoirs is exhibited in the seasonal response of zonal mean surface temperatures. Because both the (solar) forcing and observed thermal response are reasonably well known in this case, Warren and Schneider (1979) have proposed seasonal simulations as a test for uncertainties in latitude-resolved EBMs. (This is a good idea for testing GCMs as well.) Such seasonally validated models presumably could then be used with more confidence in long-term transient simulations such as the CO_2 climate problem. However, most of the Budyko-Sellers-North EBMs reported in the literature assume a single surface temperature, which makes it difficult to assess the realism of air/surface heat exchange on a seasonal scale.

However, a latitudinally and seasonally resolved transient EBM with distinct air, water, and land reservoirs was recently developed by Hsieh (1984), which illustrates the kind of validation that might be applied to test model parameterizations. Figure 5.5 shows the annual variation of $T_\ell(t)$, $T_a(t)$, and $T_m(t)$ at $\phi = 30°$N (A) and 30°S (B) computed with this model, compared with long-term monthly averages of surface air and water temperatures summarized by Oort (1983). Both the amplitude and phase of T_a and T_ℓ are simulated reasonably well at these latitudes, with the stronger damping of the Southern Hemisphere arising from its greater ocean (mixed layer) surface area. The effect of the deep

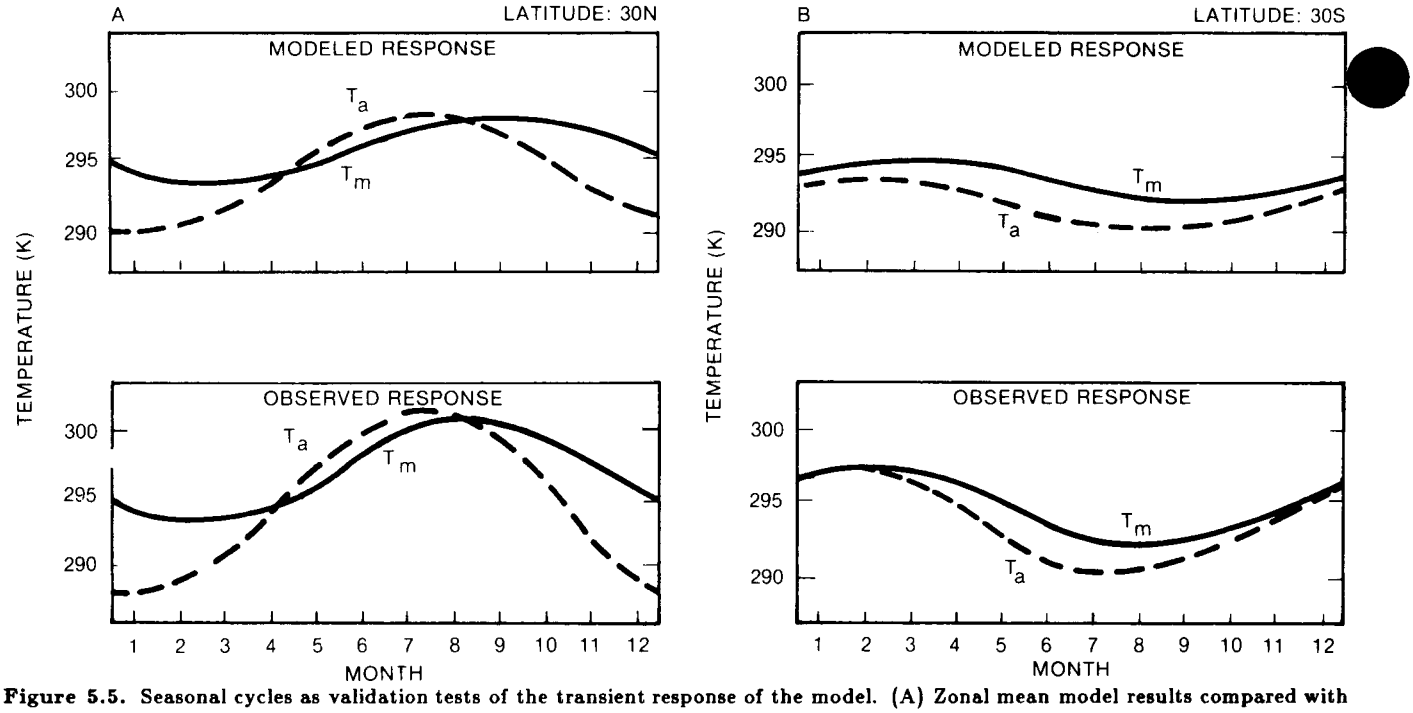

Figure 5.5. Seasonal cycles as validation tests of the transient response of the model. (A) Zonal mean model results compared with observations at 30°N latitude showing surface air (dashed) and ocean (solid) temperatures. (B) Same as A except for 30°S. Note that Southern Hemisphere water and air temperatures are more highly damped by the greater surface area of the high heat capacity surface ocean, as in Thompson and Schneider (1979) and North et al. (1984).

sea was suppressed in this simulation because its response time is much longer than a year. It should be noted that the surface temperature distribution produced by the annual mean insolation is not the same as the annual mean surface temperature driven by seasonally varying insolation. The difference arises as a result of nonlinear feedbacks from sea ice and other processes that occur during the seasonal cycle. This suggests that seasonal cycles may have to be resolved even in long-term simulations.

In modeling the century time scale CO_2 response, it is important to remember that the deep ocean does not behave as a well-mixed reservoir during its turnover time of $\simeq$ 900 years (Table 5.1). Moreover, there is a difference of at least three orders of magnitude in ocean time scales relative to the atmosphere's vertical and horizontal mixing times of the order of a year. The disparity is even greater if seasonal cycles involving the upper ocean and atmosphere must be resolved. This mismatch in time scales is the fundamental reason for computational difficulties in running coupled atmosphere/ocean GCMs with the "fast" response of the atmosphere limiting the model time step and lengthening the computer running times of the deep oceans in synchronously coupled models. This leads to unacceptably long computing times, except in the case of highly idealized land-sea geometries and forcing functions. Thus, most transient models used to study the CO_2 problem to date are of the aggregated reservoir, parameterized-transport type, which can more easily incorporate realistic land-sea fractions versus latitude. This can be an important effect because of differences in land and ocean heat capacities and internal mixing rates. Moreover, fundamental physics issues still remain unresolved in global ocean GCMs associated with the proper treatment of convection in regions of bottom water formation and of other vertical mixing processes.

Finally, the long-term cryosphere response has not yet been properly incorporated in transient models, in which a similar mismatch in thermodynamic relaxation times exists (Hoffert and Michael 1983). Typically, the time scale of snow on land is 0.01 years, of sea ice is 0.2 years, and of continental ice sheets is more than 1000 years.

The different response times of seasonal snow and ice versus land ice sheets must be accounted for in assessing transient surface albedo-temperature feedbacks. Typically, GCMs hold glacial ice extent constant while allowing seasonal ice and snow cover to vary interactively. This can be done with

latitude-resolved EBMs as well, although the simplest EBMs used in some climate sensitivity studies only compute long-term, steady-state conditions after glacial melting or freezing has occurred. Finally, some transient EBMs are designed to study oscillations of glacial land and sea ice over thousand-year time scales incorporating nonlinear feedbacks (Källén et al. 1979; Saltzman 1982). The problem of cryosphere-climate interactions is further complicated by the fact that purely thermodynamic melting may be secondary in such scenarios as the projected break-up of the West Antarctic Ice Sheet by melting at the undersea base (Mercer 1978). In general, the modeling of real-world, glacial dynamics, including viscoelastic creep and coupling with underlying lithospheric plates, requires a level of geometric detail and physical sophistication comparable to that of GCMs themselves.

5.4 FACTORS DRIVING TRANSIENT CLIMATE CHANGE

Having discussed the time scales over which climate responds, we next consider some of the external forcing components that can cause global temperature deviations (anomalies) through perturbations of the planetary radiation budget on the time scale of fossil fuel CO_2 emissions.

An essential test of the realism of transient climate models is an evaluation of their ability to reproduce observed climatic variations. To do this requires that both the forcing and the observed response are known over the time interval of interest. With the possible exception of the seasonal cycle discussed in the previous section, these conditions are seldom, if ever, satisfied in practice. In particular, it is likely that the time series of global mean surface temperature displayed in Figure 5.1 results from a combination of external forcing factors acting simultaneously, each of which may produce temperature anomalies of comparable magnitude. It is tempting to consider fluctuations unrelated to the fossil fuel CO_2 signal as random noise. The conventional wisdom is that the systematically increasing CO_2 temperature signal will emerge from the background noise in the next 10–50 years (NRC 1983). This would be a plausible conclusion from existing models if the noise were truly random, but it may not be the case if other factors influencing climate vary significantly over this time scale or if nonlinearities in the climate system affect the response. Moreover, most attempts to model recent climate changes assume that the system is perturbed relative to some preexisting steady state. Such a steady state may not, however, be the starting condition.

Accordingly, transient climate response models designed to explain historical records over the past 100 years and to project climate changes over the next 50–100 years in response to some specified scenario of greenhouse gas emissions, need to consider effects of multiple forcing. If all of the forcing factors could be modeled explicitly, it might be possible to extract the CO_2 signal from historical data sets as the residual variation, that is, removing those variations that we may be able to explain (e.g., volcanic effects) may make more apparent the CO_2 signal that would normally remain hidden in formal statistical analyses. Such superpositions of effects, for example, are the basis of transient model calculations of Hansen et al. (1981), which show apparent agreement with a particular historical data set and which have been cited widely in popular accounts as being consistent with the fossil fuel CO_2 greenhouse theory (Sullivan 1981; Revelle 1982, etc.).

The main types of forcing considered thus far that exhibit variability over time scales of years to decades are: (1) CO_2 emissions from combustion of fossil fuel and from terrestrial biospheric sources associated with large-scale deforestation; (2) anthropogenic emissions of other trace greenhouse gases; (3) variations in solar luminosity; and (4) volcanic aerosols deposited primarily in the stratosphere. A very readable, nonmathematical discussion of these factors (along with an explanation of possible causes of climate change operating over longer time scales) is provided in Chapter 7 of Schneider and Londer's (1984) book. Moreover, in addition to Hansen et al. (1981), a number of semiempirical models have been proposed in recent years that in varying degrees seem to reproduce historical records more or less successfully in terms of various combinations of these factors (Schneider and Mass 1975; Broecker 1975; Bryson and Dittberner 1976; Oliver 1976; Robock 1978, 1979; Gilliland 1982; Vinnikov and Groisman 1982). A review of these models and their relevance to the problem of detecting the effect of the increasing CO_2 concentration on climate was presented by Weller et al. (1983). These factors are

also discussed in Chapter 6 of this volume. Here we will briefly examine those aspects of the multiple forcing issue that bear directly on modeling the transient response.

5.4.1 Carbon Dioxide and Trace Gas Forcing

As discussed earlier, the time dependence of the change in equilibrium temperature from fossil fuel (and other) CO_2 emissions can be approximated by an expression of the type (cf. Equation [7.7]) $\Delta T_e(t) \simeq \beta_c \ln[c(t)/c_0]$, where $\beta_c \simeq 7.92/\lambda$ ($\simeq 3.6$ K for $\lambda \simeq 2.2$ W m^{-2} K^{-1}, corresponding to $\Delta T_e \simeq 2.5$°C for a CO_2 doubling). If we know the atmospheric concentration $c(t)$ from historical data or from a carbon cycle model driven by some emission scenario based on projection of future use of fossil fuels, this expression permits derivation of the transient temperature response by use of a climate model.

The preindustrial value of the atmospheric CO_2 concentration is thought to have been in the range of 250–290 parts per million by volume (ppm); $c_0 \simeq 270$ ppm is a reasonably representative value at the initiation of worldwide industrial emissions, nominally beginning in the year 1850 (Trabalka 1985). Scattered observations exist into the early record of this century, but the best documented part of the global atmospheric CO_2 concentration is the continuous data set from 1958 to date at Mauna Loa, Hawaii (Keeling 1983). Since that time, the record shows an approximately exponential growth in the *increase* in atmospheric CO_2 of the form $\Delta c(t) = c(t) - c_0 \simeq 44.4e^{0.019(t-1958)}$. This is consistent with the exponential growth of fossil fuel CO_2 during this period, assuming that about 50% remains in the atmosphere (the so-called airborne fraction), and the balance is absorbed by the oceans. If worldwide deforestation was a major factor during this period, the airborne fraction may have to be revised downward, which would have significant implications for oceanic transport models (see Trabalka 1985). Future emissions are impossible to predict in the sense of a physical model because they depend on the availability of coal, oil, and natural gas resources, the interplay of a variety of socioeconomic and political factors, the development cycles of alternate energy sources, and as yet unforeseen technological breakthroughs or setbacks. Under these conditions, the future is typically represented by a set of reference scenarios. These allow analysis of contingencies for purposes of assessment but should in no sense be construed as deterministic forecasts.

Nordhaus and Yohe (1983) and Wuebbles et al. (1984) have developed scenarios for $c(t)$ based on a combination of historical atmospheric CO_2 evolution and projections of emissions and using an assumed airborne fraction to estimate atmospheric concentrations. It should be stressed that predictions of future CO_2 release rates also depend on many assumptions and uncertainties, as is discussed by these authors. In particular, Wuebbles et al. (1984) propose a standard historical record and a future CO_2 growth scenario for $c(t)$ for use in modeling studies. This standard case is given in Table 5.2. Conversion of these concentrations into equilibrium temperature changes for the nominal damping coefficient ($\lambda = 2.2$ W m^{-2} K^{-1}) gives values for $\Delta T_e(t)$ shown in Figure 5.6 from 1850 to 2100 for the *high, nominal,* and *low* post-1983 emissions projections of Wuebbles et al. (1984). Clearly, in converting these values of c(t) to $\Delta T_e(t)$, additional uncertainties are introduced because the climate model is highly simplified. These uncertainties are discussed in Section 5.8 along with the results shown in Figure 5.16. However, a preliminary analysis is possible. In regions where $c/c_0 \propto e^{t'}$, where $t' = t - t_{initial}$, the time dependence of the equilibrium temperature change is approximately linear: $\Delta T_e \propto \ln(c/c_0) \propto \ln(e^{t'}) \propto t' \propto t - t_{initial}$. The solution of the simple, well-mixed reservoir model of Equation (5.6) for such linear forcing [$\Delta T_e(t') = At'$, where A is a constant and $t' \gg \tau_{rm}$] is also linear with the same slope, but lagged by the radiative relaxation time: $\Delta T(t') = A(t' - \tau_{rm})$. As a crude approximation, the effect of transient heat storage in the deep ocean is to increase τ_{rm} from the mixed-layer only value of approximately 4 y to approximately 10–20 y (Hunt and Wells 1979; Hoffert et al. 1980; Cess and Goldenberg 1981; Dickinson 1981; Schneider and Thompson 1981; Harvey and Schneider 1985a, 1985b; Harvey, in press), although some authors (e.g., Hansen et al. 1984; Wigley and Schlesinger 1985a, 1985b) have claimed oceanic lags as large as 100 y. These are discussed later in this chapter. For a $\tau_{rm} \ll t'$ lag, the surface temperature change from CO_2 follows the slope of $\Delta T_e(t')$, but decreases approximately in value by the factor

$(t' - \tau_{rm})/t'$. Also, for the nominal damping coefficient of 2.2 W m^{-2} K^{-1}, the equilibrium temperature change from 1850 to 1983 for these CO_2 scenarios is $\Delta T_e(1983) \simeq 3.6 \times \ln(341/270) \simeq 0.84°C$, although this would be doubled or halved if values of λ were 1.1 (*high* sensitivity) or 4.4 W m^{-2} K^{-1} (*low* sensitivity), respectively. Thus a nominal global temperature rise of

$$\Delta T \simeq \Delta T_e(t' - \tau_{rm})/t' \simeq 0.84 \times [(133 - 15)/133] \simeq 0.75°C$$

is indicated over the 133-year period since 1850, for $\tau_{rm} \simeq 15$ years.

Table 5.2
"Standard" Scenario of Historical and Future CO_2 Concentrations

t_0 (y)	t_1 (y)	CO_2 Concentration (ppm)
1850	1958	$c(t) = 270 \times exp[0.0014(t - t_0)]$
1958	1983	$c(t) = 270 + 44 \times exp[0.019(t - t_0)]$
1983	2100 *(high)*	$c(t) = 341.4 \times exp[0.0123(t - t_0)]$
1983	2100 *(nominal)*	$c(t) = 341.4 \times exp[0.0069(t - t_0)]$
1983	2100 *(low)*	$c(t) = 341.4 \times exp[0.0039(t - t_0)]$

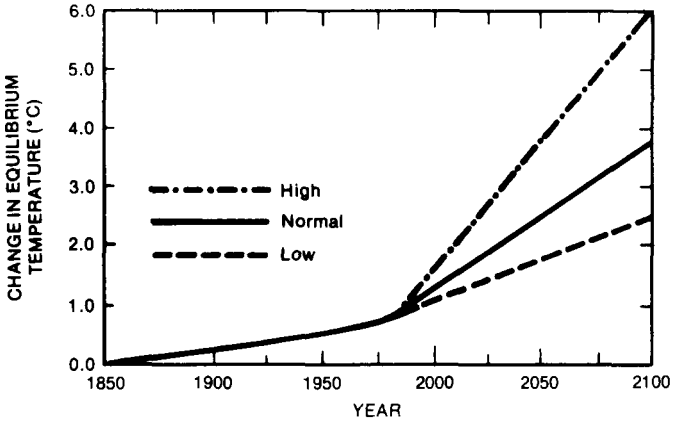

Figure 5.6. Global equilibrium temperature change versus time from CO_2 emissions for the HIGH, NOMINAL, and LOW emissions scenarios of Wuebbles et al. (1984) calibrated to a 2.5°C equilibrium warming for a CO_2 doubling; c_ϕ=270 ppm.

Admittedly, the actual response is more complex because ΔT_e in these scenarios changes slope from 1956 to 1983 and grows with different slopes thereafter for the three emission scenarios shown. In addition, the deep sea response is more complex than the well-mixed reservoir approximation. The qualitative conclusions of this analysis, however, apparently carry over to numerical models that include these effects. Again, we will look at this problem in more detail in Section 5.5.

Because of the additional warming to be expected from other greenhouse gases (Lacis et al. 1981; Hansen et al. 1981) and a possibly greater climate sensitivity than the nominal value used here, global warming of greater than 0.75°C since 1850 from increases in greenhouse gases are theoretically possible. Interestingly, Hansen et al. (1984, his Figure 18) show a current equilibrium value of $\Delta T_e \simeq 1.5°C$ from CO_2 plus trace gases, and a global surface warming of $\Delta T \simeq 1.0°C$, including the thermal inertial of a 110-m mixed layer. This value is reduced to $\Delta T \simeq 0.5°C$ when a purely diffusive deep ocean heat sink is added. As compared to other transient models, this combination of a greater equilibrium temperature change and a smaller physical temperature response for the transient change to date is possible only because of the much more vigorous heat transfer to the deep sea in Hansen's model.

The surface air temperature data shown in Figure 5.1 indicate a global warming of more than 0.5°C from the 1880s to the 1940s. This warming did not persist, however; it was followed by an apparent leveling off and decreasing trend, with substantial short-term variability superimposed. However, a number of multiply-forced transient model simulations suggest that these observations may still be consistent with a growing greenhouse effect due to contribution from fossil fuel emissions, providing account is taken of compensatory cooling by other factors.

5.4.2 Solar Forcing

Because planetary surface temperature is determined by the balance between absorbed solar and outgoing infrared radiation, it is not surprising that for many years climate modelers have theorized that climate changes are driven by changes in solar luminosity (see, e.g., Lamb 1972, for a review of early work). However, it has only recently become possible to make sufficiently accurate direct satellite measurements of the solar constant to test these theories.

In the past, estimates of the solar forcing of transient climate changes have been based on ad hoc correlations with variations in the number of sunspots per year (known to vary periodically with an 11-year cycle), changes in solar diameter, and other features observable from Earth. Historical measurements of the solar constant from the surface of the Earth have been plagued with uncertainties associated with the effect of the atmosphere on the solar irradiance observations (see, e.g., Newkirk 1983, for a recent review of solar variability). For example, although various ingenious methods have been employed in the Smithsonian Institution's long-term solar observations program to correct for atmospheric scattering, absorption, and so on, the cited uncertainties in $\Delta S/S$ are still $\simeq \pm 1.5\%$. For our nominal climate sensitivity parameter $\beta_T \simeq (238/2.2) \simeq 108°C$ in Equation (5.7), this translates as a ΔT_e uncertainty of $\simeq 1.6°C$, which is about a factor of two larger than the total observed root mean square (rms) climate variability over the past 100 years (Figure 5.1). Clearly, these ground-based solar constant measurements are not accurate enough to determine whether part of the fluctuations in the temperature record is solar driven. In the absence of hard data, a number of modelers have calculated the implications for the transient response of various assumed correlations of solar variability, and then compared their results with historical temperature records. Robock (1981), for example, using an EBM driven by $\langle S(t) \rangle$ correlated with the envelope of sunspot numbers, found such forcing gave poor predictions of the reconstructed temperature record of the last 400 years, including the inability of the so-called Maunder minimum in sunspot activity to explain the European "Little Ice Age," the outer limits of which may extend from 1430 to 1850. Hansen et al. (1981), on the other hand, found that the sunspot correlation with irradiance by Hoyt (1979) helped to explain the observational record from 1880 to 1980, when included in their transient model (see Figure 5.11). More recently, Gilliland and Schneider (1984), using Harvey and Schneider's (1985a, 1985b) transient climate model, were able to reconstruct a somewhat different observational record for the Northern and Southern Hemispheres, assuming a 76-year harmonic variation of solar flux based on an assumed solar radius variation cycle of 76 years with phase and amplitude adjusted to fit temperature data. Again, the agreement with observations looks reasonable, but on closer examination it may be fortuitous in light of discrepancies between the assumed solar variations and recent satellite observations by Willson (1984, see below).

Direct measurements of the solar constant from above the atmosphere, with an accuracy in $\Delta S/S$ of $\simeq 0.003\%$, have been available since early 1980 from the active-cavity radiometer (ACRIM) instrument onboard the NASA Solar Maximum Mission Satellite.[1] The percent change in solar irradiance, $\Delta S/S$, over an early 153-day period described by Willson et al. (1981), is shown in Figure 5.7. A major finding was that the solar constant is reduced as much as 0.2% over time scales of 5-8 days as large sunspot groups pass across the solar disk. Two such incidents are visible in Figure 5.7, peaking near days 100 and 150. Longer period variations are evident in these measurements as well, although they do not yet extend over a full solar cycle. These data have not yet been incorporated into transient climate models. As a recent example, unpublished data from Willson[2] show the ACRIM trend line for solar flux decreasing over the 1980–1984 time frame when the results of Gilliland and Schneider (1984) indicate that the solar flux should be increasing. Moreover, a new correlation with sunspots by Hoyt and Eddy (1982) based on the first year of ACRIM data, which is different from that of Hoyt (1979) and used by Hansen et al. (1981), has been developed at the National Center for Atmospheric Research (NCAR) for a period covering the last 100 years. This could give different reconstructions of climate history by transient climate models than have been obtained thus far.

Much remains to be done in unravelling the influence of solar variations on the climatic signal. Accordingly, it may be more productive to view temperature reconstructions in light of increasing data on solar forcing as narrowing the range of uncertainty by physical constraints, as opposed to validation tests as such. The best estimate, at present,

[1] R. C. Willson, Jet Propulsion Laboratory, Pasadena, CA, Principal Investigator—some problems with other instruments on "Solar Max" were corrected in orbit by Space Shuttle Challenger astronauts in April 1984, but a fairly continuous data record exists from 1980 to the present for the ACRIM.

[2] Ibid.

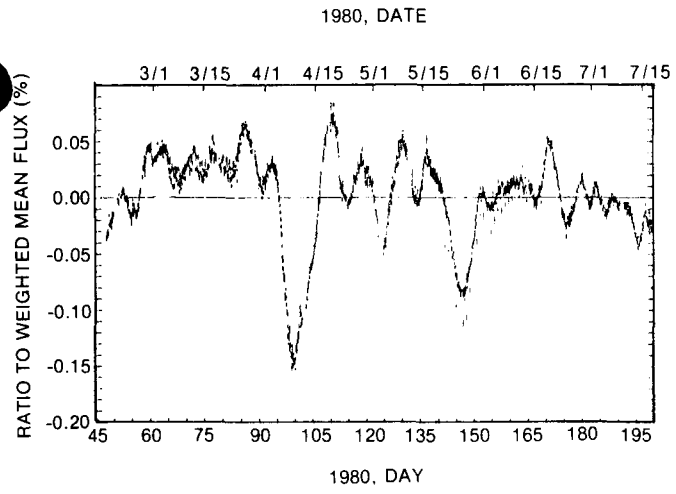

Figure 5.7. Percent change in solar irradiance over a 153-day period in 1980 (Willson et al. 1981). Weighted mean 1 A.U. irradiance for period equalled 1368.31 W m^{-2}.

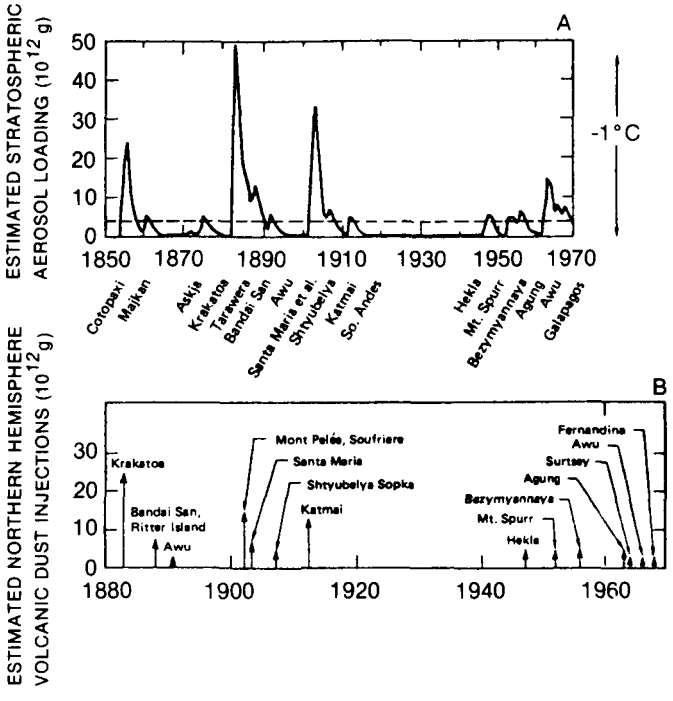

Figure 5.8. Estimates of material introduced into the atmosphere by volcanoes in the 1850 to 1970 time frame. The figures show: (A) the stratospheric loading (with the time average indicated by the horizontal dashed line and equal to 4.2×10^{12} g), as estimated by Mitchell (1970), and (B) the dust injected into the Northern Hemisphere by specific volcanoes as estimated by Oliver (1976).

is that solar variability may account for fluctuations in ΔT_e of the order of 0.1°C or less, with phase and amplitude to be determined by more careful analysis.

5.4.3 Volcanic and Stratospheric Aerosol Forcing

The basic mechanism of volcanic forcing is increased backscattering of solar radiation to space by high-altitude suspended particles—typically dust or sulfuric acid particulate matter (aerosols) formed by gas-phase reactions within the atmosphere. An observer in space would see an increased visible brightness, or albedo, as a result of the *dust veil* created by a large volcanic eruption. For an eruption to induce a significant cooling, it is important that it deposit submicron-sized aerosol particles (or gases that form such aerosols) into the stratosphere so that the solar radiation reaching the surface-troposphere system is decreased. Some 15 major volcanic eruptions have occurred at irregular intervals over the past 100 years, depositing significant amounts of stratospheric aerosols in the process (Figure 5.8). In addition to volcanoes, some authors have proposed that climatic cooling may result from dust veils created by collisions of extraterrestrial objects, such as comets or asteroids with the Earth, or from high-altitude smoke layers that could be created by the extensive fires that might be started by a nuclear war (Turco et al., 1983).

The climatic effect of such aerosol injections depends on the size and spatial distribution of the particles, the height of injection, and aerosol optical properties, such as the index of refraction, which, in turn, depend on the composition of the aerosol. In general a tropospheric layer is less likely to cool than a stratospheric one, because typical tropospheric aerosols absorb more efficiently than stratospheric aerosols, and because of a dependence on the underlying surface reflectivity (Coakley et al. 1983; Potter and Cess 1984). In addition, aerosols can induce a small compensatory thermal-blanketing effect similar to the effect of clouds. Under certain conditions, a tropospheric aerosol layer would even tend to heat the surface.

Decreases of atmospheric absorptance associated with stratospheric dust loadings from major volcanic eruptions typically induce visible albedo increases of the order of $\Delta a/a \simeq 0.2\%$, which for our nominal sensitivity of $\beta_T \simeq 108$ K corresponds to an equilibrium cooling of the order of $\Delta T_e \simeq 0.2$°C. An important consideration for transient models is that the residence time of submicron-sized stratospheric aerosol particles is a year or less, so that

the dust loading of individual volcanic eruptions is likely to have an effect on atmospheric albedo or optical depth for about that time.

The effect is more complex for very massive injections such as that proposed by Alvarez et al. (1980) from the collision of a large asteroid or comet with the Earth (or for massive injections of particles from 100 Mt or greater nuclear explosions) because severe perturbations of global wind patterns can affect aerosol residence times and spatial distributions. The transient effect on atmospheric and ocean temperatures from the Alvarez asteroid impact hypothesis was computed by Pollack et al. (1983), using a detailed time-marching aerosol physics code and assuming as an initial estimate that particle residence times were unaffected by the perturbation, that is, that the aerosol lifetime was less than one year (see Figures 5.9 and 5.10). The significance of these results in the present context is that the ocean mixed layer temperature change is rather small, compared with the massive cooling of the land surface, which drops in temperature by $\simeq 40°C$ after about 100 days. [The land heat capacity is neglected, $(\rho ch)_\ell = 0$, in these simulations.] Climatically, the system recovers rapidly—in less than 2 years. The response to volcanic injections would be similar, but considerably less intense.

A related aspect of the dust veil forcing mechanism with implications for the CO_2 transient climate problem is the argument by some authors (a minority) that a major driver of planetary cooling is anthropogenic aerosol particles produced by industrial activity, which compensates for, and may even overwhelm, the fossil-fuel CO_2 greenhouse warming. Bryson and Dittberner (1976), for example, claim to reproduce a Northern Hemisphere historical temperature data set with a model driven by volcanic plus anthropogenic aerosols, in which cooling by the latter dominates the CO_2 heating effect. However, a net cooling from industrial smokestack emissions is not very convincing because it is hard to see how submicron-sized particles emitted at the surface, or formed by chemical reactions in the troposphere, could penetrate in significant amounts into the stably stratified stratosphere. A better case can be made for stratospheric layers generated by volcanic eruptions or dust from numerous near-surface nuclear explosions carried aloft by intense thermal convection plumes induced by nuclear fireballs.

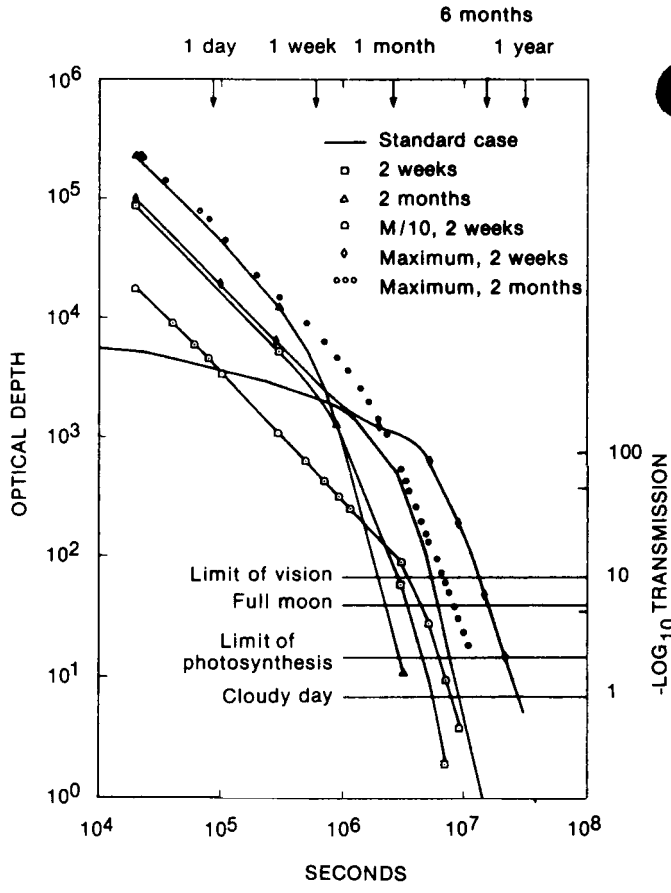

Figure 5.9. Optical depth and surface light intensity versus time after impact of an asteroid, assuming a short (<1 year) aerosol lifetime of dust in the stratosphere prior to removal by various scavenging processes. Source: Pollack et al. (1983).

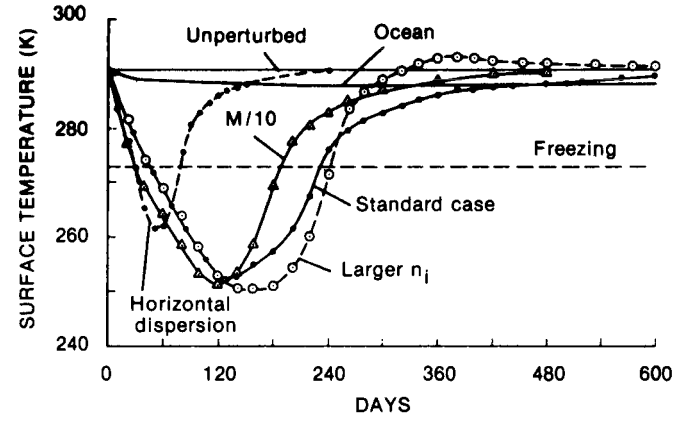

Figure 5.10. Transient ocean and land surface temperature response after impact of an asteroid. Land surface temperatures drop below freezing, whereas the ocean surface layer heat capacity provides a thermal buffer for the ocean over these time scales. Source: Pollack et al. (1983).

Major objections can (and have) been made to the Bryson-Dittberner model. But, as a thought

experiment, it is interesting to consider the implications if global cooling by anthropogenic aerosols really dominated global warming by carbon dioxide and other greenhouse gases. A sudden cessation in fossil fuel burning and associated gas and aerosol emissions would then have the curious effect of causing a near step-function warming, because the (cooling) industrial aerosols would be removed in about a year, whereas the (warming) fossil fuel CO_2 in the atmosphere would remain at elevated levels for the thousands of years needed for mixing and reequilibration with the deep oceans (Michael et al. 1981). If a significant fraction of the fossil fuel reserve is burned, then even after the reequilibration with the oceans, the atmospheric CO_2 concentration would not return to its preindustrial level, but would remain at an elevated concentration associated with a new (higher) atmosphere-ocean buffer factor (Trabalka 1985). The energy policy implications of the CO_2 climate problem would then be reversed, with a strategy of continued fossil fuel burning preventing a near-term global warming. The worst problems would come near the end of the fossil fuel era, when the increased equilibrium temperature, uncompensated for by cooling aerosols, would suddenly become very large. A more plausible, but still speculative, mitigating strategy might be intentionally to seed the stratosphere with a reflecting aerosol layer from high-altitude aircraft to compensate for CO_2 and trace gas warming [see, e.g., Budyko (1962, 1972, 1977) for discussions of intentional anthropogenic climate modification by aerosol layers]. Of course, the fallout of such layers would have to be continuously replenished for very long periods during, and virtually indefinitely after, the fossil fuel era to prevent a major latent greenhouse warming.

5.5 REVIEW OF TRANSIENT MODEL RESULTS

In reviewing results of transient models of the CO_2 climate problem that have been developed thus far, it should be remembered that the state of the art of climate modeling in general, and transient climate modeling in particular, is still essentially at the level of sensitivity studies—numerical experiments illustrating the relative importance of specific effects. The confidence level of such models is considerably less than, for example, a finite-element structural code that might be used in the design of a bridge. Even certain fairly complex fluid-mechanical processes, such as the three-dimensional flow over a supersonic vehicle like the Space Shuttle, can be simulated with some confidence because it is possible to validate and refine predictions made from numerical codes against wind-tunnel and flight test data. As indicated in Chapters 3, 4, and 5 of this volume, there has not yet evolved a comparable approach to validation and testing of transient climate models, either as a whole or with regard to their internal parameterizations, that would permit development of high confidence in model projections.

Nonetheless, the overall system is understood well enough to know that the climatic transient response from fossil fuel burning is damped mainly by heat storage in the world's oceans, as indicated by our earlier time scale analysis. All the transient models discussed here, including those currently under development, recognize this fact and include oceanic heat storage to some extent. Indeed, a natural way to characterize different transient climate models is by the amount of physical detail pertaining to ocean geometry, circulation, and mixing that they incorporate.

5.5.1 Horizontally Averaged Models

The theoretical basis of horizontally averaged multireservoir climate models was discussed in Section 5.3. Models of this type are described by Equations (5.10a) through (5.10d) and (5.12), along with their ancillary relations and boundary conditions. In most cases, for example in a radiative-convective model, the flux expression of Equation (5.10a) is run to a steady state in Equation (5.12). In some cases, even simpler approximations are used to express the equilibrium temperature variation for specified forcing of the type given here by Equation (5.5). For forcing functions that change on time scales longer than a year, this approximation is justified by the fact that the atmosphere relaxes to a steady state in much less than a year, whereas the mixed layer and deep sea relax over time scales of decades to centuries. This permits a partial decoupling of the atmospheric and oceanic calculations. Similar considerations are often invoked to justify asynchronously-coupled atmosphere-ocean GCMs (see Chapter 4 of this volume).

We consider first the transient model of Hansen et al. (1981, 1982). Conceptually simple, it was one of the early models to seriously explore the multiple forcing issue in the fossil fuel CO_2 context and was able to reproduce reasonably well the historical temperature record of the period from 1880 to 1980. This model provided the scientific framework for recent projections and analyses by the U.S. Environmental Protection Agency (EPA) on the CO_2 greenhouse problem (Seidel and Keyes 1983; Hoffman et al. 1983). These EPA reports, in turn, have themselves received considerable attention by the scientific and popular press (Abelson 1983; Shabecoff 1983) and, therefore, have influenced the popular perception of probable climatic effects of continued fossil fuel consumption. In view of its influence, it seems appropriate to reexamine the model of Hansen et al. (1981) more critically in light of the foregoing considerations.

In their early transient models, Hansen et al. (1981) treat the deep sea as a one-dimensional purely diffusive (PD) zone of specified vertical diffusivity κ. This is equivalent to Equation (5.10d) for the vertical deep sea flux with no upwelling ($w = 0$). Substitution of this into Equation (5.12) gives the unsteady one-dimensional heat-conduction equation,

$$\frac{\partial T_d}{\partial t} = \frac{\partial}{\partial z}\left[\kappa \frac{\partial T_d}{\partial z}\right], \qquad (5.23)$$

which the authors solve simultaneously with a mixed layer slab model of the form (Hoffman et al. 1983)

$$\frac{dT_m}{dt} = \frac{(T_e - T_m)}{\tau_{rm}} + \left[\frac{\kappa}{h_m} \cdot \frac{\partial T_d}{\partial z}\right]_{z=0}, \qquad (5.24)$$

where the last term represents the heat transferred across the mixed-layer thermocline interface at $z = 0$. As indicated earlier, the only steady-state ($\partial T_d/\partial t = 0$) deep ocean profile possible with the PD model is T_d equal to a depth-independent constant, not a very realistic depiction of the observed exponential depth dependence of ocean temperature profiles. It would have been relatively easy to generalize this approach to an upwelling-diffusion (UD) model (Hoffert et al. 1980; Cess and Goldenberg 1981; Harvey and Schneider 1985a, 1985b) that includes the thermohaline upwelling that Hansen's model ignores.

The results of the model of Hansen et al. for multiple forcing are illustrated in Figure 5.11. The two panels show the predicted global surface temperature anomaly for an ocean model with only a mixed layer and for an ocean model with mixed layer plus a PD deep ocean when the system is forced by exponential CO_2 growth (calibrated to $\Delta T_e = 2.8°C$ for a CO_2 doubling), compared with a surface air temperature historical time series. The effects of progressively adding volcanic dust and solar forcing according to semiempirical correlations are also shown. The final curve (bottom of panel B) shows an apparently very acceptable agreement with observations. The κ-value used here was $\simeq 3150$ m^2 y^{-1}, which Hansen et al. (1981) cite as a representative world-ocean average value of tritium-derived eddy diffusivity across the upper thermocline.

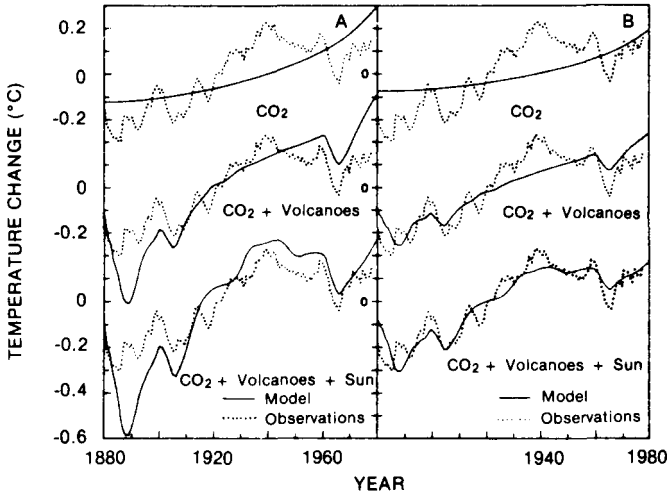

Figure 5.11. Calculation of historical surface air temperatures in response to multiple forcings. Panel (A) shows the observed temperatures (dotted) and the response of a simple mixed-layer model of the ocean to various forcings (solid curves). Panel (B) shows the response of a model having an ocean with a purely diffusive thermocline layer below the mixed layer. Source: Hansen et al. (1981).

More recently, Hansen et al. (1984) have been working with a horizontally resolved PD world ocean. In this work they utilize tritium-derived correlations for κ proportional to $1/N^4$, where N is the Brunt-Vaisala frequency of the local water column ($N = \sqrt{(g/\rho)\partial\rho/\partial z}$, where g is the gravitational acceleration and ρ the density of seawater). The correlations are derived from local transient tritium vertical profiles in the thermocline used to deduce κ's

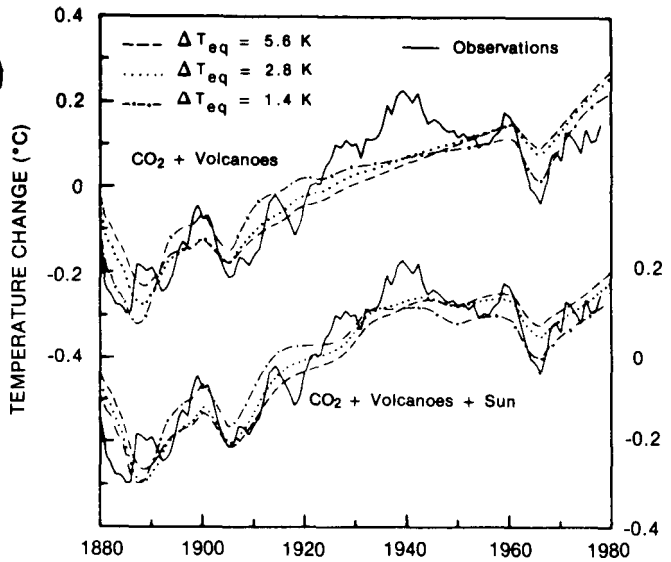

Figure 5.12. Calculation of historical surface air temperatures in response to multiple forcings using a mixed layer model of the ocean with a purely diffusive thermocline. The thermocline conductivity has been adjusted in each case to give the best possible fit to the observations (solid curves). Results are shown for models with equilibrium climate sensitivites to CO_2 doubling of 5.6°C, 2.8°C, and 1.4°C (dashed, dotted, and dot-dashed curves, respectively). Source: Hansen et al. (1982).

(by fitting PD model results in which vertical mixing balances radioactive decay of tritium to helium-3) and observations of the thermocline vertical density structure at the same location.

Although these results of Hansen et al. (1981) look impressive, so also (for example) do those of Gilliland and Schneider (1984), who compared their model output to a different data base and made different assumptions regarding the solar and volcanic forcing. Such unreconciled results demonstrate that the parameters and effects chosen, which may be chosen either intentionally or subconsciously to represent the observations, are not yet uniquely determined. How to differentiate between these different and differing approaches is the question.

In fairness, there are troublesome assumptions when we look at any historical reconstructions. What is needed to reduce the overall uncertainty is to analyze these systematically in comparison with independently known information. Examples of areas needing attention are the solar variability and volcanic dust veils used in forcing these transient models. The fact that the PD transient ocean model can only recover an unrealistic (uniform with depth) temperature profile may also be a more serious problem than it seems. The PD model has sometimes been justified on grounds that it is only being used to calculate a small perturbation of oceanic heat flux from the steady state. But a small perturbation analysis of a slightly more complex upwelling-diffusion (UD) model does not yield a PD model, but rather another UD model to represent the perturbation. Such conceptual problems cannot be resolved unless one uses a more realistic ocean model.

Moreover, the simple carryover of eddy diffusivities derived from tritium measurements for use as thermal eddy diffusivities in the oceanic thermocline is questionable. Bomb-generated tritium decays radioactively to helium-3 with a half-life of 12.3 years, which makes the effect of upwelling on the vertical profiles from which the effective diffusivities are derived fairly small. At the typical upwelling velocity of $w \simeq 4$ m y^{-1}, the profiles are pushed up only about 50 m each decay time (i.e., 12.3 years), which would be hard to identify in the GEOSECS data from which the correlations are derived. It is also known that diffusivities calibrated on the same data set using UD and PD models give different κ's [see, e.g., Hoffert et al. (1981), for a discussion of this effect on carbon cycle models calibrated on radiocarbon profiles]. Finally, it may be inappropriate to carry over the effective diffusivities for tracer mass penetration into the upper ocean, which occurs largely along isopycnals, to thermal diffusion problems in which isopycnal mixing plays a much smaller role (see Section 5.5.3). The result of making a simple analogy locally between mass and heat diffusion could well be an overestimate of κ for the transient climate problem.

In a later study, illustrated in Figure 5.12, Hansen et al. (1982) examined how κ would have to be modified to account for different values of ΔT_e for CO_2 doubling. Not surprisingly, a more sensitive climate (smaller λ) requires more vigorous heat transfer to the deep sea (bigger κ) to best fit the solution through the observations. Unlike the mixed layer relaxation time, which gets larger as λ decreases, the eddy diffusivity κ is probably a relatively fixed property of the ocean circulation. (For large perturbations in climate, ocean circulation patterns, bottom water formation zones, and so on can of course change, thereby affecting κ, which implicitly includes all of these processes.) Wigley and

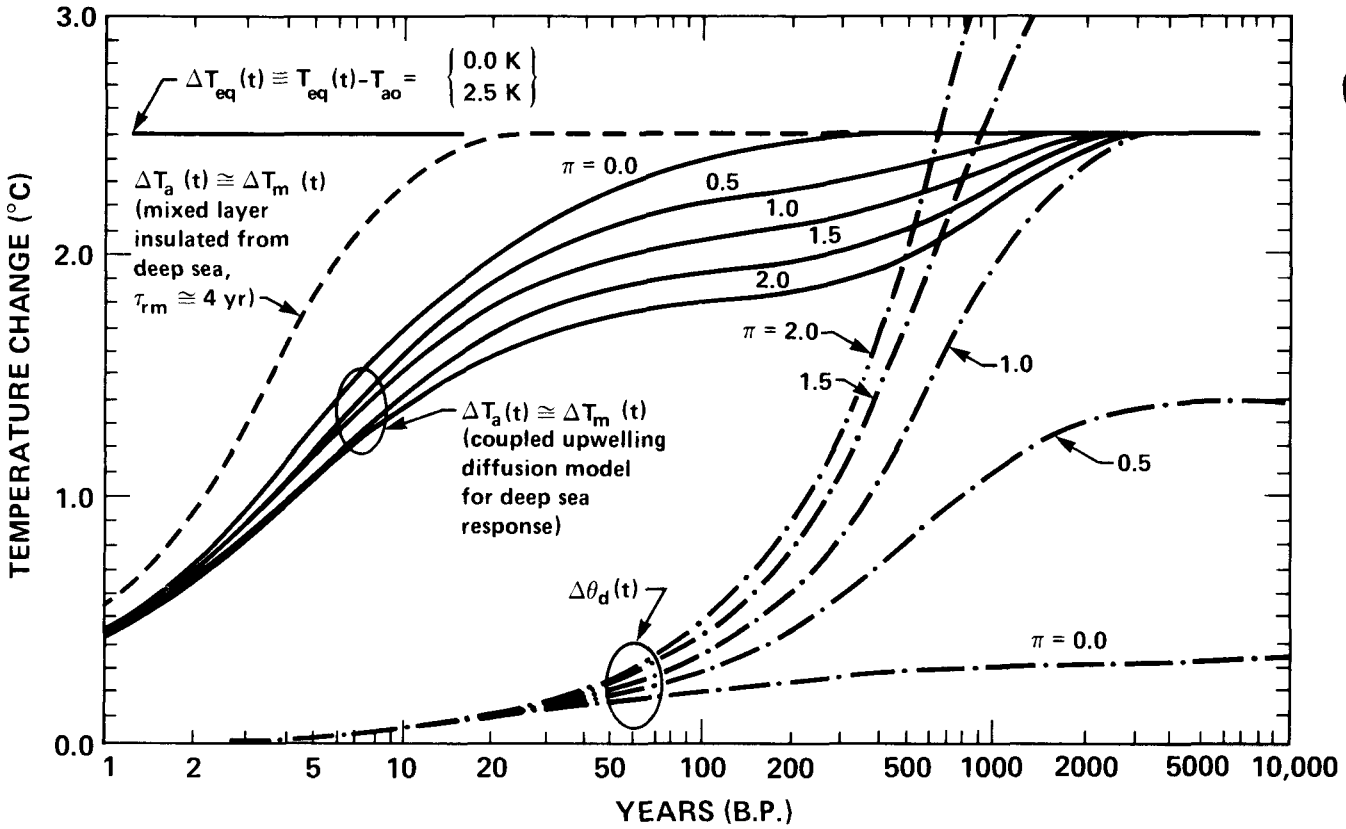

Figure 5.13. Transient temperature response to a step function forcing. Results are from the oceanic upwelling-diffusion (UD) model of Hoffert et al. (1981) assuming 100-m mixed layer depth, $\kappa = 2000$ m^2 y^{-1}, $w = 4$ m y^{-1}. Ocean temperature is shown versus time; the dashed curve is for the mixed layer only, the solid curves are for the UD model with different values of the polar warming parameter Π, and the dot-dash curves are the corresponding values of mean deep ocean temperature.

Schlesinger (1985a, 1985b) recently obtained an approximate analytic solution for the case of the transient mixed layer coupled to a purely diffusive ocean [Equations (5.23) and (5.24)]. In their solution, the diffusive flux at the mixed layer-thermocline boundary in Equation (5.24) has the form:

$$\left[\frac{\kappa}{h}\frac{\partial T}{\partial z}\right]_{z=0} \simeq -\mu f_w(\tau_d t)^{-1/2} T \ , \qquad (5.25)$$

where μ is a dimensionless coefficient that depends on the forcing $T_e(t)$, f_w is the ocean fraction, and $\tau_d \simeq \pi h^2/\kappa$ is a characteristic diffusion time that depends on the mixed layer thickness h and the vertical deep ocean eddy diffusivity κ. For step function forcing, $\mu \simeq 1.5$; for linear forcing (i.e., the exponentially increasing CO_2 concentration), $\mu \simeq 2.2$. The corresponding e-folding time for the stepfunction case is $\tau \simeq K f_w^2 \kappa (\Delta T_e)^2$, where K is a constant, and $\Delta T_e = \Delta Q_{NET}/\lambda$ is the equilibrium temperature change. Accordingly, for a given radiative perturbation, τ scales with κ/λ^2 for step forcing in the Wigley-Schlesinger model. Thus, PD ocean models with large κ's and small λ's can produce lag times as long as 100 years for step forcing, while for the variable $T_e(t)$ case characterizing the growing CO_2 component of climate forcing, they can predict global responses substantially below the local equilibrium response (e.g., Hansen et al. 1984; Schlesinger et al. 1985). The physical realism of such purely diffusive, high-κ oceans will be reviewed again in Section 5.5.3 in light of recent oceanographic research.

The response of UD and PD models to step function forcing as modeled by various authors is illustrated in Figure 5.13. In the study of Hoffert et al. (1980), the effect of varying the polar warming parameter Π—the ratio of "polar sea" to mean surface ocean temperature changes—in a UD deep sea transient model was studied. As indicated in the figure, the deep sea delayed the final approach to equilibrium relative to a model having only a mixed layer; an increase in polar warming had the largest delaying effect. Under current conditions, where high-latitude bottom water temperatures are fixed by the freezing point of seawater, Π is likely

to be near zero, although most climate models predict a polar amplification of surface air temperature. Although high-latitude ocean temperatures may not vary much due to the presence of sea ice, annual mean surface air temperatures may change by a relatively large amount as the length of the period during which sea ice is present is perturbed.

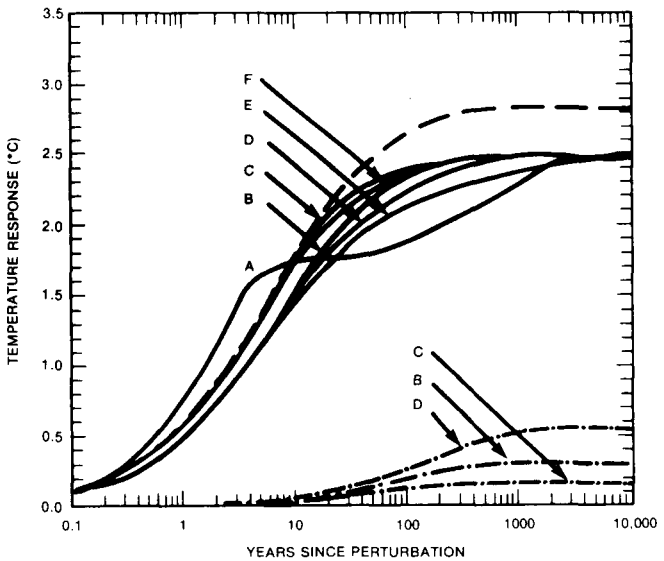

Figure 5.14. Transient temperature response to a step function forcing. Model calculations are taken from Harvey and Schneider (1985a, 1985b), with base case parameters similar to those of Hoffert et al. (1981) and with $\Pi = 0$. The solid lines are mixed layer temperatures with (A) four-box ocean model; (B) UD model, base case; (C) κ reduced by half; (D) w reduced by half; (E) $w = 0$; (F) κ and w reduced by half. The dot-dashed lines show the corresponding responses of the deep ocean and the dashed line shows the surface air temperature response.

The step function response of the UD deep ocean is characterized by an initially rapid rise, dominated by the mixed layer, followed by a slower approach to the final equilibrium. This is apparent from the results presented in Section 5.3, which suggest that the mixed layer only response scales with λ^{-1}, and from Wigley and Schlesinger's (1985a, b) results, which suggest that the long-term PD response scales with $\kappa\lambda^{-2}$. Harvey and Schneider (1985a, b) have analyzed the transient response of UD and PD ocean mixing models, including the effects of internal feedback processes in the deep sea on ocean transport processes. Figure 5.14, taken from their paper, shows the effect of varying the upwelling and diffusion parameters on the response characteristics. An important result is that setting $w = 0$ while holding κ constant at its UD value (curve E) gives the longest response time of all

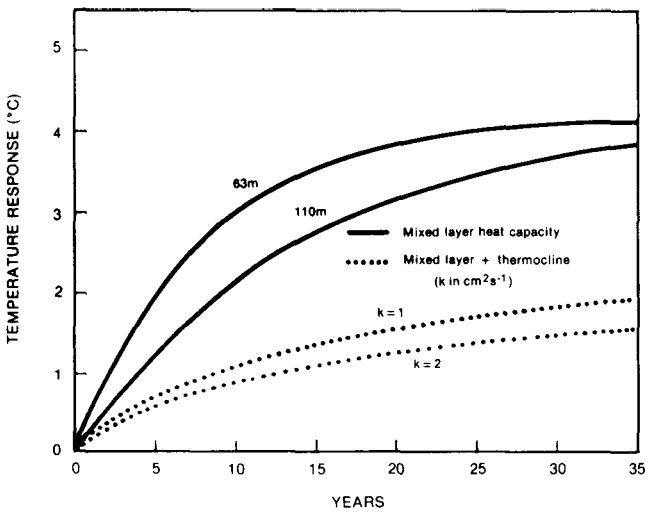

Figure 5.15. Transient temperature response to step function doubling of CO_2 found by Hansen et al. (1984). The solid lines show the surface temperature response for a model with a mixed layer ocean of the depth shown; the dotted lines show the response for a box-diffusion (BD) model with $\kappa = 3150$ and 6300 $m^2\ y^{-1}$ (1 and 2 $cm^2\ s^{-1}$), as indicated. The equilibrium sensitivity of the model is 4.2 °C.

cases studied, although a larger κ, and according to Wigley and Schlesinger (1985a, b), a smaller λ, would have delayed the response even more.

In a recent independent analysis of Hansen's long delay time (shown in Figure 5.15), Harvey (1985) used globally averaged and land-sea-resolved transient EBMs that closely duplicate the results of Hansen et al. (1984) when integrated using their assumptions. His findings indicate that Hansen et al. have overestimated the global mean transient response time scale by about 25%, and that the error at high latitudes is probably even greater, *independent of possibly spurious large ocean diffusivity.* Thus, the 350-year e-folding time that Hansen et al. obtain in the North Atlantic may be closer to 70 years. This figure could probably be reduced by another factor of two as a result of spuriously large vertical ocean diffusivities used by Hansen et al. at high latitudes.

Before leaving our review of horizontally averaged model results, it is important in confronting the CO_2 climate problem to ask: How, according to these models, is the change in global mean surface air temperature likely to vary with projected increases in the atmospheric CO_2 concentration? How, moreover, are these predictions affected by the uncertainties in climate sensitivity that are evident in present GCMs? To address these questions, the response of the Hoffert et al. (1980) UD transient

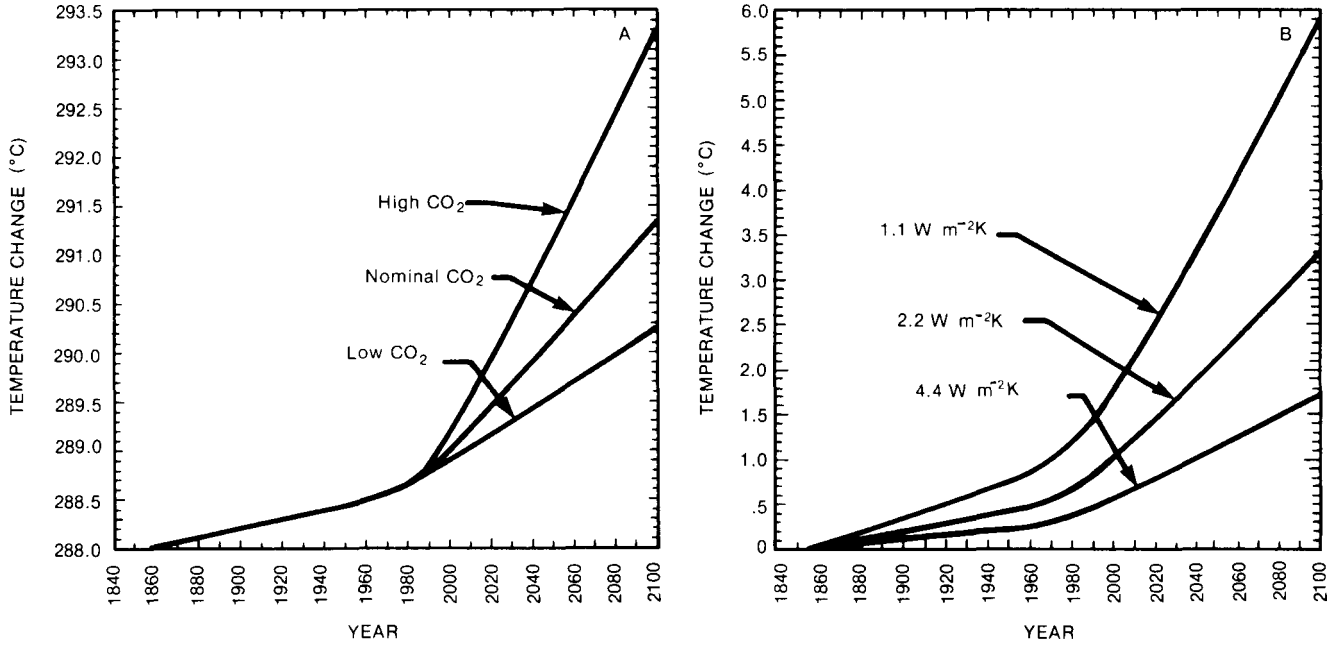

Figure 5.16. Transient temperature response to CO_2 forcing. Global surface temperature for CO_2 scenarios of Wuebbles et al. (1984) computed with transient upwelling-diffusion (UD) ocean model of Hoffert et al. (1980) with $\kappa = 2000$ m^2 y^{-1}, w = 4 m y^{-1} and $\pi = 0$. (A) $T_a(t)$ from 1850 to 2100 with the nominal damping $\lambda = 2.2$ W m^{-2} K^{-1} and three post-1983 CO_2 emission scenarios. (B) $\Delta T_a(t)$ over the same period with the nominal emission scenario, but three different damping coefficients (sensitivities); $\lambda = 1.1$, 2.2, and 4.4 W m^{-2} K^{-1}.

one-dimensional ocean model to the standard CO_2 forcing scenarios of Wuebbles et al. (1984) has been calculated. The results are shown in Figure 5.16. Figure 5.16A shows the air temperature tracking the equilibrium temperature rather closely, with a lag of $\simeq$15 y for all three scenarios, reinforcing our earlier results with the simple model forced by a linear ramp function in ΔT_e. Figure 5.16B illustrates the effect of doubling and halving λ relative to its nominal 2.2-W m^{-2} K^{-1} value. The lower λ curves correspond to a greater $\Delta T_a(t)$ response—although these do not quite scale with λ^{-1} as does ΔT_e—indicating that for the case of practical interest, the longer response times do not markedly compensate for larger equilibrium temperature perturbations in the transient response. The significance of this is that climate sensitivity must be known to a better accuracy than at present to improve the predictions of transient climate change to within a factor of two.

The foregoing results, with all their caveats, can be construed as an approximate bracketing of the consensus of transient model predictions for the next century's CO_2 greenhouse effect. In this restricted sense, they are consistent with the EPA's estimate of a 2°C warming from fossil fuel CO_2 and other greenhouse gases by the middle of the next century (Seidel and Keyes 1983). More complex scenarios than the reference one of Wuebbles et al. (1984) can be envisioned in which fossil fuel use is rapidly phased out by taxing or other policies, or in which fossil fuel use is decreased by societal feedbacks based on observations of global warming (Michael et al. 1981). Consider, for example, the finding by the Strategic Studies Staff of the EPA that:

> Worldwide taxes of up to 300% of the cost of fossil fuels (applied proportionately based on CO_2 emissions from each fuel) would delay a global 2°C warming only about 5 years beyond 2040 (Seidel and Keyes 1983, p. v).

Although this, and related, conclusions of various policy-oriented studies have important implications for the appropriate societal response to the carbon dioxide climate problem, the robustness of this type of statement is unclear at present, and should be established as an independent goal in itself. The implications of models would be more clear if it could be shown that specific predictions based on transient climate models were sufficiently robust, that is, insensitive to identified uncertainties.

A final point is that although most of the horizontally averaged transient models discussed here could be adapted to multiple climatic forcing, from

a feedback control theory viewpoint, the role of the oceans is essentially to supply passive damping to an externally imposed signal. It is possible that some of the climate variability shown in Figure 5.1 is due to short-period self-oscillations of the climate system. It is known, for example, that unforced GCMs, if left to themselves, exhibit interannual variability in their simulated climates (see, e.g., Figure 5.11). What is not clear is whether these are simulating natural internal oscillations. If such oscillations are indeed influencing the observed signal, it is important to be able to estimate their effect on the detectability and predictability of a CO_2 warming. A possible mechanism for internal short-period climate oscillations is discussed in Section 5.5.3. In any event, these processes are yet to be incorporated in simple models for the CO_2 climate problem, but could well have important, perhaps counterintuitive, effects.

5.5.2 Latitudinal Effects

Because it may be difficult to identify the global temperature increase from rising CO_2 concentrations, it would be helpful to have an estimate of the transient response with some horizontal resolution. Such models are needed for purposes of policy analysis and planning and to provide necessary input to ecological and societal impact studies. Thus, the Conclusions and Recommendations of the National Research Council's (NRC) Carbon Dioxide Assessments include:

> The lagging ocean thermal response may cause important regional differences in climatic response ... The role of the ocean in time-dependent climatic response deserves special attention in future modeling studies, stressing the regional nature of oceanic thermal inertia and atmospheric energy-transfer mechanisms (NRC 1983, p. 74–75).

However, the need for such models does not ensure their near-term availability in validated form. It was apparently not appreciated at the time by the authors of the NRC report (which cites numerical models [i.e., GCMs] as "the primary tools for investigating human impact on climate" [p. 270]) that a substantial disparity existed within the GCM community in predictions by different modelers of the long-term equilibrium, latitude-dependent warming from a CO_2 greenhouse effect. The wide range of estimates became especially clear after the study by Schlesinger (1983), whose comparison of the long-term change in zonally averaged air (or surface) temperature for a CO_2 doubling predicted by six different GCMs is reproduced here in Figure 5.17. A considerably more detailed comparison is made in Chapter 4. Not only are the global means different, but the latitude dependence—the extent of polar amplification by the model—varies from model to model. The reasons for these differences are currently under intense study and are likely to be a function of different model sensitivities associated with how each GCM parameterizes its internal feedbacks. The lack of a consensus in even the steady case underscores the potentially greater uncertainties associated with transient latitude-dependent models.

Because of uncertainties in the equilibrium response (see Chapter 4 of this volume), results of latitude-dependent transient models are often expressed as a fraction of the equilibrium temperature rise versus time attained at each latitude. Latitudinal differences in the continental and oceanic heat capacity are the most obvious cause for such a differential response. These are important effects and can be examined with latitude-resolved energy balance models (EBMs) without delving too deeply into the dynamic oceanography of the thermocline, deep sea mixing, and so forth. Schneider and Thompson (1981) conducted such a study, including the influence of different surface heat capacities versus latitude that are associated with a realistic, variable land-sea fraction (Figure 5.18). For step function forcing, they found that high latitudes equilibrate more slowly than do the tropics and that the Southern Hemisphere response lags that of the Northern Hemisphere, owing to its greater oceanic surface area.

These results suggest that a realistic characterization of continental and marine surface areas is needed to assess the latitudinal response of transient models properly. For example, simulations with the idealized topography, coupled atmosphere/ocean GCM developed at GFDL (Bryan et al. 1982; Spelman and Manabe 1984) should be interpreted carefully. These researchers modeled the transient response to an instantaneous change in CO_2 concentration. The atmosphere-ocean coupling was done synchronously (i.e., the same time step was used to integrate the air and water GCMs). Because of the

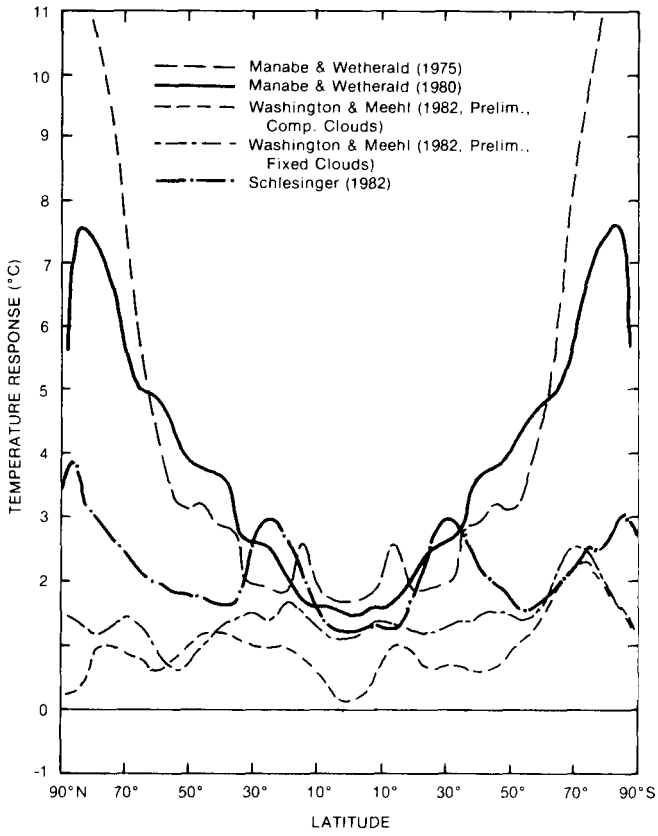

Figure 5.17. Equilibrium response of various GCMs versus latitude. Schlesinger (1983) compared the change in zonally averaged surface air (or surface) equilibrium temperature simulated by five different GCMs for doubled CO_2. The two Washington and Meehl (1983) curves are preliminary 198-day averages. The results of the Manabe and Wetherald (1975, 1980) results are plotted symmetrically about the Equator. Inclusion of the results of Hansen et al. (1984) with a 4°C global mean temperature rise would increase the scatter somewhat toward the high end, especially in low latitudes.

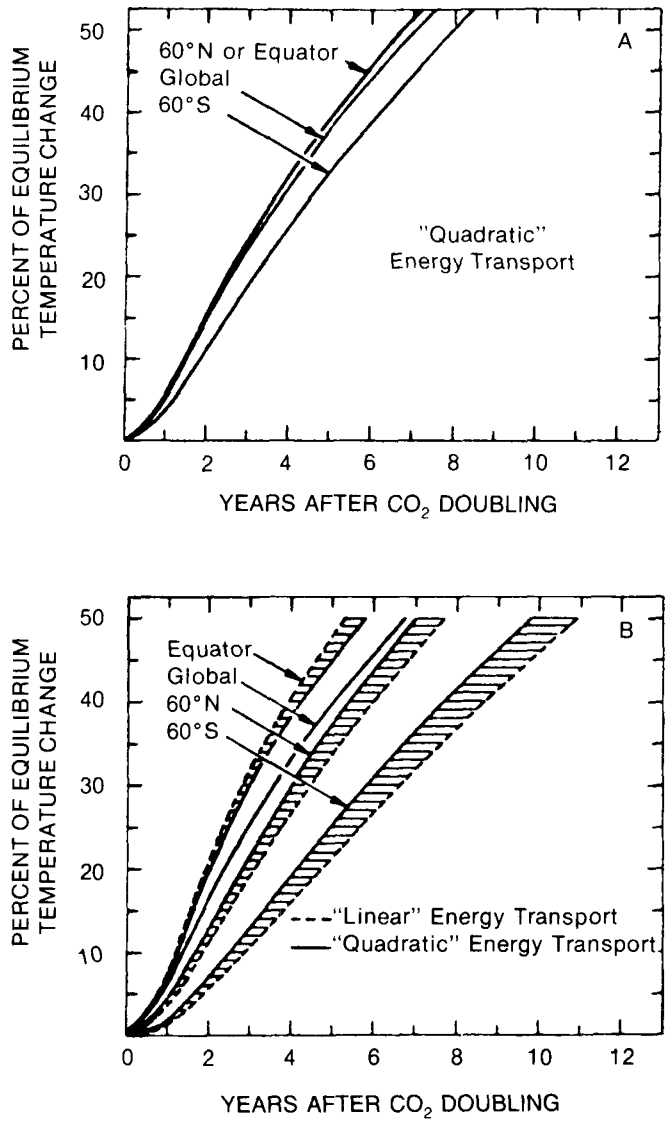

Figure 5.18. Latitudinal transient response of Schneider and Thompson's (1981) energy balance model. (A) Response of model having constant mixed layer depth and "quadratic" energy transport. (B) Response of model having latitude-dependent mixed layer depth.

widely different response times of the two domains, however, many hours of computer time would have been needed had the GFDL group not considered a highly simplified sectorized continent-ocean geometry. The model atmosphere and oceans were taken as being hemispherically symmetric and periodic in the zonal direction with land and oceans occupying adjacent 60° sectors. The transient response, globally averaged and on a latitude-by-latitude basis of this GFDL atmosphere-ocean GCM to step function forcing, is shown in Figure 5.19 [from Bryan et al. 1982; more recent results by Spelman and Manabe (1984) are somewhat different]. These results show a relatively rapid response of atmospheric temperature equatorward of 45°, but a relatively slow response poleward of that latitude; the temperature response of the ocean was only about half as rapid as that of the atmosphere. After about 10 years, the proportion of the atmospheric response became approximately independent of latitude, from which Bryan et al. (1982) concluded that while the oceans delay the signal, equilibrium GCMs could be used as an adequate guide to the nature of climate response. However, given the disparity in the latitudinal dependence of the equilibrium temperature response for different GCMs, it is not clear that this result would apply to other models. Furthermore, it is not

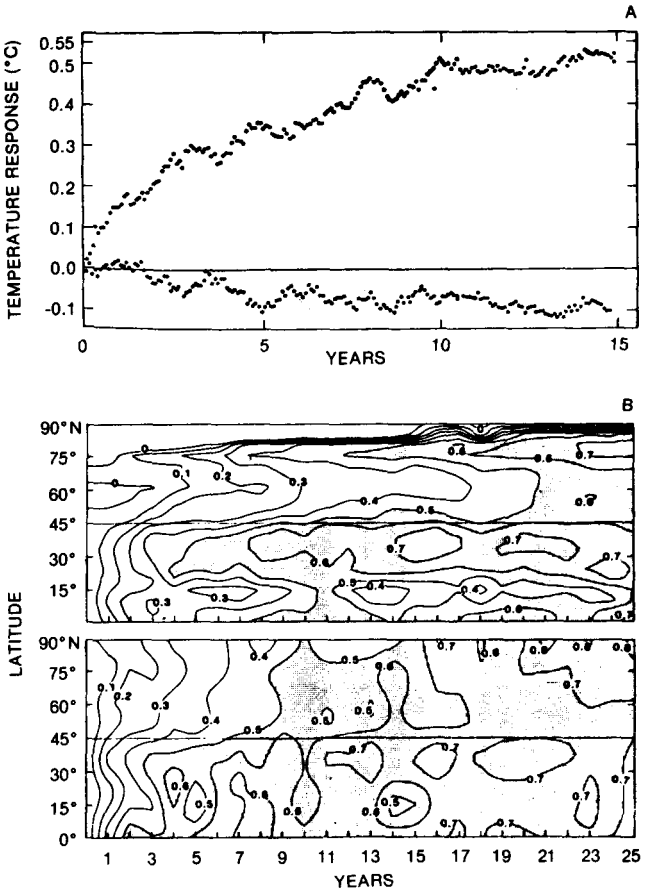

Figure 5.19. Latitudinal response of a three-dimensional atmosphere-ocean GCM. (A) Upper curve is world average SST versus time for case with sudden CO_2 doubling; lower curve is control run without CO_2 forcing. (B) Same model, normalized thermal response versus latitude and time: upper panel is for surface ocean, lower panel for surface air. Shading shows regions where the response is greater than 50% of the equilibrium response. Source: Bryan et al. (1982).

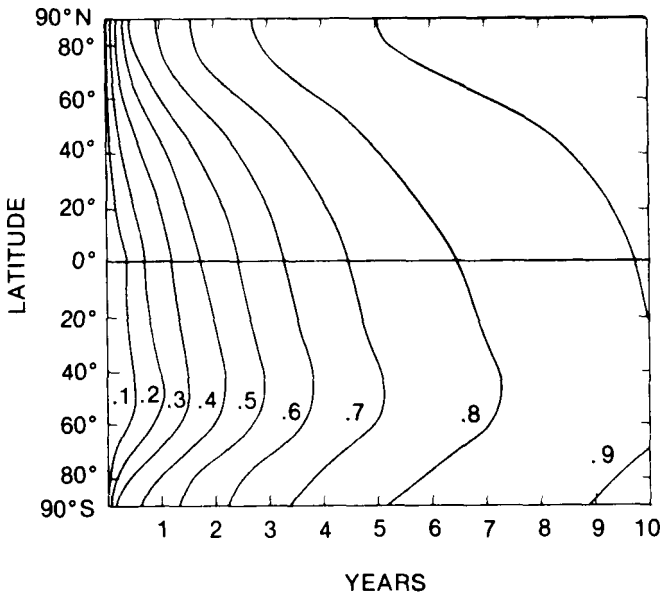

Figure 5.20. Normalized response of temperature after an instantaneous CO_2 doubling based on the study of North et al. (1984) using a two-dimensional (latitude-longitude) spherical harmonic expansion EBM with realistic geography.

evident that the same conclusion would apply to the GFDL model with realistic geography.

Shown in Figure 5.20 are predictions of transient surface temperature change versus latitude and time by North et al. (1984) using an EBM with horizontal resolution. Although it is much simpler in terms of transport processes (no dynamics), the model of North et al. (1984) incorporates a more realistic distribution of surface heat capacity (tied to the present distribution of continents and oceans) than does the GFDL model. As expected from earlier work of Thompson and Schneider (1979, 1982), there is a pronounced asymmetry in the results of North et al., with the lower-heat-capacity Northern Hemisphere warming faster than the Southern, a difference that is missing from the hemispherically symmetric GFDL model. On the other hand, the coupled GCMs show other features, such as differential response rates of surface air and water temperatures, that can be important to consider in comparison with data.

5.5.3 Testing of Transient Models: Some Recent Findings

We have repeatedly stressed the need for better methods for testing transient models against the real behavior of the climate system, particularly over the 10–100 year time scales of the CO_2 problem. What emerges from this review is that present models can provide us with semiquantitative, and sometimes only qualitative, results because they have been inadequately tested against real data. Too often, the data that are available only provide a few independent pieces of information. By judiciously choosing model parameters, reasonable or even good agreement can often be obtained. Many feedbacks and internal response mechanisms have been neglected, however, thereby introducing further uncertainty. Finally, it is worth remembering that observational data must always be interpreted in the context of some paradigm or theory, and there are still questions regarding the proper level of model at which to develop interpretations. How then is progress to be made in improving the

ability to make reliable forecasts of transient climate changes arising from CO_2 emissions? We now consider some possible new approaches to developing and testing increasingly more realistic models in light of recent research findings.

A major question in developing an appropriate model to study the transient storage and internal transport of heat by the oceans is the relative importance of mean motion, which is explicitly calculated by ocean general circulation models (OGCMs), as compared with transport by unsteady turbulent eddies below the resolution scale of the finite difference grid, which must somehow be parameterized. Wigley and Schlesinger (1985a, b) closely approximated the transient heat uptake with an appropriately calibrated one-dimensional model having both explicit and subgrid mixing parameterized as vertical eddy diffusion. This allowed more rapid integration of the transient atmosphere-ocean model, but the outstanding question, in addition to the validity of their approximations, is whether the OGCM results on which such simpler models are based can themselves be considered realistic, given the present state of the art.

The conceptual advantage of OGCMs relative to models in which transport is entirely parameterized would be clear if the explicitly computed mean motion were responsible for most of the heat transport. One measure of the importance of mean versus eddy transport is the kinetic energy of mean motions versus that in turbulent eddies. Dickson (1983) recently summarized the results of the POLYMODE ocean field experiment and related studies aimed at measuring the relative partitioning of mean and eddy kinetic energy in the oceans. These clearly indicate that eddy energy dominates mean kinetic energy in the main thermocline by factors of 3–10 almost everywhere, except for relatively narrow zones (e.g., western boundary currents) where the systematic mean flow becomes very intense. Kinetic energy profiles from current moorings in the North Atlantic are given in Table 5.3.

Major physical processes controlling the fluid dynamics of the oceans are the Coriolis force arising from the Earth's rotation, which dominates the inertial terms in the momentum conservation equations, and the generally stable density gradients in the ocean, which tend to suppress instabilities. (Local regions with unstable density gradients are responsible for the formation of high-latitude bottom water and are often treated in models by convective overturning adjustments.)

Table 5.3
Turbulent Kinetic Energy in Eddies and Mean Motion from Long-Term Current Moorings in the Saragasso Sea of the North Atlantic.

z (m)	k_{eddy} ($m^2\ s^{-2}$)	k_{mean} ($m^2\ s^{-2}$)	k_{eddy}/k_{mean}
500	9.1×10^{-4}	1.3×10^{-4}	7.0
1000	7.7×10^{-4}	2.5×10^{-4}	3.0
2000	1.1×10^{-4}	0.4×10^{-4}	3.0
4000	0.5×10^{-4}	0.5×10^{-4}	1.0

Note: Data are three-mooring averages in POLYMODE Array I, Station Δ, ~28°N, 58°W (Dickson 1983). The turbulent kinetic energies are defined $k_{mean} \equiv 1/2(\langle u\rangle^2 + \langle v\rangle^2)$, $k_{eddy} = 1/2([u'^2] + [v'^2])$.

The horizontal flow in stably stratified ocean basins is approximately accounted for by a theoretical model based on a quasi-geostrophic balance. Such a model describes a wealth of oceanic phenomena ranging from internal planetary waves to the complexities of geostrophic turbulence (Robinson 1983). Quasi-geostrophic motions are approximately hydrostatic and approximately horizontal. They generally occur in rotating stratified fluids along constant density surfaces (that is, along-isopycnals, which are generally inclined at a small angle to the horizontal and which outcrop at the surface at high latitudes). The spatial scale of the motion along isopycnals is of the order of the Rossby deformation radius—that is, the vertical scale h_v multiplied by the ratio of the Brunt-Vaisala buoyant frequency N to the Coriolis parameter f. Typical values in the thermocline are $h_v \sim 10^3$ m, $N \sim 5 \times 10^{-3}\ s^{-1}$. The corresponding spatial scale of eddies on isopycnals is $\ell_s \sim h_v N/f \sim 50$ km, which is too small to be resolved by the horizontal finite-difference grid of hundreds of kilometers employed in conventional OGCMs (Sarmiento and Bryan 1982; Schlesinger et al. 1985). These OGCMs produce steady-state mean velocity fields $[\langle u\rangle, \langle v\rangle]$, but not the eddy fluctuations $[u'(t), v'(t)]$ that contain most of the observed kinetic energy, even though it is recognized that the latter must be treated as subgrid parameterizations.

Nevertheless, because unsteady turbulence is in principle described by the unsteady, three-dimensional Navier-Stokes equations, numerical solutions with grids small enough to capture unsteady eddies should predict such eddies. Indeed, such transient eddies have been produced numerically by fine mesh eddy-resolving ocean general circulation models (EGCMs). Complete calculations would require both prohibitively long running times and very large memory capacity on current computers to deal with the flow in global scale ocean basins. In the absence of these capabilities, no EGCM as yet occupies more than a fraction of one or two ocean gyres. These findings have made a major impact on physical oceanography. As Carl Wunsch (1984) observes:

> The EGCMs have led to a shift in outlook—they made clear that the general circulation has to be obtained from the average of many realizations of the instantaneous time-dependent flow field. *Unless some as yet [undeveloped] simple parameterization of the eddy field is found, the relationship between steady models of the ocean circulation, and the time average of time-dependent models is going to remain remote, and perhaps unbridgeable* (our emphasis) (p. 198).

These considerations suggest that more work is needed in modeling the turbulent mixing processes that have important effects on the ability of the oceans to store heat during periods of transient climate change. Such studies would affect all levels of the modeling hierarchy, from one-dimensional columns to three-dimensional OGCMs. We have already remarked that the implied diffusivity normal to isopycnals, κ_n, based on global temperature profiles and upwelling estimated from global bottom water formation rates is approximately 2000 $m^2\ y^{-1}$ (see Garrett 1979; Müller 1979; and Turner 1981) for discussions of the mechanisms leading to this diffusivity). The eddy diffusivity for momentum along isopycnals in the thermocline can be estimated from mixing length arguments as (Launder and Spalding 1972) $\nu_T \sim \ell_e \times (k_{\text{eddy}})^{1/2} \sim 5 \times 10^{10}\ m^2\ y^{-1}$, where the numerical value is based on the Rossby deformation length eddy scale and the eddy kinetic energy of Table 5.3 at 500-m depth. This is about a factor of 24 less than the meridional mixed layer eddy diffusivity, $\kappa_{m,h} \sim 1.2 \times 10^{12}\ m^2\ y^{-1}$, estimated earlier from implied oceanic poleward heat transport rates, and about a factor of 5 less than the along-isopycnal eddy diffusivity for tracers deduced from radium 228 contours along isopycnals in the abyssal ocean by Sarmiento et al. (1982), that is, $\kappa_e \sim 2 \times 10^{11}\ m^2\ y^{-1}$. It may nonetheless be a reasonable estimate if we consider that poleward heat flux in the *mixed layer* is dominated by mean currents and that tracers may diffuse along isopycnals at different rates than momentum.

Because temperature perturbations in the upper ocean from transient climate changes are difficult to measure directly, and in any event are sparse, some recent models (Hansen et al. 1984; Schlesinger et al. 1985; Wigley and Schlesinger 1985a, b) use eddy diffusivities calibrated against bomb-generated radioisotope tritium data, with values of 4000-10,000 $m^2\ y^{-1}$, or more. Li et al. (1984) recently estimated the globally averaged tritium-derived vertical eddy diffusivity as $\sim 5400 \pm 600\ m^2\ y^{-1}$, although local values are substantially higher in the high latitude North Atlantic (Hoffert and Broecker 1978). The models used to fit these diffusivities to observed profiles assume that the time derivative of tritium concentration is balanced by vertical eddy diffusion and radioactive decay to helium-3. An alternative (Hoffert et al. 1980; Harvey and Schneider 1985a, b; Watts 1985) is to estimate diffusivities from steady-state global mean temperature (or density) profiles with a steady upwelling-diffusion model. As we have seen, the latter approach gives a lower global mean value, $\sim$2000 $m^2\ y^{-1}$. We now consider how eddy transport along isopycnal horizons can lead to greater apparent vertical diffusivities for transient tracers, as opposed to heat.

To date there are only three isotopic data sets suitable for global modeling: the distributions of natural radiocarbon, of bomb-produced radiocarbon, and of tritium (from data collected at the time of the GEOSECS surveys: Atlantic Ocean, 1972–1973; Pacific Ocean, 1973–1974; and Indian Ocean, 1978). However, the natural pre-bomb radiocarbon data are limited, and the GEOSECS radiocarbon data need to be corrected for the pre-bomb radiocarbon distribution. Therefore, the tritium distributions are often claimed to provide the most valuable information, under the assumption that their penetration is analogous to that of heat. Figure 5.21 compares Atlantic Ocean GEOSECS tritium contours (upper panel) with isopycnal contours zonally averaged across the Atlantic basin (lower panel).

Although both constant-property contours show effects of equatorial upwelling—which for the potential density gives rise to the characteristic double-lobed structure of isopycnals in the thermocline—the tritium is much more hemispherically asymmetric, as a consequence of more concentrated inputs from Northern Hemisphere bomb testing. One result is that, for example, at latitudes in the vicinity of 30°–40°N and depths of 200 m, tritium contours slope downward at angles of the order of $\gamma \sim -2 \times 10^{-4}$ (radians), whereas the isopycnals at approximately the same location slope upward at an angle $\alpha \sim +1 \times 10^{-4}$. The implications of tritium contours cutting isopycnals at some small angle—in this case, $\beta = \gamma - \alpha \sim -3 \times 10^{-4}$—may be very important in some regions of the ocean when calculating heat uptake.

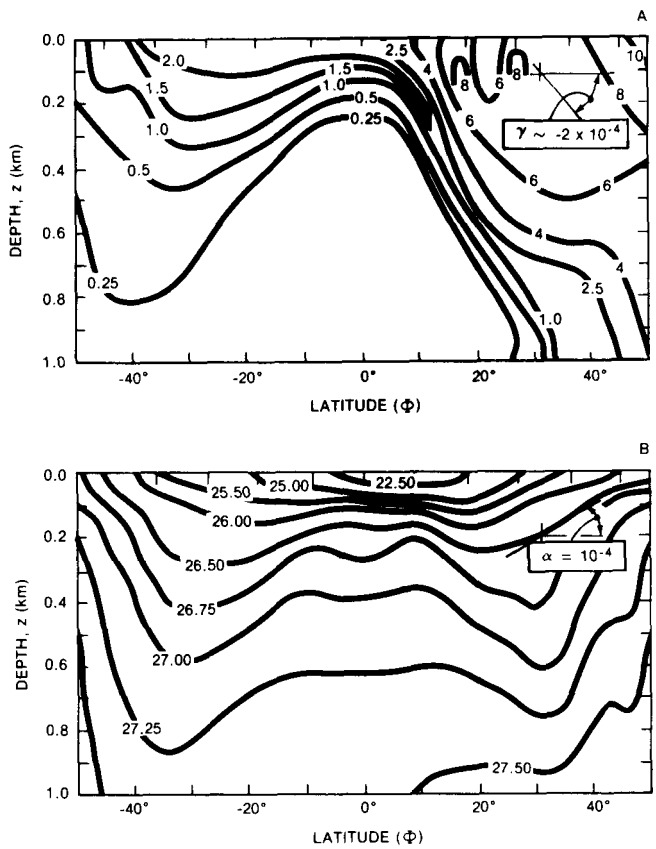

Figure 5.21. Latitude-depth contours of tracers and potential density in the Atlantic basin. (A) Transient tritium contours in tritium units (tu) from bomb testing measured in 1977 (1 tu = 10^{15} × [moles of tritium in seawater/moles of hydrogen in seawater]) from Broecker and Peng (1982). (B) Steady-state Atlantic basin isopycnals in units of $\Delta\rho = \rho - \rho_0$ (kg m^{-3}), where ρ_0 = 1000 kg m^{-3} is a reference density (Levitus 1982).

Figure 5.22 depicts a horizontal-vertical (y, z) coordinate system and a coordinate system (s, n) fixed to isopycnals, where the latter defines the principal axes for turbulent mixing in the stratified ocean. Generically then, α and γ are the angles between the horizontal (y) axis and the constant-ρ and constant-q surfaces, respectively, where $q(y, z)$ is a constant along the contour of any tracer (temperature, salt, tritium, etc.). The angle between them is $\beta = \gamma - \alpha$, and α, β, and γ are, from the geometry of ocean basins, much less than unity. From the definition of these slopes given in Figure 5.22, $\alpha = \gamma$ and $\beta = 0$ when q is a linear function of ρ. In Figure 5.23 we plot the normalized vertical profiles $q^*(z) \equiv (q - q_b)/(q_s - q_b)$, where subscripts s and b denote conditions at the surface and 4-km depths, respectively, for temperature, salinity, and potential density, horizontally averaged over the world's oceans by Levitus (1982). The variable q^* is convenient because properties that are linearly related will collapse to a single curve. Notice that, although $\rho = \rho(T, s)$ in general, the density and temperature curves are quite similar, despite a marked variation in salinity. This suggests that on a global basis density and temperature are approximately linearly related and that isotherms are nearly isopycnals. A similar conclusion is intuitively clear from the two-dimensional plots of isotherms and isopycnals in Levitus (1982).

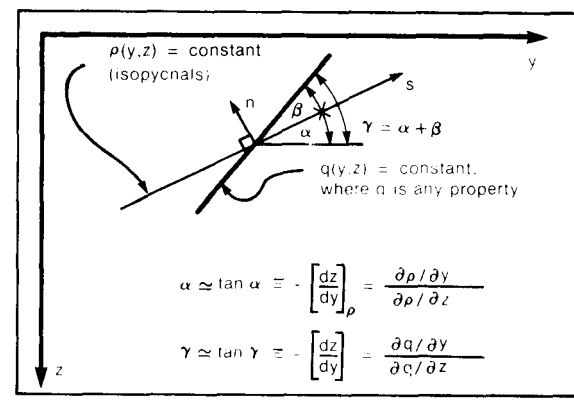

Figure 5.22. Schematic diagram of two-dimensional horizontal-vertical (y, z) and along-across isopycnal coordinate systems, where ρ = constant is an *isopycnal* surface that defines the principal axes (s, n) for turbulent mixing in stratified oceans.

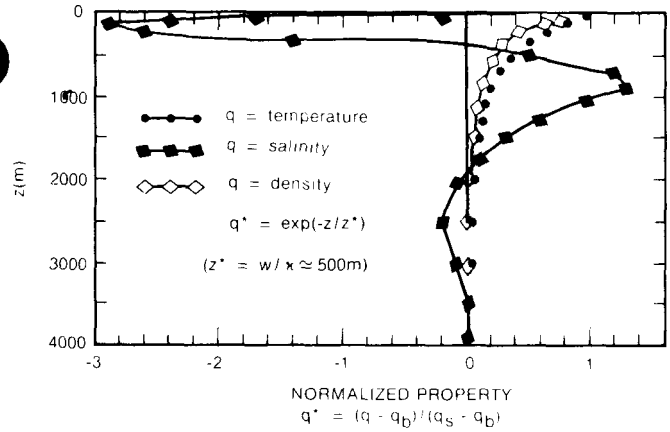

Figure 5.23. Normalized profiles of potential temperature, salinity, and density averaged over the world's oceans (from Levitus 1982). The temperature, salinity, and density are shown and compared to a theoretical exponential curve having a scale-height of 500 m (shaded).

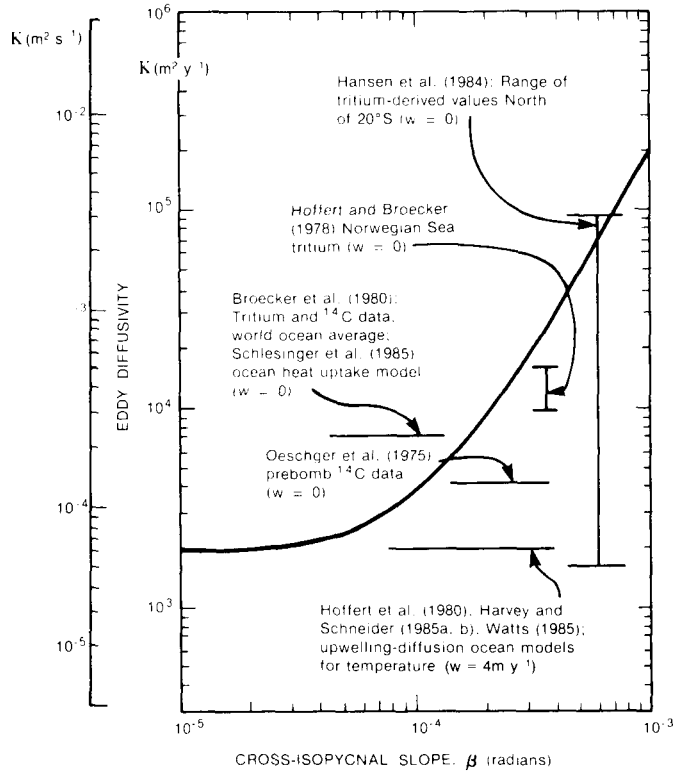

Figure 5.24. Effective vertical eddy diffusivity of an oceanic property versus its cross-isopycnal slope, β. The diffusivity is given by $\kappa(\beta) = \kappa_n + \beta^2\kappa_s$, with $\kappa_n = 2 \times 10^3$ m^2 y^{-1} (Garrett 1979) and $\kappa_s = 2 \times 10^{11}$ m^2 y^{-1} (Sarmiento et al. 1982). Some tracer-derived values of κ obtained or used by various investigators are also shown for comparison.

This apparent digression bears directly on the question of the difference between the vertical eddy diffusivities of heat and tracers in the ocean. It can be shown (Hoffert 1983) that the effective vertical eddy diffusivity of a tracer that cuts isopycnals at a local angle β is $\kappa \simeq \kappa_n + \beta^2\kappa_s$. Typical values of cross- and along-isopycnal diffusivity were discussed at the beginning of this section. Figure 5.24 shows κ versus $|\beta|$ for measured values of κ_n and κ_s. Also indicated are the ranges of vertical eddy diffusivities obtained or used by various investigators, including those used in simple transient climate models. The curve can be interpreted as follows. The smallest vertical diffusivity possible is equal to the cross-isopyncnal diffusivity and occurs when constant property surfaces are coincident (or nearly coincident at $|\beta| \ll 10^{-4}$); as $|\beta|$ increases to the order of 10^{-4}, an additional component of vertical diffusivity appears due to the projection of the along-isopycnal diffusivity on the vertical. For example, at the high latitude North Atlantic location discussed earlier where tritium contours have a $|\beta| \sim 3 \times 10^{-4}$, we expect $\kappa \sim 15{,}000$ m^2 y^{-1} from this curve, which is in the range derived by Hoffert and Broecker (1978) from vertical tritium profiles in the Norwegian Sea. (It was recognized by these authors that some of this could be due to transport along isopycnals.) However, and this is the important point in the present context, the vertical diffusivity for heat at that location could be much closer to 2000 m^2 y^{-1}, in view of the closer coincidence of isotherms and isopycnals.

Finally, these considerations lead to alternate interpretations of inverse correlations between the local vertical eddy diffusivity and the degree of stratification proposed by some authors. Some years ago, Sarmiento et al. (1976), on the basis of preliminary GEOSECS and other data, proposed a correlation of the form $\kappa \sim (\text{constant})/N^2$, whereas more recently Hansen et al. (1984) proposed an even stronger dependence of the form $\kappa \sim (\text{constant})/N^4$ based on the entire GEOSECS tritium data set. This stronger dependency is associated with the very high tritium diffusivities at high latitudes where the Vaisala frequency becomes small owing to the more nearly isothermal structure of the water column. However, $|\beta|$ can become "large" at high latitudes, which would also give a high tritium diffusivity (but not necessarily a high thermal diffusivity) for different reasons. This raises questions regarding the validity of the very large vertical diffusivities of heat at high latitudes

used in the transient climate model of Hansen et al. (1984). These questions can only be resolved by a better understanding of multidimensional oceanic eddy transport and isopycnal mixing. The main point here is that tests of ocean transport models need to be developed that are both driven by tracer data and incorporate our best understanding of the relevant physics and fluid mechanics.

More generally, it is crucial to continue comparing models with observed climatic variations from year to year in terms of a variety of external forcing and internal response mechanisms. A close and ongoing interaction between theory and observation is needed for model developers to identify essential mechanisms and to forestall the tendency of certain classes of climate models to become a world unto themselves. This objective is recognized at least implicitly by the National Climate Program, an interagency project designed to answer key climate questions under the National Climate Program Act of 1978.

In the 1983 Annual Report of this program (NOAA 1984), some important new findings were presented relating to the mechanisms of transient climate change discussed here: El Chichón, one of the most massive volcanic eruptions of the past 100 years, occurred in Mexico in April 1982 and was anticipated to affect the Earth's radiation budget in a nontrivial fashion. In response both NASA and NSF initiated coordinated observation programs in which it was established that Arctic light extinction values after the eruption increased some two orders of magnitude above background values and that extensive clouds of sulfuric acid droplets were generated at middle latitudes in the stratosphere over the western United States. Model predictions indicated that this volcanic increase of stratospheric particles should decrease the global mean surface temperature, as discussed previously in Section 5.4.3. But the expected surface cooling of a few tenths of a degree Celsius (MacCracken and Luther 1984), comparable to the volcanic effects described in the models of Hansen et al. (1981) and Gilliland and Schneider (1984), was not observed. In fact, what the transient climate models discussed here would have predicted as a major, volcanically induced cooling was entirely overwhelmed by an internal feedback not predicted by any existing model; namely, the winter 1982–1983 El Niño—an unusual warming of the eastern and midequatorial Pacific with accompanying rains in Ecuador and Peru. As it actually happened, El Niño, not El Chichón, was the most significant global climatic event of 1982–1983.

An El Niño results when the easterlies decrease and warm water in the western Pacific Ocean spreads eastward across the basin and covers the normally cool upwelling region in the eastern Pacific. Such events can be viewed climatically as quasi-periodic surfacing of localized water blobs from deeper ocean layers with 2–7 year variable cycles (Pan and Oort 1983). But the key question is what internal feedback processes produce this cycle? One possibility is internal fluid dynamic instabilities in upper ocean circulation, which can produce corresponding fluctuations in global temperature. Such processes differ from the external forcing discussed earlier because they arise from the internal dynamics and thermodynamics of short-term oceanic heat storage, and should, therefore, be predictable in principle.

To better represent such atmosphere-ocean feedbacks, Wunsch (1984) has remarked that more emphasis is needed to understand the climatic state of the ocean itself. In a recent paper, Roemmich and Wunsch (1984) reexamined vertical temperature profiles of two transatlantic sections at nominal latitudes of 24°N and 36°N, originally surveyed during the International Geophysical Year (IGY 1957–1959), and found significant warming 25 years later in an ocean-wide band from 700–3000 m depths, and subsurface cooling above this. Watts (1985) has studied this type of variation with an upwelling-diffusion transient ocean model of the type described here. He concludes:

> It seems unlikely that the variations in temperature of the deep water reported by Roemmich and Wunsch would have been caused by [surface] radiation variations. If they were caused by variations in the thermohaline circulation, then these variations might have been responsible for sizable variations in the surface temperature of the oceans, and perhaps even variations in the global climate (Watts 1985, p. 84).

The mechanism by which transient surface temperatures can be affected by upwelling rates in an upwelling-diffusion ocean model is as follows (the surface [mixed] layer temperature heating rate

dT/dt is described by Hoffert et al.[1980] and in, Section 5.3 of this review):

$$\frac{dT}{dt} \simeq \frac{T_e - T}{\tau_{rm}} + \left\{ \left(\frac{1}{h_m} \right) \left[\kappa \frac{\partial T}{\partial z} + w\,(T - T_p) \right]_{z=0} \right\}, \quad (5.26)$$

where the first term is the contribution of mixed layer thermal damping and the term in the { } braces is the contribution of heat transfer at the mixed layer-thermocline boundary. To evaluate the coupling term at the boundary, it is necessary to simultaneously solve an upwelling-diffusion equation of the form

$$\frac{\partial T}{\partial t} = \frac{\partial [\kappa \partial T/\partial z + w(T - T_p)]}{\partial z} \quad (5.27)$$

in the deep ocean numerically (or analytically, if possible). Under steady conditions—or if a hypothetical adiabatic wall separated the mixed layer from the underlying ocean—the term within braces vanishes, since upwelling balances vertical diffusion of heat. However, a sudden increase in upwelling causes the upwelling (positive) part to dominate the (negative) diffusion part of the term in braces, thus warming the surface. The system works like a heat pump for the deep ocean in which cooling of the deep sea produces surface warming. Watts (1985) imposed a periodic variation in $w(t)$ and computed the corresponding variations in $T(z,t)$ in the water column. He showed that deep sea temperature changes can be induced that are out of phase and different in magnitude with those at the surface, perhaps mimicking the changes observed by Roemmich and Wunsch (1984). Although these calculations are suggestive, they leave open the question: What drives $w(t)$?

Harvey and Schneider (1985a) have performed numerical experiments to illustrate the influence of feedbacks between surface temperature changes and upwelling rates (or bottom water source temperatures) when the system is externally forced by a step function change in surface radiation (or T_e), and found the possibility of overshooting in the response for certain parameter values. In a related work for illustrative purposes, Hoffert et al. (1985) took the analysis an additional step by proposing an ad hoc combination of stabilizing and destabilizing feedbacks between the surface temperature perturbation $\Delta T \equiv T - T_e$ and the upwelling rate, of the form

$$w = w_0 + \alpha \Delta T - \beta \Delta T^3, \quad (5.28)$$

where w_0 is the long-term upwelling rate, and α and β are coefficients chosen empirically. For small ΔT's, the system is unstable because surface warming (cooling) leads to greater (smaller) upwelling, which leads to still more warming (cooling). Indeed, a purely unstable system with $\beta = 0$ can lead to an unphysical thermal runaway if the instability becomes large enough to overwhelm the mixed layer damping. However, for large excursions in ΔT, the stabilizing term $\beta \Delta T^3$ comes into play, which prevents a runaway. It was found that this system, even without external forcing (T_e = constant), can exhibit self-excited *limit cycle* oscillations that often characterize this type of nonlinear system. Nonlinear oscillations are also produced when the system is forced by greenhouse gases, volcanic aerosol injections, or solar variations, but because of the strong nonlinearities, the principle of superposition that characterized the multiply-forced linear damping models of Hansen et al. (1981, 1982, 1984) and Gilliland and Schneider (1984) is destroyed. Instead, the system modulates the imposed signals in counterintuitive ways with unanticipated phase shifts and amplifications.

An example of the output of the Hoffert et al. (1985) model applied to the historical air temperature signal of Jones et al. (1982) is illustrated in Figure 5.25 for $w_0 = 8$ m^1 y^{-1}, α =2.6 m y^{-1} K^{-1}, and β =2.9 m y^{-1} K^{-3}. Along with the temperature anomaly data, the figure shows the response of the purely linear model to nominal CO_2 forcing with the nominal mixed layer damping (cf. Figure 5.16), and the response to the same forcing when the nonlinear feedback is allowed to operate. Perhaps fortuitously, this parameter choice gave a fairly good description of the trend of the data (not including the rapid interannual oscillations). However, we emphasize that this model was developed only to provide insight, and not to be taken too seriously in terms of predictions at this level of development. What is important at this stage is the possibility that we may be seeing internal oscillations, or nonlinear combinations of internal oscillations and external forcing, in the climate records, in contrast to

the claims of some modelers that the record is essentially explainable in terms of external forcing and linear damping by some fraction of the oceanic heat capacity. Much work remains to be done to unravel the specific mechanisms that can produce such feedback in terms of realistic physics. The resolution of these issues is of obvious importance to modeling and detecting the transient CO_2 component of the global temperature signal and eventually to predicting their future course with some confidence.

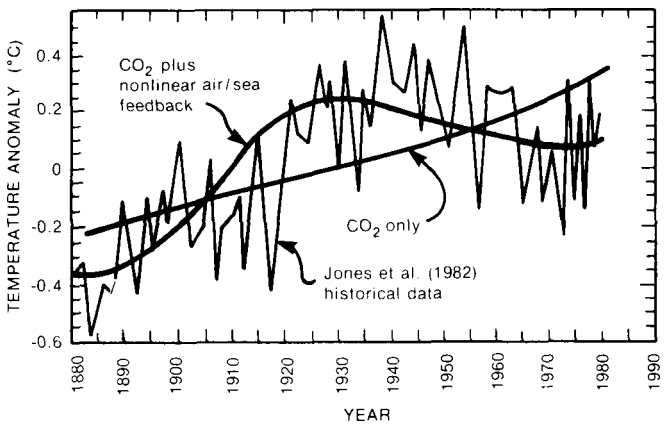

Figure 5.25. Global surface temperature anomalies from 1880 to 1980 from upwelling-diffusion model (with and without air/sea feedback) and compared to observations.

We believe that careful comparison and analysis of model results with interannual climate observations, together with a continuous and interactive development of atmosphere-ocean climate models informed by oceanographic data, is the best research strategy at present for progress in modeling transient climate change in general and fossil fuel CO_2-induced changes in particular.

5.6 CONCLUSIONS AND RESEARCH RECOMMENDATIONS

A number of approaches and levels in the climate modeling heirarchy are under active development with the goal of predicting the transient climate response from increases in CO_2. In this chapter, we have attempted to review and analyze the key issues and model results to date. The following major conclusions have emerged from the review:

- *Climatic Forcing:* The transient response of the global climate over the 10–100 year time scales of the CO_2 climate problem is probably driven by several external factors acting simultaneously—including time variations in incident solar flux, volcanic aerosols, and amounts of CO_2 and other greenhouse gases in the atmosphere, as well as internal factors such as variations in internal ocean dynamics.
- *Transient Response:* The response of global temperatures to external forcing is not instantaneous but is delayed by thermal damping, primarily by the oceanic mixed layer and upper thermocline of the ocean. Thermal storage and mixing by these reservoirs can cause a lag relative to imposed cooling or warming tendencies of the order of 10–20 years. The actual response depends on the details of the time-dependent forcing and can exhibit marked variations with latitude owing to variations in surface heat capacity associated with variations in latitudinal land-sea fractions. In hypothetical step function transitions from one steady-state climate to another, models with greater climate sensitivities take longer to reach a new, steady state, with the absolute response being relatively independent of climate sensitivity during the very early stages. However, with standard CO_2 scenarios, the more sensitive climate models predict significantly larger temperature changes during the transient as well as at the reference equilibrium state. Models with greater vertical heat transfer rates in the ocean are able to damp larger external forcing, so the relation between climate sensitivity and ocean heat transfer must be carefully considered in assessing model results for temperature histories. The observed interannual climate response may also depend on internal feedbacks of the system—El Niño, the Southern Oscillation, and so on—which have not yet been adequately represented in available climate models.
- *Testing Models:* The development of reliable predictions of transient climate change is hampered by lack of a clear validation strategy for testing models against observed data. Thus far, the testing of climatic GCMs has been confined largely to sensitivity studies and more recently to model intercomparisons that display a considerable diversity in predictions of, for example, the zonal-mean distribution of surface temperature changes from a CO_2-induced warming. Moreover, GCMs require long running

times to compute transient changes and have not been used as yet to explore the more realistic case with multiple forcing factors. Most existing transient models are simpler and involve some level of horizontal averaging of the climate system. Often the anomaly data provided to modelers for verification studies do not indicate unambiguously which physical mechanisms are responsible for the observations. Present approaches to model testing do not provide unique results. For example, a number of different models for transient climate change can apparently be constructed, by calibrating "unknown" coefficients and forcing functions such that each can reasonably reproduce a given historical data set of interannual global temperature anomalies. It is also possible to approximate a given temperature history by varying parameters such as climate sensitivity and ocean heat transfer rates simultaneously and compensatorily in a given model for a given forcing. Models still have too many degrees of freedom relative to the data available to constrain them.

- *Consensus CO_2 Warming:* Transient climate models currently available, when run with standard scenarios of fossil fuel CO_2 emissions, indicate a global warming of the order of 1°C by the year 2000, relative to the year 1850, and an additional 2°–5°C warming over the next century. However, the sensitivity of such predictions to known uncertainties of the models—that is, the robustness of CO_2 warming predictions—has not yet been extensively explored.

The resolution of uncertainties in transient climate models will require a variety of approaches, including especially closer interaction between modelers and those engaged in data analysis. Resolution and reconciliation would also be fostered by more interaction between climate modelers and physical and chemical oceanographers, whose disciplines all have something to contribute to understanding the transient climate problem. The following specific recommendations for future work are based on these findings.

- *Model Development:* In the long run, well-tested, coupled atmosphere-ocean GCMs may be able to serve as operational tools for simulating transient climate changes, but these are not now available. Work is proceeding to develop such models, but they are unlikely to be available in *reliable* form for at least the next 10 years. A major priority of near-term GCM research on the CO_2 transient climate problem should therefore be to understand and resolve the substantial differences in steady-state predictions between existing GCMs, with the eventual goal of testing the models against observations. Ocean-atmosphere GCMs having realistic geography should be further developed to incorporate properly variable heat capacity effects on the transient response and on the incorporation of efficient and accurate asynchronous coupling methods to reduce computing time. In addition, much more work is needed in modeling climate at lower levels of the modeling hierarchy to develop physical insight, to study the effects of climate sensitivity, to incorporate and make comparisons with varieties of observational data, to focus on specific mechanisms of the transient response, and to make near-term forecasts of transient climate change.
- *Oceanic Heat Storage and Mixing:* Because ocean GCMs are generally limited in their ability to resolve explicitly eddies and small-scale dynamical features responsible for vertical heat transport, more work is needed with lower level, but physically motivated, models of the dynamics and transport of the upper ocean. It is particularly important to understand the relative importance of across- and along-isopycnal mixing, and mean motion by both the thermohaline and wind stress-driven components of the ocean circulation, on the transport and storage of heat in the upper ocean. The role of convection and bottom water formation, equatorial upwelling, midlatitude gyres, and latitude-dependent oceanic mixed layers in establishing the heat uptake rates of different parts of the ocean needs to be understood as well. Such models should be tested and calibrated independently against a variety of oceanographic transient and steady-state tracers. More attention is needed in differentiating between mechanisms that act selectively on heat versus mass transport, such as isopycnal mixing. In addition, thermodynamic energy balance models should be extended to intermediate levels of complexity

to explore the role of the oceans with multiple thermodynamic reservoirs, latitude- and depth-resolved oceanic heat transfer, sea ice, and nonlinear internal feedbacks.

- *The Role of Observations:* Beyond making selective comparisons of transient model results with observations, it is essential to develop a *validation strategy* to reduce the uncertainties of the transient CO_2 climate problem. In this connection, a variety of conceptually related, but observationally independent, data sets are available through the Department of Energy Carbon Dioxide Information Center at Oak Ridge National Laboratory, including seasonal and interannual surface air and water temperatures of the Earth, data from the GEOSECs and Transient Tracers in the Ocean program on vertical profiles of oceanographic tracers, and indices of volcanic dust amounts and sunspot correlations over the past century. A careful analysis of these data in the context of climate and ocean models should be performed to reveal how the data can best be used to extract maximum information. Ideally, some data sets should be used to develop and calibrate models, and other, independent data sets should be used to validate them. A possible strategy to test a simple two-hemisphere transient climate model (e.g., Harvey and Schneider 1985a) is as follows: Use seasonal climate simulations (where both the forcing and response are known) to test overall model physics and sensitivity independent of the deep ocean, geochemical tracer data to develop and calibrate deep ocean models, satellite data on solar output plus historical sunspot observations to calibrate solar forcing, and dust veil indices plus models to calibrate greenhouse forcing. The observed temperature history of the last 100 years should then be available as an independent data set for testing the transient model. Variations of this approach, perhaps more effective, are also possible for other model types. We recommend that efforts be made to explore such strategies with the objective of systematically reducing the degrees of freedom in the models available to match data. In this way it is hoped that our ability to predict transient climate change from carbon dioxide emissions will begin to converge.

ACKNOWLEDGMENTS

We thank T. Barnett, A. Callegari, H. Ellsaesser, D. Harvey, M. MacCracken, S. Manabe, A. Robock, M. Schlesinger, S. Schneider, T. Wigley, and the anonymous referees of the American Association for the Advancement of Science review panel for their constructive comments on the manuscript; and S. Gaffin and C. T. Hsieh for their help with calculations of the reference case CO_2 scenario using the New York University upwelling-diffusion model. The contribution by MIH was supported by the Carbon Dioxide Research Division, Office of Basic Energy Sciences of the U.S. Department of Energy under contract No. DE-ACO2-81EV10610 to New York University.

REFERENCES

Abelson, P. 1983. "Carbon Dioxide Emissions." *Science 222:*879. (Editorial)

Alvarez, L. W., Alvarez, W., Asara, F., and Michel, H. V. 1980. "Extraterrestrial Causes for the Cretaceous-Tertiary Extinction." *Science 208:*1095–1108.

Augustsson, T., and Ramanathan, V. 1977. "A Radiative-Convective Model Study of the CO_2 Climate Problem." *Journal of the Atmospheric Sciences 34:*448-451.

Broecker, W. S. 1975. "Climatic Change: Are We on the Brink of a Pronounced Global Warming?" *Science 189:*460-463.

Broecker, W. S., and Peng, T. H. 1982. "Tracers in the Sea." Lamont-Doherty Geological Observatory, Columbia University, Palisades, New York.

Broecker, W. S., Peng, T. H., and Engh, P. 1980. "Modeling the Carbon Cycle." *Radiocarbon 22*(3):565–598.

Bryan, K., Komro, F. G., Manabe, S., and Spelman, M. J. 1982. "Transient Climate Response to Increasing Atmospheric Carbon Dioxide." *Science 215:*56-58.

Bryson, R. A., and Dittberner, G. J. 1976. "A Non-Equilibrium Model of Hemispheric Mean Surface Temperature." *Journal of the Atmospheric Sciences 33:*2094-2106.

Budyko, M. I. 1962. "Climatic Change and Climate Control." *Akademiia Nauk SSSR, Vestnik.* 7:33–37. Available as T-R-436, Air Force Cambridge Research Laboratories, Office of Aerospace Research, United States Air Force, L.G. Hanscom Field, Bedford, Massachusetts.

Budyko, M. I. 1969. "The Effect of Solar Radiation Variations on the Climate of the Earth." *Tellus 21:*616-619.

Budyko, M. I. 1972. "Climate Modification Techniques." *Meteorologiya i Gidrologiya 2:*91–97.

Budyko, M. I. 1977. *Climatic Changes* (Section 7.3, 236–247). American Geophysical Union, Washington, D.C.

Cess, R. D. 1976. "Climate Change: An Appraisal of Atmospheric Feedback Mechanisms Employing Zonal Climatology." *Journal of Atmospheric Sciences 33:*1831-1843.

Cess, R. D., Briegleb, B. P., and Lian, M. S. 1982. "Low-Latitude Cloudiness and Climate Feedback: Comparative Estimates from Satellite Data." *Journal of Atmospheric Sciences 21:*53–59.

Cess, R. D., and Goldenberg, S. D. 1981. "The Effect of Ocean Heat Capacity Upon Global Warming Due to Increasing Carbon Dioxide." *Journal of Geophysical Research 86:*498–602.

Coakley, J. A., Jr., Cess, R. D., and Yurevich, F. B. 1983. "The Effect of Tropospheric Aerosols on the Earth's Radiation Budget: A Parameterization for Climate Models." *Journal of the Atmospheric Sciences 40:*116–138.

Dickinson, R. E. 1981. "Convergence Rate and Stability of Ocean-Atmospheric Coupling Schemes with a Zero-Dimensional Climate Model." *Journal of the Atmospheric Sciences 38:*2112–2121.

Dickson, R. R. 1983. "Global Summaries and Intercomparisons: Flow Statistics from Long-Term Current Moorings." 278–252. In A.R. Robinson (ed.), *Eddies in Marine Science.* Springer-Verlag, New York, New York.

Folland, C. K., Parker, D. E., and Kates, F. E. 1984. "Worldwide Marine Temperature Fluctuations 1856–1981." *Nature 310:*670–673.

Garrett, C. 1979. "Mixing in the Ocean Interior." *Dynamics of Atmospheres and Oceans 3:*239–265.

Gilliland, R. L. 1982. "Solar, Volcanic and CO_2 Forcing of Recent Climatic Changes." *Climatic Change 4:*111–131.

Gilliland, R. L., and Schneider, S. H. 1984. "Volcanic, CO_2 and Solar Forcing of Recent Climatic Changes." *Nature 310:*38–41.

Hansen, J., Johnson, D., Lacis, A., Lebedeff, S., Lee, P., Rind, D., and Russell, G. 1981. "Climatic Impact from Increasing Carbon Dioxide." *Science 213:*957–966.

Hansen, J., Lacis, A., and Lebedeff, S. 1982. "Commentary on J. W. Chamberlain et al. (1982) 'Climatic Effects of Minor Atmospheric Constituents'." 284–289. In W. C. Clark (ed.), *Carbon Dioxide Review: 1982.* Oxford University Press, New York, New York.

Hansen, J., Lacis, A., Rind, D., Russell, G., Stone, P., Fung, I., Ruedy, R., and Lerner, J. 1984. "Climate Sensitivity: Analysis of Feedback Mechanisms." 130–163. In J. E. Hansen and T. Takahashi (eds.), *Climate Processes and Climate Sensitivity, Geophysical Monograph 29* (Maurice Ewing Vol. 5). American Geophysical Union, Washington, D.C.

Harvey, L. D. in press. "Effect of Ocean Mixing on the Transient Climate Response to a CO_2 Increase: Analysis of Recent Model Results." Report No. NCAR 3112–84/2. National Center for Atmospheric Research, Boulder, Colorado. *Journal of Geophysical Research.*

Harvey, L. D., and Schneider, S. H. 1985a. "Transient Climate Response to External Forcing on 10^0–10^4 Year Time Scales. 1: Experiments with Globally Averaged Coupled, Atmosphere and Ocean Models." *Journal of Geophysical Research 90*(D1):2191–2205.

Harvey, L. D., and Schneider, S. H. 1985b. "Transient Climate Response to External Forcing on 10^0–10^4 Year Time Scales. 2: Sensitivity Experiments with a Seasonal, Hemispherically Averaged, Coupled Atmosphere, Land and Ocean Energy Balance Model." *Journal of Geophysical Research 90*(D1):2207–2222.

Hoffert, M. I., and Broecker, W. S. 1978. "Apparent Vertical Eddy Diffusion Rates in the Pycnocline of the Norwegian Sea as Determined from the Vertical Distribution of Tritium." *Geophysical Research Letters 5:*502–504.

Hoffert, M. I., Callegari, A. J., and Hsieh, C. T. 1980. "The Role of Deep Sea Heat Storage in the Secular Response to Climatic Forcing." *Journal of Geophysical Research 85*(C11):6667–6679.

Hoffert, M. I., Callegari, A. J., and Hsieh, C. T. 1981. "A Box-Diffusion Carbon Cycle Model With Upwelling, Polar Bottom Water Formation and a Marine Biosphere." 287–305. In B. Bolin (ed.), *Carbon Cycle Modelling: SCOPE #16.* John Wiley & Sons, Chichester, United Kingdom.

Hoffert, M. I., Gaffin, S., Wang, Z. Y., Hsieh, C. T., and Volk, T. 1985. "Interannual Climate Oscillations in Past and Future Temperature Records." *Extended Summary Volume of the American Meteorological Society Third Conference on Climatic Variations; Symposium on Contemporary Climate 1850–2100* (January 8–11, Los Angeles, California). American Meteorological Society, Boston, Massachusetts.

Hoffert, M. I., and Michael, P. A. 1983. "Increasing Carbon Dioxide Concentrations and Climate: The Transient Response." 259–279. In W. Bach, A. J. Crane, A. L. Berger, and A. Longhetto. *Carbon Dioxide: Current Views and Developments in Energy/Climate Research.* D. Reidel Publishing Co., Hingham, Massachusetts.

Hoffert, M. I., Volk, T., and Hsieh, C. T. 1983. "A Two-Dimensional Ocean Model for Climate and Tracer Studies" (NYU/DAS 83–114). Department of Applied Science, New York University, New York, New York.

Hoffman, J. S., Keyes, D., and Titus, J. G. 1983. *Projecting Sea Level Rise: Methodology, Estimates to the Year 2100, and Research Needs.* Strategic Studies Staff, Office of Policy Analysis, U.S. Environmental Protection Agency, Washington, D.C.

Hoyt, D. V. 1979. "Variations in Sunspot Structure and Climate." *Climatic Change 2:*79–92.

Hoyt, D. V., and Eddy, J. A. 1982. *An Atlas of Variations in the Solar Constant Caused by Sunspot Blocking and Facular Emissions From 1874 to 1981* (Technical Note TN/194+ST). National Center for Atmospheric Research, Boulder, Colorado.

Hsieh, C. T. 1984. *A Three-Reservoir Latitude-Dependent Transient Climate Model With Deep Sea Heat Storage.* Doctoral Dissertation, Department of Applied Science, New York University, New York, New York.

Hunt, B. G., and Wells, N. C. 1979. "An Assessment of the Possible Future Impact of Carbon Dioxide Increases Based on a Coupled One-Dimensional Atmospheric-Oceanic Model." *Journal of Geophysical Research 84:*787–791.

Jones, P. D., Wigley, T. M. L., and Kelly, P. M. 1982. "Variations in Surface Air Temperature: Part I, Northern Hemisphere, 1881–1980." *Monthly Weather Review 111*:59–70.

Källén, E., Crafoord, C., and Ghil, M. 1979. "Free Oscillations in a Climate Model With Ice Sheet Dynamics." *Journal of Atmospheric Sciences 36*:2295–2303.

Kandel, R. S. 1983. "Simple Climate Models and the Greenhouse Effect." 179–218. In W. Bach et al. (eds.), *Carbon Dioxide: Current Views and Developments in Energy/Climate Research*. D. Reidel Publishing Co., Hingham, Massachusetts.

Keeling, C. D. 1983. "The Global Carbon Cycle: What We Know and What We Could Know From Atmospheric, Biospheric and Oceanic Observations." In *Proceedings of the Carbon Dioxide Research Conference: Carbon Dioxide, Science and Consensus* (CONF-820970). U.S. Department of Energy, Washington, D.C. Available from NTIS, Springfield, Virginia.

Kraus, E. B., and Turner, J. S. 1967. "One-Dimensional Model of the Seasonal Thermocline. II: The General Theory and Its Consequences." *Tellus 19*:98–106.

Lacis, A., Hansen, J., Lee, P., Mitchell, T., and Lebedeff, S. 1981. "Greenhouse Effect of Trace Gases, 1970–1980." *Geophysics Research Letters 8*:1035–1038.

Lamb, H. H. 1972. *Climate: Past, Present and Future, Vol. 1*. Methuen, London, United Kingdom.

Launder, B. E., and Spalding, D. B. 1972. *Mathematical Models of Turbulence*. Academic Press, New York, New York.

Levitus, S. 1982. *Climatological Atlas of the World Ocean* (NOAA Professional Paper 13). National Oceanic and Atmospheric Administration, Rockville, Maryland.

Li, Y. H., Peng, T. H., Broecker, W. S., and Ostlund, H. G. 1984. "The Average Vertical Mixing Coefficient for the Oceanic Thermocline." *Tellus 36B*:212–217.

Liou, K.-N., and Ou, S.-C. 1983. "Theory of Equilibrium Temperatures in Radiative-Turbulent Atmospheres." *Journal of the Atmospheric Sciences 40*:214–229.

MacCracken, M. C., and Luther, F. M. 1984. "Preliminary Estimate of the Radiative and Climatic Effects of the El Chichón Eruption." *Geofisica Internacional 23-3*:385–401.

MacCracken, M. C., and Luther, F. M. 1985. *Detecting the Climatic Effects of Increasing Carbon Dioxide* (DOE/ER-0235). U.S. Department of Energy, Washington, D.C. Available from NTIS, Springfield, Virginia.

Manabe, S., and Wetherald, R. T. 1975. "The Effects of Doubling the CO_2 Concentration on the Climate of a General Circulation Model." *Journal of the Atmospheric Sciences 32*:3–15.

Manabe, S., and Wetherald, R. T. 1980. "On the Distribution of Climate Change Resulting from an Increase in CO_2 Content of the Atmosphere." *Journal of the Atmospheric Sciences 37*:99–118.

Mercer, J. H. 1978. "West Antarctic Ice Sheet and CO_2 Greenhouse Effect." *Nature 271*:321–325.

Michael, P., Hoffert, M., Tobias, M., and Tichler, J. 1981. "Transient Climate Response to Changing Carbon Dioxide Concentration." *Climatic Change 3*:137–153.

Mitchell, J. M., Jr. 1970. "A Preliminary Evaluation of Atmospheric Pollution as a Cause of the Global Temperature Fluctuation of the Past Century." 139–155. In S. F. Singer (ed.), *Global Effects of Environmental Pollution*. Springer-Verlag, New York, New York.

Müller, P. 1979. "A Note on the Variability of Eddy Diffusion Coefficients in the Ocean." *Dynamics of Atmospheres and Oceans 3*:267–274.

Munk, W. H. 1966. "Abyssal Recipes." *Deep Sea Research 13*:707–736.

National Oceanic and Atmospheric Administration (NOAA). 1984. *National Climate Program: 1983 Annual Report*. NOAA, Rockville, Maryland.

National Research Council (NRC). 1982. *Carbon Dioxide and Climate: A Second Assessment: Report of the CO_2/Climate Review Panel*. National Academy Press, Washington, D.C.

National Research Council (NRC). 1983. *Changing Climate* (Report of the Carbon Dioxide Assessment Committee). Board on Atmospheric Sciences and Climate, National Academy Press, Washington, D.C.

Newkirk G., Jr. 1983. "Variations in Solar Luminosity." *Annual Reviews of Astronomy and Astrophysics 21*:429–467.

Nordhaus, W. D., and Yohe, G. W. 1983. "Future Carbon Dioxide Emissions From Fossil Fuels." 87–153. In *Changing Climate: Report of the Carbon Dioxide Assessment Committee* (W. A. Nierenberg, Committee Chairman). National Academy Press, Washington, D.C.

North, G. R., Cahalan, R. F., and Coakley, J. A. 1981. "Energy Balance Climate Models." *Reviews of Geophysics and Space Science 19*:91–121.

North, G. R., Mengle, J. C., and Short, D. A. 1984. "On the Transient Response Patterns of Climate to Time Dependent Concentrations of Atmospheric CO_2." In J. Hansen and T. Takahashi (eds.), *Climate Processes and Climate Sensitivity* (Geophysical Monograph 29, Maurice Ewing Volume 5). American Geophysical Union, Washington, D.C.

Oeschger, H., Siegenthaler, U., Shotterer, U. and Gugelmann, A. 1975. "A Box Diffusion Model to Study the Carbon Dioxide Exchange in Nature." *Tellus 27*:168–192.

Oliver, R. C. 1976. "On the Approach of Hemispheric Mean Temperature to Stratospheric Dust: An Empirical Approach." *Journal of Applied Meteorology 15*:933–950.

Oort, A. H. 1983. *Global Atmospheric Circulation Statistics 1958-1973* (NOAA Professional Paper 14). National Oceanic and Atmospheric Administration, Rockville, Maryland.

Paltridge, G., and Woodruff, S. 1981. "Changes in Global Surface Temperature From 1880 to 1977." *Monthly Weather Review 109*:2427–2434.

Pan, Y. H., and Oort, A. H. 1983. "Global Climate Variations Connected with Sea Surface Temperature Anomalies in

the Eastern Equatorial Pacific." Monthly Weather Review 111:1214–1258.

Pollack, J. B., Toon, O. B., Ackerman, T. P., McKay, C. P., and Turco, R. P. 1983. "Environmental Effects of an Impact-Generated Dust Cloud." Science 219:287–289.

Potter, G. L., and Cess, R. D. 1984. "Background Tropospheric Aerosols: Incorporation within a Statistical Dynamical Model." Journal of Geophysical Research 89(D6):9521–9526.

Revelle, R. 1982. "Carbon Dioxide and World Climate." Scientific American 287(2):35–43.

Robinson, A. R. 1983. "Overview and Summary of Eddy Science." 3–15. In A. R. Robinson (ed.), Eddies in Marine Science. Springer-Verlag, New York, New York.

Robock, A. 1978. "Internally and Externally Caused Climate Change." Journal of the Atmospheric Sciences 35:1111–1122.

Robock, A. 1979. "The 'Little Ice Age': Northern Hemisphere Average Observations and Model Calculations." Science 206:1402-1404.

Robock, A. 1981. "The Mount St. Helens Volcanic Eruption of 18 May 1980; Minimal Climatic Effect." Science 212:1383–1384.

Roemmich, D., and Wunsch, C. 1984. "Apparent Changes in the Climatic State of the Deep North Atlantic." Nature 307:447.

Saltzman, B. 1982. "Stochastically-Driven Climate Fluctuations of the Sea-Ice, Ocean Temperature, CO_2 System." Tellus 206:97–112.

Sarmiento, J. L., and Bryan, K. 1982. "An Ocean Transport Model for the North Atlantic." Journal of Geophysical Research 87:9694–9698.

Sarmiento, J. L., Feely, H. W., Moore, W. S., Bainbridge, A. E., and Broecker, W. S. 1976. "The Relationship Between Vertical Eddy Diffusion and Buoyancy Gradient in the Deep Sea." Earth and Planetary Science Letters 32:357–370.

Sarmiento, J. L., Rooth, C. G. H., and Broecker, W. S. 1982. "Radium 228 as a Tracer of Basin Wide Processes in the Abyssal Ocean." Journal of Geophysical Research 87:9694–9698.

Schlesinger, M. E. 1983. "Simulating CO_2-Induced Climate Change With Mathematical Climate Models: Capabilities, Limitations and Prospects." In Proceedings of the Carbon Dioxide Research Conference: Carbon Dioxide Research Conference: Carbon Dioxide, Science and Consensus (CONF–820970). U.S. Department of Energy, Washington, D.C. Available from NTIS, Springfield, Virginia.

Schlesinger, M. E., Han, Y. J., and Gates, L. W. 1985. "The Role of CO_2-Induced Climate Change: A Study with the OSU Coupled Atmosphere-Ocean General Circulation Model." Extended Summary Volume of the American Meteorological Society Third Conference on Climatic Variations; Symposium on Contemporary Climate 1850–2100 (January 8–11, Los Angeles, California). American Meteorological Society, Boston, Massachusetts.

Schneider, S. H., and Londer, R. 1984. The Coevolution of Climate and Life. Sierra Club Books, San Francisco, California.

Schneider, S. H., and Mass, C. 1975. "Volcanic Dust, Sunspots and Temperature Trends." Science 190:741-746.

Schneider, S. H., and Thompson, S. L. 1981. "Atmospheric CO_2 and Climate: Importance of the Transient Response." Journal of Geophysical Research 86(C4):3135-3147.

Seidel, S., and D. Keyes. 1983. Can We Delay a Greenhouse Warming? The Effectiveness and Feasibility of Options to Slow a Build-up of Carbon Dioxide in the Atmosphere. Strategic Studies Staff, Office of Policy Studies, U.S. Environmental Protection Agency, Washington, D.C.

Sellers, W. D. 1965. Physical Climatology. University of Chicago Press, Chicago, Illinois.

Sellers, W. D. 1969. "A Global Climate Model Based on the Energy Balance of the Earth-Atmosphere System." Journal of Applied Meteorology 8:329–400.

Shabecoff, P. 1983. "E. P. A. Report Says Earth Will Heat Up Beginning in 1990's." New York Times, October 18, 1983, p. A1, New York, New York.

Spelman, M. J., and Manabe, S. 1984. "Influence of Oceanic Heat Transport Upon the Sensitivity of a Model Climate." Journal of Geophysical Research 89(C1):571–586.

Sullivan, W. 1981. "Study Finds Warming Trend That Could Raise Sea Level." New York Times, August 21, 1981, pp. 1, 13, New York, New York.

Sverdrup, H. U., Johnson, M. M., and Fleming, R. H. 1942. The Oceans, Their Physics, Chemistry and General Biology,1st ed., Prentice Hall, Englewood Cliffs, New Jersey.

Thompson, S. L., and Schneider, S. H. 1979. "A Seasonal Zonal Energy Balance Climate Model With an Interactive Lower Layer." Journal of Geophysical Research 84:2401-2414.

Thompson, S. L., and Schneider, S. H. 1982. "Carbon Dioxide and Climate: The Importance of Realistic Geography in Estimating the Transient Temperature Response." Science 217:1031–1033.

Trabalka, J. R. (ed.). 1985. Atmospheric Carbon Dioxide and the Global Carbon Cycle (DOE/ER-0239). U.S. Department of Energy, Washington, D.C. Available from NTIS, Springfield, Virginia.

Turco, R. P., Toon, O. B., Ackerman, T., Pollack, J. B., and Sagan, C. 1983. "Nuclear Winter: Global Consequences of Multiple Nuclear Explosions." Science 222:1283–1292.

Turner, J. S. 1981. "Small Scale Mixing Processes." 236–262. In B. A. Warren and C. Wunsch (eds.), Evolution of Physical Oceanography: Scientific Surveys in Honor of Henry Stommel. Massachusetts Institute of Technology Press, Cambridge, Massachusetts.

Verniani, F. 1966. "The Total Mass of the Earth's Atmosphere." Journal of Geophysical Research 71:385–391.

Vinnikov, K. Y., and Groisman, P. Y. 1982. "An Empirical Study of Climate Sensitivity." Atmospheric and Oceanic Physics 18(11):1157–1167.

Vinnikov, K. Y., Gruza, G. V., Zakharov, V. F., Kirillov, K. A., Kovyneva, N. P., and Rankova E. Y. 1980. "Current Climate Estimates in the Northern Hemisphere." Meteorologiya I Gidrologiya 6:5-17. English translation by Alerton Press: Soviet Meteorology and Hydrology 6:1-10.

Warren, S. G., and Schneider, S. H. 1979. "Seasonal Simulations as a Test for Uncertainties in the Parameterization of a Budyko-Sellers Zonal Climate Model." Journal of the Atmospheric Sciences 36:1377-1391.

Washington, W. M., and Meehl, G. A. 1983."General Circulation Model Experiments on the Climatic Effects Due to a Doubling and Quadrupling of Carbon Dioxide Concentration". Journal of Geophysical Research 88:6600-6610.

Watts, R. G. 1983. "On the Absence of Self-Oscillatory Behavior in Some Zero-Dimensional Climate Models." Journal of Geophysical Research 8810829-10830.

Watts, R. G. 1985. "Climatic Transients Caused by Variations in the Thermocline Circulation." Extended Summary Volume of the American Meteorological Society Third Conference on Climatic Variations; Symposium on Contemporary Climate 1850-2100 (January 8-11, Los Angeles, California). American Meteorological Society, Boston, Massachusetts.

Weller, G., Baker, J. D., Jr., Gates, W. L., MacCracken, M. C., Manabe, S., and Vonder Haar, T. H. 1983. "Detection and Monitoring of CO_2-Induced Climate Change." 292-382. In Changing Climate (Report of the Carbon Dioxide Assessment Committee). Board on Atmospheric Sciences and Climate, National Research Council, National Academy Press, Washington, D.C.

Wigley, T. M. L., and Angell, J. K., and Jones, P. D. 1985. "Analysis of the Temperature Record." In M. C. MacCracken and F. M. Luther (eds.), Detecting the Climatic Effects of Increasing Carbon Dioxide (DOE/ER-0235). U.S. Department of Energy, Washington, D.C. Available from NTIS, Springfield, Virginia.

Wigley, T. M. L., and Schlesinger, M. E. 1985a. "Transient Response and the Detection of CO_2-Induced Climatic Change." Extended Summary Volume of the American Meteorological Society Third Conference on Climatic Variations; Symposium on Contemporary Climate 1850-2100 (January 8-11, Los Angeles, California). American Meteorological Society, Boston, Massachusetts.

Wigley, T. M. L., and Schlesinger, M.E. 1985b. "The Response of Global Mean Temperature to Changing Carbon Dioxide Levels." Nature 315: 649-652.

Willson, R. C., Gulkis, S., Jannsen, M., Hudson, H. S., and Chapman, G. A. 1981. "Observations of Solar Irradiance Variability." Science 211:700-702.

Wuebbles, D. J., MacCracken, M. C., and Luther, F. M. 1984. "A Proposed Reference Set of Scenarios for Radiatively Active Constituents" (DOE/NBB-0066). U.S. Department of Energy, Washington, D.C. Available from NTIS, Springfield, Virginia.

Wunsch, C. 1984. "The Ocean Circulation in Climate." 189-203. In J. T. Houghton, (ed.), The Global Climate. Cambridge University Press, New York, New York.

Zwally, H. J., Parkinson, C. L., and Comiso, J. C. 1983. "Variability of Antarctic Sea Ice and Changes in Carbon Dioxide." Science 220:1005-1012.

6. POTENTIAL CLIMATIC EFFECTS OF PERTURBATIONS OTHER THAN CARBON DIOXIDE

Wei-Chyung Wang
Atmospheric and Environmental Research, Inc.

Donald J. Wuebbles
Lawrence Livermore National Laboratory

Warren M. Washington
National Center for Atmospheric Research

CONTENTS

6.1 INTRODUCTION

The potential climatic effects of an increase in the carbon dioxide (CO_2) concentration have been discussed in Chapters 4 and 5 of this volume. Other factors in addition to an increased CO_2 concentration may affect the future global climate on a time scale of decades. These include increased abundance of atmospheric trace gases and aerosols, variation of incoming solar radiation, change of surface characteristics, and releases of waste heat. Study of the climatic effects of these factors is important not only because of their magnitude, but also because of their potential for masking or amplifying the effects of CO_2-induced climate change.

Tests with atmospheric numerical models have shown that atmospheric trace gases such as nitrous oxide (N_2O), methane (CH_4), and chlorocarbons (ClCs) are important in determining the Earth's longwave radiation balance (see Chapter 2 of this volume). Therefore, if increases in their concentrations continue, these trace gases could have significant effects on climate (cf. World Meteorological Organization [WMO] 1982; National Research Council [NRC] 1983). Climate model calculations suggest that, on the time scale of decades, the climatic influence of the individual trace gases is likely to be smaller than the effect of CO_2, but the combined climatic effects of increases of atmospheric N_2O, CH_4, and ClCs and their induced ozone (O_3) change from climate-chemistry interactions could be as large as those estimated for expected increases in the CO_2 concentration.

An increase in the atmospheric aerosol loading would change climate differently than would increases in the concentrations of CO_2 and trace gases (cf. WMO 1983a, 1983b). Volcanic aerosols injected into the stratosphere (for example, during the 1982 El Chichón eruption) interact more strongly with solar radiation than with terrestrial radiation and thus would be expected to warm the stratosphere and to cool the troposphere and the surface. An increase in stratospheric sulfuric aerosols from an increased carbonyl sulfide (COS) concentration would have a similar effect, but with longer term implications. The potential effects of tropospheric aerosols are much more difficult to estimate, primarily because the effects depend on the type of aerosols and environmental conditions such as the underlying surface albedo and humidity. Nevertheless, tropospheric aerosols are an important factor for consideration of regional climate change.

Solar radiation is the external driving force for the Earth's climate system. Model calculations have indicated that changes of the solar irradiance of only a few tenths of one percent would cause the global surface temperature to change a few tenths of a degree, perhaps enough to account for the temperature changes observed during the past century. The value of solar irradiance, often referred to as the solar constant, needs to be known accurately, and its possible variations on different time scales need to be understood.

Humans have been changing the characteristics of the surface of the Earth. These changes have been manifested in several ways, such as the regional albedo change resulting from changes of vegetation in several desert and tropical forested regions. Such changes of albedo and vegetation could perturb the surface energy balance and lead to climate change.

Another anthropogenic perturbation to the climate system is the addition of waste heat to the atmosphere. Substantial localized effects have resulted from this heat over many regions of the industrialized world. Also, the amount of waste heat and its effect will grow as the world's need for various forms of energy grows, particularly as the world becomes more industrialized.

The various natural and anthropogenic factors mentioned above may affect the climate on different time and space scales. The objective of this chapter is to discuss these factors and, to the extent possible, to estimate potential future effects so that CO_2-induced changes can be viewed in the context of the several types of perturbations now underway. The chapter is organized in the following way. In Section 6.2, the origins of the various natural and anthropogenic perturbations are described. The discussion centers on trace gases and aerosols because of their potentially large climatic effects. The physical and chemical processes are discussed in Section 6.3, and the interactions of these processes are illustrated through climate model sensitivity calculations. In Section 6.4, model projections of future climate changes are summarized. This is followed in Section 6.5 by a discussion of the uncertainties associated with the current understanding

TABLE 6.1
Trace Gases With Potentially Important Radiative and Chemical Effects on the Global Atmosphere

Chemical	Composition	Surface Mixing Ratio (ppm)	Estimates of Recent Annual Growth Rate (percent per year)
Carbon Dioxide	CO_2	340	0.4
Stratospheric Ozone	O_3 (strat.)	(0.1–10)[a]	0–0.3[b]
Tropospheric Ozone	O_3 (trop.)	(0.02–0.1)[a]	0–0.7[b]
Methane	CH_4	1.7	1–2
Carbon Monoxide	CO	0.12	?
Chlorocarbons	$CFCl_3$	1.9×10^{-4}	5–8
	CF_2Cl_2	3.5×10^{-4}	5–8
	CH_3CCl_3	1.3×10^{-4}	5–8
	CFC-113	0.3×10^{-4}	15–20
	CCl_4	1.5×10^{-4}	1–3
	etc.		
Hydrocarbons	C_2H_4, etc.	$\leq 10^{-3}$	?
Nitrous Oxide	N_2O	0.3	0.2
Nitrogen Oxides	$NO_x(NO + NO_2)$	$(3 \times 10^{-5} - 0.015)$[a]	?
Sulfur Compounds	COS	5×10^{-4}	?
	CS_2	0.3×10^{-4}	?
	SO_2	1.0×10^{-4}	?
Stratospheric Water Vapor	H_2O (strat.)	(3–5)[a]	?

[a] Range in concentration with altitude.
[b] Estimated based on available ozonesonde and Umkehr data.

of the non-CO_2 effect. Section 6.6 presents future research needs.

6.2 NATURAL AND ANTHROPOGENIC PERTURBATIONS

6.2.1 Trace Gases

The number of radiatively active trace gases in the atmosphere, including species that chemically influence these gases, is large. However, by limiting the discussion to source gases affecting atmospheric chemistry and to those gases most likely to have significant radiative effects in the foreseeable future, a limited list can be developed. The listing below briefly discusses each of the radiatively active gases that should be considered in order to evaluate past and potential future influences on the atmosphere. Ozone, because of its important climatic influence in the natural atmosphere, is discussed in a later section. Table 6.1 summarizes the present concentration and trend for the gases discussed below.

6.2.1.1 Methane

The current tropospheric concentration of methane (CH_4) is about 1.7 parts per million by volume (ppm). Several measurement series indicate that atmospheric CH_4 concentrations have been increasing by 1–2% per year since at least 1977 (Rasmussen and Khalil 1981; Blake et al. 1982; Fraser et al. 1982; Rowland et al. 1982) and may have been rising for a much longer period of time. The evidence for an increase in CH_4 before 1977 is less direct. Measurements have been carried out intermittently since atmospheric CH_4 was first measured 36 years ago. However, until recently, the precision, accuracy, and frequency of these measurements have generally been insufficient to permit the detection of trends. Ice core samples (Robbins et al. 1973; Craig and Chou 1982; Khalil and Rasmussen 1982) suggest that preindustrial CH_4 concentrations may have been about half the current concentration. However, further measurements are needed to clarify whether these ice core samples are representative of the past CH_4 concentration.

Most atmospheric CH_4 appears to be biological in origin. The increasing biogenic emissions connected with an increasing human population are the most likely cause of the increasing CH_4 concentration. Production from rice paddies appears to be a major CH_4 source (Ehhalt and Schmidt 1978; Cicerone and Shetter 1981). Ehhalt and Schmidt (1978) estimated that between 1964 and 1970, the area of rice paddies increased by ~45%, and Seiler (1982) suggested that a substantial part of the CH_4 increase may be due to increased emissions from

rice paddies. Enteric fermentation in mammals may also be responsible for a significant fraction of the atmospheric CH_4 increase because of the increasing populations of farm animals (Rasmussen and Khalil 1981; Blake et al. 1982; Seiler 1982). Biomass burning, particularly in the tropics, may be another major anthropogenic source of CH_4 (Crutzen et al. 1979). Direct anthropogenic sources (e.g., industrial processes, coal and lignite mining, automobile exhaust) seem to be having only a minor influence on the methane budget. The possibility that termites are a major source of atmospheric CH_4 has been the subject of recent debate (Zimmerman et al. 1982; Rasmussen and Khalil 1983b; Zimmerman and Greenberg 1983; Collins and Wood 1984; Seiler et al. 1984). Whether termite population changes are contributing to the CH_4 increase is highly uncertain. However, as described above, anthropogenic influences resulting from changes in land use, increasing human population, and the corresponding increases in animal populations may have accounted for significant changes in the CH_4 budget in recent decades.

Another possible explanation for the CH_4 increase is a decrease in the concentration of tropospheric hydroxyl radical (OH). Reaction with OH is the major sink for CH_4 in the atmosphere. An increase in tropospheric CH_4 could result from a decrease in OH concentration, which in turn might result from an increase in the concentration of carbon monoxide (CO). However, recent measurements of CO give conflicting results (see discussion on CO, Section 6.2.1.4).

The atmospheric lifetime of CH_4 is approximately 7 years. Changes in the CH_4 concentration may influence the global O_3 distribution because of its reaction with hydroxyl radicals and other trace gases and also its importance as an atmospheric source of other trace gases. Decomposition of CH_4 is an important source of atmospheric CO. Also, water vapor and odd hydrogen species (OH, HO_2) are important products of CH_4 oxidation in the stratosphere.

If changes in land use and population primarily account for the increasing CH_4 concentration, then this is likely to continue for at least the next century. In addition, atmospheric CH_4 could increase in the future through the release of CH_4 from CH_4 hydrates in continental slope sediments as the oceans respond to the atmospheric warming expected from the increasing concentrations of CO_2 and other infrared-absorbing trace gases (Bell 1982; NRC 1983). According to Revelle (NRC 1983), atmospheric methane from this source could be increased by as much as 1–2 ppm ($3.2 - 6.4 \times 10^{15}$g) over the next century. To put this value in perspective, this quantity would be almost comparable to the present rate of increase in CH_4 concentration, which is about 2–3 ppm (7×10^{15}g) per century.

6.2.1.2 Chlorocarbons

Large quantities of industrially produced ClCs are made for a variety of uses, such as solvents, refrigerants, and spray can propellants. The ClCs of primary concern currently are $CFCl_3$ (also referred to as CFC-11) and CF_2Cl_2 (CFC-12) because of their large production rates, their long atmospheric lifetimes, and the significant rate of increase in ClC concentrations (Molina and Rowland 1974; Rowland and Molina 1975; Cunnold et al. 1983a, 1983b; Wuebbles 1983a). The chlorocarbons $CFCl_3$ and CF_2Cl_2 are well mixed in the troposphere with mixing ratios of approximately 190 and 350 parts per trillion[1] by volume (ppt) (as of early 1983), respectively. Concentrations of these two chlorocarbons continue to increase by approximately 5–8% per year, although rates of emission have not increased significantly since 1976.

These species are not reactive until they are dissociated in the middle to upper stratosphere. The chlorine atoms released in the dissociated process can then react to destroy O_3. Other ClCs recognized as potentially having significant impacts on the atmosphere are CCl_4 (carbon tetrachloride), CH_3CCl_3 (methyl chloroform), $CFCl_2CF_2Cl$ (CFC-113), CF_2ClCF_2Cl (CFC-114), CF_2ClCF_3 (CFC-115), CHF_2Cl (CFC-22), and CH_3Cl (methyl chloride). Several of these chlorocarbons (CH_3CCl_3, CFC-113, CFC-22) have rapidly increasing concentrations (Table 6.1). Methyl chloride is the only chlorocarbon thought to come primarily from natural sources. An international effort has been devoted to determining the historical release rates of $CFCl_3$ and CF_2Cl_2. Unfortunately, similar efforts are not being undertaken for other chlorocarbons,

[1] One part per trillion equals 10^{-12}.

and estimates of their atmospheric release rates are of much poorer quality.

The standard scenario used in model studies (NRC 1976, 1979, 1984; WMO 1981) has assumed constant chlorocarbon emissions indefinitely at 1976 (or later) rates. Although production rates of CFC-11 and CFC-12 have not changed appreciably over the last 6 years (Chemical Manufacturers Association [CMA] 1982), there is no strong basis for selecting this scenario other than its utilization in models is straightforward. An examination of CMA (1982) data on the production of CFC-11 and CFC-12 suggests that nonaerosol spray use of these species increased by 4.0% per year from 1976 to 1982 in the companies reporting to CMA and by as much as 6.5% per year worldwide. During this time, in the companies reporting to CMA, aerosol spray use decreased from 56 to 34% of the total CFC production.

6.2.1.3 Nonmethane Hydrocarbons

Several of the nonmethane hydrocarbons (for example, C_2H_4 and C_2H_6) may be of radiative and chemical importance if significant growth in their emissions occurs. The importance of current nonmethane hydrocarbon concentrations on the global atmosphere has not been fully determined. Few measurements of these hydrocarbons currently exist, and no measured trend in their concentration is available (Singh et al. 1979; Rudolph et al. 1981; Rasmussen and Khalil 1983a; Rasmussen et al. 1983; Greenberg et al. 1984).

Budget analyses suggest that oxidation of methane and of nonmethane hydrocarbons is a major source of atmospheric CO (Seiler 1976; Zimmerman et al. 1978; Logan et al. 1981). Significant changes in the source rates of these species could affect atmospheric carbon monoxide concentrations, which in turn could affect the tropospheric ozone distribution (Fishman et al. 1979). More analysis of the role of the nonmethane hydrocarbons on the global atmosphere is needed.

6.2.1.4 Carbon Monoxide

Measurements of CO have not indicated any clearly defined difference in atmospheric global CO concentrations over the last few decades. No significant change was found in a comparison of global measurements made by Seiler (1974) during 1969–1972 and those presented by Seiler and Fishman (1981) for data from 1974. Seiler (1982) noted no significant change in his CO measurements after 1977. A more recent analysis by Seiler (private communication, 1984) indicates that the CO concentration may be increasing by as much as 1% per year. Several studies that do indicate a possible increase in CO concentration are limited in their usefulness by possible problems with accuracy, calibration, local sources, and statistical significance (Graedel and McRae 1980; Dianov-Klokov and Yurganov 1981). However, it is uncertain whether any of these problems apply to the recent work of Khalil and Rasmussen (1984), which suggests a 6% per year increase in CO at Cape Meares, Oregon, during 1980–1982.

Several earlier studies had assumed atmospheric growth of CO to be proportional to that of CO_2. However, the anthropogenic emissions of CO and CO_2 from the burning of fossil fuels come largely from different sources. An important anthropogenic source of CO_2 is from the combustion of fossil fuels in power plants (Clark et al. 1982). The anthropogenic production of the CO component comes primarily from transportation (automobiles, etc.) and industrial fossil fuel combustion processes (Seiler 1974; Logan et al. 1981), with power plants thought to be only a minor source. Carbon monoxide concentrations could be increasing through increased fossil fuel use, but not in direct proportion to the increase of CO_2. Civilization's influence on the biosphere through deforestation, biomass burning, and modification of CH_4 sources could result in changes in atmospheric CO (Crutzen et al. 1979; Logan et al. 1981). As the CH_4 concentration increases, a corresponding increase in CO would actually be expected.

6.2.1.5 Nitrous Oxide

Atmospheric measurements by Weiss (1981) indicate a possible global increase in nitrous oxide (N_2O) concentrations of approximately 0.2% per year between the years 1976 and 1980. A similar but somewhat larger increase of 0.3 ± 0.1% per year is found in the measurements of Khalil and Rasmussen (1983) for the years 1978 to 1981. Data,

attributed to Weiss (1981) but not included in his published paper, discussed in WMO (1981) suggest that N_2O concentrations may have been increasing at this rate since at least 1960. The current N_2O concentration in the troposphere is about 300 parts per billion[2] by volume (ppb). Backward extrapolation of current growth rates suggests that the N_2O concentration in the preindustrial atmosphere may have been as low as 280–285 ppb. The current concentration is about 300 ppb.

Weiss (1981) suggests that a substantial fraction (if not all) of the measured increase in N_2O may be explained by combustion of fossil fuels, and that N_2O production by fertilizer denitrification may be considerably less than previously estimated. However, the evidence supporting this explanation is limited. The dominant source of N_2O in the atmosphere is thought to be biological, with a major source being the bacterial process of nitrification (Bremner and Blackmer 1978; Breitenbeck et al. 1980; McElroy 1980; Lipschultz et al. 1981); this source also has the potential of changing the emission rate with time.

Until the N_2O budget and the reason for the current concentration increase is better understood, it will be difficult to project future N_2O growth rates. The combustion source could increase if coal usage becomes an increasingly larger fraction of total fossil fuel burning in the future. Fertilizer denitrification, even if not important now, could become a significant N_2O source in the future. Natural sources may increase as the atmosphere warms from future increases in CO_2 (and other trace gas) concentrations.

6.2.1.6 Nitrogen Oxides

Along with natural sources, nitrogen oxides (NO_x = NO + NO_2, sometimes referred to as odd nitrogen) are emitted into the atmosphere by various transportation and combustion sources at the surface and by aircraft in the upper troposphere and lower stratosphere. The major source of nitrogen oxides in the stratosphere is from the dissociation of nitrous oxide by excited oxygen atoms. Nitrogen oxides, although not important as greenhouse gases, appear to be important in determining the distribution of both tropospheric and stratospheric O_3. Current theoretical studies suggest that increased nitrogen oxide emissions in the troposphere would increase tropospheric O_3 concentrations, whereas stratospheric emissions would reduce stratospheric O_3 amounts. Large concentrations of NO_x can result in significant local heating of the atmosphere because of increased solar absorption by NO_2.

Anthropogenic production through fossil fuel combustion and biomass burning appear to be the major sources of NO_x in the lower troposphere (Crutzen et al. 1979; Bauer 1982; Liu et al. 1983; Logan 1983). The majority of the combustion component of the NO_x source occurs in midlatitudes of the Northern Hemisphere, whereas the anthropogenic component of the biomass burning occurs mostly in the tropics. Measurements of tropospheric NO_x are limited, but global concentrations appear to be in the 30–100 ppt range in nonurban areas. Model calculations (e.g., Fishman and Crutzen 1977; Liu et al. 1980; Callis et al. 1983) have indicated that more than 5 ppt of NO in the atmosphere is sufficient to influence tropospheric ozone concentrations. Nitrogen oxides can also be important in the tropospheric photochemistry of OH and HO_2 (Liu 1977; Logan et al. 1981). The OH distribution in the troposphere, in turn, is important in determining the atmospheric lifetimes of a number of trace gases such as CH_4, CH_3Cl, and CH_3CCl_3.

Results of several studies have indicated that NO_x emissions from aircraft may have had a significant impact on upper tropospheric and lower stratospheric NO_x concentrations over the last two decades (Liu et al. 1980; Wuebbles et al. 1983). However, major uncertainties exist in the actual growth rate of the aircraft emissions, in tropospheric ozone chemistry, and in the importance of tropospheric transport and removal processes.

6.2.1.7 Water Vapor

The spatial distribution of tropospheric water vapor is chiefly determined by the location and intensity of evaporation and precipitation (condensation) and by transport processes. Because evaporation and precipitation depend on the temperature and the

[2] One part per billion equals 10^{-9}.

distribution of water vapor, and the ambient temperature, and in turn the transport processes are affected by changes in water vapor, there is a strong coupling between these various processes.

The budget of water vapor is very complex and has been the subject of much study (for example, see an early work by Starr et al. 1965). Recently, Peixoto and Oort (1983) have reviewed the subject, and Salstein et al. (1983) have studied the variability in annual hemispheric water vapor during 1958–1973. However, the existing measurements of tropospheric water vapor are limited in their spatial coverage because of the problems of obtaining data over the oceans and in high latitudes. Although tropospheric water vapor measurements have been examined to determine possible global trends (e.g., Oort 1983), significant uncertainties exist because of the limited spatial coverage of such measurements. No well-defined global trend has been established.

The stratosphere is relatively dry (3–4 ppm H_2O in the lower stratosphere) compared with the troposphere, where mixing ratios can reach several parts per thousand near the surface. Although uncertainties remain, water vapor in the lower stratosphere appears to be controlled primarily by the temperature of the tropical tropopause (see Brewer 1949; Ellsaesser et al. 1980; Newell and Gould-Stewart 1981; Doherty et al. 1984). The water vapor mixing ratio increases with altitude in the stratosphere to approximately 5–6 ppm in the upper stratosphere. This increase with altitude likely is due to the oxidation of methane.

Significant changes in the amount of water vapor reaching the stratosphere could affect stratospheric ozone concentrations (Liu et al. 1976; Callis and Natarajan 1981; Wuebbles et al. 1983). Measurements of water vapor in the stratosphere are limited. However, several studies (see Ellsaesser et al. 1980) suggest a possible increase from 1954 to about 1973, a decrease to 1976, and little change thereafter. Such an increase may be associated with increased stratosphere-troposphere exchange of H_2O. In addition, an increase in CH_4 emissions may lead to an increase in upper stratospheric H_2O due to methane oxidation with subsequent climate implications due to the H_2O radiative effects.

Although anthropogenic emissions of water vapor in the troposphere (often expressed in terms of the thermal value of the latent heat and called thermal pollution) are relatively small on a global scale, anthropogenic activities may be able to modify surface characteristics in such a way as to modify the hydrologic cycle. Thus, creation of an oil film on the ocean, changes in ground characteristics, river runoff, irrigation practices, and so forth, may lead to significant changes in evaporation and precipitation.

6.2.1.8 Sulfur Species

Sulfur-based gases are the primary precursors of stratospheric aerosols (Crutzen 1976; Turco et al. 1980, 1982). Sulfur dioxide (SO_2) is an important component of volcanic effluents. SO_2 (or hydrogen sulfide [H_2S], which would be oxidized to SO_2) is often injected directly into the stratosphere by major eruptions, in which the SO_2 reacts to form sulfuric acid aerosols (Turco et al. 1982; McKeen et al. 1984). Although large amounts of SO_2 are emitted at the surface, little of this water-soluble and reactive gas actually reaches the stratosphere. In fact, during periods of low volcanic activity, carbonyl sulfide (COS) appears to be the dominant sulfur source for the stratospheric aerosol layer. Surface emissions of SO_2 may be important in the production of tropospheric aerosols, thereby introducing potential climatic implications (cf. WMO 1983a, 1983b), but the main effect is to acidify precipitation (acid rain).

The few available measurements suggest that the COS mixing ratio varies little with altitude in the troposphere, which is consistent with the fact that it has a long tropospheric lifetime (Inn et al. 1979). Current tropospheric concentrations are approximately 500 ppt. Recent measurements of carbon disulfide (CS_2) imply very low background concentrations, on the order of 30 ppt (Maroulis and Bandy 1980). There is some indication from laboratory kinetics measurements that CS_2 is converted to COS in the troposphere. Concentrations of CS_2 are also highly variable, suggesting a short lifetime for this species (Wine et al. 1981). COS concentrations are thought to decrease with altitude in the stratosphere as a result of photolysis and reaction with hydroxyl (Sze and Ko 1980; Turco et al. 1980). Dissociation of COS is thought to result in the formation of stratospheric sulfate aerosols (Crutzen 1976; Turco et al. 1980).

Major uncertainties still exist in the sources and sinks of COS and CS_2. Known sources include combustion, biomass burning and decay, and, for CS_2, industrial production (Crutzen et al. 1979; Turco et al. 1980). Volcanic sources of these species appear to be small. Anthropogenic production from combustion sources are thought to account for a large fraction of surface emissions, with coal combustion appearing to be the largest single anthropogenic source of COS (Turco et al. 1980). Whereas direct combustion is high in SO_2, the use of scrubbers (to prevent SO_2 emissions) and conversion procedures, such as synfuel production, coal gasification, and liquefication and shale oil extraction, tend to increase the fraction of the sulfur content of the fuel emitted as COS or SO_2 (Peyton et al. 1976; Hofmann and Rosen 1980; Turco et al. 1980). Conversion of CS_2 may also be an important COS source (Logan et al. 1979; Wine et al. 1981).

Because of the suspected long tropospheric lifetime of COS, future emissions from coal combustion and other anthropogenic sources may lead to substantial increases in the COS concentration. As mentioned earlier, the resultant increase in stratospheric aerosols may have important climatic implications. The anthropogenic emissions of SO_2 are of much current concern, but mainly because of their nonclimatic effects.

6.2.2 Volcanic Eruptions

Volcanic eruptions can inject large amounts of SO_2 and materials such as ash into the stratosphere (Newell and Deepak 1982). Because of the long residence time in the stratosphere, particulate matter injected into and formed within this region tends to stay long enough to be spread over much of the globe, thereby potentially affecting the heat balance and climate (Newell and Deepak 1982). Volcanic aerosols are primarily submicron-sized sulfuric acid droplets that interact strongly with solar and longwave (thermal) radiation. It is generally believed that an increase in the stratospheric aerosol loading could lead to a warming of the stratosphere and cooling of the ground and the troposphere.

A number of studies have attempted to correlate the past temperature change with volcanic activity (Lamb 1970; Baldwin et al. 1976; Pollack et al. 1976; Mass and Schneider 1977; Hansen et al. 1978, 1981; Kelly and Sear 1984). However, the results are not conclusive, primarily because the uncertainties associated with the aerosol composition and the temperature record are high.

The 1883 eruption of Krakatoa was spectacular. Symons (1888) has summarized and discussed many visual observations of abnormal twilight and skylight phenomena due to Krakatoa dust. However, available studies indicate that the subsequent climatic effect appears to be comparable in magnitude to the much smaller eruption of Agung in 1963. (Both volcanoes are located in the tropical region and are not far from each other.) This may be a result partly of the difference in the aerosol composition between the two eruptions.

The 1982 eruption of the El Chichón volcano has drawn a lot of attention and may provide the best recorded case for study of the possible effects of volcanic aerosols on climate (cf. National Aeronautics and Space Administration [NASA] 1982; Pollack et al. 1983; MacCracken and Luther 1984). Pollack and Ackerman (1983) have calculated the effects of El Chichón volcanic aerosols on the radiation budget of the northern tropics during the 6-month period following the eruption. The results indicate that the planetary albedo in this region may have increased by 10%, the total solar radiation at ground level decreased by 2–3% on cloudless days, and the temperature at an altitude of 24 km increased by 3.5 °C. They also indicated that the model calculations are compatible with relevant observations.

6.2.3 Tropospheric Aerosols

Tropospheric aerosols contribute to atmospheric opacity, but their distributions are spatially, temporally, and compositionally heterogeneous (Bach 1976). By interacting with both solar and terrestrial radiative fluxes, aerosols may either heat or cool the surface. Unlike their gaseous counterparts, they may increase planetary albedo by scattering solar radiation back to space, thus reducing the shortwave downward flux to the surface (WMO 1980, 1983b). The net radiative effect on the atmospheric heat balance because of the presence of aerosols is determined chiefly by their intrinsic optical properties including the single scattering albedo, the asymmetry parameter, and the optical depth in the visible spectrum and at 10 μm (which is representative

of the thermal radiation effect). These properties are related to both composition and particle size (Toon and Pollack 1980; WMO 1983a, 1983b). The net radiative effect depends also on extrinsic factors such as surface albedo and local relative humidity. Aerosol growth with relative humidity affects both the index of refraction and size distribution (Hänel 1972; Winkler 1973; Nilsson 1979).

The composition, size, and spatial and temporal characteristics of individually identifiable aerosol types are closely associated with specific sources. Thus, it is appropriate to discuss both aerosol optical properties and potential climatic impacts on a regional source-specific basis. Five such regional aerosol types may be identified, including soot, sulfate, desert, arctic haze, and maritime (Junge 1977; Hänel and Bullrich 1978; Shettle and Fenn 1979). An alternative approach is the specification of a global background aerosol model (Toon and Pollack 1976). Whereas aerosol measurements at background sites have generally not suggested statistically significant interannual trends (Bigg 1977, 1980; Bodhaine 1983), various indicators of subregional aerosol loading suggest that increases may be occurring (Trijonis 1979; Husar et al. 1981).

6.2.3.1 Soot

Recent studies have focused on the influence of soot (or alternatively graphitic or elemental carbon) in the troposphere (Budiansky 1980; Wolff and Klimish 1982). Soot has been measured in both urban (Rosen et al. 1978, 1980; Yasa et al. 1979) and rural (Macias et al. 1981) settings. Measurements of the absorbing and scattering coefficients of tropospheric aerosols at visible wavelengths indicate typical single scattering albedo values of 0.6–0.7 for urban and 0.8–0.9 for rural samples. The lower values in urban areas result from the carbonaceous components in the aerosol (Ackerman and Toon 1981). Additionally, soot has been shown to be present in Arctic haze (Rosen et al. 1981; Heintzenberg 1982; Rosen and Hansen 1984). Because soot is highly absorbing (Twitty and Weinman 1971), its optical properties differ considerably from most aerosol constituents, which typically absorb little radiation (cf. Weiss et al. 1979). Measurements of atmospheric aerosol absorption are subject to large differences because of the various measurement techniques employed, even for well-characterized samples (Gerber and Hindman 1981).

6.2.3.2 Sulfate Aerosols

Atmospheric sulfate aerosols are composed of a variety of compounds, including ammonium sulfate, ammonium bisulfate, sulfuric acid, and a variety of metal salts that result from the oxidation of various sulfur compounds (Graedel 1977; Charlson et al. 1978). The chemical, physical, and optical properties of sulfate aerosols have been studied extensively (Charlson et al. 1978; Whitby 1978; Waggoner et al. 1981). Sulfates have been identified as major constituents of the water soluble, submicron aerosol component in remote oceanic (Fenn et al. 1963; Flyger et al. 1973, 1976; Mészáros and Vissy 1974; Cuong et al. 1974; Mészáros 1978), continental (Mészáros 1978; Hoffer et al. 1979; Lawson and Winchester 1979; Macias et al. 1981) and urban (Altshuller 1973) areas. Concentrations are generally 1–2 $\mu g\ m^{-3}$ in remote areas, less than 10 $\mu g\ m^{-3}$ in nonurban areas, and greater than 10 $\mu g\ m^{-3}$ in urban areas based on annual average data (Altshuller 1973; Hidy et al. 1978).

Intensive studies of sulfate aerosol in major urban areas of the United States (Kneip and Lippmann 1979; Hidy et al. 1980; White et al. 1983) highlight the role of sulfate aerosol and its sources in the urban environment. Long-range transport of sulfate aerosol and its potential impact on regional air quality is of particular concern (Özkaynak et al. 1981). Because sulfate aerosols are particularly efficient scatterers of visible radiation, much attention has recently focused on the potential degradation of the visual range with increased sulfate aerosol loading on regional scales (Cass 1979; Husar et al. 1981; White et al. 1981).

6.2.3.3 Desert Aerosols

Fugitive (i.e., wind-blown) crustal material such as soil and sand contribute to the total loading of aerosol in widespread areas over the tropical Atlantic Ocean (Prospero and Carlson 1972; Prospero et al. 1981), southwestern Asia (Bryson and Baerreis 1967), and the Pacific Ocean (Prospero and Bonatti 1969; Duce et al. 1980). Optical depths

are often sufficient to permit detection by satellites (Fraser 1976). Locally, the phenomenon affects most arid regions (cf. Gillette et al. 1978). Measured size distributions indicate that crustal aerosol components are generally in the larger particle modes with particle radii greater than 1.0 μm (Gillette et al. 1972). Optical properties have been evaluated both for airborne soil and Saharan desert sand (Grams et al. 1974; Patterson et al. 1977; Carlson and Benjamin 1980; Patterson 1981).

6.2.3.4 Arctic Haze

Much effort has been spent at remote areas such as the Arctic basin to determine the characteristics of the background aerosol (cf. Flyger et al. 1973, 1980). A persistent winter diffuse haze layer in the region has been known for some time, and there have been many indications of long-range transport of anthropogenic midlatitude pollution as a potential source (Fenn et al. 1963; Robinson and Robbins 1969; Weiss et al. 1971). More recent interest in the origin of the Arctic haze layer (Rahn and McCaffrey 1980; Barrie et al. 1981; Ottar 1981; Rahn 1981; Hoff et al. 1983; Radke et al. 1984a, 1984b; Rahn and Lowenthal 1984) using elemental tracer analysis techniques has led to the characterization of the winter aerosol as being continental in origin with a major component derived from aged pollution. Source regions for this component apparently vary seasonally, with central and western Eurasian regions predominating in winter and spring, respectively (Raatz and Shaw 1984). Graphitic carbon has been identified as one elemental component (Heintzenberg 1980, 1982; Rosen et al. 1981) that is consistent with the absorbing nature of the aerosol (Patterson et al. 1982; Clarke et al. 1984).

The apparent anthropogenic source of the pollution derived component and the overall environmental sensitivity of the polar ice cap have raised concern regarding potential climatic impacts. With an absorbing aerosol overlying a high albedo surface, a surface heating effect is expected (Shaw and Stamnes 1980; Porch and MacCracken 1982; Cess 1983; Valero et al. 1984; MacCracken et al. 1986).

6.2.3.5 Maritime Aerosols

Aerosols in the marine boundary layer (Junge 1972; Podzimek 1979, 1980) include both a continental-like background type of submicron-sized particles consisting generally of water soluble sulfates (primarily ammonium) and a sea spray-generated component consisting mostly of larger sea salt particles (Junge and Jaenicke 1971; Mészáros and Vissy 1974; Patterson et al. 1980; Gras and Ayers 1983). It is likely that there is a photochemical origin for the sulfate component in remote areas (Mészáros 1973). However, the continental component may be influenced by anthropogenic sources due to long-range transport, especially above the boundary layer. Conversely, the marine boundary layer aerosol may have characteristics found over coastal regions. The sea spray component is generally limited to the lowest (1–2 km) levels of the boundary layer (Delany et al. 1973; Wells et al. 1977), being locally generated by the bursting of bubbles at the sea surface (Woodcock 1953; Blanchard and Woodcock 1957). A transient and highly wind speed-dependent fresh sea spray aerosol exists in the lowest few meters of the atmosphere just above the surface (cf. Gathman 1983; Prodi et al. 1983). Optical properties of the salt component are generally taken from Volz (1972), whereas Barnhardt and Streete (1970), Wells et al. (1977), Shettle and Fenn (1979), and Gathman (1983) have determined properties for marine aerosols.

6.2.4 Solar Constant and Solar Ultraviolet Variations

Energy from the Sun drives both the climate and the chemistry of the atmosphere. Understanding the potential effects of variations in solar irradiance are thus fundamental to determining past and future conditions.

6.2.4.1 Solar Constant Variation

There is a long (almost 150 years) history of measurements of the solar flux using ground-based instruments (e.g., Foukal 1980; Frölich 1981). After adjustment for the presence of the atmosphere and

within the limits of the accuracy of these observations (generally not better than ~1%), no systematic trends have been detected in the solar irradiance at the top of the atmosphere (see Hoyt 1979)—hence, the term solar constant. Balloon- and rocket-borne pyrheliometers have also failed to show conclusively any temporal variations in the solar constant, partly because the problems associated with the variable stratospheric transmissivity (e.g., Kondratyev and Nikolsky 1970) and the noncontinuous nature of the measurements (Willson et al. 1980). However, in recent years considerable progress has been made in improving the solar irradiance measurements, first with the Nimbus-6 and -7 satellites (Hickey et al. 1980) and lately by the Solar Maximum Mission (SMM). Both reveal that total solar irradiance is indeed at least slightly variable, that is, the solar constant is not constant.

There are several possible processes that may contribute to these variations, but a recent review by Newkirk (1983) has indicated that about 30–40% of the observed variance remains unexplained by the models used to interpret the SMM data. It is believed that sunspots dominate the variations on time scales of days to weeks and that these irradiance dips are only slightly compensated by more intense emissions from faculae (see Newkirk 1983). The present data do not lead to any definite conclusions over longer time scales, for example, over the 11- and 22-year solar cycles (Hudson 1983). Because of its strong coupling to the solar luminosity, possible changes in the solar radius can also induce changes in solar irradiance.

North et al. (1983) simulated the possible climatic effects of solar constant variations on time scales of 1 month and longer using a seasonal two-dimensional (latitude-longitude) energy balance model. The model response to the high-frequency forcing was found to be negligible (~0.01°C), whereas the solar constant variation caused by the ~11-year cycle suggested by Hoyt and Eddy (1983) could induce a temperature change of ~0.1°C. North et al. (1983) have also investigated the effect of the variation of the annual forcing caused by the Earth's eccentric orbit around the Sun, which corresponds to a variation in amplitude of the insolation by ~3.4%. The model calculated a temperature change of ~1°C in continental areas, but only ~0.2°C in mid-oceans. Besides investigating the eccentricity effect, Gage and Reid (1981) and Reid and Gage (1983) have also attempted to associate tropical tropopause height variations with variations in the sunspot cycle, but the results were not conclusive.

Molnar (1981), Schatten et al. (1982), and Pittock (1978, 1983) have investigated and reviewed several effects of solar variability on the troposphere, but no significant effects were found. Other possible tropospheric influences, such as those associated with the solar wind, the galactic cosmic ray flux modulations, and the direct solar corpuscular radiation, appear to be small (cf. Eddy 1982) and are the least likely candidates to provide the link between solar variability and terrestrial weather and climate (cf. Pittock 1983). However, further work is necessary to look into the connections between solar activity and tropospheric electricity (cf. Molnar 1981; Pittock 1983).

6.2.4.2 Solar Ultraviolet Variation

The solar ultraviolet (UV) flux, although accounting for less than 1% of the total solar irradiance, exhibits rather large fluctuations. Solar cycle-related variations are much smaller, but still appreciable, in the UV continuum (170–340 nm); the flux in this region has a very strong influence on the stratospheric O_3 content.

Variations of the UV solar flux over both the 11-year sunspot cycle and the 27-day period of solar rotation are well recognized, particularly in the Lyman α region and at wavelengths shorter than 100 nm (Brasseur and Simon 1981; Lean and Skumanich 1983). Results of several studies have indicated that variations in the UV solar flux occur at wavelengths from 150–300 nm over the 11-year cycle (Heath and Thekaekara 1977; WMO 1981; Lean 1983). Prior observational studies (Willett 1962; Hines 1974; Angell and Korshover 1976, 1978; Quiroz 1979; Nastrom and Belmont 1978) have suggested that solar activity may affect stratospheric ozone, temperature, and circulation. However, other studies have questioned the validity of some of these data and the resultant conclusions (London and Haurwitz 1963; Pittock 1978; London and Reber 1979).

Recent modeling studies have indicated that changes in the UV flux at wavelengths greater than 180 nm could affect stratospheric temperatures and the distribution of stratospheric ozone and other

minor constituents (Callis and Nealy 1978; Penner and Chang 1978, 1980; Brasseur and Simon 1981; Natarajan et al. 1981; Wuebbles 1983b; Garcia et al. 1984). Unfortunately, currently available measurements are too limited to accurately deduce the strength of the solar cycle variations at these wavelengths.

For the solar flux variability at wavelengths relevant to the stratopause and below, the analyses of Lean et al. (1982) and Lean (1983), using a three-component model of emission regions on the solar disk, derived changes in solar flux for wavelengths from 145–200 nm (Lean et al. 1982) and 200–300 nm (Lean 1983) over several solar cycles. According to the model of Lean (1983), the solar UV irradiance increased from the minimum to the maximum of solar cycle 21 (minimum, approximately 1975; maximum, end of 1979) by 25% at 200 nm, by 10% at wavelengths from 210–250 nm, and by 2% at 300 nm. This change is appreciably less than the variability suggested by Heath and Thekaekara (1977), but appears to be consistent with more recent data (Brasseur and Simon 1981).

Atmospheric modeling studies, assuming similar solar flux variations to those indicated by Lean et al. (1982) and Lean (1983), derive increases in upper stratospheric temperature of 2–5°C, increases in upper stratospheric ozone of 5–10%, and increases in total ozone of 3–4% from solar minimum to solar maximum (Brasseur and Simon 1981; Wuebbles 1983b; Garcia et al. 1984). Garcia et al. (1984) suggest that NO_x produced in the thermosphere by auroral particle precipitation is transported to the stratosphere. They calculated a significant decrease (~40%) in ozone concentration in the polar winter upper stratosphere from solar minimum to solar maximum because of this effect. Garcia et al. (1984) also have derived a small effect on stratospheric zonal winds of 2–3 m s^{-1} over the solar cycle. All of the theoretical studies suggest that insignificant solar cycle effects would be expected in the troposphere.

If the actual solar cycle effect in the stratosphere is indeed as large as that calculated, it could make detection of trends in stratospheric ozone and temperature caused by anthropogenic influences more difficult to interpret.

6.2.5 Waste Heat

Whenever energy is generated and used, the resultant energy is turned into heat. This released heat is called *waste heat* because it cannot be recaptured and put into a usable form. As pointed out by many researchers, including the review by Bach et al. (1983), this heat can be sizable for local regions. For example, energy fluxes (or power densities) for regions such as Cincinnati, West Berlin, and Los Angeles are 26.2, 21.3, and 21.0 W m^{-2}, respectively. An important question is how this energy flux compares with natural amounts of energy input into the surface-atmosphere system.

Figure 6.1 shows a summary (from Bach et al. 1983) of present and future energy fluxes from many different sources as a function of the power density and the scale of input. Also shown is the net radiation at the surface. This comparison is quite relevant because most of the waste heat enters the climate system near the surface. The main point to be made from this composite figure is that most of the highest energy fluxes are put into very small scales, for example, single cooling towers or power plants. If many more nuclear power plants were to be built, then we could expect that they would have very large energy fluxes associated with them that could have sizable effects on the small to mesoscale (10^2–10^8 m^2) climate.

Cities and metropolitan regions have energy fluxes of a few to 800 W m^{-2} over horizontal areas of 10^8 to 10^{12} m^2. Potential climatic effects on these scales will be discussed in a later section. On the larger synoptic and global scales, the energy fluxes are much smaller, on the order of 0.07 to a few W m^{-2}. Regions such as Germany, Japan, part of the United States, Italy, France, and the central U.S.S.R., for example, have energy fluxes in this range. Note also that Bach et al. (1983) show continental values (estimated for both the present and the year 2050) of approximately 0.02–0.03 W m^{-2}. Likewise their global values range from 0.015 W m^{-2} for the present to 0.6 W m^{-2} for the year 2050. These values are quite small compared with the net radiative balance at the Earth's surface. Although continental and global effects are likely to be small, the mesoscale to synoptic inputs of waste heat over industrialized regions can be a significant fraction of the net radiation budget at the surface.

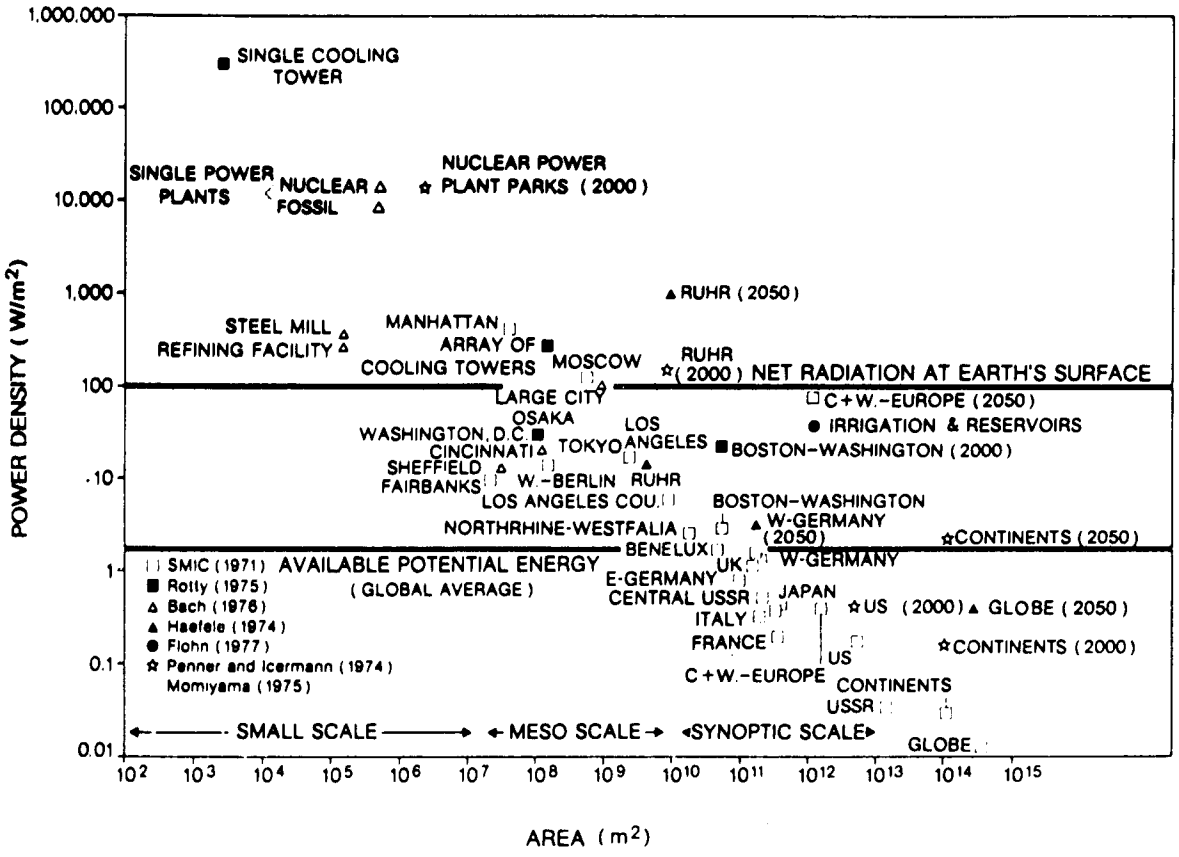

Figure 6.1. Power densities for some of society's activities circa 1970 and for some countries now and in the future. Source: Bach et al. (1983).

Therefore, society's activities could be changing the climate in these regions by the addition of waste heat.

6.2.6 Surface Albedo

Charney (1975) suggested that the creation of regional droughts and deserts, in part, may be caused by feedbacks between biological and physical (i.e., biogeophysical) processes. The hypothesis is that there could be a change in the surface albedo that would perpetuate the desert-forming process because of overgrazing and the denudation of surface vegetation. There have been several studies of the effects of unfenced and uncontrolled grazing adjacent to fenced and controlled grazing. The evidence indicates that the albedo changes are dramatic and could have significant effects over space scales much larger than the area of the albedo modification.

6.2.7 Vegetation Effects

As has been pointed out by many researchers, the surface of the Earth has been undergoing many changes caused by civilization. It has been suggested that the clearing of forests over large continental regions may reduce rainfall in those regions. Shukla and Mintz (1982) and Mintz (1984) give an account of some historical suggestions of this effect. They quote from a biography of Christopher Columbus by his son, who noted changes in the Canary, Madeira, and Azore Islands as a result of deforestation. Apparently before deforestation of these islands, there was much more rain and mist.

Shukla and Mintz (1982) point out that observed data suggest that the measured river water drainage is about one-third of the measured precipitation. This would suggest that evapotranspiration is about two-thirds of the precipitation. Furthermore, during the summer season the evapotranspiration can exceed the precipitation because of stored moisture from the earlier months. This effect may

have an impact on regional climate, especially in light of trends of deforestation. The interactions between surface albedo and vegetation preclude treatment of them as separate quantities.

6.3 PHYSICAL AND CHEMICAL PROCESSES

Increases of the atmospheric constituents such as trace gases and aerosols may have the following three effects on the physical processes of the climate system. First is a direct radiative effect. Trace gases have infrared absorption bands and could contribute to the greenhouse effect while aerosols interact with both the solar and thermal radiation and could alter both the solar albedo and the greenhouse effect. The second effect, caused by climate-chemistry interactions, arises because these atmospheric constituents play an important role in atmospheric chemistry. For example, increases in trace gas concentrations might perturb the distribution and column amount of atmospheric O_3 that could, in turn, affect the climate; some of the gases such as SO_2, COS, CS_2, and NO may undergo atmospheric chemical reactions and form particles containing nitrate and sulfate aerosols, which may affect climate by changing the radiative properties of the atmosphere. Third is the dynamical feedback effect—climate change induced by the previous effects may provide some additional feedback effects associated with changes of atmospheric dynamics. For example, the atmospheric constituent abundances may be altered because of changes in the winds caused by climate changes. On the other hand, changes of the solar constant, surface albedo, and vegetation and increases of waste heat affect directly the energy balance and thus could lead to climate changes.

We discuss the various aspects in this section. Included in this discussion are various model sensitivity studies of possible climate perturbations.

6.3.1 Trace Gases

Study of the climatic effects of trace gases requires a complete treatment of the physical processes of chemistry, dynamics, and radiation and of their interactions, and is therefore more complex than the CO_2 climate problem. Comprehensive three-dimensional models that can include proper treatment of these coupled processes are in an early stage of development. Therefore, whereas the climatic effects of CO_2 have been investigated with a variety of one- to three-dimensional climate models, present knowledge about the climatic effects of trace gases is gathered mainly through the use of one-dimensional models. Two-dimensional models have only recently been used to investigate the problem (cf. Wang and Molnar 1985).

6.3.1.1 Direct Radiative Effect

The radiation budget and the thermal structure of the atmosphere are influenced by the presence of trace gases. The main radiative effect of the gases is modulation of the solar radiation and thermal emission. The principal gaseous absorbers of solar radiation are water vapor in the troposphere and O_3 in the stratosphere. Water vapor absorbs primarily in the near-infrared spectral region, whereas O_3 is most effective in the UV and visible regions. Because of the significant influence of atmospheric chemical processes on O_3, a more thorough discussion of the climatic influence of O_3 is given in the following section.

In the infrared, H_2O effectively blocks thermal emission from the surface except for the window region between 7 and 12 μm (800–1400 cm^{-1}) where O_3, CO_2, and several trace gases (notably N_2O, CH_4, and ClCs with strong absorption bands) contribute additional atmospheric opacity (Figure 6.2; see Wang et al. 1976). Absorption of outgoing thermal radiation in the atmosphere, followed by reradiation at the local temperature, can lead to an increase of the surface temperature, the so-called greenhouse effect. In fact, these trace gases, together with clouds, are mainly responsible for the globally averaged temperature of the Earth being 288 K, some 35 K warmer than the calculated temperature for the planet with its existing albedo. Consequently, a change of trace gas concentrations in the atmosphere can affect the global climate, as demonstrated in the climate model sensitivity studies discussed below.

One-dimensional model sensitivity calculations are in good agreement on the surface temperature increase due to direct radiative effects associated

with increases of trace gas concentrations. Table 6.2 presents a brief summary of these model results, and details can be found in the cited references. Note that the surface-warming effect of individual trace gases could be small, but the total combined effect may be substantial. More discussion of the total effect and comparison with the CO_2-induced warming will be given in Section 6.4.

Wang and Molnar (1985) have used a coupled high and low latitude radiative-dynamical model to study the effect of surface temperature resulting from increases of atmospheric N_2O, CH_4, $CFCl_3$ and CF_2Cl_2. Comparisons of the climate change calculations among the one-dimensional radiative-convective model and the two-dimensional model indicate that the one-dimensional model with the commonly used 6.5°C km^{-1} lapse rate for convective adjustment tends to calculate a much larger surface warming effect than the two-dimensional model. On the other hand, the radiative-convective model based on the use of a moist-adiabatic lapse rate, although not simulating present temperature and humidity distributions realistically, calculates the surface warming induced by trace gases in close agreement with the two-dimensional model. The two-dimensional model results also suggest that the combined effect on surface temperature of increases of these gases is comparable to that due to the CO_2 increase.

Dickinson et al. (1978) have investigated the effects of increased chlorofluoromethanes on regional, zonal, and global climate. A version of the National Center for Atmospheric Research (NCAR) General Circulation Model (GCM) with 5° latitude-longitude horizontal grid and 12 vertical layers was used. This model adopted realistic continental outlines, specified (observed) ocean temperatures, used smoothed orography and surface albedoes derived empirically from satellite observations. The effect of a 20 ppb ClC concentration was included by a supplementary heating term and an additional downward flux of infrared energy at the surface. This additional heating acted like other trace gases in contributing to the greenhouse effect. There was a net radiative cooling in the lower troposphere and heating of the upper troposphere in the model. When changes in surface temperature were neglected, a

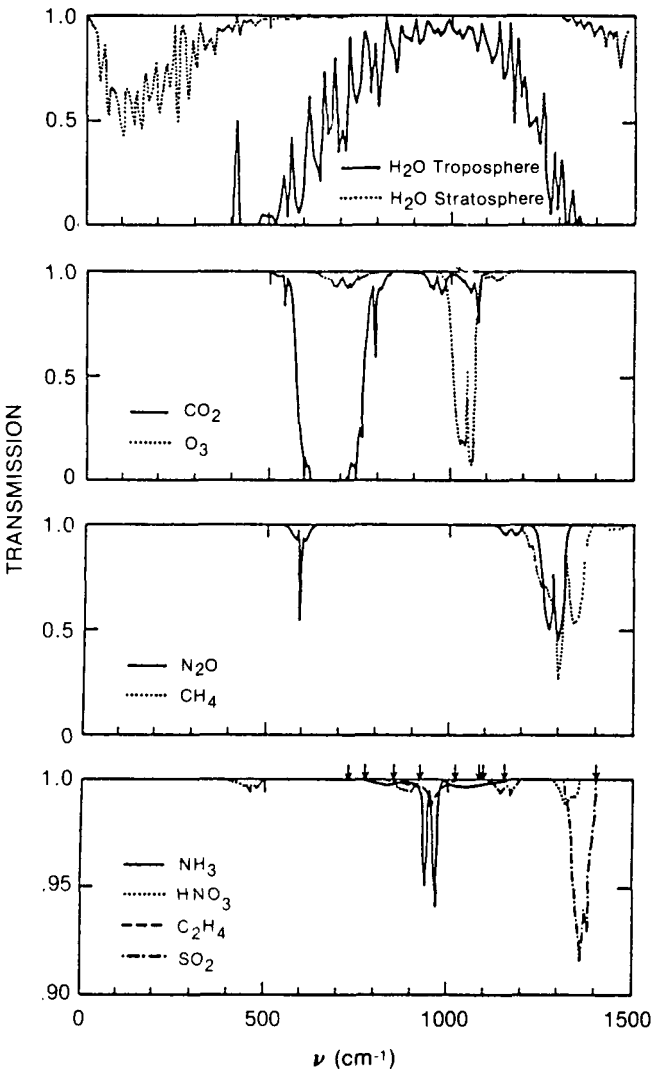

Figure 6.2. Transmission of thermal radiation by atmospheric gases for present-day abundances. Source: Wang et al. (1976).

net cooling near the surface and warming in the upper troposphere occurred. In a more realistic simulation, warming of the ocean and land temperatures would be expected because of the increased downward infrared radiation; this would offset the lower tropospheric cooling rates.

To estimate this latter effect, Dickinson and Chervin (1979) increased the ocean surface temperature in a separate model experiment. They did not compute explicitly the ocean surface temperature response but estimated it by using results from (1) Ramanathan's (1975) energy balance climate model with 10 ppb ClCs, (2) the GCM studies of Manabe and Wetherald (1975) for a doubled CO_2 concentration, and (3) Wetherald and Manabe (1975)

Table 6.2
Sensitivity Studies in Chemical and Climate Models of Potential Trace Gas Influences on Surface Temperature and Total Ozone Column

Chemical	Sensitivity Study	Change in Surface Temperature (°C)	Change in Total Ozone (percent)
CO_2	330 → 660 ppm	+1.5 to +4.5[a]	+3.1[b]
CH_4	1.7 → 3.4 ppm	+0.2 to +0.4[c]	+2.1 to +3.3[b]
$CFCl_3$	Constant emissions	+0.5[d]	−3.3 to −5.5[e]
CF_2Cl_2	at 1977 rates:		
	0 → 1.0 ppb, $CFCl_3$;		
	0 → 2.7 ppb, CF_2Cl_2		
	Constant emissions	+1.0[d]	−15.7[b]
	at double 1983 rates:		
	0 → 1.8 ppb, $CFCl_3$;		
	0 → 5.0 ppb, CF_2Cl_2;		
	0 → 1.5 ppb, CH_3CCl_3		
N_2O	0.3 → 0.6 ppm	+0.3 to +0.4[f]	−8.7 to −10.7[b]
O_3	2 × tropospheric distribution	0.9[g]	
H_2O	Stratosphere 3 → 6 ppm	0.6[h]	

[a] NRC (1983).
[b] Wuebbles (1983b); Wuebbles (unpublished results, 1984).
[c] Wang et al. (1976); Donner and Ramanathan (1980); Lacis et al. (1981).
[d] Estimated based on WMO (1982); for detailed discussion of individual ClCs, see WMO (1982).
[e] NRC (1984).
[f] Wang et al. (1976); Donner and Ramanathan (1980).
[g] Fishman et al. (1980); Hameed et al. (1980).
[h] Wang et al. (1976).

results for a 2% solar constant variation. Instead of directly computing the ocean temperature, Dickinson and Chervin estimated that the ocean temperature change would be 2.0°C in the tropics, increasing up to 4°C at 60°N and 60°S. This should be viewed as a preliminary experiment to the one in which the ocean temperature is explicitly computed. The continental surface temperatures were computed, however. They found that there were large, statistically significant changes in the Northern Hemisphere winter planetary waves. Results of their experiments strongly suggest that many of the regional changes in large-scale planetary patterns may be sensitive to the ocean temperature patterns imposed as boundary conditions. They cautioned about making any definitive statements about the potential climatic impact of increased ClCs from these experiments until physically reasonable coupled ocean-atmospheric models could be used.

6.3.1.2 Climate-Chemistry Interactions

Much of the concern about impacts of chemical processes on the global atmosphere has been directed to possible changes in the O_3 distribution of the troposphere and stratosphere and its subsequent effect on biologically important UV flux and on climate. There are also a number of other ways (see Wang et al. 1980; Wang and Sze 1980; Callis et al. 1983; Owens et al. 1985; and others) in which atmospheric chemical processes can influence climate, particularly through interactions with species that affect the temperature distribution.

The chemistry of the global troposphere is complex, with both homogeneous and heterogeneous processes playing important roles. The homogeneous chemistry is governed by coupling among carbon-, nitrogen-, hydrogen-, and oxygen-containing species. Global tropospheric chemistry is generally considered to have more uncertainties and to be more complex than the chemistry of the stratosphere because of the presence of higher hydrocarbons, long photochemical relaxation times, higher total atmospheric pressure, and a higher water vapor mixing ratio (NASA Panel for Data Evaluation 1983). The hydroxyl radical (OH) is probably the single most important trace gas in tropospheric chemistry because of its importance as a reactive sink for CH_4, CO, CH_3Cl and many hydrocarbons. Hydrogen oxide ($HO_x = OH + HO_2$) chemistry also

appears to be the primary chemical sink for O_3 in the troposphere.

Several mechanisms for interactive tropospheric chemical-climatic effects are now recognized. For example, an increase in the amount of water vapor as a result of a warmer climate should result in an increase in the OH concentration, which can affect CH_4 and O_3 concentrations. There is a close relationship among OH, CH_4, and CO concentrations (a major source of CO is CH_4 oxidation and CO is a major chemical sink for OH); therefore, an increase of any one of these species has significant effects on the others and on other important trace gases (Levy 1971, 1972; Wofsy et al. 1972; Wofsy 1976; Sze 1977; Chameides et al. 1977; Cess 1982). Hameed and Cess (1983) discuss how increased CH_4 levels may result from biogenic sources in an atmosphere with a warmer climate and with an increased CO_2 concentration. In addition, changes in temperature, the amount of clouds, and the amount of rainfall will affect the chemical kinetics rates, which are important to tropospheric chemical processes.

Carbon dioxide and most of the other radiatively active trace gases (e.g., ClCs) that can have an impact on climate are not chemically reactive in the troposphere, where they have their largest climatic impact. However, O_3 is much more complicated. Not only is O_3 chemically reactive, but changes in both tropospheric and stratospheric O_3 can affect climate. The discussion below is devoted to giving an overview of what is known about O_3 climate-chemistry interactions.

Ozone is produced primarily in the middle and upper stratosphere as a result of photolysis of molecular oxygen (O_2) by solar radiation of wavelengths less than 242 nm. The resultant oxygen atoms react rapidly with O_2 to produce O_3. The destruction of O_3 comes about primarily through the catalytic effects of various free radical species, including nitrogen oxides, chlorine oxides, and hydrogen oxides. The spatial distribution of stratospheric O_3 is strongly influenced by stratospheric circulation processes, which are affected by tropospheric dynamics. Tropospheric O_3 is derived in part from the transport of O_3 from the stratosphere, and in part from in situ photochemical production involving nitrogen oxides.

Ozone is of major importance in maintaining the thermal structure in the stratosphere through its absorption of solar radiation in the UV by the Hartley (200–290 nm) and Huggins (290–340 nm) bands and in the visible by the Chappuis (500–700 nm) band. The Hartley band provides the major heating at altitudes above ~45 km. Below ~30 km, absorption by the Chappuis band dominates the heating. In fact, it is believed that stratospheric O_3 is largely responsible for the existence of the tropopause, a nearly isothermal region separating the radiatively equilibrated stratosphere from the more dynamically controlled troposphere. For a moderate change in the column integral of O_3, the changes in UV flux at the surface are confined to the spectral region near 290 to 340 nm.

In the infrared, O_3 has a number of vibration-rotation absorption bands that tend to cool the middle and upper stratosphere and provide a greenhouse effect for the lower stratosphere and the troposphere. In particular, the narrow 9.57-μm (1045 cm^{-1}) absorption band is the most effective because it lies inside the atmospheric window where H_2O is almost transparent. Furthermore, the Planck function at the surface temperature also peaks in this spectral region (near 10 μm). Hence, O_3 can absorb a large quantity of heat emitted from the surface; simultaneously, it radiates heat downward to the troposphere and surface and upward into space. Ramanathan and Dickinson (1979) studied the role of seasonally and latitudinally varying O_3 in the troposphere-surface energy balance and found that on an annual and global basis, O_3 contributes about 20% of the total thermal downward flux from the stratosphere to the troposphere. Thus, it is quite clear that O_3 plays a key role in the atmospheric heat balance.

Results of studies based on the one-dimensional models indicate that the computed temperature profile is sensitive to both the vertical distribution and the column amount of O_3 (Manabe and Wetherald 1967; Reck 1975; Ramanathan et al. 1976; Ramanathan 1980; Wang et al. 1980). The results suggest that the larger the total O_3 column or the lower the height of the maximum O_3 concentration, the warmer the temperatures of the troposphere and the surface.

Wang et al. (1980) investigated further the separate solar and thermal effects of atmospheric O_3

in determining the surface temperature for a typical midlatitude atmosphere. To do this, the O_3 radiative contributions to the thermal cooling and solar heating were excluded in computing the thermal structure. Exclusion of the strong thermal greenhouse effect causes the surface temperature to decrease by 2.6°C, whereas omission of the solar effect warms the surface by only 0.2°C. The results indicate that the thermal effect of O_3 is far more important than the solar effect in influencing the tropospheric and surface temperatures.

These simple model results suggest that O_3 has an important influence on the current climate. Certainly, a perturbation of the O_3 amount in the atmosphere will perturb the thermal structure and heat balance of the surface-atmosphere system and eventually could have direct and indirect climatic effects.

Direct climatic effects may follow from the fact that a change in O_3 may change the way it modulates the solar and thermal radiation. For example, a reduction of stratospheric O_3 may lower the stratospheric temperature, but would produce the following competing effects on the temperatures of the troposphere and surface. First, more solar UV and visible radiation could reach the troposphere and the surface, thus causing a warming effect. Second, the strength of the greenhouse effect would be reduced which, in turn, would induce a cooling effect. Consequently, the effects on the troposphere ultimately depend on the difference between the two opposing effects.

Studies based on one-dimensional radiative-convective models show a cooling of a few tenths of a degree Celsius if the stratospheric O_3 concentration is uniformly reduced by 20–30% (Reck 1975; Wang et al. 1976; Ramanathan et al. 1976). A more detailed study by Ramanathan and Dickinson (1979), who considered the latitudinal and seasonal variation of O_3, confirms the cooling effect, although the effect is found to be smaller because the perturbations in solar and thermal fluxes into the surface-troposphere system nearly cancel. In addition, they have indicated that the tropospheric climate may be as sensitive to a relatively small vertical redistribution of O_3 as it is to a large uniform reduction of stratospheric O_3.

Fishman et al. (1980) have studied the effect of a tropospheric O_3 perturbation on climate. By varying the tropospheric O_3 amount, they examined the change in the net radiative energy input to the surface-troposphere system and estimated that halving the tropospheric O_3 concentration may cool the surface by 0.5°C and doubling may warm it by 0.9°C.

A sensitivity study has been performed by Wang et al. (1980) (Figure 6.3) to examine the surface temperature sensitivity as a function of O_3 perturbations at various altitudes for a midlatitude and a tropical atmosphere. On a per molecule basis, O_3 changes in the lower stratosphere and upper troposphere are more effective than changes in other regions of the atmosphere in causing a surface temperature change. Furthermore, the results suggest that the magnitude of the surface temperature change also depends on the latitude region, with larger changes found in the tropics. The fact that the tropics have a smaller O_3 column and higher surface temperature contributes to the larger surface temperature sensitivity. These results further demonstrate that a perturbation to the O_3 profile itself may affect the climate even if the total column amount remains relatively unchanged, and that investigation of the climatic effects of an O_3 perturbation require consideration of latitudinal effects (two- or three-dimensional models).

Many of the assessment studies in recent years have been directed toward determining the influence of emissions of the chlorocarbons $CFCl_3$ and CF_2Cl_2 on stratospheric ozone (WMO 1981). Of the potential anthropogenic influences on atmospheric O_3, surface emissions of these chlorocarbons remain the most immediate and largest concern (WMO 1981; NRC 1984). Stolarski and Cicerone (1974) postulated the potential role of inorganic chlorine species (ClO_x) in influencing O_3, and Molina and Rowland (1974) determined that the industrially produced chlorocarbons $CFCl_3$ and CF_2Cl_2 have sufficiently long atmospheric lifetimes that they are dissociated in the stratosphere to produce inorganic chlorine, thereby affecting stratospheric O_3. Other chlorocarbons have also been recognized as being potentially significant sources of stratospheric chlorine (Rowland and Molina 1975; Molina et al. 1976; Crutzen et al. 1978; McConnell and Schiff 1978; WMO 1981; Wuebbles 1983a).

A number of other potential influences on stratospheric O_3 have been identified. Crutzen (1970)

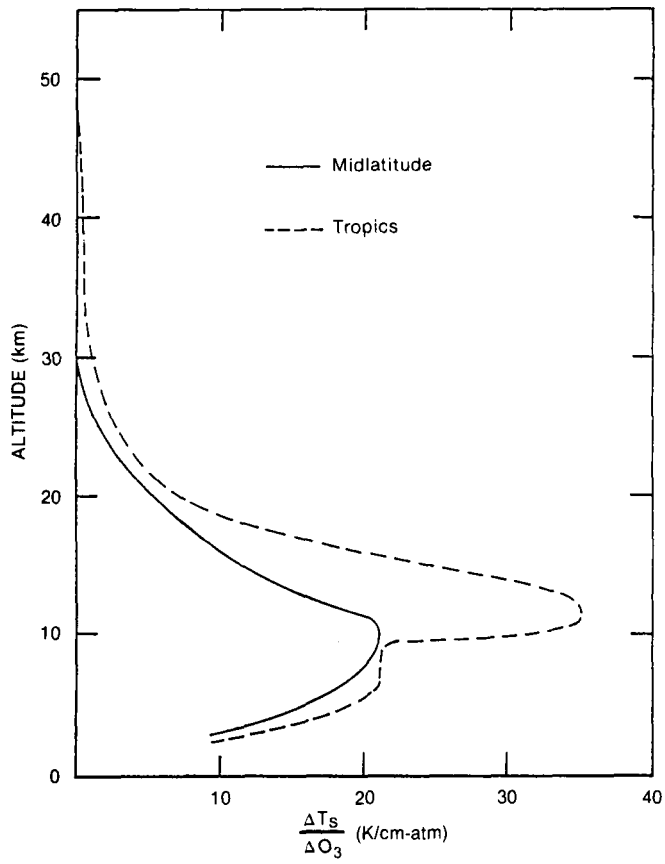

Figure 6.3. Sensitivity of change in surface temperature to changes in O_3 concentration for midlatitude and tropical atmospheres. Source: Wang et al. (1980).

recognized the important role of NO_x in regulating stratospheric O_3, and Johnston (1971) and Crutzen (1971) suggested that the NO_x emitted by high-flying aircraft could affect O_3. Foley and Ruderman (1973) suggested that the atmospheric nuclear weapons tests of the late 1950s and early 1960s should have reduced stratospheric O_3 because of the NO_x produced by the explosions. Crutzen (1974) noted that increases in the global emissions of N_2O could lead to increased stratospheric NO_x, thereby reducing ozone.

Chameides et al. (1977) discussed the possible effects of increased methane levels on tropospheric and stratospheric O_3. Bromine could affect stratospheric O_3 levels (Wofsy et al. 1975), but current bromine concentrations are too small to be important. Tropospheric O_3 concentrations may change indirectly because of changes in stratospheric O_3 and/or changes in the stratospheric-tropospheric exchange rate, but they also may change directly because of chemical influences, such as from anthropogenic sources of NO_x, CO, or hydrocarbons (Liu 1977; Logan et al. 1981; Callis et al. 1983). It has also been estimated that the concentration of ozone in the upper troposphere might have increased as a result of emissions of nitrogen oxides from subsonic aircraft (Liu et al. 1980; Wuebbles et al. 1983). Many recent studies have examined the past and potential future effects of these chemical influences on O_3 (e.g., Chang et al. 1979; Wuebbles 1983b; Wuebbles et al. 1983).

Besides direct chemical interaction with O_3, changes in the stratospheric amount of radiatively important species such as CO_2 can indirectly affect stratospheric O_3 by altering the temperature distribution, which in turn can affect the temperature-dependent chemical reaction rates influencing O_3. Increases in CO_2 concentration reduce stratospheric temperatures, resulting in an increase in total ozone by slowing down the rates of chemical loss reactions involving ozone (Boughner and Ramanathan 1975; Luther et al. 1977). Because the O_3 perturbation caused by CO_2 increase peaks at about 40 km and is very small below ~25 km, the associated effect on surface temperature from CO_2-induced O_3 change has been calculated to be very small. Recent model-calculated steady-state changes in the total O_3 column for assumed changes of CO_2, CH_4, ClCs, and N_2O concentrations are shown in Table 6.2.

6.3.1.3 Dynamical Feedback

As changes occur in the distribution of radiatively active atmospheric constituents such as O_3 and CO_2, the resultant changes in temperature structure could influence tropospheric and stratospheric dynamical processes. Changes in the dynamics could, in turn, affect trace gas distribution. Only a few studies have attempted to examine these complex feedbacks.

The GCM results of Fels et al. (1980) for perturbations of CO_2 and O_3 suggest that, whereas large radiative changes in the atmosphere are calculated, transport processes through most of the stratosphere may not be significantly altered. Their results for a nonrealistic, uniform 50% O_3 reduction suggest that changes in wave activity could occur in the tropical lower stratosphere. Such changes could conceivably further alter the distribution of

O_3 and other trace gases. The results of Geller and Alpert (1980) indicate that for significant changes in the zonal winds below 35 km, corresponding changes in tropospheric wave structure could occur. These results could provide a possible mechanism for stratospheric-tropospheric dynamical interactions. If tropospheric temperature changes can affect tropospheric-stratospheric exchange processes, such effects could be important to the budgets of ozone and other trace gases. Unfortunately, a definitive study of perturbation to the coupled radiative-dynamic-chemical system has yet to be done.

6.3.2 Aerosols

A complete treatment of aerosols would require consideration of microphysical processes (such as coagulation and scavenging), chemical and radiative processes, and the dynamical interactions with the atmosphere. As is the case for trace gases, the problem is more complex than is the CO_2 climate problem. We will limit the discussion here to those aspects of aerosol processes most directly related to potential climate change, rather than also considering processes affecting the atmospheric lifetime of the aerosols.

6.3.2.1 Direct Radiative Effect

Aerosols interact strongly with both solar and thermal radiation. An increase of atmospheric aerosol loading could cause either cooling or heating of the surface-atmosphere system, depending on the altitude and composition of the aerosol layer, the characteristics of the underlying surface, and other factors. The effects of aerosols on the radiation budget have already been discussed in some detail in Chapter 2 of this volume. In this chapter we concentrate on the potential climatic effects of aerosols. Because the climatic effects of aerosols depend significantly on the aerosol optical properties, we briefly discuss the important radiative parameters, and then the model-calculated climatic effects.

Whether there will be a warming or a cooling of the surface-atmosphere system depends on the compensating changes of the solar albedo (cooling) and thermal greenhouse (warming) effects (as discussed in Sections 6.2.2 and 6.2.3). The solar and thermal radiative effects in turn depend on the aerosol single scattering albedo $\tilde{\omega}_0$, the asymmetry factor g, and the extinction coefficients σ_e at 0.55 and 10 μm. Physically, $\tilde{\omega}_0$ is the fraction of energy scattered by the aerosols and g describes the amount of energy scattered in the forward direction. Consequently, larger values of $\tilde{\omega}_0$ and smaller values of g contribute to a larger reflected energy and a larger planetary albedo.

Table 6.3
Range of the Aerosol Radiative Characteristics

	Radiative Characteristics[a]			
Aerosol type	$\tilde{\omega}_0$ (0.55 μm)	1 − g	$\tilde{\omega}_0$ (10 μm)	$\frac{\sigma_e(10\ \mu m)}{\sigma_e(0.55\ \mu m)}$
Soot	0.209	0.66	0.0	0.038
Oceanic	1.0	0.22	0.692	0.250
Dust-like	0.653	0.12	0.558	1.08
Water Soluble	0.957	0.37	0.209	0.019
Maritime	0.989	0.26	0.680	0.19
Continental	0.891	0.36	0.486	0.097
Urban	0.647	0.41	0.173	0.033
H_2SO_4 (75%)	1.0	0.27	0.010	0.050
Volcanic	0.947	0.30	0.130	0.035

[a] σ_e is the volume extinction coefficient (m^{-1}); $\tilde{\omega}_0$ is the single scattering albedo; and g is the asymmetry factor, so that the backscattering fraction $\approx 1 - g$. Source: WMO (1983b).

The thermal greenhouse effect depends strongly on the values of σ_e at 10 μm. The larger the σ_e at 10 μm, the stronger the greenhouse effect. Values of these parameters, presented in Table 6.3, provide some clues to their potential climatic effects, but quantitative evaluations must rely on climate model calculations.

A summary of the climatic effects of stratospheric and tropospheric aerosols is given in Table 6.4. Note that the calculations are based on a variety of climate models for different aerosol compositions and locations, and therefore it is very difficult to compare these model results. Nevertheless, these results strongly suggest that aerosols can significantly affect the climate.

There have been relatively few sensitivity studies of the effects of aerosols on the climate system using GCMs. Recently, Coakley and Cess (1985) performed a study of changes due to the inclusion of tropospheric aerosols in a GCM. Covey et al. (1984) and Aleksandrov and Stenchikov (1983) published studies using GCM model calculations of the potential climatic effects of a large-scale nuclear war. In these studies the solar radiation treatment was

Table 6.4
Change in the Average Surface Temperature ΔT_s and of the Stratospheric Temperature ΔT_{strat} Due to an Aerosol Layer

Sources	Aerosol Location	Climate Model	$\tilde{\omega}_0$	$\Delta\tau_{0.55}$	ΔT_s (°C)	ΔT_{strat} (°C)
Rasool and Schneider (1971)	Homogeneous layer	Energy balance	0.90	0.2	−2.3	
			0.99	0.2	−3.4	
Yamamoto and Tanaka (1972)	Elterman et al. (1969) profile	Energy balance (solar energy)	0.90	0.2	−2.3	
			0.99	0.2	−3.9	
Wang and Domoto (1974)	Elterman et al. (1969) profile	Radiative-convective		0.25	−2.1	
Reck (1976)	Low layers	Radiative-convective		0.26	−1.0	
Harshvardan and Cess (1976)	Stratosphere	Energy balance	1.00	0.03	−1.1	
Charlock and Sellers (1980)	Toon and Pollack (1976) profile for stratosphere	Radiative-convective	0.994	0.125	−1.5	
			0.993	0.1275	−1.4	+1.9
Pollack et al. (1981)	Stratosphere	Radiative-convective	1.00	0.003	+0.01	
			0.98	0.003	+0.1	
Lenoble et al. (1982)	Stratosphere	Energy balance	0.998	0.003	1.1	
			0.944	0.003	−0.45	
Coakley et al. (1983)	Troposphere	Energy balance (solar only)	0.96	Varying with latitude	−3.0	
			0.08	0.16	−3.3	
			0.01	0.07	−2.0	

Source: WMO (1983b).

modified to account for aerosol loading, albeit in a simplified manner.

The effects of tropospheric aerosols are usually ignored in GCMs, an assumption made both because of the simplification of the calculation and because the aerosol burden is often assumed to remain constant. Based on the experiments of Coakley and Cess (1985), about 5 W m^{-2} too much solar radiation may be reaching the surface in the models and the upward flux at the top of the atmosphere may be underestimated by 3.5 W m^{-2}. This amount of energy is roughly comparable to that induced by a doubling of the CO_2 concentration. In their modeling study, a control experiment without aerosols was compared with a second experiment with aerosols. However, the snow cover, sea ice, and ocean surface temperature distributions were held fixed. Therefore, it cannot be compared directly with CO_2 experiments or other climate sensitivity experiments in which these feedback mechanisms would be allowed to interact. The solar heating rates are the principal forcing terms that are modified.

Coakley and Cess (1985) ran experiments for about 400 days. As expected, they found in their July simulation less solar flux arriving at the surface and also less net flux at the top of the atmosphere. The surface temperature cooled by about 0.1–0.2°C over most latitudes. If ocean temperatures were allowed to change, it is expected that the response would be much larger. In the vertical dimension, the largest cooling occurred close to 300 to 400 mb. They compared their results with those of other modeling studies using simpler energy balance models such as those of North et al. (1981) and Coakley et al. (1983) and found similar results for the same feedback restrictions.

A second series of experiments concerns the aerosol loading of the atmosphere because of large-scale nuclear war. Initial studies were carried out by Turco et al. (1983) using a one-dimensional model. The studies with full three-dimensional GCMs are quite recent and should be viewed as preliminary because of the many ad hoc and simplified assumptions about aerosol distributions and poorly known physical processes. The study by Covey et al. (1984) used a version of the NCAR community climate model (CCM), and the Soviet study by Aleksandrov and Stenchikov (1983) made use of

a modified version of the model developed at Oregon State University. A two-dimensional (latitude-height) model study has also been performed by MacCracken (1983a). In all of these experiments there was virtually complete atmospheric absorption of solar radiation by the smoke emitted by fires caused by a major nuclear war. This absorpton acted to heat the upper troposphere and to cool the surface significantly. The distribution and optical treatment of the dust and smoke was highly simplified. There was no attempt to consider the removal of aerosols by various physical processes such as precipitation in these early three-dimensional modeling studies, which are now being improved (e.g., MacCracken and Walton 1984; Malone et al. 1985; Cess et al. 1985).

Typical optical depths being considered are of the order of 3.0. This would cause flux changes of greater than 100 W m^{-2}, which is significantly larger than the CO_2 effect. With this strong solar heating, the entire atmospheric circulation is altered much more significantly than found in typical enhanced CO_2 experiments. These experiments are, in some ways, not comparable to CO_2-induced climate change experiments in that it is assumed that effects will probably be transitory while the change brought about by CO_2 will be essentially permanent. These nuclear war experiments do, however, give a measure of the sensitivity of the climate models to significant changes in the aerosol loading of the atmosphere.

6.3.2.2 Climate-Chemistry Interactions

Several mechanisms have been proposed in which the SO_2 from volcanic eruptions could affect O_3 and other stratospheric chemistry as the SO_2 is converted to sulfuric acid aerosol. Crutzen and Schmailzl (1983) suggest that the photolysis of SO_2 following a major volcanic eruption may locally lead to much enhanced O_3 concentrations.

McKeen et al. (1984) state that although current theory indicates that a decrease in stratospheric OH radicals could conceivably result after a major eruption, a small change in OH concentration appears to be most consistent with the data from the El Chichón eruption. There is no direct indication of a change in O_3 concentration from available atmospheric measurements (at this time there are conflicting results from available ozone measurements following the El Chichón eruption) and no available measurements of OH within a volcanic cloud. Little is known about the direct chemical interactions between aerosols and trace gases in either the troposphere or stratosphere.

6.3.2.3 Dynamical Feedback

Dunkerton (1983) points out that a tropically confined volcanic aerosol heat source can generate an upward residual mean meridional circulation which, given the best current estimate of radiative heating, is capable of retarding the descent of the downward-propagating quasi-biennial mean zonal wind regimes. This mechanism is suggested as a possible explanation for a strong, persistent easterly shear zone during the quasi-biennial oscillation following the Agung eruption in 1963.

6.3.3 Waste Heat

General circulation models have been used to study the effects of waste heat on the climate system. Using an NCAR grid point GCM, Washington (1971) added 24 W m^{-2} of waste heat to all continental areas as an additional term in the net energy balance at the surface. The rationale for such a large (and unrealistic) input was to see whether urban heat island effects could be detected easily with exaggerated forcing. A more realistic experiment (Washington 1972) was performed a year later using the heat input suggested by Weinberg and Hammond (1970), which was proportional to an estimated future population density. The amount of waste heat input was six times less than that used in the earlier studies.

Several experiments performed by Murphy et al. (1976) and Williams et al. (1977a, 1977b, 1979) were different from the earlier NCAR studies (see Llewellyn and Washington 1977), in that ocean energy parks were simulated. An energy park is a small localized region where electrical or thermal energy is produced. Most of the energy eventually would be released as heat. If the energy park were

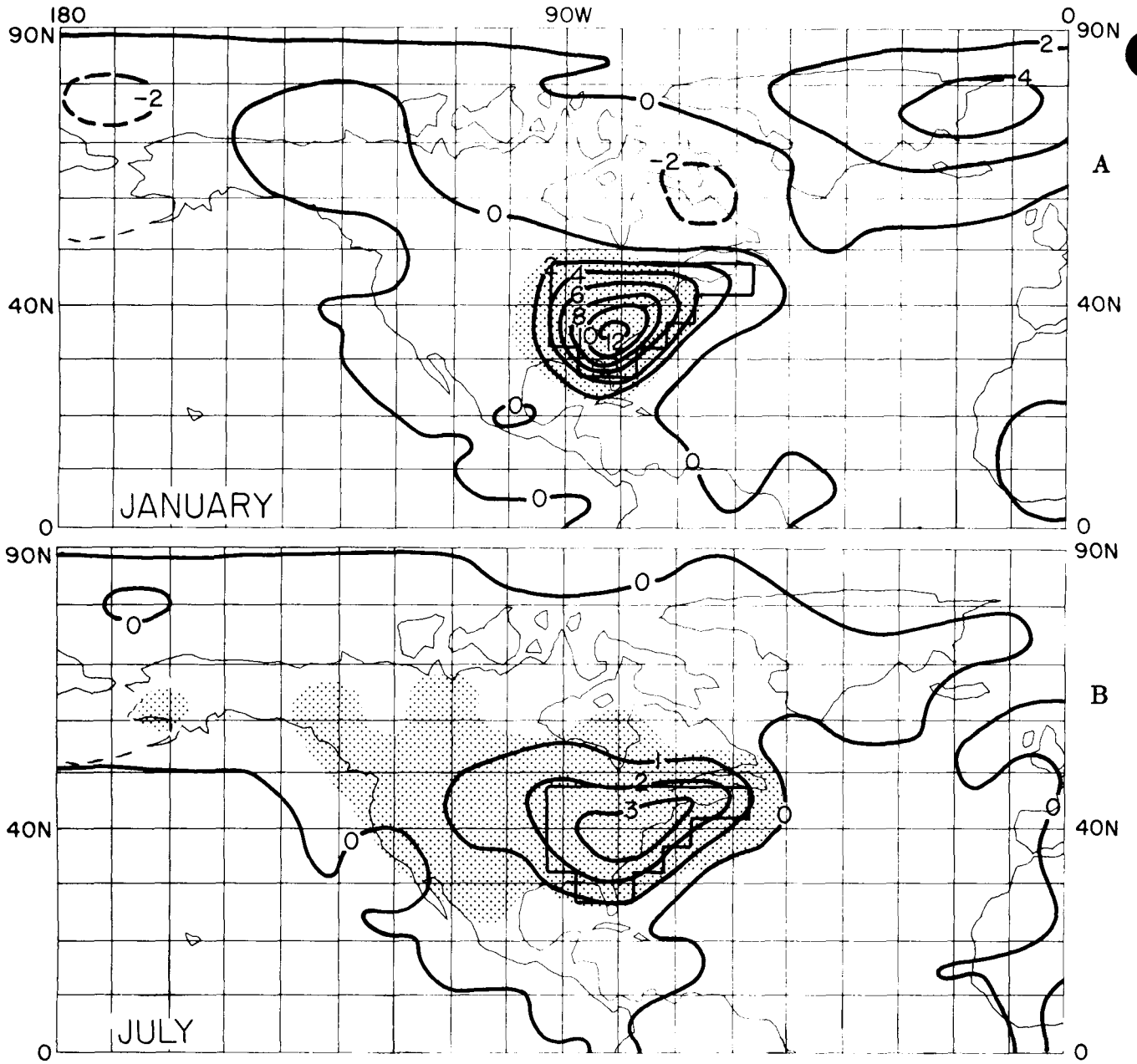

Figure 6.4. Response of ground surface temperature to a waste heat input of 90 W m^{-2} over the eastern United States for (A) January and (B) July. The stippled areas indicate statistically significant differences at the 5% level. Source: Chervin (1980).

over the ocean, then a sizable portion of waste heat would go into evaporative heat flux.

Washington and Chervin (1979) and Chervin (1980) showed in a later series of experiments that when Manhattan Island energy fluxes of 90 W m^{-2} were injected along the east coast of the United States in the GCM, the temperature increase went up to a maximum of about 12°C in January over the region of the prescribed change (Figure 6.4A). The response of the model in July was about 3°C less (Figure 6.4B). The reason the response was larger in winter than summer was that the input due to waste heat was a larger fraction of the net energy balance at the surface during winter and that surface air is more stable in winter. In summer the solar flux is much larger and the fraction of the waste heat compared with the solar flux would be smaller and thus associated with a reduced temperature change.

Statistical tests showed that the results were highly statistically significant. In fact, most of the

response showed a significance level of 5% or less. Another important aspect was that no teleconnection was found with other regions of the globe. Most of the temperature change due to the added waste heat occurred over the prescribed regions where the changes were present.

Robock (1978) has performed waste heat experiments using a zonal energy balance model. The model does not explicitly compute motions; instead, the model relates the meridional sensible heat flux to the meridional temperature gradient. His results showed the waste heat effect to be about 10% of the warming due to a CO_2 increase over the period 1860–2000, during which time it was assumed that the CO_2 concentration would change from 290 to 375 ppm.

6.3.4 Solar Constant

In studying the climate sensitivity to solar constant variations, a convenient and often used measure is the parameter β, defined as

$$\beta = S\frac{d\overline{T}_s}{dS} \times 100,$$

where $\overline{T}_s$ is the global mean surface temperature, and S is the present solar constant. This climate sensitivity parameter is a measure of the change in global average surface temperature expected in response to a 1% change in the solar constant (multiplied by 100). It is important to compare β between different climate models, because the sensitivity of a model to other climate perturbations is roughly proportional to β (cf. North et al. 1981). Table 6.5 presents values of β for several climate models.

These simple model results suggest that a 1% increase in S could warm the surface by 1.1–1.5°C for fixed cloud altitude and no ice albedo-temperature feedback (i.e., β is in the range of 110–150). However, the surface warming may be augmented by the feedbacks from ice albedo and clouds. Ice albedo-temperature feedback results from the possible decrease in polar ice cover that may occur when surface temperature increases. This could result in a further increase in surface temperature because of decreases in the reflected solar radiation from the ground. Thus, ice albedo-temperature feedback may further enhance the model climate sensitivity shown in the model calculations cited in Table 6.5.

Table 6.5
Model Climate Sensitivity to Solar Constant Change

	β (K)			
	No Ice-Albedo Feedback		Ice-Albedo Feedback	
Model				
A. Zonal Energy Balance Models				
Budyko (1969)	155		400	
Sellers (1969)	150		326	
Lian and Cess (1977)	147		184	
Coakley (1979)	152		207	
North and Coakley (1979)	—		163 (167)[a]	
	FCA[b]	FCT[b]	FCA[b]	FCT[b]
B. Vertical Energy Balance Models				
Rodgers and Walshaw (1966)	113			
Manabe and Wetherald (1967)	128	(65)[c]		
Cess (1974)	125	231		
Ramanathan (1976)	121	197		
Wang et al. (1976)	—	160		
Wang and Stone (1980)	110	135	138	188
	Fixed Clouds		Variable Clouds	
C. General Circulation Models				
Wetherald and Manabe (1975)	~185[d]			
Wetherald and Manabe (1980)	200		205	

[a] For the seasonal model.
[b] FCA = fixed cloud altitude, FCT = fixed cloud temperature.
[c] Fixed absolute humidity (all other model results in B use fixed relative humidity).
[d] Averaged from experimental results for changes in solar constant of ± 2%.

Knowledge of the cloud feedback is lacking primarily because of the inadequate understanding of the processes that determine the formation, persistence, and dissipation of clouds. This is one of several key areas identified to be stumbling blocks in climate research (cf. NRC 1983). The one-dimensional radiative-convective models usually assume either fixed cloud altitude (FCA) or fixed cloud temperature (FCT) for climate studies. In the case of a warming climate, the cloud temperatures are lower in the FCT treatment than in the FCA treatment. Consequently, the FCT parameterization calculates a smaller outgoing thermal radiation flux from clouds than the FCA parameterization and thus can yield a larger surface warming, as can be seen in the model results.

Clouds are generated in the GCMs. However, Wetherald and Manabe (1980) have compared the model sensitivity between fixed clouds and clouds that were generated based on their computed climate. These early results indicate that the cloud feedback effect appears to be small, primarily because of the small changes in overall cloudiness and the compensating changes of cloud solar albedo and

the thermal greenhouse effect. Hansen et al. (1984), however, suggest that the cloud feedback processes may be important. This disagreement will not be resolved easily.

6.3.5 Surface Albedo

There have been several sensitivity studies on the impact of surface albedo changes on the climate. Original studies by Charney (1975) involved the use of a simple theoretical model of the directly driven circulation caused by a change in the heating pattern induced by a surface albedo change. Because this study required many assumptions, Charney et al. (1977) performed a more realistic experiment with the NASA Goddard Institute for Space Studies (GISS) GCM. In this experiment the albedo over desert regions was increased from 0.14 to 0.35. Separate experiments were carried out assuming fixed ground wetness and surface hydrology. The precipitation with each type of surface wetness decreased over the deserts, resulting in an increase of surface albedo. The surface albedo increased to the south of the deserts.

Similar experiments were performed with the two-dimensional zonal average atmospheric model by Ellsaesser et al. (1976). They found that increased albedo in the region led to pronounced decreases of precipitation over and around deserts and increases in precipitation to the south of the desert. Chervin (1979) conducted similar experiments with the NCAR third-generation GCM in which the surface albedo over the modeled United States and Sahara desert regions was increased from 0.07 to 0.17 for the former region and from 0.08 to 0.45 for the latter. Chervin also found changes in the pattern of precipitation similar to those of earlier studies. By using standard methods of measuring statistical significance, he found that the differences were significant at the 5% level. In summary, the results support the general hypothesis that biogeophysical processes involving increased surface albedo can lead to further drying, which in turn can lead to an even higher surface albedo.

6.3.6 Vegetation Effects

Shukla and Mintz (1982) performed two climate sensitivity experiments on the role of evapotranspiration on the climate system with the GCM at the NASA Goddard Laboratory for Atmospheres (GLA). They assumed extreme conditions for the changes in evaporative processes at the surface. In one experiment it was assumed that the land surface was completely saturated as if it were a swamp (i.e., perpetually wet). In the second experiment, the surface was assumed to be completely dry so that no evaporation took place. In reality, of course, nature is usually somewhere between the two. Shukla and Mintz (1982) found very large changes in many of the model variables, including surface pressure, precipitation, and temperature. For example, the local precipitation dropped by a factor of three or more and the temperature increased by 15–25°C in the dry case. The reason for the large changes can be understood in terms of simple thermodynamics, in that the dry soil experiment did not have evaporative cooling taking place, and the surface temperature increased as a consequence. Furthermore, Shukla and Mintz (1982) found that the cloudiness changes also provided a feedback in that less cloudiness in the dry experiment resulted in increased solar flux at the surface.

The important point to be made here is that CO_2-induced climate changes could be masked by changes in the surface vegetation, which would have a large effect on the evapotranspiration. These latter changes are not well understood, although there are some suggestions that deforestation may play an important role. Experiments should be conducted with models that have more realistic parameterizations of vegetation and surface processes such as soil moisture, as suggested by Dickinson (1984).

Mintz (1984) has reviewed other GCM experiments and has found similar climate sensitivity to surface processes that is above the model-simulated natural variability. However, because of many compensating mechanisms, such as changes in cloud cover, which are poorly understood and represented, the uncertainty of the model response is quite substantial.

6.4 MODEL PROJECTIONS

It is important to make projections of the possible climate change that may result from the above-mentioned perturbations to provide a reference and comparison to the expected CO_2 climatic effects. However, it is an extremely difficult task because of the many factors involved. For example, one of the major uncertainties for the projected effects of trace gas changes on climate is the projected emission rate of these radiatively and chemically active gases, because the emission rates depend highly on the growth rate of energy consumption, agricultural development, land use, and other factors. A few studies have attempted to estimate growth rates and then, using models, to investigate the possible effects on the atmosphere. Several of these studies are discussed in this section.

6.4.1 Trace Gases

Analyses of calculated trends in O_3 and temperature for past decades and for potential future changes in trace gas concentrations have been performed primarily with one-dimensional vertical coupled radiative-chemical-transport models (Lacis et al. 1981; Wuebbles 1983b; Wuebbles et al. 1983; Wang et al. 1984; Owens et al. 1985; Ramanathan et al. 1985). These various model results tend to be in good agreement with each other. In this section, for illustrative purposes, discussions focus mainly on the results calculated from the Lawrence Livermore National Laboratory (LLNL) and Atmospheric and Environmental Research, Inc. (AER) models.

It should be noted, however, that these one-dimensional models represent only the global and annual mean conditions. Therefore, comparisons of model-calculated O_3 and temperature with data measured at selected sites or averaged over limited regions should not be expected to be totally compatible. Nevertheless, these comparisons are useful as a consistency check of the hypothesis that several different anthropogenic influences are affecting the present global atmosphere.

6.4.1.1 Past Trends in Ozone and Temperature

Global data with which to compare calculated trends in the O_3 and temperature distributions have only been available for the last few decades. Comparisons of these data with model simulations have been performed based on the LLNL model (Wuebbles 1984b). Calculated trends in total O_3 for the 1970s (approximately a 0.45% global increase for the decade) based on increasing CO_2, CH_4, N_2O, ClCs and NO_x concentrations (discussed in Section 6.2.2) compare well with the small increase determined by statistical analysis of Dobson data (see Table 6.6).

A small increase also was calculated for the 1960s. However, it is necessary to consider the effect of the atmospheric nuclear test series during this earlier period. Calculations examining effects from the nitrogen oxides produced in the nuclear tests gave a decrease in total O_3 of about 2.5% (Wuebbles 1983b), which is consistent with analyses of the available O_3 measurements from that period (Reinsel 1981). This consistency cannot, however, be considered as proof of an anthropogenic effect on O_3 because of the limited O_3 data that are available.

Table 6.6
Summary of Comparison Between Calculated and Observed Trends for 1970–1980

	Calculated	Observed	Source
Total Ozone	+0.45%	+0.49 ± 1.35%	Reinsel (1981)
Ozone Distribution			
2–8 km	~ +6%	~ +7%	Angell (1982a)
8–16 km	~ +3%	Some +	Angell (1982a)
16–31 km	~ +1%	Little change	Angell (1982a)
38–43 km	−3.0 to −4.4%	−3 to + 4%	Reinsel et al. (1984)
Stratospheric Temperature			
26–35 km	−0.2 to +0.6°C	−1.5 to +3°C	Angell (1982b)
38–45 km	−1.2 to +1.7°C	−2.5 to +3.5°C	Angell (1982b)
48–55 km	−1.4 to +1.5°C	−3.5 to +5°C	Angell (1982b)

Source: Wuebbles (1983b).

Although the total O_3 column was calculated to have increased during the 1970s, this increase was a result of the cancellation of substantial, but opposing, changes in O_3 with altitude. A maximum decrease of 4.4% in upper stratospheric O_3 was calculated near 40 km for the 1970s. This result compares well with recent, but preliminary, trend estimates from satellite and Umkehr data (see Figure 6.5). In the model calculations, this decrease in O_3 resulted largely from the effect of ClC emissions over

this period. The increasing CO_2 concentrations reduced the ClC impact. When only ClC emissions were considered, a 5.6% decrease in O_3 at 40 km was calculated for the 1970s. The case with ClC emissions only appears to be incompatible with the measured trends in the vertical O_3 distribution.

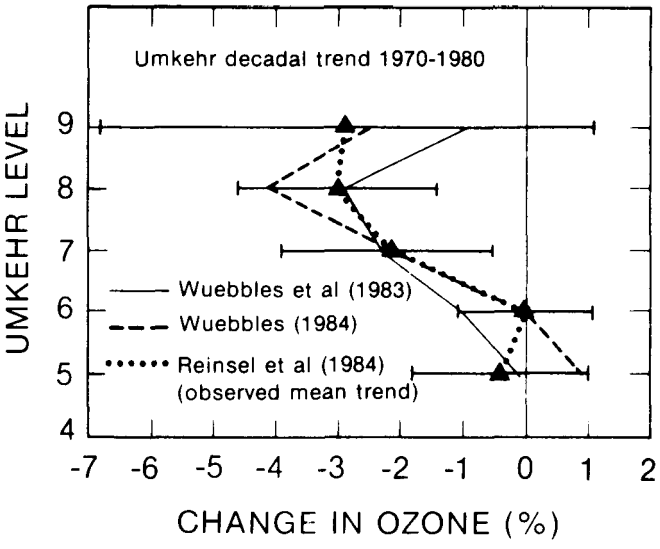

Figure 6.5. Comparison of trend estimate of total O_3 column from Umkehr data for 1970–1980 with LLNL model calculations.

The calculated decrease in upper stratospheric O_3 during the 1970s was approximately balanced by an increase in O_3 concentrations at altitudes below about 30 km. The O_3 concentration at 25 km was calculated to have increased by about 1% during the 1970s. Because this is the altitude of maximum O_3 concentration, this small percentage of change contributed significantly to the overall increase in total O_3 over the decade. Increasing CO_2 and CH_4 concentrations, plus the O_3 recovery mechanism (increased photolysis of molecular oxygen producing O_3 at altitudes below an O_3 decrease), contributed to the calculated O_3 increase at this altitude.

In the upper troposphere, an increase in O_3 during the 1970s of 6.7% (at 8–9 km) was calculated for the Northern Hemisphere because of aircraft emissions and an increasing CH_4 concentration. Little change at these altitudes would be expected in the Southern Hemisphere during the 1970s. By comparison, ozonesonde measurements in the tropospheric layer from 2–8 km in northern temperate latitudes suggest nearly a 7% ozone increase during the last decade, with little change found in the Southern Hemisphere. However, the limited amount of data makes interpretation of these analyses highly uncertain. In general, ozonesonde and Umkehr data suggest similar observed trends to those calculated below 30 km, but there are few stations and the tentatively identified trends must be considered to have large uncertainties at this time (Angell and Korshover 1983a; Reinsel et al. 1984).

The calculated decrease in upper air temperatures during the 1970s is in good qualitative agreement with available observations (Angell and Korshover 1983b). However, the calculated decrease in temperature of 1.7°C at 2.4 mb was appreciably smaller than the 2.5–3.5°C decrease determined from rocketsonde data. The measured decrease of 3.5–5°C near the stratopause is unexplained by current theory. Calculations for the first 3 years of the 1980s suggest that trends in O_3 and temperature are continuing at similar rates to those calculated for the 1970s.

6.4.1.2 Future Projections

The possible effect of future emissions of ClCs, CO_2, CH_4, N_2O, and NO_x were also calculated with the LLNL model (Wuebbles et al. 1984; Wuebbles 1984a). Model calculations that include the effect of chlorocarbon emissions only (scenario D in Figure 6.6a) result in a steady decline in the total O_3 column. These results, which assume constant emissions of the ClCs at 1982 levels, give a steady-state O_3 change of −4.6%, including temperature feedback effects.

As shown in Figure 6.6a, when the effects of other trace gases (CO_2, CH_4, N_2O, NO_x) known to now have increasing concentrations are included, a small increase in total O_3 is calculated for the next 70 years. However, significant decreases in total O_3 could result if chlorocarbon emissions were to increase by as much as 3% per year (scenario B in Figure 6.6b). Declining chlorocarbon emissions (scenario C) would add slightly to the increases in total O_3.

Although the calculated O_3 column shows little change over the next 70 years for scenario A, the calculated O_3 distribution is significantly affected in the troposphere and stratosphere. The change in O_3 with pressure level over this period is shown in Figure 6.7. Similarly, a significant temperature decrease of approximately 12°C at about 40 km is

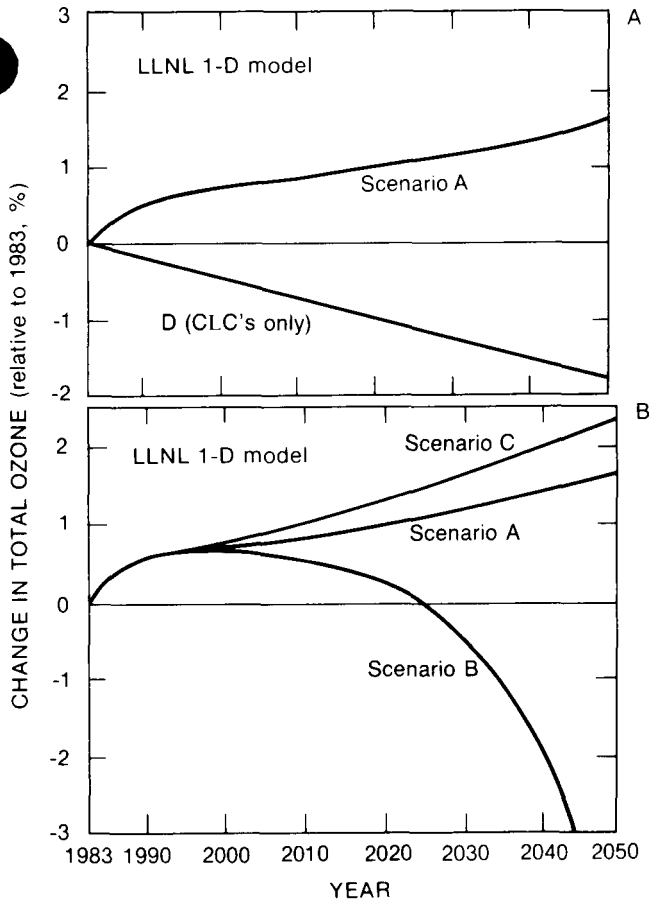

Figure 6.6. (a) Calculated changes in the total O_3 column resulting from chlorocarbon emissions only (scenario D) and from ClCs, CO_2, CH_4, N_2O, and NO_x emissions using the LLNL model. (b) Calculated changes in total ozone for constant ClC emissions at 1983 levels (scenario A), 3% per year increase in ClC emissions after 1983 (scenario B), and 3% per year decline in emissions (scenario C) using the LLNL model.

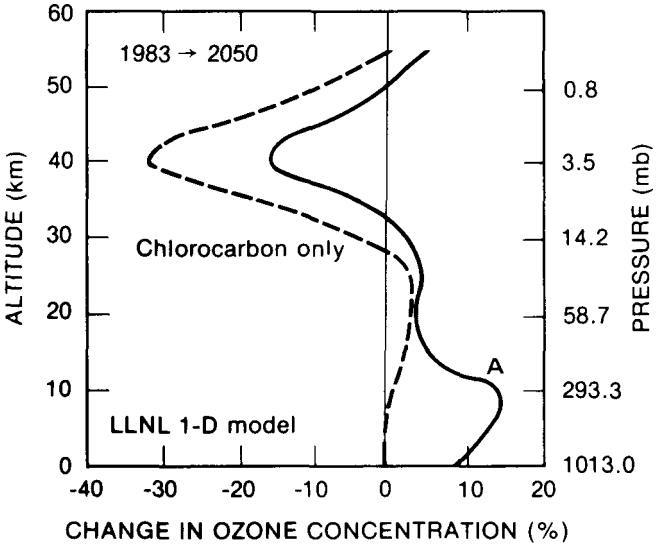

Figure 6.7. Calculated changes in the O_3 distribution resulting from assumed future emissions of chlorocarbons only and with CO_2, CH_4, N_2O, and NO_x emission scenarios using the LLNL model.

calculated for the upper stratosphere over the period from 1983 to 2050 in scenario A.

The potential combined effects on O_3 and tropospheric and stratospheric temperature because of past and projected releases of atmospheric NO_x, CH_4, N_2O, CO_2 and $CFCl_3$ and CF_2Cl_2 have also been estimated using the AER model (cf. Wang 1984; Wang et al. 1984). Particular emphasis has been placed on the effect on tropospheric climate of the O_3 change induced by climate-chemistry interactions. In the AER calculations, both the CH_4 and N_2O concentrations are assumed to increase with growth rates at 1.2 and 0.2% per year, respectively, after 1960. The calculated surface mixing ratios at about 2010 are 2.4 ppm for CH_4 and 0.32 ppm for N_2O. The growth rate for CO_2 after 1980 is assumed to be 0.5% per year, which is regarded as a conservative estimate (see Clark et al. 1982). At 2010, the CO_2 concentration would reach 389 ppm, an increase of 27 and 15%, respectively, when compared with 1950 and 1980 values. The emission rate for ClCs between the years 1950 and 1980 was based on historical data from the Chemical Manufacturers Association (1982). The emission rate after 1980 is assumed to be constant at the 1980 production rate. The past and projected NO_x injection rates were taken from Bauer (1982) and Oliver et al. (1977), who estimated that the NO_x emission was 5.4×10^7 kg y^{-1} in 1950 and could reach 2.64×10^9 kg y^{-1} in 1990 and then remain constant afterwards. These scenarios are qualitatively similar to those of the LLNL study.

Based on these scenarios, the O_3 perturbation calculated for the period 1950–2010 is shown in Figure 6.8. It can be seen that O_3 increases below ~26 km and decreases above it. The maximum O_3 increase of ~36% occurs around 7 km due, in part, to aircraft NO_x emissions and, in part, to the elevated level of tropospheric CH_4. The maximum O_3 depletion of about 22%, however, is found at 42 km because of the increase of ClCs. Because of the compensating changes in O_3 in the stratosphere and troposphere, the net increase in the O_3 column is small (~1.0%). The O_3 column increases for the periods 1950–1980 and 1980–2010 are calculated to

be +0.5 and +0.4%, respectively. For the latter period, the altitude distribution of the changes (Figure 6.9) is very similar to the total change over the period 1950–2010, but with smaller magnitude. A maximum depletion of 15% at 42 km and a maximum increase of 16% at 7 km were calculated.

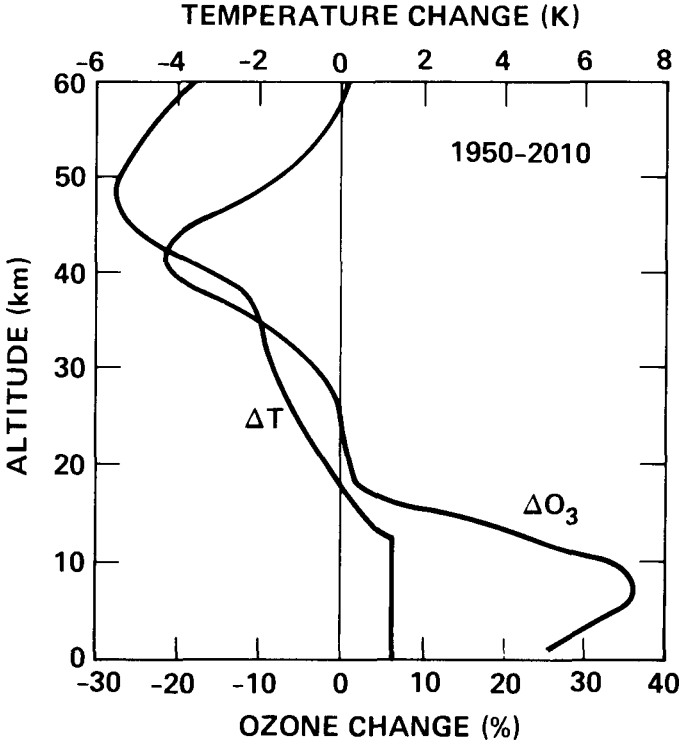

Figure 6.8. One-dimensional model-calculated changes of atmospheric O_3 and temperature between 1950 and 2010 from combined anthropogenic emissions of NO_x, CH_4, N_2O, CO_2 and ClCs. Source: Wang et al. (1984).

The effect on surface temperature due to such an O_3 perturbation is, however, not small because of the large increases of O_3 in the upper troposphere and lower stratosphere, where surface temperature sensitivity is high (see Figure 6.3). Table 6.7 shows the computed surface temperature change ΔT_s for the periods 1950–1980 and 1980–2010 from anthropogenic emissions of CO_2 only (case A) and of NO_x, CH_4, N_2O, CO_2, and ClCs (case B). Note that the latter case includes the effect due to the associated O_3 perturbations.

The results indicate that increases of CO_2 alone could increase the surface temperature by 0.25 and 0.39°C respectively, for the two periods. However, the results also suggest that the surface warming caused by increases of other gases is the same as that caused by CO_2 in the 1950–1980 period and

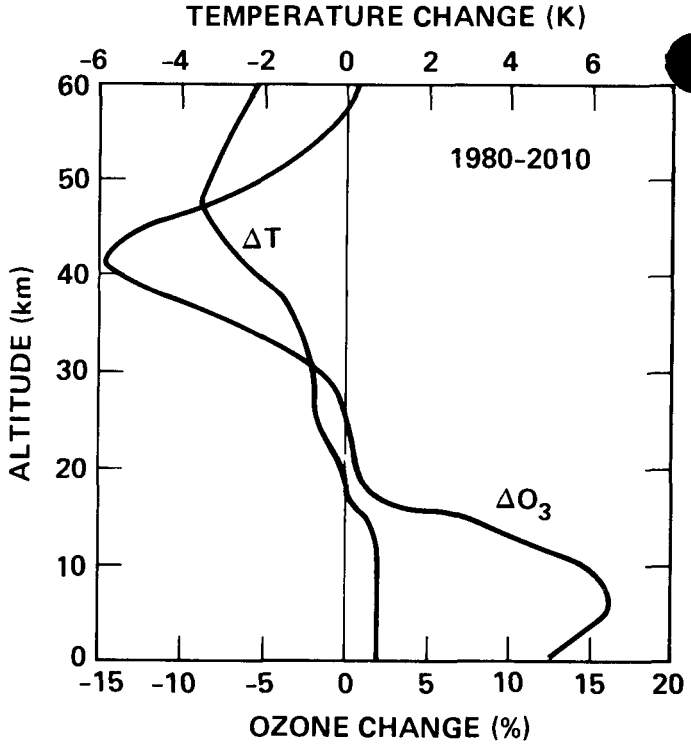

Figure 6.9. Same as in Figure 6.8, but between 1980 and 2010. Source: Wang et al. (1984).

Table 6.7
Calculated Surface Temperature Change ΔT_s for the Periods 1950–1980 and 1980–2010 Caused by the Combined Effect of Simultaneous Increases of Atmospheric Trace Gases and the Associated O_3 Perturbation

Case	Scenario	ΔT_s(°C) 1950–1980	ΔT_s(°C) 1980–2010
A	CO_2	+0.25	+0.39
B	CO_2 + NO_x + CH_4 + N_2O + O_3 + ClCs	+0.50	+0.80

Note: Physical parameterizations used in the one-dimensional model are fixed cloud altitude, fixed relative humidity, and no ice-albedo feedback. Source: Wang et al. (1984).

becomes slightly larger in the 1980–2010 period; for example, for the latter period, anthropogenic emissions other than CO_2 could warm the surface by 0.41°C. It is important to note that the warming effect for changes other than that of the CO_2 concentration can be attributed (roughly) equally to the direct radiative effects of NO_x, CH_4, N_2O, and ClCs and to the indirect radiative effect associated with the induced O_3 perturbations of these anthropogenic emissions.

The combined effect on stratospheric temperature for the period 1950–2010 is shown in Figure

6.8. It can be seen that a small warming is calculated between 12 and 18 km while the middle and upper stratosphere is cooled, with a maximum cooling of 5.5°C occurring at about 48 km, which is a few kilometers higher than the point of maximum O_3 depletion. The distribution of the temperature change for the period 1980–2010 (Figure 6.9) is very similar to that for the total period shown in Figure 6.6. The magnitude of stratospheric temperature change is smaller, however, with a maximum temperature decrease of 3.5°C at about 48 km. These results suggest that to detect anthropogenic influences on the stratosphere, it may be more useful to monitor changes in the vertical distribution of ozone and temperature distribution than to rely primarily on measurements of the total ozone column.

Recently, Wang and Molnar (1985) have used a simple two-dimensional (latitude-altitude) model to estimate the potential greenhouse effects due to increases of N_2O, CH_4, and CFCs on the time scale of decades. In this study, the effect of O_3 perturbations associated with the increases of these trace gas concentrations was not included. The results suggest that these trace gases could potentially augment the surface warming due to a CO_2 increase by more than 60%.

6.4.2 Aerosols

Both stratospheric and tropospheric aerosols have the potential to induce significant climatic effects. However, at present, the primary factors preventing reliable prediction of the future effect of aerosols on climate are large uncertainties about aerosol optical properties, particularly anthropogenic aerosols, and lack of knowledge of how these will change in the future.

6.4.3 Waste Heat

The waste heat experiments that have been performed thus far with general circulation models are limited. Because the amount of energy flux over large regions is small for present energy use levels, no experiments have been carried out that consider future projections of energy use.

6.5 UNCERTAINTIES AND DISAGREEMENTS OF MODEL RESULTS

6.5.1 Simple Models

The vast majority of model calculations of the potential climate-chemical effects on the global atmosphere have been done with one-dimensional models of atmospheric processes. Although such models can include detailed representations of the vertical distribution of atmospheric chemical and radiative processes, these models only crudely represent the effects of transport processes and do not consider adequately the variations with season and latitude that may be important in determining long-term trends in O_3 levels and temperature. However, more limited studies with higher-dimensional models have generally verified the results from one-dimensional model studies.

Much effort has been put into attempts to validate the diagnostic and prognostic capabilities of these simple models. However, measurements of the distribution of radiative properties and trace species concentrations in the global atmosphere are limited. The results of comparisons with the present atmosphere are inconclusive because of the limited number of measurements. Such comparisons, while necessary, are not a sufficient condition for the validity of a model's prognostic capabilities. Attempts at validating the prognostic capability have also been inconclusive, although these attempts have provided some increased confidence in the overall representativeness of the models in treating atmospheric processes.

Analyses of the effects on O_3 chemistry from solar particle capture events (Crutzen et al. 1975; Heath et al. 1977), the nuclear test series (Chang et al. 1979; Wuebbles 1983b), solar eclipses (Wuebbles and Chang 1979; Starr et al. 1980), and the few comparisons with measurements of diurnal variations of trace gases have helped the validation process. Comparisons of the observed trends in ozone and other gases over recent decades with model calculations have been surprisingly good (Wuebbles 1983b; Wuebbles et al. 1983; Reinsel et al. 1984), but unfortunately, the incompleteness of the data base greatly limits the significance of such comparisons. Likewise, comparisons of model results with observed trends in upper atmospheric temperatures

are also limited by the available data (Wuebbles 1983b).

A number of studies have attempted to analyze historical records to determine actual global changes in surface temperature over the last century (see Chapter 4 of the SOA on Detection of Climate Change). Hansen et al. (1981) and others have invoked changes in atmospheric CO_2, stratospheric aerosols from volcanic eruptions, and solar activity to attempt to explain many of the general features of the global temperature variations over the last 100 years. However, as discussed by NRC (1983) and MacCracken (1983b), there are many uncertainties associated with these analyses (see Wigley et al. 1985).

6.5.2 Trace Gases

Although it is quite clear that perturbation of trace gas concentrations and their associated changes in O_3 can influence the climate; the magnitude, and sometimes (particularly for the effect of O_3 change) even the sign, however, remains uncertain.

From the discussion presented in the previous sections and in Chapter 2 of this volume, it is evident that the accuracy of the trace gas climate-chemistry calculations depends on the accuracy of the spectroscopic data, radiation approximations adopted in the models, atmospheric chemistry, the abundance and distribution of the trace gases, and other dynamical and physical processes. The available spectroscopic data and radiative transfer algorithms used in the models have always been assumed to be adequate. However, model comparison studies (cf. Luther 1982) have indicated that the range of uncertainty in the CO_2 thermal radiation flux calculations between different models is quite large, because of the differences in the gaseous absorption data as well as the approximate radiation treatments adopted in the models. Similar reasons were found for the large difference in the calculated climatic effect of increasing concentrations of ClCs between different models (see Ramanathan 1975; Wang et al. 1976; Hansen et al. 1981; Clark et al. 1982).

In addition, model-calculated trace gas climatic effects also depend on the model parameterizations of humidity, cloud, and ice albedo feedbacks. For example, the range of the calculated surface warming in one-dimensional models caused by an increase of ClC concentrations from 0 to 2 ppb is found to lie in the range of 0.3–0.9°C (see Table 6.8). The difference in model results depends on the parameterizations of the physical processes that are used. Because the physical processes influencing the concentrations of radiatively important chemical trace gases are not well understood, proper analysis of the radiative effect involves complex consideration of radiative, dynamical, and chemical processes and their interactions. Particular regard must be paid to stratospheric-tropospheric exchange mechanisms and to the atmospheric water budget.

Table 6.8
Effects of Physical Parameterizations on One-Dimensional Vertical Radiative-Convective Model-Calculated Surface Temperature Increase ΔT_s Caused by Increases of ClCs from 0 to 2 ppb

Case	ΔT_s (°C)	
	Calculation with Data of Kagann et al. (1983)	Calculation by Wang et al. (1976) with Data of Varanasi and Ko (1977)
1. 6.5 °C km^{-1} critical lapse rate		
A. FRH + FCA + No IAT	0.46	0.39
B. FRH + FCA + IAT	0.52	
C. FRH + FCT + No IAT	0.68	0.57
D. FRH + FCT + IAT	0.94	
2. Moist-adiabatic critical lapse rate		
A. FRH + FCA + No IAT	0.26	

Abbreviations: FRH, fixed relative humidity; FCA, fixed cloud altitude; FCT, fixed cloud temperature; IAT, ice albedo-temperature feedback. Source: Wang et al. (1984).

It is difficult to assess quantitatively uncertainties in the model-calculated climate-chemistry interactions, especially based on one-dimensional model results. However, sources of uncertainties in the model-calculated effects on O_3 and climate may arise from (1) the treatment of humidity, clouds, and the use of the average critical lapse rate to approximate the vertical transport of heat by atmospheric motions; (2) the complexity and incomplete understanding of the atmospheric chemistry; and (3) the inadequacies in the basic formulation of one- and two-dimensional models. Presumably some of the uncertainties discussed here may be narrowed when more atmospheric data and more sophisticated models become available (e.g., Wang and Molnar 1985).

One of the most significant uncertainties in analyses of effects from past and possible future changes in trace gas concentrations has been the choice of scenarios used in model calculations of the trace gas effects. Significant uncertainties remain in understanding the budgets and global trends of such gases as CH_4, N_2O, CO, several of the chlorocarbons, most of the hydrocarbons, and NO_x emissions from surface and aircraft sources. A regularly updated reference set of scenarios would provide a common basis for model intercomparisons.

Despite recent improvements in the understanding of overall stratospheric chemistry, much remains to be done, for example, to quantify errors, to identify preferred reaction pathways, and to measure reactions under atmospheric conditions. These uncertainties are particularly relevant in the lower stratosphere where pressure and temperature dependencies of rate coefficients are most critical. Many of the changes in the sensitivity of perturbation results for O_3 over recent years have been because of changes in rate coefficients involving HO_x species. Significant uncertainties remain in the chemistry of these species.

Despite the importance of global tropospheric chemistry to understanding the composition of both the troposphere and stratosphere, many uncertainties remain. The most important sink for many of the important trace gases is reaction with OH, yet very few measurements of OH exist either in the troposphere or stratosphere. The role of nonmethane hydrocarbons in determining the troposphere OH distribution is essentially unknown. Lack of data on the NO_x content of the troposphere, is another significant uncertainty. The controlling factors in the origin and destruction of tropospheric O_3 have been controversial for some time (Chameides and Walker 1973; Pruchniewiez 1973; Crutzen 1974; Chatfield and Harrison 1976; Fishman and Crutzen 1977; Liu et al. 1980; Fishman 1981; Logan et al. 1981). The distribution of O_3 in the troposphere depends critically on the amount of NO_x and on the role of dynamical processes that are not yet well understood.

Many of the feedbacks between trace gases and the global chemical-climate system are poorly understood. As an example, the removal rates of water soluble gases and their dependence on tropospheric water content are only crudely known.

6.5.3 Aerosols

It is very difficult to compare model calculations of aerosol climatic effects because the optical properties used in the different models are quite different, as discussed in Section 6.3.2. However, in recognizing the importance of aerosols on climate, a model intercomparison program has been recently organized to compare the results from climate models with specified aerosol inputs (cf. WMO 1983b).

6.5.4 Waste Heat

Future changes in waste heat are strongly influenced by uncertainties in future energy growth. In addition, past model studies have inserted the waste heat in the surface energy balance, whereas it really should be put in as a component to the surface boundary layer parameterization. This would allow for immediate dispersion of heat (or moisture) as lofted plumes. There is also large seasonal and daily variation in waste energy that has not been included in modeling studies. Perhaps these effects could be modeled with smaller-scale models and then put into GCMs in parameterized form because the details cannot be adequately accounted for with the available GCM grid sizes.

6.6 SUMMARY

In this chapter the various natural and anthropogenic factors (other than CO_2) that may affect the climate have been reviewed. The purpose is to summarize our understanding of these factors and their potential future climatic effects so that, on the time scale of a few decades, CO_2-induced climate change can be viewed in a proper context. The factors we discussed include trace gases, anthropogenic and volcanic aerosols, variation of the solar constant, change of surface characteristics, and releases of waste heat.

We have discussed the origins of the various natural and anthropogenic perturbations, the physical and chemical processes and their interactions, model sensitivity calculations, and model projections of their potential future climatic effects. The discussions center on trace gases and aerosols because of their potentially large climatic effects.

It appears that the increases of atmospheric trace gases could have important climatic effects. The model calculations suggest that the combined effect of increasing atmospheric trace gases and the associated change of atmospheric ozone and water vapor distributions could potentially warm the climate to a magnitude comparable to that from the increase in CO_2. Aerosols of anthropogenic origins may have substantial effects on regional climate whereas volcanic aerosols may have an effect on large-scale climate for up to a few years after injection into the atmosphere.

Changes of surface characteristics and releases of waste heat may also have substantial effects on the regional climate, but these effects are most likely to be small when compared with the effect of a CO_2 increase. Changes in the solar constant could have an effect on the global scale, but the time scale is much longer.

There is much more that needs to be learned with regard to the natural and anthropogenic factors mentioned above that may affect the climate. A brief summary of those needs is presented in the next section.

6.7 FUTURE RESEARCH NEEDS

In this section, some of the most important research needs are outlined (based on the prior discussion) before an adequate analysis of the role of trace gases and other perturbations can be addressed within the CO_2 assessment program. We restrict our discussion to those that differ from the needs to study the climatic effects of CO_2 already recognized. Some of the most important needs are listed under each research area. The ordering does not imply relative priority.

6.7.1 Modeling Activities

Modeling will continue to play an essential role in evaluating future perturbations. A number of activities must be pursued:

1. The development of multidimensional (two- and three-dimensional) models that include the feedback processes affecting atmospheric chemistry, dynamics, and radiation.
2. The development of trace gas (CO_2, CH_4, N_2O, CO_2, ClCs, NO_x, COS, etc.) scenarios for estimating quantitatively their climatic effects and for model intercomparison purposes (see below).
3. Better understanding of the source and sink processes affecting trace gas concentrations and aerosols.
4. Intercomparison of models and data to better understand the agreements and disagreements between models and between models and data.
5. Model sensitivity calculations to link causes and effects associated with trace gases, aerosols, waste heat, and changes of surface characteristics.

6.7.2 Laboratory Measurements

Laboratory measurements are needed in order to provide input data for modeling chemical and radiative processes. The following tasks are of special importance.

1. Refined techniques for measuring HO_x kinetics under tropospheric and stratospheric conditions.
2. Measurements of the temperature and pressure dependences of trace gas infrared absorption band strengths.
3. Evaluation of the possible importance of molecule-molecule reactions under tropospheric and stratospheric conditions.
4. Measurements of aerosol optical properties such as the index of refraction.
5. Refined techniques for studying heterogeneous and liquid phase chemistry.

6.7.3 Atmospheric Measurements

Some quantities and processes must be measured in the environment. The information is necessary both to carry out the modeling calculations and to verify that the calculations are correct. The following observations are of particular importance.

1. Long-term trends of important trace gases, including CH_4, CO_2, N_2O, ClCs, COS, O_3, and other species.
2. Geographical distributions of tropospheric and stratospheric temperatures and O_3 concentrations.
3. Surface fluxes of trace gases.

4. Tropospheric and stratospheric concentrations of short-lived gases (e.g., NO, NO_2, OH, HO_2 SO_2) and the longer-lived reservoir gases (e.g., chlorine nitrate [$ClONO_2$]).
5. Accurate measurements of the solar constant.
6. Measurements of atmospheric aerosol loadings, waste heat release, and surface albedo and vegetation changes.
7. Measurements to establish the important processes governing tropospheric-stratospheric exchange of atmospheric constituents.

REFERENCES

Ackerman, T. P., and Toon, O. B. 1981. "Absorption of Visible Radiation in Atmosphere Containing Mixtures of Absorbing and Nonabsorbing Particles." *Applied Optics 20:*3661–3668.

Aleksandrov, V. V., and Stenchikov, G. L. 1983. "On the Modeling of the Climatic Consequences of the Nuclear War." *Proceedings on Applied Mathematics.* The Computing Centre of the USSR Academy of Sciences, Moscow.

Altshuller, A. 1973. "Atmospheric Sulfur Dioxide and Sulfate Distribution of Concentration at Urban and Nonurban Sites in the United States." *Environmental Science and Technology 7:*709–712.

Angell, J. K. 1982a. "Trends in Total Ozone and Vertical Ozone Distributions." 197–200. In R. R. Reck and J. R. Hummel (eds.), *Interpretation of Climate and Photochemical Models, Ozone, and Temperature Measurements.* American Institute of Physics, New York, New York.

Angell, J. K. 1982b. "Trend in Surface and Upper Air Temperatures." 241–245. In R. R. Reck and J. R. Hummel (eds.), *Interpretation of Climate and Photochemical Models, Ozone, and Temperature Measurements.* American Institute of Physics, New York, New York.

Angell, J. K., and Korshover, J. 1976. "Global Analysis of Recent Total Ozone Fluctuations." *Monthly Weather Review 104:*63–75.

Angell, J. K., and Korshover, J. 1978. "Recent Rocketsonde-Derived Temperature Variations in the Western Hemisphere." *Journal of the Atmospheric Sciences 35:*1758–1764.

Angell, J. K., and Korshover, J. 1983a. "Global Variations in Total Ozone and Layer-Mean Ozone: An Update Through 1981." *Journal of Climate and Applied Meteorology 22:*1611–1627.

Angell, J. K., and Korshover, J. 1983b. "Global Temperature Variations in the Troposphere and Stratosphere 1958–1982." *Monthly Weather Review 111:*901–921.

Bach, W. A. 1976. "Global Air Pollution and Climatic Change." *Reviews of Geophysics and Space Physics 14:* 429–474.

Bach, W. A., Crane, J., Berger, A. L., and Longhetto, A. (eds.) 1983. *Carbon Dioxide: Current Views and Developments in Energy/Climate Research.* D. Reidel Publishing Company, Dordrecht, The Netherlands.

Baldwin, B., Pollack, J. B., Summers, A., and Toon, O. B. 1976. "Stratospheric Aerosols and Climatic Change." *Nature 263:*551–555.

Barnhardt, E. A., and Streete, J. L. 1970. "A Method for Predicting Atmospheric Aerosol Scattering Coefficients in the Infrared." *Applied Optics 9:*1337–1344.

Barrie, L. A., Hoff, R. M., and Daggupaty, S. M. 1981. "The Influence of Mid-Latitudinal Pollution Sources on the Haze in the Canadian Arctic." *Atmospheric Environment 15:*1407–1419.

Bauer, E. 1982. "Natural and Anthropogenic Sources of Oxides of Nitrogen (NO_x) for the Troposphere." Department of Transportation, Federal Aviation Administration Report No. FAA-EE-82-7, Washington, D.C.

Bell, P. R. 1982. "Methane Hydrate and the Carbon Dioxide Question." 401–406. In W. C. Clark (ed.), *Carbon Dioxide Review: 1982.* Oxford University Press, New York, New York.

Bigg, E. K. 1977. "Some Properties of the Aerosol at Mauna Loa Observatory." *Journal of Applied Meteorology 16:*262–267.

Bigg, E. K. 1980. "Comparison of Aerosol at Four Baseline Atmospheric Monitoring Stations." *Journal of Applied Meteorology 19:*521–533.

Blake, D. R., Mayer, E. W., Tyler, S. C., Makide, Y., Montague, D. C., and Rowland, F. S. 1982. "Global Increase in Atmospheric Methane Concentrations between 1978 and 1980." *Geophysical Research Letters 9:*477–480.

Blanchard, D. C., and Woodcock, A. H. 1957. "Bubble Formation and Modification in the Sea and its Meteorological Significance." *Tellus 9:*145–158.

Bodhaine, B. A. 1983. "Aerosol Measurements at Form Background Sites." *Journal of Geophysical Research 88 (C15):*10753–10768.

Boughner, R. E., and Ramanathan, V. 1975. "Climatic Consequence of Increasing CO_2: A Study of the Feedback Mechanisms Between Increasing CO_2 Concentrations and the Atmospheric Ozone, Water Vapor, and Thermal Structure Balance." Presented at *Second Conference on Atmospheric Radiation, October 29–31.* American Meteorological Society, Arlington, Virginia.

Brasseur, G., and Simon, P. C. 1981. "Stratospheric Chemical and Thermal Response to Long-Term Variability in Solar UV Irradiance." *Journal of Geophysical Research 86:*7343–7362.

Breitenbeck, G. A., Blackmer, A. M., and Bremner, J. M. 1980. "Effects of Different Nitrogen Fertilizers on Emissions of Nitrous Oxide from Soil." *Geophysical Research Letters 7:*85–88.

Bremner, J. M., and Blackmer, A. M. 1978. "Nitrous Oxide: Emission From Soils During Nitrification of Fertilizer Nitrogen." *Science 199:*295–296.

Brewer, A. W. 1949. "Evidence for a World Circulation Provided by Measurements of Helium and Water Vapor Distribution in the Stratosphere." *Quarterly Journal of the Royal Meteorological Society 75:*351–363.

Bryson, R. A., and Baerreis, D. A. 1967. "Possibilities of Major Climatic Modification and Their Implications: Northwest India, A Case Study." *Bulletin of the American Meteorological Society 48:*132–142.

Budiansky, S. 1980. "New Attention for Atmospheric Carbon." *Environmental Science and Technology 14:*1430–1432.

Budyko, M. I. 1969. "The Effect of Solar Radiation Variations on the Climate of the Earth." *Tellus 21:*611–619.

Callis, L. B., and Natarajan, M. 1981. "Atmospheric Carbon Dioxide and Chlorofluoromethanes: Combined Effects on Stratospheric Ozone, Temperature, and Surface Temperature." *Geophysical Research Letters 8:*587–590.

Callis, L. B., Natarajan, M., and Boughner, R. E. 1983. "On the Relationship Between the Greenhouse Effect, Atmospheric Photochemistry and Species Distribution." *Journal of Geophysical Research 88:*1401–1426.

Callis, L. B., and Nealy, J. E. 1978. "Solar UV Variability and Its Effect on Stratospheric Thermal Structure and Trace Constituents." *Geophysical Research Letters 5:*239–252.

Carlson, T. N., and Benjamin, S. G. 1980. "Radioactive Heating Rates for Saharan Dust." *Journal of the Atmospheric Sciences 37:*193–213.

Cass, G. R. 1979. "On the Relationship Between Sulfate Air Quality and Visibility with Examples in Los Angeles." *Atmospheric Environment 13:*1069–1084.

Cess, R. D. 1974. "Radiative Transfer Due to Atmospheric Water Vapor: Global Considerations of the Earth's Energy Balance." *Journal of Quantitative Spectroscopy and Radiative Transfer 14:*861–871.

Cess, R. D. 1982. "Increased Atmospheric Carbon Dioxide and Climate Feedback Mechanisms." In J. D. Hall, Jr. (compiler), *Earth Radiation Science Seminar* (NASA Conference Publication 2239). NASA, Washington, D.C.

Cess, R. D. 1983. "Arctic Aerosols: Model Estimates of Interactive Influences Upon the Surface-Atmosphere Clear-Sky Radiation Budget." *Atmospheric Environment 17*(12):2555–2564.

Cess, R. D., Potter, G. L., Ghan, S., and Gates, W. L. 1985. "The Climatic Effects of Large Injections of Atmospheric Smoke and Dust: A Study of Climate Feedback Mechanisms With One- and Three-Dimensional Climate Models." *Journal of Geophysical Research* (in press).

Chameides, W. L., Liu, S. C., and Cicerone, R. J. 1977. "Possible Variations in Atmospheric Methane." *Journal of Geophysical Research 82:*1795–1798.

Chameides, W. L., and Walker, J. C. G. 1973. "A Photochemical Theory of Tropospheric Ozone." *Journal of Geophysical Research 78:*8751–8760.

Chang, J. S., Duewer, W. H., and Wuebbles, D. J. 1979. "The Atmospheric Nuclear Tests of the 1950s and 1960s: A Possible Test of Ozone Depletion Theories." *Journal of Geophysical Research 84:*1755–1765.

Charlock, T., and Sellers, W. D. 1980. "Aerosol Effects on Climate: Calculations with Time-Dependent and Steady-State Radiative Convective Models." *Journal of the Atmospheric Sciences 37:*1327–1341.

Charlson, R. J., Cover, D. J., Larom, T. V., and Waggoner, A. D. 1978. "Chemical Properties of Tropospheric Sulfur Aerosols." *Atmospheric Environment 12:*39–53.

Charney, J. G. 1975. "Dynamics of Deserts and Drought in the Sahel." *Quarterly Journal of the Royal Meteorological Society 101:*193–202.

Charney, J. G., Quirk, W. J., Chow, S., and Kornfield, J. 1977. "A Comparative Study of the Effects of Albedo Change on Drought in Semi-Arid Regions." *Journal of the Atmospheric Sciences 34:*1366–1385.

Chatfield, R., and Harrison, H. 1976. "Ozone in the Remote Troposphere: Mixing Versus Photochemistry." *Journal of Geophysical Research 81:*421–423.

Chemical Manufacturers Association (CMA). 1982. "World Production and Release of Chlorofluorocarbons 11 and 12 Through 1981" (Report FPP 83-F). Chemical Manufacturers Association, Washington, D.C.

Chervin, R. M. 1979. "Response of the NCAR Atmospheric General Circulation Model to Changed Albedo." 563–581. In *Report of the JOC Study Conference on Climate Models: Performance, Intercomparison and Sensitivity Studies* (GARP Publication Series No. 22). World Meteorological Organization, Geneva, Switzerland.

Chervin, R. M. 1980. "Computer Simulation Studies of the Regional and Global Climatic Impacts of Waste Heat Emission." 399–415. In W. Bach (ed.), *Interactions of Energy and Climate.* D. Reidel Publishing Company, Dordrecht, The Netherlands.

Cicerone, R. J., and Shetter, J. D. 1981. "Sources of Atmospheric Methane: Measurements in Rice Paddies and a Discussion." *Journal of Geophysical Research 86:*7203–7209.

Clark, W. C. (ed.) 1982. *Carbon Dioxide Review: 1982.* Oxford University Press, New York, New York.

Clark, W. C., Cook, K. H., Marland, G., Weinberg, A. M., Rotty, R. M., Bell, P. R., Allison, L. J., and Cooper, C. L. 1982. "The Carbon Dioxide Question: Perspectives for 1982." 3–44. In W. C. Clark (ed.), *Carbon Dioxide Review: 1982.* Oxford University Press, New York, New York.

Clarke, A. D., Charlson, R. J., and Radke, L. F. 1984. "Airborne Observations of Arctic Aerosol. 4. Optical Properties of Arctic Haze." *Geophysical Research Letters 11:*405–408.

Coakley, J. A. 1979. "A Study of Climate Sensitivity Using a Simple Energy Balance Climate Model." *Journal of the Atmospheric Sciences 36:*260–269.

Coakley, J. A., Jr., and Cess, R. D. 1985. "Response of the NCAR Community Climate Model to the Radiative Forcing by the Naturally Occurring Tropospheric Aerosol." *Journal of the Atmospheric Sciences 42:*1677–1692.

Coakley, J. A., Jr., Cess, R. D., and Yurevich, F. B. 1983. "The Effect of Tropospheric Aerosols on the Energy's

Radiation Budget: A Parameterization for Climate Models." *Journal of the Atmospheric Sciences 40:*116–138.

Collins, N. M., and Wood, T. G. 1984. "Termites and Atmospheric Gas Production." *Science 224:*84–86.

Covey, C., Schneider, S. H., and Thompson, S. L. 1984. "Global Atmospheric Effects of Massive Smoke Injections from a Nuclear War: Results from General Circulation Model Simulations." *Nature 308:*21–25.

Craig, H., and Chou, C. C. 1982. "Methane: The Record in Polar Ice Cores." *Geophysical Research Letters 9:*1221–1224.

Crutzen, P. J. 1970. "The Influence of Nitrogen Oxides on the Atmospheric Ozone Content." *Quarterly Journal of the Royal Meteorological Society 96:*320–325.

Crutzen, P. J. 1971. "Ozone Production Rates in an Oxygen-Hydrogen-Nitrogen Oxide Atmosphere." *Journal of Geophysical Research 76:*7311–7327.

Crutzen, P. J. 1974. "Estimates of Possible Variations in Total Ozone Due to Natural Causes and Human Activities." *Ambio 3:*301–310.

Crutzen, P. J. 1976. "The Possible Importance of CSO for the Sulfate Layer of the Stratosphere." *Geophysical Research Letters 3:*73–76.

Crutzen, P. J., Heidt, L. E., Krasnel, J. P., Pollock, W. H., and Seiler, W. 1979. "Biomass Burning as a Source of Atmospheric Gases CO_2, H_2, N_2O, NO, CH_3Cl, and COS." *Nature 282:*253–256.

Crutzen, P. J., Isaksen, I. S. A., and McAfee, J. R. 1978. "The Impact of the Chlorocarbon Industry on the Ozone Layer." *Journal of Geophysical Research 83:*345–363.

Crutzen, P. J., Isaksen, I. S. A., and Reid, G. R. 1975. "Solar Proton Events: Stratospheric Sources of Nitric Oxides." *Science 189:*457–458.

Crutzen, P. J., and Schmailzl, U. 1983. "Chemical Budgets of the Stratosphere." *Planetary and Space Science 9:*1009–1032.

Cunnold, D. M., Prinn, R. G., Rasmussen, R. A., Simmonds, P. G., Alyea, F. N., Cardelino, C. A., Crawford, A. J., Fraser, P. J., and Rosen, R. D. 1983a. "The Atmospheric Lifetime Experiment 3: Lifetime Methodology and Application to Three Years of $CFCl_3$ Data." *Journal of Geophysical Research 88:*8379–8400.

Cunnold, D. M., Prinn, R. G., Rasmussen, R. A., Simmonds, P. G., Alyea, F. N., Cardelino, C. A., and Crawford, A. J. 1983b. "The Atmospheric Lifetime Experiment. 4. Results for CF_2Cl_2 Based on Three Years of Data." *Journal of Geophysical Research 88:*8401–8414.

Cuong, N.-B., Bonsang, B., and Lambert, G. 1974. "The Atmospheric Concentration of Sulfur Dioxide and Sulfate Aerosols over the Antarctic, Subantarctic Areas and Oceans." *Tellus 26:*241–249.

Delany, A. C., Pollock, W. H., and Shedlovsky, J. P. 1973. "Tropospheric Aerosol: The Relative Contribution of Marine and Continental Components." *Journal of Geophysical Research 78:*6249–6265.

Dianov-Klokov, V. I., and Yurganov, L. N. 1981. "A Spectroscopic Study of the Global Space-Time Distribution of Atmospheric CO." *Tellus 33:*262–273.

Dickinson, R. E. 1984. "Modeling Evaporation for Three-Dimensional Global Climate Models." 58–72. In J. Hansen and T. Takahashi (eds.), *Climate Porcesses and Climate Sensitivity* (Geophysical Monograph 29, Maurice Ewing, Vol. 5). American Geophysical Union, Washington, D.C.

Dickinson, R. E., and Chervin, R. M. 1979. "Sensitivity of a General Circulation Model to Changes in Infrared Cooling Due to Chlorofluoromethanes With and Without Prescribed Zonal Ocean Surface Temperature Change." *Journal of the Atmospheric Sciences 36:*2304–2319.

Dickinson, R. E., Liu, S. C., and Donahue, T. M. 1978. "Effect of Chlorofluoromethane Infrared Radiation on Zonal Atmospheric Temperature." *Journal of the Atmospheric Sciences 35:*2142–2152.

Doherty, G. M., Newell, R. E., and Danielson, E. F. 1984. "Radiative Heating Rates Near the Stratospheric Fountain." *Journal of Geophysical Research 89:*1380–1384.

Donner, L., and Ramanathan, V. 1980. "Methane and Nitrous Oxide: Their Effects on the Terrestrial Climate." *Journal of the Atmospheric Sciences 37:*119–124.

Duce, R. A., Unni, C. K., Ray, B. J., Prospero, J. M., and Merrill, J. T. 1980. "Long-Range Atmospheric Transport of Soil Dust from Asia to the Tropical North Pacific: Temporal Variability." *Science 209:*1522–1524.

Dunkerton, T. J. 1983. "Modification of Stratospheric Circulation by Trace Constituent Changes?" *Journal of Geophysical Research 88:*10831–10836.

Eddy, J. A. (ed.). 1982. *Solar Variability, Weather, and Climate.* Geophysics Study Committee, Geophysics Research Board, Studies in Geophysics Series, National Academy Press, Washington, D.C.

Ehhalt, D. H., and Schmidt, U. 1978. "Sources and Sinks of Atmospheric Methane." *Pure and Applied Geophysics 116:*452–464.

Ellsaesser, H. W., Harries, J. E., Kley, D., and Penndorf, R. 1980. "Stratospheric H_2O." *Planetary and Space Science 28:*827–835.

Ellsaesser, H. W., MacCracken, M. C., Potter, G. L., and Luther, F. M. 1976. "An Additional Model Test of Positive Feedback from High Desert Albedo." *Quarterly Journal of the Royal Meteorological Society 102:*655–666.

Elterman, L., Wexler, R., and Chang, D. T. 1969. "Features of Tropospheric and Stratospheric Dust." *Applied Optics 8:*893–902.

Fels, S. B., Mahlman, J. D., Schwarzkopf, M. D., and Sinclair, R. W. 1980. "Stratospheric Sensitivity to Perturbations in Ozone and Carbon Dioxide: Radiative and Dynamical Response." *Journal of the Atmospheric Sciences 37:*2265–2297.

Fenn, R. W., Gerber, H. E., and Wasshausen, D. 1963. "Measurement of the Sulfur and Ammonium Component of the Arctic Aerosol of the Greenland Ice Cap." *Journal of the Atmospheric Sciences 20:*466–468.

Fishman, J. 1981. "The Distribution of NO_x and the Production of Ozone: Comments on 'The Origin of Tropospheric Ozone' by S.C. Liu et al." *Journal of Geophysical Research 86:*12161–12164.

Fishman, J., and Crutzen, P. J. 1977. "A Numerical Study of Tropospheric Photochemistry Using a One-Dimensional Model." *Journal of Geophysical Research 82:*5897–5906.

Fishman, J., Ramanathan, V., Crutzen, P. J., and Liu, S. C. 1980. "Tropospheric Ozone and Climate." *Nature 282:*818–820.

Fishman, J., Solomon, S., and Crutzen, P. J. 1979. "Observational and Theoretical Evidence in Support of a Significant In Situ Photochemical Source of Tropospheric Ozone." *Tellus 31:*432–446.

Flyger, H., Hansen, K., Megaw, W. J., and Cox, L. C. 1973. "The Background Level of the Summer Tropospheric Aerosol Over Greenland and the North Atlantic Ocean." *Journal of Applied Meteorology 12:*161–174.

Flyger, H., Heidam, N., Hansen, K., Megaw, W. J., Walther, E., and Hogan, A. 1976. "The Background Level of the Summer Tropospheric Aerosol, Sulfur Dioxide, and Ozone Over Greenland and the North Atlantic Ocean." *Journal of Aerosol Science 7:*103–140.

Flyger, H., Heidam, N. Z., Hansen, K. A., Rasmussen, L., and Megaw, W. J. 1980. "The Background Level of the Summer Tropospheric Aerosol and Trace Gases in Greenland." *Journal of Aerosol Science 11:*95–110.

Foley, H. M., and Ruderman, M. A. 1973. "Stratospheric NO Production from Past Nuclear Explosions." *Journal of Geophysical Research 78:*4441–4450.

Foukal, P. 1980. "Solar Luminosity Variation on Short Time Scales; Observational Evidence and Basic Mechanisms." 29–44. In R. O. Pepin, J. A. Eddy, and R. B. Merill (eds.), *The Ancient Sun.* Pergamon Press, New York.

Fraser, P. J., Khalil, J. A. K., Rasmussen, R. A., and Crawford, A. J. 1982. "Trends of Atmospheric Methane in the Southern Hemisphere." *Geophysical Research Letters 9:*461–464.

Fraser, R. S. 1976. "Satellite Measurement of Mass of Sahara Dust in the Atmosphere." *Applied Optics 15*(10):2471–2479.

Frölich, C. 1981. "The Variability of the Solar Output." 37–44. In S. Sofia (ed.), *Variations in the Solar Constant.* (NASA Conference Publication 2191) NASA, Washington, D.C.

Gage, K. S., and Reid, G. C. 1981. "Solar Variability and the Secular Variation in the Tropical Tropopause." *Geophysical Research Letters 8:*187–190.

Garcia, R. R., Solomon, S., Roble, R. G., and Rusch, D. W. 1984. "A Numerical Study of the Response of the Middle Atmosphere to the 11-Year Solar Cycle." *Planetary and Space Science 32:*411–424.

Gathman, S. G. 1983. "Atmospheric Properties of the Marine Aerosol as Predicted by the Navy Aerosol Model." *Optical Engineering 22:*57–62.

Geller, M. A., and Alpert, J. C. 1980. "Planetary Wave Coupling Between the Troposphere and the Middle Atmosphere as a Possible Sun-Weather Mechanism." *Journal of the Atmospheric Sciences 37:*1197–1215.

Gerber, H. E., and Hindman, E. E. 1981. "First International Workshop on Light Absorption by Aerosol Particles: Background, Activities and Preliminary Results." *Bulletin of the American Meteorological Society 62:*1321–1327.

Gillette, D. A., Blifford, I. H., and Fenster, C. R. 1972. "Measurements of Aerosol Size Distributions and Vertical Fluxes of Aerosols on Land Subject to Wind Erosion." *Journal of Applied Meteorology 11:*977–987.

Gillette, D. A., Clayton, R. N., Mayeda, T. K., Jackson, M. L., and Sridhar, K. 1978. "Tropospheric Aerosols from Some Major Dust Storms of the Southwestern United States." *Journal of Applied Meteorology 17:*832–845.

Graedel, T. E. 1977. "The Homogeneous Chemistry of Atmospheric Sulfur." *Reviews of Geophysics and Space Physics 15*(4):421–428.

Graedel, T. E., and McRae, J. E. 1980. "On the Possible Increase of the Atmospheric Methane and Carbon Monoxide Concentrations During the Last Decade." *Geophysical Research Letters 7:*977–979.

Grams, G. W., Blifford, I. H., Gillette, D. A., and Russell, P. B. 1974. "Complex Index of Refraction of Airborne Soil Particles." *Journal of Applied Meteorology 13:*459–471.

Gras, J. L., and Ayers, J. P. 1983. "Marine Aerosol at Southern Mid-latitudes." *Journal of Geophysical Research 88:*10661–10666.

Greenberg, J. P., Zimmerman, P. R., Heidt, L., and Pollock, W. 1984. "Hydrocarbon and Carbon Monoxide Emissions for Biomass Burning in Brazil." *Journal of Geophysical Research 89:*1350–1354.

Hameed, S., and Cess, R. D. 1983. "Impact of a Global Warming on Biospheric Sources of Methane and Its Climatic Consequences." *Tellus 35B:*1–7.

Hameed, S., Cess, R. D., and Hogan, J. S. 1980. "Response of the Global Climate to Changes in Atmospheric Chemical Composition Due to Fossil Fuel Burning." *Journal of Geophysical Research 85:*7537–7545.

Hänel, G. 1972. "Computation of the Extinction of Visible Radiation by Atmospheric Aerosol Particles as a Function of the Relative Humidity Based Upon Measured Properties." *Journal of Aerosol Science 3:*377–386.

Hänel, G., and Bullrich, K. 1978. "Physico-Chemical Property Models of Tropospheric Aerosol Particles." *Beitrage Zur Physik Der Atmosphare 51:*129–138.

Hansen, J., Johnson, D., Lacis, A., Lebedeff, S., Lee, P., Rind, D., and Russell, G. 1981. "Climate Impact of Increasing Atmospheric Carbon Dioxide." *Science 213:*957–966.

Hansen, J., Lacis, A., Rind, D., Russell, G., Stone, P., Fung, I., Ruedy, R., and Lerner, J. 1984. "Climate Sensitivity: Analysis of Feedback Mechanisms." 130–163. In J. Hansen and X. Takahashi (eds.), *Climate Processes and Climate Sensitivity* (Geophysical Monograph 29, Maurice Ewing, Vol. 5). American Geophysical Union, Washington, D.C.

Hansen, J. E., Wang, C.-W. and Lacis, A. A. 1978. "Mount Agung Eruption Provides Test of a Global Climate Perturbation." *Science 199:*1065–1068.

Harshvardhan, and Cess, R. D. 1976. "Stratospheric Aerosols: Effect Upon Atmospheric Temperature and Global Climate." *Tellus 28:*1–10.

Heath, D. F., Krueger, A. J., and Crutzen, P. J. 1977. "Solar Proton Events: Influence on Stratospheric Ozone." *Science 197:*886–889.

Heath, D. F., and Thekaekara, M. P. 1977. "The Solar Spectrum between 1200 and 3000 Å." 193–212. In O. R. White (ed.), *The Solar Output and Its Variation.* Colorado Associated University Press, Boulder, Colorado.

Heintzenberg, J. 1980. "Particle Size Distribution and Optical Properties of Arctic Haze." *Tellus 32:*251–260.

Heintzenberg, J. 1982. "Size-Segregated Measurements of Particulate Elemental Carbon and Aerosol Light Absorption at Remote Arctic Locations." *Atmospheric Environment 16:*2461–2470.

Hickey, J. R., Stowe, L. L., Jacobowitz, H., Pellegrino, P., Marschoff, R. H., House, F., and Vonder Haar, T. H. 1980. "Initial Solar Irradiance Determination from NIMBUS 7 Cavity Radiometer Measurements." *Science 208:*281–283.

Hidy, G. M., Mueller, P. K., Gradjean, D., Appel, B. R., and Wesolowsky, J. J. (eds.). 1980. *Character and Origins of Smog Aerosols: A Digest of Results from the California Aerosol Characterization Experiment (ACHEX).* Wiley-Interscience, New York, New York.

Hidy, G. M., Mueller, P. K., and Tong, E. Y. 1978. "Spatial and Temporal Distributions of Airborne Sulfates in Parts of the U.S." *Atmospheric Environment 12:*735–752.

Hines, C. O. 1974. "A Possible Mechanism for the Production of Sun-Weather Correlations." *Journal of the Atmospheric Sciences 31:*589–591.

Hoff, R., Leaitch, W., Fellin P., and Barrie, L. 1983. "Mass Size Distributions of Chemical Constituents of the Winter Arctic Aerosol." *Journal of Geophysical Research 88*(C15):10947–10956.

Hoffer, T., Kliwer, J., and Moyer, J. 1979. "Sulfate Concentrations in the South Western Desert of the United States." *Atmospheric Environment 13:*619–627.

Hofmann, D. J., and Rosen, J. M. 1980. "Stratospheric Sulfuric Acid Layer: Evidence for an Anthropogenic Component." *Science 208:*1368–1370.

Hoyt, D. V. 1979. "The Smithsonian Astrophysical Observatory Solar Constant Program." *Reviews of Geophysics and Space Physics 17:*427–458.

Hoyt, D. V., and Eddy, J. A. 1983. "Solar Irradiance Modulation by Active Regions from 1969 through 1981." *Geophysical Research Letters 10:*509–512.

Hudson, S. H. 1983. "Variations of the Solar Radiation Input." 31. In B. M. McCormac (ed.), *Weather and Climate Responses to Solar Variations.* Colorado Associated University Press, Boulder, Colorado.

Husar, R. B., Holloway, J. M., Patterson, D. E., and Wilson, W. E. 1981. "Spatial and Temporal Pattern of Eastern U.S. Haziness: A Summary." *Atmospheric Environment 15:*1919–1928.

Inn, E. C. Y., Vedder, J. F., and Tyson, B. J. 1979. "COS in the Stratosphere." *Geophysical Research Letters 6:*191–193.

Johnston, H. S. 1971. "Reduction of Stratospheric Ozone by Nitrogen Oxide Catalysts from Supersonic Transport Exhaust." *Science 173:*517–522.

Junge, C. E. 1972. "Our Knowledge of the Physico-Chemistry of Aerosols in the Undisturbed Marine Environment." *Journal of Geophysical Research 77:*5183–5200.

Junge, C. 1977. "Tropospheric Aerosols." 2–5. In J. H. Bolle (ed.), *Radiation in the Atmosphere.* Science Press, Princeton, New Jersey.

Junge, C., and Jaenicke, R. 1971. "New Results in Background Aerosols Studies from the Atlantic Expedition of the R.V. Meteor." *Journal of Aerosol Science 2:*305–314.

Kagann, R. H., Elkins, J. W., and Sams, R. L. 1983. "Absolute Band Strengths of Halocarbons F-11 and F-12 in the 8- to 16-μm Region." *Journal of Geophysical Research 88:*1427–1432.

Kelly, P. M., and Sear, C. B. 1984. "Climatic Impact of Explosive Volcanic Eruptions." *Nature 311:*740–743.

Khalil, M. A. K., and Rasmussen, R. A. 1982. "Secular Trends of Atmospheric Methane (CH_4)." *Chemosphere 11:*877–883.

Khalil, M. A. K., and Rasmussen, R. A. 1983. "Increase and Seasonal Cycles in the Atmospheric Concentration of Nitrous Oxide (N_2O)." *Tellus 35B:*161–169.

Khalil, M. A. K., and Rasmussen, R. A. 1984. "Carbon Monoxide in the Earth's Atmosphere: Increasing Trend." *Science 224:*54–56.

Kneip, T. J., and Lippmann, M. (eds.). 1979. "New York Summer Aerosol Study, 1976." *Annals of the New York Academy of Sciences 322:*1–153.

Kondratyev, K., and Nikolsky, G. A. 1970. "Solar Radiation and Solar Activity." *Quarterly Journal of the Royal Meteorological Society 98:*509–522.

Lacis, A., Hansen, J., Lee, P., Mitchell, T., and Lebedeff, S. 1981. "Greenhouse Effect of Trace Gases, 1970–1980." *Geophysical Research Letters 8:*1035–1038.

Lamb, H. H. 1970. "Volcanic Dust in the Atmosphere with a Chronology and Assessment of Its Meteorological Significance." *Philosophical Transactions of the Royal Society of London, Series A 266:*425–533.

Lawson, D., and Winchester, J. 1979. "Atmospheric Sulfur Aerosol Concentrations and Characteristics from the South American Continent." *Science 205:*1267–1269.

Lean, J. L. 1983. "Estimating the Variability of the Solar Flux Between 200 and 300 nm." Cooperative Institute for Research in Environmental Science. University of Colorado, Boulder, Colorado.

Lean, J. L., and Skumanich, A. 1983. "Variability of the Lyman Alpha Flux with Solar Activity." *Journal of Geophysical Research 88:*5751–5759.

Lean, J. L., White, O. R., Livingston, W. C., Heath, D. F., Donnelly, R. F., and Skumanich, A. 1982. "A Three Component Model of the Variability of the Solar Ultraviolet Flux: 145–200 nm." *Journal of Geophysical Research 87:*10307–10317.

Lenoble, J., Tanre, D., Deschamps, P. Y., and Herman, M. 1982. "A Simple Method to Compute the Change in the Earth-Atmosphere Radiative Balance Due to a Stratospheric Aerosol Layer." *Journal of the Atmospheric Sciences 39:*2565–2576.

Levy, H. 1971. "Normal Atmosphere: Large Radical and Formaldehyde Concentrations Predicted." *Science 173:* 141–143.

Levy, H. 1972. "Photochemistry of the Lower Troposphere." *Planetary Space Science 20:*919–935.

Lian, M. S., and Cess, R. D. 1977. "Energy Balance Climate Models: A Reappraisal of Ice-Albedo Feedback." *Journal of the Atmospheric Sciences 34:*1058–1062.

Lipschultz, F., Zafiriou, O. C., Wofsy, S. C., McElroy, M. B., Valois, F. W., and Watson, S. W. 1981. "Production of NO and N_2O by Soil Nitrifying Bacteria." *Nature 294:*641–643.

Liu, S. C. 1977. "Possible Effects on Tropospheric O_3 and OH Due to NO Emissions." *Geophysical Research Letters 4:*325–328.

Liu, S. C., Donahue, T. M., Cicerone, R. J., and Chameides, W. L. 1976. "Effect of Water Vapor on the Destruction of Ozone in the Stratosphere Perturbed by Cl_x or NO_x Pollutants." *Journal of Geophysical Research 81:*3111–3118.

Liu, S. C., Kley, D., McFarland, M., Mahlman, J. D., and Levy, H., II 1980. "On the Origin of Tropospheric Ozone." *Journal of Geophysical Research 85:*7546–7552.

Liu, S. C., McFarland, M., Kley, D., Zafiriou, O., and Huebert, B. 1983. "Tropospheric NO_x and O_3 Budgets in the Equatorial Pacific." *Journal of Geophysical Research 88:*1360–1368.

Llewellyn, R. A., and Washington, W. M. 1977. "Regional and Global Aspects." 106–118. In *Energy and Climate, Studies in Geophysics.* National Academy of Sciences, Washington, D.C.

Logan, J. A. 1983. "Nitrogen Oxides in the Troposphere Global and Regional Budgets." *Journal of Geophysical Research 88:*10785–10807.

Logan, J. A., McElroy, M. B., Wofsy, S. C., and Prather, M. J. 1979. "Oxidation of CS_2 and COS: Sources for Atmospheric SO_2." *Nature 281:*185–188.

Logan, J. A., Prather, M. J., Wofsy, S. C., and McElroy, M. B. 1981. "Tropospheric Chemistry: A Global Perspective." *Journal of Geophysical Research 86:*7210–7254.

London, J., and Haurwitz, M. W. 1963. "Ozone and Sunspots." *Journal of Geophysical Research 68:*795–801.

London, J., and Reber, C. A. 1979. "Solar Activity and Total Atmospheric Ozone." *Geophysical Research Letters 6:*869–872.

Luther, F. M. 1982. "Radiative Effects of a CO_2 Increase: Results of a Model Comparison" (Report UCRL-88121). Lawrence Livermore National Laboratory, Livermore, California.

Luther, F. M., Wuebbles, D. J., and Chang, J. S. 1977. "Temperature Feedback in a Stratospheric Model." *Journal of Geophysical Research 82:*4935–4942.

MacCracken, M. C. 1983a. "Nuclear War: Preliminary Estimates of the Climatic Effects of a Nuclear Exchange." 161–183. In *Proceedings of the International Seminar on Nuclear War, 3rd Session: The Technical Basis for Peace.* August 19–24, 1983, "E. Majorana" Centre for Scientific Culture, Erice, Italy.

MacCracken, M. C. 1983b. "Climatic Effects of Atmospheric Carbon Dioxide." *Science 220:*873–874.

MacCracken, M. C., Cess, R. D., and Potter, G. L. 1986. "Preliminary Estimate of the Effect of Arctic Soot on the Seasonal Climate of a Zonal Statistical Dynamic Model" (Report UCRL-93806). Lawrence Livermore National Laboratory, Livermore, California.

MacCracken, M. C., and Luther, F. M. 1984. "Radiative and Climatic Effects of the El Chichón Eruption." *Geofisica Internacional 23-3:*385–401.

MacCracken, M. C., and Walton, J. J. 1984. "The Effects of Interactive Transport and Scavenging of Smoke on the Calculated Temperature Change Resulting from Large Amounts of Smoke." *Proceedings of the International Seminar on Nuclear War, 4th Session: The Nuclear Winter and the New Defense Systems: Problems and Perspectives.* August 19–24, 1984, Erice, Italy.

Macias, E. S., Zwicker, J. O., Ouimette, J. R., Hering, S. V., Friedlander, S., Cahill, T., Kuhlmey, G., and Richards, L. W. 1981. "Regional Haze Case Studies in the Southwestern U.S.—I. Aerosol Chemical Composition." *Atmospheric Environment 15:*1971–1986.

Malone, R. C., Auer, L. H., Glatzmaier, G. A., Wood, M. C., and Toon, O. B., 1985. "Influence of Solar Heating and Precipitation Scavenging on the Simulated Lifetime of Post-Nuclear War Smoke." *Science 230:*317–319.

Manabe, S., and Wetherald, R. T. 1967. "Thermal Equilibrium of the Atmosphere with a Given Distribution of Relative Humidity." *Journal of the Atmospheric Sciences 24:*241–259.

Manabe, S., and Wetherald, R. T. 1975. "The Effects of Doubling the CO_2 Concentration on the Climate of a General Circulation Model." *Journal of the Atmospheric Sciences 32:*3–15.

Maroulis, P. J., and Bandy, A. R. 1980. "Measurements of Atmospheric Concentrations of CS_2 in the Eastern United States." *Geophysical Research Letters 7:*681–684.

Mass, C., and Schneider, S. H. 1977. "Statistical Evidence on the Influence of Sunspots and Volcanic Dust on Long-Term Temperature Records." *Journal of the Atmospheric Sciences 34:*1995–2004.

McConnell, J. C., and Schiff, H. I. 1978. "Methyl Chloroform: Impact on Stratospheric Ozone." *Science 199:*1974–1977.

McElroy, M. B. 1980. "Sources and Sinks for Nitrous Oxide" (Report FAA-EE-80-20). U. S. Department of Transportation, Washington, D.C.

McKeen, S. A., Liu, S. C., and Kiang, C. S. 1984. "On the Chemistry of Stratospheric SO_2 from Volcanic Eruptions." *Journal of Geophysical Research 89:*4873–4881.

Mészáros, A., and Vissy, K. 1974. "Concentration, Size Distribution and Chemical Nature of Atmospheric Aerosol Particles in Remote Oceanic Areas." *Journal of Aerosol Science 5:*101–109.

Mészáros, E. 1973. "Evidence of the Role of Indirect Photochemical Processes in the Formation of Atmospheric Sulphate Particulate." *Journal of Aerosol Science 4*:429–434.

Mészáros, E. 1978. "Concentration of Sulfur Compounds in Remote Continental and Oceanic Areas." *Atmospheric Environment 12*:699–707.

Mintz, R. 1984. "The Sensitivity of Numerically Simulated Climate to Land-Surface Boundary Conditions." 79–103. In John T. Houghton (ed.), *The Global Climate*. University Press, Cambridge, United Kingdom.

Molina, M. J., and Rowland, F. S. 1974. "Stratospheric Sink for Chlorofluoromethanes: Chlorine Atom Catalyzed Destruction of Ozone." *Nature 249*:810–812.

Molina, M. J., Rowland, F. S., Chou, C. C., Smith, W. S., Vera Ruiz, H., Cresentini, G., and Milstein, R. J. 1976. "Atmospheric Chemistry of Several Chlorofluorocarbon Compounds—Fluorocarbon 21, 22, 31, 13, 113, 114, 115." In *12th International Symposium on Free Radicals*. January 4–9, Laguna Beach, California.

Molnar, G. 1981. "A Survey of Possible Effects of Long-Lasting Absence of Solar Activity on Climate and Some Speculations on Possible Mechanisms." *Climatic Change 3*:189–203.

Murphy, A. H., Gilchrist, A., Häfele, W., Krömer, G., and Williams, J. 1976. "The Impact of Waste Heat Release on Simulated Global Climate" (Report RM-76-79). International Institute for Applied Systems Analysis, Laxenburg, Austria.

Nastrom, G. D., and Belmont, A. D. 1978. "Preliminary Results on 27-Day Solar Rotation Variation in Stratospheric Zonal Winds." *Geophysical Research Letters 5*:665–668.

Natarajan, M., Callis, L. B., and Nealy, J. E. 1981. "Solar UV Variability: Effects on Stratospheric Ozone, Trace Constituents and Thermal Structure." *Pure and Applied Geophysics 119*:750–779.

National Aeronautics and Space Administration (NASA). 1982. "Radiative Effects of the El Chichón Volcanic Eruption: Preliminary Results Concerning Remote Sensing" (NASA TM 84959). NASA, Washington, D.C.

National Aeronautics and Space Administration (NASA) Panel for Data Evaluation. 1983. "Chemical Kinetics and Photochemical Data for Use in Stratospheric Modeling" (Report JPL83-62). Jet Propulsion Laboratory, Pasadena, California.

National Research Council. 1976. "Halocarbons: Effect on Stratospheric Ozone." National Academy Press, Washington, D.C.

National Research Council. 1979. "Stratospheric Ozone Depletion by Halocarbons: Chemistry and Transport." National Academy Press, Washington, D.C.

National Research Council. 1983. "Changing Climate" (Board on Atmospheric Sciences and Climate). National Academy Press, Washington, D.C.

National Research Council. 1984. "Causes of Effects of Changes in Stratospheric Ozone: Update 1983." National Academy Press, Washington, D.C.

Newell, R. E., and Deepak, A. (eds.) 1982. *Mount St. Helens Eruptions of 1980: Atmospheric Effects and Potential Climatic Impact*. (NASA SP–458) NASA, Washington, D.C.

Newell, R. E., and Gould-Stewart, S. 1981. "A Stratospheric Fountain." *Journal of the Atmospheric Sciences 38*:2789–2796.

Newkirk, G., Jr. 1983. "Variations in Solar Luminosity." *American Review of Astronomy and Astrophysics 21*:429–467.

Nilsson, B. 1979. "Meteorological Influence on Aerosol in the 0.2–40.0 ¯m Wavelength Range." *Applied Optics 18*:3457–3473.

North, G. R., Cahalan, R. F., and Coakley, J. A., Jr. 1981. "Energy Balance Climate Models." *Reviews of Geophysics and Space Physics 19*:91–121.

North, G. R., and Coakley, J. A. 1979. "Differences Between Seasonal and Mean Annual Energy Balance Model Calculations of Climate and Climate Sensitivity." *Journal of the Atmospheric Sciences 36*:1189–1204.

North, G. R., Mengel, J. G., and Short, D. A. 1983. "Climatic Response to a Time Varying Solar Constant." 243. In B. M. McCormac (ed.), *Weather and Climate Responses to Solar Variations*. Colorado Associated University Press, Boulder, Colorado.

Oliver, R. C., Bauer, E., Hidalgo, H., Gardner, K. A., and Wasylkiwskyz, W. 1977. "Aircraft Emissions: Potential Effects on Ozone and Climate." (Report No. EQ-77–3). Federal Aviation Administration, Washington, D.C.

Oort, A. H. 1983. "Global Atmospheric Circulation Statistics, 1958–1973." NOAA Professional Paper 14. U.S. Government Printing Office, Washington, D.C.

Ottar, B. 1981. "The Transfer of Airborne Pollutants to the Arctic Region." *Atmospheric Environment 15*:1439–1445.

Owens, A. J., Hales, C. H., Filkin, D. L., Miller, C., Steed, J. M. and Jesson, J. P. 1985. "A Coupled One-Dimensional Radiative-Convective Chemistry-Transport Model of the Atmosphere. I. Model Structure and Steady State Perturbation Calculations." *Journal of Geophysical Research 90*:2283–2311.

Özkaynak, H., Mohnen, V. A., Spengler, J. D., Isaacs, R. G., Ryan, P. B., Shannon, J. D., Sze, N. D., Ko, M. K. W., and Bosart, L. 1981. *Study of the Role of Transport in Fine and Total Suspended Particulate Air Quality*. National Commission on Air Quality, Washington, D.C.

Patterson, E. M. 1981. "Optical Properties of the Crustal Aerosol: Relation to Chemical and Physical Properties." *Journal of Geophysical Research 86*:3236–3246.

Patterson, E. M., Gillette, D. A., and Stockton, B. H. 1977. "Complex Index of Refraction Between 300 and 900 nm for Saharan Aerosols." *Journal of Geophysical Research 82*:3153–3160.

Patterson, E. M., Kiang, C. S., Delaney, A. C., Wartburg, A. F., Leslie, A. C. D., and Hueber, B. J. 1980. "Global Measurements of Aerosols in Remote Continental and Marine Regions: Concentrations, Size Distributions, and Optical Properties." *Journal of Geophysical Research 85*:7361–7376.

Patterson, E. M., Marshall, B. T., and Rahn, K. A. 1982. "Radiative Properties of the Arctic Aerosol." *Atmospheric Environment 16:*2967–2977.

Peixoto, J. P., and Oort, A. H. 1983. "The Atmospheric Branch of the Hydrologic Cycle and Climate." 5–65. In A. Street-Perrott, M. Beran, and R. Ratcliffe (eds.), *Variations in the Global Water Budget.* D. Reidel Publishing Company, Dordrecht, The Netherlands.

Penner, J. E., and Chang, J. S. 1978. "Possible Variations in Atmospheric Ozone Related to the 11-Year Solar Cycle." *Geophysical Research Letters 5:*817–820.

Penner, J. E., and Chang, J. S. 1980. "The Relation Between Atmospheric Trace Species Variability and Solar UV Variability." *Journal of Geophysical Research 85:*5523–5528.

Peyton, T. O., Steele, R. V., and Mabey, W. R. 1976. "Carbon Disulfide, Carbonyl Sulfide: Literature Review and Environmental Assessment." (Report 68-01-2940). Stanford Research Institute, Menlo Park, California. Available from NTIS (Publication PB-257947), Springfield, Virginia.

Pittock, A. B. 1978. "A Critical Look at Long-Term Sun-Weather Relationships." *Review of Geophysical Space Physics 16:*400–420.

Pittock, A. B. 1983. "Solar Variability, Weather and Climate: An Update." *Quarterly Journal of the Royal Meteorological Society 109:*23–55.

Podzimek, J. 1979. "Literature Survey of Marine Aerosol Research" (Report CR78-03). Naval Environmental Prediction Research Facility, Monterey, California.

Podzimek, J. 1980. "Advances in Marine Aerosol Research." *Journal de Recherches Atmospheriques 14:*35–61.

Pollack, J. B., and Ackerman, T. P. 1983. "Possible Effects of the El Chichón Volcanic Cloud on the Radiation Budget of the Northern Tropics." *Geophysical Research Letters 10:*1057–1060.

Pollack, J. B., Toon, O. B., Danielsen, E. F., Hoffman, D. J., and Rosen, J. M. 1983. "The El Chichón Volcanic Cloud: An Introduction." *Geophysical Research Letters 10:*989–992.

Pollack, J. B., Toon, O. B., Sagan, C., Summers, A., Baldwin, B., and Van Camp, W. 1976. "Volcanic Explosions and Climatic Change: A Theoretical Assessment." *Journal of Geophysical Research 81:*1071–1083.

Pollack, J. B., Toon, O. B., and Wiedman, D. 1981. "Radiative Properties of Stratospheric Aerosols." *Geophysical Research Letters 8:*26–34.

Porch, W. M., and MacCracken, M. C. 1982. "Parametric Study of the Effects of Arctic Soot in Solar Radiation." *Atmospheric Environment 16:*1365–1371.

Prodi, F., Santachiara, G., and Oliosi, F. 1983. "Characterization of Aerosols in Marine Environments." *Journal of Geophysical Research 88*(C15):10957–10968.

Prospero, J. M., and Bonatti, E. 1969. "Continental Dust in the Atmosphere of the Eastern Equatorial Pacific." *Journal of Geophysical Research 74:*3362–3371.

Prospero, J. M., and Carlson, T. N. 1972. "Vertical and Areal Distribution of Saharan Dust Over the Western Equatorial North Atlantic Ocean." *Journal of Geophysical Research 77:*5255–5265.

Prospero, J. M., Glaccum, R. A., and Nees, R. T. 1981. "Atmospheric Transport of Soil Dust from Africa to South America." *Nature 289:*570–572.

Pruchniewicz, T. G. 1973. "The Average Tropospheric Ozone Content and Its Variation with Seasons and Latitudes as a Result of Global Ozone Circulation." *Pure and Applied Geophysics 106–108:*1058–1073.

Quiroz, R. S. 1979. "Stratospheric Temperatures During Solar Cycle 20." *Journal of Geophysical Research 84:*2415–2420.

Raatz, W. E., and Shaw, G. E. 1984. "Long Range Tropospheric Transport of Pollution Aerosols into the Alaskan Arctic." *Journal of Climate and Applied Meteorology 23:*1052–1064.

Radke, L. F., Hobbs, P. V., and Bailey, I. H. 1984a. "Airborne Observations of Arctic Aerosols. 3. Origins and Effects of Airmasses." *Geophysical Research Letters 11:*401–404.

Radke, L. F., Lyons, J. H., Hegg, D. A., Hobbs, P. V., and Bailey, I. H. 1984b. "Airborne Observations of Arctic Aerosols. 1. Characteristics of Arctic Haze." *Geophysical Research Letters 11:*393–396.

Rahn, K. A. 1981. "Relative Importance of North America and Eurasia as Sources of Arctic Aerosol." *Atmospheric Environment 15:*1447–1455.

Rahn, K. A., and Lowenthal, D. H. 1984. "Elemental Tracers of Distant Regional Pollution Aerosols." *Science 223:*132–139.

Rahn, K. A., and McCaffrey, R. J. 1980. "On the Origin and Transport of Winter Arctic Aerosol." *Annals of the New York Academy of Sciences 338:*486–503.

Ramanathan, V. 1975. "Greenhouse Effect Due to Chlorofluorocarbons: Climatic Implications." *Science 190:*50–52.

Ramanathan, V. 1976. "Radiative Transfer Within the Earth's Troposphere and Stratosphere: A Simplified Radiative-Convective Model." *Journal of the Atmospheric Sciences 33:*1330–1346.

Ramanathan, V. 1980. "Climatic Effects of Anthropogenic Trace Gases." 269–280. In W. Bach, J. Pankrath, and J. Williams (eds.), *Interactions of Energy and Climate.* D. Reidel Publishing Company, Dordrecht, The Netherlands.

Ramanathan, V., Callis, L. B., and Boughner, R. E. 1976. "Sensitivity of Surface Temperature and Atmospheric Temperature to Perturbations in the Stratospheric Concentrations of Ozone and Nitrogen Dioxide." *Journal of the Atmospheric Sciences 33:*1092–1112.

Ramanathan, V., and Dickinson, R. E. 1979. "The Role of Stratospheric Ozone in the Zonal and Seasonal Radiative Energy Balance of the Earth-Troposphere System." *Journal of the Atmospheric Sciences 36:*1084–1104.

Ramanathan, V., Singh, H. B., Cicerone, R. J., and Kiehl, J. T. 1985. "Trace Gas Trends and Their Potential Role in Climate Change." *Journal of Geophysical Research 90:*5547–5566.

Rasmussen, R. A., and Khalil, M. A. K. 1981. "Increase in the Concentration of Atmospheric Methane." *Atmospheric Environment 15:*883–886.

Rasmussen, R. A., and Khalil, M. A. K. 1983a. "Atmospheric Benzene and Toluene." *Geophysical Research Letters 10:*1096–1099.

Rasmussen, R. A., and Khalil, M. A. K. 1983b. "The Global Production of Methane by Termites." *Nature 301:*700–702.

Rasmussen, R. A., Khalil, M. A. K., and Fox, R. J. 1983. "Altitudinal and Temporal Variations of Hydrocarbons and Other Gaseous Tracers of Arctic Haze." *Geophysical Research Letters 10:*144–147.

Rasool, S. I., and Schneider, S. H. 1971. "Atmospheric Carbon Dioxide and Aerosols: Effects of Large Increases on Global Climate." *Science 173:*138–141.

Reck, R. 1975. "Stratospheric Ozone Effects on Temperature." *Science 192:*557–559.

Reck, R. 1976. "Thermal and Radiative Effects of Atmospheric Aerosols in the Northern Hemisphere Calculated Using a Radiative Convective Model." *Atmospheric Environment 10:*611–617.

Reid, G. C., and Gage, K. S. 1983. "Solar Variability and the Height of the Tropical Tropopause." 569. In B. M. McCormac (ed.), *Weather and Climate Responses to Solar Variations.* Colorado Associated University Press, Boulder, Colorado.

Reinsel, G. C. 1981. "Analysis of Total Ozone Data for the Detection of Recent Trends and the Effects of Nuclear Testing During the 1960s." *Geophysical Research Letters 8:*1227–1230.

Reinsel, G. C., Tiao, G. C., Miller, A. J., Mateer, C. L., Deluisi, J. J., and Frederick, J. E. 1984. "Analysis of Upper Stratospheric Umkehr Ozone Profile Data for Trends and the Effects of Stratospheric Aerosols." *Journal of Geophysical Research 89:*4833–4840.

Robbins, R. C., Cavanaugh, L. A., Salos, L. J., and Robinson, E. 1973. "Analysis of Ancient Atmospheres." *Journal of Geophysical Research 78:*5341–5344.

Robinson, E., and Robbins, R. C. 1969. "Atmospheric CO Concentrations on the Greenland Ice Cap." *Journal of Geophysical Research 74:*1968–1973.

Robock, A. 1978. "Internally and Externally Caused Climate Change." *Journal of the Atmospheric Sciences 35:*1111–1122.

Rodgers, C. D., and Walshaw, C. D. 1966. "The Computation of Infrared Cooling Rate in Planetary Atmospheres." *Quarterly Journal of the Royal Meteorological Society 92:*67–92.

Rosen, H., and Hansen, A. D. A. 1984. "Role of Combustion-Generated Carbon Particles in the Absorption of Solar Radiaton in Arctic Haze." *Geophysical Research Letters 11:*461–464.

Rosen, H., Hansen, A. D. A., Dod, R. L., and Novakov, T. 1980. "Soot in Urban Atmospheres: Determination by an Optical Absorption Technique." *Science 208:*741–743.

Rosen, H., Hansen, A. D. A., Gundel, L., and Novakov, T. 1978. "Identification of the Optically Absorbing Component in Urban Aerosol." *Applied Optics 17:*3859–3861.

Rosen, H. A., Novakov, T., and Bodhaine, B. A. 1981. "Soot in the Arctic." *Atmospheric Environment 15:*1371–1374.

Rowland, F. S., Mayer, E. W., Blake, D. R., and Makide, Y. 1982. "Trends in Atmospheric Methane Concentrations Since 1978." *Symposium on the Composition of the Nonurban Troposphere.* May 25–28, Williamsburg, Virginia.

Rowland, F. S., and Molina, M. J. 1975. "Chlorofluoromethanes in the Environment." *Reviews of Geophysics and Space Physics 13:*1–35.

Rudolph, J., Ehhalt, D. H., and Tonnissen, A. 1981. "Vertical Profiles of Ethane and Propane in the Stratosphere." *Journal of Geophysical Research 86:*7267–7272.

Salstein, D. A., Rosen, R. D., and Peixoto, J. P. 1983. "Modes of Variability in Annual Hemispheric Water Vapor and Transport Fields." *Journal of the Atmospheric Sciences 40:*788–803.

Schatten, K. H., Miller, N., Sofia, S., and Oster, L. 1982. "Solar Irradiance Modulation by Active Regions from 1969 through 1980." *Geophysical Research Letters 9:*49–51.

Seiler, W. 1974. "The Cycle of Atmospheric CO." *Tellus 26:*116–135.

Seiler, W. 1976. "The Cycle of Carbon Monoxide in the Atmosphere." *Proceedings of the International Conference on Environmental Sensing and Assessment.* Institute of Electrical and Electronic Engineers, New York, New York.

Seiler, W. 1982. "The Cycle of Methane in the Troposphere." *Symposium on the Composition of the Nonurban Troposphere.* May 25–28, Williamsburg, Virginia.

Seiler, W., Conrad, R., and Scharffe, D. 1984. "Field Studies of Methane Emission from Termite Nests into the Atmosphere and Measurements of Methane Uptake by Tropical Soils." *Journal of Atmospheric Chemistry 1:*171–186.

Seiler, W., and Fishman, J. 1981. "The Distribution of Carbon Monoxide and Ozone in the Free Troposphere." *Journal of Geophysical Research 86:*7255–7265.

Sellers, W. D. 1969. "A Climate Model Based on the Energy Balance of the Earth-Atmosphere System." *Journal of Applied Meteorology 8:*392–400.

Shaw, G. E., and Stamnes, K. 1980. "Arctic Haze: Perturbations of the Polar Radiation Budget." *Annals of the New York Academy of Sciences 338:*533–539.

Shettle, E. P., and Fenn, R. W. 1979. "Models for the Aerosols of the Lower Atmosphere and the Effects of Humidity Variations on Their Optical Properties" (AFGL-TR-79-0214). Air Force Geophysics Laboratory, Bedford, Massachusetts.

Shukla, J., and Mintz, Y. 1982. "Influence of Land-Surface Evaportranspiration on the Earth's Climate." *Science 215:*1498–1500.

Singh, H. B., Salas, L. J., Shigeishi, H., and Scribner, E. 1979. "Atmospheric Halocarbons, Hydrocarbons, and

Sulfur Hexafluoride: Global Distributions, Sources, and Sinks." *Science 203:*899–903.

Starr, W. L., Craig, R. A., Loewenstein, M., and McGhan, M. E. 1980. "Measurements of NO, O_3, and Temperature at 19.8 km During the Total Solar Eclipse of 26 February 1979." *Geophysical Research Letters 7:*553–555.

Starr, V. P., Peixoto, J. P., and Crisi, A. R. 1965. "Hemispheric Water Balance for the IGY." *Tellus 17:*463–472.

Stolarski, R. S., and Cicerone, R. J. 1974. "Stratospheric Chlorine: A Possible Sink for Ozone." *Canadian Journal of Chemistry 52:*1610–1615.

Symons, G. J. 1888. *The Eruption of Krakatoa and Subsequent Phenomena.* Report of the Krakatoa Committee, Truebner and Co., London, United Kingdom.

Sze, N. D. 1977. "Anthropogenic CO Emissions: Implications for the Atmospheric CO-OH-CH_4 Cycle." *Science 195:*673–675.

Sze, N. D., and Ko, M. K. W. 1980. "Photochemistry of COS, CS_2, CH_3SCH_3 and H_2S: Implications for the Atmospheric Sulfur Cycle." *Atmospheric Environment 14:*1223–1239.

Toon, O. B., and Pollack, J. B. 1976. "A Global Average Model for Atmospheric Aerosols for Radiative Transfer Calculations." *Journal of Applied Meteorology 15:*225–246.

Toon, O. B., and Pollack, J. B. 1980. "Atmospheric Aerosols and Climate." *American Scientist 68:*268–278.

Trijonis, J. 1979. "Visibility in the Southwest — An Exploration of the Historical Data Base." *Atmospheric Environment 13:*833–843.

Turco, R. P., Toon, O. B., Ackerman, T. P., Pollack, J. B., and Sagan, C. 1983. "Nuclear Winter: Global Consequences of Multiple Nuclear Explosions." *Science 222:*1283–1292.

Turco, R. P., Whitten, R. C., and Toon, O. B. 1982. "Stratospheric Aerosols: Observation and Theory." *Reviews of Geophysics and Space Physics 20:*233–279.

Turco, R. P., Whitten, R. C., Toon, O. B., Pollack, J. B., and Hamill, P. 1980. "COS, Stratospheric Aerosols and Climate." *Nature 283:*283–286.

Twitty, J. T., and Weinman, J. A. 1971. "Radiative Properties of Carbonaceous Aerosols." *Journal of Applied Meteorology 10:*725–731.

Valero, F. P. J., Ackerman, T. P., and Gore, W. J. Y. 1984. "The Absorption of Solar Radiation by the Arctic Atmosphere During the Haze Season and Its Effect on the Radiation Balance." *Geophysical Research Letters 11:*465–468.

Varanasi, P., and Ko, F. K. 1977. "Intensity Measurements in Freon Bands of Atmospheric Interest." *Journal of Quantitative Spectroscopy and Radiative Transfer 17:*385–389.

Volz, F. E. 1972. "Infrared Refractive Index of Atmospheric Aerosol Substances." *Applied Optics 11:*755–759.

Waggoner, A. P., Weiss, R., Ahlquist, N., Covert, D., Will, S., and Charlson, R. 1981. "Optical Characteristics of Atmospheric Aerosols." *Atmospheric Environment 15:*1891–1909.

Wang, W.-C. 1984. "Climatological Effects of Atmospheric Ozone: A Review." 98-102. In C. S. Zerefos and A. Ghazi (eds.), *Atmospheric Ozone.* D. Reidel Publishing Company, Dordrecht, Holland.

Wang, W.-C., and Domoto, G. A. 1974. "The Radiative Effects of Aerosols in the Earth's Atmosphere." *Journal of Applied Meteorology 13:*521–534.

Wang, W.-C., and Molnar, G. 1985. "A Model Study of the Greenhouse Effects Due to Increasing Atmospheric CH_4, N_2O, CF_2Cl_2 and $CFCl_3$." *Journal of Geophysical Research.* (In press).

Wang, W.-C., Pinto, J. P., and Yung, Y. L. 1980. "Climatic Effects Due to Halogenated Compounds in the Earth's Atmosphere." *Journal of the Atmospheric Sciences 37:*333–338.

Wang, W.-C., and Stone, P. H. 1980. "Effect of Ice-Albedo Feedback on Global Sensitivity in a One-Dimensional Radiative-Convective Model." *Journal of the Atmospheric Sciences 37:*545–552.

Wang, W.-C., and Sze, N. D. 1980. "Coupled Effects of Atmospheric N_2O and O_3 on the Earth's Climate." *Nature 286:*589–590.

Wang, W.-C., Sze, N. D., Goldenberg, S., and Ko, M. K. W. 1984. "Possible Effects of CFCs and O_3 on Atmospheric Temperatures." Report to Fluorocarbon Program Panel, Chemical Manufacturers Association, Washington, D.C.

Wang, W.-C., Yung, Y. L., Lacis, A. A., Mo, T., and Hansen, J. E. 1976. "Greenhouse Effects Due to Man-Made Perturbations of Trace Gases." *Science 194:*685–690.

Washington, W. M. 1971. "On the Possible Uses of Global Atmospheric Models for the Study of Air and Thermal Pollution." 265–276. In W. H. Matthews et al. (eds.), *Man's Impact on the Climate.* MIT Press, Cambridge, Massachusetts.

Washington, W. M. 1972. "Numerical Climatic-Change Experiments: The Effect of Man's Production of Thermal Energy." *Journal of Applied Meteorology 11:*768–772.

Washington, W. M., and Chervin, R. M. 1979. "Regional Climatic Effects of Large Scale Thermal Pollution: Simulation Studies with the NCAR General Circulation Model." *Journal of Applied Meteorology 18:*3–18.

Weinberg, A. M., and Hammond, R. P. 1970. "Limits to the Use of Energy." *American Scientist 58:*412–418.

Weiss, H. V., Koide, M., and Goldberg, E. D. 1971. "Selinium and Sulfur in a Greenland Ice Sheet: Relation to Fossil Fuel Combustion." *Science 172:*261–263.

Weiss, R. E., Waggoner, A. P., Charlson, R. J., Thorsell, D. L., Hall, J. S. and Riley, L. A. 1979. "Studies of the Optical, Physical, and Chemical Properties of Light Absorbing Aerosols." 257–262. In T. Novakov (ed.), *Proceedings of the Conference on Carbonaceous Particles in the Atmosphere.* (Report LDL-9037). Lawrence Berkeley Laboratory, Berkeley, California.

Weiss, R. F. 1981. "The Temporal and Spatial Distribution of Tropospheric Nitrous Oxide." *Journal of Geophysical Research 86:*7185–7195.

Wells, W. C., Gal, G., and Munn, M. W. 1977. "Aerosol Distributions in Maritime Air and Predicted Scattering Coefficients in the Infrared." *Applied Optics 16:*654–659.

Wetherald, R. T., and Manabe, S. 1975. "The Effects of Changing the Solar Constant on the Climate of a General Circulation Model." *Journal of the Atmospheric Sciences 32:*2044–2059.

Wetherald, R. T., and Manabe, S. 1980. "Cloud Cover and Climate Sensitivity." *Journal of the Atmospheric Sciences 37:*1485–1510.

Whitby, K. T. 1978. "The Physical Characteristics of Sulfur Aerosols." *Atmospheric Environment 12:*135–159.

White, W. H., Moore, D. J., and Lodge, J. P., Jr., (eds.) 1981. "Proceedings of the Symposium on Plumes and Visibility Measurements and Model Components." *Atmospheric Environment 15:*1785–2406.

White, W. H., Patterson, D. E., Wilson, W. E. 1983. "Urban Exports to the Non-Urban Troposphere: Results from Project MISTT." *Journal of Geophysical Research 88*(C15):10745–10752.

Wigley, T. M. L., Angell, J. K., and Jones, P. D. 1985. "Analyses of the Temperature Record." In M. C. MacCracken and F. M. Luther (eds.), *Detecting the Climatic Effects of Increasing Carbon Dioxide.* (DOE/ER-0235). U.S. Department of Energy, Washington, D.C. Available from NTIS, Springfield, Virginia.

Willett, H. C. 1962. "The Relationship of Total Atmospheric Ozone to the Sunspot Cycle." *Journal of Geophysical Research 67:*661–670.

Williams, J., Kromer, G., and Gilchrist, A. 1977a. "Further Studies of the Impact of Waste Heat Release on Simulated Global Climate: Part I." (Report RM-77-15). International Institute for Applied Systems Analysis, Laxenburg, Austria.

Williams, J., Kromer, G., and Gilchrist, A. 1977b. "Further Studies of the Impact of Waste Heat Release on Simulated Global Climate: Part II." (Report RM-77-34). International Institute for Applied Systems Analysis, Laxenburg, Austria.

Williams, J., Kromer, G., and Gilchrist, A. 1979. "The Impact of Waste Heat Release on Climate: Experiments with a General Circulation Model." *Journal of Applied Meteorology 18:*1501–1511.

Willson, R. C., Duncan, C. H., and Geist, J. 1980. "Direct Measurements of Solar Luminosity Variation." *Science 207:*177–179.

Wine, P. H., Chameides, W. L., and Ravishonkara, A. R. 1981. "Potential Role of CS_2 Photo-Oxidation in Tropospheric Sulfur Chemistry." *Geophysical Research Letters 8:*543–546.

Winkler, P. 1973. "The Growth of Atmospheric Aerosol Particles as a Function of the Relative Humidity. II. An Improved Concept of Mixed Nuclei." *Aerosol Science 4:*373–387.

Wofsy, S. C. 1976. "Interactions of CH_4 and CO in the Earth's Atmosphere." *Annual Reviews of Earth and Planetary Science 4:*441–469.

Wofsy, S. C., McConnell, J. C., and McElroy, M. B. 1972. "Atmospheric CH_4, CO, and CO_2." *Journal of Geophysical Research 77:*4477–4493.

Wofsy, S. C., McElroy, M. B., and Yung, Y. L. 1975. "The Chemistry of Atmospheric Bromine." *Geophysical Research Letters 2:*215–218.

Wolff, G. T., and Klimish, R. L. (eds.) 1982. *Particulate Carbon: Atmospheric Life Cycle.* Plenum Press, New York, New York.

Woodcock, A. H. 1953. "Salt Nuclei in Marine Air as a Function of Altitude and Wind Force." *Journal of Meteorology 10:*362–371.

World Meteorological Organization (WMO). 1980. "Meeting of JSC Experts on Aerosols and Climate" (Report WCP–12). 27–31 October 1980, Geneva. WMO, Geneva, Switzerland.

World Meteorological Organization (WMO). 1981. "The Stratosphere 1981: Theory and Measurements" (WMO Global Ozone Research and Monitoring Project Report No. 11). WMO, Geneva, Switzerland.

World Meteorological Organization (WMO). 1982. "Potential Climatic Effects of Ozone and Other Minor Trace Gases" (Report No. 14). WMO, Geneva, Switzerland.

World Meteorological Organization (WMO). 1983a. "Tropospheric Aerosols: Review of Current Data on Physical and Optical Properties" (Report WCP-43). WMO, Geneva, Switzerland.

World Meteorological Organization (WMO). 1983b. "Report of the Expert Meeting on Aerosols and Their Climatic Effects" (Report WCP-55). WMO, Geneva, Switzerland.

Wuebbles, D. J. 1983a. "Chlorocarbons Emission Scenarios: Potential Impact on Stratospheric Ozone." *Journal of Geophysical Research 88:*1433–1443.

Wuebbles, D. J. 1983b. "A Theoretical Analysis of the Past Variations in Global Atmospheric Composition and Temperature Structure" (Report UCRL-53423). Lawrence Livermore National Laboratory, Livermore, California.

Wuebbles, D. J. 1984a. "Future Scenarios and Ozone Change" (Report UCID-20128). Lawrence Livermore National Laboratory, Livermore, California.

Wuebbles, D. J. 1984b. "Trends in Ozone and Temperature Structure: Comparison of Theory and Measurements." 87–91. In C. S. Zerefos and A. Ghazi (eds.), *Atmospheric Ozone.* D. Reidel Publishing Company, Dordrecht, The Netherlands.

Wuebbles, D. J., and Chang, J. S. 1979. "A Theoretical Study of Stratospheric Trace Species Variations During a Solar Eclipse." *Geophysical Research Letters 6:*179–182.

Wuebbles, D. J., Luther, F. M., and Penner, J. E. 1983. "Effect of Coupled Anthropogenic Perturbations on Stratospheric Ozone." *Journal of Geophysical Research 88:* 1444–1456.

Wuebbles, D. J., MacCracken, M. C., and Luther, F. M. 1984. "A Proposed Reference Set of Scenarios for Radiatively Active Atmospheric Constituents" (DOE/NBB-0066). U. S. Department of Energy, Carbon Dioxide Research Division, Washington, D.C.

Yamamoto, G., and Tanaka, M. 1972. "Increase of Global Albedo Due to Air Pollution." *Journal of the Atmospheric Sciences 29:*1405–1412.

Yasa, Z., Arner, N. M., Rosen, H., Hansen, A. D. A., and Novakov, T. 1979. "Photoacoustic Investigation of Urban Aerosol Particles." *Applied Optics 18:*2528–2530.

Zimmerman, P. R., and Greenberg, J. P. 1983. "Termites and Methane." *Nature 302:*354.

Zimmerman, P. R., Chatfield, R. B., Fishman, J., Crutzen, P. J., and Hanst, P. L. 1978. "Estimates on the Production of CO and H_2 from the Oxidation of Hydrocarbon Emissions from Vegetation." *Geophysical Research Letters 5:*679–682.

Zimmerman, P. R., Greenberg, J. P., Wondiga, S. D., and Crutzen, P. J. 1982. "Termites: A Potentially Large Source of Atmospheric Methane, Carbon Dioxide, and Molecular Hydrogen." *Science 218:*563–565.

7. WHAT PAST CLIMATES CAN INDICATE ABOUT A WARMER WORLD

T. Webb III
Brown University

T. M. L. Wigley
University of East Anglia

CONTENTS

7.1 INTRODUCTION

The study of past climates contributes key information to the understanding of how future increases in atmospheric concentrations of carbon dioxide (CO_2) and other trace gases may affect the climate. Research using long-term instrumental and noninstrumental records can (1) illustrate the natural variability of past climates on several temporal and spatial scales, (2) provide data that may be used in developing scenarios for possible future climates, (3) increase the fundamental understanding of the causes of climatic change, and (4) provide independent data for testing mathematical models that simulate climatic conditions.

Recent climate model simulations indicate that the global mean temperature may increase by 1.5 to 4.5°C if the atmospheric concentration of CO_2 is doubled over the next 50 to 150 years (National Research Council 1983; Schlesinger 1983; Chapter 4 of this volume). The time scale of this predicted change has stimulated detailed studies of instrumental records of temperature from the past 100 years (Wigley et al. 1985). These records show that the predicted change is much larger than any recorded change in hemispheric or global average temperature from this time period (Clark 1982). This fact has led to studies of paleoclimatic records for times interpreted as possibly having a higher global mean temperature than today, for example, the mid-Holocene—8000 to 4000 years Before Present (B.P.) (Kellogg 1978; Butzer 1980). Even though the global mean temperature for this mid-Holocene period may never have been as much as 1.5°C higher than today, study of this and other periods with warm climates or with increasing temperatures (e.g., 16,000 to 10,000 B.P.) may reveal potentially useful information for understanding the characteristics of future warm climates. Such information, when portrayed as maps showing the magnitude and spatial scale of changes in temperature, precipitation, and moisture balance which might be associated with an increase in the global mean temperature, complements the output of general circulation climate model simulations of a future high-CO_2 world (such as those of Manabe and Stouffer 1980; Manabe et al. 1981; and other studies reported in Chapters 4 and 5 of this volume).

Knowledge of how variations in the global mean temperature are related to variations in regional climate is fundamental to understanding climate change. From such knowledge can come the ability to construct useful scenarios for possible future warm climates. Current attempts at constructing scenarios require caution, however, because many of the factors and processes active during previous large (1–5°C) changes in the global mean temperature will not be applicable to the next 50 to 150 years when the CO_2-induced changes are projected to occur. For example, during the period of major temperature rise from 16,000 to 10,000 B.P., both the global ice extent and seasonal insolation changed markedly. CO_2 concentrations may also have changed by 40–80 parts per million by volume (ppm) (Neftel et al. 1982), but the role of these changes is not yet fully understood.

The main portion of this chapter is broken into three sections. The first provides a background discussion of (1) the evidence that past climate changes may have been induced by changes in atmospheric CO_2 concentrations, (2) the development of climate scenarios, and (3) model validation with paleoclimatic data. The second section describes climate scenarios that are based on instrumental data, and the third section describes the global data base for 6000 B.P. and its initial use for validating the results of a global circulation model.

7.2 BACKGROUND

7.2.1 Possible Role of Carbon Dioxide in Past Climate Change

Interpretation of past data, especially in searching for causes of climate change, requires an understanding of how the climate system works. Such an understanding is essential in order to isolate CO_2 effects from other causal factors. In recent years CO_2 has become implicated as a potentially important causal factor in explaining past changes in climate on a variety of time scales. To illustrate this fact, we consider examples which involve CO_2 as a possible forcing mechanism and demonstrate the ubiquity of changing atmospheric CO_2 levels.

In the late 1970s the CLIMAP (Climate: Long-Range Investigation, Mapping And Prediction) Program demonstrated that changes in the Earth's orbital parameters must have been the primary factor in causing the quasi-regular glacial-interglacial cycles that have affected the global climate for at least the past 1.7 million years (Hays et al. 1976). Modeling exercises, however, have not always been able to simulate the magnitude of the observed changes between today and full glacial conditions at 18,000 B.P. This lack of success has been attributed either to model deficiencies or to the neglect of some other causal factor. The latter possibility was recently demonstrated by the analysis of air samples trapped in bubbles extracted from ice cores which showed that, at the peak of the last glaciation, CO_2 levels were around 200 ppm, a value considerably lower than the preindustrial level (Neftel et al. 1982).

The direct effects of a glacial-interglacial CO_2 change of 40–80 ppm are subject to some uncertainty. They can be estimated using the logarithmic relationship for the equilibrium temperature change (ΔT) that would result from a CO_2 concentration change from c_0 to c (viz. $\Delta T = \Delta T_{2\times} \ell n(c/c_0)/\ell n2$, where $\Delta T_{2\times}$ is the projected temperature change for a doubling of the CO_2 concentration; see Augustsson and Ramanathan 1977). This relationship gives a range of possible ΔT values between 0.4 and 2.2°C, when uncertainty in changes in CO_2 concentration and in ΔT_{2x} are considered. More detailed modeling suggests that the range in ΔT because of the effects of CO_2 alone may be smaller than this, perhaps only 0.3–0.6°C (Hansen et al. 1984). These values are considerably less than the observed glacial-interglacial ΔT of 4–6°C and indicate that CO_2 is not the whole answer to the problem of explaining the magnitude of glacial-interglacial temperature changes. There is, nevertheless, a possibility that CO_2 is an important factor in the feedback mechanisms that may amplify the orbital forcing of glacial-interglacial climate change (Hansen et al. 1984; Kerr 1984; Pisias and Shackleton 1984).

Processes that might cause the observed changes in CO_2 concentration have been suggested a several authors, including most recently Broecker and Takahashi (1984), Knox and McElroy (1984), Sarmiento and Toggweiler (1984), and Siegenthaler and Wenk (1984). These works outline mechanisms through which CO_2 changes of the order of 50 ppm could occur on time scales of the order of centuries, much less than the glacial-interglacial time scale. Observational evidence from ice cores supports the possibility of such rapid CO_2 fluctuations (Stauffer et al. 1984). These data show that CO_2 levels were not only low during the last glacial period, but also may have varied continually on the 10- to 1000-year time scale. At the shorter end of this range, stable carbon isotopes in tree rings provide evidence of frequent fluctuations of about ± 15 ppm in CO_2 concentrations during the last 2000 years (Stuiver et al. 1984). At the long end of the range, the ice core data have been supported by stable carbon isotope data from deep sea sediment cores (Shackleton et al. 1983) that show, for example, that the concentration of CO_2 during at least part of the last interglacial period (around 120,000 B.P.) was as high as or higher than the preindustrial (late Holocene) level.

On a much longer time scale, the Cretaceous period (about 100 million years ago) was a time of global warmth, with high latitude regions being more than 10°C warmer than they are today (Frakes 1979; Wigley 1981). Because the continents then were in different positions, Barron et. al. (1981) postulated that the Cretaceous warmth probably resulted from the different continental positions, coupled with a different latitudinal distribution of albedo and a necessarily very different system of ocean currents. When, however, attempts were made to simulate the climate of the period using a general circulation model, the predicted global mean temperature fell well short of that implied by the paleoclimatic evidence (Barron et al. 1981; Barron and Washington 1982, 1984). Although several explanations exist for this discrepancy, the most probable is that, during the Cretaceous, atmospheric CO_2 levels were substantially above those existing today. Independent geological evidence supports this possibility (Berner et al. 1983; see also Schneider and Londer 1984, pp. 241–247; Trabalka et al. 1985).

Other examples (e.g., Owen et al. 1979; Hunt 1984), together with the cases described above, indicate that, far from being a constant, atmospheric CO_2 levels in the past have probably varied continuously on all time scales from ~100 years upwards (Trabalka et al. 1985). Studies of past climates must, therefore, seriously consider CO_2 as a

possible causal factor. Paleoclimatology, in its delineation of the details of past climate and the mechanisms of climate change, is intimately linked with the study of the influences of CO_2 on the global climate system. In this light, future anthropogenic emissions of atmospheric CO_2 and trace gases and the anticipated changes in climate that may occur as a result can be viewed as an escalation of the natural processes of climatic change.

7.2.2 Climate Scenarios

The most significant effects of increased atmospheric CO_2 on climate will be manifest in regional changes of moisture and temperature patterns. The increase in available energy in the lower troposphere resulting from CO_2-induced changes in the radiation balance will perturb the whole atmospheric circulation system. Changes in pressure patterns, both geographical and seasonal, will in turn affect rainfall, temperatures, and winds: all the meteorological variables that contribute to the overall climate at a given place. To assess the effects of such changes in climate on human activities, detailed regionally and seasonally specific simulations of future CO_2-induced climate change are required. Increasing concentrations of other radiatively active trace gases (methane, ozone, nitrous oxide and chlorofluorocarbons) may well add significantly to any CO_2-induced warming. Because such trace gas effects cannot easily be distinguished from the effects of CO_2, most references to CO_2 in this chapter should be considered as applying to the combined effects of CO_2 and other trace gases.

Because reliable regional and seasonal detail cannot yet be obtained by modeling the future climate with appropriate general circulation models (GCM), there has been interest in using past climate data as an analog for the future. Pittock and Salinger (1982) have distinguished three different approaches to analog-based scenario developments. The first is to use a suitably defined ensemble of warm years from the recent instrumental record and to compare this either with the long-term mean or with a similarly defined cold-year ensemble (Wigley et al. 1980; Williams 1980; Namias 1980; Jäger and Kellogg 1983). The second is to use regional reconstructions of paleoclimate during past warm periods. Flohn (1977) suggested a number of possible periods: the Medieval Warm Epoch (ca. 800–1200 A.D.); the time of proposed maximum Holocene warmth (often referred to as the Hypsithermal, ca. 8000 to 4000 B.P.); and the last (Eemian) interglacial about 120,000 B.P. A third approach is to use atmospheric dynamical arguments together with a knowledge of empirical climatic relationships and correlations to develop a scenario by an educated guess (Bryson 1974; Flohn 1979; Pittock and Salinger 1982).

Of these possibilities, instrumentally based scenarios have been most extensively developed and will be discussed in depth in Section 7.3. Kellogg (1977, 1978), Kellogg and Schware (1981), and Butzer (1980) have all pursued the second approach and mapped the climatic conditions from the mid-Holocene (4000 to 8000 B.P.) as a possible analog for future warm climates. This work is critically reviewed in Section 7.4. The other two possible warm-world analogs mentioned above (the Medieval Warm Epoch and the Eemian) have not been extensively discussed in the literature, largely because of incomplete data coverage. Williams and Wigley (1983) have shown that the former period was not one of consistent warmth even in the Northern Hemisphere. The warmth was largely confined to the North Atlantic basin region (the region with most data!) and was interspersed by shorter time scale (<100 years) changes in climate that show little spatial coherence. Flohn (1980, 1981) has considered the Eemian as a warm-world analog, and the recently published CLIMAP (1984) data may allow more detailed interpretations of this period. It is of particular interest because of the evidence of higher sea levels at this time, thought to be the result of partial melting of Antarctic ice. A similar sea level rise has been suggested as a possible extreme future consequence of CO_2-induced warming (Mercer 1978).

Flohn (1980, 1981) has also considered more distant climates as possible analogs for a future CO_2-warmed world. These include the period 2.4 million years ago when ice was completely absent from the Arctic (Shackleton et al. 1984). With unipolar glaciation, the global climate system would become even more asymmetrical than today with possible northward displacements of the intertropical convergence zone (ITCZ) and subtropical anticyclones

by 2° latitude or more. The possibility that Arctic ice might disappear, at least seasonally, was first suggested by Budyko (1962, 1969). Complete disappearance is now thought to be unlikely for any future anticipated CO_2 level. However, because of the simplified nature of sea ice models applied to this problem (see, e.g., Semtner 1984), and the general difficulties in modeling long-term sea ice variations (Sear 1984), the question remains open.

7.2.3 Model Validation

Although paleoclimatic data may have only limited value in developing scenarios for CO_2-induced climate change, such data may be of considerable value in testing climate models because past climates provide independent data sets for model validation. The credibility of models used to estimate future climates would be considerably enhanced if they were able to produce reasonable simulations of past climates.

Work toward this goal of simulating past climates has only recently begun, and much of the initial work has focused on simulations of ice age (18,000 B.P.) climates (Williams et al. 1974; Gates 1976; Manabe and Hahn 1977; Hansen et al. 1984). The research to simulate interglacial climates is even more recent (Kutzbach 1981; Kutzbach and Otto-Bliesner 1982; Kutzbach and Guetter 1984a, 1984b), and the methods and criteria for verifying the results of this work are still being formulated. Difficulties can arise because of uncertainties concerning both the causal factors influencing past climates and the correct estimation of the differences between past and present climates. These uncertainties need to be decreased or better understood before the model performance can be fully judged. An iterative approach will probably be necessary in which a series of experimental simulations are completed and tested against paleoclimatic data. If properly implemented, this approach will lead to greater certainty concerning both the causes and the observations of past climatic patterns (see Hansen et al. 1984, pp. 153–154). Key tests of model performance may then be possible.

7.3 CLIMATE SCENARIOS BASED ON INSTRUMENTAL DATA

7.3.1 Background

The use of past warm periods as potential analogs of a world with high CO_2 concentrations is based on the assumption that, given similar boundary conditions (as represented by the state of the oceans, the land surface, and the cryosphere), the general circulation of the lower atmosphere will respond in a similar way, even with different forcing mechanisms (Wigley et al. 1980). If this were correct, then past climate patterns or patterns of climate change could be used as CO_2 analogs, even if the causes of these patterns were unknown. Manabe and Wetherald (1980) and Hansen et al. (1984) have provided some evidence to support this assumption in their numerical modeling work. They applied two different forcing mechanisms to their GCMs: increased levels of CO_2 and increased values of solar insolation. In both cases, the near-surface response of the model climate was similar. In Manabe and Wetherald's case, however, they used a relatively simple GCM with highly idealized geography and without seasonal dependence, and thus their results are not easily transferred to the real world.

There is additional model and observational evidence both for and against the assumption that the patterns of climate change are largely independent of the underlying forcing. The model evidence against the assumption comes from studies of the transient response of the climate system. Most model studies of CO_2 effects, including the work cited above, have considered only the equilibrium response to a specified (e.g., doubling or quadrupling) step-function increase in atmospheric CO_2 concentration. In reality, the changes in CO_2 are continual, and it is the time-dependent evolution of climate that is important, more than the final state yielded by an equilibrium response study. Because of the thermal inertia of the ocean, the climatic response to external forcing is significantly damped, and the response at any given time may lag considerably behind the instantaneous equilibrium response (Hansen et al. 1984; Wigley and Schlesinger 1985; and Chapter 5 of this volume). The amount of lag itself may be time varying, but it should be of the order of decades. Because the response

time of the ocean is a function of location (see, e.g., Hansen et al. 1984), the spatial patterns of the transient response to a steadily increasing level of CO_2 should differ from those for the steady-state, asymptotic response to a step-function CO_2 change. This possibility was first pointed out by Schneider and Thompson (1981). Later work by Bryan et al. (1982) and Spelman and Manabe (1984), using a model with highly idealized geography, suggested that the magnitude of the differences in the latitudinal distribution of changes might be quite small. Thompson and Schneider (1982) have carefully defended their position in a response to the paper by Bryan et al., noting in addition, that it is the longitudinal detail that is most important.

These model-based arguments are complemented by observational evidence. In the early decades of the 20th century, the available instrumental records show that the Earth warmed at the same time that CO_2 levels rose (see Wigley et al. 1985), and it is possible that a part of the warming was due to this CO_2 increase. Wigley and Jones (1981, Figure 3 therein) have shown that, in the Northern Hemisphere, the zonal and seasonal patterns of this early 20th century warming were remarkably similar to those predicted by the equilibrium response in the GCM study of Manabe and Stouffer (1979, 1980). If this similarity were a result of CO_2 forcing, then it would indicate that equilibrium models can give realistic results, and that the transient response influence on spatial detail is relatively small, at least when one considers seasonal data and zonal averages covering about 30° of latitude. However, when longitudinal details are considered, the patterns of climate change show little temporal stability. Jones and Kelly (1983) compared the patterns of temperature change during the early 20th century warming with the patterns of change during the cooling from 1940 to the mid-1960s and with those for the warming that has occurred subsequently. They found marked differences between these periods. Against this, however, one can argue that the noisiness of the climate system may obscure the spatial signal on the scale of Jones and Kelly's study, given the relatively small temperature changes involved.

In summary then, the scenario approach is neither convincingly supported nor contradicted by available theoretical evidence or observational data. Although the issue has not yet been fully resolved, there are strong arguments to suggest that, when both longitudinal and latitudinal details are considered, transient patterns of change may differ from that for the equilibrium response. If this is correct, then the patterns of climatic response may differ according to the type of forcing, and may depend crucially on the time scale of the forcing. This casts doubt, not only on the validity of instrumental scenarios as analogs for the future, but also on the usefulness of equilibrium general circulation model calculations in providing insight into future climatic conditions. Neither method can reliably predict the details of future climate, which is why we deliberately use the word scenario here. Scenarios are not meant to be predictions of future climate; rather they are intended to be internally consistent pictures of a plausible future climate that provide a basis for other workers to evaluate the possible range of impacts of climate change on society.

7.3.2 Scenario Construction

Instrumental scenarios are based on differences between past warm and cold periods, as indicated in records of average global surface air temperature. Because global mean temperatures are not known, however, they are usually estimated from Northern Hemisphere data. The basic method is to select a set of warm years and a set of cold years and to produce regional composites of the differences in pressure, temperature, and precipitation between the two sets. In that way, spatially detailed scenarios can be produced down to the monthly time scale (although published works have considered only seasonal or annual scenarios).

There are a number of different factors that must be considered when selecting years for scenario construction, imposed by the need to simulate as closely as possible conditions in a high-CO_2 world. First, the temperature difference in the instrumental record should be maximized. Although Williams (1980) constructed scenarios by comparing warm years with the long-term mean, most other workers have compared a set of warm years with a set of cold years to produce the greatest possible temperature contrast from the available data.

Second, the gradual but steady rise in the atmospheric CO_2 concentration will cause the climatic effects to develop relatively slowly and to be

associated with important changes in oceanic and cryospheric boundary conditions. The method of selecting individual warm or cold years and forming these into a composite, as followed by Wigley et al. (1980), Williams (1980), Namias (1980), and Pittock and Salinger (1982), fails to allow for this problem because interannual climate fluctuations occur on too short a time scale (Pittock and Salinger 1982). One way to simulate the effects of the gradual increase in atmospheric CO_2 is to extract blocks of warm and cold years from the instrumental record rather than individual extreme years, an approach used by Jäger and Kellogg (1983), Lough et al. (1983), and Palutikof et al. (1984). (As it happens, because the individual years used in the studies mentioned above tend to be closely grouped, they may also reflect slow changes.)

Finally, an appropriate data set must be chosen from which to select the sample years. Because numerical modeling work suggests that the effect of increased CO_2 concentrations on temperatures will be manifest most strongly at high latitudes, Wigley et al. (1980) used annual surface air temperatures for high northern latitudes (65°–85°N) as their source data set. Modeling work also shows temperature increases to be greatest in the winter season (December through February) so that winter temperature data might be more appropriate for defining warm (and cold) years on the grounds that this season shows the greatest sensitivity to changes in CO_2. However, even though the proposed CO_2 signal may be highest in high latitudes and in winter, this region and season need not be the most suitable as an indicator of climatic change. A choice might be more appropriately based on the signal-to-noise ratio, which is highest in midlatitude summer (June through August) or Northern Hemisphere annual temperatures (Wigley and Jones 1981).

An alternative approach to scenario construction has been employed by workers in the Soviet Union (Budyko et al. 1978; Groisman 1981; and Vinnikov and Kovyneva 1983), based on earlier work by Drozdov (1966, 1974) and on the empirical modeling results of Vinnikov and Groisman (1979) and Groisman (1979). Essentially, linear relationships are developed between local, seasonally specific climate data and the Northern Hemisphere (17.5°–87.5°N) surface air temperature record of Borzenkova et al. (1976) and Vinnikov et al. (1980):

$$C_i = aT_i + b + \epsilon_i \,, \tag{7.1}$$

where C_i is the year-i value of a chosen local climate variable (e.g., temperature or precipitation), T_i is the Northern Hemisphere temperature averaged over the 12 preceding months, a and b are regression coefficients, and ϵ_i is an error term. Having determined a and b, the change in the chosen climate variable can be estimated for any given Northern Hemisphere temperature change, and regionally and seasonally specific scenarios can be developed. As noted by Palutikof et al. (1984), the results produced by this method must be similar to those produced by the method of compositing the differences between warm and cold years.

Some Soviet results have been presented as forecasts rather than scenarios. For the case where C_i is local temperature, Jones and Kelly (1983) have shown that the correlation coefficient between C_i and T_i (and hence the regression coefficient, a) depends critically on the time period considered. This temporal instability casts doubt on the validity of Equation (7.1) as a forecasting tool (and on the validity of all instrumentally based scenarios as forecasts). However, whereas empirically based forecasts of future climate change are of doubtful reliability, this fact does not preclude the use of empirical data for the construction of climate scenarios.

The most detailed scenarios produced to date are those of Lough et al. (1983) and Palutikof et al. (1984). These workers compared the results obtained by a variety of methods for choosing analog years. They placed greatest confidence on scenarios that exploit the early 20th century warming, which as already noted may have been partially caused by increasing CO_2 levels. Warm and cold year ensembles were chosen using the warmest and coldest 20-year periods from the Northern Hemisphere surface air temperature record of Jones et al. (1982), viz. 1934 to 1953 and 1901 to 1920. Lough et al. (1983) presented regional scenarios for Europe and discussed the implications of these for energy demand and for agriculture. Their most surprising result is that winter temperatures over a substantial part of Europe were colder and showed greater interannual variability during the hemispherically warm period, probably as a result of increased blocking

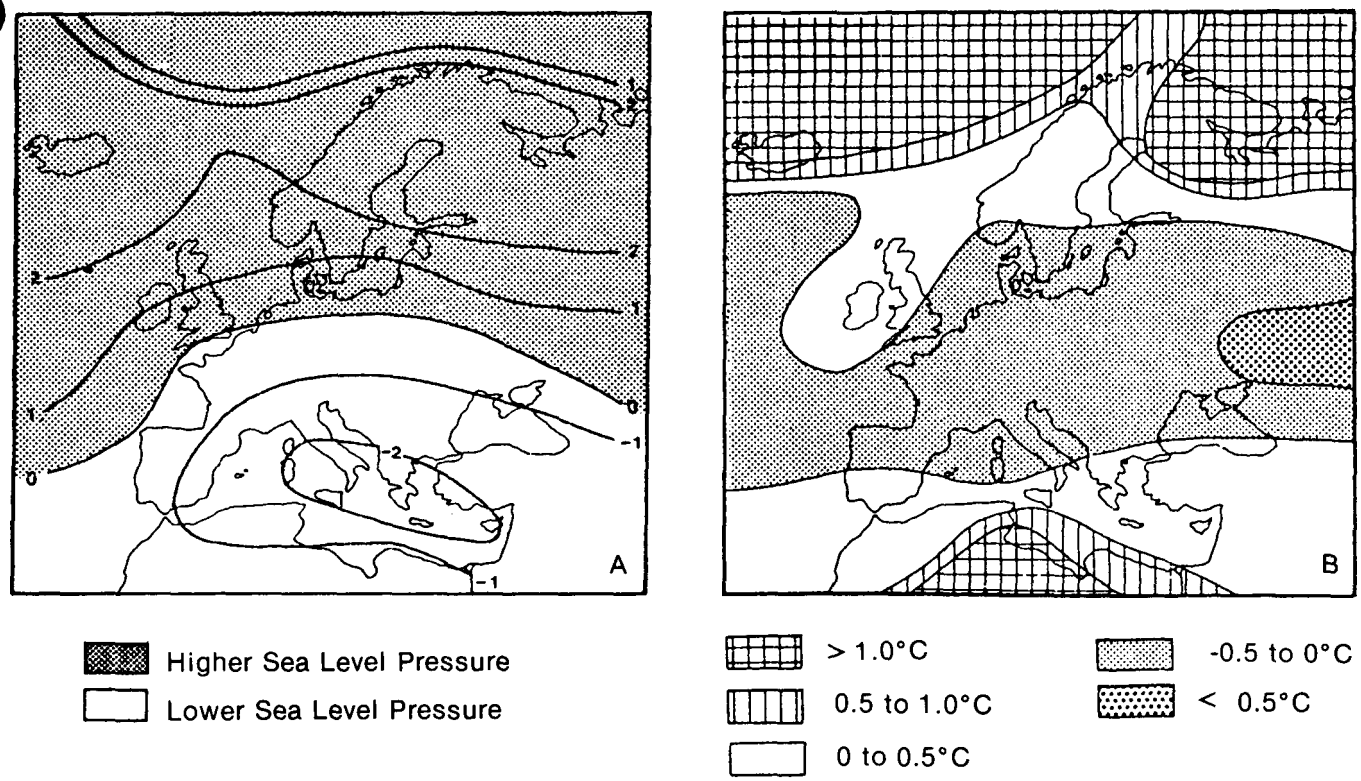

Figure 7.1. Winter pressure (A) and temperature (B) scenarios for Europe showing higher pressure in the north and a band of cooler conditions across central Europe. Isobars are given in millibars (1000 mb = 100 kPa). The values shown here are differences between the 1934–1953 and 1901–1920 mean values and correspond to a warming of the Northern Hemisphere of about 0.5°C. Source: Palutikof et al. (1984.)

(Figure 7.1). Rainfall patterns showed overall decreases during springs and summers of warm years, and increases in autumns and winters.

Further details of these European scenarios are given by Palutikof et al. (1984), along with similar scenarios for North America. The North American scenarios for temperature and pressure exhibit much less interseasonal contrast than is the case for Europe. Temperatures are shown to be generally higher and less variable throughout the year in a warm world, although there is a band of cooler conditions that runs across the continent between about 50° and 60°N in all seasons. Most of the continent south of 50°N shows considerable warming, especially in summer (Figure 7.2). Precipitation patterns are complex with substantial areas of increase and decrease (Figure 7.2).

A disadvantage of the instrumental scenario method is that the scenarios are based on relatively small hemispheric temperature changes compared with those expected to result from future increases in the atmospheric CO_2 concentration. Manabe and Stouffer's (1979, 1980) model, for example, shows temperature increases ranging from about 3°C at the equator to over 13°C in high northern latitudes for a quadrupling of atmospheric CO_2. Because the temperature response to CO_2 changes is approximately logarithmic, these results imply a range of from 1.5° to 6.5°C for a CO_2 doubling. By comparison, the instrumental record for the Northern Hemisphere yields maximum warm-cold differences of about 2°C for Arctic latitudes and 0.5°C for the Northern Hemisphere as a whole. Thus, instrumental scenarios can only be taken as being indicative of conditions during the early phase of CO_2-induced warming, changes which are expected to take place by the early decades of the 21st century.

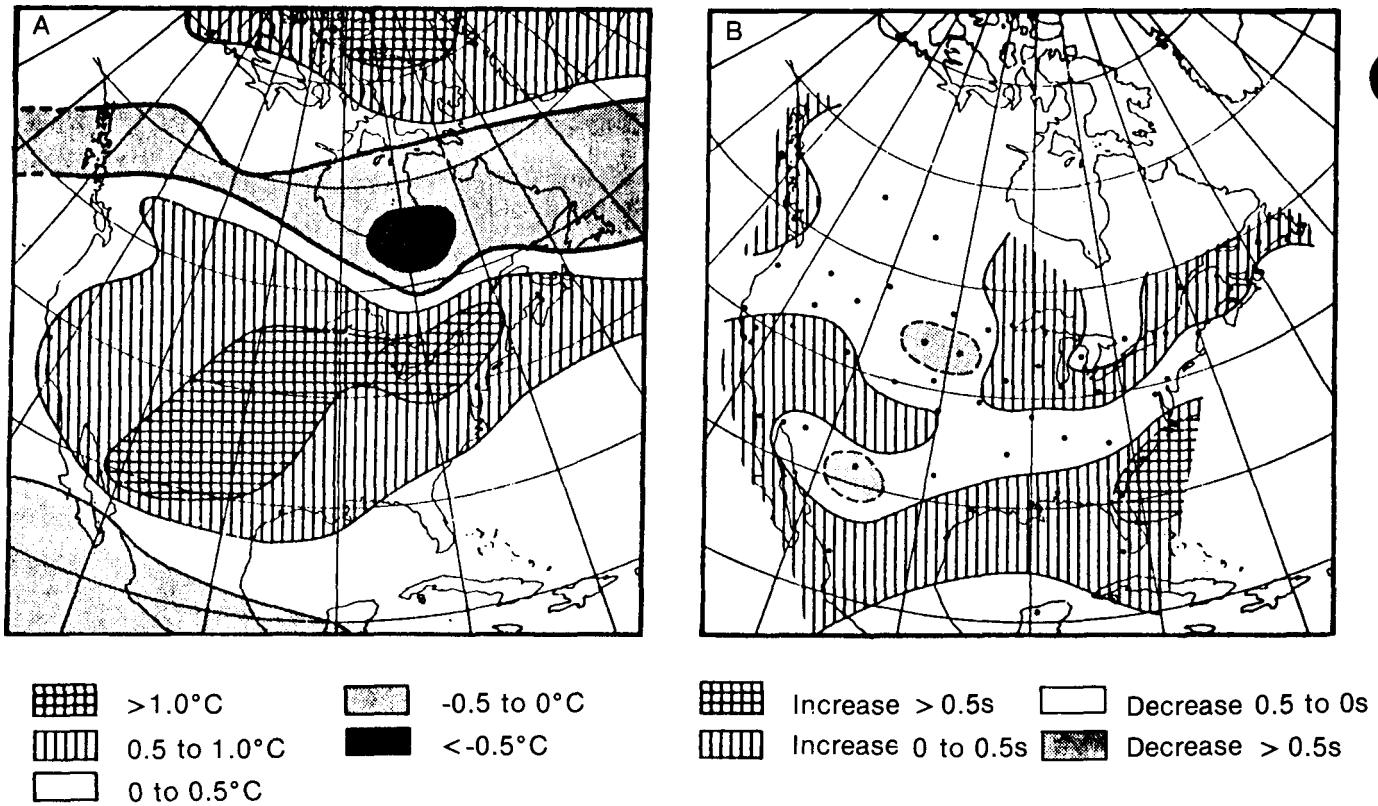

Figure 7.2. Summer temperature (A) and precipitation (B) scenarios for North America. The precipitation changes are shown in multiples of the local standard deviation (s). The dots on the lower diagram show the locations of precipitation stations used. The values shown here are differences between the 1934–1953 and 1901–1920 mean values and correspond to a warming of the Northern Hemisphere of about 0.5°C. Source: Palutikof et al. (1984.)

7.4 GLOBAL CLIMATE DATA BASE FOR 6000 YEARS AGO

7.4.1 Purpose

A program to map the climate patterns at 6000 B.P. has been under way for some time. The initial goal in assembling a global set of paleoclimatic data for this time period was to study certain of the regional climatic implications of a rise in the global mean temperature. The plan was to produce a computer tape of the data used, to map the climate patterns derived from this data set, and to provide quantitative estimates for the regional climatic differences between today and 6000 B.P., a time when the global mean temperature might have been higher than that of today. Kellogg (1977, 1978) and Butzer (1980) pioneered studies of this type and have published global maps of possible moisture differences between today and the mid-Holocene, which began at 8000 B.P. and ended at 5000 B.P. (Butzer 1980) or 4500 B.P. (Kellogg 1978). Their studies produced qualitative maps without full documentation of the data used and mixed together data from a 3000- or 3500-year period when the regional climates varied in major ways, the Laurentide ice sheet retreated and disappeared, and the seasonal solar radiation at the top of the atmosphere changed significantly (Berger 1978). The reason that more recent efforts have focused on 6000 B.P. was to narrow the time interval represented by the data and to avoid mixing data from after 6000 B.P. with data from 8000 and 7000 B.P. when the Laurentide ice sheet still covered a significant area of North America (Denton and Hughes 1981). This research is just reaching its first major stage of synthesis and is described below.

A second goal in compiling data from 6000 B.P. was to gain average temperature estimates for regions, continents, and even the globe to show how much the temperatures differed between 6000 B.P. and now. The major work on this goal has yet to begin and awaits the description and publication

of the global data base. A third goal has recently arisen. From model simulation studies, Kutzbach (1981) has shown the potential importance of the Earth's orbital variations in affecting regional climatic patterns during the Holocene. This work has identified one of the potential causes for the differences in climate between 6000 B.P. and today and has created a new critical use for the global data set from 6000 B.P.: that of testing climate model simulations. Work toward this third goal is just beginning and is described in Section 7.4.4.

7.4.2 Data and Analysis

The current global data set of paleoclimatic data from 6000 B.P. (Webb 1984, 1985a, 1985b) includes pollen, lake-level, and marine plankton data (Figure 7.3). Coverage is most dense in North America, Europe, Africa, and New Zealand and is incomplete in southeast Asia, Antarctica, and Greenland and the central Pacific Ocean. Data are only included if they are reliably dated (usually by interpolation of radiocarbon dates) and are known to date from 6000 B.P. The data base includes full documentation about the dating and location of the samples with each type of data and can be easily updated or edited. Unlike Kellogg's (1978) data which came variously from 4500 to 8000 B.P. (Kellogg and Schware 1981), the current data set is more time specific with data from just 6000 B.P. with an average uncertainty of ±300 years for terrestrial data (Webb 1982) and ±1000 years for marine plankton data. With further work, global data sets for other dates, e.g. 9000, 8000, or 3000 B.P., can be compiled, and Andrews (1984) has recently compiled an annotated bibliography that will aid this task. CLIMAP (1976, 1981), Sarnthein (1978), and Peterson et al. (1979) have already described and mapped the available data for 18,000 B.P.

The data compilation has focused on pollen, lake-level, and marine plankton data because all three types of data come from continent-wide to ocean-wide networks of samples and can be calibrated in climatic terms to produce quantitative estimates of past temperature or precipitation (Webb 1985a). Energy budget-hydrological models exist for the estimation of precipitation from lake-level information (Kutzbach 1980), and multiple regression techniques have been developed for the calibration of pollen and marine plankton data (Imbrie and Kipp 1971; Kipp 1976; Sachs et al. 1977; Imbrie and Webb 1981; Howe and Webb 1983). The global isotherm map of sea-surface temperatures for 18,000 B.P. (CLIMAP 1976) was developed by use of these multivariate techniques on marine plankton data.

7.4.3 Regional Climate Estimates

For 6000 B.P., Bartlein and Webb (1985) used a series of multiple regression equations to produce isotherm maps from the pollen data in eastern North America (Figure 7.4). Huntley and Prentice (1986) have done the same for Europe, and Peterson (1983, 1984) has calculated temperature estimates from pollen data at four sites in the western Soviet Union (Table 7.1). Other temperature estimates from pollen data at isolated sites in the Canadian Arctic (Andrews et al. 1981), British Columbia (Mathewes and Heusser 1981), and Chile (Heusser and Streeter 1980) are described in Webb (1985a). Kay and Andrews (1983) and Heusser et al. (1985) have added estimates for the Arctic and western North America. Ruddiman and Mix (1986) and Marvil and Prell (1986) have produced estimates of sea-surface temperatures from the marine plankton data in the Atlantic and Indian Oceans. The standard errors of estimate for the temperature equations range from 0.8° to 1.7°C and are of the same magnitude as the estimated temperature differences between 6000 B.P. and today. Confidence in the sign and even the magnitude of the estimates is gained from maps and time series plots that show that independent results from widely separated cores are both spatially and temporally consistent.

Table 7.1
Estimates for Mean July Temperature from the Western Soviet Union.

Site	Latitude	Longitude	Temperature Present	Temperature 6000 B.P.
Orshinskii Mokh	56°57'N	36°20'E	18.2°C	19.8°C
Osechenskoe	57°31'N	34°50'E	18.0°C	19.4°C
Ivanovskoe	57°50'N	30°00'E	18.4°C	19.8°C
Polovetsko-Kupanskoe	57°34'N	37°54'E	18.2°C	20.2°C

Source: Peterson (1983)

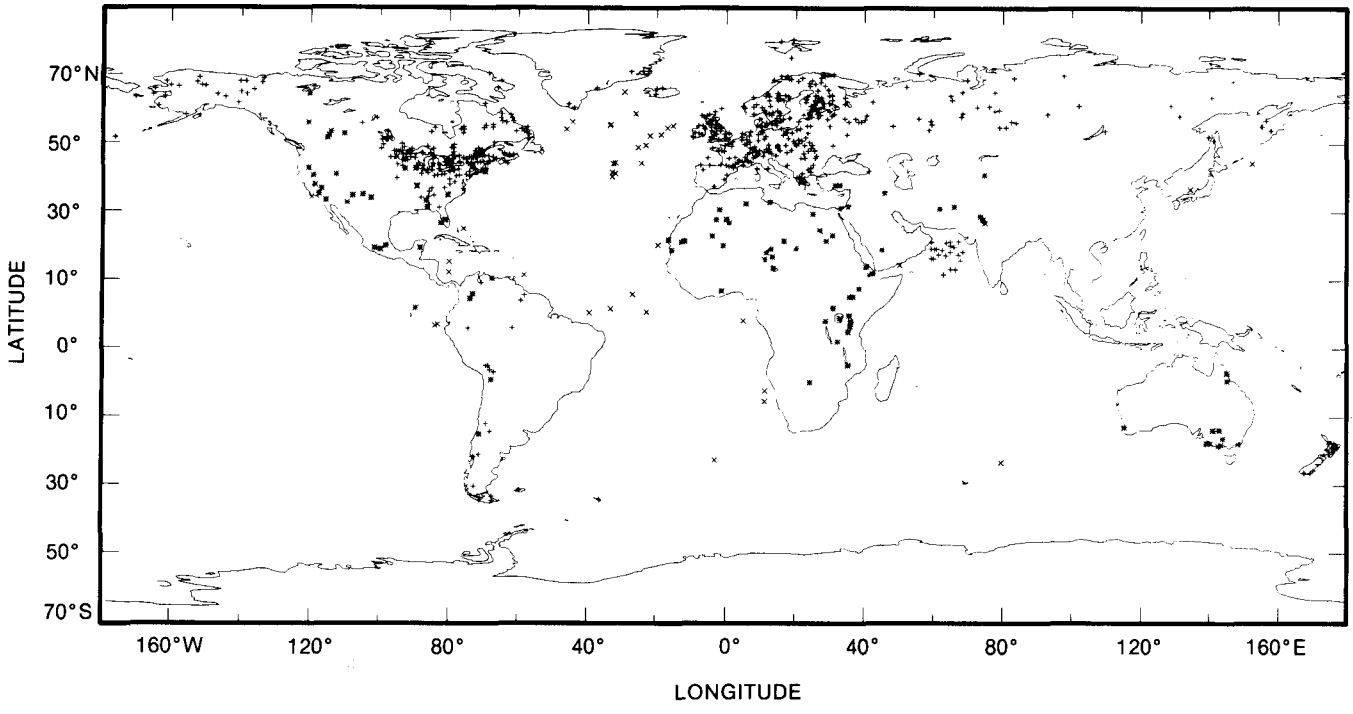

Figure 7.3 Location of sites with paleoclimatic data for 6000 B.P. (Webb 1985a, 1985b): pollen data (+), marine plankton data (×), and lake-level data (*). Pollen data from South America are being added to the data set. All of the sites shown have met prescribed standards for radiocarbon dating.

Estimates of precipitation at 6000 B.P. (Figure 7.5; Table 7.2) are available from pollen data in central North America (Bartlein et al. 1984) and northwest India (Swain et al. 1983) and from lake-level data in central and east Africa (Kutzbach 1980; Hastenrath and Kutzbach 1983) and northwest India (Swain et al. 1983). In a comparison of the calibration methods, Swain et al. (1983) showed that both the pollen and lake-level data yielded a similar estimate of about 200 mm more rainfall at 6000 B.P. in northwest India (Table 7.2). Bartlein et al. (1984) have described independent paleoclimatic evidence within the Midwest that agrees with their climatic reconstructions there.

7.4.3.1 Temperature Estimates for Eastern North America and Europe

In eastern North America, the estimated mean July temperatures for 6000 B.P. display a north-to-south gradient from 8° to 27°C just like those for today (Figure 7.4). The region with the steepest temperature gradient, however, was much farther to the north at 6000 B.P. than it is today. This band, from 12° to 21°C, lay between the United States and Canadian border and central Quebec at 6000 B.P. (Figure 7.4A), but today it is between the 18° and 22°C isotherms and is located south from the United States and Canadian border to Pennsylvania and southern Michigan (Figure 7.4).

The estimated mean July temperatures for 6000 B.P. were higher than those of today in a region from central Quebec to the southern United States (Figure 7.4). This region of higher temperatures narrows to the west and extends across Manitoba into Saskatchewan. The temperature estimates were much lower than those observed today in northern Quebec and Labrador. A small residual ice sheet of insignificant size still existed in the center of this region, and its presence might be tied to the colder conditions that were estimated for this area of the north. The pattern of temperature change for Europe is broadly similar to that in eastern North America, except that the temperature differences were not negative in the north (I. C. Prentice and B. Huntley[1]). The Scandinavian ice sheet had long since disappeared by 6000 B.P. The temperature patterns for North America and

[1] I. C. Prentice and B. Huntley, personal communications.

Table 7.2
Precipitation Estimates for East Africa and India for 6000 B.P.

Site	Annual Precipitation: Today	Annual Precipitation: 6000 B.P.	Data Source	Reference
Lake Naivasha, Kenya	900 mm	990–1055 mm[a]	Water level	Hastenrath and Kutzbach 1983
Sambhar Lake, India	470 mm	500–670 mm[b]	Water level	Swain et al. 1983
Lunkaransar Lake, India	340 mm	519 mm[b]	Pollen	Swain et al. 1983
Lake Chad, Chad	350 mm	650 mm[c]	Water level	Kutzbach 1980

[a] Estimates apply to 5650 to 9200 B.P.
[b] Estimates apply to 3500 to 10,500 B.P.
[c] Estimates apply to 5000 to 10,000 B.P.

Europe differ from those simulated by general circulation models for a world with higher CO_2 concentrations. These simulations show temperature differences that increase from mid to high latitudes (Manabe and Stouffer 1980; Wetherald and Manabe 1981).

7.4.3.2 Sea Surface Temperature Estimates

The maps of estimated sea surface temperature in the Atlantic Ocean show anomaly patterns between 6000 B.P. and today that are similar for both February and August (Ruddiman and Mix 1986). Temperatures north of 60°N and south of 20°S were much higher than the temperatures today, but temperatures in between are similar to those for today. More sites are needed to fill in the data base, but enough data exist to indicate that at 6000 B.P. sea surface temperatures were not uniformly higher than today's temperatures.

7.4.3.3 Precipitation Estimates for the American Midwest

Between 8000 and 2000 B.P., the prairie-forest border was east of its current location in Minnesota, Iowa, and Illinois (Figure 7.5). Bartlein et al. (1984) have recently updated the work of Webb and Bryson (1972) and have shown that this vegetational change was associated with annual precipitation values 10–20% below those of today. This pattern of change, along with the implied increase in the frequency and duration of dry western air masses, is similar to the climate changes during the 1930s dust bowl years in this area (Borchert 1950).

7.4.3.4 Global Maps of Lake Levels

The global maps show that the water levels in lakes in Australia, India, Saudi Arabia, and northern and eastern Africa were higher at 6000 B.P. than at present (Figure 7.6). These modern arid to subhumid regions had much different climatic conditions at 6000 B.P. than occur there today. The Sahara and Rajasthan deserts probably were replaced by dry savannas and steppes at 6000 B.P. In Africa and India estimates of annual precipitation were as much as 300 mm (or 50 to 100%) higher than today (Table 7.2).

7.4.4 Was the Earth Warmer Than Today at 6000 B.P.?

The period of 6000 B.P. was chosen for study because it fell within the time interval usually associated with the Altithermal or Hypsithermal, but was late enough that the Laurentide ice sheet had shrunk to insignificant size (Denton and Hughes 1981). Kellogg and Schware (1981, p. 157) claimed that "During the Altithermal the Earth was generally several degrees warmer than the present . . ." Was it? What is the geological evidence that supports this statement? Local and regional evidence

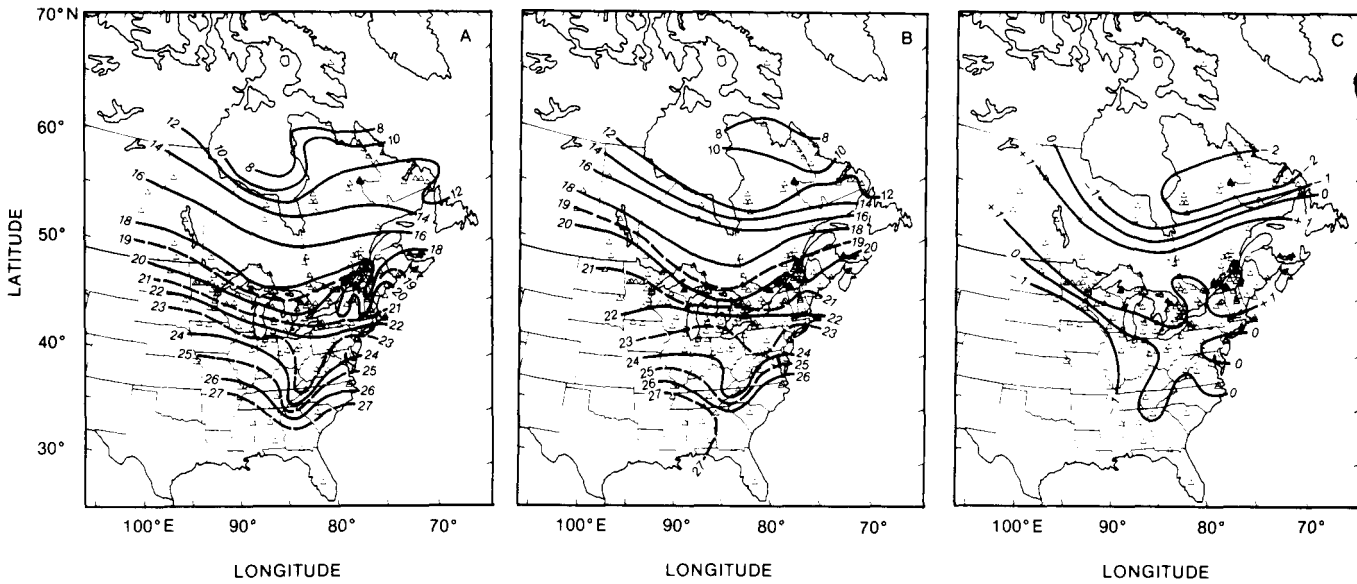

Figure 7.4. Isotherm maps: (A) for the present climate, (B) for 6000 yr B.P., and (C) for the difference between 6000 yr B.P. and the present (in °C) estimated from pollen data (Bartlein and Webb 1985). Positive differences indicate that the estimated temperatures at 6000 yr B.P. were higher than those today. Sites with pollen data are indicated by triangles.

for hypsithermal conditions is abundant, but what about evidence for a global hypsithermal state?

A search of the literature showed that little direct evidence exists, although the idea that a period of maximum global warmth had occurred during the present interglacial period has long been accepted (Deevey and Flint 1957). Terms like altithermal, xerothermic, postglacial, and climatic optimum were coined to describe it. Deevey and Flint (1957) formally defined the term Hypsithermal, which is climatically descriptive of high temperature conditions, but they gave it a chronostratigraphic definition as the time period during which certain Danish pollen zones formed. Since then its chronostratigraphic usage (i.e., reference to a specific time period) has been neither strict nor frequent, and its most common application is as a regional climatostratigraphic term (i.e., reference to a climatic condition) of somewhat vague definition (Wright 1976). In fact, Watson and Wright (1980) have demonstrated why it cannot be applied both chronostratigraphically and climatostratigraphically when descriptive of local and regional paleoclimatic data. A way out of this dilemma is to use the term Hypsithermal in the climatic sense that Deevey and Flint (1957) intended, i.e., as the time period during the Holocene when the global mean temperature was higher than it is today, and to cease using it to describe local evidence for a thermal maximum. Local or regional hypsithermal conditions may be quite unrelated to the timing of such conditions globally.

The problem is to find evidence from the past 10,000 years for a time when the global mean temperature was higher than it is today, because no data are known that provide direct information about the global mean temperature. Most claims for a Hypsithermal period in the mid-Holocene (Deevey and Flint 1957; Wright 1976) are based on regional or local data from northern midlatitudes where July temperatures may have been 1° to 3°C higher than those of today. These regional estimates are from a small area of the globe and can hardly be cited as representative of the annual global mean temperature.

Oxygen isotope data from deep-sea cores provide data interpreted to reflect global climatic variations (Shackleton and Opdyke 1973; Hays et al. 1976). The major Quaternary variations in these data reflect the changes in global ice volume, and over an appropriately long time scale the global mean temperature should be proportionately related to global ice volume. The main decrease in the ratio of ^{18}O to ^{16}O ended about 6000 ± 2000 B.P. (see Figure 1 in Shackleton et al. 1983), which is about the time when the Laurentide ice sheet finally disappeared. No clear trend is evident in the oxygen isotope data since then, and most variations within the past 6000 years are within $0.2^0/_{00}$, which is close to the noise level for the measurements. The

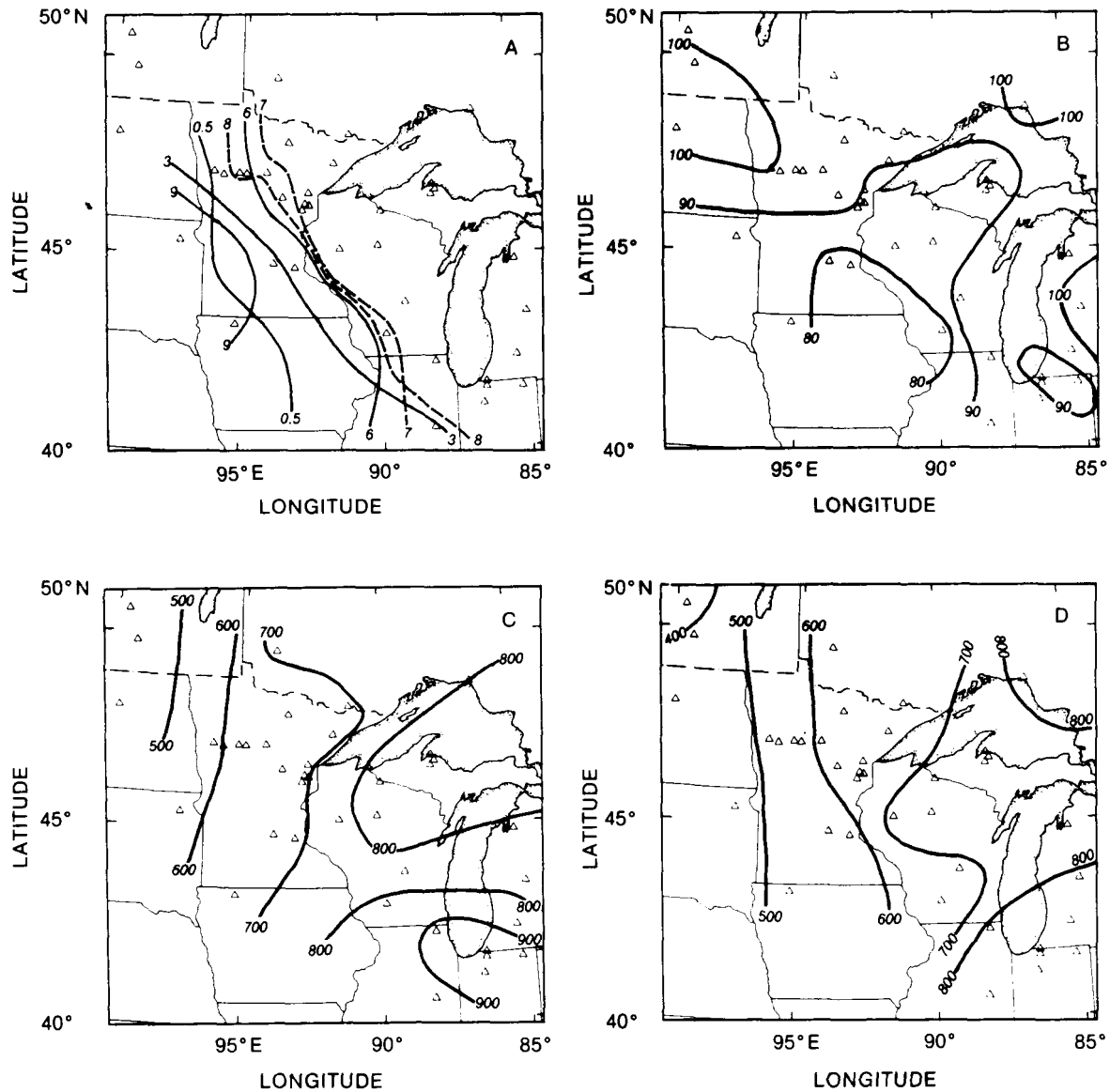

Figure 7.5 (A) Isochrone map (contour values are in thousands of years) for 20% prairie forb pollen *Artemisia* + *Ambrosia* + *Compositae* + *Chenopodiaceae/Amaranthaceae* = sage + ragweed + daisy family + pigweed family) that shows the eastward and then westward movement of the prairie-forest border. (B) Ratio between estimated annual precipitation at 6000 B.P. and observed annual precipitation at present. (C) Observed values of annual precipitation in mm. (D) Estimates of annual precipitation at 6000 B.P. calculated from pollen data by regression analysis. Source: Bartlein et al. (1984, reprinted by permission of *Quaternary Research 22*, 361–374.)

recent variations in $\delta^{18}O$ are small in comparison to the 1.7 $\pm$ 0.1‰ decrease that occurred since the last glacial maximum at 18,000 B.P. and coincided with a decrease in global ice volume and an estimated increase in the global mean temperature by 5° $\pm$ 1°C (Manabe and Hahn 1977). A change in the global mean temperature by more than 1°C since 6000 B.P., therefore, seems unlikely.

7.4.5 Climate Model Validation

An important use for the paleoclimatic maps for 6000 B.P. will be in testing the results from model simulations. In work in progress, Webb et al.[2] have shown that the pattern of temperature differences for eastern North America is similar to the pattern generated with the National Center for Atmospheric

[2] T. Webb, P. J. Bartlein, and J. E. Kutzbach, unpublished data.

Research (NCAR) atmospheric GCM by Kutzbach and Guetter (1984a). Their experiment was similar to the work of Kutzbach (1981), Kutzbach and Otto-Bliesner (1982), and Kutzbach and Guetter (1984b) for 9000 B.P. They ran the model using the July solar radiation values for 6000 B.P. which were about 5 to 6% higher than today for all latitudes of the Northern Hemisphere. (This amplification of the seasonal cycle of solar radiation at 6000 B.P. was related to the different time of perihelion and different inclination of the Earth's axis then. January solar radiation values were 5% lower than they are today.) The model results also yielded higher rainfall in Africa and India, where lake-level data (Figure 7.5) and other climate estimates indicate more moist conditions at both 9000 and 6000 B.P. (Table 7.2).

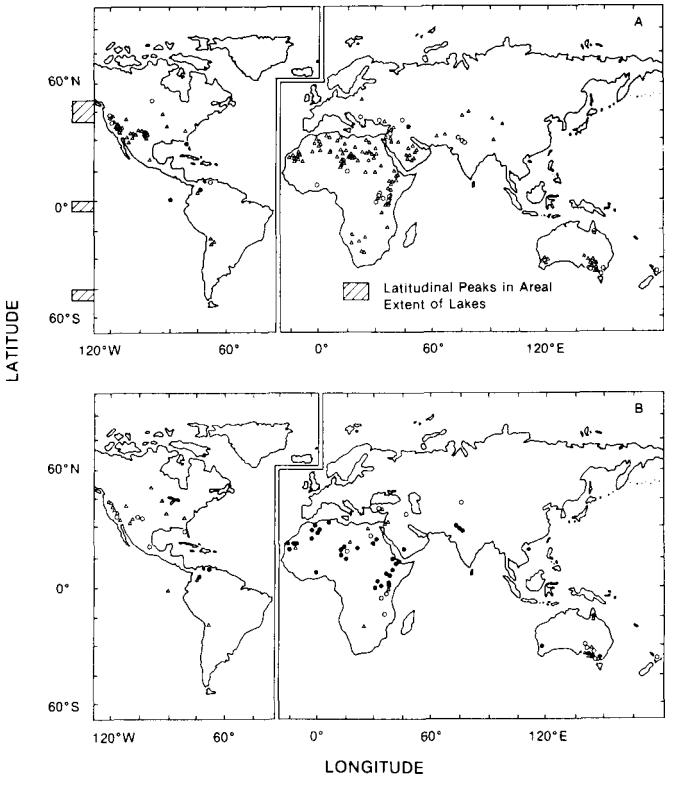

Figure 7.6. Water levels in lakes for the present (A) and 6000 B.P. (B). Symbols indicate high water levels (above 70% of the maximum level recorded for the basin) (•); intermediate levels (○); and low water levels (below 15% of the maximum level recorded for the basin) (Δ). Source: Street-Perrott and Harrison (1985, reprinted by permission of J. Wiley & Sons, Inc.)

Full evaluation of this first model experiment for conditions at 6000 B.P. is still in progress, but the work so far demonstrates the promise for using paleoclimatic data in testing the results simulated by GCMs. One of the main effects of increased amounts of CO_2 in the atmosphere is to change the radiative forcing and energy balance of the climate system. Tests are needed to show how well the models can simulate climate patterns when the radiative forcing is changed. Because the orbital variations alter this forcing, the experiments with the paleoclimatic data provide just such a test.

The paleoclimatic data and modeling results for 9000 and 6000 B.P. show that the 5–7% change in Northern Hemisphere summer radiation between then and now had a major effect on climate. The demonstration of the climatic significance of these relatively small changes in radiation is one important consequence of this synthesis of modeling and paleoclimatic research. The different seasonal radiation conditions at 6000 B.P. are also an important reason why the climate for 6000 B.P. cannot serve as an exact analog for the climates that may occur when CO_2 concentrations double.

7.4.6 Conclusions

The climate around 6000 B.P. was significantly different from today, and maps of estimated mean July temperatures show patterns with regions of higher as well as lower temperatures in northern middle to high latitudes. More data (and derived temperature estimates) are needed before it can be demonstrated that the global mean temperature was higher at 6000 B.P. than it is today. The current data suggest that the global mean temperature at 6000 B.P. was probably within 1°C of today's temperature. If this estimate is correct, then the data for moisture conditions at 6000 B.P. are impressive because they show that large changes in both precipitation and the extent of deserts and grasslands can be associated with relatively small variations in the global mean temperature. Further study of this and other periods with warm climates or with increasing temperatures (e.g., 16,000 to 10,000 B.P.) should be helpful in producing potentially useful information for improving our understanding of future warm climates. This type of study should include preparation of maps showing the magnitude and spatial

scale of changes in temperature, precipitation, and moisture balance that might be associated with a relatively small change in the global radiation budget. Such information should be used cautiously until the exact causes of past and future climate changes are known.

7.5 RESEARCH RECOMMENDATIONS

The most important conclusions and recommendations arising from this review and from research to date are:

1. The magnitude of the predicted changes in global mean temperature that may be induced by increasing CO_2 and trace gas concentrations over the next 100 years may be similar to or greater than changes observed over the past 10,000 years. Specific knowledge of past climatic variability on time scales of 10^2 to 10^4 years is therefore relevant to the greenhouse gas issue. More data are required for selected intervals during the past 10,000 years in order to demonstrate and quantify the past "natural" variability of climate in both time and space and to obtain estimates for the global mean temperature and its variation.
2. Information from past climates can help in constructing climate scenarios, but past climates cannot serve as exact analogs for future climate changes. Studies of past climates are, nevertheless, required in order to show the geographical patterns of climate change associated with past periods of global warming or cooling on different time scales. Such studies will allow possible similarities in the patterns of climate change that have been identified on different time scales to be more firmly established and understood.
3. Data about past climates are needed for use in validating the results of climate models, including general circulation models. Tests are required to show how well the models can simulate climate patterns when the radiation patterns are changed and when the changes in climate are large relative to those recorded by instruments over the past 100 years. Global sets of paleoclimatic data are needed to make these tests possible.

ACKNOWLEDGMENTS

We thank J. E. Kutzbach and R. S. Bradley for comments on an early draft of this chapter. NSF Climate Dynamics funding to COHMAP (Cooperative Holocene Mapping Project) as well as DOE Contracts DE-ACO2-79EV 10097 and 10098 supported much of the research described in this chapter. We thank P. M. Anderson, R. Arigo, J. Avizinis, P. J. Bartlein, S. Klinkman, R. M. Mellor, I. C. Prentice, M. Ryall, and S. Suter for technical assistance.

REFERENCES

Andrews, J. T., Davis, P. T., Mode, W. N., Nichols, H., and Short, S. K. 1981. "Relative Departures in July Temperatures in Northern Canada for the Past 6000 Yr." *Nature 289*:164–167.

Andrews, M. 1984. *Holocene Paleoclimates: An Annotated Bibliography* (Occasional Paper 41), Institute of Arctic and Alpine Research, University of Colorado, Boulder, Colorado.

Augustsson, T., and Ramanathan, V. 1977. "A Radiative, Convective Model Study of the CO_2 Climate Problem." *Journal of the Atmospheric Sciences 34*:448–451.

Barron, E. J., Sloan, J. L., and Schneider, S. H. 1981. "An Ice-Free Cretaceous? Results from Climate Model Simulations." *Science 212*:501–508.

Barron, E. J., and Washington, W. M. 1982. "The Atmospheric Circulation During Warm Geologic Periods: Is the Equator to Pole Temperature Gradient the Controlling Factor?" *Geology 10*:633–636.

Barron, E. J., and Washington, W. M. 1984. "The Role of Geographic Variables in Explaining Paleoclimates: Results from Cretaceous Climate Model Sensitivity Studies." *Journal of Geophysical Research 89*:1267–1279.

Bartlein, P. J., and Webb, T., III. 1985. "Mean July Temperature at 6000 yr BP in Eastern North America: Regression Equations for Estimates from Fossil-pollen Data." *Syllogeus 55*:301–342.

Bartlein, P. J., Webb, T., III, and Fleri, E. C. 1984. "Holocene Climatic Change in the Northern Midwest: Pollen-Derived Estimates." *Quaternary Research 22*:361–374.

Berger, A. L. 1978. "Long-Term Variations of Daily Insolation and Quaternary Climatic Changes." *Journal of the Atmospheric Sciences 35*:2362–2367.

Berner, R. A., Lasage, A. C., and Garrels, R. M. 1983. "Carbonate Silicate Geochemical Cycle and its Effect on Atmospheric Carbon Dioxide Over the Past One Hundred Million Years." *American Journal of Science 283*:641–683.

Borchert, J. R. 1950. "The Climate of the Central North America Grassland." *Annals of the American Association of Geographers 40*:1–29.

Borzenkova, I. I., Vinnikov, K. Ya., Spirina, L. P., and Stekhnovskii, D. I. 1976. "Variation of Northern Hemisphere Air Temperature from 1881 to 1975" [in Russian]. *Meteorologiya i Gidrologiya 1976*(7):27–35.

Broecker, W. S., and Takahashi, T. 1984. "Is There a Tie Between Atmospheric CO_2 Content and Ocean Circulation?" 314–326. In J. E. Hansen and T. Takahashi (ed.), *Climate Processes and Climate Sensitivity.* Geophysical Monograph 29, Maurice Ewing Volume 5, American Geophysical Union, Washington, D.C.

Bryan, K., Komro, S., Manabe, S., and Spelman, M. J. 1982. "Transient Climate Response to Increasing Atmospheric Carbon Dioxide." *Science 215:*56–58.

Bryson, R. A. 1974. "A Perspective on Climatic Change." *Science 184:*753–760.

Budyko, M. I. 1962. "Polar Ice and Climate" [in Russian]. *Izvestia Ak. Nauk. SSR, Ser. Geog. 1962*(6):3–10.

Budyko, M. I. 1969. "The Effect of Solar Radiation Variations on the Climate of the Earth." *Tellus 21:*611–619.

Budyko, M. I., Vinnikov, K. Ya., Drozdov, O. A., and Efimova, N. A. 1978. "The Forthcoming Climatic Change" [in Russian]. *Izvestia Ak. Nauk. SSR, Ser. Geog. 1978*(6):-5–20.

Butzer, K. W. 1980. "Adaptation to Global Environmental Change." *Professional Geographer 32:*269–278.

Clark, W. C. (ed.) 1982. *Carbon Dioxide Review: 1982.* Oxford University Press, New York, New York.

CLIMAP Project Members. 1976. "The Surface of the Ice Age Earth." *Science 191:*1131–1137.

CLIMAP Project Members. 1981. "Seasonal Reconstructions of the Earth's Surface at the Last Glacial Maximum." *GSA Map and Chart Series,* (MC-36, 1–18). Geological Society of America, Boulder, Colorado.

CLIMAP Project Members. 1984. "The Last Interglacial Ocean." *Quaternary Research 21:*123-224.

Deevey, E. S., Jr., and Flint, R. F. 1957. "Postglacial Hypsithermal Interval." *Science 125:*285–288.

Denton, G. H., and Hughes, T. J. (eds.). 1981. *The Last Great Ice Age.* John Wiley Intersciences, New York, New York.

Drozdov, O. A. 1966. "On the Precipitation Changes in the Northern Hemisphere When the Temperature of the Polar Basin Changes" [in Russian]. *Trudy GGO 1966*(198):3–16.

Drozdov, O. A. 1974. "Anthropogenic Impact on the Hydrological Cycle" [in Russian]. *Trudy GGO 1974* (316):83–103.

Flohn, H. 1977. "Climate and Energy: A Scenario to a 21st Century Problem." *Climatic Change 1:*5–20.

Flohn, H. 1979. "A Scenario of Possible Future Climates—Natural and Man-Made." 243–266. *Proceedings of the World Climate Conference* (WMO-No. 537). World Meteorological Organization, Geneva, Switzerland.

Flohn, H. 1980. *Possible Climatic Consequences of a Man-Made Global Warming* (IIASA publication RR-80-30). International Institute for Applied Systems Analysis, Laxenburg, Austria.

Flohn, H. 1981. *Major Climatic Events Associated with a Prolonged CO_2-Induced Warming.* (ORAU/IEA-81-8[m]). Institute for Energy Analysis, Oak Ridge Associated Universities, Oak Ridge, Tennessee.

Frakes, L. A., 1979. *Climates Throughout Geologic Time.* Elsevier, Amsterdam, The Netherlands.

Gates, W. L. 1976. "Modeling the Ice-Age Climate." *Science 191:*1138–1144.

Groisman, P. Ya. 1979. "Algorithm of Estimation of Linear Structural Relation between Macroclimatic Parameters" [in Russian]. *Trudy GGI 1979*(257):76–80.

Groisman, P. Ya. 1981. "The Empirical Estimates of the Relationship between the Processes of Global Warming and Cooling and the Moisture Regime Over the Territory of the USSR" [in Russian]. *Izvestia Ak. Nauk. SSR, Ser. Geog. 1981*(5):86–95.

Hansen, J. E., Lacis, A., Rind, D., Russell, G., Stone, P., Fung, I., Ruedy, R., and Lerner, J. 1984. "Climate Sensitivity: Analysis of Feedback Mechanisms." 130–163. In J. E. Hansen and T. Takahashi (eds.), *Climate Processes and Climate Sensitivity* (Geophysical Monograph 29, Maurice Ewing Volume 5). American Geophysical Union, Washington, D.C.

Hastenrath, S., and Kutzbach, J. E. 1983. "Paleoclimatic Estimates From Water and Energy Budgets of East African Lakes." *Quaternary Research 19:*141–153.

Hays, J. D., Imbrie, J., and Shackleton, N. J. 1976. "Variations in the Earth's Orbit: Pacemaker of the Ice Ages." *Science 194:*1121–1132.

Heusser, C. J., and Streeter, S. S. 1980. "A Temperature and Precipitation Record of the Past 16,000 Years in Southern Chile." *Science 210:*1345–1347.

Heusser, C. J., Heusser, L. E., and Peteet, D. M. 1985. "Late-Quaternary Climatic Change on the American North Pacific Coast." *Nature 315:*485–487.

Howe, S. E., and Webb, T., III. 1983. "Calibrating Pollen Data in Climatic Terms: Improving the Methods." *Quaternary Science Reviews 2:*17–51.

Hunt, B. G. 1984. "Polar Glaciation and the Genesis of Ice Ages." *Nature 308:*48–51.

Huntley, B. and Prentice, I. C. 1986. "Pollen Data and Climate Estimates for 6000 and 9000 yr B.P. from Europe." COHMAP Members (ed.) *Global Climates 6000 and 9000 yr B.P.* University of Minnesota Press, Minneapolis, Minnesota.

Imbrie, J., and Kipp, N. G. 1971. "A New Micropaleontological Method for Quantitative Paleoclimatology: Application to a Late Pleistocene Caribbean Core." 71–181. In K. Turekian (ed.), *The Late Cenozoic Glacial Ages.* Yale University Press, New Haven, Connecticut.

Imbrie, J., and Webb, T., III. 1981. "Transfer Functions: Calibrating Micropaleontological Data in Climatic Terms." 125–134. In A. Berger (ed.), *Climatic Variations and Variability: Facts and Theories.* D. Reidel Publishing, Dordrecht, The Netherlands.

Jäger, J., and Kellogg, W. W. 1983. "Anomalies in Temperature and Rainfall During Warm Arctic Seasons." *Climatic Change 5:*39–60.

Jones, P. D., and Kelly, P. M. 1983. "The Spatial and Temporal Characteristics of Northern Hemisphere Surface Air

Temperature Variations." *Journal of Climatology 3*:243–252.

Jones, P. D., Wigley, T. M. L., and Kelly, P. M. 1982. "Variations in Surface Air Temperature: Part 1. Northern Hemisphere 1881–1980." *Monthly Weather Review 110*:59–70.

Kay, P. A. and Andrews, J. T. 1983. "Re-evaluation of Pollen-Climate Transfer Functions in Keewaitin, Northern Canada." *Annals of the Association of American Geographers 73*:550–559.

Kellogg, W. W. 1977. "Effects of Human Activities on Climate." *WMO Technical Note 156 (WMO No. 486)*. World Meteorological Organization, Geneva, Switzerland.

Kellogg, W. W. 1978. "Global Influences of Mankind on Climate," 205–227. In J. Gribbin (ed.), *Climatic Change*, Cambridge University Press, Cambridge, United Kingdom.

Kellogg, W. W., and Schware, R. 1981. *Climate Change and Society*. Westview Press, Boulder, Colorado.

Kerr, R. A. 1984. "Carbon Dioxide and the Control of the Ice Ages." *Science 223*:1053–1054.

Kipp, N. G. 1976. "New Transfer Function for Estimating Past Sea-Surface Conditions from Sea-Bed Distribution of Planktonic Foraminiferal Assemblages in the North Atlantic." *Geological Society of America Memoir 145*:3–41.

Knox, F., and McElroy, M. B. 1984. "Changes in Atmospheric CO_2: Influence of the Marine Biota at High Latitude." *Journal of Geophysical Research 89*:4629–4637.

Kutzbach, J. E. 1980. "Estimates of Past Climate at Paleolake Chad, North Africa, Based on a Hydrological and Energy Budget Model." *Quaternary Research 14*:210–223.

Kutzbach, J. E. 1981. "Monsoon Climate of the Early Holocene: Climate Experiment with the Earth's Orbital Parameters for 9000 Years Ago." *Science 214*:59–61.

Kutzbach, J. E., and Guetter, P. J. 1984a. "Sensitivity of Late-Glacial and Holocene Climates to the Combined Effects of Orbital Parameter Changes and Lower Boundary Condition Changes: Snapshot Simulations with a General Circulation Model for 18,000, 9000, and 6000 Years Ago." *Annals of Glaciology 5*:85–87.

Kutzbach, J. E., and Guetter, P. J. 1984b. "The Sensitivity of Monsoon Climates to Orbital Parameter Changes for 9000 yr B.P.: Experiments with the NCAR General Circulation Model," 801–820. In J. Imbrie and A. Berger (eds.), *Milankovitch and Climatic Change*. D. Reidel Publishing Co., Dordrecht, The Netherlands.

Kutzbach, J. E., and Otto-Bliesner, B. 1982. "The Sensitivity of the African-Asian Monsoonal Climate to Orbital Parameter Changes for 9000 Years BP in a Low-Resolution General Circulation Model." *Journal of the Atmospheric Sciences 39*:1177-1188.

Lough, J. M., Wigley, T. M. L., and Palutikof, J. P. 1983. "Climate and Climate Impact Scenarios for Europe in a Warmer World." *Journal of Climate and Applied Meteorology 22*:1673–1684.

Manabe, S., and Hahn, D. G. 1977. "Simulation of an Ice Age." *Journal of Geophysical Research 82*:3889–3911.

Manabe, S., and Stouffer, R. J. 1979. "A CO_2-Climate Sensitivity Study with a Mathematical Model of the Global Climate." *Nature 282*:491–493.

Manabe, S., and Stouffer, R. J. 1980. "Sensitivity of a Global Climate Model to an Increase of CO_2 Concentration in the Atmosphere." *Journal of Geophysical Research 85*:5529–5554.

Manabe, S., and Wetherald, R. T. 1980. "On the Distribution of Climate Change Resulting from an Increase in CO_2 Content of the Atmosphere." *Journal of the Atmospheric Sciences 37*:99–118.

Manabe, S., Wetherald, R. T., and Stouffer, R. J. 1981. "Summer Dryness Due to an Increase of Atmospheric CO_2 Concentration." *Climatic Change 3*:347–386.

Marvil, R., and Prell, W. L. 1986. "The Northwest Indian Ocean at 6000 and 9000 Yr B.P." In COHMAP Members (eds.), *Global Climates 6000 and 9000 Yr B.P.* University of Minnesota Press, Minneapolis, Minnesota.

Mathewes, R. W., and Heusser, L. E. 1981. "A 12,000 Year Palynological Record of Temperature and Precipitation Trends in Southwestern British Columbia." *Canadian Journal of Botany 59*:707–710.

Mercer, J. H. 1978. "West Antarctic Ice Sheet and CO_2 Greenhouse Effect: A Threat of Disaster." *Nature 271*:-321–325.

Namias, J. 1980. "Some Concomitant Regional Anomalies Associated with Hemispherically Averaged Temperature Variations." *Journal of Geophysical Research 85*:1580–1590.

National Research Council 1983. *Changing Climate* (Report of the Carbon Dioxide Assessment Committee). Board on Atmospheric Sciences and Climate. National Academy Press, Washington, D.C.

Neftel, A., Oeschger, H., Schwander, J., Stouffer, B., and Zumbrunn, R. 1982. "Ice Core Sample Measurements Give Atmospheric CO_2 Content During the Past 40,000 Years." *Nature 295*:220–223.

Owen, T., Cess, R. D., and Ramanathan, V. 1979. "Enhanced CO_2 Greenhouse to Compensate for Reduced Solar Luminosity on Early Earth." *Nature 277*:640–642.

Palutikof, J. P., Wigley, T. M. L., and Lough, J. M. 1984. *Seasonal Climate Scenarios for Europe and North America in a High-CO_2, Warmer World* (DOE/EV/10098-5 Report). U.S. Department of Energy, Washington, D.C. Available from NTIS, Springfield, Virginia.

Peterson, G. M. 1983. *Holocene Vegetation and Climate in the Western USSR*. Doctoral Dissertation, University of Wisconsin, Madison, Wisconsin.

Peterson, G. M. 1984. "Recent Pollen Spectra and Zonal Vegetation in the Western USSR." *Quaternary Science Reviews 2*:281–321.

Peterson, G. M., Webb, T., III, Kutzbach, J. E., vander Hammen, T., Wijmstra, T. A., and Street, F. A. 1979. "The Continental Record of Environmental Conditions at 18,000 yr B.P.: An Initial Evaluation." *Quaternary Research 12*:47–82.

Pisias, N. G., and Shackleton, N. J. 1984. "Modeling the Global Climate Response to Orbital Forcing and Atmospheric Carbon Dioxide." *Nature 310:*757–759.

Pittock, A. B., and Salinger, J. M. 1982. "Towards Regional Scenarios for a CO_2-Warmed Earth." *Climatic Change 4:*23–40.

Ruddiman, W. F., and Mix, A. C. 1986. "The North and Equatorial Atlantic Ocean at 6000 and 9000 Yr B.P." COHMAP Members (eds.), *Global Climates 6000 and 9000 Yr B.P.* University of Minnesota Press, Minneapolis, Minnesota.

Sachs, H. M., Webb, T., III, and Clark, D. R., 1977. "Paleoecological Transfer Functions." *Annual Review of Earth and Planetary Sciences. 5:*159–178.

Sarmiento, J. L., and Toggweiler, J. R. 1984. "A New Model for the Role of the Oceans in Determining Atmospheric pCO_2." *Nature 308:*621–624.

Sarnthein, M. 1978. "Sand Deserts During Glacial Maximum and Climatic Optimum." *Nature 272:*43–46.

Schlesinger, M. E. 1983. "Simulating CO_2-Induced Climate Change with Mathematical Climate Models Capabilities, Limitations and Prospects." *Proceedings of the Carbon Dioxide Research Conference: Carbon Dioxide, Science and Consensus.* (Document CONF-820970). U.S. Department of Energy, Washington, D.C. Available from NTIS, Springfield, Virginia.

Schneider, S. H., and Londer, R. 1984. *The Coevolution of Climate and Life.* Sierra Club Books, San Francisco, California.

Schneider, S. H., and Thompson, S. L. 1981. "Atmospheric CO_2 and Climate: Importance of the Transient Response." *Journal of Geophysical Reseach 86:*3135–3147.

Sear, C. B. 1984. *Atlantic Arctic Sea Ice Variations: A Modeling Experiment with Relevance to the Carbon Dioxide Problem.* (Doctoral Dissertation). University of East Anglia, Norwich, United Kingdom.

Semtner, A. J. 1984. "On Modeling the Seasonal Thermodynamic Cycle of Sea Ice in Studies of Climatic Change." *Climatic Change 6:*27–37.

Shackleton, N. J., and Opdyke, N. D. 1973. "Oxygen Isotope and Paleomagnetic Stratigraphy of Equatorial Pacific Core V28-328: Oxygen Isotope Temperatures and Ice Volumes on a 10^5 Year and 10^6 Year Scale." *Quaternary Research 3:*39–55.

Shackleton, N. J., Backman, J., Zimmerman, H., Kent, D. V., Hall, M. A., Robert, D. G., Schnitker, D., Baldauf, J. G., Desprairies, A., Homrighausen, R., Huddlestun, P., Keene, J. B., Kaltenback, A. J., Krumsiek, K. A. O., Morton, A. C., Murray, J. W., and Westberg-Smith, J. 1984. "Oxygen Isotope Calibration of the Onset of Ice-Rafting and History of Glaciation in the North Atlantic Region." *Nature 307:*620–623.

Shackleton, N. J., Hall, M. A., Line, Jr., and Cang Shuxi 1983. "Carbon Isotope Data in Core V19-30 Confirms Reduced Carbon Dioxide of the Ice-Age Atmosphere." *Nature 306:*319–322.

Siegenthaler, U., and Wenk, T. 1984. "Rapid Atmospheric CO_2 Variations and Ocean Circulation." *Nature 308:*-624–626.

Spelman, M. J., and Manabe, S. 1984. "Influence of Oceanic Heat Transport Upon the Sensitivity of a Model Climate." *Journal of Geophysical Research 89:*571–586.

Stauffer, B., Hofer, H., Oeschger, H., Schwander, J. and Siegenthaler, U. 1984. "Antarctic CO_2 Concentration During the Last Glaciation." *Annals of Glaciology 5:*160–164.

Street-Perrott, F. A., and Harrison, S. 1985. "Lake-Level Fluctuation." In A. D. Hecht (ed.), *Paleoclimate Analysis and Modeling.* J. Wiley & Sons, New York, New York.

Stuiver, M., Burk, R. L., and Quay, P. D. 1984. "$^{13}C/^{12}C$ Ratios and the Transfer of Biospheric Carbon to the Atmosphere." *Journal of Geophysical Research: 89:*11731–11748.

Swain, A. M., Kutzbach, J. E., and Hastenrath, S. 1983. "Estimates of Holocene Precipitation for Rajasthan, India, Based on Pollen and Lake-Level Data." *Quaternary Research, 19:*1–17.

Thompson, S. L., and Schneider, S. H. 1982. "Carbon Dioxide and Climate: The Importance of Realistic Geography in Estimating the Transient Temperature Response." *Science 217:*1031–1033.

Trabalka, J. R., Edmonds, J. A., Reilly, J., Gardner, R. H., and Voorhees, L. D. 1985. "Human Alterations of the Global Carbon Cycle and the Projected Future." In J. Trabalka (ed.), *Atmospheric Carbon Dioxide and the Global Carbon Cycle* (DOE/ER-0239). U.S. Department of Energy. Washington, D.C. Available from NTIS, Springfield, Virginia.

Vinnikov, K. Ya., and Groisman, P. Ya. 1979. "Empirical Model of Modern Climatic Change" [in Russian]. *Meteorologiya i Gidrologiya 1979* (3):25–36.

Vinnikov, K. Ya., Gruza, G. V., Zakharov, V. F., Kirillov, A. A., Kovyneva, N. P., and Ran'kova, E. Ya. 1980. "Current Climatic Changes in the Northern Hemisphere" [in Russian]. *Meteorologiya i Gidrologiya 1980* (6):5–17.

Vinnikov, K. Ya., and Kovyneva, N. P. 1983. "Global Warming: The Distribution of Climatic Change" [in Russian]. *Meteorologiya i Gidrologiya 1983* (5):10–19.

Watson, R. A., and Wright, H. E., Jr. 1980. "The End of the Pleistocene: A General Critique of Chronostratigraphic Classification." *Boreas 9:*153–163.

Webb, T., III. 1982. "Temporal Resolution in Holocene Pollen Data." *Third North American Paleontological Convention Proceedings. 2:*569–572.

Webb, T., III. 1984. "A Global Paleoclimatic Database for 6 and 9 ka BP." *Annals of Glaciology 5:*236–237.

Webb, T., III 1985a. "Holocene Palynology and Climate." In A.D. Hecht (ed.), *Paleoclimate Analysis and Modeling. 163–195,* J. Wiley & Sons, New York, New York.

Webb, T., III. 1985b. *A Global Paleoclimatic Data Base for 6000 yr B.P.* (Report DOE/EV/10097-6). U.S. Department of Energy, Washington, D.C. Avaliable from NTIS, Springfield, Virginia.

Webb, T., III, and Bryson, R. A. 1972. "Late- and Postglacial Climatic Change in the Northern Midwest, USA Quantitative Estimates Derived from Fossil Pollen Spectra by Multivariate Statistical Analysis." *Quaternary Research 2:*70–115.

Wetherald, R. T., and Manabe, S. 1981. "Influence of Seasonal Variation Upon the Sensitivity of a Model Climate." *Journal of Geophysical Research 86:*1194–1204.

Wigley, T. M. L. 1981. "Climate and Paleoclimate: What We Can Learn About Solar Luminosity Variations." *Solar Physics 74:*435–471.

Wigley, T. M. L., Angell, J., and Jones, P. D. 1985. "Analysis of the Temperature Record." In M. C. MacCracken and F. M. Luther (eds.), *Detecting the Climatic Effects of Increasing Carbon Dioxide* (DOE/ER-0235). U.S. Department of Energy, Washington, D.C. Available from NTIS, Springfield, Virginia.

Wigley, T. M. L., and Jones, P. D., 1981. "Detecting CO_2-Induced Climatic Change." *Nature 292:*205–208.

Wigley, T. M. L., Jones, P. D., and Kelly, P. M. 1980. "Scenarios for a Warm, High-CO_2 World." *Nature 283:*17–21.

Wigley, T. M. L., and Schlesinger, M. E. 1985. "Analytical Solution for the Effect of Increasing CO_2 on Global Mean Temperature." *Nature 315:*649–652.

Williams, J. 1980. "Anomalies in Temperature and Rainfall During Warm Arctic Seasons as a Guide to the Formulation of Climate Scenarios." *Climatic Change 2:*249–266.

Williams, J., Barry, R. G., and Washington, W. M. 1974. "Simulation of the Atmospheric Circulation Using the NCAR Global Circulation Model with Ice Age Boundary Conditions." *Journal of Applied Meteorology 13:*305–317.

Williams, L. D., and Wigley, T. M. L. 1983. "A Comparison of Evidence for Late Holocene Summer Temperature Variations in the Northern Hemisphere." *Quaternary Research 20:*286–307.

Wright, H. E., Jr. 1976. "The Dynamic Nature of Holocene Vegetation." *Quaternary Research 6:*581–596.

8. PROJECTING THE CLIMATIC EFFECTS OF INCREASING CARBON DIOXIDE: VOLUME SUMMARY

Frederick M. Luther
Lawrence Livermore National Laboratory

CONTENTS

8.1 INTRODUCTION

For almost a century, it has been recognized that changes in the atmospheric carbon dioxide (CO_2) concentration could alter the Earth's climate. Preliminary compilations of measurements indicated a CO_2 increase starting in the 19th century. More definitive measurements made since the International Geophysical Year (IGY) in 1957–1958 have confirmed about a 25% increase in CO_2 concentration since about 1850, caused in its initial stages by deforestation and now primarily by fossil fuel combustion. Initial studies of the potential climatic consequences of increasing CO_2 concentration indicated that substantial warming would occur, but important approximations and simplification in the early studies introduced many uncertainties. The need to resolve these uncertainties and to carry out more accurate and complete assessments prompted the initiation of a carbon dioxide research program by the U.S. Department of Energy. Progress in these areas is described in these State-of-the-Art reports.

A more thorough assessment of the potential climatic effects of the increasing CO_2 concentration will require a better understanding of the various components of the climate system and their interactions. Because of the complex coupling among physical, chemical, radiative, and dynamical processes in the climate system, it is not possible to derive an analytic expression that describes how the climate parameters will change as the composition of the atmosphere is changed. Rather, the system of nonlinear equations that is used to describe the climate system must be solved numerically. The resulting system of equations and solution techniques is referred to as a climate model, and models vary greatly in complexity, depending on their intended application. To address the many climate related questions associated with an increase in atmospheric CO_2 concentration, a hierarchy of models has been developed ranging from the simpler energy balance models to complex, three-dimensional general circulation models (GCMs) of the atmosphere and the oceans. Some models provide steady-state solutions, whereas others provide transient solutions. Each class of models has made valuable contributions to the understanding of the potential climatic effects of the increasing CO_2 concentration.

Observational data play an important role in the validation of the climate models and as input to the model calculations. The study of past climates is useful for illustrating the natural variability of the climate on several temporal and spatial scales. Confidence in the models' ability to simulate the potential climatic effects of changes in atmospheric composition is derived from the ability of the models to simulate the present climate and observed climate variations for which the perturbations are known. Validation of the models includes testing the accuracy of the treatment of each process separately as well as testing the model as a whole. For this purpose, data with broad spatial and temporal coverage and with sufficient accuracy are needed. Unfortunately, most data sets do not meet all of these conditions.

Over the past 10 years, significant progress has been made in our understanding of the various processes that make up the climate system. These processes include physical, chemical, radiative, and dynamical processes that affect the atmosphere, the hydrosphere (the oceans and water distributed on the land), the cryosphere (the snow and ice on, at, or beneath the Earth's surface), and the biosphere. Improvements have been made in our ability to model these processes through a combination of theoretical research and the collection and interpretation of observational data. This chapter summarizes the significant progress that is reported in more detail and with complete references in the earlier chapters of this volume.

8.2 CLIMATE SYSTEM COMPONENTS AND PROCESSES (CHAPTER 1)

The global energy balance provides a physical basis for relating energy transfer processes to the state of the climate system. Perturbations to the climate system originate as perturbations to one or more energy transfer processes. In the case of increasing CO_2 concentration, the forcing mechanism leading to climate change is a perturbation to the radiation balance of the Earth/atmosphere system. Other energy transfer processes within the atmosphere include the transfer of sensible and latent heat by convection and by the winds. The processes of evaporation and condensation affect the transfer of latent heat between the surface and the

atmosphere. The exchange of energy between the atmosphere and the surface (land and oceans) also depends on the large-scale circulation and mixing within the oceans and on the surface characteristics such as sea ice, snow cover, soil moisture, and type of vegetation. These processes are coupled by physical, chemical, radiative, and dynamical interactions.

Changes in atmospheric composition (radiatively active gases, clouds, or aerosols) affect local heating rates within the atmosphere and change the energy balance at the Earth's surface and at the top of the atmosphere. Changes in the radiative fluxes at the surface affect the rates of evaporation and convection of heat away from the surface, which in turn affect the amount of moisture in the atmosphere and the precipitation rates. The resulting change in temperature affects chemical rates of reaction within the atmosphere, leading to further changes in composition that also affect radiative processes. The changes in temperature structure and radiative heating rates affect the large-scale dynamics, which in turn changes on the distribution of species concentrations within the atmosphere, thereby altering further the temperature and chemical rates of reaction. Thus, the climate system responds to perturbations in a complex, coupled manner until a balance is restored in both the net energy budget and in the budgets of the various chemical species.

Progress has been made in understanding the radiative properties of CO_2, trace gases, and aerosols and in the ability to treat the basic radiative effects of these constituents in climate models. The basic radiative properties of CO_2 have been known for many years, but there is a need to understand better how to treat the overlap of the longwave absorption bands of CO_2 with those of water vapor (H_2O) and ozone (O_3). Improvements have been made in compilations of the spectral line data for CO_2, H_2O, and O_3, and spectroscopic measurements have been made for many trace gases for the first time. As a result, it has been possible to assess the radiative importance of CO_2, H_2O, O_3, and many of the other trace gases in terms of their role in the present atmosphere and their potential climatic impact in the future as their concentrations increase.

With the development of larger and faster computers, it has been possible to incorporate more-detailed representations of the energy transfer processes into climate models. In many models the solar and longwave radiation transfer routines have been upgraded to include the current understanding of the radiative properties of the gases and improved solution techniques. Improvements have been made in the parameterization of boundary layer processes in GCMs, and there have been major improvements in the treatment of oceans in these models. Early versions of these models used fixed sea surface temperatures. Later the sea surface temperatures were calculated by assuming that they were shallow layers without a circulation (swamp model). Oceans were next treated as having a fixed mixed-layer depth but no heat transport by ocean currents. Models have progressed and varied in complexity to the extent that some models now have variable mixed-layer depth or even full three-dimensional resolution in which the ocean circulation is driven by ocean interactions with the atmosphere.

Models have also progressed in their ability to treat the transient effects of the increasing CO_2 concentration. Until a few years ago, climate models treated only annual-mean steady-state conditions; GCMs were generally run for fixed seasons (usually January and July), and their results were interpolated to cover the rest of the year. The models are now able to handle seasonal variations, and the time response of the oceans is being included with increasing sophistication; the ability to treat ocean currents is also being added. Some of the simplified models are able to investigate the transient effects of a time-dependent increase in the CO_2 concentration. However, in the most physically complete models such calculations are very expensive and are not likely to be repeated frequently; therefore, they have been postponed until the recent model improvements have been more completely tested and verified.

By comparing results from different climate models, it has been possible to assess the effects of various modeling approaches on the ability of the models to simulate the present climate and their sensitivity to a doubling of the CO_2 concentration. Although there is relatively good agreement among models on the change in global mean surface air

temperature for a doubling of the CO_2 concentration, there are significant differences in the latitudinal and regional patterns of the calculated changes in temperature. The models also differ in their assessments of the latitudinal and regional changes in precipitation. The causes of these differences are under active investigation. The treatment of the oceans has been shown to have a significant effect, and differences in the cloud cover prescriptions are likely to be important contributors to the differences.

It is generally agreed that improvements need to be made in the cloud cover prescriptions and in the prescription of the radiative properties of clouds, but there has not been an adequate data base from which new prescriptions could be developed. In recent years there has been significant improvement in the understanding of the effects of the finite sizes of clouds. Although parameterizations have been developed to include the effects of the finite sizes of clouds in radiation transfer calculations, these parameterizations have not been adapted in climate calculations because the geographical distribution of the required cloud parameters is largely unknown. Recently, the International Satellite Cloud Climatology Project (ISCCP) was initiated by the World Meteorological Organization with the scientific objectives of (1) producing a global infrared and visible radiance data set from which cloud parameters can be derived, (2) deriving and validating a global cloud climatology, and (3) improving parameterizations of clouds in climate models. This project promises to provide the needed data and parameterizations for improving the climate models.

The research conducted in recent years has led to a better understanding of the climate system and how the climate might change in the future. Despite these improvements, significant uncertainties remain in assessments of the climate sensitivity to an increased CO_2 concentration. In the following sections, current understanding of various aspects of the potential changes resulting from the increasing CO_2 concentration is summarized.

8.3 RADIATIVE EFFECTS OF CARBON DIOXIDE AND TRACE GASES (CHAPTER 2)

Many gases have absorption bands in the longwave region (wavelengths greater than 4 μm). Among these, CO_2, H_2O, and O_3 are the most important. Carbon dioxide has strong absorption bands in the 15-μm region and weak absorption bands near 10 μm. Water vapor absorption bands span most of the longwave region, but the absorption is weak in the 8–12 μm region. Ozone has two narrow absorption bands centered near 9.6 μm and a weak band centered at 14 μm that overlaps the strong 15-μm band of CO_2. There is relatively little atmospheric absorption in the region between 8 and 12 μm compared with the rest of the longwave spectrum. Because the atmosphere is essentially transparent in this portion of the longwave regime, this region is called the atmospheric window. However, the absorption bands of many trace gases lie within the atmospheric window. Because they do not overlap strong absorption bands of other constituents, absorption bands in the window region can be very effective in decreasing the longwave radiation emitted to space. Many of the trace gases have band strengths that are greater than the band strength of the 15-μm CO_2 band, but because of their small concentrations, these gases do not have radiative effects as large as that of CO_2. Although the radiative effects of trace gases currently are small, they could increase significantly in the future because the concentrations of many of the gases are projected to increase dramatically as a result of anthropogenic activity.

The three techniques used to calculate the radiative effects of gases in the longwave regime include the line-by-line technique, narrow band models, and wide band models. The line-by-line technique is the most accurate. Comparisons of laboratory-measured transmittances with line-by-line calculated transmittances for CO_2 have generally shown agreement to within 5–10% over narrow spectral intervals and to within several tenths of a percent for total band absorption. Each of the approaches has an application to climate modeling. The line-by-line calculations provide a reference against which the less sophisticated techniques can be checked. The narrow band model calculations are particularly

useful for one-dimensional model studies requiring high relative accuracy. The wide band model calculations are best suited for the rapid calculations necessary for many climate studies, particularly those involving GCMs.

A comparison of model calculations (the Intercomparison of Radiation Codes in Climate Models) showed that the line-by-line models were in very good agreement with each other; that is, typically to within a few W m^{-2} or about 1%. The narrow band models showed a spread of 10–15% in the calculations of the downward flux at the surface for five reference atmospheres. Calculations of the change in net flux at the tropopause when the CO_2 concentration is doubled ranged from -4.3 to -7.4 W m^{-2} for cloud-free conditions. The wide band model results were very similar to the narrow band model results, in spite of the fact that the wide band models are designed to achieve high computational efficiency. The comparison of calculations with flux observations from within the atmosphere generally have shown agreement of the order of $\pm 5\%$ for cloud-free, low aerosol content conditions. In terms of overall climate model performance, there is less discrepancy among calculated radiation budgets and flux perturbations than there is between elements of the hydrologic cycle, calculated humidity fields, and cloud amounts and their spatial distribution.

Model calculations show that most of the downward emission by CO_2 to the surface comes from the central portion of the 15-μm band in which there are many strong spectral lines. Because of saturation of strong lines, most of the change in longwave absorption and emission resulting from an increase in CO_2 occurs in the weaker absorption regions on either side of the 15-μm band. As a result, the change in radiative forcing due to an increase in the CO_2 concentration varies logarithmically with respect to CO_2 concentration. On the other hand, the absorption lines of trace gases are not saturated (because the gas concentrations are small). Consequently, the radiative effects of trace gases essentially are directly proportional to their concentrations.

Because convective mixing leads to strong coupling between the upper and lower troposphere, as well as between the troposphere and the Earth's surface, changes in the net flux at the tropopause affect temperatures throughout the troposphere and at the surface. A basis for estimating the climate change resulting from a perturbation to the atmospheric composition is to calculate the effect that the perturbation has on the net flux at the tropopause. The direct radiative heating of the surface/troposphere system resulting from a doubling of CO_2 concentration, assuming that atmospheric temperatures and water vapor amount do not change, is about 4 W m^{-2} averaged hemispherically, ranging from nearly 5 W m^{-2} at low latitudes to about 2 W m^{-2} at high latitudes. This forcing has a seasonal variation with little amplitude at low latitudes and a range of about 1 W m^{-2} at high latitudes. Because of the atmospheric temperature and water vapor distribution, the maximum heating occurs in summer and the minimum in winter.

The trace gases that have the largest radiative effects (although still small) in the present atmosphere are methane (CH_4), nitrous oxide (N_2O), and chlorocarbons ($CFCl_3$ and CF_2Cl_2). The current tropospheric concentration of CH_4 is about 1.7 parts per million by volume (ppm), and measurements indicate that the concentration has been increasing at a rate of about 1% per year. Anthropogenic influences resulting from changes in land use, increasing human population, and the corresponding increasing animal populations may hav accounted for significant changes in the atmospheric CH_4 budget. The current tropospheric concentration of N_2O is about 300 parts per billion by volume (ppb), and measurements indicate that N_2O is increasing at a rate of about 0.2% per year. A substantial fraction of the increase in N_2O is attributed to the combustion of fossil fuels. Chlorocarbons $CFCl_3$ and CF_2Cl_2 are well mixed in the troposphere and have concentrations of about 190 and 350 parts per trillion by volume (ppt), respectively. Although the production of $CFCl_3$ and CF_2Cl_2 has remained almost constant since about 1974, the atmospheric concentrations of these species continue to increase because of their long lifetimes. The combined radiative effect of these four trace gases over the past decade has been estimated to be nearly equal to that of the change in CO_2 concentration over the same period. The relative effect of trace gases and CO_2 will continue to shift toward trace gases in the near future.

8.4 METHODS FOR DETERMINING THE CLIMATIC RESPONSE (CHAPTER 3)

Analyses of the climate of the last 100 years indicate the presence of both short-term variations and long-term trends. These analyses alone, however, do not provide unique identification of the possible roles of various causal factors, such as volcanic, CO_2, and solar variations. Because we cannot determine the causes of past climate changes, it is not possible to predict the future climate by simply extrapolating trends from the recent past. Attempts have been made to determine empirically the sensitivity of the climate system by examining the changes in radiative fluxes and temperature that occur during the normal change of seasons and as the result of small-scale perturbations. These approaches have not proved successful because the time and space domains of these analyses have not been comparable to those associated with the increasing CO_2 concentration. The only way known to study the details of the many physical processes responsible for the structure and variation of climate, and to develop a reliable capability for projecting future climates, is to construct mathematical models based on the full set of fundamental physical principles governing the climate system.

The basic physical laws governing the behavior of most of the components of the climate system (and on which a climate model therefore can be based) are relatively well known, as are the physics of the various interactive processes that serve to link the components. In the atmosphere these laws are expressed by the equations for the conservation of heat, momentum, mass, and moisture. Small-scale processes that cannot be explicitly resolved in the model must be treated parametrically.

Simplified climate models are developed by averaging over one or more dimensions. Averaging over all dimensions yields a model for the globally averaged climate in which the globally averaged temperature and water vapor amounts are the dependent variables and the motion of the atmosphere is implicitly included. Such a global energy balance model is developed using a budget equation for the fluxes of radiation (solar and longwave) and sensible and latent heat at the surface. Other energy balance models have been developed by averaging only in the vertical and longitudinal directions, in which case the zonal mean temperature and water vapor amounts are determined as functions of latitude. In this model the meridional transports of heat and moisture must be parameterized. Radiative-convective models resolve only the variation of the temperature with respect to altitude. They combine the effects of solar and longwave radiative heat transfer along with that due to vertical convection.

The most complex climate models are those in which no explicit spatial averaging is introduced. The governing equations are integrated in time over the globe in these three-dimensional GCMs. These models have a horizontal resolution of several hundred kilometers, but transport processes on smaller scales must be parameterized. These models calculate the changes in atmospheric dynamics (resulting from various perturbations), which are not calculated explicitly in the one- and two-dimensional models. The computer costs associated with running GCMs can be up to several orders of magnitude greater than that of the one- and two-dimensional models because of their larger computational requirements.

Because the GCMs actually resolve large-scale eddies that make up the day-to-day weather, it is necessary to average their results over sufficient time periods to acquire representative and stable climate statistics in the presence of these essentially short-term fluctuations. This makes the detection of the regional details (and even the latitudinal variation of some variables) of a simulated climate change a formidable statistical task.

When used with prescribed boundary conditions based on observational data, atmospheric GCMs are capable of simulating almost all of the observed large-scale features of the climate, including the average distribution of the pressure, temperature, and wind speed both near the surface and aloft. These models also reproduce the seasonal changes of the circulation from winter to summer. The GCMs do not yet, however, adequately represent all of the observed regional features needed for making detailed climate projections.

Models also have been developed for the oceanic, cryospheric, and land surface components of the climate system. In modeling the oceans, the continuity equation for salinity replaces that for water vapor. Oceanic GCMs successfully portray the average large-scale distribution of oceanic temperature, salinity, and current speed in response to realistic surface forcing and realistic basin geometry, but they are not yet particularly successful in representing observed oceanic fluctuations and vertical motions. The observed average seasonal distribution of sea ice also has been successfully simulated by specialized sea models, but not yet completely adequately by simplified models of the surface mixed layer of the ocean. Only a few models have included coupling of the atmospheric and oceanic general circulations, and assessments of their success in representing the observed conditions are now under way.

8.5 CLIMATIC SENSITIVITY TO AN INCREASED CARBON DIOXIDE CONCENTRATION (CHAPTER 4)

A hierarchy of climate models has been used to simulate the change in the equilibrium climate of the Earth resulting from an abrupt increase in the CO_2 concentration, such as a doubling from 300 ppm (characteristic of the early 20th century) to 600 ppm (a value projected for late in the next century). The earliest estimates of the CO_2-induced temperature change were obtained from surface energy balance models, wherein the energy balance condition was applied at the Earth's surface. Later, planetary energy balance models were used, wherein the balance condition was applied at the top of the atmosphere. The change in global mean surface air temperature resulting from an increased CO_2 concentration determined by these early studies differed significantly because of the neglect of certain energy fluxes in some models (so that energy was not conserved) and the inability of these models to adequately include feedback processes.

The first study with a radiative-convective model of CO_2-induced temperature change was carried out in 1967. Subsequently there have been many calculations with radiative-convective models that have differed in their treatments of physical processes. The differences are mainly in the treatment or assumed behavior of the surface energy fluxes, the response of water vapor (relative humidity) to temperture changes, the effect of convection on tropospheric lapse rates, the treatment of clouds, and the variation of surface albedo as the surface temperature changes. The changes in surface air temperature simulated by radiative-convective models for a doubling of CO_2 show a range of from 0.48 to 4.2°C. They also show that temperatures increase in the troposphere and decrease in the stratosphere. Calculations of the temperature change without feedbacks show very good agreement among models, being in the range 1.2–1.3°C for a doubling of the CO_2 concentration. In this case, the surface and tropospheric temperatures are assumed to change by the same amount, but the boundary conditions and composition of the atmosphere are kept constant (no change in water vapor or cloudiness). The difference between model results is due to differences in the treatment of feedback processes, which are generally positive (tending to increase the change in temperature) when they act individually. Variable cloud cover and variable cloud optical depth feedbacks may act as negative feedback mechanisms when they are included along with the positive water vapor feedback.

GCMs require extensive computer time to simulate the transient climate response to a perturbation lasting several decades or more. In order to reduce the computer time required for the calculations, simulations have most often been made of the equilibrium change in climate due to a sudden increase in CO_2 concentration (usually a doubling) rather than of the time-dependent (transient) changes that would result from a gradual rise in the CO_2 concentration.

For a doubling of the CO_2 concentration, the change in global mean surface air temperature calculated by GCMs has ranged from 1.5 to 4.5°C. Results from the most recent GCM calculations tend to fall near the high end of this range. The model results have been shown to be rather sensitive to the treatment of the oceans (e.g., swamp ocean versus mixed layer) and of cloud feedback processes.

The computed changes in global mean conditions are similar for the GCM calculations, but the latitudinal and regional distributions of the changes reveal significant differences. The GCM results are generally similar in that most show greater warming at high latitudes than at low latitude, but the

magnitude of the polar amplification differs among the models. The models project a warming of 2–3°C near the equator, but the maximum zonal-average warming at high northern latitudes ranges from 4 to 16°C in winter. The models are consistent in showing a maximum warming in winter at middle and high latitudes and a minimum in summer. The warming is generally greater over land than it is over the oceans.

The models predict warming in the troposphere and cooling in the stratosphere. Most models project a maximum warming in the upper troposphere at equatorial latitudes. There are major differences in the projected latitudinal distribution of changes in lapse rate in the lower troposphere.

There is less agreement among the model calculations for the projected changes in precipitation resulting from a doubling of the CO_2 concentration. The models project an increase in global mean precipitation, but there are significant areas where precipitation decreases. There are major differences in the regional patterns of the change in precipitation, but precipitation generally increases at middle and high latitudes and decreases at low latitudes. Because the precipitation data are noisy (i.e., large natural variations), the statistical significance of the projected patterns of precipitation change can be low, particularly at high latitudes.

8.6 RATE OF CLIMATE CHANGE FROM THE INCREASING CARBON DIOXIDE CONCENTRATION (CHAPTER 5)

Records show that the climate has exhibited variability over a wide range of time scales and that the climate is rarely, if ever, in a steady state. The climate record over the past 100 years shows a complex picture including interannual variability and, perhaps, some systematic trends. From 1880 to 1940 Northern Hemisphere surface air temperatures over land areas warmed by more than 0.5°C. This was followed by a gradual temperature drop of about half this amount between 1940 and 1970, after which the surface air temperature has increased, nearly reaching the 1940 peak. This record shows no clear indication of a monotonic warming over this period, as might be anticipated from the apparently continuous buildup of CO_2 in the atmosphere. These and other changes are described more fully in the companion State-of-the-Art volume entitled *Detecting the Climatic Effects of Increasing Carbon Dioxide.*

This variable pattern likely reflects the effect of forcing by factors in addition to the increasing CO_2 concentration, with variations in incident solar flux, volcanic aerosol loading, trace gases, and internal ocean dynamics probably being the most influential factors. Transient climate models are needed to address whether historical records are consistent with predictions of past warming from the increasing CO_2 concentration, as well as where and when a climate change is likely to occur in the future. External and internal forcing factors acting simultaneously with increasing CO_2 must also be included in these assessments.

Determination of the rate of climate change requires that proper account be taken of not only the rate at which the atmospheric CO_2 concentration is changing and will change, but also of the various climate system mechanisms that control the rate at which the climate changes. The coupling of the various thermal reservoirs of the climate system that can store heat is a central feature of the transient problem, along with the relaxation times of the heat storage reservoirs. On the time scale of the CO_2 problem, these reservoirs should include at least the atmosphere, land surface, upper mixed layer of the oceans (including sea ice), and the deep sea.

In the long term, well-tested, coupled atmosphere-ocean GCMs may be able to serve as operational tools for simulating transient climate changes, but these are not yet available. A hierarchy of climate models is under development with the goal of predicting the transient climate response from increases in the CO_2 concentrations. Certain essential features of the problem, however, can be illustrated with simpler energy balance models. Energy balance models that incorporate horizontal averaging depict global mean conditions, and these models are useful for studying the time scales associated with the various energy storage reservoirs in the climate system, particularly with regard to the response of the oceans. These models have shown that the response of global temperatures to external forcing is not instantaneous but is delayed by thermal damping, primarily by the oceanic mixed layer and the upper thermocline of the ocean. Thermal storage

and mixing by these reservoirs can cause a lag relative to imposed cooling or warming tendencies of about 10–20 years (although some models indicate ocean lags as large as 100 years). The results depend on the way that the ocean heat transport is modeled and the values assumed for the coefficients, since the heat diffusion rate into the deep sea significantly affects the temperature evolution at the Earth's surface. Although the heat capacity and response time of the ocean do not affect the eventual equilibrium climate change, this equilibrium may never be achieved because of changes in other factors.

A class of zonally averaged energy balance models has been developed to study the latitudinal variation of the transient climate response. Model studies show that the transient climate response can vary markedly with latitude owing to variations in surface heat capacity associated with variations in latitudinal land/sea fractions. Positive and negative feedback processes have a significant effect on model sensitivity and response time. Models with greater climate sensitivity take longer to reach a new equilibrium state.

The development of reliable predictions of transient climate change is hampered by the lack of a clear validation strategy for testing models against observed data. The seasonal response can be used as a test for latitude-resolving models since both the solar forcing and the observed thermal response are reasonably well known. However, other means must be developed to test the response of the models on the longer time scale associated with the increase in CO_2 concentration. It has been noted that the surface temperature distribution produced by the annual mean insolation is not the same as the annual mean surface temperature driven by the seasonally varying insolation. This suggests that seasonal cycles may have to be resolved in long-term simulations.

Transient climate models, when run with standard scenarios of fossil fuel CO_2 emissions, indicate that there will be a global warming of about 1°C by the year 2000 relative to the year 1850, and an additional warming of a few degrees Celsius over the next century. Estimates of the rise in surface air temperature between 1850 and the present resulting from CO_2 alone range from 0.5°C to more than 1.0°C, reflecting differences in the sensitivity of the models and differences in the lag time of the oceans as depicted in the models. It is estimated that variations in solar forcing (measured to be about 0.2%) may account for fluctuations in surface air temperatures of a few tenths of a degree Celsius. Decreases in atmospheric absorptance resulting from stratospheric dust loadings from major volcanic eruptions are estimated to cause surface cooling of a few tenths of a degree Celsius for periods of a few years. These estimates indicate that the climatic effects of solar variations and volcanic aerosols are considerably smaller in magnitude and shorter in duration than that projected for an increase in CO_2 concentration.

8.7 CLIMATIC EFFECTS OF TRACE GASES (CHAPTER 6)

Trace gases may affect the climate either directly by their own radiative properties or indirectly by interacting chemically or climatically with species that are radiatively important. The trace gases N_2O, CH_4, $CFCl_3$, and CF_2Cl_2 are the most important radiatively-active gases, each having strong absorption bands in the longwave regime. In addition, these gases interact chemically so as to affect O_3 either directly or indirectly through their influence on other species that affect O_3. Nitrous oxide is an important source of nitric oxide (NO) and nitrogen dioxide (NO_2) in the stratosphere. Although NO and NO_2 are not important radiatively, they are important in determining the distribution of both tropospheric and stratospheric O_3 and in the tropospheric photochemistry of hydroxyl (OH) and perhydroxyl (HO_2). These oxides of hydrogen provide the primary sink for O_3 in the troposphere, and the OH distribution in the troposphere is important in determining the atmospheric lifetimes of a number of trace gases, such as CH_4, methyl chloride (CH_3Cl), and methyl chloroform (CH_3CCl_3). Reaction with OH is the major sink for CH_4 in the atmosphere. Degradation of CH_4 is an important source of atmospheric carbon monoxide (CO). In the stratosphere, H_2O, OH, and HO_2 are also important products of CH_4 oxidation. Increases in CO due to anthropogenic emissions would be expected to reduce the OH concentration, which in

turn would lead to an increase in CH_4. In the stratosphere, $CFCl_3$ and CF_2Cl_2 are photolyzed, producing Cl and ClO, which destroy O_3. Thus, many of the trace gases interact photochemically through many reaction pathways. Modeling the chemistry of the atmosphere requires the simultaneous determination of the concentrations of dozens of chemical species and includes treatment of over a hundred photochemical reactions.

Changes in climate can affect the concentrations of chemical species by changing temperature-dependent chemical reaction rates. In addition, the concentration of water vapor in the atmosphere is expected to change in response to the climate perturbation, which in turn affects atmospheric chemistry. Significant changes in the amount of water vapor reaching the stratosphere could affect stratospheric O_3 concentrations. Increased water vapor in the troposphere as a result of a warmer climate should result in an increased OH concentration, which would affect the CH_4 and O_3 concentrations. Changes in atmospheric dynamics (i.e., wind patterns) resulting from climate perturbations could also affect the concentrations of the trace gases. Thus, there is a coupling among radiative, chemical, and dynamical processes in the atmosphere. Comprehensive three-dimensional models that can include proper treatment of these coupled processes are in an early stage of development. Consequently, most of the present knowledge about the climatic effects of trace gases has been gathered through the use of one-dimensional models.

Climate model calculations suggest that, on the time scale of decades, the combined climatic effects of increases of atmospheric N_2O, CH_4, $CFCl_3$, and CF_2Cl_2 concentrations and their induced change in O_3 from climate-chemistry interactions could be at least as large as that estimated from the expected increase in the CO_2 concentration alone. The computed temperature profile is sensitive to both the vertical distribution and the column amount of O_3; the larger the total O_3 column or the lower the height of the maximum O_3 concentration, the warmer the temperature of the troposphere and the surface. Estimates of the change in O_3 in the year 2010, assuming constant emission rates for $CFCl_3$ and CF_2Cl_2 and using projected emissions of other trace gases, show only a small net increase in the O_3 column (~1%), but there is a significant change in the vertical distribution of O_3. The O_3 concentration decreases in the upper stratosphere and increases in the lower stratosphere and troposphere. If $CFCl_3$ and CF_2Cl_2 emissions are assumed to increase at a rate of 3% per year, then a significant decrease in total O_3 could result.

8.8 LESSONS FROM THE PAST (CHAPTER 7)

The study of past climates contributes to the understanding of how future increases in the atmospheric CO_2 concentration may affect the climate. No close analog to the projected CO_2 warming exists in the paleoclimatic records, but there have been a few periods in the past 200,000 years that have apparently been as much as a few degrees Celsius warmer than the present over broad geographical regions. Three such periods have been considered: (1) the Medieval Warm Epoch (ca. 800–1200 A.D.), (2) the time of maximum warmth during the Holocene period (4000 to 8000 years B.P.), and (3) the last interglacial period around 120,000 years B.P. Periods (1) and (3) have not been analyzed as much as period (2), the reason being that the data coverage is less complete for these periods and the warmth may not have been global in extent during the Medieval Warm Epoch.

The current global set of paleoclimatic data for the mid-Holocene period includes pollen, lake-level, and marine plankton data. During the mid-Holocene period (also referred to as the Hypsithermal), the global mean temperature may have been 1°C warmer than at present, but limited data coverage makes precise determination of the global mean temperature difficult. However, the climate during this period was significantly different from that of today, and maps of estimated July temperatures show patterns with regions of higher as well as lower temperatures in northern middle to high latitudes. Patterns of precipitation show larger changes than do the temperature patterns. In the U.S. Midwest, the annual precipitation was 10–20% less than it is today. This pattern of change, along with the implied increase in the frequency and duration of dry western air masses, is similar to the climate changes during the 1930s Dust Bowl period in the Midwest. In Africa and India, estimates of annual precipitation were as much as 300 mm (or 50 to

100%) higher than current levels. The present Sahara and Rajasthan Deserts probably were covered by dry savannas and steppes. The moisture data are impressive because they show that large changes in both precipitation and the extent of deserts and grasslands can be associated with relatively small variations in the global mean temperature.

Another approach to the analysis of past climates is to use the instrumental records of climate parameters over the past 100 years and compare differences between warm and cold periods. This approach has the advantage that it does not require the use of noninstrumental data to estimate temperature and precipitation, but it has the disadvantage in that over this rather short time period the differences tend to be small. By using ensembles of data from warm and cold years (chosen using the warmest and coldest 20-year periods from the Northern Hemisphere surface air temperature record), detailed patterns of change have been developed. A surprising result was that winter temperatures over a substantial part of Europe were colder and showed greater interannual variability during the hemispherically warm period, probably as a result of increased blocking. Rainfall patterns showed overall decreases in spring and summer and increases in autumn and winter during periods of global warming. The North American patterns for temperature and pressure showed much less interseasonal contrast than was the case for Europe. Temperatures generally were shown to be higher and less variable throughout the year in a warm world. Changes in precipitation patterns are complex, with substantial areas of increase and decrease. The instrumental record for the Northern Hemisphere yields maximum warm-cold differences of about 2°C for Arctic latitudes and 0.5°C for the Northern Hemisphere as a whole, which is in qualitative agreement with model simulations that show an amplification of the temperature change at high latitudes.

8.9 CONCLUSIONS

The climatic effects of increasing CO_2 and trace gas concentrations are complex and not fully understood. Nevertheless, there are aspects of the projected climatic effects that are well studied, so changes in future assessments in most instances will be quantitative rather than qualitative in nature. Consequently, some conclusions can be made that are not likely to change in the future.

- CO_2 is an effective absorber (and emitter) of longwave radiation, but a weak absorber of solar radiation.
- As the CO_2 concentration increases, CO_2 acts to reduce the outgoing longwave radiation emitted to space at the top of the atmosphere and increases the downward longwave radiation incident at the Earth's surface. The change in net incoming solar radiation at the top of the atmosphere would be negligible unless significant changes in cloud cover were to occur.
- If the outgoing longwave radiation at the top of the atmosphere is reduced, then the global average emitting temperature of the climate system must increase to restore the equilibrium between the outgoing longwave radiation and the net incoming solar radiation.
- Because over 90% of the longwave radiation emitted to space comes from the troposphere (~80%) and the surface (~12%), an increase in global average emitting temperature implies that the combined emission to space from the troposphere and surface must increase.
- Because of convection and mixing within the troposphere, a strong coupling exists between the temperature changes at the surface and those occurring throughout the troposphere; thus the changes in global mean surface and tropospheric temperatures both will have the same sign. Consequently, the requirement to increase longwave radiation to space leads to warming of the troposphere and the surface (the greenhouse effect).
- When the CO_2 concentration increases, the increase in longwave emission from the stratosphere (upward to space and downward to the troposphere) is greater than the increase in absorption of longwave radiation received from below. Consequently, there is a net loss of radiative energy and the stratosphere cools.
- As the atmosphere warms, the ability of the atmosphere to hold water vapor increases and the rate of evaporation at the surface also increases. Consequently, the amount of water vapor present in the atmosphere increases.

- Because water vapor is also a greenhouse gas, an increase in the amount of water vapor also leads to warming of the troposphere and surface. Consequently, the increase in water vapor enhances the warming that would be experienced if CO_2 alone were to increase (the enhancement is estimated to be about a factor of 2).
- An increase in global mean temperature does not mean that every location on the Earth will experience the same change. There also can be regions of cooling and amplified warming.
- To maintain equilibrium between the input and output of moisture in the atmosphere, the global rate of precipitation must increase in response to an increase in the rate of evaporation. The increase, however, will be nonuniform and may increase or decrease at particular locations.
- As the climate warms, the amount of sea ice and the extent of snow cover will generally be reduced. In very cold regions (for example, in Antarctica), snowfall may acutally increase during the early stages of the warming because of increased moisture content of the air, at least until the increased snowfall is melted as a result of further warming.
- Because of the large reflectivity of snow and ice relative to their underlying surfaces, reductions in sea ice and snow cover will lead to increased solar absorption at the surface. This increase in solar absorption leads to warming of the troposphere and surface, thereby amplifying the warming due to the radiative effects of the increasing CO_2 concentration, especially at high latitudes. This polar amplification also occurs because of the near-surface temperature inversion at high latitudes and the insulating effect of snow and ice.
- Clouds may play an important role in further amplifying or moderating climate changes. In summer, increases in polar stratus clouds may increase albedo and help compensate for snow and ice changes, whereas in winter such clouds may warm the surface by trapping infrared radiation. Changes in cloud amount, optical thickness, and vertical extent all may induce temperature changes, and these processes may be introducing large uncertainties into the model simulations.
- Feedbacks and interactions of many other types can also occur among elements of the climate system. For example, drying of the land surface can lead to warming because of reduced evapotranspiration or cooling due to a higher albedo and lessened solar absorption; usually the former effect dominates, depending on the atmospheric response. While many processes have been identified, it is likely that others have not. The uncertainties introduced into CO_2 assessments by the probable lack of complete knowledge about and treatment of the climate system are not possible to evaluate directly. Successful comparison of model results with observations can, however, provide indirect evidence that the uncertainties are modest.
- Numerical models have been developed that attempt to calculate the coupled effect of the most important feedback processes. These models have been used to simulate the present climate, including the seasonal cycle, and their representation of large-scale climatic features is quite reasonable. For the simulation of regional features, the model results are not yet adequate and projections of such features must be viewed as highly uncertain.
- These model results suggest that global average temperatures will warm by 1.5 to 4.5°C once equilibrium is achieved after the CO_2 concentration has doubled. Continuing increases in the CO_2 concentration above those levels would warm the Earth still further. Such changes would be large in comparison to the decadal average temperature changes of the last 10,000 years, during which prolonged, global-scale variations have probably only rarely been more than about 1°C.
- On a molecule-for-molecule basis, a number of trace gases have even more potential than CO_2 to induce warming. Although the concentrations of these gases currently are small, their concentrations are increasing rapidly. Model studies indicate that the warming due to trace gases could augment the potential CO_2 perturbation by form 50% to more than 100% over the next century. It is essential that the potential effects of trace gases be investigated further.
- The large heat capacity of the oceans will act to slow the climate system response to changes

in atmospheric composition and other forcing factors. The vertical behavior of the oceans is not understood well enough, however, to permit precise estimation of this effect, but estimates are that the atmosphere requires from 20 to 100 years to achieve two-thirds of the expected equilibrium temperature response. As a result, substantial further warming may occur, even if CO_2 and trace gas concentrations do not increase above their present concentrations as the climate attempts to fully reach a new equilibrium state.

In summary, we have a sound qualitative understanding of the causes of the warming that is occurring and is projected to occur as a result of the increasing CO_2 and trace gas concentrations. Our quantitative understanding remains limited, particularly regarding the regional and seasonal pattern of the warming and the rate at which it will be occurring. Chapter 9 summarizes the research that must be done to reduce uncertainties sufficiently for useful assessments to be undertaken.

9. RECOMMENDATIONS FOR RESEARCH AND MODELING ACTIVITIES FOR PROJECTING THE CLIMATIC EFFECTS OF INCREASING CARBON DIOXIDE

Frederick M. Luther
Lawrence Livermore National Laboratory

Michael C. MacCracken
Lawrence Livermore National Laboratory

CONTENTS

9.1 INTRODUCTION

To provide a basis for informed decision making, a capability to accurately project the climatic effects of the increasing carbon dioxide (CO_2) concentration and other perturbations is needed. Considering long-term effects, CO_2, trace gases, and aerosols have the greatest potential for affecting the climate. Coupling of these factors through chemical, radiative, and dynamical interactions makes the problem very complex. Projections of the climatic effects of the increasing CO_2 concentration over the next several decades must consider the combined effects of many simultaneous perturbing factors along with the many feedback processes that are operative. Because of this complexity, we will continue to rely on numerical models as the primary means for making these projections.

Although significant progress has been made over the last decade in improving the understanding of individual processes and the roles of various perturbing factors, it is not yet possible to project the climatic effects of coupled perturbations with adequate confidence or accuracy. The detailed projections of changes in atmospheric parameters that are particularly relevant to estimating societal impacts cannot be provided at this time; in particular, projections of climate changes cannot yet be provided on a regional and seasonal basis. To project the impact on agriculture, for example, changes in the occurrence of situations that are particularly stressful to crops (such as the frequency and intensity of drought and the time of the first and last freezes) must be estimated. The goal of the research that is currently ongoing and that is recommended for the future is to provide a stronger scientific and technical basis for making projections in these areas. The emphasis up until now has been mainly on projecting changes in hemispheric and global mean conditions. Research during the next decade will move more toward making projections on smaller spatial scales and toward consideration of higher order statistical variations in climatic parameters.

Improvement of climate modeling capabilities requires a research effort spanning a broad range of activities. The strategy to improve our understanding of climate processes and the capability to project future climate change is based on the use of a hierarchy of models. Each class of model has its particular strengths and weaknesses, and each is best suited to particular specialized applications. For this hierarchy of models, model improvement will come about through a combination of studies directed toward improved understanding of climate processes and feedback mechanisms (and their roles in the climate system), inclusion of these processes and mechanisms in the climate models (including improvements in the parameterization of subgrid scale processes in the models), and detailed analysis of model simulations carried out to examine the climatic sensitivity to increasing concentrations of CO_2 and trace gases and to changes in other factors. In association with these activities, the testing and validation of the models by comparison with observations is essential. Confidence in the ability of the models to simulate the present climate and its variation (including the sensitivity of the climate to various perturbations) rests on proper validation of the climate models.

The research that is recommended for the major areas of scientific investigation is described in the following sections. It is not the intent of this chapter to provide a detailed research plan for accomplishing these tasks. Rather, the purpose of this chapter is to present the overall picture of the major research needs and priorities, highlighting those areas where special emphasis and effort should be directed to address key issues. More detailed recommendations for specific research in the various research areas can be found at the end of each chapter in this volume.

9.2 UNDERSTANDING OF CLIMATE PROCESSES AND FEEDBACK MECHANISMS

Models require accurate representation of all important climate processes and feedback mechanisms. The highest priority should be placed on improved understanding of how oceans and clouds affect energy transport processes in the climate system. Once the roles of the oceans and clouds are better understood, then they can be more accurately represented in the climate models. Progress in these two areas will require coordinated field experiments and modeling activities. The World Ocean Circulation Experiment (WOCE) and the International

Satellite Cloud Climatology Project (ISCCP) provide the potential for gathering the data that will enable oceanic and cloud processes to be simulated more accurately in climate models. Improvements in the representations of the planetary boundary layer, precipitation, and surface hydrology must also be made if estimates of the equilibrium sensitivity of models are to be made with greater confidence and less disagreement between models.

Goal 1. Evaluate and improve representations of important climate processes and feedback mechanisms in climate models.

9.2.1 Oceanic Processes

Oceanic processes are important because they have a significant effect on the time rate of change of the climate in response to a perturbation. Efforts to simulate the changes in climate that have occurred since the middle of the last century caused by variations in the concentrations of CO_2, trace gases, and aerosols and efforts to project future changes in climate over the next several decades both require proper representation of the thermal inertia and heat transfer effects of the oceans. For these reasons, it is important that oceanic processes and ocean-atmosphere coupling be treated more accurately in climate models.

Recommendation 1A.

The dynamics and thermodynamics of the ocean must be included in climate models. Currents, upwelling, and bottom water formation must be represented so that potential changes can be investigated. The transport of heat from the mixed layer to deeper levels in the oceans must be explicitly treated. Field observations are probably required to gather the data needed to achieve better understanding of ocean processes.

9.2.2 Cloud Processes

Improvements need to be made to the treatment of feedback processes in climate models. Cloud feedback processes are the least understood of the major climate feedback mechanisms. Depending on how cloud properties change in response to a climate perturbation, the climatic response may either be enhanced or diminished. Clouds may change in a combination of ways, including changes in cloud cover (amount), cloud altitude and thickness, and cloud optical properties.

Recommendation 1B.

The potential for clouds to amplify or moderate climate perturbations must be investigated thoroughly. Better representations must be developed for projecting changes in the physical and radiative properties of clouds as other climatic parameters change.

9.2.3 Sea Ice and Snow Cover

The climate model simulations of the warming caused by an increase in the CO_2 concentration show an amplification at high latitudes. This amplification is caused in part by the reduction in extent of sea ice and snow cover in response to the warming caused by the increased CO_2 concentration. With less snow and ice, more solar radiation is absorbed at the Earth's surface, which leads to further warming. The enhanced warming at high latitudes results in a change in the meridional gradient of temperature in the lower troposphere, which can significantly affect atmospheric circulation. The coupling between changes in ice and snow extent and changes in surface temperature is one of the strongest feedback mechanisms affecting the sensitivity of the climate to perturbations.

Recommendation 1C.

More accurate treatment of the growth and melting of sea ice and snow cover and the concomitant effect on energy exchange in the boundary layer is required in models so that the high-latitude temperature changes can be accurately projected.

9.2.4 Coupling of Climate System Components

Because of the importance that feedback processes have been shown to have on climate sensitivity, it is essential that the many coupled processes and feedback mechanisms present in the climate system be included in the climate models. For example, as has already been discussed, atmospheric and oceanic processes must be considered together.

The problem that this presents is that the atmosphere and the oceans have much different thermal response times. In time-dependent calculations, the time step is adjusted according to the response time of the system; systems with longer response times can use larger time steps, thereby reducing the computational burden. When processes with much different response times are coupled, the shorter time step must be used, which is numerically inefficient for treating the process with a long time constant. Some approaches developed to treat the coupling between the atmosphere and oceans so as to reduce overall computer time usage have inadvertently affected the representation of energy transfer between these two systems. How best to calculate the effects of coupling between system components having characteristically different response times must be determined.

Recommendation 1D.

Research is needed to develop better numerical approaches for coupling climate system components and processes with characteristically different time constants, such as coupling between small-scale, large-scale, and vertical transport in the oceans and between the oceans and the atmosphere.

9.3 COUPLED MODELING OF SIMULTANEOUS PERTURBATIONS TO THE CLIMATE

Several factors (such as CO_2, trace gases, volcanic emissions, and solar variations) are simultaneously affecting the climate. An accurate estimate of their coupled effects cannot be determined by evaluating the perturbations separately and adding them together. The climatic effects resulting from these forcings must be treated simultaneously because of the strong coupling between radiative, chemical, and dynamical processes in the atmosphere. The strong coupling requires that these processes and feedback mechanisms be integrated together in the models. As more coupled processes have been incorporated into the models, previously unrecognized feedback mechanisms have been uncovered. Further investigation is needed to ensure that important processes and mechanisms are not still being overlooked. Specialized models (rather than general circulation models) can help address some aspects of these issues, with particular emphasis being placed on radiative, chemical, and dynamical processes as appropriate.

Goal 2. Develop models that include all identified and relevant feedback mechanisms and that accurately treat the coupling between radiative, chemical, and dynamical processes.

9.3.1 Trace Gases

Model calculations indicate that increasing trace gas concentrations could substantially amplify the expected warming from the increasing CO_2 concentration. It is estimated that the increase in surface temperature caused by trace gases for the next 50 years could be at least as large as that due to the increased CO_2 concentration. Therefore, it is essential that the emissions, transformations, radiative interactions, and chemical removal mechanisms related to these species be thoroughly investigated so that these processes can eventually be included in the climate models. To improve assessments of the effects of trace gases, attention must be given to their radiative and chemical properties. Input data to the calculations could be improved by laboratory measurements of absorption bands and kinetics rates. The variation of the absorption band parameters with respect to changes in temperature and pressure particularly needs to be addressed.

Recommendation 2A.

Projections of the sensitivity of future climate to increasing trace gas concentrations must be coordinated and integrated with projections of the effects of the increasing CO_2 concentration.

Recommendation 2B.

Methods for treating the radiative, chemical, and climatic interactions of the many trace gases must be developed, tested, and included in climate models.

Recommendation 2C.

Monitoring and laboratory programs are required to provide the data needed to determine the global fluxes, balances, and trends of the important trace gases.

9.3.2 Other Perturbations to the Climate

Perturbing factors in addition to the increasing concentrations of CO_2 and trace gases also have potentially significant climatic effects. Aerosols resulting from volcanic eruptions and variations in the solar irradiance may affect the climate over periods lasting months to decades. It is not possible to predict what the climatic forcing from these perturbations will be in the future, but understanding the role of perturbations such as these on the climate of the past 100 years is important. Until the climate changes that have been observed over this time period are adequately explained, there will be significant uncertainty about the ability of models to project future climate change.

Recommendation 2D.

The causes of observed climate variations over the past 100 years must be adequately explained. Research must be directed at simulations of simultaneous coupled perturbations and must also address the issue of climatic fluctuations internal to the climate system.

9.4 TESTING AND VALIDATION OF MODELS

Differences in results among models pose a serious problem in developing confidence in sensitivity calculations. Models must be thoroughly compared to understand the basis for differences in model behavior and to evaluate the accuracy of submodels. Differences can arise because of different approximations in representing the present climate; for example, inclusion of seasonal variations in climate simulations has led to increased sensitivity compared to models averaging over the annual cycle. The effect of including finer scale spatial variations in the climate model assessments also needs to be determined.

The issue of how best to test and validate climate models has received repeated (although sometimes less than adequate) attention. Over the past few years, activity has become much more vigorous in this area. The two basic approaches have been to compare models with observational data and to conduct comparisons of different models or different versions of the same model. By comparing models, it has been possible to identify effects of various assumptions and approaches and to isolate areas of model performance that need more attention. The accuracy of the treatment of individual processes in climate models can be evaluated by comparing highly accurate calculations with the parameterized subroutines used in the climate models. The radiation transfer subroutines are already undergoing such a comparison in the Intercomparison of Radiation Codes in Climate Models (ICRCCM) study.

9.4.1 Simulation of Present and Past Climate Behavior

The observational data that are useful for model validation include the annual, seasonal, and monthly variations of climate parameters, including the frequency of anomalies and extreme events. The variations in these parameters in response to known perturbations could also be useful, but, with the exception of a few volcanic eruptions, the perturbing conditions for the perturbations are usually not well enough known for such cases to serve as definitive model validation tests. Another problem is that the perturbations that have occurred during times when observations were made have not lasted for time periods appropriate to the CO_2 problem. Thus, these cases cannot adequately serve to test model response to long-term forcing.

Although data bases are limited in both temporal and spatial coverage, the study of past climates can contribute to the understanding of how future increases in the atmospheric CO_2 concentration may affect the climate. The climate reconstructions contribute to such studies by providing information about the climatic pattern during warm (or cold) periods in the Earth's past and by providing conditions that can be used to test the ability of the models to simulate climatic variations on a range of time scales. The historical climate record has been extended back to about 1850, but there is a sparsity of data over many regions of the Earth, particularly prior to 1900 and in the Southern Hemisphere. Data are primarily for Northern Hemisphere continental locations, so it is difficult to determine accurate global average or latitudinal average perturbations. Efforts to improve and extend the historical record would aid in the evaluation of the temporal

response of the climate to increases in the CO_2 concentration and other climatic factors over the past 150 years.

Goal 3. The ability of climate models to simulate observed climate behavior must be more thoroughly investigated.

Recommendation 3A.

The results of climate models must be more thoroughly compared with observations of the present climate. It is of special importance to improve the ability of climate models to simulate the regional and seasonal variations of climate parameters.

Recommendation 3B.

The substantial differences in the character of the results of different climate models when present and perturbed climates are simulated must be identified and resolved.

Recommendation 3C.

To the extent data can be assembled, climate models should be tested to determine if they can simulate past variations in climate. The potential importance of such a test justifies a program to assemble data and investigate the causes of past climate changes.

9.4.2 Regional and Seasonal Climatic Variability and the Frequency of Extreme Events

Many societal activities (e.g., agriculture, water resources) are more influenced by climatic extremes and variations (e.g., freeze, floods, drought) than by small changes in the mean. It is essential to develop the capability to project how the frequency and magnitude of extreme events may change.

Developing and evaluating this capability will be extremely difficult. The first task will be to determine how well (or poorly) available models represent such variability. Determining the ability to simulate storm tracks is now an important aspect of the verification of weather forecast models, and should be extended to climatological time scales. At the time scale of months to a few years, the ability of the models to represent global scale ocean-atmosphere coupling can be investigated by comparison with observational data for events such as El Niño and the Southern Oscillation. Attempts to simulate the effects of changes in solar irradiance and aerosol concentrations over time periods of years or longer need to be pursued.

In the past, emphasis has been placed on the comparison of parameters averaged over large areas (hemispheric average or latitudinal variations), but future research must place increasing emphasis on the projection of changes on a regional basis. This will require comparison of regional climate records with model simulations. Attention should also move toward comparison of higher order statistical variations on these scales (e.g., the frequency and intensity of anomalies and extreme events) rather than simply annual and seasonal averages.

Goal 4. Increased effort must be devoted to projection of regional and seasonal climate changes and associated changes in climatic variability, the frequency of extreme events, and other aspects of interest for impact studies.

Recommendation 4A.

The ability of ocean-atmosphere climate models to represent the regional and seasonal variability of the present climate must be improved.

Recommendation 4B.

Consideration must be given to the development of new methodologies for projecting changes in the frequency of extreme events. Statistical and analog methods may prove to be useful.

Recommendation 4C.

Means of summarizing future climate projections must be enriched so that changes in the variability and details of climate projections can be of greater value for impact studies.

9.5 SUMMARY

A broad program of research has been outlined to address the key issues relating to projection of the climatic effects of increasing CO_2 concentration and other perturbing influences. The research involves coordination between theoretical and empirical research approaches. Progress made over the last decade has contributed to the expectation that continued efforts over the coming decade will lead to significant contributions to the goal of providing a stronger scientific basis for the assessment studies that could provide the basis for decision making.

APPENDIX A
ANALYSIS OF RESULTS FROM ENERGY BALANCE AND RADIATIVE-CONVECTIVE MODELS

Michael E. Schlesinger
Oregon State University

CONTENTS

A.1 INTRODUCTION

Three different types of climate models have been used to simulate the change in the equilibrium climate resulting from an increase in the carbon dioxide (CO_2) concentration: energy balance models (EMBs), radiative-convective models (RCMs), and general circulation models (GCMs). This appendix presents a detailed analysis of the results from EBMs and RCMs. A summary of this analysis is presented in Section 4.2 of Chapter 4 of this volume. The discussion of the GCM simulations of the change in equilibrium climate resulting from an increase in CO_2 concentration is included in Chapter 4. The discussion in this appendix places emphasis on the quantitative understanding of climate feedback processes. For this reason, the discussion necessarily involves a highly mathematical approach. This approach is helpful for analyzing the differences in sensitivity among climate models.

A.2 ENERGY BALANCE MODELS

Energy balance models predict the change in temperature at the Earth's surface that results from a change in heating based on the requirement that the net flux of energy does not change. The earliest estimates of the CO_2-induced temperature change were obtained from surface energy balance models (SEBMs) wherein the energy balance condition was applied at the Earth's surface. Later, planetary energy balance models (PEBMs) were used to determine the CO_2-induced temperature change from the balance condition applied at the top of the atmosphere. In this section we review these EBM studies of CO_2-induced temperature change, beginning with the historically first SEBMs, and concluding with PEBMs. This formulation also facilitates the quantitative evaluation of feedback, thus enabling comparison of EMBs among themselves and with the RCMs and GCMs.

A.2.1 Generalized Formulation

Energy balance models predict the change in temperature at the Earth's surface (ΔT_*) from the requirement that $\Delta N = 0$, where N is the net energy flux expressed by

$$N = N(\underline{E}, T_*, \underline{I}) \; . \qquad \text{(A.1)}$$

Here $\underline{E}$ is a vector of quantities that can be regarded as external to the climate system, that is, quantities whose change can lead to a change in climate, but which are independent of climate. $\underline{I}$ is a vector of quantities that are internal to the climate system, that is, quantities that can change as the climate changes and, in so doing, feed back to modify the climate change. The external quantities include, for example, the solar constant, the optically active ejecta from volcanic eruptions, trace gas concentrations and, for purposes of this report, the CO_2 concentration (although eventually the CO_2 concentration also may change in response to climate change). The climatic effects of the first three external factors are discussed further in Chapter 6 of this volume.

The internal quantities include all the variables of the climate system other than T_*. Because T_* is the only dependent variable in an EBM, the internal quantities must be represented therein by

$$\underline{I} = \underline{I}(T_*) \; . \qquad \text{(A.2)}$$

A small change in the energy flux ΔN, therefore, can be expressed by Equations (A.1) and (A.2) as

$$\Delta N = \sum_i \frac{\partial N}{\partial E_i} \Delta E_i + \left(\frac{\partial N}{\partial T_*} + \sum_j \frac{\partial N}{\partial I_j} \frac{dI_j}{dT_*} \right) \Delta T_* \; . \qquad \text{(A.3)}$$

This can be written in a more convenient and instructive way as

$$\Delta N = \Delta Q - G_f^{-1} \Delta T_* \; , \qquad \text{(A.4)}$$

where

$$\Delta Q = \sum_i \frac{\partial N}{\partial E_i} \Delta E_i \qquad \text{(A.5)}$$

is the change in N due to a change in one or more external quantities (ΔE_i), and

$$G_f^{-1} = -\frac{dN}{dT_*} = -\frac{\partial N}{\partial T_*} - \sum_j \frac{\partial N}{\partial I_j} \frac{dI_j}{dT_*} \qquad \text{(A.6)}$$

is the change in N resulting from a temperature change ΔT_*. From Equation (A.4) the energy balance requirement, $\Delta N = 0$, gives

$$\Delta T_* = G_f \, \Delta Q \; , \qquad \text{(A.7)}$$

from which it is seen that G_f is the gain (output/input) of the system.

It is useful to express G_f as

$$G_f^{-1} = G_0^{-1} - F \ , \tag{A.8}$$

where

$$G_0 = -\left(\frac{\partial N}{\partial T_*}\right)^{-1} \tag{A.9}$$

is the climate system gain in the absence of feedbacks and

$$F = \sum_j \frac{\partial N}{\partial I_j} \frac{dI_j}{dT_*} \tag{A.10}$$

represents the feedbacks. Then, by Equation (A.7),

$$\Delta T_* = \frac{G_0}{1 - G_0 F} \Delta Q \ . \tag{A.11}$$

This relation can be represented by a system block diagram as shown in Figure A.1. If N is independent of the internal quantities $\underline{I}$, or if $\underline{I}$ is independent of T_*, then $F = 0$ and the input ΔQ to the system is directly transferred to the output

$$\Delta T_* = (\Delta T_*)_0 \equiv G_0 \Delta Q \tag{A.12}$$

by means of only those processes for which N explicitly depends on T_*. However, if N also depends implicitly on T_*, through its dependence on the internal quantities and their dependence on T_*, part of the output is transferred through a feedback loop back to the input. Then, as can be seen from Figure A.1, the input to the climate system J is

$$J = \Delta Q + \Delta J \ , \tag{A.13}$$

where ΔQ is the external forcing and

$$\Delta J = F \Delta T_* \tag{A.14}$$

is the contribution of the feedbacks, and the output of the climate system is

$$\Delta T_* = G_0 J = G_0 (\Delta Q + F \Delta T_*) \ . \tag{A.15}$$

Solving for ΔT_* then gives Equation (A.11). Consequently, the response of the surface temperature

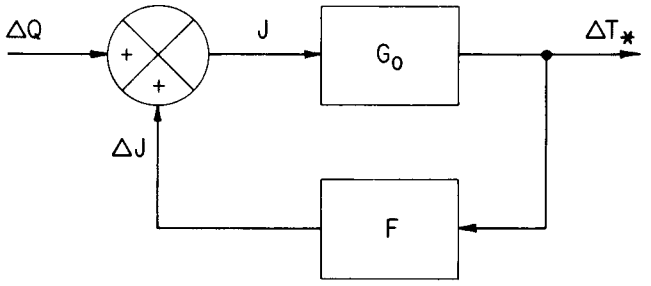

Figure A.1. Block diagram of the climatic system with a feedback loop.

ΔT_* to the forcing ΔQ is analogous to that of a system with feedback.

The effect of the feedback can be characterized on the basis of the ratio of the ΔT_* with feedback to that without feedback. Thus, by Equations (A.7), (A.11), and (A.12), we define the feedback gain ratio

$$R_f \equiv \Delta T_*/(\Delta T_*)_0 = G_f/G_0 = \frac{1}{1 - f} \ , \tag{A.16}$$

where

$$f = G_0 F \tag{A.17}$$

is the feedback factor (Bode 1975, p. 32) or, here, simply the feedback.[1] For $f = 0$, $R_f = 1$; hence $(\Delta T_*)_0$ represents the zero-feedback temperature change. Because $0 < R_f < 1$ for $f < 0$, the latter represents negative feedback (see Figure A.2). As negative feedback increases indefinitely, $R_f \to 0$ and $\Delta T_* \to 0$; however, it is important to note that ΔT_* does not change sign as $f \to -\infty$. Because $R_f > 1$ for $0 < f < 1$, the latter represents positive feedback. As positive feedback approaches unity, $R_f \to \infty$ and $\Delta T_* \to \infty$. If the positive feedback could be extended beyond unity, R_f would change sign and approach zero from negative values as $f \to \infty$. Clearly, the region $f > 1$ is physically meaningless.[2] However, as we shall see, one SEBM has estimated *de facto* such strong positive feedbacks that $f > 1$ and a temperature decrease $\Delta T_* < 0$ was obtained for heating $\Delta Q > 0$!

[1] Hansen et al. (1984) call f (their g) the system gain and R_f (their f) the net feedback factor.

[2] If $f > 1$, an increase in energy $\Delta Q > 0$ for example from an increase in the solar constant, would result in a cooling $\Delta T_* < 0$, and a decrease in energy $\Delta Q < 0$ in a warming $\Delta T_* > 0$.

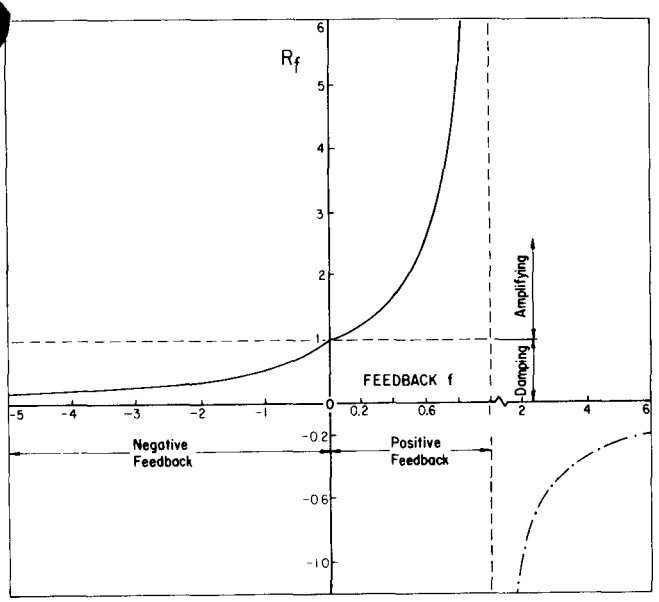

Figure A.2. The feedback gain ratio R_f versus the feedback f.

From Equations (A.5), (A.9), (A.10), (A.16), and (A.17) we can write

$$\Delta T_* = \frac{G_0}{1-f}\,\Delta Q \quad , \tag{A.18}$$

where

$$f = G_0 \sum_j \frac{\partial N}{\partial I_j}\,\frac{dI_j}{dT_*} \, , \tag{A.19}$$

$$G_0 = \left(\frac{\partial N}{\partial T_*}\right)^{-1} \tag{A.20}$$

and

$$\Delta Q = \sum_i \frac{\partial N}{\partial E_i}\Delta E_i \, . \tag{A.21}$$

Thus, the determination of ΔT_* induced by an increase in CO_2 concentration requires knowledge of the associated thermal forcing ΔQ, the zero-feedback gain of the system G_0, and the feedback f. These in turn require knowledge of the partial derivatives of N with respect to the CO_2 concentration, the temperature, and the internal quantities, as well as the total derivative of the internal quantities with respect to the temperature. In the next section we examine the SEBMs from this vantage point.

A.2.2 Surface Energy Balance Models

The net downward energy flux at the Earth's surface (N_s) can be expressed by

$$N_s = S_s - R_s - E_s - H_s \quad , \tag{A.22}$$

where S_s is the net downward solar radiation flux, R_s is the net upward longwave radiation flux, E_s is the net upward flux of latent heat due to evaporation of water and sublimation of snow and ice, and H_s is the net upward sensible heat flux. In SEBMs the temperature T_* is the temperature of the Earth's surface, T_s.

The results from three SEBMs are presented in Table A.1 in terms of the thermal forcing ΔQ for a fractional increase in CO_2 concentration $\Delta C/C$, the system gain G_f, and the surface temperature response ΔT_s. The table shows that the values of ΔT_s for a CO_2 doubling range over almost two orders of magnitude, from about 0.2°C to almost 10°C. This wide range is due to differences in both ΔQ and G_f among the models, with ΔQ varying by a factor of about 7, and G_f by a factor of about 30. Because the differences shown in Table A.1 for ΔQ can be virtually eliminated by the use of contemporary line-by-line or calibrated band models of radiative transfer (see Chapter 2 and Luther 1984), we restrict attention here to an examination of the reasons for the large variation of G_f.

Table A.1
Forcing, Gain, and Response of Selected SEBMs

Model	$\Delta C/C$	ΔQ (W m^{-2})	G_f °C(W m^{-2})$^{-1}$	ΔT_s (°C)
Callendar (1938)	1.0	6.72	0.195	1.3
Möller (1963)	1.0	3.08	3.113	9.6
Newell and Dopplick (1979)	0.8	1.0	0.237	0.24

A.2.2.1 Callendar

One of the earliest calculations of CO_2-induced warming was performed by Callendar (1938) with an SEBM. In his study S_s, E_s, and H_s were ignored so that Equation (A.22) becomes

$$N_s = R_s^{\downarrow}(C) - \sigma T_s^4 \, , \tag{A.23}$$

where $R_s^{\downarrow}$ and σT_s^4 are the downward and upward longwave fluxes, respectively, C represents the CO_2

Table A.2
Gain and Feedback Characteristics of Selected Surface Energy Balance Models

Model	Fluxes Included	V_s (m s^{-1})	G_0 (°C(W m^{-2})$^{-1}$)	Feedbacks					G_f (°C(W m^{-2})$^{-1}$)
				f_{TR}	f_{WR}	f_{WE}	f_{TH}	f	
Callendar (1938)	$R_s^\downarrow$, σT_s^4	—	0.1950	0	0	0	0	0	0.195
Möller (1963)	$R_s^\downarrow$, σT_s^4, S_s	—	0.1850	0.6122	0.3284	0	0	0.9406	3.113
Newell and Dopplick (1979)	$R_s^\downarrow$, σT_s^4, S_s, E_s, H_s	0	0.1633	0.8411	0	0	0	0.8411	1.028
		3	0.0260	0.1342	0	0	0	0.1342	0.030
		6	0.0142	0.0733	0	0	0	0.0733	0.015
Illustration Based on Newell and Dopplick (1979)	$R_s^\downarrow$, σT_s^4, S_s, E_s, H_s	0	0.1633	0.8411	0	0	0	0.8411	1.028
		3	0.0260	0.1342	0	0.6431	0.1958	0.9731	0.967
		6	0.0142	0.0733	0	0.7024	0.2139	0.9896	1.365

concentration, and σ is the Stefan-Boltzmann constant (5.6687×10^{-8} W m^{-2} K^{-4}). Because $R_s^\downarrow$ is not explicitly a function of T_s, the zero feedback gain is, by Equations (A.20) and (A.23),

$$G_0 = (4\sigma T_s^3)^{-1} \quad . \tag{A.24}$$

Thus, G_0 rapidly decreases with increasing T_s. For $T_s = 283$ K, as assumed by Callendar, $G_0 = 0.195$°C (W m^{-2})$^{-1}$. Callendar did not consider any feedback, hence as shown in Table A.2, $f = 0$ and $G_f = G_0 = 0.195$°C (W m^{-2})$^{-1}$.

A.2.2.2 Möller

Möller (1963) considered three SEBMs. First, Möller assumed that the surface energy flux was

$$N_s = R_s^\downarrow(C, T_a) - \sigma T_s^4 \ , \tag{A.25}$$

where T_a represents the vertical profile of atmospheric temperature. Again, because $R_s^\downarrow$ is not explicitly a function of T_s, the zero feedback gain is given by Equation (A.24) as $G_0 = 0.185$°C (W m^{-2})$^{-1}$ for the assumed $T_s = 288$ K. The internal variables in this model are the atmospheric temperatures, so by Equations (A.19) and (A.25)

$$f = G_0 \sum \frac{\partial R_s^\downarrow}{\partial T_a} \frac{dT_a}{dT_s} = G_0 \frac{dR_s^\downarrow}{dT_s} \ . \tag{A.26}$$

Möller prescribed $T_a = -55$°C in the stratosphere and $T_a = T_s - \Gamma z$ in the troposphere, where z is altitude, with lapse rate $\Gamma = 6.5$°C km^{-1}. Instead of determining f by Equation (A.26), Möller determined $dN_s/dT_s = dR_s^\downarrow/dT_s - 4\sigma T_s^3$ by computing N_s from a radiation diagram for several values of T_s, each with the attendant change in T_a, and then by expressing the result as $N_s(T_s)$ by an approximate interpolation formula. The result can be written by Equation (A.6) as

$$G_f \equiv \left(\frac{dN_s}{dT_s}\right)^{-1} = 0.477\text{°C (W m}^{-2})^{-1} \ , \tag{A.27}$$

which is in agreement with the value found similarly by Plass (1956). Then by Equation (A.16) we find that

$$f = f_{TR} = 1 - \frac{G_0}{G_f} = 0.6122 \ . \tag{A.28}$$

Because this positive feedback is due to the increase in $R_s^\downarrow$ that occurs when T_a increases, the latter as a result of the increase in T_s, we shall call it a temperature/radiation feedback (f_{TR}) (Table A.2).

As a second SEBM, Möller assumed that

$$N_s = R_s^\downarrow(C, T_a, W) - \sigma T_s^4 \quad , \tag{A.29}$$

where

$$W = \int_0^\infty \rho_a q_a \, dz \tag{A.30}$$

represents the total amount of water vapor in the atmospheric column, with ρ_a being air density and q_a being specific humidity. The internal variables are T_a and W, and

$$f = f_{TR} + G_0 \frac{\partial R_s^\downarrow}{\partial W} \frac{dW}{dT_s} \ . \tag{A.31}$$

Again Möller did not determine f from Equation (A.31), but instead he determined dN_s/dT_s by computing N_s from a radiation diagram for several values of T_s with the relative humidity (RH) assumed to be constant at 75%. In this case, T_a and W increase as T_s increases, the latter by Equation (A.30) because $q_a = RH \ q^*(T_s, p)$, where q^* is the saturation specific humidity, and q^* increases rapidly with

T_s. From an approximate interpolation formula for $N_s(T_s, W)$, Möller obtained $G_f = -2.864°C$ (W $m^{-2})^{-1}$. Then by Equations (A.28) and (A.31) we find $f = 1.0646$ and

$$f_{WLR} \equiv G_0 \frac{\partial R_s^{\downarrow}}{\partial W} \frac{dW}{dT_s} = 0.4524 , \qquad (A.32)$$

where f_{WLR} is a water vapor/longwave radiation feedback caused by the increase in $R_s^{\downarrow}$ as W increases, that is, the greenhouse effect for water vapor, and the increase in W with T_s caused by the constant RH.

The combination of f_{TR} and f_{WLR} is larger than unity, hence these positive feedbacks combine to yield the physically unrealistic result that $\Delta T_s < 0$ for $\Delta Q > 0$. Möller realized this inconsistency and therefore proposed a third SEBM, namely,

$$N_s = S_s(W) + R_s^{\downarrow}(C, T_a, W) - \sigma T_s^4 . \qquad (A.33)$$

Then,

$$f = f_{TR} + f_{WLR} + f_{WSR} , \qquad (A.34)$$

where

$$f_{WSR} \equiv G_0 \frac{\partial S_s}{\partial W} \frac{dW}{dT_s} \qquad (A.35)$$

is a water vapor-solar radiation feedback. Möller determined dN_s/dT_s from his radiation diagram and a model for the solar radiation and found $G_f = 3.113$ °C (W $m^{-2})^{-1}$. Then by Equations (A.28), (A.32), and (A.34), $f = 0.9406$ and $f_{WSR} = -0.1240$. The water vapor-solar radiation feedback is negative because S_s decreases as W increases, and W increases with T_s for fixed RH. The two effects of water vapor on radiation can be combined into a single water vapor-solar radiation feedback (f_{WR}) as

$$f_{WR} = f_{WLR} + f_{WSR} = 0.3284 . \qquad (A.36)$$

The combined effect of the temperature-radiation and water vapor-radiation feedbacks is strongly positive (see Table A.2).

A.2.2.3 Newell and Dopplick

Newell and Dopplick (1979), concerned about the 2–3°C warming of the tropical oceans simulated by radiative-convective and general circulation models for a CO_2 doubling, investigated the effects of the latent and sensible heat fluxes on the CO_2-induced temperature change. Their SEBM is described by

$$N_s = S_s(C, q_a) + R_s^{\downarrow}(C, T_a, q_a) - \sigma T_s^4 - E_s(T_s, q_a) - H_s(T_s, T_a) , \qquad (A.37)$$

where

$$E_s = 6080\, V_s (q_s^* - q_a) , \qquad (A.38)$$

and

$$H_s = 2.51\, V_s (T_s - T_a) . \qquad (A.39)$$

Here T_a and q_a represent the temperature and specific humidity of the surface air, V_s the surface wind speed (m s^{-1}), and q_s^* the saturation specific humidity at T_s and surface pressure p_s (mb^3). From Equation (A.20) we find

$$G_0 = -\left(\frac{\partial N_s}{\partial T_s}\right)^{-1} = \left[4\sigma T_s^3 + V_s\left(6080 \frac{\partial q_s^*}{\partial T_s} + 2.51\right)\right]^{-1} \qquad (A.40)$$

Comparing this with Equation (A.24) shows that G_0 depends on which fluxes are included in the surface energy budget; here, it depends on V_s as well as T_s. (This definition of G_0 is not unique. Alternatively, G_0 can be defined as in Equation (A.27) with E_s and H_s then contributing only to f.) From Equation (A.19)

$$f = f_{TR} + f_{WR} + f_{WE} + f_{TH} , \qquad (A.41)$$

where

$$f_{TR} = G_0 \frac{\partial R_s^{\downarrow}}{\partial T_a} \frac{dT_a}{dT_s} , \qquad (A.42)$$

$$f_{WR} = G_0 \left(\frac{\partial R_s^{\downarrow}}{\partial q_a} + \frac{\partial S_s}{\partial q_a}\right) \frac{dq_a}{dT_s} , \qquad (A.43)$$

$$f_{WE} = -G_0 \frac{\partial E_s}{\partial q_a} \frac{dq_a}{dT_s} = G_0 (6080\, V_s) \frac{dq_a}{dT_s} , \qquad (A.44)$$

and

[3] 100 mb equals 10 kPa.

$$f_{TH} = -G_0 \frac{\partial H_s}{\partial T_a} \frac{dT_a}{dT_s}$$
$$= G_0 (2.51 V_s) \frac{dT_a}{dT_s} . \quad (A.45)$$

f_{WE} represents a water vapor-evaporation feedback, and f_{TH} is a temperature-sensible heat feedback.

Following the approach taken by Plass (1956) and Möller (1963), Newell and Dopplick determined the equivalent value for f_{TR}/G_0 from an expression for $\sigma T_s^4 - R_s^{\downarrow}(T_s, q_a)$ given by Privett (1960). The result can be written as

$$f_{TR} = G_0 \left(0.474 + 0.075\sqrt{q_a p_s/0.622}\right) 4\sigma T_s^3 . \quad (A.46)$$

In so doing, because $R_s^{\downarrow}$ is not explicitly a function of T_s, it was implicitly assumed that T_a is not constant, but rather changes as T_s changes. However, Newell and Dopplick otherwise explicitly assumed that both T_a and q_a do not change as T_s changes; hence by Equations (A.43)-(A.45), it was assumed that $f_{WR} = f_{WE} = f_{TH} = 0$ and, therefore, $f = f_{TR}$. It is evident that $f_{TR} \neq 0$ and $f_{TH} = 0$ are consistent for this model only for $V_s = 0$.

For $T_s = 300$ K, $q_a = 15 \times 10^{-3}$, as selected by Newell and Dopplick, and $p_s = 1000$ mb

$$G_0 = (6.122 + 10.757 V_s)^{-1} \quad (A.47)$$

and

$$f = f_{TR} = 5.16 G_0 \quad (A.48)$$

with the values shown in Table A.2 for $V_s = 0$, 3 and 6 m s^{-1}. For $V_s = 0$, G_0 is smaller than the values given by Callendar (1938) and Möller (1963) as a result of the large (tropical) value for T_s. Also, f_{TR} is larger than the values given by Callendar (1938) and Möller (1963) because of the large (tropical) values for q_a. Consequently, for the case of no latent and sensible heat transfer, that is, $V_s = 0$, G_f obtained by Newell and Dopplick is comparable to that obtained by Möller (1963) with only the temperature/radiation feedback. However, as evident from Equations (A.46) and (A.47) and Table A.2, both G_0 and f_{TR} rapidly decrease as V_s increases, resulting in the decrease of G_f from 1.028 to 0.030°C (W m^{-2})$^{-1}$ as the wind increases from 0 to only 3 m s^{-1}. This decrease in G_f with increasing V_s when the latent and sensible heat fluxes are included in the SEBM has sometimes been called negative feedback. However, as shown in Table A.2, the feedback $f = f_{TR}$ is actually positive. The decrease in G_f is predominantly the result of the decrease in the zero-feedback gain G_0 with increasing V_s.

The value of $G_f = 0.24$ given by Newell and Dopplick (Table A.1) was obtained as a weighted average of the 3 m s^{-1} value of $G_f = 0.030$ for the 92% tropical ocean area, and the value by Möller of $G_f = 0.477$ for $f = f_{TR}$ for the 8% tropical land area. This result was then multiplied by a factor of 3.5 to account for the effect of a nonzero water vapor-radiation feedback. The climatic gain obtained by Newell and Dopplick has been cited by Idso (1980) in support of his empirical result (see Appendix B of this volume).

The cause of the dramatic decrease in G_f with increasing V_s is the assumption that T_a and q_a do not change. This fact can be demonstrated by choosing what could be called the other limit, namely, that $T_s - T_a$ and $q_s^* - q_a$ do not change. In this limit, by Equations (A.44) and (A.45),

$$f_{WE} = 6080 V_s \frac{\partial q_s^*}{\partial T_s} G_0 = 8.244 V_s G_0 , \quad (A.49)$$

and

$$f_{TH} = 2.510 V_s G_0 , \quad (A.50)$$

with the results shown in Table A.2. For $V_s = 0$, hence no latent or sensible heat, G_f is as before. However, for $V_s \neq 0$, both f_{WE} and f_{TH} are positive, with $f_{WE} = 3.3 f_{TH}$, and increase with increasing V_s. Even ignoring f_{WR}, the sum of the feedbacks now increases with V_s. G_f still decreases from $V_s = 0$ to $V_s = 3$ m s^{-1}, but much less than for the Newell and Dopplick limit, and now increases from $V_s = 3$ to $V_s = 6$ m s^{-1}.

A.2.2.4 Summary

The wide range in the values of G_f obtained from SEBMs shown in Tables A.1 and A.2 is, in part, a consequence of the nonlinear dependence of G_f on f. From Equation (A.6)

$$\frac{\partial G_f}{\partial f} = \frac{G_0}{(1-f)^2} , \quad (A.51)$$

hence, the change in G_f resulting from a given change in f rapidly increases as $f \rightarrow 1$ (Figure A.2)

This sensitivity of G_f to f means that f must be determined with both high accuracy and precision. The difficulty of achieving this has been due to the neglect of certain fluxes in the earlier SEBMs, and to the inability of SEBMs in general to determine the behavior of the climate system away from the surface energy balance level.

The surface and the troposphere are strongly coupled; hence, neither the surface nor the atmosphere can be considered in isolation. Because of the inherent difficulty of specifying the behavior of the atmosphere in terms of the surface temperature in SEBMs, that is, $I(T_s)$, and the large sensitivity of ΔT_s in SEBMs to this specification, it is preferable to use models that calculate the atmosphere's behavior based on the fundamental laws of physics.

A.2.3 Planetary Energy Balance Models

The planetary radiative energy budget is

$$N_0 = \frac{1-\alpha_p}{4} S_0 - R_0 , \qquad \text{(A.52)}$$

where N_0 is the net radiation at the top of the atmosphere, S_0 is the solar constant ($\sim$1370 W m^{-2}), R_0 is the upward longwave radiation flux at the top of the atmosphere, and α_p is the planetary albedo ($\sim$0.3 To balance the planetary radiative energy budge: requires that $N_0 = 0$; hence,

$$R_0 = \frac{1-\alpha_p}{4} S_0 \sim 240 \text{ W m}^{-2} . \qquad \text{(A.53)}$$

An effective radiating temperature of the Earth (T_e) can be defined by

$$T_e = \left(\frac{R_0}{\sigma}\right)^{1/4} \sim 255 \text{ K} . \qquad \text{(A.54)}$$

Hence, by Equations (A.52) and (A.54),

$$N_0 = \frac{1-\alpha_p}{4} S_0 - \sigma T_e^4 . \qquad \text{(A.55)}$$

N_0 can be expressed in terms of T_s rather than T_e by introducing an effective planetary emissivity (ϵ_p) as

$$\epsilon_p = \left(\frac{T_e}{T_s}\right)^4 \sim 0.6 . \qquad \text{(A.56)}$$

Then by Equation (A.55)

$$N_0 = \frac{1-\alpha_p}{4} S_0 - \epsilon_p \sigma T_s^4 . \qquad \text{(A.57)}$$

Letting $T_* = T_s$, the zero-feedback gain G_0 is given by Equations (A.9) and (A.57) as

$$G_0 = \left(4\epsilon_p \sigma T_s^3\right)^{-1} , \qquad \text{(A.58a)}$$

and

$$G_0 = \frac{T_s}{(1-\alpha_p)S_0} , \qquad \text{(A.58b)}$$

which can be compared with Equation (A.24). It can be seen that G_0 depends on T_s and ϵ_p (or α_p and S_0) of the unperturbed climate and, in contrast to SEBMs, does not depend on the type and treatment of the physical processes in the model. Taking T_s as being approximately equal to the observed surface air temperature, $T_a = 288$ K, gives $G_0 \sim 0.3$°C (W m^{-2})$^{-1}$.

The feedback f is given by

$$f = G_0 \sum_j \frac{\partial N}{\partial I_j} \frac{dI_j}{dT_s} , \qquad \text{(A.59)}$$

where the I_j are again the internal variables of the climate system. It can be seen here that the feedback depends on the specification of the behavior of the atmosphere and the Earth's surface. Thus, PEBMs also have the same problem as SEBMs, namely, the need to treat the behavior of the climate system away from the energy balance level. In PEBMs this has been done semi-empirically following the initial studies by Budyko (1969) and Sellers (1969). The equilibrium surface temperature change for a CO_2 doubling ranges in PEBMs from 0.6°C (Rasool and Schneider 1971) to 3.3°C (Ramanathan et al. 1979).

A.3 RADIATIVE-CONVECTIVE MODELS

As was evident from the discussion of the preceding section, the essential difficulty in using EBMs to determine climatic change lies in their inability to accurately and precisely determine the feedbacks. This occurs because of the limited set of internal variables that can be selected in these models and because of the limited knowledge of the relationships of the chosen internal variables to the surface

temperature. Simply stated, EBMs are limited because they do not have a physically based model of the atmosphere.

What physical processes must be included in such a model of the atmosphere if the objective is to simulate the change in the surface temperature ΔT_s induced by a change in the CO_2 concentration ΔC? If we knew ΔT_s observationally, as presumably we will in the future, then we could answer the question by sequentially inserting different processes into the model and retaining only those that significantly contribute to ΔT_s. Because we cannot do this yet, we can take the not unreasonable approach of determining which processes are required in the model to reproduce the present-day temperature profile of the atmosphere, $T(z)$. Proceeding in this way, however, does not guarantee that some physical processes essential to the determination of ΔT_s may not be important for the reproduction of $T(z)$, and, therefore, that some essential physical processes (and feedbacks) are not left out of the model. We will discuss this issue later.

A.3.1 Model Formulation

The transfers of solar and longwave radiation are essential physical processes in establishing the atmospheric temperature profile. Accordingly, a thermodynamic climate model based solely on the thermodynamic energy equation can be developed that includes only the heating and cooling by solar and longwave radiation, respectively, that is,

$$\rho c_p \frac{\partial T}{\partial t} = \frac{\partial S}{\partial z} - \frac{\partial R}{\partial z}, \qquad \text{(A.60)}$$

where t is time, z is altitude, ρ is density, c_p is the heat capacity at constant pressure, S is the downward solar radiation flux and R is the net upward longwave radiation flux. The calculation of the radiative fluxes requires a radiative transfer model (see Chapter 2) and knowledge of the vertical distributions of the gaseous absorbers—principally water vapor, carbon dioxide, ozone, and clouds—which may be prescribed along with the solar constant, the solar zenith angle, and the albedo of the Earth's surface. The atmosphere may then be subdivided vertically into layers, and the radiative-equilibrium temperature for each layer may be determined by integrating Equation (A.60) in time from an arbitrary initial temperature until $\partial T/\partial t = 0$ for all layers. Such a purely radiative thermodynamic climate model is successful in reproducing the observed vertical temperature distribution of the stratosphere, but it gives temperatures that are colder in the upper troposphere and warmer near the surface than those observed (Manabe and Strickler 1964). The resultant tropospheric temperature lapse rate, $\Gamma = -\partial T/\partial z$, is larger than the dry adiabatic lapse rate, $\Gamma_{da} \approx 10°\text{C km}^{-1}$, which defines the neutral stratification for the vertical displacement of unsaturated air. This superadiabatic stratification $\Gamma > \Gamma_{da}$ is unstable and cannot persist in the actual atmosphere due to the ameliorating processes of convection. Accordingly, Equation (A.60) must be modified to include the nonradiative transfer of energy from the surface to the atmosphere (Q_{sfc}), as well as the convective redistribution of energy within the atmosphere (Q_{conv}), that is,

$$\rho c_p \frac{\partial T}{\partial t} = \frac{\partial S}{\partial z} - \frac{\partial R}{\partial z} + Q_{\text{sfc}} + Q_{\text{conv}}. \qquad \text{(A.61)}$$

The physical processes that comprise Q_{sfc} and Q_{conv} are complex because they involve the turbulent transfer of energy in both unsaturated and saturated conditions, and would, if explicitly treated, place an impractical computational burden on the model. Consequently, simplified (parameterized) treatments of these processes have been in use since the pioneering work of Manabe and Strickler (1964), in which Q_{sfc} was determined as an equivalent radiative energy exchange and Q_{conv} was determined by convective adjustment. In the latter, the temperatures of consecutive model layers are adjusted in an energetically conservative manner such that the lapse rate is restored to a prescribed value Γ_p whenever $\Gamma > \Gamma_p$. This type of model is called a radiative-convective model or RCM and, as first shown by Manabe and Strickler (1964), is capable of reproducing many of the observed features of the temperature profiles in both the stratosphere and troposphere.

Since the development of the first RCM by Manabe and Strickler (1964), a large number of RCMs have been constructed with different radiative transfer models, different parameterizations of Q_{sfc} and Q_{conv}, and additional physical processes

and feedbacks of potential importance for CO_2-induced (and other) climate changes. It will be useful in what follows to tabulate in Table A.3 the physical processes whose treatments differ among the RCMs, along with a brief descriptor and abbreviation of these different treatments.

In the following sections we first present the results for CO_2-induced temperature changes obtained by RCMs and then analyze these results in terms of the feedbacks associated with the physical processes shown in Table A.3.

Table A.3
Physical Processes Whose
Treatments Differ Among RCMs

Physical Process	Treatment	Abbreviation
Surface energy flux	Equivalent radiative exchange	ERE
	Bulk aerodynamic exchange	BAE
Water vapor	Fixed absolute humidity	FAH
	Fixed relative humidity	FRH
	Variable relative humidity	VRH
Convection	Fixed lapse rate	FLR
	Moist adiabatic lapse rate	MALR
	Baroclinic adjustment	BADJ
	Penetrative convection	PC
Clouds	No cloud	CLR
	Fixed cloud altitude	FCA
	Fixed cloud pressure	FCP
	Fixed cloud temperature	FCT
	Predicted clouds	PCL
	Fixed cloud cover	FCC
	Variable cloud cover	VCC
	Fixed optical depth	FOD
	Variable optical depth	VOD
Surface albedo	Fixed albedo	FAL
	Predicted albedo	PAL

A.3.2 Results

The first study of CO_2-induced temperature change with an RCM was carried out by Manabe and Wetherald (1967). In their RCM, the cosine of the solar zenith angle and the length of the day were taken equal to their respective annual mean values for the globe. The surface energy flux was treated as an equivalent radiative exchange, convection was parameterized by convective adjustment with a fixed critical lapse rate, the atmospheric water vapor mixing ratio was calculated assuming a fixed profile of relative humidity, and three cloud layers with fixed pressure were prescribed along with a fixed surface albedo. The equilibrium vertical temperature profiles computed for prescribed CO_2 concentrations of 150, 300 and 600 ppm are shown in Figure A.3. Each profile exhibits a troposphere between the surface and about 13 km with a lapse rate Γ_p, and a stratosphere from 13 to 42 km where the temperature is first isothermal and then increases with increasing altitude. The stable stratification in the stratosphere shows that it is in pure radiative equilibrium, whereas the critical lapse rate of the troposphere indicates that it is in radiative-convective equilibrium. Figure A.3 shows that doubling the CO_2 concentration, either from 150 to 300 ppm or from 300 to 600 ppm, increases the temperture at the surface and in the troposphere, and decreases the temperature in the stratosphere above 20 km.

The surface temperature changes simulated by 17 RCMs for a doubled CO_2 concentration are presented in Table A.4. The values are all positive and range from a minimum of 0.48°C to a maximum of 4.20°C. In the next section we analyze the physical processes that result in this wide range of simulated surface temperature change induced by a doubling of the CO_2 concentration.

A.3.3 Analysis and Interpretation of the Results

Why does the temperature increase in the troposphere and decrease in the stratosphere when the CO_2 concentration is doubled, and why do the estimated surface temperature changes vary by almost a factor of 10? We will attempt to answer these questions in the following sections. To answer these questions, we will first examine the direct radiative forcing caused by the increased CO_2 concentration. Next we will estimate the temperature response in the absence of feedbacks, and finally, we will examine the CO_2-induced temperature change with feedbacks as revealed by the RCM studies presented in Table A.4.

A.3.3.1 Direct Radiative Forcing Due to Increased CO_2

Because about 95% of the direct radiative forcing occurs in the longwave radiation emitted by the Earth and only 5% in the shortwave solar radiation (Ramanathan et al. 1979), we consider here only the former. Figure A.4 shows the change in the net

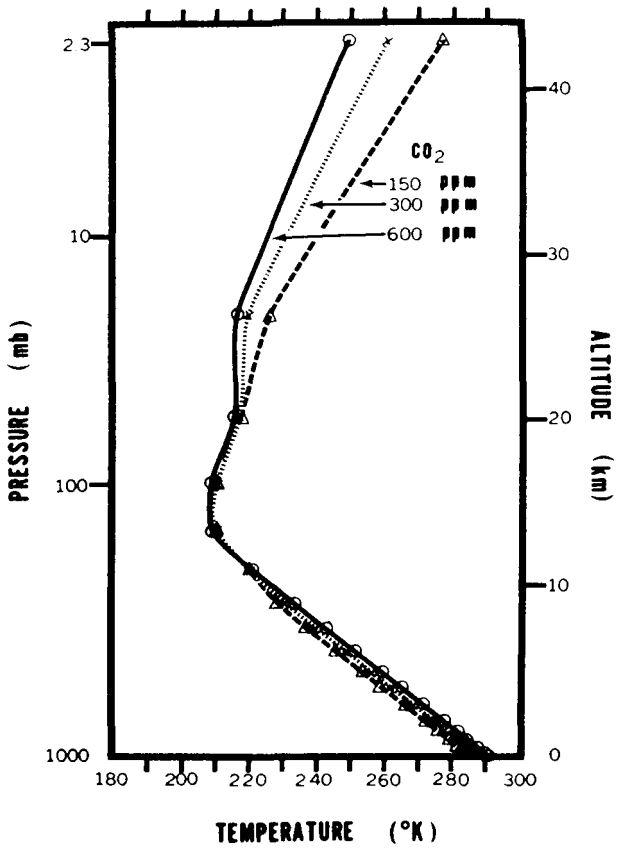

Figure A.3. Vertical distribution of temperature in a radiative-convective model for fixed relative humidity (FRH) and fixed cloud cover (FCL). The surface temperature change is 2.88°C for a CO_2 doubling from 150 to 300 ppm and 2.36°C for 300 to 600 ppm. Source: Manabe and Wetherald (1967).

Table A.4
Surface Temperature Change Induced by a Doubled CO_2 Concentration as Calculated by Selected Radiative-Convective Models

Study	ΔT_s(°C)
Manabe and Wetherald (1967)	1.33–2.92
Manabe (1971)	1.9
Augustsson and Ramanathan (1977)	1.98–3.2
Rowntree and Walker (1978)	0.78–2.76
Hunt and Wells (1979)	1.82–2.2
Wang and Stone (1980)	2.00–4.20
Charlock (1981)	1.58–2.25
Hansen et al. (1981)	1.22–3.5
Hummel and Kuhn (1981a)	0.79–1.94
Hummel and Kuhn (1981b)	0.8–1.2
Hummel and Reck (1981)	1.71–2.05
Hunt (1981)	0.69–1.82
Wang et al. (1981)	1.47–2.80
Hummel (1982)	1.29–1.83
Lindzen et al. (1982)	1.46–1.93
Lal and Ramanathan (1984)	1.8–2.4
Somerville and Remer (1984)	0.48–1.74

upward longwave radiation flux ΔR as a function of altitude when the CO_2 concentration is doubled from 300 to 600 ppm and the temperatures are held fixed. These changes represent the direct radiative forcing due to the CO_2 doubling and were obtained from the 33-layer Oregon State University radiative transfer model in which the vertical profiles of temperature, water vapor, and ozone were prescribed from the midlatitude summer atmosphere of McClatchey et al. (1971) and in which there were no clouds. Figure A.4 shows $\Delta R < 0$ everywhere, with values decreasing from about -2 W m^{-2} at the surface to -4.5 W m^{-2} at the tropopause ($p = 179$ mb and $z = 13$ km) and then increasing at varying rates to about -2 W m^{-2} at the stratopause ($p = 1$ mb and $z = 50$ km) and above; that is, the net upward fluxes decreased at all levels. Using Equation (A.60) to give the temperature change ΔT when ΔS is neglected gives

$$\rho c_p \frac{\partial \Delta T}{\partial t} = -\frac{\partial \Delta R}{\partial z} . \qquad \text{(A.62)}$$

This shows that the direct radiative forcing of the increased CO_2 level acts to cool the stratosphere because $\partial \Delta R/\partial z > 0$ and to warm the troposphere because $\partial \Delta R/\partial z < 0$. At the surface the decreased net upward longwave radiation $\Delta R < 0$ acts to warm the surface.

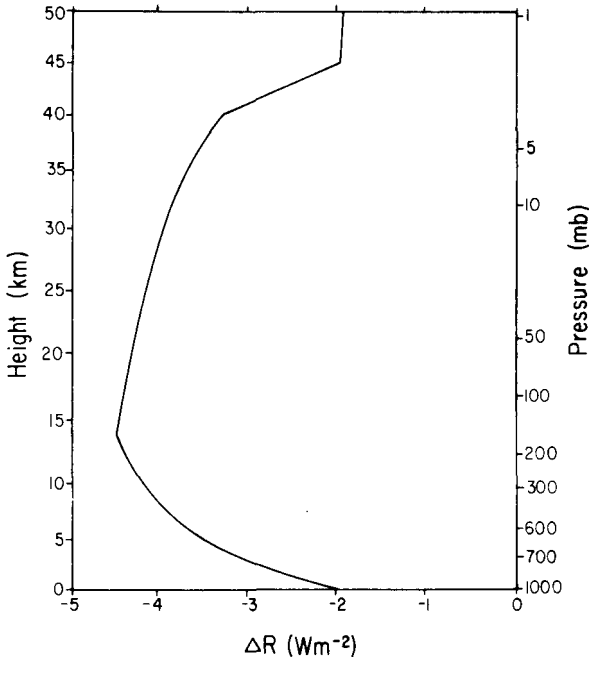

Figure A.4. The change in the net upward longwave radiation flux caused by an abrupt doubling of the CO_2 concentration.

Why is $\Delta R < 0$ at the surface (and elsewhere), and why is $\partial \Delta R / \partial z$ negative in the troposphere and positive in the stratosphere? These questions can be answered with the simple two-layer atmospheric model shown in Figure A.5. In this figure levels 0 and 2 represent the top of the atmosphere and the top of the troposphere (the tropopause), respectively, level 1 is the upper (stratospheric) layer with temperature T_1 and longwave transmissivity τ_1, level 3 is the lower (tropospheric) layer with temperature T_3 and longwave transmissivity τ_3, and level 4 is the Earth's surface with temperature T_s and longwave emissivity of unity. The flux of solar radiation at even level k is S_k. Longwave radiation is emitted by the surface and each atmospheric layer. The flux emitted by the surface, $B_s = \sigma T_s^4$, is attenuated by atmospheric absorption through the lower layer with absorptivity $a_3 = 1 - \tau_3$, such that the flux at level 2 is $\tau_3 B_s$. This flux is further attenuated by atmospheric absorption through the upper layer with absorptivity $a_1 = 1 - \tau_1$ such that the flux at level 0 is $\tau_1 \tau_3 B_s$. Because the emissivity ϵ_3 is equal to the absorptivity a_3 by Kirchhoff's law, the lower layer emits radiation both upward and downward with magnitude $a_3 B_3 = a_3 \sigma T_3^4$. The upward flux is attenuated by absorption through the upper layer such that the flux at level 0 is $\tau_1 a_3 B_3$. Finally, the upper layer emits radiation both upward and downward with magnitude $a_1 B_1 = a_1 \sigma T_1^4$. The downward flux is attenuated by absorption through the lower layer such that the flux at the surface is $\tau_3 a_1 B_1$.

Using the fluxes described above and the hydrostatic relation $\partial p / \partial z = -\rho g$, we can write the thermodynamic energy Equation (A.60) for the atmospheric layers as

$$\frac{\delta_1 p}{g} c_p \frac{\partial T_1}{\partial t} = (S_0 - S_2) + Q_1 \qquad \text{(A.63)}$$

and

$$\frac{\delta_3 p}{g} c_p \frac{\partial T_3}{\partial t} = (S_2 - S_4) + Q_3 \,, \qquad \text{(A.64)}$$

where

$$\begin{aligned} Q_1 &= (1 - \tau_1)\tau_3 B_s \\ &\quad + (1 - \tau_1) a_3 B_3 - 2 a_1 B_1 \\ &= a_1 (\tau_3 B_s + a_3 B_3 - 2 B_1) \end{aligned} \qquad \text{(A.65)}$$

and

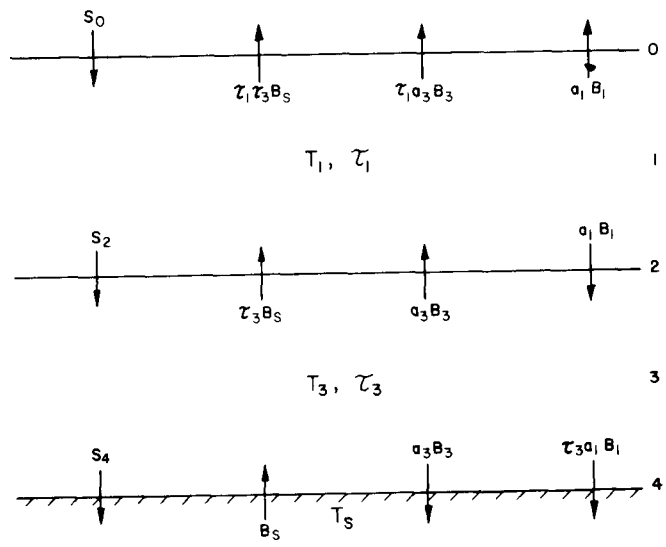

Figure A.5. Two-layer model representation of the atmosphere-surface climate system. See text for nomenclature.

$$\begin{aligned} Q_3 &= (1 - \tau_3) B_s - 2 a_3 B_3 \\ &\quad + (1 - \tau_3) a_1 B_1 \\ &= a_3 (B_s - 2 B_3 + a_1 B_1) \end{aligned} \qquad \text{(A.66)}$$

are the longwave radiation heating rates for the upper and lower layers with pressure thicknesses $\delta_1 p$ and $\delta_3 p$, respectively. Similarly, the thermodynamic energy equation for the surface is

$$C_s \frac{\partial T_s}{\partial t} = S_4 + Q_4 \,, \qquad \text{(A.67)}$$

where

$$Q_4 = -B_s + a_3 B_3 + \tau_3 a_1 B_1 \qquad \text{(A.68)}$$

is the longwave radiation heating rate for the surface with bulk heat capacity C_s. In the thermodynamic equilibrium prior to the change in the CO_2 concentration, $\partial T_1 / \partial t = \partial T_3 / \partial t = \partial T_s / \partial t = 0$ so that

$$Q_1 = -(S_0 - S_2) < 0 \,, \qquad \text{(A.69)}$$

$$Q_3 = -(S_2 - S_4) < 0 \,, \qquad \text{(A.70)}$$

$$Q_4 = -S_4 < 0 \,, \qquad \text{(A.71)}$$

and the longwave radiation heating of the atmosphere and surface is negative, that is, a cooling.

When the radiative equilibrium is disturbed by the abrupt doubling of the CO_2 concentration, the

thermodynamic energy Equations (A.63), (A.64), and (A.67) become

$$\frac{\delta_1 p}{g} c_p \frac{\partial \Delta T_1}{\partial t} = \Delta(S_0 - S_2) + \Delta Q_1 \ , \quad \text{(A.72)}$$

$$\frac{\delta_3 p}{g} c_p \frac{\partial \Delta T_3}{\partial t} = \Delta(S_2 - S_4) + \Delta Q_3 \ , \quad \text{(A.73)}$$

and

$$C_s \frac{\partial \Delta T_s}{\partial t} = \Delta S_4 + \Delta Q_4 \ , \quad \text{(A.74)}$$

where by Equations (A.65), (A.66), (A.68), and $\Delta\tau_k = -\Delta a_k$,

$$\begin{aligned} \Delta Q_1 &= a_1(\Delta\tau_3 B_s + \Delta a_3 B_3) \\ &\quad + \Delta a_1(\tau_3 B_s + a_3 B_3 - 2B_1) \\ &= -a_1(B_s - B_3)\Delta a_3 \\ &\quad + \frac{Q_1}{a_1} \Delta a_1 \ , \end{aligned} \quad \text{(A.75)}$$

$$\begin{aligned} \Delta Q_3 &= a_3 \Delta a_1 B_1 \\ &\quad + \Delta a_3(B_s - 2B_3 + a_1 B_1) \\ &= a_3 B_1 \Delta a_1 + \frac{Q_3}{a_3} \Delta a_3 \ , \end{aligned} \quad \text{(A.76)}$$

and

$$\begin{aligned} \Delta Q_4 &= \Delta a_3 B_3 + \Delta\tau_3 a_1 B_1 \\ &\quad + \tau_3 \Delta a_1 B_1 \\ &= (B_3 - a_1 B_1)\Delta a_3 \\ &\quad + \tau_3 B_1 \Delta a_1 \ . \end{aligned} \quad \text{(A.77)}$$

Here ΔT_k and ΔQ_k are the temperature and heating perturbations from their respective undisturbed equilibrium values, with Δa_k and $\Delta\tau_k$ the perturbed absorptivity and transmissivity due to the doubled CO_2 concentration. In Equations (A.75)–(A.77) the temperatures on the right-hand sides in $B_k = \sigma T_k^4$ are held at their undisturbed values so that the direct radiative forcing due to the doubled CO_2 concentration can be determined.

The direct radiative forcing of the stratosphere is given by Equations (A.72) and (A.75). Because $B_s > B_3$, $\Delta a_3 > 0$, $Q_1 < 0$ and $\Delta a_1 > 0$, both terms on the right-hand side of Equation (A.75) are negative, hence $\Delta Q_1 < 0$. Although $\Delta(S_0 - S_2) > 0$ in Equation (A.72) because of the weak solar absorption bands of CO_2, it is dominated by ΔQ_1 so that the direct radiative forcing acts to cool the stratospheric layer. Figure A.5 shows that this cooling tendency occurs primarily because of the greater upward and downward emission from the stratosphere itself.

The direct radiative forcing of the troposphere-surface system is given by Equations (A.73), (A.74), (A.76), and (A.77) as

$$\begin{aligned} \frac{\delta_3 p}{g} c_p \frac{\partial \Delta T_3}{\partial t} + C_s \frac{\partial \Delta T_s}{\partial t} \\ = \Delta S_2 - \Delta R_2 \ , \end{aligned} \quad \text{(A.78)}$$

where

$$\Delta R_2 = -(B_s - B_3)\Delta a_3 - B_1 \Delta a_1 \quad \text{(A.79)}$$

is the change in the net upward longwave flux at the tropopause. Because $B_s > B_3$, $\Delta a_3 > 0$, and $\Delta a_1 > 0$, then $\Delta R_2 < 0$. Again, although $\Delta S_2 < 0$ in Equation (A.78), it is dominated by $-\Delta R_2$ so that the direct radiative forcing acts to warm the troposphere-surface system. Figure A.5 and Equation (A.79) show that this warming tendency occurs because of both the increased downward flux from the stratosphere and the decreased upward flux from the troposphere.

The direct radiative forcing of the surface is given by Equations (A.74) and (A.77). Because $B_3 > B_1$, $\Delta a_3 > 0$, and $\Delta a_1 > 0$, both terms on the right-hand side of Equation (A.77) are positive, hence $\Delta Q_4 > 0$. Although $\Delta S_4 < 0$, ΔQ_4 dominates ΔS_4 so that the direct radiative forcing acts to warm the surface. As can be seen from Figure A.5, this warming tendency occurs primarily because of the greater downward emission from the troposphere.

Finally, the direct radiative forcing of the troposphere is given by Equations (A.73) and (A.76). Because $\Delta a_1 > 0$, $Q_3 < 0$, and $\Delta a_3 > 0$, the first term on the right-hand side of Equation (A.76) is positive and the second term is negative. Because $\Delta(S_2 - S_4) > 0$ but small, the fact that the direct radiative forcing of the troposphere is a warming tendency (Figure A.4) is seen from Equation (A.76) and Figure A.5, as noted by Schneider (1975), to be primarily caused by the increased downward flux from the stratosphere.

Kiehl and Ramanathan (1982) have shown that the direct radiative forcing of the surface strongly depends on the water vapor absorption in the 12–18 μm region, which overlaps and competes with the 15-μm absorption band of CO_2. However, th

direct radiative forcing of the troposphere-surface system does not strongly depend on the water vapor absorption in this spectral region. Kiehl and Ramanathan found that the direct radiative forcing of the surface ΔR_s decreased from 1.56 to 0.55 W m^{-2} when the continuum absorption was added to the line absorption between 12 and 18 μm. The corresponding change in the direct radiative forcing of the troposphere-surface system, that is, the change in net upward flux at the tropopause ΔR_T, was from 4.18 to 3.99 W m^{-2}. Consequently, the inclusion of the 12–18 μm continuum absorption increases the direct radiative forcing of the troposphere, $\Delta R_T - \Delta R_s$, from 2.62 to 3.44 W m^{-2}.

As the stratosphere cools in response to its direct radiative forcing, it is expected that radiation emitted downward into the troposphere will decrease and, in effect, will reduce the direct radiative forcing of the troposphere-surface system. However, Ramanathan et al. (1979) found that this effect is negligibly small because most of the contribution to the downward flux at the tropopause comes from the region within 5 km above the tropopause where the final temperature change is small. More recently, Lal and Ramanathan (1984) found that the direct radiative forcing of the troposphere-surface system of 4.1 W m^{-2} was decreased to 4.0 W m^{-2} after the stratospheric temperatures alone were allowed to cool to their radiative equilibrium values. Of this 4.0 W m^{-2}, 2.7 W m^{-2} was contributed by the reduction in upward flux from the troposphere, 1.55 W m^{-2} by the increased downward flux from the stratospheric CO_2 increase, and -0.15 W m^{-2} by the decreased solar flux at the tropopause. In the following we shall consider that the direct radiative forcing of the troposphere-surface system is $\Delta R_T = 4$ W m^{-2}.

A.3.3.2 Response of the Climate System Without Feedbacks to Increased CO_2

The response of the climate system to increased CO_2 when only the temperature changes is given by Equation (A.18), with $f = 0$ and $\Delta Q = \Delta R_T$, and Equation (A.58b) as

$$(\Delta T_s)_0 = G_0 \Delta R_T = \frac{T_s(1 \times CO_2)}{(1 - \alpha_p) S_0} \Delta R_T \, . \qquad \text{(A.80)}$$

Taking $\Delta R_T = 4$ W m^{-2} and $G_0 = 0.3$°C (W m^{-2})$^{-1}$ gives $(\Delta T_s)_0 = 1.2$°C. This value is in excellent agreement with the value of $\Delta T_s = 1.22$°C obtained by Hansen et al. (1981) using an RCM with no feedbacks—that is, with fixed lapse rate (FLR, Table A.3), fixed absolute humidity (FAH), fixed cloud altitude (FCA), fixed cloud cover (FCC), fixed cloud optical depth (FOD) and fixed surface albedo (FAL)—and in which $\Delta R_T = 4.0$ W m^{-2}. However, because $T_s(1 \times CO_2)$ was not reported by Hansen et al. (1981), the actual value of G_0 may not have been the 0.3°C (W m^{-2})$^{-1}$ assumed here. The value of $(\Delta T_s)_0 = 1.2$°C is also in close agreement with the values of $\Delta T_s = 1.33$ and 1.29°C obtained, respectively, by Manabe and Wetherald (1967) and Rowntree and Walker (1978) using different RCMs, but with the same characteristics as those of Hansen et al. (1981) described above. However, the values of ΔR_T were not reported in these earlier studies and so may have been different from the 4 W m^{-2} assumed here. Therefore, to test the validity of Equation (A.80) we used the two-layer Oregon State University RCM, which has been described by Hall et al. (1982) and has been modified here to include a single cloud layer at 500 mb with a 45% cloud cover. For the zero-feedback configuration described above, this model with $S_0 = 1370$ W m^{-2} gives $\alpha_p = 0.3128$, $T_s = 288.38$ K and $\Delta R_T = 4.17$ W m^{-2}. Thus, $G_0 = 0.306$°C (W m^{-2})$^{-1}$ by Equation (A.58b) and $(\Delta T_s)_0 = 1.276$°C by Equation (A.80). Because this value is within 6% of the actual $(\Delta T_s)_0 = 1.354$°C, it is seen that Equation (A.80) does provide an accurate estimate of $(\Delta T_s)_0$.

A.3.3.3 Response of the Climate System With Feedbacks to Increased CO_2

The RCM results presented in Table A.4 can be characterized in terms of the feedback f by making use of Equation (A.18) written as

$$f = 1 - \frac{(\Delta T_s)_0}{\Delta T_s} \qquad \text{(A.81)}$$

and our estimate of $(\Delta T_s)_0 = G_0 \Delta Q = 1.2$°C based on $\Delta Q = 4$ W m^{-2} and $G_0 = 0.3$°C (W m^{-2})$^{-1}$. Thus, $-1.5 \leq f \leq 0.7$. Several physical mechanisms are thought to be the cause of this wide range in the feedback of these models. As T_s increases these mechanisms include the following: (1) the increase

in the amount of water vapor in the atmosphere as a consequence of the quasi-constancy of the relative humidity, (2) the decrease in the temperature lapse rate, (3) the increase in the cloud altitude as (or if) the clouds maintain their temperature, (4) the change in cloud amount, (5) the change in the cloud optical depth, and (6) the decrease in surface albedo due to the decrease in ice and snow. If the feedbacks of these individual mechanisms were all mutually independent, the total feedback would be equal to the sum of the individual feedbacks. In such a case the contribution of each mechanism to the total feedback could be individually determined and ranked. An intercomparison of the models of these ranked feedback mechanisms would then reveal the sources for the wide range in the RCM results. However, if the total feedback is not equal to the sum of the individual feedbacks, two or more of the feedbacks would be dependent. In this case the dependent feedbacks should be considered as only one feedback, such that it is independent of the remaining feedbacks. Then the contribution of each independent mechanism to the total feedback can be determined, ranked, and intercompared as described above.

To investigate the independence of the six mechanisms listed above, we have carried out a quantitative feedback evaluation using the Oregon State University two-layer RCM. The results presented in Table A.5 show that although $T_s(1 \times CO_2)$ changes when some of the individual feedback mechanisms are activated, $(\Delta T_s)_0$ is essentially constant and equal to 1.28°C. For the case with no feedback mechanisms, ΔT_s differs from $(\Delta T_s)_0$ by 0.07°C and therefore gives a small apparent feedback. This apparent feedback may represent the neglected second- and higher-order terms in Equation (A.3) and will be discounted below. Of all the individual feedback mechanisms, only that of the variable (moist adiabatic) lapse rate gives a negative feedback. (It is likely that the two-layer model exaggerates this negative feedback.) The individual positive feedback mechanisms are in decreasing order of magnitude: water vapor, cloud altitude, surface albedo, cloud optical depth, and cloud cover. The latter two are sufficiently small compared with the small apparent feedback for the zero-feedback case that they can be regarded as essentially zero. Table A.5 shows that the feedbacks of water vapor and either lapse rate, cloud altitude, or surface albedo are additive (within the small nonzero apparent feedback value for the zero-feedback case). Thus, these feedbacks are independent. This is not the case for the water vapor feedback with either the cloud cover or cloud optical depth feedbacks, because the resultant feedback is substantially less than the sum of the individual feedbacks. Thus, it appears that both variable cloud cover and variable cloud optical depth are negative feedback mechanisms when they act in conjunction with the positive water vapor feedback. Consequently, cloud cover and cloud optical depth, when allowed to vary within an RCM, should be considered together with water vapor as a single feedback mechanism.

Table A.5
Feedback Analysis Using the
Oregon State University Two-Layer RCM

Feedback Mechanism	$T_s(1\times CO_2)$ (°C)	$(\Delta T_s)_0$[a] (°C)	ΔT_s (°C)	f[b]
None	15.28	1.28	1.35	0.058
Water Vapor[c]	14.53	1.28	1.94	0.340
Lapse Rate[d]	9.53	1.24	0.88	−0.409
Cloud Altitude[e]	15.28	1.28	1.73	0.261
Cloud Cover[f]	15.28	1.28	1.38	0.074
Cloud Optical Depth[g]	15.28	1.28	1.39	0.079
Surface Albedo[h]	15.43	1.28	1.56	0.181
Water Vapor[c] and Lapse Rate[d]	9.38	1.25	1.19	−0.043 (−0.069)
Cloud Altitude[e]	14.20	1.28	2.79	0.543 (0.601)
Cloud Cover[f]	15.12	1.29	1.81	0.291 (0.414)
Cloud Optical Depth[g]	15.39	1.28	1.70	0.248 (0.419)
Surface Albedo[h]	14.58	1.28	2.39	0.466 (0.521)
Water vapor,[c] cloud altitude,[e] and surface albedo[h]	14.14	1.28	3.85	0.668 (0.782)

[a] $(\Delta T_s)_0$ is calculated by Equation (A.80).
[b] The values in parentheses are the algebraic sum of the individual feedbacks.
[c] With the fixed relative humidity profile of Manabe and Wetherald (1967).
[d] With the moist adiabatic lapse rate.
[e] With fixed cloud temperature prescribed equal to that of the $1 \times CO_2$ simulation with no feedback.
[f] With variable cloud cover prescribed similarly to that of Wang et al. (1981).
[g] With variable optical depth τ prescribed similarly to that of Wang et al. (1981) and cloud albedo, absorptivity and transmissivity parameterized in terms of τ following Stephens et al. (1984).
[h] With variable surface albedo prescribed as in Wang and Stone (1980).

It is useful to consider here the effect of the three positive feedback mechanisms of water vapor, cloud altitude, and surface albedo. Table A.5 shows that these feedbacks essentially are independent (allowing for the apparent feedback of the zero-feedback case for each of the two additional feedback mechanisms) and combine to produce a 3.85°C surface warming. This value is close to the 4.2°C maximum warming simulated by Wang and Stone (1980) using an RCM with these feedbacks (Table A.4) and close to the values simulated for the global-mean surface air temperature by Hansen et al. (1984), Washington and Meehl (1984) and Wetherald and Manabe (1986) with general circulation models (see Section 4.3 of Chapter 4). We will consider this result again later.

Next we will analyze those RCM studies in Table A.4 that have reported the data necessary to quantitatively evaluate individual water vapor, lapse rate, cloud altitude, and surface albedo feedbacks and the joint cloud cover-water vapor and cloud optical depth-water vapor feedbacks. However, before doing this we will consider the influence of the different surface energy flux parameterizations used in RCMs.

Surface energy flux. In RCM studies of the equlibrium climate change induced by increased CO_2 concentrations, the heat capacity of the surface C_s is taken to be zero to minimize the computer time required to establish equilibrium. The thermodynamic energy equation for the surface is then

$$C_s \frac{\partial T_s}{\partial t} = S_s + R_s^{\downarrow} - \sigma T_s^4 - H_s = 0 \ , \qquad \text{(A.82)}$$

where S_s is the absorbed solar radiation, $R_s^{\downarrow}$ is the downward longwave radiation, σT_s^4 is the upward longwave radiation emitted by the surface with temperature T_s, and H_s is the upward flux of sensible and latent heat. Two treatments or parameterizations of H_s have been used in RCMs. Manabe and Wetherald (1967) and others have assumed that $T_s = T_a$, where T_a is the surface air temperature and is taken to be equal to the temperature of the model's lowest layer. In this case, by Equation (A.82),

$$H_s = S_s + R_s^{\downarrow} - \sigma T_a^4 \ . \qquad \text{(A.83)}$$

This is identified as the equivalent radiative exchange treatment in Table A.3. In such RCM studies as that by Hunt and Wells (1979), H_s is parameterized using the bulk aerodynamic exchange method, that is,

$$H_s = \rho c_p c_D V_s (T_s - T_a) + \rho L c_D V_s [q^*(T_s) - q_a] \ . \qquad \text{(A.84)}$$

Here the first term represents the sensible heat flux, with c_D being a drag coefficient and V_s being the surface wind speed, and the second term represents the latent heat flux with L being the latent heat of vaporization, $q^*(T_s)$ being the saturation mixing ratio of water vapor at temperature T_s, and q_a being the water vapor mixing ratio of the surface air, which is taken to be equal to the mixing ratio of the model's lowest layer. In using Equation (A.84), T_s is not constrained to be equal to T_a as it is in Equation (A.83), but it is necessary to prescribe $c_D V_s$.

Do these different treatments of the surface energy flux in RCMs account for the differences in the results presented in Table A.4? Only the study by Lindzen et al. (1982) investigated this question. Using their RCM with fixed relative humidity (FRH), a fixed lapse rate of 6.5°C km^{-1} [FLR(6.5)], and no cloud cover, Lindzen et al. found a surface temperature warming for doubled CO_2 of 1.98°C with the equivalent radiative exchange and 1.93°C with the bulk aerodynamic exchange and $c_D V_s$ = 0.0124 m s^{-1}. Furthermore, in an RCM with FRH, moist adiabatic lapse rate (MALR), fixed cloud altitude (FCA) and bulk aerodynamic exchange, Hunt (1981) found that ΔT_s for a CO_2 doubling varied from 1.89 to 1.79°C as V_s varied from 2 to 10 m s^{-1} with $c_D = 1.5 \times 10^{-3}$. Consequently, from these results it appears that the different treatments of the surface energy flux in RCMs has a negligible effect on the CO_2-induced warming of the surface ΔT_s.

Water vapor feedback. In their pioneering RCM study of CO_2-induced climate change, Manabe and Wetherald (1967) argued on the basis of seasonal observations that the atmosphere tends to maintain the climatological distribution of relative humidity (RH) rather than absolute (specific) humidity (q). Accordingly, Manabe and Wetherald (1967)

Table A.6
Water Vapor Feedback f_W Determined From Selected Radiative-Convective Models

Study	Model Attributes[a]	Water Vapor Treatment	$T_s(1\times CO_2)$ (° C)	ΔT_s[b] (°C)	Estimated Feedback f_W[c]
Manabe and Wetherald (1967)	ERE; FLR(6.5); CLR; —, —; FAL	FAH	26.89	1.36*	
		FRH[d]	34.04	2.92	0.534
	ERE; FLR(6.5); FCC, FCP(3), FOD; FAL	FAH	17.89	1.33*	
		FRH[d]	15.23	2.36	0.436
Rowntree and Walker (1978)	BAE; FLR(6.5); CLR; —, —; FAL	FAH		1.29*	
		FRH[d]	32.84	2.76	0.533[e]
Hansen et al. (1981)	BAE; FLR(6.5); FCC, FCA(1), FOD; FAL	FAH		1.22*	
		FRH[d]		1.94	0.371

[a] Surface energy flux; convection; cloud cover, altitude (number of layers), optical depth; surface albedo. See Table A.3 for definition of the abbreviations.
[b] * indicates the value of $(\Delta T_s)_0$.
[c] $f_W = 1 - (\Delta T_s)_0/\Delta T_s$.
[d] The prescribed relative humidity profile is given by Equation (A.85).
[e] $(\Delta T_s)_0$ and ΔT_s were obtained with $\cos\zeta = 0.225$ and 0.250, respectively.

prescribed the vertical profile of relative humidity on the basis of observations to be

$$RH(p) = RH(p_s)\,\frac{p/p_s - 0.02}{1 - 0.02}\,, \qquad \text{(A.85)}$$

where p is pressure, p_s is the surface pressure, and $RH(p_s) = 0.77$ and calculated the specific humidity from

$$q(T,p) = RH(p)\; q^*(T,p)\,, \qquad \text{(A.86)}$$

where $q^*(T,p)$ is the saturation specific humidity given with the aid of the Clausius-Clapeyron relation as

$$q^*(T,p) = \frac{a}{p}\, e^{-b/T}\,, \qquad \text{(A.87)}$$

where a and b are constants. This fixed relative humidity treatment of water vapor is identified in Table A.3 as FRH. For comparison Manabe and Wetherald (1967) also performed a calculation with fixed absolute humidity (FAH). The results of this study are shown in Table A.6 for two cases, one with no clouds (CLR) and the other with three cloud layers with fixed cloud altitude (FCA) and fixed optical depth (FOD). By taking $(\Delta T_s)_0$ for each cloud condition as ΔT_s for the corresponding FAH case, the water vapor feedback for FRH is by Equation (A.81) $f_W = 0.534$ for the clear case and $f_W = 0.436$ for the cloudy case.

What is the physical cause of this positive water vapor feedback, and why does its value differ for the clear and cloudy cases? These questions can be answered by considering the amount of water vapor per unit horizontal area between two vertical levels k and ℓ,

$$W_{k,\ell} = \int_{z_k}^{z_\ell} q(z)\rho dz = \frac{1}{g}\int_{p_\ell}^{p_k} q(p)dp\,. \qquad \text{(A.88)}$$

The last term is obtained by substituting the hydrostatic equation $dp/dz = -\rho g$. For FAH, $W_{k,\ell}$ is determined solely by the prescribed absolute humidity profile and is constant. For FRH, $W_{k,\ell}$ is given by Equation (A.88) with Equations (A.86) and (A.87) as

$$W_{k,\ell} = \frac{1}{g}\int_{p_\ell}^{p_k} RH(p)\,\frac{a}{p}\, e^{-b/T}dp \qquad \text{(A.89)}$$

and is therefore determined not only by the prescribed relative humidity profile, but also by the temperature. Because

$$T = T_s(p/p_s)^{R\Gamma/g} \qquad \text{(A.90)}$$

for the particular case of a fixed tropospheric lapse rate Γ adopted by Manabe and Wetherald (1967), it can be seen from Equation (A.89) that $W_{k,\ell}$ depends on $RH(p)$ and T_s. Consequently, when CO_2 is increased, the initial warming of the surface in response to the direct radiative forcing results in an increase in $W_{k,\ell}$ between any levels k and ℓ. This increases the atmospheric absorptivities and decreases the transmissivities (Figure A.5) beyond and in the same directions as the changes in these quantities resulting from the increased CO_2 concentration and thereby acts to enhance the radiative forcing. This in turn leads to further warming of the surface and further increases in $W_{k,\ell}$ in a feedback

loop as shown in Figure A.1. The positive feedback is less than unity; hence, the amplification of the loop is finite (Figure A.2). However, the feedback increases nonlinearly with increasing T_s because of the $e^{-b/T}$ term, in part, in Equation (A.89), which arises from the Clausius-Clapeyron relation. This dependence explains the difference in f_W between the clear and cloudy cases: the $1 \times CO_2$ surface temperature is lower in the cloudy case than in the clear case because of the larger planetary albedo; hence, the feedback is lower in the cloudy case than in the clear case. However, if there is a large lapse-rate feedback as in the case of penetrative convection (discussed in the next subsection), ΔT_s may be practically independent of T_s.

Table A.6 shows results from two other RCM studies using the Manabe and Wetherald (1967) prescribed relative humidity profile [Eq. (A.85)]. The water vapor feedback ranges from 0.371 to 0.534. This range is probably caused by the dependence of f_W on $T_s(1 \times CO_2)$ as described above, and the differences in the $T_s(1 \times CO_2)$ values of the models. This is supported by the fact that the $T_s(1 \times CO_2)$ and f_W values of Rowntree and Walker (1978) are nearly the same as those of Manabe and Wetherald (1967). Because the present global mean surface air temperature is 14.2°C (Jenne 1975), the results in Tables A.5 and A.6 suggest a probable value of $f_W \sim 0.3$ to 0.4. This is a moderate positive feedback which, acting alone, would multiply the zero feedback temperature change by an R_f of ~ 1.4 to 1.7 (see Figure A.2). However, it should be noted that the concept of constant relative humidity is an idealization. If the relative humidity increased with temperature as investigated by Augustsson and Ramanathan (1977) and Rowntree and Walker (1978), f_W would exceed the value above, and f_W would be smaller if the relative humidity decreased with temperature. Interestingly, general circulation model studies of climate changes induced by both CO_2 and changes in the solar constant have shown that the relative humidity is not constant (see Section 4.3.4.2 of Chapter 4).

Temperature lapse rate feedback. In the first RCM study of CO_2-induced climate change by Manabe and Wetherald (1967), it was assumed, based on early observations (Brunt 1933; Goody 1964), that the tropospheric temperature lapse rate $\Gamma = -dT/dz$ was 6.5°C km^{-1}. A more recent analysis by Stone and Carlson (1979), using the observations of Oort and Rasmusson (1971), showed that a better estimate of the global mean tropospheric lapse rate is $\Gamma = 5.1$°C km^{-1}. Is this difference in prescribed critical lapse rate important?

Cess (1975) investigated this question with a PEBM and found that the outgoing infrared flux F and $\partial F/\partial T_s$ were insensitive to Γ in the range 6.0 to 7.0°C km^{-1}. Rowntree and Walker (1978) investigated this question with an RCM and found that varying the fixed lapse rate from 5 to 6.5°C km^{-1} affected the results little. Quantitative results were presented by Chýlek and Kiehl (1981), shown in Table A.7, who concluded that the choice of the lapse rate within an interval from 5.5 to 6.5°C km^{-1} has no significant effect on the results obtained using radiative-convective models. Nevertheless, Table A.7 shows a 12% decrease in ΔT_s for $\Gamma = 5.0$°C km^{-1}. This decrease probably represents a smaller water vapor feedback, although this cannot be verified because the requisite data were not reported.

Stone and Carlson (1979) also found that the lapse rate varies systematically with latitude and is governed by the vertical heat transports by cumulus convection and baroclinic eddies. In low latitudes cumulus convection dominates and the lapse rate closely agrees with the moist adiabatic lapse rate

$$\Gamma_m = \Gamma_d \frac{1 + \frac{Lq^*}{RT}}{1 + \frac{Lq^*}{RT}\frac{\epsilon L}{c_p T}}, \qquad \text{(A.91)}$$

where $\Gamma_d = g/c_p \sim 9.8$°C km^{-1} is the dry adiabatic lapse rate, R is the gas constant for dry air, $\epsilon = 0.622$ and the other symbols have their previously assigned meanings. In high latitudes baroclinic eddies dominate and the lapse rate agrees with the critical lapse rate established by the baroclinic adjustment mechanism (Stone 1978). Recently, however, Yang and Smith (1985) showed that the lapse rate in the midlatitudes of the Southern Hemisphere follows the critical lapse rate for baroclinic adjustment with a 15° latitude lag. Both the moist adiabatic lapse rate (MALR) and the baroclinic adjustment lapse rate (BADJ) depend on temperature and therefore can produce a temperature lapse rate feedback.

Table A.7
Lapse Rate Feedback f_{LR} Determined From Selected Radiative-Convective Models

Study	Model Attributes[a]	Convection Treatment	ΔT_s $2\times CO_2-1\times CO_2$ (°C)	Estimated Feedback f_{LR}
Chýlek and Kiehl (1981)	ERE;FRH;FCC, FCA(1),FOD;FAL	FLR(6.5)	100%[b]	
		FLR(6.0)	98%	
		FLR(5.5)	94%	
		FLR(5.0)	88%	
		BADJ[c]	184%	Positive
		MALR[c]	75%	Negative
Hunt and Wells (1979)	BAE;FRH;FCC, FCP(3),FOD;FAL	FLR(6.5)	2.2	
		MALR	1.82	Negative
Hummel and Kuhn (1981a)	ERE;FRH;FCC,FCP(1) (500 mb), FOD;FAL	FLR(6.5)	1.94	
		MALR	0.79	Negative
	ERE;FRH;FCC,FCP(1) (800 mb),FOD;FAL	FLR(6.5)	1.82	Negative
		MALR	1.53	Negative
Wang et al. (1981)	BAE;FRH;FCC, FCA(17),FOD;FAL	FLR(6.5)	2.06	
		MALR	1.49	Negative
Hummel (1982)	ERE;FRH;FCC, FCP(3),FOD;FAL	FLR(6.5)	1.83	
		MALR	1.29	Negative
Lindzen et al. (1982)	BAE;FRH;CLR, —,—;FAL	FLR(6.5)	1.93	
		MALR	1.51	Negative
		PC	1.46	Negative
Rowntree and Walker (1978)	BAE;FAH;CLR, —,—;FAL	PC	0.78	-0.654[d]
Hansen et al. (1981)	BAE;FRH;FCC, FCA(1),FOD;FAL	MALR	1.37	-0.262[e]

[a] Surface energy flux; water vapor; cloud cover, altitude (number of cloud layers), optical depth; surface albedo. See Table A.3 for definition of abbreviations.
[b] ΔT_s for $\Gamma = 6.5°C\ km^{-1}$ is taken to be 100%.
[c] BADJ is baroclinic adjustment defined as $d\Gamma/d\Delta T_s = 0.125\ km^{-1}$ and MALR is defined here as $d\Gamma/d\Delta T_s = -0.092\ km^{-1}$.
[d] $f_{LR} = 1 - (\Delta T_s)_0/\Delta T_s$ with $(\Delta T_s)_0$ from Table A.6.
[e] $f_{LR} = [1 - (\Delta T_s)_0/\Delta T_s] - f_W$ with $(\Delta T_s)_0$ and f_W from Table A.6.

Chylek and Kiehl (1981) investigated the feedbacks of the BADJ and MALR lapse rates which they defined as

$$\Gamma_{BADJ} = 6.5 + 0.125\Delta T\ ,\quad °C\ km^{-1}\ ,\quad (A.92)$$

and

$$\Gamma_{MALR} = 6.5 - 0.092\Delta T\ ,\quad °C\ km^{-1}\ .\quad (A.93)$$

Their results are presented in Table A.7 and show a positive lapse-rate feedback for BADJ and a negative lapse-rate feedback for MALR. These lapse-rate feedbacks are illustrated schematically in Figure A.6 for the simplified case where ΔT in Equations (A.92) and (A.93) is taken to be equal to ΔT_s. In Figure A.6A the critical lapse rate is independent of temperature, hence $\Gamma_{1\times CO_2} = \Gamma_{2\times CO_2} = 6.5°C\ km^{-1}$, and the CO_2-induced warming is uniform throughout the troposphere; in this case there is no lapse-rate feedback. In the Figure A.6B the critical lapse rate increases with ΔT_s so that $\Gamma_{2\times CO_2} > \Gamma_{1\times CO_2} = 6.5°C\ km^{-1}$. If ΔT_s in this case were less than or equal to the ΔT_s of the zero-feedback case, the tropospheric temperatures for a doubled CO_2 concentration with feedback would be colder everywhere than the corresponding temperatures without feedback. But then the infrared radiation emitted by the surface and the troposphere would be less than the equilibrium values of the zero-feedback case, and the atmosphere/surface system would not be in equilibrium. Therefore, to achieve equilibrium, ΔT_s with this feedback must exceed the ΔT_s without feedback, and the lapse-rate feedback with $d\Gamma/dT_s > 0$ is positive. However, when $d\Gamma/dT_s < 0$ as shown in Figure A.6C, ΔT_s with feedback is less than the ΔT_s without feedback, and the lapse-rate feedback is negative. The temperature changes are actually more complex than those shown in Figure A.6 because the lapse rates for BADJ and MALR vary with altitude.

Because the baroclinic adjustment process occurs in middle and high latitudes, whereas cumulus convection is dominant in low latitudes, BADJ should enhance the CO_2-induced middle and high latitude surface warming, and MALR should diminish the surface temperature increase in low latitudes. This latitudinal variation in the surface temperature warming is what is simulated by the general circulation models. Therefore, it is of interest to quantify the feedbacks of the baroclinic adjustment and cumulus convection processes. Unfortunately, we are able to do this from the RCM studies only for cumulus convection.

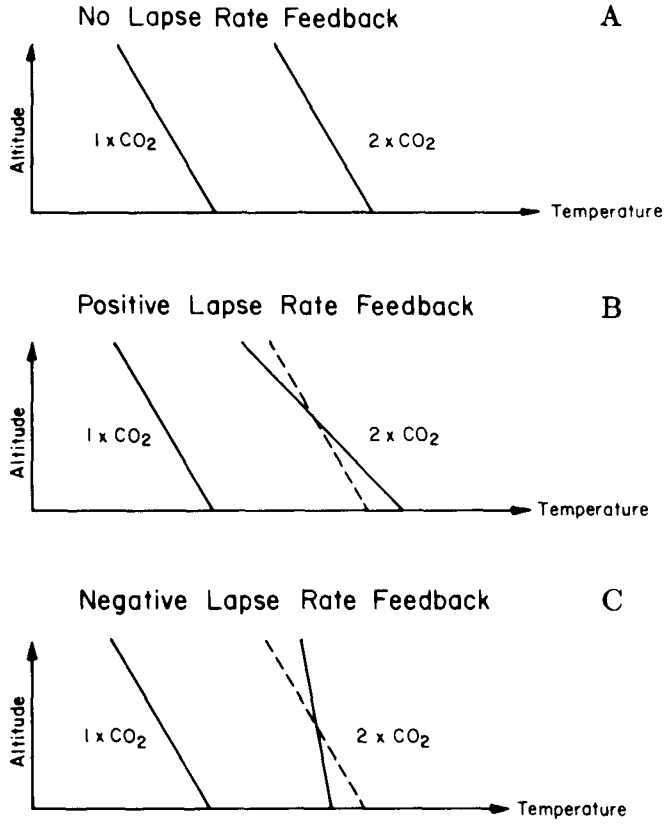

Figure A.6. Schematic representation of CO_2-induced warming with (A) no lapse rate feedback, (B) positive lapse rate feedback and (C) negative lapse rate feedback.

The MALR Γ_m given by Equation (A.91) decreases with increasing temperatures (Figure A.7) because of the increase of $q*$ with temperature and the fact that $\epsilon L/c_pT > 1$ for the temperatures in the Earth's atmosphere. Thus, based on the result shown in Figure A.6C, it is expected that the MALR feedback is negative. This is confirmed qualitatively by the studies of Hunt and Wells (1979), Hummel and Kuhn (1981a), Wang et al. (1981), Hummel (1982), and Lindzen et al. (1982) shown in Table A.7. A quantitative estimate of this negative feedback can be obtained from the study of Hansen et al. (1981) assuming that the water vapor and lapse-rate feedbacks are independent as suggested by the results of Table A.5. It is thereby estimated that $f_{\mathrm{MALR}} = -0.262$, which, as expected, is smaller than the value given by the Oregon State University two-layer RCM (Table A.5). This is a moderately negative feedback, which, acting alone, would multiply the zero feedback temperature change by $R_f = 0.79$ (see Figure A.2).

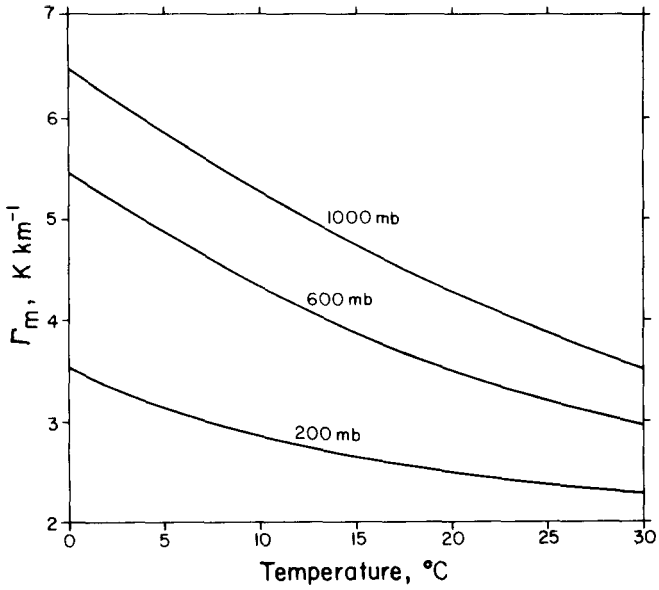

Figure A.7. Moist adiabatic lapse rate (Γ_m) as a function of temperature for selected pressures.

In general circulation model studies of CO_2-induced climate change, the physical processes of cumulus convection are too small to be explicitly resolved and therefore are incorporated in a parameterized form. Two types of cumulus parameterization have been employed in GCMs: moist convective adjustment based on restoring a super moist adiabatic lapse rate to the moist adiabatic lapse rate, and penetrative convection (PC). The PC parameterization differs from the MALR in that convection can take place between two noncontiguous atmospheric layers that are convectively unstable with respect to each other, even though the intervening atmospheric layers are not convectively unstable. Lindzen et al. (1982) investigated a simple

PC parameterization and found that f_{PC} is negative (Table A.7). These authors concluded that this negative feedback is caused by two factors: (1) the surface sensible and latent heat loss is deposited at higher altitudes by cumulus clouds than by a fixed critical lapse rate and is therefore more effectively radiated to space; and (2) the variable lapse rate resulting from the PC allows local radiative perturbations near the tropopause to be compensated by changes in local temperature without having these changes being carried to the surface by a fixed lapse rate. However, the surface and tropospheric warming induced by a doubled CO_2 concentration for this simple PC parameterization is similar to that for the MALR (Figure A.8). Rowntree and Walker (1978) used the PC parameterization of the United Kingdom Meteorological Office 11-layer GCM (Saker 1975) and found that $f_{PC} = -0.654$ (Table A.7). This value is larger in magnitude than f_{MALR} of the two-layer RCM (Table A.5) and, acting alone, would reduce the zero-feedback temperature change by almost 40%.

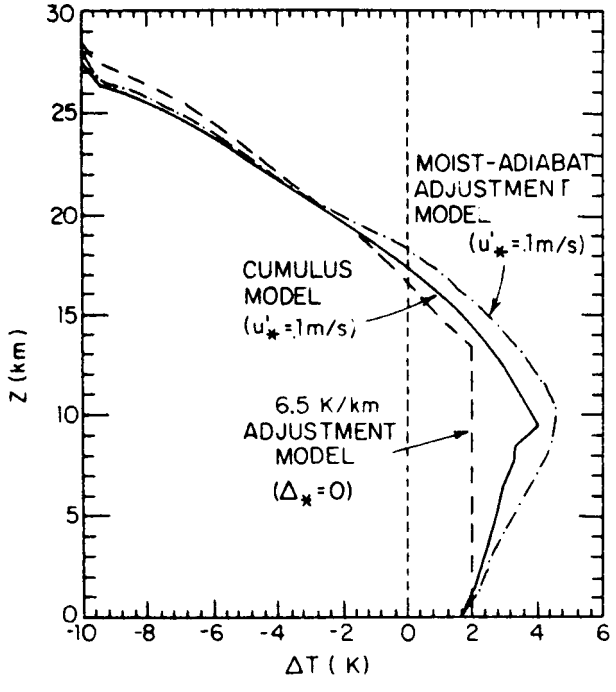

Figure A.8. Temperature changes induced by doubled CO_2 for FLR(6.5), MALR and PC (cumulus model) from Lindzen et al. (1982). u'_* is a surface wind parameter used in the calculation of the surface sensible and latent heat fluxes.

In summary it is seen that $f_{BADJ} > 0$, $f_{MALR} < 0$ with values between about -0.25 and -0.4, and $f_{PC} < 0$ with values that, although dependent on the particular parameterization of penetrating convection, are likely to give $f_{PC} \leq f_{MALR} < 0$.

Cloud feedbacks. Changes in the altitude, cover and optical depth of clouds induced by a change in CO_2 concentration can give rise to the three cloud feedbacks shown in Table A.5. In this section we will describe these feedbacks and will evaluate them quantitatively, insofar as possible, from the RCM results.

Cloud altitude feedback. In the first RCM study of CO_2-induced climate change, Manabe and Wetherald (1967) prescribed the location of three cloud layers at what was stated to be 10, 4.1, and 1.7 to 2.7 km for both the $1 \times CO_2$ and $2 \times CO_2$ simulations. Consequently, this treatment of the altitudes of the clouds has come to be known as constant or fixed cloud altitude (FCA). In actuality, however, the pressures of the cloud layers were fixed (FCP) rather than the altitudes in the Manabe and Wetherald (1967) RCM[4]. The reason for this is that the vertical structure of the Manabe and Wetherald (1967) RCM is based on the σ-coordinate system, which, in this case, is equal to the pressure p divided by the surface pressure p_s. Because the clouds were defined at fixed σ-levels and p_s was fixed, the pressures of the cloud layers were fixed. Subsequently, other RCM studies also employed the FCP assumption (e.g., Rowntree and Walker 1978; Hunt and Wells 1979; Charlock 1981; Hummel and Kuhn 1981a, 1981b; Hummel and Reck 1981; Hunt 1981; Hummel 1982; Lal and Ramanathan 1984; Somerville and Remer 1984), but these studies also have been misinterpreted as employing the FCA assumption. Several RCM studies actually have employed the FCA assumption (e.g., Augustsson and Ramanathan 1977; Wang and Stone 1980; Hansen et al. 1981; Wang et al. 1981) but, as we will show below, the FCA and FCP assumptions about the vertical location of clouds give results that are not strictly comparable. Another assumption was proposed by Cess (1974, 1975) from an examination of the outgoing infrared flux from the Earth-atmosphere system written as $F = c_1 - c_2 A_c$, where

[4] R. T. Wetherald, personal communication.

A_c is the fractional cloud cover, $c_1 = c_1(T_s, \Gamma)$, $c_2 = c_2(T_s, \Gamma, T_c)$, and T_c is the cloud-top temperature. Cess found that $\partial c_2/\partial T_s$ for either a single effective cloud or for three cloud layers agreed with the empirical findings of Budyko (1969) if the cloud-top temperature was fixed (FCT) rather than the cloud altitude.

We can compare the FCA, FCP, and FCT assumptions about the vertical location of clouds by determining the partial derivatives of cloud altitude, z_c, cloud pressure, p_c, and cloud temperature, T_c, with respect to the surface temperature T_s. This can be done simply by assuming that the temperature lapse rate Γ is constant. Then

$$T_c = T_s - \Gamma z_c \ , \tag{A.94}$$

and by integrating the hydrostatic equation from the surface to the cloud we can obtain

$$p_c = \left(\frac{T_c}{T_s}\right)^{\frac{g}{R\Gamma}} p_s \ , \tag{A.95}$$

and by Equation (A.94)

$$z_c = \frac{1 - (p_c/p_s)^{\frac{R\Gamma}{g}}}{\Gamma} T_s \ . \tag{A.96}$$

From these expressions we can obtain the following:

FCA

$$\frac{\partial z_c}{\partial T_s} = 0 \ , \tag{A.97a}$$

$$\frac{\partial p_c}{\partial T_s} = \frac{g z_c}{R T_c} \frac{p_c}{T_s} \ , \tag{A.97b}$$

and

$$\frac{\partial T_c}{\partial T_s} = 1 \ . \tag{A.97c}$$

FCP

$$\frac{\partial z_c}{\partial T_s} = \frac{1 - (p_c/p_s)^{\frac{R\Gamma}{g}}}{\Gamma} \ , \tag{A.98a}$$

$$\frac{\partial p_c}{\partial T_s} = 0 \ , \tag{A.98b}$$

and

$$\frac{\partial T_c}{\partial T_s} = \left(\frac{p_c}{p_s}\right)^{\frac{R\Gamma}{g}} \ . \tag{A.98c}$$

FCT

$$\frac{\partial z_c}{\partial T_s} = \frac{1}{\Gamma} \ , \tag{A.99a}$$

$$\frac{\partial p_c}{\partial T_s} = -\frac{g}{r\Gamma} \left(\frac{T_c}{T_s}\right)^{\frac{g}{R\Gamma}} \frac{p_s}{T_s} \ , \tag{A.99b}$$

and

$$\frac{\partial T_c}{\partial T_s} = 0 \ . \tag{A.99c}$$

Numerical values for these partial derivatives are shown in Table A.8 for the case where $p_s = 1000$ mb, $T_s = 288°C$, $\Gamma = 6.5°C\ km^{-1}$ and $p_c = 500$ mb. Of course $\partial z_c/\partial T_s$, $\partial p_c/\partial T_s$, and $\partial T_c/\partial T_s$ are zero for the FCA, FCP, and FCT assumptions, respectively. For the FCA assumption, both T_c and p_c increase as T_s increases. This is shown schematically in Figure A.9. For the FCP assumption, both T_c and z_c increase as T_s increases, whereas for the FCT assumption, z_c increases and p_c decreases as T_s increases. These changes also are shown schematically in Figure A.9. In comparing the three assumptions, it can be seen that for a small change in surface temperature δT_s

$$0 = (\delta z_c)_A < (\delta z_c)_P < (\delta z_c)_T = \Gamma^{-1} \delta T_s \ , \tag{A.100a}$$

$$(\delta p_c)_T < 0 = (\delta p_c)_P < (\delta p_c)_A = \alpha \delta T_s \ , \tag{A.100b}$$

and

$$0 = (\delta T_c)_T < (\delta T_c)_P < (\delta T_c)_A = \delta T_s \ , \tag{A.100c}$$

where $\alpha > 0$ and subscripts A, P, and T denote constant altitude, pressure, and temperature, respectively.

Table A.8
Partial Derivatives of Cloud Altitude, Pressure, and Temperature With Respect to Surface Temperature for the FCA, FCP, and FCT Assumptions

Cloud Altitude Treatment	$\frac{\partial z_c}{\partial T_s}$ (m °C^{-1})	$\frac{\partial p_c}{\partial T_s}$ (mb °C^{-1})	$\frac{\partial T_c}{\partial T_s}$ (°C °C^{-1})
FCA	0	1.29	1.0
FCP	19.0	0	0.876
FCT	154	−9.12	0

Note: See text for the parameter values.

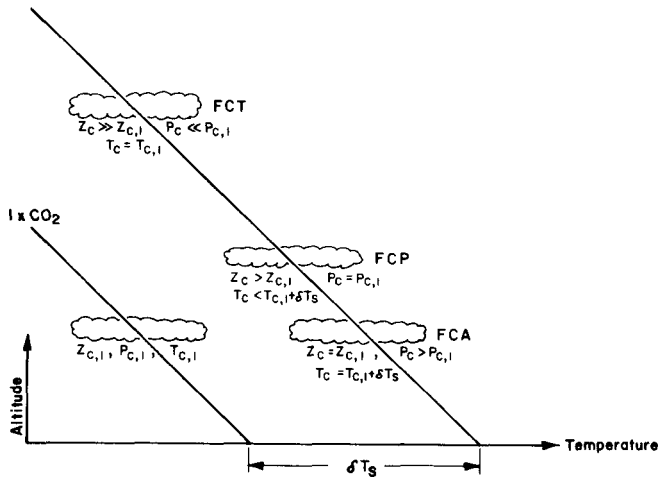

Figure A.9. Schematic representation of changes in cloud altitude, z_c, pressure, p_c, and temperature, T_c, in response to a change in surface temperature, δT_s, for FCA, FCP, and FCT assumptions.

We can now consider the feedback of the change in cloud altitude in the FCP and FCT assumptions. First, consider that the cloud altitude is fixed, the CO_2 concentration is doubled, and the climate system reaches the new equilibrium where surface temperature has increased by $(\Delta T_s)_A$ compared with the 1 × CO_2 equilibrium value. Then by Equation (A.100c), $(\Delta T_c)_A = (\Delta T_s)_A$. Now consider that the cloud temperature is fixed, the CO_2 concentration is doubled, and suppose that the new equilibrium is reached in which $\Delta T_s = (\Delta T_s)_A$. But $(\Delta T_c)_T = 0 < (\Delta T_c)_A$ by Equation (A.100c); hence, the amount of radiation emitted upward by the cloud for FCT is less than that for FCA; therefore the climate system with FCT cannot be in equilibrium with $\Delta T_s = (\Delta T_s)_A$. To achieve equilibrium with FCT, a necessary condition is $(\Delta T_s)_T > (\Delta T_s)_A$. The FCT assumption amplifies the surface temperature change of the FCA assumption and therefore is a positive feedback process. Following similar reasoning it can be seen that the FCP assumption also is a positive feedback process. However, comparison of the $\partial T_c/\partial T_s$ derivatives in Table A.8 indicates that the FCP feedback is small compared with the FCT feedback.

A quantitative assessment of the FCT feedback f_{CA} is presented in Table A.9. The ratio of ΔT_s with FCT to ΔT_s with FCA or FCP varies from 1.43 to 1.62 in the four studies shown in the table. Because each of these studies was performed with the water vapor feedback of the fixed relative humidity assumption, it is possible to estimate f_{CA} only for the two studies for which f_W can be estimated. The resultant estimated cloud altitude feedback varies from 0.168 to 0.203, which is smaller than the value of 0.261 shown in Table A.5.

Cloud cover feedback. To begin our discussion of cloud cover feedback, it is helpful to consider again the planetary radiative energy budget given by Equation (A.52) as

$$N_0 = \frac{1 - \alpha_p}{4} S_0 - R_0 .$$

Following the procedure in Section A.2.1, we can write that the change in N_0 due to a change in the CO_2 concentration ΔC and the induced surface temperature change $(\Delta T_s)_{\Delta C}$ is

$$\Delta N_0 = \frac{\partial N_0}{\partial C} \Delta C + \frac{\partial N_0}{\partial T_s} (\Delta T_s)_{\Delta C} + \left(\sum_j \frac{\partial N_0}{\partial I_j} \frac{dI_j}{dT_s} + \frac{\partial N_0}{\partial A_c} \frac{dA_c}{dT_s} \right) (\Delta T_s)_{\Delta C}$$

where $\partial N_0/\partial T_s$ is the change in N_0 caused by the change in T_s when all the internal quantities I_j are constant, $(\partial N_0/\partial A_c)(dA_c/dT_s)$ is the change in N_0 caused by the change in the internal quantity cloud cover A_c through its dependence on T_s, and $\sum_j (\partial N_0/\partial I_j)(dI_j/dT_s)$ is the change in N_0 caused by the changes in all the other internal quantities through their dependences on T_s. Setting $\Delta N_0 = 0$ in the equation above gives the equilibrium $(\Delta T_s)_{\Delta C}$ as

$$(\Delta T_s)_{\Delta C} = \frac{\frac{\partial N_0}{\partial C} \Delta C}{\left(-\frac{\partial N_0}{\partial T_s} - \sum_j \frac{\partial N_0}{\partial I_j} \frac{dI_j}{dT_s} - \frac{\partial N_0}{\partial A_c} \frac{dA_c}{dT_s} \right)} \quad \text{(A.101a)}$$

or

$$(\Delta T_s)_{\Delta C} = \frac{G_0}{\left(1 - \sum_j f_j - f_{CC}\right)} \frac{\partial N_0}{\partial C} \Delta C , \quad \text{(A.101b)}$$

where

$$G_0 = -\left(\frac{\partial N_0}{\partial T_s}\right)^{-1} ,$$

$$f_j = \frac{\partial N_0}{\partial I_j} \frac{dI_j}{dT_s} ,$$

Table A.9
Cloud Altitude Feedback f_{CA} Determined From Selected Radiative-Convective Models

Study	Model Attributes[a]	Cloud Altitude Treatment (layers)	ΔT_s $2\times CO_2$-$1\times CO_2$ (°C)	Estimated Feedback f_{CA}
Augustsson and Ramanathan (1977)	ERE;FRH;FLR(6.5); FCC,FOD;FAL	FCA(1)	1.98	
		FCT(1)	3.2	Positive
Wang and Stone (1980)	BAE;FRH;FLR(6.5); FCC,FOD;FAL	FCA(1)	2.00	
		FCT(1)	3.00	Positive
Reck (1979a)	ERE;FRH;FLR(6.5); FCC,FOD;FAL	FCT(3)	1.426 to 1.561 times the response for FCP	0.168 to 0.203[b]
Hansen et al. (1981)	BAE;FRH;FLR(6.5); FCC,FOD;FAL	FCA(1)	1.94	
		FCT(1)	2.78	0.190[c]

[a] Surface energy flux; water vapor; lapse rate; cloud cover, optical depth; surface albedo. See Table A.3 for definition of abbreviaions.
[b] $f_{CA} = [1 - (\Delta T_s)_0/\Delta T_s] - f_W$ with $(\Delta T_s)_0$ and f_W from Table A.6 for Manabe and Wetherald (1967) with FCC.
[c] As in footnote *b*, except values from Hansen et al. (1981).

and the cloud cover feedback f_{CC} is given by

$$f_{CC} = \delta \frac{dA_c}{dT_s} G_0 , \qquad \text{(A.102)}$$

with

$$\delta = \frac{\partial N_0}{\partial A_c} = -\frac{S_0}{4} \frac{\partial \alpha_p}{\partial A_c} - \frac{\partial R_0}{\partial A_c} , \qquad \text{(A.103)}$$

as first defined by Schneider (1972). From Equation (A.102) it can be seen that cloud cover feedback depends on the three quantities: δ, dA_c/dT_s, and G_0. Assuming that

$$\alpha_p = (1 - A_c)\alpha_s + A_c\alpha_c , \qquad \text{(A.104)}$$

where α_s is the clear sky albedo and α_c is the albedo with cloud cover, Equation (A.103) can be written as

$$\delta = -\frac{S_0}{4} (\alpha_c - \alpha_s) - \frac{\partial R_0}{\partial A_c} . \qquad \text{(A.105)}$$

Because $\alpha_c > \alpha_s$ in the global mean, the change in albedo caused by a change in cloud cover contributes negatively to δ. On the other hand, $\partial R_0/\partial A_c < 0$ because the upward emission from clouds is less than that from the warmer ground. Thus, the changes in longwave radiation caused by a change in cloud cover contributes positively to δ. If $\delta > 0$ the longwave radiation effect dominates the albedo effect and vice versa if $\delta < 0$. This is summarized in Table A.10, together with the dependence of the sign of the cloud cover feedback on dA_c/dT_s.

Table A.10
Characteristics of Cloud Cover Feedback f_{CC}

$\frac{dA_c}{dT_s}$	δ	Dominant Effect	f_{CC}
+	+	Longwave	+
	0	Neither	0
	−	Albedo	−
0	+	Longwave	0
	0	Neither	0
	−	Albedo	0
−	+	Longwave	−
	0	Neither	0
	−	Albedo	+

Only one CO_2 study has been performed with an RCM in which the cloud cover has been a predicted quantity. (We shall describe this study subsequently.) In all the other RCM CO_2 studies, $dA_c/dT_s = 0$; hence, as shown in Table A.10, $f_{CC} = 0$. However, a few non-CO_2 studies have been carried out to determine the effects of prescribed changes in cloud cover. In these studies A_c is an external quantity, hence

$$\Delta N_0 = \frac{\partial N_0}{\partial A_c} \Delta A_c + \left(\frac{\partial N_0}{\partial T_s} + \sum_j \frac{\partial N_0}{\partial T_s} \frac{dI_j}{dT_s} \right) (\Delta T_s)_{\Delta CL} ,$$

and the equilibrium $(\Delta T_s)_{\Delta CL}$ is then

$$(\Delta T_s)_{\Delta CL} = \frac{\delta \Delta A_c}{-\dfrac{\partial N_0}{\partial T_s} - \sum_j \dfrac{\partial N_0}{\partial I_j}\dfrac{dI_j}{dT_s}} . \quad \text{(A.106)}$$

This can be written by Equation (A.6) as

$$(\Delta T_s)_{\Delta CL} = G_f \, \delta \, \Delta A_c . \quad \text{(A.107)}$$

Thus, δ can be determined from

$$\delta = \frac{(\Delta T_s)_{\Delta CL}}{G_f \Delta A_c} , \quad \text{(A.108)}$$

if G_f for the model is known. In addition, a few RCM studies have been performed in which both the CO_2 concentration and the fractional cloudiness were changed. In this case

$$\Delta N_0 = \frac{\partial N_0}{\partial C} \Delta C + \delta \, \Delta A_c + \left(\frac{\partial N_0}{\partial T_s} + \sum_j \frac{\partial N_0}{\partial I_j}\frac{dI_j}{dT_s} \right) (\Delta T_s)_{\Delta C, \Delta CL} .$$

Setting $\Delta N_0 = 0$ at equilibrium and solving for $(\Delta T_s)_{\Delta C, \Delta CL}$ then gives

$$(\Delta T_s)_{\Delta C, \Delta CL} = \frac{\dfrac{\partial N_0}{\partial C}\Delta C + \delta \, \Delta A_c}{-\dfrac{\partial N_0}{\partial T_s} - \sum_j \dfrac{\partial N_0}{\partial I_j}\dfrac{dI_j}{dT_s}} \quad \text{(A.109)}$$

and

$$(\Delta T_s)_{\Delta C, \Delta CL} = (\Delta T_s)_{\Delta C} + G_f \, \delta \, \Delta A_c , \quad \text{(A.110)}$$

the latter by Equation (A.101a) with $dA_c/dT_s = 0$ and the definition of G_f [Equation (A.6)]. Thus δ can be determined from

$$\delta = \frac{(\Delta T_s)_{\Delta C, \Delta CL} - (\Delta T_s)_{\Delta C}}{G_f \Delta A_c} \quad \text{(A.111)}$$

if G_f is known for the model.

An analysis of δ based on either Equation (A.108) or Equation (A.111) has been made for six RCM studies, and the necessary input data and results are presented in Table A.11 together with the attributes and cloud characteristics of the models. These results are categorized in Table A.12 in terms of the vertical location of the clouds, that is, low, middle, and high clouds as defined within the altitude bounds of 0.75 and 2.7 km, 3.5 and 5.5 km, and 7.5 and 11 km, respectively. It can be seen that these RCMs give negative values of δ for low and middle clouds, with more negative values for the low clouds than for the middle clouds, and positive values of δ for high clouds. Thus, from Table A.10, the albedo effect dominates the longwave effect for low and middle clouds, while the opposite is true for high clouds. From Equation (A.105) it can be seen that the dominance of the albedo effect over the longwave effect in low and middle clouds occurs because α_c is large (see Table A.11) and $\partial R_0/\partial A_c$ is small (and negative), the latter because the cloud-top temperature is not much colder than the ground. However, as the cloud altitude increases, the difference between the cloud-top and ground temperatures grows and $\partial R_0/\partial A_c$ becomes more negative. Also α_c decreases as the optical thickness of the cloud decreases with increasing altitude (see Table A.11). Both of these effects cause δ to increase with increasing altitude and eventually to become positive for the high clouds. For the latter, α_c is small and close to α_s, so the value of δ is largely determined by $\partial R_0/\partial A_c$. This, in turn, depends on the emissivity ϵ of the high cloud as well as on the difference between the cloud-top and ground temperatures. Because $\partial R_0/\partial A_c$ increases in magnitude with increasing ϵ, δ increases with ϵ for high clouds as generally shown in Table A.12.

The values of δ shown in Table A.12 for each cloud differ among the models for several reasons including differences in the atmospheric composition of the models, other feedback processes, the actual location of clouds within the altitude bounds of low, middle, and high clouds, and probably most importantly the cloud optical properties of the models. All of the models except that of Stephens and Webster (1981) prescribe the optical properties of the clouds on the basis of limited and nonsimultaneous observations. However, Stephens and Webster (1981) calculate all of the cloud optical properties in a consistent manner for the prescribed cloud liquid water path (LWP) or ice water path (IWP) and the solar zenith angle from parameterizations of multiple scattering calculations. Figure A.10 shows $(\Delta T_s)_{\Delta CL}$ as a function of the LWP or IWP for the three cloud layers of Stephens and Webster (1981) defined in Table A.11. Because δ is

Table A.11
Analysis of $\delta = \partial N_0/\partial A_c$ From RCM Simulations of $(\Delta T_s)_{\Delta CL}$ and $(\Delta T_s)_{\Delta C,\Delta CL}$

Study	Model Attributes[a]	Cloud Altitude (km)	Cloud Emissivity	Cloud Albedo	Cloud Absorptivity	ΔA_c	G_f (°C(W m^{-2})$^{-1}$)	$(\Delta T_s)_{\Delta CL}$ or $(\Delta T_s)_{\Delta C,\Delta CL}$, $(\Delta T_s)_{\Delta C}$ (°C)	δ (W m^{-2})
Manabe and Strickler (1964)	ERE; FAH; FLR(6.5); FOD;FAL	20	0.5	0.21	0.005	1	0.34[b]	~5	14.7[c]
		11	0.5	0.21	0.005	1	0.34[b]	~5	14.7[c]
		7.5	1	0.21	0.005	1	0.34[b]	~ −2	−5.9[c]
		3.7	1	0.48	0.020	1	0.34[b]	~ −22	−65[c]
		1.4–2.0	1	0.69	0.035	1	0.34[b]	~ −50	−147[c]
Manabe and Wetherald (1967)	ERE; FRH; FLR(6.5); FOD;FAL	10	0.5	0.20	0	1	0.73[d]	4	5.5[c]
		10	1	0.20	0	1	0.73[d]	39	53[c]
		4.1	1	0.48	0	1	0.73[d]	−39	−53[c]
		1.7–2.7	1	0.69	0	1	0.73[d]	−82	−112[c]
Reck (1979b)	ERE;FRH;FLR(6.5); FOD;FAL	10	1	0.20	0	−0.05	0.425[e]	0, 1.7	80[f]
		1.7–2.7	1	0.69	0	0.03	0.425[e]	0, 1.7	−133[f]
Hummel and Reck (1981)	ERE;FRH;MALR; FOD;FAL	3.5–5.5	1	0.32	0	−0.212	0.512[g]	2.56, 2.05	−4.7[f]
		3.5–5.5	1	0.32	0	0.176	0.512[g]	1.89, 2.05	−1.8[f]
Hunt (1981)	BAE,FRH,FLR(6.5); FOD;FAL	10	1	0.21	0.005	0.018	0.455[h]	2.19, 1.82	45[f]
		4.1	1	0.48	0.020	0.008	0.455[h]	1.59, 1.82	−63[f]
		1.7–2.7	1	0.69	0.035	0.030	0.455[h]	0.01, 1.82	−133 [f]
Stephens and Webster (1981)	ERE;FRH;FLR(6.5); FOD;FAL	7.5–9	IWP = 20 g m^{-2}[i]			1	0.52[j]	16	31[g]
		3.75–5	LWP = 140 g m^{-2}[i]			1	0.52[j]	−22	−42[g]
		0.75–1.5	LWP = 140 g m^{-2}[i]			1	0.52[j]	−40	−77[g]

[a] Surface energy flux; water vapor; convection; cloud optical depth; surface albedo. See Table A.3 for definition of abbreviations.
[b] $G_f = (\Delta T_s)_{2\times CO_2}/\Delta Q$ with $(\Delta T_s)_{2\times CO_2} = 1.36$ °C from Table A.6 for Manabe and Wetherald (1967) with CLR and FAH, and assumed $\Delta Q = 4$ W m^{-2}.
[c] Determined from Equation (A.108).
[d] As in footnote *b*, except with $(\Delta T_s)_{2\times CO_2} = 2.92$ °C from Table A.6 for Manabe and Wetherald (1967) with CLR and FRH.
[e] As in footnote *b*, except with $(\Delta T_s)_{2\times CO_2} = 1.7$ °C.
[f] Determined from Equation (A.111).
[g] As in footnote *b*, except with $(\Delta T_s)_{2\times CO_2} = 2.05$ °C.
[h] As in footnote *b*, except with $(\Delta T_s)_{2\times CO_2} = 1.82$ °C.
[i] Cloud emissivity, albedo and absorptivity determined from the cloud liquid-water and ice-water paths (LWP and IWP) shown, based on Stephens (1978) and Stephens and Webster (1981), respectively.
[j] $G_f = \beta/(1 - \alpha_p/4)S_0)$ with $\alpha_p = 0.3$, $S_0 = 1370$ W m^{-2}, and $\beta = S_0(\Delta T_s/\Delta S_0) = 125$ °C from Stephens and Webster (1981).

related to $(\Delta T_s)_{\Delta CL}$ by Equation (A.108), in this case for which $\Delta A_c = 1$ and $G_f = 0.52$ (see Table A.11), $\delta \simeq 2(\Delta T_s)_{\Delta CL}$. Therefore, Figure A.10 shows that δ decreases with increasing LWP and IWP. As shown by Stephens and Webster (1981) and Equation (A.105), this occurs because α_c increases with LWP(IWP), but ϵ rapidly reaches unity for small LWP(IWP) and thereafter cannot increase with increasing LWP. Figure A.10 also shows that δ increases with altitude for fixed LWP(IWP), as was also shown in Table A.12, and increases with latitude in winter for fixed LWP(IWP) and altitude. The latter occurs because of the dependence of δ on insolation and the decrease of insolation with latitude in the winter hemisphere. It can be concluded from the above that the feedback effect of a CO_2-induced change in cloud cover depends on the latitude, altitude, LWP(IWP)—or equivalently optical depth—of the clouds and on the sign and magnitude of dA_c/dT_s.

We now will consider the RCM study by Wang et al. (1981) in which the cloud cover is a predicted quantity. The cloud model is based on the conservation equation for the cloud liquid water mixing ratio ℓ,

$$\frac{\partial \ell}{\partial t} = C - P \,, \qquad \text{(A.112)}$$

where C and P are the condensation and precipitation rates per unit mass of air. The precipitation rate is parameterized as

$$P = f_1 \ell \,, \qquad \text{(A.113)}$$

where f_1^{-1} is a prescribed conversion time (~2 h) of cloud droplets to precipitation. The condensation is obtained from

$$(1 + B)LC = H_c \,, \qquad \text{(A.114)}$$

Table A.12
$\delta = \partial N_0/\partial A_c$ (W m^{-2}) for Low, Middle, and High Cloud Summarized From the Analysis of Table A.11

Study	Low Cloud (0.75, 1.7 km)[a]	Middle Cloud (3.5, 5.5 km)[a]	High Cloud[b] (7.5, 11 km)[a]
Manabe and Strickler (1964)	−147	−65	14.7 (0.5)
Manabe and Wetherald (1967)	−112	−53	5.5 (0.5) 53 (1.0)
Reck (1979b)	−133		80 (0.5)
Hummel and Reck (1981)		−4.7, −1.8[c]	
Hunt (1981)	−133	−63	45 (1.0)
Stephens and Webster (1981)	−77	−42	31 (0.86)
Hummel (1982)	−143	−50	36 (1.0)

[a] Altitude bounds between which the particular cloud type is located.
[b] The cloud emissivity is shown in parentheses.
[c] For $\Delta A_c = -0.212$ and 0.176, respectively.

where H_c is the convective heating rate given by the convective adjustment. This is equal to the latent heating rate, LC, plus the sensible heating rate, $B(LC)$, where B is the Bowen ratio of the sensible to latent heating rates. Combining Equations (A.112)–(A.114) and setting $\partial \ell/\partial t = 0$ for equilibrium gives

$$\ell = \frac{H_c}{f_1(1+B)L} . \qquad \text{(A.115)}$$

The Bowen ratio is taken to be independent of altitude to satisfy the vertically integrated conservation of water substance and energy, and the relative humidity is assumed fixed. The Bowen ratio is then given by the surface value

$$B = \frac{\frac{1}{4}\frac{c_p}{L}}{RH_s\left(\frac{\partial q^*}{\partial T}\right)_{T_s}} , \qquad \text{(A.116)}$$

where the derivative of saturation mixing ratio q^* with respect to temperature is evaluated at the surface temperature, and the factor 1/4 is introduced to match the global mean value of B given by Budyko (1956). Finally, it is assumed that the cloud cover A_c increases with increasing precipitation rate, hence

$$A_c = \ell/f_2 , \qquad \text{(A.117)}$$

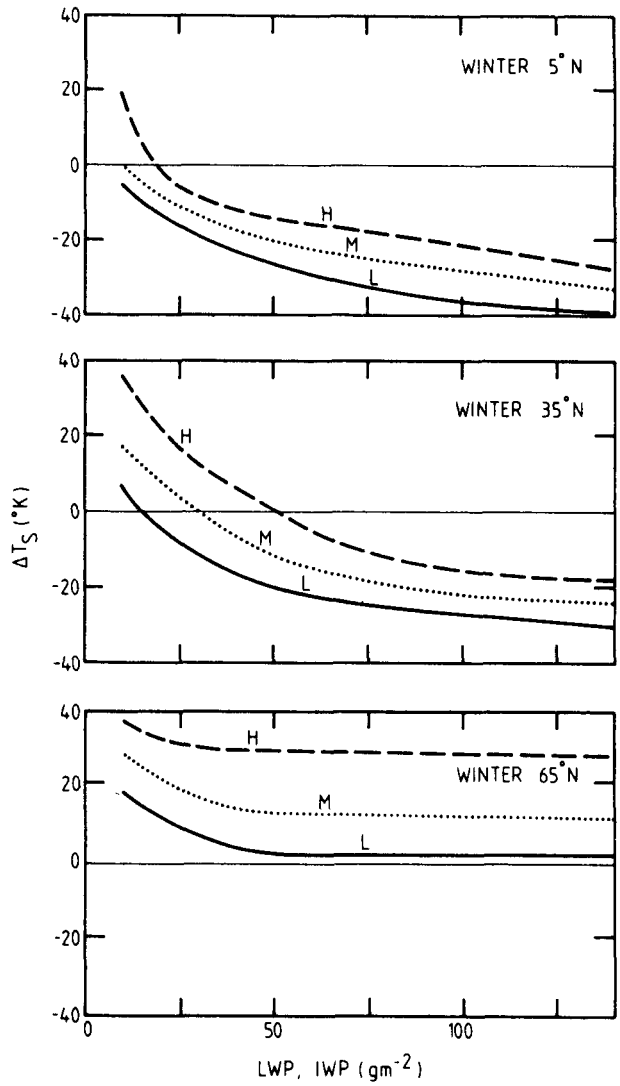

Figure A.10. Change in surface temperature $(\Delta T_s)_{\Delta CL}$ for $\Delta A_c = 1$ at different latitudes as a function of liquid water and ice water path (LWP and IWP) for high (7.5–9 km), middle (3.75–5 km) and low (0.75–1.5 km) clouds. Source: Stephens and Webster (1981).

where f_2 is a typical mixing ratio for precipitating cloud systems (5.5×10^{-4}). Combining Equations (A.115) and (A.117) gives

$$A_c = \frac{H_c}{f_1 f_2(1+B)L} \qquad \text{(A.118)}$$

from which

$$\frac{dA_c}{dT_s} = \frac{1}{f_1 f_2 L(1+B)}\left(\frac{dH_c}{dT_s} - \frac{H_c}{1+B}\frac{dB}{dT_s}\right) . \qquad \text{(A.119)}$$

Because B decreases with increasing T_s, the last term in Equation (A.119) contributes positively to

dA_c/dT_s. However, because dH_c/dT_s can be either positive or negative, dA_c/dT_s can also be of either sign.

The RCM of Wang et al. (1981) has 17 vertical layers from the surface to 50 km altitude with attributes of ERE, FRH, FLR(6.5), FCA, FOD, and FAL (see Table A.3). Thus, the results with and without cloud cover feedback also include water vapor feedback, and a precise evaluation of f_{CC} cannot be obtained because $(\Delta T_s)_0$ is not known. The optical depth in the experiments discussed below was fixed with values of 16, 6, and 2 for the altitude ranges 0–3 km, 3–8 km, and above 8 km, respectively.

Results from Wang et al. (1981) are shown in Table A.13 for both a CO_2 doubling and a 2% increase in the solar constant S_0. For fixed cloud cover, these different external forcings give comparable surface warmings of about 2°C. Both external forcings give nearly the same increase in the total cloud cover of about 0.02 on a scale from 0 (no clouds) to 1 (overcast). Because ΔT_s is also positive, dA_c/dT_s is positive for both forcings. However, ΔT_s for the CO_2 doubling increases with the increased cloud cover, but ΔT_s for the increased solar constant decreases with the increased cloud cover. Table A.13 shows an estimate of the cloud cover feedback defined as

$$\tilde{f}_{CC} = 1 - \frac{(\Delta T_s)_{\Delta CL=0}}{(\Delta T_s)_{\Delta CL\neq 0}} .$$

This parameter is different from the actual cloud feedback f_{CC} because both $(\Delta T_s)_{\Delta CL=0}$ and $(\Delta T_s)_{\Delta CL\neq 0}$ have water vapor feedback. It can be seen that $\tilde{f}_{CC}$ is positive for the CO_2 doubling and is negative and of comparable magnitude for the increased solar constant.

Table A.13
Cloud Cover Feedback Analysis for the Study by Wang et al. (1981)

External Forcing	ΔA_c	ΔT_s (°C)	$\tilde{f}_{CC}$[a]
$\Delta C/C = 1$	0	1.96	
	0.0178	2.68	0.269
$\Delta S_0/S_0 = 0.02$	0	2.28	
	0.021	1.87	−0.219

[a] $\tilde{f}_{CC} = 1 - \frac{(\Delta T_s)_{\Delta CL=0}}{(\Delta T_s)_{\Delta CL\neq 0}}$

To understand these apparently contradictory results, Figure A.11 shows the vertical distribution of the changes in cloud cover for both external forcings. This figure shows cloud cover increases below about 2 km and above about 5 km, with cloud cover decreases between these altitudes. The changes in cloud cover of both signs are generally larger in magnitude for the CO_2 doubling than for the solar constant increase. In Table A.14 we present an estimate of the contribution of these changes in cloud cover to the feedback f_{CC}. For this purpose we have estimated the values of δ for the three layers of constant τ (0–3 km, 3–8 km, and above 8 km) based on the results of Manabe and Wetherald (1967) shown in Table A.12. The values of ΔA_c are estimated from Figure A.11 for each of these constant τ layers. Table A.14 shows that both the increased high cloud cover and decreased low cloud cover give positive contributions to the positive cloud cover feedback of the CO_2 doubling, with the contribution from the low cloud being about twice that of the high cloud, and no contribution from the middle cloud. On the other hand, the increased low and middle cloud cover in the increased solar constant forcing give negative contributions to the cloud cover feedback, which dominate the positive contribution from the increased high cloud.

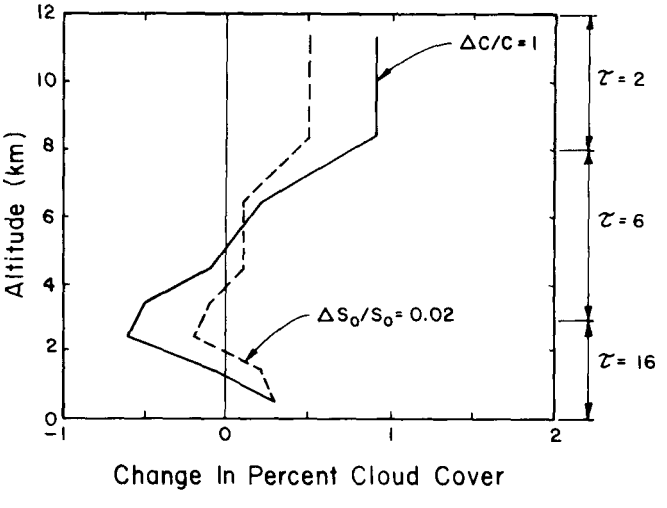

Figure A.11. Change in percent cloud cover as a function of altitude for a 2% increase in the solar constant and a doubling of the CO_2 concentration. Source: Wang et al. (1981).

Table A.14
Contributions to f_{CC} by the Changes in the Low, Middle, and High Clouds in the Study by Wang et al. (1981)

External Forcing	Cloud	τ	δ[a] (W m^{-2})	ΔA_c[b]	$\tilde{f}_{CC}$[c]
$\Delta C/C = 1$	High ($z > 8$ km)	2	6	0.01	0.0090
	Middle ($3 < z < 8$ km)	6	−50	0	0
	Low ($z < 3$ km)	16	−100	−0.0015	0.0225
	Total Effect				0.0315
$\Delta S_0/S_0 = 0.02$	High ($z > 8$ km)	2	6	0.005	0.0045
	Middle ($3 < z < 8$ km)	6	−50	0.002	−0.0150
	Low ($z < 3$ km)	16	−100	0.0007	−0.0105
	Total Effect				−0.0210

[a] Based on the study of Manabe and Wetherald (1967) shown in Table A.12.
[b] Estimated from Figure A.11.
[c] $f_{CC} = \delta\ (\Delta A_c/\Delta T_s) G_0$ with ΔT_s taken as 2°C based on Table A.13 and $G_0 = 0.3$°C (W m^{-2})$^{-1}$.

These results from the study performed by Wang et al. (1981) clearly show that it is the vertical integral throughout the atmosphere of $\delta \Delta A_c$ that determines the sign and magnitude of the cloud cover feedback. Because this integral includes the changes in the vertical location of clouds through the vertical distribution of ΔA_c, it is seen that cloud altitude feedback is subsumed in cloud cover feedback.

Cloud optical depth feedback. We now consider the third and final feedback mechanism of clouds, namely, that caused by the change in cloud optical depth, τ_c. As in the preceding section it is useful to consider this feedback from the viewpoint of the planetary radiative energy budget. Doing so we can obtain

$$(\Delta T_s)_{\Delta C} = \frac{G_0}{\left(1 - \sum_j f_j - f_{OD}\right)} \frac{\partial N_0}{\partial C} \Delta C \ , \quad \text{(A.120)}$$

where the cloud optical depth feedback f_{OD} is given by

$$f_{OD} = \phi \frac{d\tau_c}{dT_s} G_0 \ , \quad \text{(A.121)}$$

and

$$\phi = \frac{\partial N_0}{\partial \tau_c} = -\frac{S_0}{4} \frac{\partial \alpha_p}{\partial \tau_c} - \frac{\partial R_0}{\partial \tau_c} \ . \quad \text{(A.122)}$$

These three equations are analogous to Equations (A.101)–(A.103), from which they may be obtained by replacing f_{CC} by f_{OD} and A_c by τ_c. Equation (A.121) shows that f_{OD}, like f_{CC}, depends on three quantities: ϕ, $d\tau_c/dT_s$, and G_0. As in the preceding section, we assume that

$$\alpha_p = (1 - A_c)\alpha_s + A_c \alpha_c \ , \quad \text{(A.104)}$$

and we also assume that R_0 can be approximated as

$$R_0 \doteq (1 - A_c) R_{0,s} + A_c [R_{0,s}(1 - \epsilon_c) + \epsilon_c \sigma T_c^4] \ , \quad \text{(A.123)}$$

where $R_{0,s}$ is the clear-sky value of R_0, ϵ_c is the upward effective cloud emissivity (Stephens 1978), and T_c is the cloud top temperature. Substituting Equations (A.104) and (A.123) into Equation (A.122) then gives

$$\phi = -A_c \left[\frac{S_0}{4} \frac{\partial \alpha_c}{\partial \tau_c} + (\sigma T_c^4 - R_{0,s}) \frac{\partial \epsilon_c}{\partial \tau_c}\right] . \quad \text{(A.124)}$$

This shows that ϕ, like δ, has both an albedo effect and a longwave radiation effect and depends on the cloud cover amount A_c. Because $\partial \epsilon_c/\partial \tau_c = 0$ for black clouds, while $\partial \alpha_c/\partial \tau_c > 0, \phi < 0$ for most low and middle clouds. On the other hand, because $\partial \epsilon_c/\partial \tau_c > 0$ for nonblack clouds, and σT_c^4 can be smaller than $R_{0,s}$, ϕ may be either negative or positive for cirrus clouds. Thus if $d\tau_c/\partial T_s > 0$ for the reasons described below, the cloud optical depth feedback f_{OD} is negative for low and middle clouds and may be either negative or positive for cirrus clouds.

Because τ_c depends on LWP and IWP for water and ice (cirrus) clouds, respectively (e.g., Stephens 1978; Stephens et al. 1984), we also can write Equations (A.121) and (A.124) as

$$f_{OD} = \tilde{\phi} \frac{dWP}{dT_s} G_0 \ , \quad \text{(A.125)}$$

$$\tilde{\phi} = -A_c \left[\frac{S_0}{4} \frac{\partial \alpha_c}{\partial WP} + (\sigma T_c^4 - R_{0,s}) \frac{\partial \epsilon_c}{\partial WP}\right] , \quad \text{(A.126)}$$

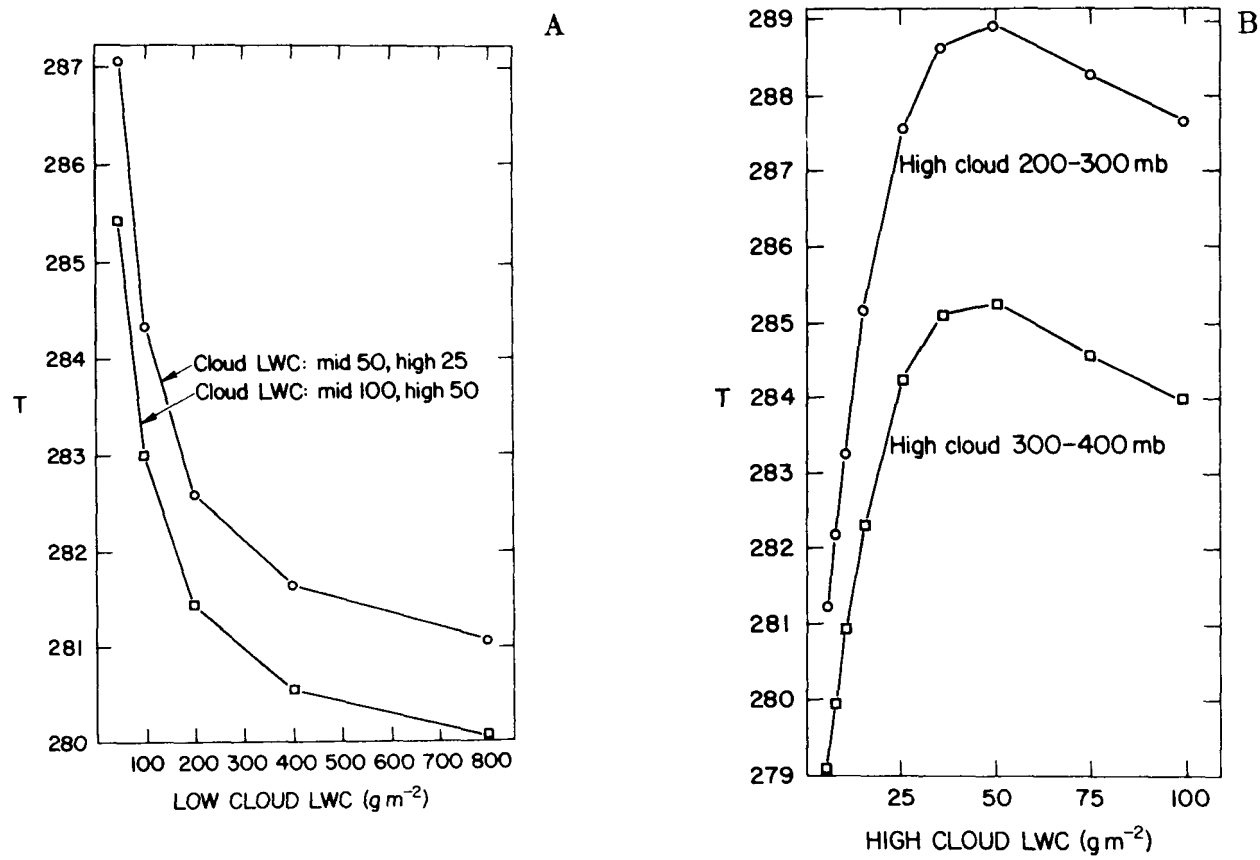

Figure A.12. Surface temperature T (K) as a function of (A) low cloud liquid water content (LWC) and (B) high cloud LWC with the high cloud at two different altitudes. Fractional area of each cloud type is 0.20. Source: Charlock (1982).

where WP represents LWP or IWP. Following the development of the preceding section leading to Equation (A.108), we can write that

$$\tilde{\phi} = \frac{(\Delta T_s)_{\Delta WP}}{G_f \Delta WP} . \qquad \text{(A.127)}$$

Estimates of $\tilde{\phi}$ for low and high clouds can be obtained from the results by Charlock (1982) using a RCM (Figure A.12) and $G_f \sim 0.5°C$ (W m^{-2})$^{-1}$ based on the 2.253°C warming obtained by Charlock (1981) for a CO_2 doubling with an assumed $\Delta N_0 = 4$ W m^{-2}. For low cloud with $A_c = 0.2$, Figure A.12 and Equation (A.127) show that $\tilde{\phi}$ varies from about -0.1 W m^{-2} (g m^{-2})$^{-1}$ for WP between 50 and 100 g m^{-2} to about -0.003 W m^{-2} (g m^{-2})$^{-1}$ for WP between 400 and 800 g m^{-2}. For high cloud with $A_c = 0.2$, $\tilde{\phi}$ varies from about $+0.8$ W m^{-2} (g m^{-2})$^{-1}$ for WP between 10 and 20 g m^{-2} to about -0.05 W m^{-2} (g m^{-2})$^{-1}$ for WP between 50 and 100 g m^{-2}. This transition from positive to negative values of $\tilde{\phi}$ with increasing WP represents the dominance of the longwave effect in Equation (A.126) for thin cirrus clouds and the dominance of the albedo effect in thick cirrus clouds, the latter because $\partial \epsilon_c / \partial WP$ becomes zero once ϵ_c becomes unity.

Three RCM studies of the effect of variable cloud optical depth or cloud water path on CO_2-induced temperature change have been performed by Wang et al. (1981), Charlock (1982), and Somerville and Remer (1984). The results of these studies are shown in Table A.15 along with the characteristics of the RCMs used therein. The optical depth feedback defined as $\tilde{f}_{OD} = 1 - (\Delta T_s)_{FOD}/(\Delta T_s)_{VOD}$ ranges from essentially zero to about -1.3. These values depend not only on ϕ, as previously discussed, but also on $d\tau_c/dT_s$ or dWP/dT_s as shown by Equations (A.121) and (A.127). Each of the three studies parameterized these latter quantities differently.

Table A.15
Cloud Optical Depth Feedback Determined From Selected Radiative-Convective Models

Study	Model Attributes[a]	Cloud Optical Depth Treatment	ΔT_s $2\times CO_2-1\times CO_2$ (°C)	Estimated Feedback $\tilde{f}_{OD}$[b]
Wang et al. (1981)	BAE;FRH;FLR(6.5);	FOD	2.06	
	FCC,FCA(17);FAL	VOD	2.08	0.0096
	BAE;FRH;FLR(MA)[c]	FOD	2.26	
	FCC;FCA(17);FAL	VOD	2.09	−0.08
Charlock (1981)	ERE;VRH[d];FLR(6.5);	FOD	2.253	
	FCC;FCA(3);FAL	VOD	1.579	−0.427
Somerville and Remer (1984)	BAE;FRH,MALR;	FOD	1.74	
	FCC;FCA(1);FAL	VOD	0.85 to 0.75	−1.05 to −1.32[e]

[a] Surface energy flux; water vapor; lapse rate; cloud cover, altitude (number of cloud layers); surface albedo. See Table A.3 for definition of abbreviations.
[b] $\tilde{f}_{OD} = 1 - [(\Delta T_s)_{FOD}]/[(\Delta T_s)_{VOD}]$.
[c] Lapse rate fixed equal to the moist adiabatic value for the initial conditions.
[d] From Charlock (1982), $RH(p) = RH(p_s)[(p/p_s - -0.02)/(1 - -0.02)]^{\Omega}$ with $RH(p_s) = 0.77$ and $\Omega = 1 - -0.03(T_s - -288)$.
[e] See Figure A.14.

Wang et al. (1981) used the model described in the preceding subsection with cloud cover A_c prescribed, instead of computed by Equation (A.117) and τ_c given by

$$\tau_c = f_3 \ell \,, \tag{A.128}$$

with $f_3 = 3.09 \times 10^4 (z < 3 \text{ km}), 1.15 \times 10^4 (3 \leq z < 8 \text{ km})$, and $2.75 \times 10^3 (z \geq 8 \text{ km})$. Substituting Equation (A.128) into Equation (A.115) then gives

$$\tau_c = \frac{f_3 H_c}{f_1 (1 + B) L} \tag{A.129}$$

from which we can obtain

$$\frac{d\tau_c}{dT_s} = \frac{f_3}{f_1 L (1 + B)} \left(\frac{dH_c}{dT_s} - \frac{H_c}{1 + B} \frac{dB}{dT_s} \right) . \tag{A.130}$$

This has the same form as dA_c/dT_s given by Equation (A.119), hence $d\tau_c/dT_s$, like dA_c/dT_s, can be either positive or negative. The vertical profile of the change in τ_c for both a CO_2 doubling and a 2% increase in solar constant is shown in Figure A.13, together with the vertical profile of the prescribed cloud cover. This figure shows that τ_c increased at both low and high altitudes and decreased at middle altitudes for both the CO_2 and solar constant increases. If we assume that $\phi < 0$ for the low, middle, and high clouds, then $\phi d\tau_c/dT_s$ is negative at low and high altitudes and positive at middle altitudes. It is not possible to quantitatively evaluate the vertical integral of $\phi d\tau_c/dT_s$, but the zero value of $\tilde{f}_{OD}$ in Table A.15 does not appear to be inconsistent with the profile shown in Figure A.11 for the CO_2 doubling. Furthermore, the larger increase of τ_c at low altitudes in the 2% solar constant increase experiment indicates that $\tilde{f}_{OD}$ for this experiment should be smaller than that for the CO_2 doubling experiment; that is, it should be negative. Indeed, such a negative value was obtained by Wang et al. (1981) because ΔT_s for the 2% solar constant increase experiment decreased from 2.26°C to 1.95°C when τ_c was changed from a prescribed to a predicted quantity. These results from Wang et al. (1981) show that, as for the cloud cover feedback, the cloud optical depth feedback depends on the vertical integral of $\phi d\tau_c/dT_s$ throughout the atmosphere.

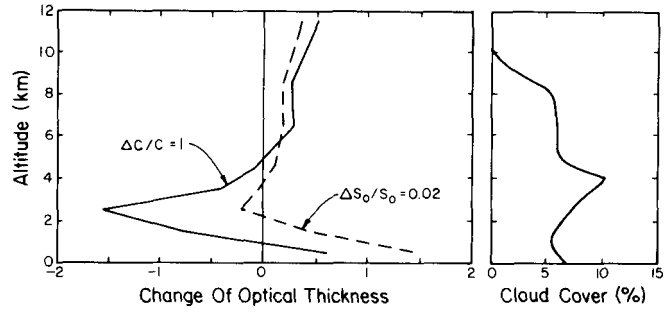

Figure A.13. Change in the optical thickness (left) for prescribed cloud cover (right) is shown as a function of altitude for a 2% increase in the solar constant ($\Delta S_0/S_0 = 0.02$) and a doubling of the CO_2 concentration ($\Delta C/C = 1$). Source: Wang et al. (1981).

Charlock (1981) used a simpler model than Wang et al. (1981) to compute the change in the cloud water path (WP) induced by doubling CO_2,

$$\frac{\Delta WP}{WP} = \frac{\Delta q}{q} , \qquad \text{(A.131)}$$

where q is the water vapor mixing ratio. Charlock prescribed the relative humidity profile as

$$RH(p) = RH(p_s)\left(\frac{p/p_s - 0.02}{1 - 0.02}\right)^{\Omega} \qquad \text{(A.132)}$$

with

$$\Omega = 1 - 0.03(T_s - 288) . \qquad \text{(A.133)}$$

Thus, $RH(p)$ increases slightly with T_s, q and WP increase rapidly with increasing T_s, and $dWP/dT_s > 0$ everywhere. Furthermore, because Charlock assumed $\partial\epsilon_c/\partial WP = 0, \tilde{\phi} < 0$ (see Equation [A.126]). Consequently, $\tilde{\phi}\, dWP/dT_s < 0$ for each of the three cloud layers in Charlock's study, with the result that $\tilde{f}_{OD} < 0$ as shown in Table A.15.

Somerville and Remer (1984) also used a simple model for the change in the cloud optical thickness,

$$\Delta\tau_c = \mu\Delta T , \qquad \text{(A.134)}$$

where

$$\mu = \frac{1}{\rho_c}\frac{\partial\rho_c}{\partial T} , \qquad \text{A.135)}$$

and ρ_c is the cloud water density. Somerville and Remer assumed μ to be a positive constant, hence $\partial\tau_c/\partial T > 0$. Furthermore, they assumed their single cloud to be black, $\epsilon_c = 1$, hence $\partial\epsilon_c/\partial\tau_c = 0$ and $\phi < 0$ by Equation (A.122). Consequently, $\tilde{f}_{OD} = \phi\, d\tau_c/dT = \phi\mu < 0$ as shown in Figure A.14. From this figure it appears that $\phi = -26.3°C$. If μ is as large as 0.1, then $\Delta T_s = 0.48°C$. This is the minimum surface air temperature warming shown in Table A.4 for all the RCMs. This minimum warming is the result of both the large negative cloud optical depth feedback and the negative lapse rate feedback, which results from the MALR used in this model (see Table A.15). However, based on Soviet observations of $\rho_c(T)$ as summarized by Feigelson (1978), Somerville and Remer conclude that $\mu \simeq 0.04$ to 0.05. Thus, as shown in Figure A.14 and Table A.15, this range gives $\Delta T_s = 0.75$ to 0.85°C.

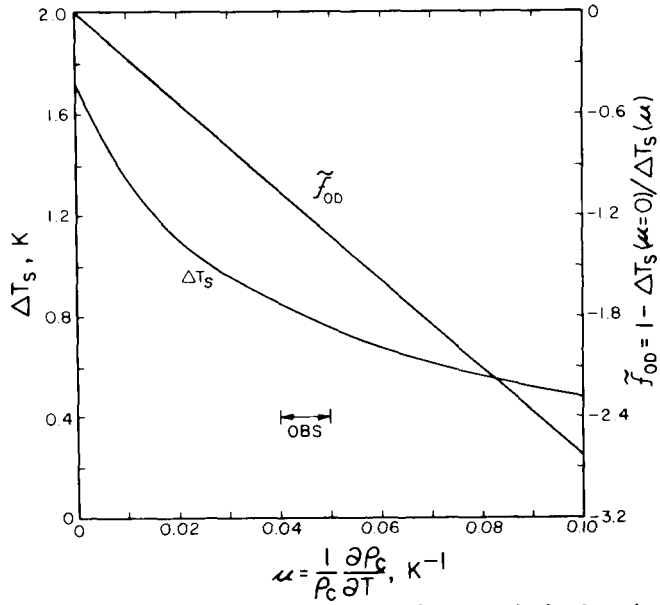

Figure A.14. Surface temperature change and cloud optical depth feedback for CO_2 doubling versus the prescribed cloud parameter μ. Source: Somerville and Remer (1984).

Surface albedo feedback. During a CO_2-induced climate change, surface albedo feedback can occur as a result of alterations in the amount of sea ice, land ice, and snow as first proposed by Budyko (1969) and Sellers (1969) or in the amount and type of vegetation. As in the preceding two subsections, we can analyze this surface albedo feedback from the viewpoint of the planetary energy budget and obtain

$$(\Delta T_s)_{\Delta C} = \frac{G_0}{(1 - \sum_j f_j - f_{SA})}\frac{\partial N_0}{\partial C}\Delta C , \qquad \text{(A.136)}$$

where the surface albedo feedback f_{SA}) is given by

$$f_{SA} = \psi\frac{d\alpha_s}{dT_s}G_0 , \qquad \text{(A.137)}$$

and

$$\psi = \frac{\partial N_0}{\partial\alpha_s} = -\frac{S_0}{4}\frac{\partial\alpha_p}{\partial\alpha_s} - \frac{\partial R_0}{\partial\alpha_s}$$

or

$$\psi = -\frac{S_0}{4}\frac{\partial\alpha_p}{\partial\alpha_s} , \qquad \text{(A.138)}$$

the latter because $\partial R_0/\partial\alpha_s = 0$.

Wang and Stone (1980) investigated the effect of ice-albedo feedback on CO_2-induced warming. Following North (1975), Wang and Stone assumed that

the annual mean, zonal mean surface air temperature can be represented by

$$T_s(x) - \overline{T}_s + T_2 P_2(x) = \overline{T}_s + \frac{T_2}{2}(3x^2 - 1) \quad \text{(A.139)}$$

where x is the sine of the latitude, $\overline{T}_s$ is the global mean surface air temperature, P_2 is the Legendre polynomial of degree two, and $T_2 = -32.1$. The latter is chosen so that the sine of the latitude of the ice edge is $x_s = 0.95$ at $T_s(x_s) = -13°C$ for the current climate for which $\overline{T}_s = 14.2°C$. Assuming that $T_s(x_s) = -13°C$ is invariant under a climate change, Equation (A.139) can be solved for x_s to obtain

$$x_s = (d + e\overline{T}_s)^{1/2}, \quad \text{(A.140)}$$

where $d = 0.6035$ and $e = 0.02078$. Then assuming that

$$\alpha_s = \begin{cases} a, & 0 \le x < x_s \\ b, & x_s \le x \le 1 \end{cases} \quad \text{(A.141)}$$

where $a = 0.087$ is the ice-free zonal mean surface albedo and $b = 0.55$ is the ice-covered zonal mean surface albedo, and that the surface insolation has the same latitudinal distribution as the insolation at the top of the atmosphere given by

$$S(x) = [1 + \frac{S_2}{2}(3x^2 - 1)]\overline{S}, \quad \text{(A.142)}$$

where $\overline{S}$ is the global mean and $S_2 = -0.482$, the global mean albedo is given by

$$\overline{\alpha}_s = b(1 - x_s) + ax_s + \frac{S_2}{2}(b - a)(x_s - x_s^3). \quad \text{(A.143)}$$

From Equations (A.140) and (A.143) it can be shown that

$$\frac{d\overline{\alpha}_s}{d\overline{T}_s} = -\frac{(b-a)e}{2} \frac{1 + S_2[1 - 3(d + e\overline{T}_s)]/2}{(d + e\overline{T}_s)^{1/2}}. \quad \text{(A.144)}$$

Combining this with Equation (A.137) gives

$$\frac{f_{SA}}{\partial\alpha_p/\partial\alpha_s} = \left[\frac{S_0}{4} \frac{(b-a)e}{2}\right] \times \left[\frac{1 + S_2[1 - 3(d + e\overline{T}_s)]/2}{(d + e\overline{T}_s)^{1/2}}\right] G_0. \quad \text{(A.145)}$$

This is shown plotted in Figure A.15 versus $\overline{T}_s$ and the ice edge latitude x_s for an assumed value of $G_0 = 0.3°C\ (W\ m^{-2})^{-1}$. Because $\partial\alpha_p/\partial\alpha_s > 0, f_{SA} > 0$. If $\partial\alpha_p/\partial\alpha_s$ is independent of $\overline{T}_s$, then f_{SA} decreases with increasing temperature as the ice edge of the control climate retreats toward the pole. This effect has been demonstrated in the GCM study of Spelman and Manabe (1984). However, in the formulation of Wang and Stone, f_{SA} does not approach zero as the ice edge retreats to the pole and the ice disappears.

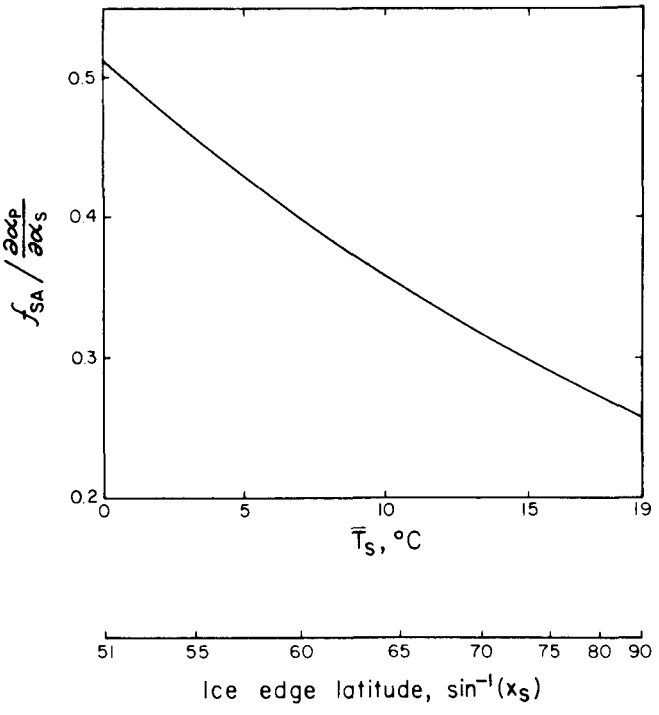

Figure A.15. Surface albedo feedback divided by $\partial\alpha_p/\partial\alpha_s$ for CO_2 doubling versus the surface air temperature and ice edge latitude of the control from the study by Wang and Stone (1980).

The results of Wang and Stone (1980) are summarized in Table A.16. Although we cannot estimate f_{SA} for this study because $(\Delta T_s)_0$ is not known, the feedback $\tilde{f}_{SA} = 1 - (\Delta T_s)_{FAL}/(\Delta T_s)_{VAL}$ is positive. In fact, the case with fixed cloud top temperature (FCT), along with fixed relative humidity (FRH), produces the maximum warming of all the RCMs shown in Table A.4. Because this 4.2°C warming is also the maximum global mean surface air temperature increase simulated by GCMs for a CO_2 doubling (see Table A.18), it appears that ice-albedo feedback is important in GCM simulations of CO_2-induced climate change.

Finally, Hansen et al. (1981) also studied the ice-albedo effect, apparently with the ice-albedo parameterization of Wang and Stone (1980). Because we have an estimate of $(\Delta T_s)_0$ and f_W for

Table A.16
Surface Albedo Feedback From Selected Radiative-Convective Models

Study	Model Attributes[a]	Surface Albedo Treatment	ΔT_s $2\times CO_2-1\times CO_2$ (°C)	Estimated Feedback $\tilde{f}_{SA}$[b]	Estimated Feedback f_{SA}
Wang and Stone (1980)	BAE;FRH;FLR(6.5); FCC,FCA(3),FOD	FAL	2.00		
		VAL	2.51	0.203	
	BAE;FRH;FLR(6.5); FCC,FCT(3),FOD	FAL	3.00		
		VAL	4.20	0.286	
Hansen et al. (1981)	BAE;FRH;FLR(6.5); FCC,FCA(3),FOD	FAL	1.94		
		VAL	2.5–2.8	0.224–0.307	0.141–0.193[c]

[a] Surface energy flux; water vapor; lapse rate; cloud cover, cloud layer, altitude (number of cloud layers), optical depth. See Table A.3 for definition of abbreviations.
[b] $\tilde{f}_{SA} = 1 - [(\Delta T_s)_{FAL}]/[(\Delta T_s)_{VAL}]$.
[c] $f_{SA} = 1 - [(\Delta T_s)_0]/[(\Delta T_s)_{VAL}] - f_W$ with $(\Delta T_s)_0 = 1.22$°C and $f_W = 0.371$ from Table A.6.

the RCM of Hansen et al. (see Table A.6), we can estimate f_{SA} for this model. As shown in Table A.16, $f_{SA} \sim 0.141$ to 0.193. This is close to the value of $f_{SA} = 0.135$ that one obtains from Figure A.15 at $\overline{T}_s = 15$°C using $\partial\alpha_p/\partial\alpha_s = 0.45$ obtained from the Oregon State University two-layer RCM. The value of $f_{SA} = 0.181$ obtained from that model (Table A.5) also agrees with the result of Hansen et al. (1981).

A.4 SUMMARY

The pioneering RCM study of Manabe and Wetherald (1967) showed that doubling the CO_2 concentration results in a warming of the surface and the troposphere and a cooling of the stratosphere above 20 km. This and other RCM studies give a surface temperature warming induced by doubled CO_2 that ranges from 0.48 to 4.2°C. These CO_2-induced surface temperature changes can be understood in terms of the direct radiative forcing, the response to this forcing in the absence of feedbacks, and the amplification and damping of the response that results from positive and negative feedbacks, respectively.

The direct radiative forcing occurs predominantly in the longwave radiation and is characterized by a decrease in the net upward flux at the surface and throughout the atmosphere. The decrease at the surface acts to warm the surface. In the troposphere the magnitude of the decrease in the net upward longwave flux increases with altitude, which acts to warm the troposphere. In the stratosphere the magnitude of the decrease in the net upward longwave flux decreases with altitude which acts to cool the stratosphere. This cooling tendency occurs primarily because of the greater upward and downward emission from the stratosphere itself. The warming tendency of the troposphere primarily is caused by the increased downward flux from the stratosphere, and the warming tendency of the surface primarily occurs because of the greater downward emission from the troposphere.

The surface temperature response of the climate system without feedbacks to the radiative forcing caused by increased CO_2, ΔR_T, can be characterized by a zero-feedback surface temperature change $(\Delta T_s)_0 = G_0 \Delta R_T$, where G_0 is the climate system gain without feedbacks. G_0 can be estimated from a PEBM as 0.3°C (W m^{-2})$^{-1}$. Thus, $(\Delta T_s)_0 = 1.2$°C for the nominal value of $\Delta R_T = 4$ W m^{-2}. This estimate of $(\Delta T_s)_0$ is in agreement with several RCM studies that were made without feedbacks.

The surface temperature response of the climate system with feedbacks can be characterized by

$$\Delta T_s = \frac{G_0}{1 - f} \Delta R_T ,$$

where f is the feedback, which varies from −1.5 to 0.7 in the RCM studies of CO_2-induced climate change. The physical mechanisms that contribute to this range include, as T_s increases: the increase in the amount of water vapor in the atmosphere as a consequence of the quasi-constancy of the relative humidity; the decrease in the lapse rate; the changes in cloud altitude, cloud cover, and cloud optical depth; and the decrease in surface albedo.

A study with the Oregon State University two-layer RCM was performed to determine the independence of the above feedbacks. This study shows that the individual feedbacks of water vapor, cloud

altitude, and surface albedo are positive, the individual cloud cover and cloud optical depth feedbacks are essentially zero, and the individual MALR feedback is negative. This study also shows that the feedbacks of water vapor and either lapse rate, cloud altitude, or surface albedo are additive; hence, these feedbacks are independent. This is not the case for the water vapor feedback with either the cloud cover or cloud optical depth feedbacks. Both variable cloud cover and variable optical depth act as negative feedback mechanisms when they act in conjunction with the positive water vapor feedback.

A positive water vapor feedback occurs when the relative humidity is held fixed because then the absolute humidity increases nonlinearly with increasing temperature due to the Clausius-Clapeyron relation, and the increased water vapor reduces the atmospheric transmissivity, which enhances the CO_2 greenhouse effect. A positive feedback f_W = 0.340 was obtained by the Oregon State University RCM, and values from 0.371 to 0.533 were obtained by the other RCMs, with their actual values depending on the temperatures of the control simulation and whether the atmosphere was clear or cloudy. A reasonable estimate allowing for these dependencies is $f_W = 0.3 - 0.4$. The value of f_W would be larger (smaller) than this if the relative humidity were not constant and instead increased (decreased) with increasing temperature.

Radiative-convective model studies have shown that the CO_2-induced warming decreases by 12% as the prescribed temperature lapse rate is decreased from 6.5 to 5.0°C km^{-1}. When the lapse rate is allowed to vary, a lapse rate feedback is obtained. A positive feedback is found for the BADJ, which should be applicable in middle and high latitudes where baroclinic adjustment is prevalent. From Table A.7 we can estimate $f_{BADJ} = 1 - 1/1.84 - f_W \sim 0.15$ if $f_W = 0.3$. A negative feedback is found for the MALR with values of −0.409 and −0.262 from the Oregon State University and other RCMs, respectively. Because the former value is probably an overestimate by the two-layer RCM, a reasonable estimate of this feedback is $f_{MALR} \simeq -0.25$ to −0.4. A negative feedback is also found when the lapse rate is determined by penetrative convection with a value of $f_{PC} = -0.654$ given by one RCM. One or both of these negative feedbacks are likely to be found in the tropics where cumulus convection is prevalent.

Cloud feedback can occur from changes in cloud altitude, cloud cover, and cloud optical depth. Three treatments of cloud altitude have been used in RCMs: FCA, FCP, and FCT. Fixed cloud altitude and FCP have frequently been taken to be synonymous even though this strictly is not the case. For FCA the cloud temperature increases by the same amount as the surface temperature, and there is no feedback. For FCP the cloud temperature increases less than the surface temperature; hence to achieve equilibrium the CO_2-induced surface temperature warming must be greater with FCP than with FCA. Therefore, FCP is a positive feedback process; however, there is insufficient information to evaluate this quantitatively. For FCT the cloud temperature does not change with a change in the surface temperature; hence, its CO_2-induced surface temperature warming must be even larger than that required for FCP to achieve equilibrium. The FCT feedback f_{CA} is 0.261 from the Oregon State University RCM and 0.168 to 0.203 from another RCM; the latter is in comparison with the FCP case. Thus, a reasonable range of f_{CA} is perhaps from 0.15 to 0.30.

The feedback caused by changes in cloud cover A_c depends in part on the quantity

$$\delta = -\frac{S_0}{4}\frac{\partial \alpha_p}{\partial A_c} - \frac{\partial R_0}{\partial A_c},$$

which itself depends on the competing effects of changes in the planetary albedo, α_p, and in the net upward longwave flux at the top of the atmosphere, R_0. An analysis of several RCM studies shows that $\delta \simeq -100$ W m^{-2} for low clouds, $\delta \simeq -50$ W m^{-2} for middle clouds, and $\delta \simeq$ 5–80 W m^{-2} for high clouds, the latter generally increasing with cloud emissivity. Thus, for the case $dA_c/dT_s > 0$, low and middle clouds make a positive contribution to the cloud cover feedback f_{CC}, and high clouds make a negative contribution, while the sign of these contributions reverses for $dA_c/dT_s < 0$. A single RCM study of cloud cover feedback gave a positive value f_{CC} for doubled CO_2, but a negative value for a 2% solar constant increase. These seemingly contradictory findings can be understood on the basis of the changes in the vertical cloud cover profile, which demonstrates that it is the vertical integral

of $\delta\Delta A_c$ that determines the sign and magnitude of the cloud cover feedback. Because of this, cloud altitude feedback is subsumed in cloud cover feedback.

The feedback due to changes in cloud optical depth, τ_c, depends in part on the quantity

$$\phi = -\frac{S_0}{4}\frac{\partial \alpha_p}{\partial \tau_c} - \frac{\partial R_0}{\partial \tau_c} ,$$

which also depends on the competing albedo and longwave effects. For radiatively black clouds, $\partial R_0/\partial \tau_c = 0$ and $\phi < 0$. For nonblack clouds, $\partial R_0/\partial \tau_c < 0$ and ϕ may be positive or negative. Thus, for the case of $d\tau_c/dT_s > 0$, low and middle clouds make a negative contribution to the cloud optical depth feedback f_{OD}, and high clouds can make either a positive or negative contribution, while the sign of these contributions reverses for $d\tau_c/dT_s < 0$. Two RCM studies, each with a single cloud layer, found that f_{OD} was negative with values of –0.427 and of –1.05 to –1.32. Another study found that f_{OD} was essentially zero for doubled CO_2, but was negative for a 2% solar constant increase. This latter study, as for the cloud cover feedback, showed that the cloud optical depth feedback depends on the vertical integral of $\phi d\tau_c/dT_s$ throughout the atmosphere.

Finally, the feedback due to changes in the extent of ice depends in part on

$$-\frac{S_0}{4}\frac{\partial \alpha_p}{\partial \alpha_s}\frac{d\alpha_s}{dT_s} .$$

Because the amount of ice decreases as the surface temperature increases, $d\alpha_s/dT_s < 0$. Consequently, because $\partial \alpha_p/\partial \alpha_s > 0$, the ice-albedo feedback f_{SA} is positive. A single RCM study gives values of f_{SA} from 0.141 to 0.193.

Based on the RCM studies reviewed in this section we can summarize our knowledge of water vapor, lapse rate, cloud altitude, cloud cover, cloud optical depth, and surface albedo feedbacks as

$$\begin{aligned} f_W &= 0.3 \text{ to } 0.4 , \\ f_{BADJ} &\simeq 0.15, \\ f_{MALR} &= -0.25 \text{ to } -0.4 , \\ f_{PC} &\simeq -0.65, \\ f_{CA} &\simeq 0.15 \text{ to } 0.30 , \\ f_{CC} &= \text{unknown}, \\ f_{OD} &\simeq 0 \text{ to } -1.32 , \text{ and} \\ f_{SA} &= 0.14 \text{ to } 0.19 . \end{aligned}$$

However, we cannot be highly confident of these quantitative results because RCMs are not models of the global climate system and, more importantly, because RCMs need to prescribe the behavior of much of that system. In particular, water vapor feedback is predicted on the basis of constant relative humidity, lapse rate feedback generally is predicted on the basis of baroclinic or moist adiabatic adjustment, cloud feedbacks are predicted on the basis of greatly simplified cloud models, and surface albedo is predicted on the basis of assumed constant temperature of the equatorward position of the ice extent. However, the relative humidity may not be constant, the lapse rate may differ from those given by baroclinic and moist adiabatic adjustment, the altitude of clouds may not conform to FCA, FCP, or FCT; the cloud cover and cloud optical depth may vary vertically in a complex manner; and the change in surface albedo depends on snow and ice, which may not have a constant dependence on temperature for the equatorward position of their extent. These changes can be predicted credibly only by a physically based global model that includes the essential dynamical and thermodynamical processes in addition to radiative transfer. Nevertheless, RCMs are extremely valuable because their comparative simplicity permits a more complete understanding of their feedbacks than the more comprehensive, and therefore more complex, GCMs.

ACKNOWLEDGMENTS

I would like to thank Jai-Ho Oh and Dean Vickers for performing some of the calculations and graphics herein; Larry Holcomb and John Stark for drafting; and Monica Cox, Dee Dee Reynolds, Leah Riley, and especially Naomi Zielinski for typing the manuscript. I express my appreciation to Fred Luther and Michael MacCracken for their editing, and to Robert Dickinson, James Hansen, Syukuro Manabe, Gerald Meehl, Stephen Schneider, Richard Wetherald, Warren Washington and several anonymous referees for their constructive reviews of this appendix. This study was supported by the Department of Energy under contract number DE-AC03-76SF00098, and by the National Science Foundation and the Department of Energy under grants ATM 82-05992 and ATM–8511889.

REFERENCES

Augustsson, T., and Ramanathan, V. 1977. "A Radiative-Convective Model Study of the CO_2 Climate Problem." *Journal of the Atmospheric Sciences, 34:*448–451.

Bode, H. W. 1975. *Network Analysis and Feedback Amplifier Design.* Krieger, New York, New York.

Brunt, D. 1933. "The Adiabatic Lapse Rate for Dry and Saturated Air." *Quarterly Journal of the Royal Meteorological Society 59:*351–360.

Budyko, M. I. 1956. Heat Balance of the Earth's Surface." *Gidrometeoizdat,* Leningrad [in Russian]. Translation by N. A. Steanova, MGA 13E-286, U.S. Weather Bureau, Washington, D.C., 11B-25.

Budyko, M. I. 1969. "The Effect of Solar Radiation Variations on the Climate of the Earth." *Tellus 21:*611–619.

Callendar, G. S. 1938. "The Artificial Production of Carbon Dioxide and Its Influence on Temperature." *Quarterly Journal of the Royal Meteorological Society 64:*223–240.

Cess, R. D. 1974. "Radiative Transfer Due to Atmospheric Water Vapor: Global Considerations of the Earth's Energy Balance." *Journal of Quantitative Spectroscopy and Radiative Transfer 14:*861–871.

Cess, R. D. 1975. "Global Climate Change: An Investigation of Atmospheric Feedback Mechanisms." *Tellus 27:*193–198.

Charlock, T. P. 1981. "Cloud Optics as a Possible Stabilizing Factor in Climate Change." *Journal of the Atmospheric Sciences 38:*661–663.

Charlock, T. P. 1982. "Cloud Optical Feedback and Climate Stability in a Radiative-Convective Model." *Tellus 34:*245–254.

Chýlek, P., and Kiehl, J. T. 1981. "Sensitivity of Radiative-Convective Climate Models." *Journal of the Atmospheric Sciences 38:*1105–1110.

Feigelson, E. M. 1978. "Preliminary Radiation Model of a Cloudy Atmosphere. 1. Structure of Clouds and Solar Radiation." *Beitr. Phys. Atmos. 51:*203–229.

Goody, R. M. 1964. *Atmospheric Radiation, Vol. I.* Clarendon Press.

Hall, M. C. G., Cacuci, D. G., and Schlesinger, M. E. 1982. "Sensitivity Analysis of a Radiative-Convective Model by the Adjoint Method." *Journal of the Atmospheric Sciences 39:*2038–2050.

Hansen, J., Johnson, D., Lacis, A., Lebedeff, S., Lee, P., Rind, D., and Russell, G. 1981. "Climate Impact of Increasing Atmospheric Carbon Dioxide." *Science 213:*957–966.

Hansen, J., Lacis, A., Rind, D., Russell, G., Stone, P., Fung, I., Ruedy, R., and Lerner, J. 1984. "Climate Sensitivity: Analysis of Feedback Mechanisms." 130–163. In J. E. Hansen and T. Takahashi (eds.), *Climate Processes and Climate Sensitivity* (Maurice Ewing Series, 5) American Geophysical Union, Washington, D.C.

Hummel, J. R., 1982. "Surface Temperature Sensitivities in a Multiple Cloud Radiative-Convective Model With a Constant and Pressure Dependent Lapse Rate." *Tellus 34:*203–208.

Hummel, J. R., and Kuhn, W. R. 1981a. "Comparison of Radiative-Convective Models With Constant and Pressure-Dependent Lapse Rates." *Tellus 33:*254–261.

Hummel, J. R., and Kuhn, W. R. 1981b. "An Atmospheric Radiative-Convective Model With Interactive Water Vapor Transport and Cloud Development." *Tellus 33:*372–381.

Hummel, J. R., and Reck, R. A. 1981. "Carbon Dioxide and Climate: The Effects of Water Transport in Radiative-Convective Models." *Journal of Geophysical Research 86:*12035–12038.

Hunt, B. G. 1981. "An Examination of Some Feedback Mechanisms in the Carbon Dioxide Climate Problem." *Tellus 33:*78–88.

Hunt, B. G., and Wells, N. C. 1979. "An Assessment of the Possible Future Climatic Impact of Carbon Dioxide Increases Based on a Coupled One-Dimensional Atmospheric-Oceanic Model." *Journal of Geophysical Research 84:*787–791.

Idso, S. B. 1980. "The Climatological Significance of a Doubling of Earth's Atmospheric Carbon Dioxide Concentration." *Science 207:*1462–1463.

Jenne, R. L. 1975. "Data Sets for Meteorological Research" (NCAR-TN/IA-111). National Center for Atmospheric Research, Boulder, Colorado.

Kiehl, J. T., and Ramanathan, V. 1982. "Radiative Heating Due to Increased CO_2: The Role of H_2O Continuum Absorption in the 12-μm Region." *Journal of the Atmospheric Sciences 39:*2923–2926.

Lal, M., and Ramanathan, V. 1984. "The Effects of Moist Convection and Water Vapor Radiative Processes on Climate Sensitivity." *Journal of Atmospheric Science 41:*2238–2249.

Lindzen, R. S., Hou, A. Y., and Farrell, B. F. 1982. "The Role of Convective Model Choice in Calculating the Climate Impact of Doubling CO_2." *Journal of Atmospheric Science 39:*1189–1205.

Luther, F. M. 1984. *The Intercomparison of Radiation Codes in Climatic Models (ICRCCM): Longwave Clear-Sky Calculations.* World Climate Research Programme, WCP-93, International Council of Scientific Unions and World Meteorological Organization, Geneva, Switzerland.

Manabe, S. 1971. "Estimate of Future Changes in Climate Due to Increase of Carbon Dioxide Concentration in the Air." 249–264. In W. H. Mathews, W. W. Kellogg, and G. D. Robinson (eds.), *Man's Impact on the Climate,* MIT Press, Cambridge, Massachusetts.

Manabe, S., and Strickler, R. F. 1964. "Thermal Equilibrium of the Atmosphere With a Convective Adjustment." *Journal of the Atmospheric Sciences 21:*361–385.

Manabe, S., and Wetherald, R. T. 1967. "Thermal Equilibrium of the Atmosphere with a Given Distribution of Relative Humidity." *Journal of the Atmospheric Sciences 24:*241–259.

McClatchey, R. A., Fenn, R. W., Selby, J. E. A., Volz, F. E., and Garing, J. S. 1971. *Optical Properties of the Atmosphere* (AFCRL-71-0279). Air Force Cambridge Research Laboratories, Bedford, Massachusetts.

Möller, F. 1963. "On the Influence of Changes in CO_2 Concentration in Air on the Radiative Balance of the Earth's Surface and on the Climate." *Journal of Geophysical Research 68:*3877–3886.

Newell, R. E., and Dopplick, T. G. 1979. "Questions Concerning the Possible Influence of Anthropogenic CO_2 on Atmospheric Temperature." *Journal of Applied Meteorology 18:*822–825.

North, G. R. 1975. "Theory of Energy-Balance Climate Models." *Journal of the Atmospheric Sciences 32:*2033–2043.

Oort, A. H., and Rasmusson, E. M. 1971. *Atmospheric Circulation Statistics* (NOAA Professional Paper No. 5). U.S. Government Printing Office, Washington, D.C.

Plass, G. N. 1956. "The Influence of the 15 μm Carbon-Dioxide Band on the Atmospheric Infra-Red Cooling Rate." *Quarterly Journal of the Royal Meteorological Society 82:*310–324.

Privett, D. W. 1960. "The Exchange of Energy Between the Atmosphere and the Oceans of the Southern Hemisphere." *Geophysics Memo 13, No. 104,* Meteorological Office, London, United Kingdom.

Ramanathan, V., Lian, M. S. and Cess, R. D. 1979. "Increased Atmospheric CO_2: Zonal and Seasonal Estimates of the Effects on the Radiation Energy Balance and Surface Temperature." *Journal of Geophysical Research 84:*4949–4958.

Rasool, S. I., and Schneider, S. H. 1971. "Atmospheric Carbon Dioxide and Aerosols: Effects of Large Increases on Global Climate." *Science 173:*138–141.

Reck, R. A. 1979a. "Comparison of Fixed Cloud-Top Temperature and Fixed Cloud-Top Altitude Approximations in the Manabe-Wetherald Radiative-Convective Atmospheric Model." *Tellus 31:*400–405.

Reck, R. A. 1979b. "Carbon Dioxide and Climate: Comparison of One- and Three-Dimensional Models." *Environment International 2:*387–391.

Rowntree, P. R., and Walker, J. 1978. "The effects of doubling the CO_2 concentration on Radiative-Convective Equilibrium." 181–191. In J. Williams, (ed.), *Carbon Dioxide, Climate and Society,* Pergamon Press, Oxford, United Kingdom.

Saker, N. J. 1975. "An 11-Layer General Circulation Model." (Met 020 Tech. Note No. II/30). Meteorological Office, Bracknell, United Kingdom.

Schneider, S. H. 1972. Cloudiness as a Global Climatic Feedback Mechanism The Effects on the Radiation Balance and Surface Temperature of Variations in Cloudiness. *Journal of the Atmospheric Sciences 29:*1413–1422.

Schneider, S. H. 1975. "On the Carbon Dioxide-Climate Confusion." *Journal of the Atmospheric Science 32:*2060–2066.

Sellers, W. D. 1969. "A Global Climate Model Based on the Energy Balance of the Earth-Atmosphere System." *Journal of Applied Meteorology 8:*392–400.

Somerville, R. C. J., and Remer, L. A. 1984. "Cloud Optical Thickness Feedbacks in the CO_2 Climate Problem." *Journal of Geophysical Research, 89:*9668–9672.

Spelman, M. J., and Manabe, S. 1984. "Influence of Oceanic Heat Transport Upon the Sensitivity of a Model Climate." *Journal of Geophysical Research 89:*571–586.

Stephens, G. L. 1978. "Radiation Profiles in Extended Water clouds, 2, Parameterization Schemes." *Journal of the Atmospheric Sciences 35:*2123–2132.

Stephens, G. L., and Webster, P. J. 1981. "Clouds and Climate: Sensitivity of Simple Systems." *Journal of the Atmospheric Sciences 38:*235–247.

Stephens, G. L., Ackerman, S., and Smith, E. A. 1984. "A Shortwave Parameterization Revised to Improve Cloud Absorption." *Journal of the Atmospheric Sciences 41:*687–690.

Stone, P. H. 1978. "Baroclinic Adjustment." *Journal of the Atmospheric Sciences 35:*561–571.

Stone, P. H., and Carlson, J. H. 1979. "Atmospheric Lapse Rate Regimes and Their Parameterization." *Journal of the Atmospheric Sciences 36:*415–423.

Wang, W.-C., and Stone, P. H. 1980. "Effect of Ice-Albedo Feedback on Global Sensitivity in a One-Dimensional Radiative-Convective Climate Model." *Journal of the Atmospheric Sciences 37:*545–552.

Wang, W.-C., Rossow, W. B., Yao, M. S., and Wolfson, M. 1981. "Climate Sensitivity of a One-Dimensional Radiative-Convective Model with Cloud Feedback." *Journal of the Atmospheric Sciences 38:*1167–1178.

Washington, W. M., and Meehl, G. A. 1983. "General Circulation Model Experiments on the Climatic Effects Due to a Doubling and Quadrupling of Carbon Dioxide Concentration." *Journal of Geophysical Research 88:*6600–6610.

Washington, W. M., and Meehl, G. A. 1984. "Seasonal Cycle Experiment on the Climate Sensitivity Due to a Doubling of CO_2 With an Atmospheric General Circulation Model Coupled to a Simple Mixed-Layer Ocean Model." *Journal of Geophysical Research 89:*9475–9503.

Wetherald, R. T., and Manabe, S. 1986. "An Investigation of Cloud Cover Change in Response to Thermal Forcing." *Climatic Change 8,* in press.

Yang, S.-K., and Smith, G. L. 1985. "Further Study on Atmospheric Lapse Rate Regimes." *Journal of the Atmospheric Sciences 42:*961–965.

APPENDIX B
REVIEW OF THE RECENT CARBON DIOXIDE-CLIMATE CONTROVERSY

Frederick M. Luther
Lawrence Livermore National Laboratory

Robert D. Cess
State University of New York

CONTENTS

B.1 INTRODUCTION

Model calculations of the climatic impact of the increasing atmospheric carbon dioxide (CO_2) concentration consistently suggest that a doubling of the CO_2 concentration would lead to a warming of global average surface air temperatures by as much as several degrees Celsius (National Research Council [NRC] 1979, 1982, 1983; also see Chapter 4). Nevertheless, a controversy arose in 1979 when Newell and Dopplick (1979) concluded that climate models were overestimating the sensitivity of the climate to a doubled CO_2 concentration. This position has also been expressed by S. B. Idso in a series of articles (summarized below). These articles prompted a series of replies from several authors and counter-responses by Idso, primarily, and by Newell and Dopplick.

In this appendix, this controversy about the effect of CO_2 on climate is reviewed. Because the surface energy balance approach to estimating climate sensitivity has been the source of much of the controversy, a review of this approach is presented. It is shown that prior applications of this approach violate the law of conservation of energy (the first law of thermodynamics); therefore, these results are incorrect.

Empirical data indicating the relationship between atmospheric emittance and surface vapor pressure and surface air temperature are shown to be consistent with climate model calculations. Consequently, it is not the experimental data that are the basis of the controversy, but rather the analysis and interpretation of these data.

B.2 CHRONOLOGY OF THE CARBON DIOXIDE-CLIMATE CONTROVERSY

As has already been mentioned, a controversy arose in 1979 when Newell and Dopplick (1979) concluded, based on a surface energy balance analysis, that climate models were overestimating the sensitivity of the climate to a doubled CO_2 concentration. An exchange of comments (Watts 1980, 1982; Newell and Dopplick 1981) and articles by Kandel (1981) and Crane (1981) have made it clear that Newell and Dopplick neglected the consequences of small energy differences and did not carry their calculation through to achieve convergence to a new equilibrium. When this further calculation was done, the increase in tropical sea surface temperature was 1.08°C (Watts 1982) instead of 0.03°C, as originally calculated by Newell and Dopplick. It was also shown that the reduced sensitivity that Newell and Dopplick (1981) derived for tropical land and sea combined ($\Delta T < 0.25$°C) applied only to tropical oceans, not to the entire planet, as was implied in the abstract of their article. However, these follow-up analyses have shown that model results in tropical regions are quite sensitive to the various assumptions that have been used in model representations of the convection and boundary layer processes (Kandel 1981; Lindzen et al. 1982). Newell and Dopplick (1981) also pointed out that observations indicate that tropical temperatures have apparently been very stable, even during periods of extreme glaciation—a result in apparent conflict with some model results and an issue being investigated by a number of research groups.

The controversy was further fueled by Idso (1980a), who also claimed that the CO_2 climate response would be small, based on his analysis of data from three series of observations. Letters to *Science* by Schneider et al. (1980) and by Leovy (1980) attempted a technical rebuttal of Idso's article (1980a), and the response from Idso (1980b) attempted to further discredit the theoretical studies. Other responses to Idso's article appeared in papers by Kandel (1981), Crane (1981), Hansen et al. (1981), and Ramanathan (1981).

Letters by Idso appeared in *Environmental Science and Technology* (Idso 1980c), *Journal of the Air Pollution Control Association* (Idso 1980d), and *Weatherwise* (Idso 1981a). A response by MacCracken (1981) to the last of these letters suggested a number of alternative experiments that, when interpreted in terms of Idso's analysis technique, gave results quite different from Idso's. Further alternative experiments were proposed in other rebuttals to Idso's analysis, including that from the NRC (1982).

Ramanathan (1981) studied the final equilibrium that would arise from the oversimplified situation posed by Newell and Dopplick (1979). Ramanathan's results using a one-dimensional model indicated that Newell and Dopplick's results were understandable in terms of their assumptions, and that if these were made less restrictive, the sensitivity to CO_2 remained as suggested by the NRC

(1979). Ramanathan's one-dimensional model focused on global average conditions, however, and so did not consider surface temperatures in the range considered by Newell and Dopplick (1979), a factor critical to their argument concerning temperature changes in the tropics.

Idso's original article (1980a) was brief and did not include a detailed description of the data analysis approach used to determine the climate's sensitivity. His analysis approach was later described in journal articles and conference proceedings (Idso 1981b, 1981c, 1981d, 1981e, 1982a). In addition to his three analyses of empirical data, Idso (1981d, 1982a) presented a fourth argument that appeared to contradict model results. This fourth argument was a theoretical assessment that involved contrasting the present climate with the hypothetical case of the Earth without an atmosphere.

As part of its congressionally mandated review of the national CO_2 program, the Climate Research Committee of the National Research Council undertook a review of all of these arguments and counterarguments. Published in 1982 (NRC 1982), the report devoted considerable attention to the papers of Idso and Newell and Dopplick. Although the Climate Research Committee encouraged use of empirical approaches, they found that the techniques used by both Idso and Newell and Dopplick ignored many important interactions of the climate system. The NRC arguments were based on both technical reasons and refutation by counterexample. Idso's response appeared in *Carbon Dioxide, Friend or Foe?*, a book he published in 1982 (Idso 1982b).

Idso put forth the contention that the climate model projections were not consistent with the historical temperature record (Idso 1982b, 1983a, 1983b). Observational data indicate that the climate of the Northern Hemisphere has cooled since 1945, and he suggested that during this time CO_2 concentrations have been undergoing a "rapid increase." He postulated that the decrease in temperature was actually the result of the increasing CO_2 concentration, indicating that he now expects increased CO_2 concentrations will lead to a cooling rather than a warming. This idea was amplified further in additional articles (Idso 1983b, 1984a, 1984b), in which the claim was made that CO_2 operates as an "inverse greenhouse gas."

Cess and Potter (1984) carefully rebutted these arguments, showing that the climate changes from 1945 to the present must have been dominated by climate variability due to causes other than CO_2 and cannot be attributed to anthropogenic CO_2. Idso's basis for the argument that CO_2 could operate as an inverse greenhouse gas is that at low latitudes a doubling of the CO_2 concentration (with no change in air temperature) would cause a decrease in the net solar flux at the Earth's surface that is greater than the increase in the downward longwave flux. This analysis approach ignores the increased heating that would occur in the atmosphere as a result of the doubling of the CO_2 concentration. As pointed out by Cess and Potter (1984) and others, the surface temperature response depends on the net forcing of the surface-troposphere system, not just the forcing at the Earth's surface.

Cess and Potter (1984) presented a critical evaluation of the approaches used by Newell and Dopplick (1979), Idso (1980a), and others who have carried out surface energy balance analyses that have indicated that increased CO_2 levels will produce negligible warming of the Earth's surface. Cess and Potter found that these analyses were founded on various violations of the first law of thermodynamics; consequently, they did not conserve energy.

Webster (1984) evaluated the relative merits of the arguments put forth by Idso (1982b) and the NRC (1982). These two publications were selected because they reflect the diametrically opposed arguments on both sides of the CO_2-climate controversy. Webster concluded that both empirical and numerical modeling studies possess weaknesses and both show a certain utility.

Much of the CO_2-climate controversy centers around the surface energy balance approach used to estimate climate sensitivity. In the following sections the surface energy balance approaches used by Newell and Dopplick and by Idso are summarized, and it is shown that, with careful consideration of assumptions, their results can be reconciled with those from the detailed climate models being used to study the CO_2 issue.

B.3 THE SURFACE ENERGY BALANCE

The surface energy balance may be expressed on a global annual average as

$$Q = F + LH + SH \ , \qquad \text{(B.1)}$$

where F is the net upward longwave flux, LH is the upward latent heat flux, SH is the upward sensible heat flux, and Q is the net downward solar flux, all of which are evaluated at the Earth's surface. Now consider the case in which the surface energy balance is perturbed by an energy flux G. At equilibrium, the changes in the components of the surface energy balance sum to G:

$$G = \Delta F + \Delta LH + \Delta SH - \Delta Q \ . \qquad \text{(B.2)}$$

We next define a surface response function, λ, relating the change in surface temperature, ΔT_a, to the surface flux perturbation such that

$$\Delta T_a = \lambda G \ . \qquad \text{(B.3)}$$

From Equation (B.2) it readily follows that for relatively small changes in surface temperature,

$$\frac{1}{\lambda} = \frac{dF}{dT_a} + \frac{d(LH)}{dT_a} + \frac{d(SH)}{dT_a} - \frac{dQ}{dT_a} \ . \qquad \text{(B.4)}$$

The surface temperature is employed in this formulation to be consistent with the procedure of Newell and Dopplick (1979). The formulation could also be expressed in terms of changes in surface air temperature as Idso has done. This difference has no significant effect on the results of the calculation.

One method for evaluating the response function is to use Equation (B.3), which requires knowledge of both the initial forcing (i.e., assuming all other parameters are fixed so that there is not a climatic response) and the final change in temperature after a new equilibrium has been established. In concept, this could be done empirically. For example, the past climatic record might be examined for situations in which a factor such as solar radiation has changed and a new equilibrium climate has been established.

The response function may alternatively be evaluated by using Equation (B.4), in which each of the terms is determined from changes in the climate system after that particular forcing has been applied. Equations (B.2) and (B.4) are simply statements of conservation of energy (the first law of thermodynamics). If any terms in Equation (B.4) are neglected in evaluating λ, then the analysis would violate the fundamental conservation of energy requirement.

B.4 NEWELL AND DOPPLICK'S SURFACE ENERGY BALANCE ANALYSIS

For an increase in atmospheric CO_2, G denotes the increase in downward surface radiation without allowing the surface and atmosphere to respond to the perturbation. Newell and Dopplick (1979) calculated values of G in the range of 0.8 to 1.5 W m^{-2} for a doubling of the CO_2 concentration, with the smallest values occurring at low latitudes. In calculating G, they included both the decrease in net solar flux at the surface and the increase in downward longwave flux. Other model calculations in which global mean conditions are used generally fall within this range of values (Hansen et al. 1981; Ramanathan 1981).

Newell and Dopplick (1979) also incorporated potential changes in LH and SH in their assessment, but these quantities were evaluated by assuming that the atmospheric temperature and the water vapor concentration were constant. These assumptions have the effect of replacing the total derivatives of LH and SH in Equation (B.4) with partial derivatives (Ramanathan 1981; Cess and Potter 1984). In calculating their surface response function, λ_{ND}, Newell and Dopplick also assumed that Q did not change as the climate system responded to the initial perturbation, so that Equation (B.4) became

$$\frac{1}{\lambda_{ND}} = \frac{dF}{dT_a} + \frac{\partial(LH)}{\partial T_a} + \frac{\partial(SH)}{\partial T_a} \ . \qquad \text{(B.5)}$$

Cess and Potter have calculated values for the partial derivatives in Equation (B.5) and the total derivatives in Equation (B.4) as a means of evaluating the effect of Newell and Dopplick's assumptions on the estimate of ΔT_a for a doubling of CO_2 concentration. Using Equation (B.5) to evaluate λ_{ND}, Cess and Potter calculated a value for ΔT_a of 0.02°C, which agrees very well with the value of 0.03°C calculated by Newell and Dopplick (1979).

However, when the complete Equation (B.4) was used, Cess and Potter obtained a value of 1.87°C for ΔT_a.

The use of Equation (B.5) instead of Equation (B.4) results in a violation of the first law of thermodynamics because energy is not conserved. According to Equation (B.5), energy is added to the atmosphere, but atmospheric temperatures are not allowed to change. Additionally, as surface temperature increases, the rate of evaporation increases, but the amount of water vapor in the atmosphere is not allowed to increase. This example illustrates the importance of properly treating the atmospheric energy balance, even when the equations are formulated based on a surface energy balance and do not directly include all of the elements of the atmospheric energy balance.

B.5 IDSO'S SURFACE ENERGY BALANCE ANALYSIS

A surface energy balance approach was used in other studies to estimate the climate's sensitivity to changes in radiative forcing (Idso 1981d, 1982a). Surface air temperature rather than surface temperature was used in these analyses, but this in itself had no significant effect on the results other than to change the definition of T_a in the above equations to indicate surface air temperature. However, the choice of other variables did have a significant effect.

The studies included analyses of temperature changes arising from changes in atmospheric dust, atmospheric water vapor, and the seasonal solar cycle (Idso 1981d, 1981e, 1982a). In the first study, the occurrence and persistence of temperature inversions in summer and winter over the metropolitan Phoenix area were investigated. The difference in air temperature between the level of the city and the top of a nearby 450-meter-high mountain was measured. In the second study, daily maximum and minimum air temperatures and concurrent water vapor pressures were extracted from the records of the National Weather Service Forecast Office in Phoenix for all cloudless days during the period from June 10 to July 25 over the past 30 years. The last study considered the temperature change resulting from the seasonal variation of solar radiation received at the Earth's surface at various locations in the United States. Monthly mean data for surface air temperature and solar radiation incident at the Earth's surface from 105 stations were used in the analysis.

All of these empirical evaluations employed nonequilibrium observations. For example, the seasonal temperature response is delayed by the large heat capacity of the ocean. Because Equations (B.3) and (B.4) apply only to equilibrium conditions, it is not appropriate to use these equations with data from nonequilibrium situations to determine climate sensitivity. These equations were used nonetheless.

Among these three empirical studies, the case of the seasonal solar cycle is the only one for which it is possible to compare model simulations with empirical data. From the empirical data that were available for locations in the interior of the United States, Idso (1980a, 1981d) determined the average sensitivity of surface air temperature to changes in radiative flux at the surface, λ_I, to be

$$\lambda_I = \frac{\Delta T_a}{\Delta Q} = 0.175°\text{C (W m}^{-2})^{-1} . \qquad \text{(B.6)}$$

The value over the oceans was estimated to be reduced by a factor of 2 or more.

Hansen et al. (1981) used a three-dimensional general circulation model to calculate the range of surface air temperature resulting from the seasonal variation of insolation. Their model results ranged from 0.2°C (W m^{-2})$^{-1}$ in midcontinent to about 0.1°C (W m^{-2})$^{-1}$ on the coast, which is in good agreement with the empirical results. A similar calculation for the midcontinental United States using the Geophysical Fluid Dynamics Laboratory (GFDL) general circulation model (Manabe and Stouffer 1980; Cess and Potter 1984) is also in good agreement with the empirical results, giving a value of 0.15°C (W m^{-2})$^{-1}$. Consequently, the empirical results actually confirm the seasonal response of the models.

The disagreement between Idso and the modeling results that he criticizes arises when the results from this study of events occurring under nonequilibrium conditions are used to estimate the equilibrium change in global mean surface air temperature for a doubling of the CO_2 concentration. Idso (1981d) estimated that the increase in surface air temperature caused by a doubling of the CO_2 concentration would be no greater than 0.31°C

whereas the equilibrium model calculations give values from about 2°C (Manabe and Stouffer 1980) to about 4°C (Hansen et al. 1981).

B.6 THE HYPOTHETICAL CASE OF THE EARTH WITHOUT AN ATMOSPHERE

The hypothetical case of the Earth without an atmosphere is often used to estimate the magnitude of the greenhouse effect of the atmosphere. The calculated change in surface temperature in going from an airfree Earth to present conditions is used to estimate the climatic effect of the radiatively active gases present in the atmosphere.

By assuming that the same amount of solar energy is absorbed by the airfree Earth as by the present atmosphere (i.e., no change in planetary albedo, although without an atmosphre there would be no highly reflective clouds), a new equilibrium temperature can be calculated. This temperature is that which would have to exist everywhere on the Earth to make the thermal emission from the surface equal to the solar radiation absorbed globally. Making this calculation for an airfree Earth, the equilibrium surface temperature is calculated to be 254.4 K (Idso 1982a) compared with the current global mean surface air temperature of about 288 K. Consequently, the Earth would be 33.6°C colder than present if the atmosphere were removed.

The results of this calculation were used to estimate the value of the surface response function, λ_I. Idso (1982a) calculated an average value of 348 W m^{-2} for the downward longwave radiative flux received at the surface under present conditions, a value that is reasonable. It was assumed that the increase in downward longwave flux from 0 to 348 W m^{-2} constituted the forcing G, so the response function was determined to be $\lambda_I = 33.6/348 = 0.097$°C (W m^{-2})$^{-1}$. This value for λ_I, incidentally, is about half that obtained from the three empirical studies (Idso 1981d) discussed in Section B.5.

This theoretical value of λ_I is in error because of mistakes made in calculating the initial forcing G. As pointed out by Ramanathan,[1] instead of using the initial change in longwave radiative flux that would be present with an atmosphere above a surface at 254.4 K, Idso (1982a) used the value of the flux that results when the new equilibrium temperature of 288 K has been reached. Thus, the change of 348 W m^{-2} in downward longwave flux that Idso used included both the effect of the initial forcing when the atmosphere was first introduced and the effect of changes in atmospheric temperature and water vapor amount resulting from this forcing; that is, the 348 W m^{-2} is the sum of the forcing and the response.

The difficulty with calculating the radiative forcing when the atmosphere is introduced with $T_a = 254.4$ K is that many atmospheric conditions have to be assumed. The value calculated for the initial forcing depends critically on the temperature profile, water vapor profile, and cloud amount. These quantities are determined by the fluxes of sensible and latent heat from the Earth's surface and by dynamical and convective processes, none of which is known for such an initial state. Ramanathan[1] assumed that the amount of cloudiness and the relative humidity profile were the same as present-day values and calculated the temperature profile assuming radiative-convective equilibrium (i.e., no net flux divergence of the sum of radiative and convective heat fluxes in the atmosphere). With these assumptions, Ramanathan calculated a downward longwave flux at the surface of 165 W m^{-2} as the initial longwave forcing for a surface temperature of 254 K. The solar and longwave flux components are diagrammed in Figure B.1.

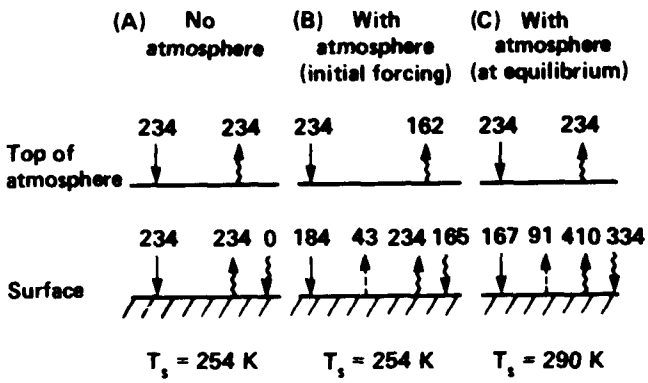

Figure B.1. Initial forcing and ultimate equilibrium warming of the surface from the radiative properties of the atmosphere as calculated by Ramanathan (private communication, 1982). Net solar flux (downward minus upward) components are indicated by straight lines, longwave flux components are indicated by wavy lines, and the convective flux of latent and sensible heat is indicated by a dashed line. All flux quantities are in W m^{-2}. In all three cases, the planetary albedo was held fixed at 0.30. Cases (B) and (C) include the radiative effects of H_2O, CO_2, CH_4, N_2O, and clouds.

[1] V. Ramanathan, personal communication, 1982.

The change in the net solar flux at the surface should be included in evaluating the radiative forcing term, G, but it was neglected in the analysis of Idso (1982a). With the assumption of a surface albedo of 0.30 without an atmosphere (in contrast to the present surface value of about 0.13), the net solar flux at the Earth's surface without an atmosphere was 234 W m^{-2} (see Figure B.1). When the atmosphere was initially introduced, the net solar flux at the surface was reduced to 184 W m^{-2}. Thus, the net solar flux was reduced by 50 W m^{-2}, which, when combined with the longwave forcing of 165 W m^{-2}, leaves an initial radiative forcing of 115 W m^{-2}.

The introduction of the atmosphere also causes changes in the surface fluxes of latent heat (LH) and sensible heat (SH). Ramanathan[2] estimated $SH + LH$ to be 43 W m^{-2} when the atmosphere is first introduced. When these contributions are considered, the value of G becomes only 72 W m^{-2} rather than the value of 348 W m^{-2} used by Idso (1982a). Using Ramanathan's results, the response function would then be $\lambda = 0.50°C\ (W\ m^{-2})^{-1}$, which is larger than Idso's value by about a factor of 5.

Although Ramanathan's approach to estimating the value of λ is an improvement over Idso's, it still has major shortcomings that make it an unreliable method for estimating climate sensitivity. Because it is a hypothetical experiment, many assumptions must be made. Thus, the value for λ that was determined for this case applies to just one set of assumptions, and a wide range of results could be obtained by varying these assumptions. Another problem is that nonlinear processes are not taken into account in the analysis. The two equilibrium states differ by a large amount, and ΔT_a is about an order of magnitude greater than that expected for a doubling of CO_2. Because this value of λ represents the average climate sensitivity over the range of ΔT_a, it may not be representative of the value at the warmer end. This is a particular concern because nonlinear processes cause the climate sensitivity to vary as surface temperature changes.

[2] Ibid.

B.7 LINEAR VERSUS NONLINEAR CLIMATE RESPONSE

The claim has been made (Idso 1982b) that a linear climate response is more accurate than the nonlinear responses obtained from climate models. The issue of linear versus nonlinear climate response is a major point of departure between Idso and the climate modelers. Both sides of this issue are summarized below, and an attempt is made to resolve this issue by comparing the two approaches with observational data.

Figure B.2 shows three different types of surface temperature variations, starting with the Earth without an atmosphere and progressing to present conditions. The abscissa is atmospheric emittance, ϵ, which is defined as the ratio of the downward longwave flux at the Earth's surface, $F_{\downarrow}(0)$, to the flux emitted by a black body at the surface air temperature:

$$\epsilon = \frac{F_{\downarrow}(0)}{\sigma T_a^4} . \qquad \text{(B.7)}$$

Without an atmosphere, the atmospheric emittance is zero. As the concentrations of radiatively active gases in the atmosphere are increased, the atmospheric emittance increases, reaching a value of about 0.89 for present global-mean conditions (Idso 1982a). Other authors give somewhat lower values for the atmospheric emittance; see Table B.1.

According to Idso (1982b), curve C in Figure B.2 is the type of curve suggested by the majority of the CO_2-climate models, curve B is the type of response implied by his theoretical analysis (assumed to be linear), and curve A depicts an extreme case of little change in surface temperature for limited deviations in atmospheric emittance from present conditions. These curves represent equilibrium states for a given atmospheric emittance, and they are referred to here as climate response curves.

The climate sensitivity at any given temperature is indicated by the slope of the response curve. The nonlinear nature of the climate response is indicated by comparing the slope of the curve at the present atmospheric emittance with the average slope between zero emittance and present conditions. Idso assumes a linear response (i.e., constant slope), so the slope of curve B in Figure B.2 is

$$\frac{dT_a}{d\epsilon} = \frac{\Delta T_a}{\Delta \epsilon} = \frac{33.6}{0.89} = 38°C . \qquad \text{(B.8)}$$

Table B.1
Comparison of the Sensitivity of Atmospheric Emittance, ϵ, Downward Longwave Flux at the Earth's Surface, $F_\downarrow(0)$, and Net Upward Longwave Flux at the Earth's Surface, $F(0)$, to Changes in Surface Air Temperature, T_a.

Source	T_a (K)	Surface Relative Humidity	ϵ	$\frac{dT_a}{d\epsilon}$ (°C)	$\frac{dF_\downarrow(0)}{dT_a}$ (W m^{-2} °C^{-1})	$\frac{dF(0)}{dT_a}$ (W m^{-2} °C^{-1})
Manabe and Wetherald (1967) Model (Constant Relative Humidity)	288.4	0.77	0.783	180	6.4	−1.0
Manabe and Wetherald (1975) Model (Hydrologic Cycle Included)	294.0	0.7–0.8	0.850	240	6.8	−1.0
Ramanathan (1981) Model (Constant Relative Humidity)	290.1	0.8	0.832	210	6.5	−1.9
Hansen et al. (1981) Model (Constant Relative Humidity)	287.5	0.75	0.852	180	5.7	−0.3
Empirical Results (Constant Relative Humidity)	288.0	0.77	0.894	220	6.6	−1.2
Empirical Results (Constant Absolute Humidity)	288.0	0.77	0.894	−620	4.2	1.2
Idso's Theoretical Analysis (curve B, Figure B.2)	288.0	—	0.892	38	15.2	−9.8

Note: The CO_2 concentration is constant in all cases.

To evaluate the slope of the response curve for typical climate models, it is necessary to determine how the downward longwave flux at the surface would change as atmospheric emittance is varied. The value of $dT_a/d\epsilon$ will differ, depending on how the climate is perturbed. For a particular perturbation, there would be a subsequent change in the atmospheric water vapor and temperature profiles as the climate responds to the initial perturbation. The resultant ΔT_a and $\Delta F_\downarrow(0)$ at equilibrium could then be used to determine $dT_a/d\epsilon$ for this perturbation, as shown below.

The expression for $dT_a/d\epsilon$ is derived from the definition of ϵ (see Equation B.7):

$$\frac{d\epsilon}{dT_a} = \frac{d}{dT_a}\left(\frac{F_\downarrow(0)}{\sigma T_a^4}\right) = \frac{1}{\sigma T_a^4}\frac{dF_\downarrow(0)}{dT_a} - \frac{4F_\downarrow(0)}{\sigma T_a^5}. \tag{B.9}$$

Substituting $F_\downarrow(0) = \epsilon\sigma T_a^4$ leads to

$$\frac{dT_a}{d\epsilon} = \frac{\sigma T_a^4}{\frac{dF_\downarrow(0)}{dT_a} - 4\epsilon\sigma T_a^3}. \tag{B.10}$$

Substituting $dF_\downarrow(0)/dT_a \approx \Delta F_\downarrow(0)/\Delta T_a$ and $\sigma T_a^4 = F_\downarrow(0)/\epsilon$ then leads to

$$\frac{dT_a}{d\epsilon} = \frac{\Delta T_a}{\epsilon\left(\frac{\Delta F_\downarrow(0)}{F_\downarrow(0)} - \frac{4\Delta T_a}{T_a}\right)}. \tag{B.11}$$

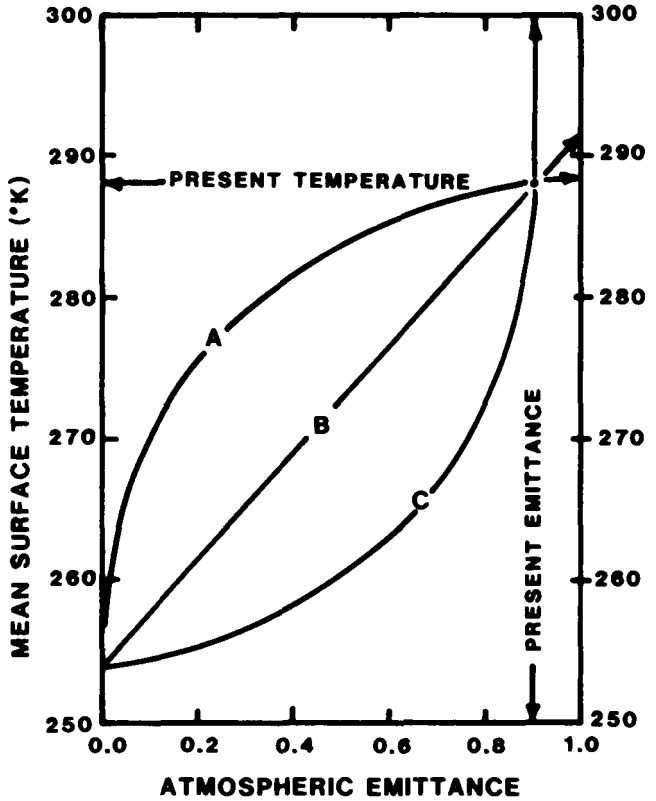

Figure B.2. Three different types of surface air temperature response to an increasing atmospheric emissivity. The atmospheric emissivity increases as the Earth conceptually travels from a condition of no atmosphere to one characteristic of today and beyond assuming no variation in solar radiation absorbed by the system. Source: Idso (1982b).

Values of $dT_a/d\epsilon$ can be determined using either Equation (B.10) or (B.11), depending on the data available. Values of $dT_a/d\epsilon$ as determined from several climate models are given in Table B.1. For the models listed in Table B.1, $dT_a/d\epsilon$ ranges from 180 to 240°C. These values are much greater than the value of 38°C obtained by assuming a linear response. Indeed, the model results are consistent with curve C in Figure B.2, which has a large slope at the present value of ϵ, as Idso has asserted.

The model results and Idso's analysis differ significantly in terms of the estimated values of $dT_a/d\epsilon$. Observational data on the variation of atmospheric emittance in response to changes in water vapor amounts and air temperature can be used to test these analyses to determine which estimate is more consistent with observations.

The variation in atmospheric emittance has been measured for cloudfree conditions, and the following equation for atmospheric emittance, ϵ_0, was shown to fit the empirical data (Idso 1981b):

$$\epsilon_0 = 0.70 + 5.95 \times 10^{-5} e_s exp(1500/T_a) \ , \quad \text{(B.12)}$$

where e_s is the surface water vapor pressure. The global mean atmospheric emittance, including the effect of clouds, can be calculated according to the following expression (Idso 1980a),

$$\epsilon = \epsilon_0 + \eta(1 - \epsilon_0)\left(\frac{T_c}{T_a}\right)^4 \ , \quad \text{(B.13)}$$

where ϵ_0 is given by Equation (B.12), η is the mean fractional cloud cover, T_c is the cloud base temperature, and T_a is the surface air temperature. For current climatic conditions, Idso (1980a) used $\eta = 0.54$, $T_c = 255$ K, and $T_a = 288$ K. Changes in T_c are related to changes in T_a in the following analysis by assuming that the tropospheric lapse rate and the cloud base altitude are constant (i.e., $T_a - T_c =$ constant).

Curves of ϵ versus T_a obtained from Equations (B.12) and (B.13) are plotted in Figure B.3 for the cases of constant relative humidity and constant absolute humidity. Note that these curves are based on observational data. Constant absolute humidity assumes that there is no change in water vapor concentration as temperature increases. Such a condition is possible but would not be expected because $d(LH)/dT_a$ is positive. As T_a increases, the latent heat flux increases, thereby adding more water vapor to the atmosphere. It is generally agreed that the curve for constant absolute humidity (i.e., constant water vapor concentration) would tend to underestimate the water vapor feedback effect on atmospheric emittance.

Constant relative humidity is generally assumed in modeling the climate response in one-dimensional radiative-convective models in which the hydrologic cycle is not explicitly represented. This assumption is based on observational evidence (Manabe and Wetherald 1967). Other analyses of the seasonal and latitudinal variations in water vapor concentration indicate a variation in moisture that is not as strong as holding relative humidity constant (Ellsaesser 1984). Accepting constant relative humidity and constant absolute humidity as upper and lower

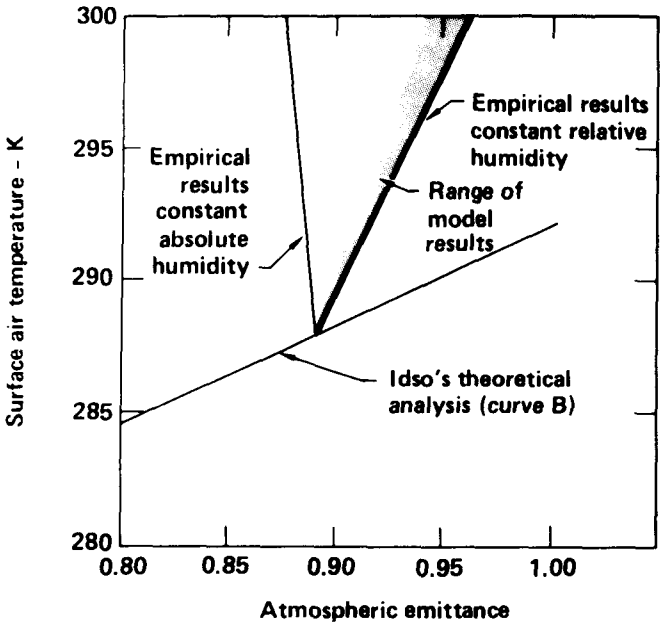

Figure B.3. The relationship between surface air temperature and atmospheric emittance as determined from empirical data, numerical models, and the analysis of Idso (1982b).

bounds would appear to be a conservative approximation of where the actual climate response might be.

Curve C in Figure B.2, which Idso attributes to the majority of the climate models, falls within the range of empirical results (see Figure B.3). On the other hand, curve B, which is Idso's theoretical analysis, falls well outside the range of empirical results. Consequently, the empirical results and the model results are in agreement, but Idso's theoretical analysis is not consistent with his own measurements.

An interesting feature of the empirical results is that the curve for constant absolute humidity has a negative slope, whereas the curve for constant relative humidity has a positive slope. Consequently, the range of responses between the two cases includes the case with $dT_a/d\epsilon$ equal to infinity. Since the empirical data include the situation where $dT_a/d\epsilon$ equals infinity, why did the empirical data not show large temperature variations in response to slight changes in atmospheric emittance? The answer to this question is provided in the next section, which explains the relationship between $dT_a/d\epsilon$ and climate sensitivity.

B.8 INTERPRETATION OF CLIMATE RESPONSE CURVES

As was shown in Section B.2, the climate sensitivity (i.e., response function λ) is defined by Equation B.4, which relates λ to a sum of derivative terms. To evaluate λ, it must be known how the net upward longwave flux F, upward latent heat flux LH, upward sensible heat flux SH, and net downward solar flux Q at the Earth's surface vary as the surface air temperature changes.

The relationship between dF/dT_a and $dT_a/d\epsilon$ is derived from the definition of atmospheric emittance given in Equation (B.7). Because $F = F_\uparrow(0) - F_\downarrow(0)$, it is necessary to determine $dF_\uparrow(0)/dT_a$ and $dF_\downarrow(0)/dT_a$. Differentiating Equation (B.7) with respect to T_a gives

$$\frac{dF_\downarrow(0)}{dT_a} = 4\epsilon\sigma T_a^3 + \frac{\sigma T_a^4}{dT_a/d\epsilon} . \qquad \text{(B.14)}$$

The upward longwave flux at the surface is defined by the Stefan-Boltzmann law,

$$F_\uparrow(0) = \sigma T_s^4 , \qquad \text{(B.15)}$$

where T_s is the ground temperature. It has been assumed for convenience in Equation (B.15) that the emissivity of the Earth's surface is unity, but any value could be used. The value of the surface emissivity is not critical to the discussion.

The expression for dF/dT_a is determined by differentiating Equation (B.15) and combining the result with Equation (B.14) to get

$$\frac{dF}{dT_a} = 4\sigma\left[T_s^3\frac{dT_s}{dT_a} - \epsilon T_a^3\right] - \frac{\sigma T_a^4}{dT_a/d\epsilon} . \qquad \text{(B.16)}$$

Note that $dT_a/d\epsilon$ appears in the denominator of the last term. Consequently, if $dT_a/d\epsilon$ were to approach infinity, then the last term would approach zero and the value of dF/dT_a would remain finite.

In general, the surface temperature, T_s, and the surface air temperature, T_a, are different. The expression for dF/dT_a could be simplified by assuming that $T_a = T_s$, as is frequently done in one-dimensional radiative-convective models. Such an assumption does not have a very significant effect on model sensitivity (Ramanathan 1981).

Table B.2.
Values of Terms in the Energy Balance Equation for a Doubling of CO_2

Reference	G (W m^{-2})	$\frac{dF}{dT_a}$ (W m^{-2}°C^{-1})	$\frac{dLH}{dT_a}$ (W m^{-2}°C^{-1})	$\frac{dSH}{dT_a}$ (W m^{-2}°C^{-1})	$-\frac{dQ}{dT_a}$ (W m^{-2}°C^{-1})	λ (°C(W m^{-2})$^{-1}$)	ΔT_a (°C)
Manabe and Wetherald (1975)	0.8	−0.3	0.1[a]		0.5	0.3	2.7
Hansen et al. (1981)	0.9	−1.0	1.9	−0.7	0.1	0.3	2.9
Ramanathan (1981)	0.9	−1.9	3.5	−1.6	0.4	0.4	2.2

[a] The low value for the change in convective flux results from not including a surface boundary layer as is done in the other models listed. Without a boundary layer, the surface air temperature and ground temperature are the same value.

Substituting dF/dT_a from Equation (B.16) into Equation (B.4) gives

$$\lambda = \left[4\sigma\left(T_s^3\frac{dT_s}{dT_a} - \epsilon T_a^3\right) - \frac{\sigma T_a^4}{dT_a/d\epsilon} + \right] \frac{d(LH)}{dT_a} + \frac{d(SH)}{dT_a} - \frac{dQ}{dT_a}\Bigg]^{-1}. \quad \text{(B.17)}$$

To assess the effect of the value of $dT_a/d\epsilon$ on λ, it is necessary to know the value of each of the terms in Equation (B.17). Values for each of the derivative terms are shown in Table B.2. Although there is considerable uncertainty about the value of each term, observational and modeling studies are consistent in their description of the relative magnitude of the terms.

The sum of the terms must be a positive number because λ must be positive (if λ were negative, then adding heat to the surface would cool rather than warm the surface). The upward latent heat flux at the surface increases when the surface air temperature increases, so $d(LH)/dT_a > 0$, even though this increased heat loss will tend to push the temperature lower. As T_a increases, the upward flux of sensible heat decreases, so $d(SH)/dT_a < 0$. Although $d(LH)/dT_a$ and $d(SH)/dT_a$ are of opposite sign, their sum is a positive number (see Table B.2). As the surface and atmosphere warm, the amount of water vapor in the atmosphere increases, which reduces the amount of solar radiation reaching the Earth's surface; thus $dQ/dT_a < 0$. Since dQ/dT_a is negative and is subtracted from the sum of the other terms, it actually adds to the positive value of the sum; thus $[d(LM)/dT_a + d(SH)/dT_a - dQ/dT_a]$ is a positive quantity.

The derivative dF/dT_a may be either positive or negative depending on how the atmospheric water vapor amount varies. If absolute humidity is held fixed, then dF/dT_a is positive (Kandel 1981). However, if the amount of atmospheric water vapor is allowed to change as the atmosphere warms, then dF/dT_a is negative (see Table B.2). Regardless of whether dF/dT_a is positive or negative,

$$\frac{dF}{dT_a} < \left[\frac{d(LH)}{dT_a} + \frac{d(SH)}{dT_a} - \frac{dQ}{dT_a}\right]$$

because λ must be positive. We now address the effect of varying $dT_a/d\epsilon$.

Because processes affecting atmospheric composition and energy fluxes are coupled, it is not generally appropriate to vary one derivative in Equation (B.17) independent of the others. Varying $dT_a/d\epsilon$ would be expected to affect other derivatives in addition to dF/dT_a, but there is no empirical capability for quantitatively assessing the corresponding changes in the other terms. Nevertheless, some qualitative indications of the variation may be deduced.

Increasing $dT_a/d\epsilon$ has the effect of reducing $dF_\downarrow(0)/dT_a$ (making dF/dT_a a smaller negative number), so the positive feedback mechanism leading to increased back radiation to the surface would be diminished. The change would imply a lessened increase in the atmospheric emittance. Because the increase in atmospheric emittance when T_a increases is caused in part by an increase in atmospheric water vapor content, the reduction in

$dF_{\downarrow}(0)/dT_a$ would imply a reduction in evaporation rates and, therefore, a reduction in $d(LH)/dT_a$. With a reduction in $d(LH)/dT_a$, an increase might be expected in $d(SH)/dT_a$. The last term in Equation (B.17), dQ/dT_a, is normally a small negative quantity reflecting a reduction in solar flux reaching the Earth's surface because of increased atmospheric water vapor. With a smaller increase in atmospheric water vapor, dQ/dT_a would be expected to be reduced in magnitude.

The effect of increasing $dT_a/d\epsilon$ can be illustrated using model results, but the particular values used are not critical to the illustration. For the climate to be extremely sensitive to perturbations, the value of λ must be very large. For this to happen, the sum

$$\left[\frac{dF}{dT_a} + \frac{d(LH)}{dT_a} + \frac{d(SH)}{dT_a} - \frac{dQ}{dT_a}\right]$$

must approach zero. The issue is whether or not this sum approaches zero as $dT_a/d\epsilon$ approaches infinity.

Using the results from Ramanathan's model (1981) as an example, for the unperturbed atmosphere (see Table B.2):

$$\frac{dF}{dT_a} = -1.9 \text{ W m}^{-2} \text{ °C}^{-1} \qquad \text{(B.18)}$$

and

$$\left[\frac{d(LH)}{dT_a} + \frac{d(SH)}{dT_a} - \frac{dQ}{dT_a}\right] = 2.3 \text{ W m}^{-2} \text{ °C}^{-1} . \qquad \text{(B.19)}$$

For the unperturbed atmosphere, $dT_a/d\epsilon = 220$ K according to this model. From Equation (B.16) it follows that as $dT_a/d\epsilon$ approaches infinity, then dF/dT_a approaches -0.1 W m^{-2} °C^{-1}. If there were no change in the remaining heat flux derivatives, then λ would increase from 0.4 to 2.2°C (W m^{-2})$^{-1}$, making the model less sensitive rather than more sensitive. Consequently, if a response curve has a large slope, even one approaching or equaling infinity, this is not an adequate basis alone for asserting that the climate should be extremely sensitive. To claim that the climate is more sensitive when $dT_a/d\epsilon$ is large, it must be shown that the sum

$$\left[\frac{dF}{dT_a} + \frac{d(LH)}{dT_a} + \frac{d(SH)}{dT_a} - \frac{dQ}{dT_a}\right]$$

approaches a small value. This is equivalent to having to show that as $dT_a/d\epsilon$ increases, it becomes harder to remove excess heat from the surface. We know of no physical basis for making such an argument. In fact, the empirical data are evidence that such an instability does not occur, since those data include the case where $dT_a/d\epsilon$ equals infinity.

B.9 CONCLUSIONS

It would clearly be desirable to design an empirical experiment that would provide a more accurate determination of the surface air temperature response function. The complicating factor, however, is that the value of the response function will differ depending on the type of perturbation. It would make a significant difference, for example, whether the perturbing radiative energy were to be deposited in the atmosphere or at the Earth's surface.

As an illustration, consider the difference between two perturbations: (1) an increase in solar radiation incident at the top of the atmosphere and (2) a doubling of the CO_2 concentration. In the first case, the change in solar heating would occur primarily at the Earth's surface, because the atmosphere is relatively transparent to solar radiation. On the other hand, most of the increased thermal flux convergence due to a doubling of CO_2 would occur in the troposphere (Kiehl and Ramanathan 1982). Energy deposited in the atmosphere also contributes to heating of the troposphere-surface system. For the CO_2 perturbation, the additional atmospheric heating would contribute to a larger increase in temperature beyond that due to just the initial increase in thermal flux at the Earth's surface. Consequently, basing the response function on the change in radiative flux at the Earth's surface leads to different values of the response function for different perturbations, depending on how much energy would be deposited in the atmosphere relative to how much would be deposited at the surface.

The problem of where the change in heating occurs is partly eliminated by considering changes in the energy balance of the troposphere-surface system rather than just that of the Earth's surface. As emphasized by Kiehl and Ramanathan (1982) and others (Ramanathan et al. 1979; Manabe and Wetherald 1980; Potter and Cess 1984), it is the surface-troposphere CO_2 heating rather than surface heating that dominates the surface temperature response. Long-term monitoring of radiative

fluxes at the tropopause, however, would be difficult. An alternative might be to measure changes in radiative fluxes out the top of the atmosphere by using satellite systems (Kiehl 1983).

In summary, although papers continue to be published indicating order-of-magnitude shortcomings of model results, when these arguments have been carefully considered, they have been found to be based on improper assumptions or incorrect interpretations. Although the models are by no means perfect, where it has generally been possible to compare large-scale results from model simulations with measurements, the agreement has been good. These comparisons have been on mainly seasonal time scales, however. Testing model responses to long-term forcing is a more difficult matter and may require simulation of past climate changes on time scales of hundreds or thousands of years.

ACKNOWLEDGMENTS

The authors gratefully acknowledge the helpful suggestions made by Michael MacCracken, V. Ramanathan, Hugh Ellsaesser, Fred O'Hara, and the various reviewers for AAAS.

REFERENCES

Cess, R. D., and Potter, G. L. 1984. "A Commentary on the Recent CO_2-Climate Controversy." *Climatic Change 6:*365–376.

Crane, A. J. 1981. "Comments on Recent Doubts About the CO_2 Greenhouse Effect." *Journal of Applied Meteorology 20:*1547–1549.

Ellsaesser, H. W. 1984. "The Climatic Effect of CO_2: A Different View." *Atmospheric Environment 18:*431–434.

Hansen, J., Johnson, D., Lacis, A., Lebedeff, S., Lee, P., Rind, D., and Russell, G. 1981. "Climate Impact of Increasing Atmospheric Carbon Dioxide." *Science 213:*957–966.

Idso, S. B. 1980a. "The Climatological Significance of a Doubling of Earth's Atmospheric Carbon Dioxide Concentration." *Science 207:*1462–1463.

Idso, S. B. 1980b. "Carbon Dioxide and Climate." *Science 210:*7–8.

Idso, S. B. 1980c. "CO_2 Modeling." *Environmental Science and Technology 14:*760.

Idso, S. B. 1980d. "The Global CO_2 Problem." *Journal of the Air Pollution Control Association 30:*848.

Idso, S. B. 1981a. "CO_2 and Climate." *Weatherwise 34:*142.

Idso, S. B. 1981b. "A Set of Equations for Full Spectrum and 8–14 ¯m and 10.5–12.5 ¯m Thermal Radiation from Cloudless Skies." *Water Resources Research 17:*295–304.

Idso, S. B. 1981c. "An Experimental Determination of the Radiative Properties and Climatic Consequences of Atmospheric Dust Under Nonduststorm Conditions." *Atmospheric Environment 15:*1251–1259.

Idso, S. B. 1981d. "An Empirical Evaluation of Earth's Surface Air Temperature Response to an Increase in Atmospheric Carbon Dioxide Concentration." 119–134. In R. A. Reck and J. R. Hummel (eds.), *Interpretation of Climate and Photochemical Models, Ozone and Temperature Measurements,* AIP Conference Proceedings No. 82.

Idso, S. B. 1981e. "Carbon Dioxide—An Alternative View." *New Scientist 90:*444–446.

Idso, S. B. 1982a. "A Surface Air Temperature Response Function for Earth's Atmosphere." *Boundary Layer Meteorology 22:*227–232.

Idso, S. B. 1982b. *Carbon Dioxide: Friend or Foe?* IBR Press, Tempe, Arizona.

Idso, S. B. 1983a. "Carbon Dioxide and Global Temperature: What the Data Show." *Journal of Environmental Quality 12:*159–163.

Idso, S. B. 1983b. "Do Increases in Atmospheric CO_2 Have a Cooling Effect on Surface Air Temperature?" *Climatological Bulletin 17:*22–26.

Idso, S. B. 1984a. "What if Increases in Atmospheric CO_2 Have an Inverse Greenhouse Effect? I. Energy Balance Considerations Related to Surface Albedo." *Journal of Climatology 4:*399–409.

Idso, S. B. 1984b. "The Case for Carbon Dioxide." *Journal of Environmental Science 27:*19–22.

Kandel, R. S. 1981. "Surface Temperature Sensitivity to Increased Atmospheric CO_2." *Nature 293:*634–636.

Kiehl, J. T. 1983. "Satellite Detection of Effects Due to Increased Atmospheric Carbon Dioxide." *Science 222:*504–506.

Kiehl, J. T., and Ramanathan, V. 1982. "Radiative Heating Due to Increased CO_2: The Role of H_2O Continuum Absorption in the 12–18 ¯m Region." *Journal of the Atmospheric Sciences 39:*2923-2326.

Leovy, C. B. 1980. "Carbon Dioxide and Climate." *Science 210:*7.

Lindzen, R. S., Hou, A. Y., and Farrell, B. F. 1982. "The Role of Convective Model Choice in Calculating the Climate Impact of Doubling CO_2." *Journal of the Atmospheric Sciences 39:*1189–1205.

MacCracken, M. C. 1981. "CO_2 Concentration." *Weatherwise 34:*236–237.

Manabe, S., and Stouffer, R. J. 1980. "Sensitivity of a Global Climate Model to an Increase of CO_2 Concentration in the Atmosphere." *Journal of Geophysical Research 85:*5529–5554.

Manabe, S., and Wetherald, R. T. 1967. "Thermal Equilibrium of the the Atmosphere with a Given Distribution of Relative Humidity." *Journal of the Atmospheric Sciences 24:*241–259.

Manabe, S., and Wetherald, R. T. 1975. "The Effects of Doubling the CO_2 Concentration on the Climate of a General Circulation Model." *Journal of the Atmospheric Sciences 32:*3–15.

APPENDIX C
ESTIMATING THE RELIABILITY OF CLIMATE MODEL PROJECTIONS— STEPS TOWARD A SOLUTION

Matthew C. G. Hall
Oak Ridge National Laboratory

CONTENTS

C.1 BACKGROUND

Recent reviews (e.g., National Research Council, 1979, 1982) of the potential effects of an increasing carbon dioxide (CO_2) concentration have developed their estimates of the climate's temperature sensitivity by considering the range of modeling results that are available. Of overriding importance in considering the validity of such assessments is the issue of whether any of the projections are real. Although comparison of results of models with today's climate is instructive, such an approach has many shortcomings as a technique for validating projections of future climates. For example, a model could be "tuned" to simulate today's climate well, but still fail to include the slowly evolving feedbacks that are important in predicting climate change. Comparison of the projections of various climate models is also instructive, but reconciliation of the different projections should be a prerequisite for trusting them. The important issue, however, is whether the projections of the models will agree with reality, not whether they can be made to agree with each other.

Climate changes have occurred in the past, so there is the possibility of determining how well climate models simulate reconstructions of past warmer climates. However, from available data we can only reconstruct limited aspects of these warmer climates, and to what extent these climates were warmer because of an increased CO_2 concentration is not known. On the other hand, the atmospheric CO_2 concentration has risen by about 14% over the last 100 years. Thus, we should be able to start looking for a CO_2 warming effect now, although it could be decades before the CO_2 warming is clearly distinguishable from variations in temperature that may be unrelated to the CO_2 increase (see MacCracken and Luther 1985). Moreover, even if a global CO_2 warming is clearly identified, it would only validate the gross projections of climate models for relatively small changes in CO_2 concentration. Validation of projections of regional and seasonal climate change for larger changes in CO_2 level is needed.

Theoretical uncertainty analyses can play an important part in aiding in the validation of climate models. The purpose of this appendix is to show what can be done to estimate the reliability of climate model projections using this approach. It should be recognized however, that this effort represents only one step, although an important one, to accomplishment of a proper assessment of climate models. The main conclusion drawn here is that meaningful steps toward a solution can be achieved by embarking on a systematic uncertainty analysis supported by a comprehensive sensitivity analysis. Section C.2 develops a terminology for discussing the various aspects of uncertainty analysis. Section C.3 reviews existing methods of model validation in the context of CO_2 climate modeling. Sections C.4 and C.5 review methods of sensitivity analysis, and Section C.6 illustrates methods of quantifying sources of uncertainty. Conclusions and recommendations appear in Section C.7.

C.2 TERMINOLOGY

A variety of terms will be used in this appendix. A *source of uncertainty* is an approximation, assumption, simplification, coding error, numerical technique, or other factor that can cause the results of a model to be unrealistic. The potential effect that a source of uncertainty has on the model's result is called the *uncertainty in the result.* The process of quantifying sources of uncertainty and evaluating the consequential uncertainties in the results is called *uncertainty analysis.* An essential component of uncertainty analysis is *sensitivity analysis,* that is, determination of the sensitivity of the results to each source of uncertainty.

The different approximations, assumptions, and simplifications made in developing different models can (and usually do) lead to *disagreements among the results.* The process of analyzing and reconciling the disagreements among the results of different models is called *model intercomparison.* Model intercomparison is an essential component for establishing the reliability of climate models, because until the disagreements can be reconciled, nobody will know which model, if any, can be believed. However, the disagreement among the results of different models is only one aspect of determining the uncertainty in the results. For example, when a collection of models all make the same assumptions or have been tuned to agree with each other, the disagreement can be small while the uncertainty is large. On the other hand, when one model is much more reliable than the rest, the disagreement can be

large while the uncertainty (at least for the reliable model) is small. To date, most estimates of uncertainty in the results of climate models have been based on the magnitude of disagreements among models: such estimates could be quite misleading.

Uncertainty analysis is a valuable component of an effective model intercomparison. It is precisely the magnitude of the combined uncertainty in two results that can reconcile their disagreement. A tempting, but dangerous, approach to model intercomparison is to make ad hoc adjustments to the models until they agree with each other. The removal of disagreement does not necessarily reduce uncertainty. The best way to reduce uncertainty is to reduce or eliminate sources of uncertainty.

An important issue in uncertainty analysis is which sources of uncertainty it is possible to quantify. Therefore, it is useful to distinguish among various sources of uncertainty. *Process uncertainties* refer to the uncertainties arising in the data needed for, and in the simplifications associated with, the representation of various processes (e.g., radiation transfer, cloud formation, sea ice formation, surface heat transfer). The accuracy of these representations can be evaluated by comparison with focused laboratory or field experiments. *Model uncertainties* are uncertainties that are characteristic of the model as a whole, for example, numerical method approximations, aggregation error, coding errors, or physical processes that have been neglected. Comparison with observations of the contemporary climate gives some idea of the overall influence of model uncertainties. For example, a model that uses an unstable numerical method or has a major coding error will not accurately simulate the observed climate, although on the other hand a model may simulate the observed climate well while neglecting important feedback processes. *Statistical uncertainties* arise because of the spontaneous fluctuations that occur both in climate models and in the observations. The climatic means obtained from climate models must be taken over sufficiently long time periods for the changes in these means to be statistically significant. *Forcing uncertainties* arise in making projections into the future because we do not know how CO_2 and trace gas concentrations, volcanic aerosol injections, and other factors will actually change.

C.3 MODEL VALIDATION

There are guidelines for model validation in several different areas of mathematical modeling. For example, Weisbin et al. (1981) developed and applied a set of guidelines for assessing a long-term energy analysis model used for the 1978 Energy Information Administration report to Congress. The purpose of this section is to provide background information about applying some of the customary components of model validation to CO_2-climate modeling.

C.3.1 The Hierarchy of Climate Models

The simplest example of a climate model is an energy balance equation that relates solar radiation absorbed on the Earth to outgoing infrared radiation. However, such a model does not take into account the radiative processes in the atmosphere that make it warmer nearer the surface nor the regional differences in the absorbed solar radiation. One-dimensional radiative-convective models (RCMs) take into account the vertical distribution of heat and radiation in the atmosphere, whereas one- or two-dimensional energy balance models (EBMs) take into account global effects such as latitudinal differences in surface albedos (i.e., fraction of solar radiation reflected). Three-dimensional general circulation models (GCMs) take into account both vertical and global effects, including horizontal transport by winds. The GCMs generally are regarded as the most reliable because they treat the three spatial dimensions, the temporal evolution of the atmosphere, and usually attempt to represent the many processes with more rigor than in simpler models.

The principal groups in the United States that apply GCMs to make CO_2-climate projections are at the Geophysical Fluids Dynamics Laboratory, the Goddard Institute for Space Studies, the National Center for Atmospheric Research, and Oregon State University. Each group is separately developing and applying one or more climate models. Despite the fact that these GCMs are attempting to represent the same physical system, there are disagreements between the results of the models applied to CO_2 studies by the various research groups.

One reason for this is that these models necessarily involve assumptions and approximations, and the various modeling groups make them in different ways.

C.3.2 Identifying the Results that Users Require of Climate Models

Three-dimensional climate models simulate selected meteorological variables (e.g., winds, temperature, water vapor mixing ratio) throughout the atmosphere. However, only a limited subset of such a simulation is required to assess the impacts of the simulated climate change on society. Therefore, it is helpful to define the results that users require of climate models in order to focus on the uncertainties that should be investigated before an adequate basis can exist for planning decisions.

As far as the CO_2 problem is concerned, climate models estimate the relationship between the future atmospheric CO_2 concentration and the induced climate change that could affect society. Both the future atmospheric CO_2 concentration and the potential direct and indirect effects of climate change are discussed in detail in companion State-of-the-Art reports. These reports essentially define the problem that climate models need to solve. By way of illustration, a typical result required of climate models is the projected effect that a doubling of the atmospheric CO_2 concentration over the next 100 years will have on regional temperature and precipitation; to be of use, the projected changes need to have at least the correct sign and order of magnitude.

Figure C.1 shows the observed annual precipitation over North America. Superimposed on the figure is a $10° \times 10°$ grid, which is about double the grid size found in many GCMs. Bearing in mind that the detailed structure within each GCM grid square must be represented by a single number, we can understand both the difficulty of simulating regional climate and the importance of how the term *regional* is defined, even with $5° \times 5°$ spatial resolution. Ultimately, the results of global climate models will have to be subjected to detailed interpretation to provide useful regional information.

C.3.3 Model Documentation

All three-dimensional climate models are implemented as computer programs, and the results of interest for the CO_2 problem are based on analyses of the output of these programs. Model documentation explains and references the path of reasoning that leads from the laws of physics to an executable computer program (Table C.1). This path includes the following steps: the physical assumptions and approximations that must be made to formulate and solve the conservation equations of mass, energy, and momentum; the acquisition and processing of physical data; and the numerical approximations required to formulate the computer program. It is the sources of uncertainty and the variety of plausible alternatives along this path that can cause disagreements among climate models.

Ideally, uncertainty analysis requires that up-to-date model documentation should be available and understandable to those not involved in the development of the model. Such an ideal, however, presents practical problems because providing more widely accessible documentation requires extensive preparation. Also, climate models are continually changing, and frequent updates of documentation can be prohibitively time consuming to prepare. Nevertheless, the importance of model documentation to uncertainty analysis is paramount. The intelligent interpretation of good model documentation can provide a supportable and comprehensive list of the sources of uncertainty in climate models.

C.3.4 Analyzing the Validity of Assumptions and Approximations

A central issue in uncertainty analysis of climate models is the degree to which the uncertainty in the results is caused by assumptions and approximations. Many assumptions and approximations arise because computing power restricts the spatial resolution of climate models (typically to about 500 km for multi-year simulations), and processes on scales smaller than this must be represented parametrically. For example, even if the microscopic processes of cloud formation were well understood, climate models do not have a fine enough resolution to model these processes. Instead, climate modelers typically assume that cloud formation depends

Table C.1
Major Headings in the Documentation for the Oregon State University Atmospheric GCM

I. INTRODUCTION
II. MODEL DESCRIPTION—VERTICAL DIFFERENCING AND PHYSICS
  A. DYNAMICAL SYSTEM OF EQUATIONS
    1. Notation and Vertical Layering
    2. Differential Equations in σ-Coordinates
    3. Vertically-Differenced Equations
  B. CONDITIONS AT THE EARTH'S SURFACE
    1. Orography and Surface Type
    2. Sea-Surface Temperature and Sea Ice
    3. Surface Albedo
    4. Ground Hydrology
    5. Ground Temperature
    6. Snow Mass
  C. TREATMENT OF THE BOUNDARY LAYER
    1. Surface Fluxes
    2. Determination of Surface Air Temperature and Mixing Ratio
  D. FRICTION TERMS
  E. DIABATIC HEATING AND MOISTURE SOURCES
    1. Convective Adjustment
    2. Large-scale Condensation and Evaporation
    3. Cumulus Convection
    4. Cloud types
    5. Long-wave Radiation
    6. Short-wave Radiation
    7. Total Heating and Moisture Budget
III. MODEL DESCRIPTION - HORIZONTAL DIFFERENCING AND INTEGRATION
  A. TIME FINITE DIFFERENCES
    1. The General Scheme of Time Integration
    2. Matsuno Time Step — Predictor
    3. Matsuno Time Step — Corrector
    4. Leapfrog Time Step
    5. Final Estimate of the Dependent Variables
  B. HORIZONTAL FINITE DIFFERENCES
    1. Horizontal Finite-Difference Grid
    2. Finite-Difference Notation
    3. Preparation for Time Steps
  C. SOLUTION OF THE FINITE-DIFFERENCE EQUATIONS
    1. Mass Flux
    2. Continuity Equation
    3. Horizontal Flux of Momentum
    4. Vertical Flux of Momentum
    5. Coriolis Force
    6. Pressure-Gradient Force
    7. Horizontal Flux of Heat
    8. Vertical Flux of Heat and Energy Conversion Terms
    9. Horizontal Flux of Moisture
    10. Vertical Flux of Moisture
    11. Forcing Terms
    12. Surface Variables
  D. SMOOTHING
  E. GLOBAL MASS CONSERVATION
  F. CONSTANTS AND PARAMETERS
IV. LISTING OF MATHEMATICAL SYMBOLS
V. MODEL PROGRAM
  A. DIRECTORY OF SUBPROGRAMS
  B. PROGRAM LISTING
VI. FORTRAN DICTIONARY
VII. PHYSICS DICTIONARY
VIII. MODEL USE AND OPERATION
  A. INITIALIZATION
    1. Sea-Surface Temperatures and Sea Ice
    2. Initial Conditions
  B. RUNNING THE MODEL
    1. Operating Characteristics
    2. Model Output
  C. POST-PROCESSING
    1. Recovery of Source Terms
    2. Post-Processing Language
IX. SAMPLE MODEL PERFORMANCE
  A. GRID-POINT MAPS
  B. ZONAL-MEAN PLOTS
REFERENCES

Source: Ghan et al. (1982).

on the values of meteorological variables averaged over distances of $\sim$ 500 km in the horizontal and of about 100 mb[1] in the vertical.

The uncertainty arising from an assumption usually depends on two factors: how large a source of uncertainty the assumption causes and how sensitive the model results are to this source of uncertainty. Typically the size of process uncertainties can be estimated by comparison with observation. For example, average cloud cover simulated on 500 km $\times$ 500 km grid squares can be compared with that which is observed, although observations can also introduce an important source of uncertainty. The sensitivity of model results to various assumptions and approximations can be difficult to estimate, especially if the model requires a large amount of computing time and many different sensitivities need to be estimated.

C.3.5 Verification of Model Results

Although projections of climate change cannot easily be validated against observations, there are checks to verify that a climate model is behaving as intended. For example, global conservation of mass and energy can be checked routinely during model runs. A more stringent check for climate models

[1] Because millibars are used as a vertical coordinate in some climate models, this unit will be retained in these discussions (1000 mb = 100 kPa).

Figure C.1. Observed annual precipitation (in millimeters) over North America (Korzoun et al. 1977). The grid resolution of typical GCMs is about 5° by 5°, as compared to the 10° by 10° grid shown here.

is a comparison of the simulated contemporary climate with observations (Figure C.2). The purpose of such a comparison is to verify that the model simulates the main features of the global climate and to provide evidence that the physical assumptions and approximations underlying the model are reasonable.

Climate models do simulate many of the features of the global climate, although there are obvious regional discrepancies. But what does this tell us about the uncertainties in results estimated by using these climate models? There is always a danger that precisely those parts of the model that are most highly approximated have been adjusted to produce a good simulation of a subset of the variables representative of the contemporary climate, and that these variables are the only ones that the model simulates well. As for the discrepancies between the observed and simulated climates, they indicate that some of the sources of uncertainty must be large enough to be causing the discrepancies. But which sources of uncertainty are to blame? Even for an experienced modeler it can be difficult to tell.

There are systematic methods that can be helpful in comparing model results with observations and that assess objectively which uncertainties are most likely to be causing the discrepancies (e.g., Marable et al. 1980). These methods require that modelers quantify sources of uncertainty and evaluate sensitivities of results to these uncertainties. With such information, it may be possible to calculate the most likely set of adjustments that would tend to remove the discrepancies. Most importantly, however, these methods also provide an objective test of whether the adjustments to the model

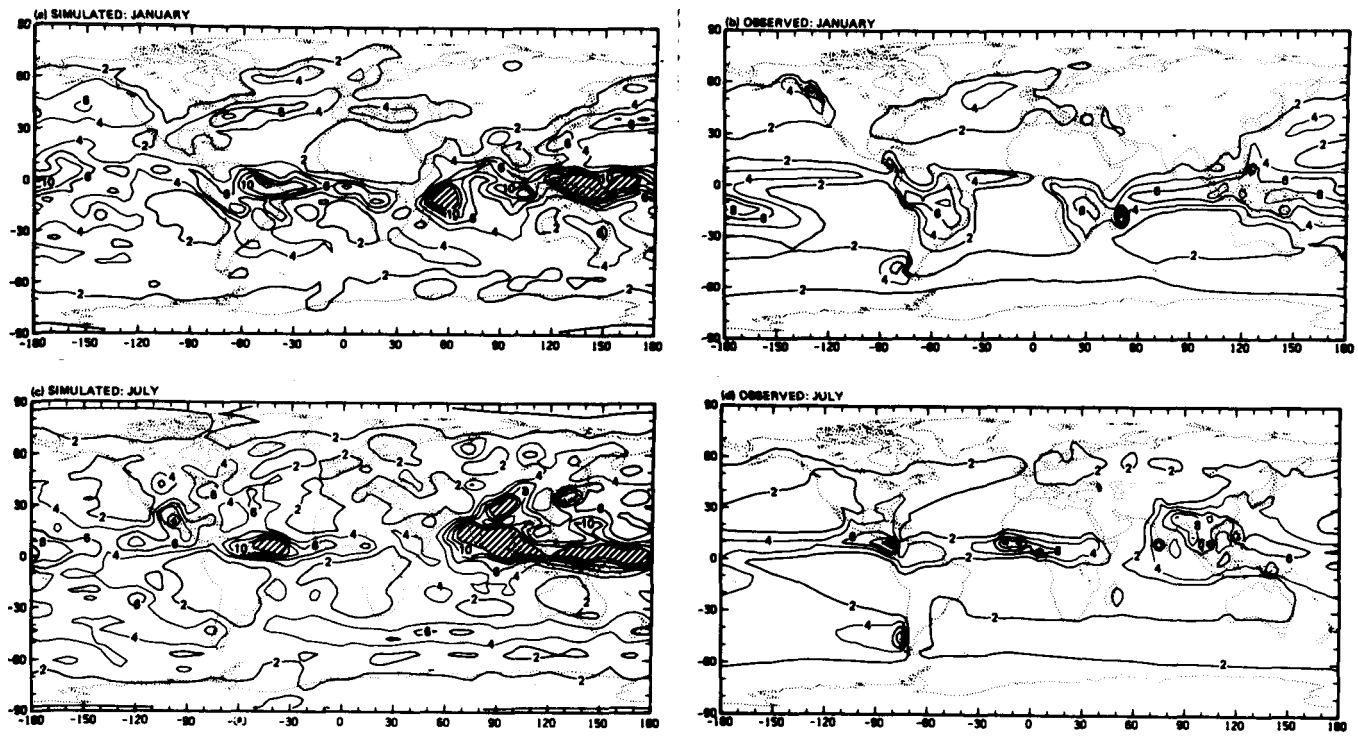

Figure C.2. Comparison of surface air temperature (K) simulated by the National Center for Atmospheric Research GCM for (A) January and (C) July compared to observations for (B) January and (D) July. Source: Pitcher et al. (1983).

represent heuristic tuning or whether the adjustments are physically important and are necessary for the model results to agree with observations.

C.3.6 Sensitivity Analysis

For a single climate simulation, three-dimensional climate models typically require many hours of computing time on the most powerful computers available. Therefore, although it has been attempted (e.g., Hansen et al. 1983, 1984), it is generally prohibitively expensive to determine sensitivity by simply rerunning the model for every variation of interest. Nevertheless, sensitivities are needed to determine the effect that sources of uncertainty have on model results. Consequently, although sensitivities to variations in solar radiation and CO_2 concentration are usually determined by rerunning the model, there is an important role to be played by more efficient methods capable of determining sensitivity to a wide variety of different effects.

C.3.7 Quantitative Expression of Uncertainties

Uncertainties in climate models arise for a variety of different reasons: physical assumptions are made, some processes are entirely neglected, and other processes involve parameters with uncertain values. Nevertheless, many sources of uncertainty can be expressed by introducing new parameters specifically designed to identify the importance of the uncertainty. The uncertainty can then be quantified by specifying numerical ranges or distributions for these new parameters.

An example of quantifying uncertainties in this way occurs when data in the model are subject to uncertainty. For instance, the value of the surface albedo in climate models is subject both to experimental and aggregation error. This uncertainty can be expressed by multiplying the albedo in the model by a coefficient that is allowed to vary from unity by a specified percentage. The effect of this variation can then be estimated using sensitivity analysis.

A more complicated example occurs when an attempt is made to express a process uncertainty, such as the use of a simple mixed-layer ocean model instead of a fully interactive three-dimensional ocean model. Some aspects of this uncertainty can be investigated by introducing sources of heat into the ocean model in a way that represents schematically the effect of ocean currents and by introducing sources of momentum into the atmosphere in a

Table C.2
Examples of Uncertainties (and Their Effects) in the Goddard Institute for Space Studies GCM

Changes of Model Physics from Model I to Model II		
Test Run	Physics Change	Major Effect
I-6	Coriolis/metric terms at pole	Strengthened polar cell
I-10	Drag in top model layer	Reduced stratospheric winds; realistic tropopause at high latitudes
I-13,14	Nine layers in vertical	Improved definition of jet stream and tropopause; more longwave generation
I-24	Alternative infrared radiation algorithm	Faster computation; higher accuracy
I-25	Realistic surface emissivities	No large effect
I-29	No subgrid-scale temperature variation for moist convection	Increased eddy kinetic energy: reduced upper level humidity and temperature; narrowed Hadley cell
I-34	Moist convection can start below condensation level	Stronger high-latitude winter temperature inversion at low levels
I-36	Large-scale rain every 5 h	Increased large-scale cloud cover
I-40	Local $T = -40°C$ for saturation over ice	Fewer cirrus clouds at low latitudes
I-42,43	Cloud optical thickness modified	Reduced net heat into ground
I-44	Snow density decreased	Warmer ground in winter
I-45	Ground thermal conductivity changed	Reduced vertical temperature gradient in ground
I-46, 47,49	Altered hydrology based on vegetation; intermediate runoff formulation	Early summer moisture increased and temperature decreased
I-50	Realistic vegetation masking depths	Reduced albedo in snow-covered areas
I-51	Ground albedo based on vegetation	Small albedo increase in subtropics
I-52	Modified ocean ice coverage	Local effects on T and evaporation
I-54	Modified ocean temperatures	No large effects
I-55	New lower limit for surface roughness	No large effect
I-59	Ekman surface wind formulation	Increased eddy kinetic energy and eddy transports
I-61	Modified cross-isobar angle	Sharpened intertropical convergence zone

Source: Adapted from Hansen et al. (1983).

way that represents the effect of additional viscous drag at the ocean surface. The magnitude of the uncertainty can then be roughly quantified by placing constraints on these source terms. Once again sensitivity analysis is used to estimate the effect of introducing these terms.

A particularly difficult type of uncertainty to quantify is one in which the model projections influence the expected magnitude of the uncertainty; for example, when the uncertainty is involved in a feedback mechanism. This is true for the ocean example given above because atmospheric changes can influence ocean currents. Cacuci and Hall (1984) and Hall (1986) have developed an efficient method for estimating the effect of these feedback uncertainties.

Some other sources of uncertainty in climate models are illustrated in Table C.2. Although the original purpose of this table was to summarize the results of a sensitivity analysis, the "Physics Change" column indicates some of the aspects of the model that are subject to uncertainty. Quantifying sources of uncertainty in climate models in this way is a difficult and expensive task, but it does seem to be possible. Also, the careful interpretation of sensitivity analyses can eliminate some sources of uncertainty from consideration.

C.3.8 Model Intercomparison

One use of model intercomparison studies is to test the results of a fast and economical model against the results of a slower-running model that is known to be reliable. For example, the relatively simple radiation calculations that must be used in GCMs can be compared with more sophisticated and accurate radiation models (see Chapter 2 of this volume). In CO_2-climate research, however, model intercomparison also refers to comparison of the overall results of different GCMs.

Of the GCMs used in CO_2-climate studies, there is no hard evidence to suggest that any one of them

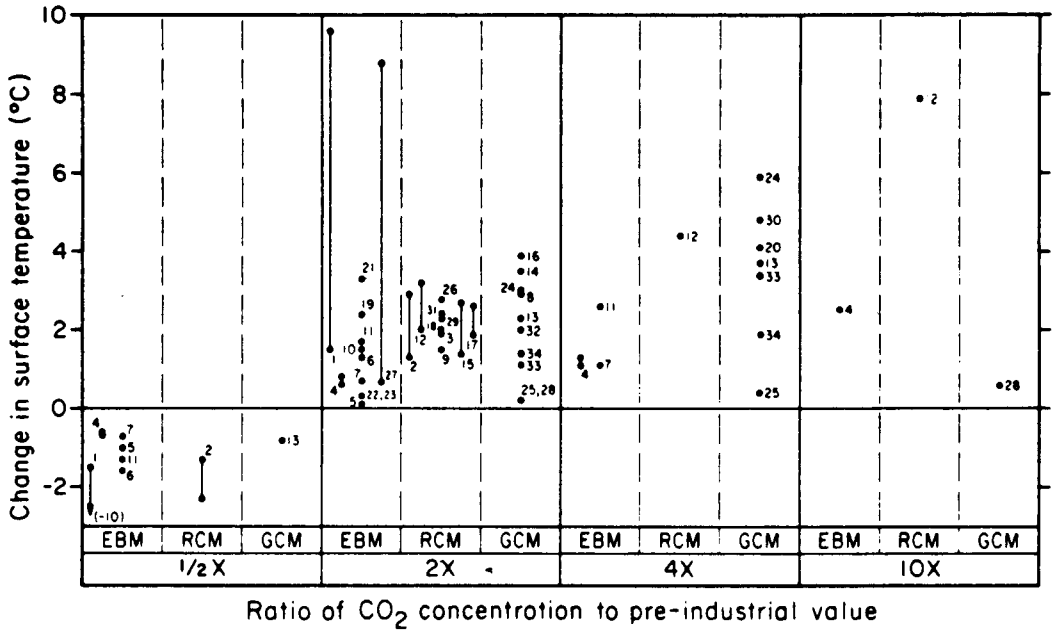

1. Möller (1963)
2. Manabe and Wetherald (1967)
3. Manabe (1971)
4. Rasool and Schneider (1971)
5. Sellers (1973)
6. Sellers (1974)
7. Weare and Snell (1974)
8. Manabe and Wetherald (1975)
9. Ramanathan (1975)
10. Schneider (1975)
11. Temkin and Snell (1976)
12. Augustsson and Ramanathan (1977)
13. Potter (1978, 1980)
14. Hansen, personal communication
15. Rowntree and Walker (1978)
16. Hansen (1979)
17. Hummel and Reck (1979)
18. Hunt and Wells (1979)
19. MacDonald et al. (1979)
20. Manabe and Stouffer (1979, 1980)
21. Ramanathan et al. (1979)
22. Newell and Dopplick (1979)
23. Idso (1980)
24. Manabe and Wetherald (1980)
25. Gates et al. (1981)
26. Hansen et al. (1981)
27. Kandel (1981)
28. Mitchell (1983)
29. Ramanthan (1981)
30. Wetherald and Manabe (1981)
31. Hall et al. (1982)
32. Schlesinger (1983)
33. Washington and Meehl (1983)
34. Aleksandrov et al. (1983)

Figure C.3. The change in surface temperature induced by halving (0.5×), doubling (2×), quadrupling (4×) and decupling (10×) the preindustrial CO_2 concentration as simulated by energy balance models (EBMs), radiative-convectivemodels (RCMs), and general circulation models (GCMs). Source: Schlesinger (1983).

is the most reliable for projecting climate change (see Chapter 4 of this volume). Therefore, we cannot deduce from the disagreements between the models how much they disagree with reality. For example, the changes in equilibrium surface temperatures projected for different changes in CO_2 concentration are compared in Figure C.3 for various models. As Schlesinger (1983) points out in the original discussion of this figure, however, not all of the results are comparable, and the uncertainty is not necessarily as large as the disagreement between the results. Even if we eliminate the results that are not precisely comparable, the disagreement still does not indicate the uncertainty. For example, all GCMs have a limited spatial resolution (of about 500 km). Therefore, it is not only possible but probable that the models make approximations that result in similar errors, and there is always the danger that the results have more in common with each other than they do with reality.

An important conclusion is that the value of model intercomparison is greatly enhanced if coupled with some form of uncertainty analysis that is aimed at explaining why the disagreements among results occur. Furthermore, it is equally important to explain why models adopting a variety of different approaches *agree* with each other in many important respects. Explaining and understanding the agreements and disagreements between different models is perhaps the most fruitful goal of model intercomparison studies.

C.3.9 Overall Model Evaluation

To be of value to decision makers, an overall evaluation of climate model projections needs to be simple to understand yet supportable. Climate models, however, are highly sophisticated, so preparation of a useful model evaluation is not easy. A structured

approach to model validation, as, for example, outlined in this section, helps because it identifies self-contained steps that are relatively easy to comprehend.

In the short term, the most valuable contribution of an overall model evaluation is likely to be identification of the most important uncertainties in CO_2-climate modeling and to provide an assessment of how best to proceed with modeling research. The long-term objective of model evaluation, however, is to provide a convincing argument of why both global and regional projections of climate change can be trusted.

C.4 CONVENTIONAL SENSITIVITY ANALYSIS

There are so many different sources of uncertainty in climate models that it is useful, if not essential, to sort out the important from the unimportant. It is often possible to separate the importance of an uncertainty into two factors: first, how large the source of uncertainty is; second, how sensitive the model is to that source of uncertainty. This separation is useful because the sensitivity of a model is a mathematical and objective quantity, whereas the size of an uncertainty usually is open to discussion and is sometimes difficult even to define. Therefore, sensitivities provide the focus for a discussion of uncertainties. For example, one of the most widespread sources of uncertainty in climate models is the practice of representing parametrically those physical processes that cannot be resolved by the model's spatial grid (i.e., parameterization of subgrid processes). Sensitivity analysis determines whether a subgrid process has a large influence on the model, consequently determining whether scrutiny of the uncertainty in the parametric representation is called for.

Conventional methods of determining the sensitivity of climate models to uncertainties are reviewed in the following sections.

C.4.1 Comparison of Results of Different Models

As has already been discussed, comparison of the results of models is, on its own, unsatisfactory as a method of uncertainty analysis. However, a comparison of model results is a form of sensitivity analysis because it indicates how sensitive the results are to a combination of model differences. A difficulty with this type of sensitivity analysis is the identification of which model differences are causing which differences in the results. For example, in Figure C.4 the regional changes in surface temperatures after a doubling of the CO_2 concentration in three different models are compared. Although it is interesting to compare the net effect of all of the differences among the three models, the main effect of Figure C.4 is bewilderment. Provided that the simulations really are comparable (e.g., they represent equilibrium results of physically comparable models), and provided that the differences in the simulations are statistically significant, then a sensitivity analysis of specific differences between the models can help to identify the importance of the differences in the results.

The need for sensitivity analysis in the intercomparison of sophisticated models is underlined by intercomparisons that focus on models of specific processes. For example, in Table C.3 Luther (1982) illustrates the range of radiative flux changes due to a doubling of the CO_2 concentration in eight different radiation models. Although Luther points out that radiative models must be compared with observations to evaluate their accuracy, his comparison does provide an estimate of the size of the uncertainty in radiative flux changes (see also Chapter 2 of this volume). In addition, however, it is important that we know how sensitive the overall climate models are to uncertainties in radiative fluxes. For example, different models can have different sensitivities to radiative fluxes, depending on the strength of the water vapor feedback mechanism.

C.4.2 Multiple Simulations With the Same Model

Most CO_2-climate projections are based on estimation of the sensitivity of the equilibrium climate to a doubling of the atmospheric CO_2 concentration. This sensitivity is estimated by comparing a doubled CO_2 concentration simulation with a control run. This method of rerunning can be extended to estimate other sensitivities, as illustrated in Table C.4. An important disadvantage of this method

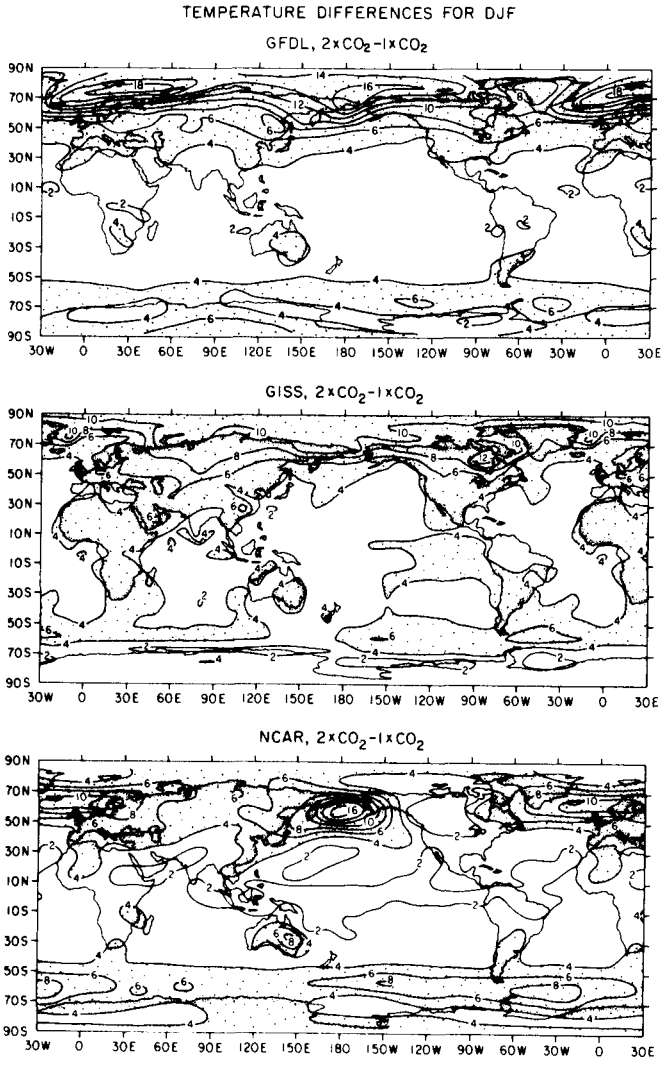

Figure C.4. The increase in surface air temperature (°C) for December-January-February (DJF) after a doubling of the CO_2 concentration based on GCM simulations by researchers at the Geophysical Fluid Dynamics Laboratory (GFDL), the Goddard Institute for Space Studies (GISS), and the National Center for Atmospheric Research (NCAR). Source: Schlesinger and Mitchell (1985).

is its computational expense. For example, the 60 sensitivity experiments shown in Table C.4, despite being run for much shorter times than the control run, required the equivalent of 900 hours of computing time on an IBM 360 computer. Although a reduction of the simulated time for each rerun does reduce the computational expense of rerunning the model, it also raises doubts about whether the simulations have reached equilibrium. An alternative approach is to use simpler and faster-running models for sensitivity studies, but such an approach introduces even more assumptions.

Table C.3
Comparison of Net Flux Changes at the Tropopause Due to Doubling of CO_2 for Different Radiation Calculations

Case	Change in CO_2 (ppm)	Range of Values (Wm^{-2})	Central Value and Range (%)
All models (8 models)	600–300	−3.15 to −6.11	−4.63(±32)
	1200–600	−4.87 to −6.69	5.78(±16)
15 μm band only using McClatchey et al. (1973) data (3 models)	600–300	−4.73 to −5.49	−5.11(±7)
	1200–600	−4.87 to −5.58	−5.22(±7)

Note: Differences in model calculations of the change in net flux at the tropopause (13 km) due to doubling CO_2 with all other atmospheric constituents included. Source: Luther (1982).

C.4.3 Simplified Models

Mathematical models are not always intended to be realistic, but sometimes they are formulated to illustrate the outcome of using a particular set of physical assumptions. For example, one of the simplest climate models applies the Stefan-Boltzmann law and the energy balance on a sphere of radius r having uniform absolute temperature T:

$$4\pi r^2 \sigma T^4 = \pi r^2 S(1-\alpha) \; . \qquad \text{(C.1)}$$

Using values of $S = 1367$ W m^{-2} for the solar constant, $\alpha = 0.3$ for the planetary albedo (i.e., fraction of solar radiation reflected back into space by both the ground and the atmosphere), and $\sigma = 5.69 \times 10^{-8}$ W m^{-2} K^{-4} for the Stefan-Boltzmann constant, Equation (C.1) gives a temperature of 255 K. We can interpret this as the effective mean temperature of the surface-atmosphere system required to achieve radiative equilibrium. Schneider and Mass (1975) have defined the sensitivity β of the temperature T to changes in solar constant S as

$$\beta = S \, \frac{\partial T}{\partial S} \; . \qquad \text{(C.2)}$$

For this simple model, the value of β is 64 K, that is, an increase of 1% in the solar constant would increase T by 0.64°C.

Because of the greenhouse warming (see Chapter 2 of this volume), the observed global temperature at the Earth's surface (288 K) is considerably higher than the effective mean temperature (255 K). Radiative-convective models take into account this greenhouse warming and simulate a global surface

Table C.4
Sensitivity Experiments Performed with the Goddard Institute for Space Studies GCM

Model Run	Numbers of Months Simulated	Experiment Description
I-1	60	Control run for most experiments, 8° × 10° resolution, 7 layers
I-2	9	C grid
I-3	3	C grid with *smoothing* of the horizontal pressure gradient force
I-4	3	C grid, 4° × 5° resolution
I-5	9	C grid, potential enstrophy conservation
I-6	9	*Coriolis and metric terms* included at poles
I-7	12	Momentum drag in top model layer
I-8	12	Model I with surface physics and radiation of Model II
I-9	3	I-8 with drag in *strratosphere*, $C_{DN} = 10^{-5}$
I-10	3	I-8 with drag in stratosphere, $C_{DN} = 10^{-4}(5 + 0.5U)$
I-11	3	I-8 with drag in stratosphere, $C_{DN} = 10^{-3}$
I-12	3	I-8 with *model top* at 0.01 *mb*, 21 layers, *no* drag in stratosphere
I-13	18	10-layer model, 3 layers added in upper troposphere and stratosphere
I-14	18	12-layers; 2 layers added in planetary boundary layer to Run I-13
I-15	3	Matsuno TASU time stepping
I-16	3	No smoothing toward poles, 2 minute time step
I-17	3	No sea level pressure filter
I-18	3	GFDL *horizontal* diffusion
I-19	3	NCAR horizontal diffusion
I-20	3	25% limit on horizontal advection of water vapor
I-21	3	Vertical advection of water vapor uses arithmetric mean at layer edges
I-22	3	No friction, i.e., no surface drag or momentum mixing by convection
I-23	3	Aerosols omitted
I-24	9	IR radiation of Model II (single k-distribution for each gas)
I-25	9	Realistic IR emissivities for deserts, snow, and ice
I-26	9	Radiation computed at all gridpoints; run I-1 uses 2-point mean
I-27	9	Complete radiation calculation every hour
I-28	3	Daily average solar insolation, i.e., no diurnal cycle
I-29	9	No subgrid-scale temperature variance for moist convection
I-30	9	Moist adiabatic adjustment
I-31	9	Moist convection cloud constant (γ) tripled
I-32	3	Radiation computed separately in cloudy/noncloudy areas of gridbox
I-33	9	No mixing of momentum by convection
I-34	9	Moist convection can start below the condensation level
I-35	9	No subgrid-scale temperature variance for supersaturation clouds
I-36	3	Large-scale rainfall calculated every 5 hours
I-37	9	Fixed annually-averaged clouds
I-38	3	Fixed annually-averaged and longitudinally averaged clouds
I-39	3	Local temperature 0°C criterion for saturation over water or ice
I-40	3	Local temperature −40°C criterion for saturation over water or ice
I-41	3	Local temperature −65°C criterion for saturation over water or ice
I-42	12	Optical thickness of cirrus clouds reduced to $\tau = 1/3$
I-43	12	Optical thickness of other non-convective clouds reformulated
I-44	21	Snow density decreased from 0.25 to 0.1 g cm^{-3}
I-45	9	Modified thermal conductivity in deserts and vegetated areas
I-46	9	Increased field capacity based on vegetation type; I-8 is control
I-47	9	Instant upward water diffusion from root zone; I-46 is control
I-48	9	No runoff until first ground layer is saturated; I-47 is control
I-49	11	Intermediate runoff formulation; I-47 is control
I-50	9	Increased masking depths based on vegetation type
I-51	9	Modified ground albedo based on vegetation type
I-52	3	Ocean ice coverage based on Walsh and Johnson (1979)
I-53	24	No fractional grid for land/water
I-54	12	Ocean surface temperature based on Robinson and Bauer (1981)
I-55	9	Lower limit for surface roughness based on vegetation
I-56	3	Surface layer height of 30 m used over the ocean
I-57	9	Ekman surface wind formulation with specified α_0
I-58	9	First layer wind employed for Ekman wind calculation
I-59	3	Varying boundary layer height for Ekman wind calculation
I-60	3	Geostrophic wind used for Ekman wind calculation
I-61	9	Modified cross-isobar angle calculation; I-59 is control

Source: Hansen et al. (1983).

air temperature close to its observed value. These models also include positive feedbacks that increase the value of β. For example, the RCM used in a sensitivity analysis by Hall et al. (1982) gave a value for β of 108 K.

Sensitivities for the two models described above are summarized in Table C.5. As shown in this table, the extremely simple model represented by Equation (C.1) accounts for the order of magnitude of the sensitivities in the much more complex RCM (consisting of several hundred lines of FORTRAN coding). On the other hand, Equation (C.1) totally neglects important processes and sensitivities (for example, the effect of changes in the CO_2 concentration).

Table C.5
Comparison of Sensitivities Obtained by Using an Energy Balance Equation and a RCM

Change in Forcing Factor	Change in Temperature (°C)	
	Equation (C.1)	RCM
1% Increase in Solar Constant	0.64	1.08
	(β = 64 K)	(β = 108 K)
Increase of 0.01 in Albedo	−0.91	−0.85
Doubling of CO_2 Concentration	0	2.42

There is a complete range of climate models, from the simplest energy balance equation to the most complex GCM. Each of these models has a role in helping us to understand different physical processes and sensitivities.

C.4.4 Specialized Methods of Sensitivity Analysis

Even for the most complex models, it is possible to extract sensitivity information without actually rerunning the model. For example, Manabe and Wetherald (1980) performed an analysis to elucidate the net contribution of cloud feedback for a quadrupling of the CO_2 concentration (Table C.6). Their method involved noting the changes in temperature (T), mixing ratio of water vapor (r), surface albedo (A), and cloud cover (C) after a quadrupling of the CO_2 concentration. They then calculated the partial effects of each of these changes on the net solar radiative flux (S), the net terrestrial flux (F), and the net downward radiation (R), all at the top of the atmosphere. From the cloud column (C), they concluded that the change in terrestrial radiation (-2.06 W m^{-2}) was almost compensated by an accompanying change in solar radiation (2.26 W m^{-2}), indicating a small net contribution of cloud cover feedback.

Table C.6
Example of Specialized Method of Sensitivity Analysis Designed to Assess the Feedback Effects of Clouds

$Y \setminus x$	$\overline{\delta_x Y}^A$					$\sum$	δ_y
	CO_2	T	r	A	C		
S	0.35	—	1.12	2.10	2.26	5.83	5.72
$-F$	4.26	−16.74	6.68	—	−2.06	−7.86	−5.72
R	4.61	−16.74	7.80	2.10	0.20	−2.03	0

Note: Partial change in S, F, and R (W m^{-2}) of the standard model atmosphere attributable to separate changes in various relevant factors, i.e., CO_2, T, r, A, and C. Σ denotes the sum of all of these partial changes. δY is the change in a radiative flux Y (i.e., S, F or R) due to the simultaneous changes in all relevant variables resulting from a quadrupling of CO_2 concentration. Source: Manabe and Wetherald (1980).

Such specialized methods of sensitivity analysis can be effective, although they must be applied piecemeal and are time consuming to apply to the analysis of a wide variety of processes. This is a drawback for application to uncertainty analyses in which it is not known at the outset which uncertainties are important.

C.5 ADJOINT SENSITIVITY ANALYSIS

Conventional methods of sensitivity analysis focus on specific uncertainties in climate models and assess the effect of these uncertainties on any result that is of interest. On the other hand, the new method of adjoint sensitivity analysis focuses on specific results of the model and assess how these results are influenced by any uncertainty that can be expressed mathematically. Therefore, while conventional sensitivity analysis requires prior knowledge of which uncertainties might be important, adjoint sensitivity analysis only requires a knowledge of which results are important. The advantage of the adjoint method for analyzing uncertainties in climate models is that we generally know which are the critical results whereas we usually do not generally know which are the critical uncertainties.

The practical difference between conventional and adjoint methods of sensitivity analysis can be illustrated by comparing Tables C.2 and C.7. Hansen et al. (1983) constructed Table C.2 by identifying 20 different changes in the model, calculating the effects of these changes on the model results, and noting the major effects. Calculating these effects required about five times the computing time of the control run. On the other hand, Hall et al. (1982) constructed Table C.7 by identifying the global surface air temperature as the result of interest and using the adjoint method to calculate sensitivities for all 312 of the parameters in the model. The sensitivities were ranked by their relative sensitivities (i.e., fractional change in result divided by fractional change in parameter). Calculating these sensitivities required about 1.5 times the computing time of the control run.

The advantage of the adjoint approach is that it makes it practical to calculate all of the sensitivities, with hope even for models as complex as GCMs. Thus, by looking at, for example, the first 20 entries in Table C.7, we can be sure that we are looking at the 20 most sensitive parameters. By contrast, the conventional approach restricts the number of sensitivity experiments that can be performed, so it is always possible that important sensitivities will be overlooked when this method is used. Because the adjoint approach is new, however, it is relatively unfamiliar to atmospheric scientists; it is therefore reviewed here.

C.5.1 Basic Concepts Underlying the Adjoint Method

The purpose behind the adjoint method of sensitivity analysis is illustrated with a very simple time-dependent energy balance equation described by

$$C\dot{T} + \sigma T^4 = \frac{S(1-\alpha)}{4} \qquad \text{(C.3)}$$

with $T = T_0$ at $t = 0$. In this differential equation, C is the heat capacity per unit area, T is the time-dependent absolute temperature ($\dot{T} = dT/dt$), σ is the Stefan-Boltzmann constant, S is the solar constant, α is the planetary albedo, and T_0 is the initial temperature. The result of interest is the average temperature $\overline{T}$ given by

$$\overline{T} = (1/\tau)\int_0^\tau T dt\ , \qquad \text{(C.4)}$$

where τ is the final time. The value of $\overline{T}$ can be calculated by solving the differential equation for the time dependence of T and then by evaluating the integral for $\overline{T}$.

The objective of sensitivity analysis is to estimate the change in $\overline{T}$ arising from changes in the parameters C, S, α, and T_0. The conventional method of sensitivity analysis is to recalculate, that is, to specify the new values of the parameters, then to solve for the new time dependence of T, and finally to reevaluate $\overline{T}$. A possible alternative to recalculation involves differentiating the equations for T and $\overline{T}$:

$$\delta\dot{T} + \frac{4\sigma T^3 \delta T}{C} = \frac{\left\{-\dot{T}\delta C + (1-\alpha)\delta S - S\delta\alpha\right\}}{4C}\ ; \qquad \text{(C.5)}$$

with $\delta T = \delta T_0$ at $t = 0$, and

$$\delta\overline{T} = (1/\tau)\int_0^\tau \delta T dt\ . \qquad \text{(C.6)}$$

In these equations,[2] δT is the first-order change in the unperturbed temperature T arising from the parameter changes δC, δS, $\delta\alpha$, and δT_0. Once the parameter changes have been specified, then Equation (C.5) can be solved for the time dependence of δT, and finally $\delta\overline{T}$ can be evaluated. However, this offers no advantage over recalculation other than that the differential equation for δT is linear and therefore easier to solve than the original differential equation for T.

The adjoint method of sensitivity analysis uses a different approach. It involves finding an operator adjoint to the operator acting on δT in Equation (C.5). The operator acting on δT is $(d/dt + 4\sigma T^3/C)$. Its adjoint is the operator $(-d/dt + 4\sigma T^3/C)$, since these two operators satisfy the equation defining the adjoint operator:

$$\int_0^\tau u\left(-\frac{d}{dt} + \frac{4\sigma T^3}{C}\right) v dt =$$

[2] Strictly speaking, these equations are obtained by taking the Gateaux differential of operators representing the equations for T and $\overline{T}$ (e.g., see Cacuci and Hall [1984]).

Table C.7

Comprehensive Sensitivities for a Radiative Convective Model[a]

Ranking	Parameter Description[b]	Relative Sensitivity[c]
1	Coefficient $A_{1,3} = 1.43 - 2$ mb $(°C)^{-2}$ in equation for saturation vapor pressure of water	1.19
2	Coefficient $A_{1,2} = 4.44 - 1$ mb $(°C)^{-1}$ in equation for saturation vapor pressure of water	−1.04
3	Coefficient $A_{1,4} = 2.65 - 4$ mb $(°C)^{-3}$ in equation for saturation vapor pressure of water	−9.49 − 1
4	Conversion constant 273.155 from K to °C	−6.80 − 1
5	F_d =(total daylight hours)/24 = 0.5	4.16 − 1
6	Average cosine of solar zenith angle $\overline{\cos \zeta} = 0.5$	4.16 − 1
7	Coefficient $A_{1,5} = 3.03 - 6$ mb $(°C)^{-4}$ in equation for saturation vapor pressure of water	4.03 − 1
8	Stefan-Boltzman constant $\sigma = 1.17 - 7$ cal cm^{-2} d^{-1} K^{-1}	−4.00 − 1
9	Constant 0.930 in CO_2 transmission function τ_{CO_2} for terrestrial radiation [see Eq. (II.38) of Katayama (1972)]	−3.93 − 1
10	Constant 1.09 in CO_2 transmission function τ_{CO_2} for terrestrial radiation [see Eqs. (II.40, 41) of Katayama (1972)]	−3.92 − 1
11	Solar constant $S_0 = 2793.6$ cal cm^{-2} d^{-1}	3.81 − 1
12	Earth-Sun distance factor $(\bar{r}_e/r_e)^2 = 1$	−3.80 − 1
13	Coefficient $A_{1,1}$= 6.11 mb in equation for saturation vapor pressure of water	3.68 − 1
14	Constant 0.29 in water vapor transmission function $\tilde{\tau}_{H_2O}$ for terrestrial radiation [see Eq. (II.37) of Katayama (1972)]	−2.34 − 1
15	Constant 0.373 in water vapor transmission function $\tau^A_{H_2O}$ for terrestrial radiation [see Eq. (II.34) of Katayama (1972)]	−1.13 − 1
16	Coefficient $A_{1,6} = 2.03 - 8$ mb $(°C)^{-5}$ in equation for saturation vapor pressure of water	−1.09 − 1
17	Constant 0.028 in water vapor transmission function $\tilde{\tau}_{H_2O}$ for terrestrial radiation [see Eq. (II.37) of Katayama (1972)]	−8.13 − 2
18	Tropospheric pressure difference $p_4 - p_0 = 800$ mb	7.61 − 2
19	Constant 0.259 in water vapor transmission function $\tau^A_{H_2O}$ for terrestrial radiation [see Eq. (II.34) of Katayama (1972)]	−7.09 − 2
20	Fraction of solar insolation subject to water vapor absorption [constant $1 - f = 0.366$ [see Eq. (33) and Eq. (34) of Schlesinger and Gates (1979)]	6.00 − 2
21	Constant 0.194 in water vapor transmission function $\tilde{\tau}_{H_2O}$ for terrestrial radiation [see Eq. (II.37) of Katayama (1972)]	−4.15 − 2
22	Pressure $p_0 = 200$ mb	−4.01 − 2
23	Stratospheric temperature $T_{st} = 218$ K for terrestrial radiation calculation [see Eq. (27a) of Schlesinger and Gates (1979)]	3.81 − 2
24	Constant 0.247 in albedo α_O of cloudless sky due to Rayleigh scattering [see Eq. (39) of Schlesinger and Gates (1979)]	−3.73 − 2
25	Acceleration of gravity $g = 9.8$ m s^{-2}	−3.68 − 2
26	Constant 0.066 in CO_2 transmission function τ_{CO_2} for terrestrial radiation [see Eq. (II.38) of Katayama (1972)]	−3.40 − 1
27	Constant 0.16 in water vapor plus CO_2 transmission function $\tilde{\tau}\bar{\tau}$ for terrestrial radiation [see Eqs. (II. 18, 23, 27) of Katayama (1972)]	3.34 − 2
28	Constant 9.0 − 5 in CO_2 transmission function τ_{CO_2} for terrestrial radiation [see Eqs. (II.40, 41) of Katayama (1972)]	3.23 − 2
29	Surface albedo $\alpha_s = 0.1$	−2.99 − 2
30	Constant 0.622 in the saturation mixing ratio equation	2.86 − 2
31	Relative humidity at the surface, set equal to 0.77	2.86 − 2
32	Gas constant $R = 287$ m^2 s^{-2} K^{-1}	2.47 − 2
33	Critical lapse rate $\Gamma_c = 6.5$°C km^{-1}	2.47 − 2
34	Constant 0.9 in calculation of effective amount of water vapor $U^*_{H_2O}$ [see Eq. (29a) of Schlesinger and Gates (1979)]	−2.33 − 2
35	Constant 0.085 in albedo α_0 of cloudless sky due to Rayleigh scattering [see Eq. (39) of Schlesinger and Gates (1979)]	−2.13 − 2
36	Constant $f = 0.634$ in the ozone transmission function T_{O_3} for solar radiation [see Eq. (A.108) of Schlesinger (1976)]	2.07 − 2
37	Constant $(1 - f) = 0.366$ in the water vapor transmission function T_{H_2O} for solar radiation [see Eq. (A.100) of Schlesinger (1976)]	−1.52 − 2
38	Constant $p_{st} = 100$ mb in the calculation of the water vapor mixing ratio profile [see Eq. (30) of Schlesinger and Gates (1979)]	−1.49 − 2
39	Surface heat transfer coefficient C_s =10 cal cm^{-2} d^{-1} K^{-1}	−1.49 − 2

Table C.7
Continued

Ranking	Parameter Description[b]	Relative Sensitivity[c]
40	Constant −1.66 in water vapor plus CO_2 transmission function $\bar{\tau}_n^+$ for terrestrial radiation [see Eqs. (II.19, 23, 24) of Katayama (1972)]	−1.37 − 2
41	Coefficient $A_{1,7} = 6.14 - 11$ mb $(°C)^{-6}$ in equation for saturation vapor pressure of water	1.28 − 2
42	CO_2 concentration $\mu_{CO_2} = 320$ ppm	1.21 − 2
43	CO_2 molecular weight $\times 10^{-7}(44 \times 10^{-7})$ in calculation of total CO_2 amount [see Eq. (IV.18) of Katayama (1972)]	1.21 − 2
44	CO_2 density at NTP $\times 10^3$ (1.977 g cm^{-3}) in calculation of total CO_2 amount [see Eq. (IV.18) of Katayama (1972)]	−1.21 − 2
45	Molecular weight of air (28.966) in calculation of total CO_2 amount [see Eq. (IV.18) of Katayama (1972)]	−1.21 − 2
46	Constant in calculation of total CO_2 amount [see Eq. (IV.18) of Katayama (1972)]	1.21 − 2
47	Coefficient $b = 4.08 - 2$ (cm-NTP)$^{-1}$ in O_3 absorption function A'_{O_3} for solar radiation [see Table A.5 of Schlesinger (1976)]	−1.18 − 2
48	Total ozone $\Omega = 0.367$ atm-cm	−1.17 − 2
49	Coefficient $b = 1.44 - 1$ (g cm^{-2})$^{-1}$ in water vapor absorption function A'_{H_2O} for solar radiation [see Table A.4 of Schlesinger (1976)]	1.14 − 2
50	Constant 15.78 in water vapor plus CO_2 transmission function $\bar{\tau}_i$ for terrestrial radiation [see Eqs. (II.19,23,27) of Katayama (1972)]	1.13 − 2
51	Constant −42.59 in water vapor plus CO_2 transmission function $\bar{\tau}_i$ for terrestrial radiation [see Eqs. (II.19,23,27) of Katayama (1972)]	−1.01 − 2
52–89	Remaining parameters, which are mostly constants in transmission functions — magnitude between	−1.01 − 2
	and	1.00 − 3
90–152	magnitude between	1.00 −3
	and	0.0
153–312		0.0

Source: Hall et al. (1982).

[a] Surface air temperature (control) = 283.28 K.

[b] In giving values for various parameters, the second part of each value represents a power of 10; e.g., 9.49 − 1 = 9.49×10^{-1}. Where an unreferenced equation is referred to, see Hall et al. (1982).

[c] The second part of each value represents a power of 10.

$$\int_0^\tau v\left(\frac{d}{dt} + \frac{4\sigma T^3}{C}\right) u dt + uv]_0^\tau , \qquad \text{(C.7)}$$

where u and v are arbitrary functions of time. The adjoint method involves calculating an adjoint function T^*. This adjoint function is so called because it satisfies an equation involving the adjoint operator:

$$\left(-\frac{d}{dt} + \frac{4\sigma T^3}{C}\right) T^* = \left(\frac{1}{\tau}\right) \qquad \text{(C.8)}$$

with $T^* = 0$ at $t = \tau$. The left side of this equation is the adjoint operator acting on the adjoint function, and the right side is the coefficient of δT in the expression for $\delta\overline{T}$; the adjoint boundary condition is satisfied at the final time τ.

The Equation (C.7) defining the adjoint operator holds for the particular case when $u = \delta T$ and $v = T^*$:

$$\int_0^\tau \delta T\left(-\frac{d}{dt} + \frac{4\sigma T^3}{C}\right) T^* dt$$

$$= \int_0^\tau T^*\left(\frac{d}{dt} + \frac{4\sigma T^3}{C}\right) \delta T dt + [\delta T\, T^*]_0^\tau . \qquad \text{(C.9)}$$

From Equation (C.8), the term $(-d/dt + 4\sigma T^3/C)T^*$ is equal to $(1/\tau)$. Also, from Equation (C.5), the term $(d/dt + 4\sigma T^3/C)\delta T$ is equal to $\{-\dot{T}\delta C + (1 - \alpha)\delta S - S\delta\alpha\}/4C$. Moreover $\delta T = \delta T_0$ at $t = 0$, and $T^* = 0$ at $t = \tau$. Thus, Equation (C.9) gives the following expressions for $\delta\overline{T}$:

$$\delta\overline{T} = \int_0^\tau \delta T(1/\tau) dt = \delta T_0 T^*(0) +$$

$$\int_0^\tau T^*\left\{-\dot{T}\delta C + (1 - \alpha)\delta S - S\delta\alpha\right\}(1/4C) dt . \qquad \text{(C.10)}$$

The adjoint method starts by solving for the time dependence of T^*. Then $\delta\overline{T}$ can be evaluated for any parameter change by using Equation (C.10). For example, we can evaluate the sensitivity β by considering a constant change δS and setting all other parameter changes to zero. Then, the adjoint expression for β is

$$\beta = S\frac{\delta T}{\delta S} = \int_0^\tau T^*(1 - \alpha) S(1/4C) dt \qquad \text{(C.11)}$$

The advantage of the adjoint method is that the parameter variations do not have to be specified until after all of the differential equations have been solved. Thus the change in the result arising from changes in individual parameters can be identified and evaluated easily. The two different expressions for $\delta\overline{T}$ illustrate this point well. The expression for $\delta\overline{T}$ in terms of T^* in Equation (C.10) shows the relative importance of all of the parameters, including initial conditions, whereas the conventional expression in terms of δT,

$$\delta\overline{T} = (1/\tau)\int_0^\tau \delta T dt\ , \qquad \text{(C.12)}$$

is not so physically revealing.

The adjoint function has a useful physical interpretation that can be understood as follows. When the initial temperature T_0 is the only parameter to be changed, then the adjoint expression for δT becomes $\delta T = \delta T_0 T^*(0)$, or equivalently $T^*(0) = \delta\overline{T}/\delta T_0$. Thus, the value of the adjoint function at time zero is the sensitivity of the result $\overline{T}$ to perturbations in the initial temperature T_0. More generally, the adjoint function T^* at an arbitrary time is the sensitivity of the result $\overline{T}$ to an instantaneous perturbation in dependent variable T at that arbitrary time. This interpretation of the adjoint function helps us to understand the adjoint expression for β. The sensitivity β can be interpreted as the first-order increase in average temperature resulting from a doubling of the solar constant. The term $(1-\alpha)S(1/4C)$ in the expression for β is the rate of change of temperature T due to this doubling of the solar constant. The resultant rate of change in the average temperature in $\overline{T}$ is thus $T^*(1-\alpha)S(1/4C)$. The integration of this expression over time gives the change in average temperature arising from a doubling of the solar constant, giving the adjoint expression for β. Thus, the term $T^*(1-\alpha)S(1/4C)$ gives the importance of increases in solar constant as a function of time. Similar terms can be derived for the time-dependent importance of other parameter changes.

In practice, climate models are much more complicated than the simple energy balance equation considered here. For example, a GCM solves conservation equations of mass, momentum, and energy throughout the global atmosphere. Nevertheless, even the most complex climate models are based on first-order nonlinear differential equations, like the differential energy balance equation. Thus, the basic concepts and interpretations discussed above apply to all climate models.

The adjoint method has been successfully applied to a RCM (Hall et al. 1982) and, recently, to the Oregon State University atmospheric GCM[3]. The following sections review the results from these applications.

C.5.2 Parameter Sensitivities

Sensitivities calculated using the adjoint method can be used to predict the actual effect of changing parameters (predicted effect = parameter change × sensitivity). Because of second-order effects, however, the effect of small parameter changes will be predicted accurately, while the effect of large changes in some parameters will be predicted less accurately. For example, Table C.8 compares predicted and actual changes in the surface air temperature after various changes in several input parameters of a RCM. Table C.8 illustrates that, for this model, the adjoint method accurately predicts the effect of most physically reasonable parameter changes. The only significant discrepancy is for the doubling of the CO_2 concentration. This is because the predicted change assumes a linear relationship between CO_2 concentration and surface air temperature, while the true relationship is recognized to be logarithmic. Thus, for a doubling of the CO_2 concentration, the predicted and actual changes differ by a factor of $\log_e 2 \sim 0.7$.

Having established that the sensitivities calculated by the adjoint method are generally correct, we can take advantage of the method's analytical power. Table C.7 has shown that the adjoint method makes it possible to rank the importance of all the parameters in a RCM. The following discussion presents some of the sensitivity information that has recently been obtained by applying the adjoint method to the Oregon State University atmospheric GCM.

The version of this model currently being analyzed has been comprehensively documented by Ghan et al. (1982). The particular version of this

[3] M. C. G. Hall, "Application of Adjoint Sensitivity Theory to an Atmospheric General Circulation Model." Accepted for publication in the *Journal of the Atmospheric Sciences.*

Table C.8
Comparison of Adjoint Estimated Sensitivities of Equilibrium Surface Temperature with Results from Model Reruns

Parameter Description	Relative Sensitivity	Fractional Variation in Parameter (%)	Change in Temperature: Adjoint Estimate (° C)	Change in Temperature: Rerun Method (° C)
Solar Constant	0.381	0.1	0.108	0.108
		10	10.8	10.8
Surface Albedo	−0.0299	0.1	−0.00847	−0.00850
		10	−0.847	−0.853
Relative Humidity at Surface	0.0285	0.1	0.00807	0.00811
		10	0.807	0.795
Atmospheric CO_2 Concentration	0.0121	0.1	0.00343	0.00343
		100	3.43	2.42

Note: Equilibrium surface temperature = 283.28 K.
Source: Hall et al. (1982).

model that we will consider has *prescribed* sea surface temperatures (SST) and sea ice extent. The sensitivity information in Table C.9 illustrates the dominating effect of the SST on the global average surface air temperature. When all feedback processes are neglected and SST is held fixed, an increase in the SST of 0.5°C has a much larger effect than a doubling of the CO_2 concentration. In fact, the sensitivity to the CO_2 concentration in this version of the model is much lower than that which is usually reported, precisely because the surface air temperature is so closely tied to the prescribed SST. The sensitivity of 0.126°C to a doubling of the CO_2 concentration is smaller than that reported by Gates et al. (1981) using the same model because in the present analysis the model was run for only 10 days, and this did not allow parameter changes to have their full equilibrium effect.

Table C.9
Adjoint Estimated Sensitivities for the Oregon State University Atmospheric GCM

Change in Model Parameter	Change in Global Surface Air Temperature (° C)
Increase Global SST by 0.5°	0.292
Increase Surface Albedos by 0.03	−0.131
Double Atmospheric CO_2	0.126
Increase Solar Constant by 2%	0.090
Double Stratospheric Ozone	−0.067

We can understand the sensitivities in Table C.9 by analyzing the adjoint expressions for these sensitivities (along the same lines as for β in the energy balance equation). The GCM is spatially dependent and has several types of state variables (surface pressure, wind velocity, atmospheric temperature, atmospheric humidity, ground temperature, ground wetness, snow amount). Thus, the adjoint expression for the effect of parameter variations has the form:

$$\begin{pmatrix}\text{change}\\ \text{in}\\ \text{result}\end{pmatrix} = \int_{\text{time}} \int_{\text{space}} \sum_{\substack{\text{variable}\\ \text{types}}} \begin{pmatrix}\text{adjoint}\\ \text{function}\\ \text{for}\\ \text{variable}\end{pmatrix} \times \begin{pmatrix}\text{effect of}\\ \text{parameter}\\ \text{change on}\\ \text{variable}\end{pmatrix} \qquad \text{(C.13)}$$

Integrating over space and summing over variable types gives the time-dependent importance of the parameter change (e.g., Figure C.5A), integrating over time and space gives the contribution from each variable type (e.g., Figure C.5B), and integrating over time and summing over variable types gives the spatial importance of the parameter change (e.g., Figure C.5C).

Figure C.5 shows a breakdown of the sensitivity of global air temperature to a doubling of atmospheric CO_2. As Figure C.5A indicates, while the contribution to the sensitivity is steadily decreasing, the effect is not complete at ten days. In fact, if we extrapolate Figure C.5A to longer times and estimate the additional area under the curve, we might expect the equilibrium sensitivity to be about twice the 10-day sensitivity. This is consistent with the equilibrium sensitivity of 0.2°C for the fixed sea surface temperature experiment reported by Gates et al. (1981). Figure C.5B shows that in this model, CO_2 affects the globally averaged surface air temperature entirely through its effect on atmospheric and ground temperature. The absence of any contribution from atmospheric humidity shows that the water vapor feedback mechanism is virtually nonexistent in this model (no doubt as a consequence of the prescribed ocean temperatures). The ice-albedo feedback mechanism is also absent, as illustrated by the absence of large sub-arctic contributions to the sensitivity in Figure C.5C. Comparison of information such as in Figure C.5 between different models is a powerful way of analyzing why models exhibit

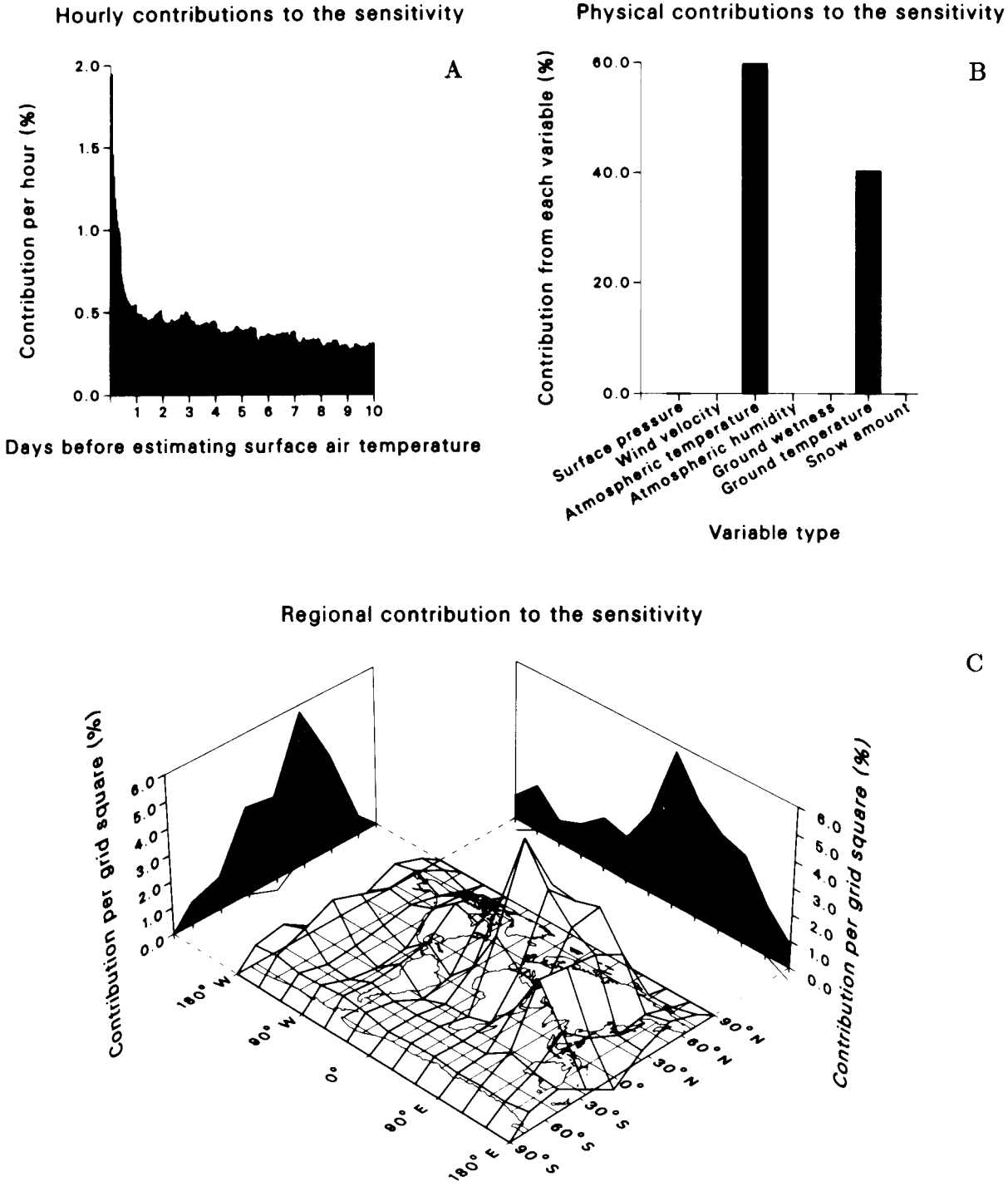

Figure C.5. Analysis of the sensitivity of global surface air temperature (SAT) to atmospheric CO_2 concentration. When the atmospheric CO_2 concentration is doubled, ten days later the global SAT is estimated to increase by 0.126°C. The percentage contribution to this sensitivity is resolved above (A) as a function of time, (B) as a function of physical process, and (C) as a function of spatial location.

different sensitivities. Moreover, this type of information can be made available not only for CO_2 sensitivity, but also for sensitivities to any parameter or group of parameters in a model.

Implementation of the adjoint method for a GCM requires considerable investment, but once the method has been implemented, it is computationally very efficient. The main computational

expense of the adjoint method is the numerical evaluation of the adjoint operator. This evaluation takes about the same amount of computation time as the original run. The 10-day GCM simulation chosen as an initial test of the adjoint method required about 1 hour of computing time on an IBM 3033 computer. Use of the adjoint method to calculate detailed sensitivity information for a wide variety of parameters required a little over an hour of additional computing time. To obtain the same sensitivity information by rerunning would have required hundreds of hours of computing time.

To check the sensitivities obtained by the adjoint method, some of these reruns have actually been performed. Even for large parameter changes (e.g., a doubling of the CO_2 concentration) the agreement has been within 30%. The adjoint method has been applied successfully to a general circulation model only very recently (M. C. G. Hall[4]), and it is hoped that its analytical power will be taken advantage of increasingly as time progresses.

C.5.3 Sensitivity to Feedback

Feedback occurs in a climate model when physical quantities that influence the climate (e.g., albedo, humidity, cloud cover, ocean currents, sea ice) are themselves influenced by the climate. Positive feedbacks play an important role in climate change because of their amplifying effect. For example, as much as half of the estimated CO_2 warming is attributable to the water vapor feedback mechanism (higher temperatures → more atmospheric water vapor → stronger water vapor greenhouse effect → higher temperatures). Also, some of the severity of ice ages can likely be attributed to the ice albedo feedback (lower temperatures → more sea ice → higher albedo → lower temperatures).

Since feedback is so important in determining the magnitude of the climate change, different feedback strengths between climate models are likely to account for many of the differences between results. Therefore, to understand these differences in results, it is particularly useful to isolate the effects of individual feedbacks. One approach is to remove the feedbacks, then add them individually, noting their effect. Hansen et al. (1984) used this approach to generate Figure C.6, which illustrates the effect of various feedbacks in a RCM. The disadvantage of this approach is that it requires rerunning the model several times, which is prohibitively expensive for GCM climate simulations.

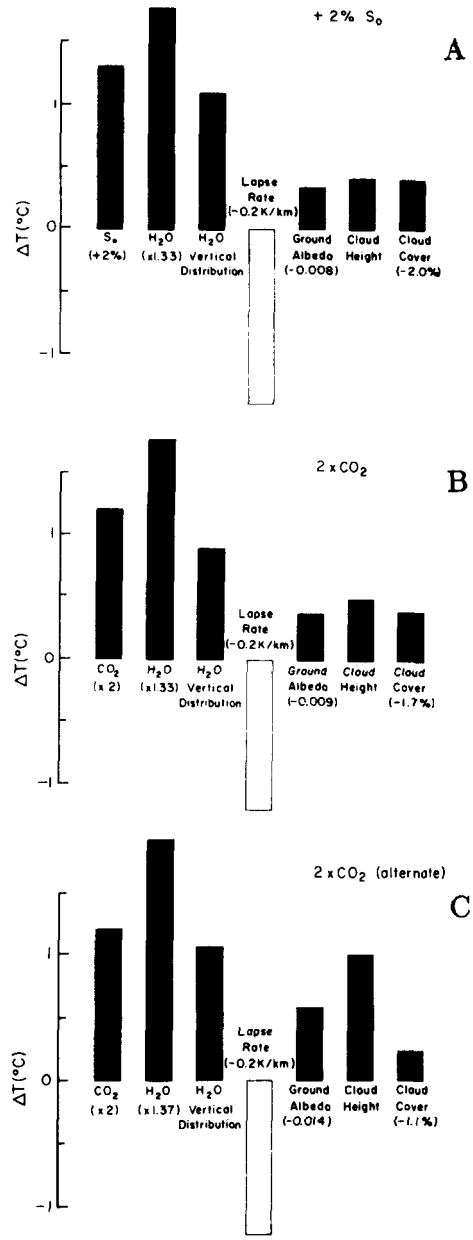

Figure C.6. Contributions to the global mean temperature rise in the S_0 and CO_2 experiments as estimated by inserting changes obtained in the three-dimensional experiments into a one-dimensional radiative-convective model. (A) +2% S_0 experiment, (B) experiment with a doubled CO_2 concentration, and (C) experiment with a doubled CO_2 concentration for the alternate control run with greater sea ice (Hansen et al. 1984).

[4] Ibid.

Table C.10
Feedback Effects in a Radiative Convective Model Using Different Analysis Methods[a]

Feedback Description	Prescribed Relative Humidity Feedback	Surface Air Temperature (T) and Surface Albedo (α) Feedback			
		$\partial\alpha/\partial T =$ 0.005 K^{-1}	$\partial\alpha/\partial T =$ 0.0005 K^{-1}	$\partial\alpha/\partial T =$ −0.0005 K^{-1}	$\partial\alpha/\partial T =$ −0.005 K^{-1}
Sensitivity to Feedback by Adjoint Method (°C)	0.67	−0.51	−0.051	0.051	0.51
Result with Feedback Estimated by Recalculation (°C)	2.78	1.27	1.615	1.717	2.40
Result with Feedback Estimated by Summing a Geometric Progression (°C)	2.77	1.27	1.614	1.717	2.39

Source: Cacuci and Hall (1984).
[a] Model sensitivity without feedback (i.e., surface air temperature increase after doubling CO_2) is equal to 1.644°C.

The adjoint method provides a much more efficient method of estimating the effect of feedback. To explain this method, we return to the energy balance equation described in Section C.5.3. Allowing the albedo α to depend on the temperature introduces an albedo feedback mechanism. In terms of sensitivities, this feedback can be thought of as a temperature-dependent change ($\delta\alpha$) in the albedo. Thus, we can express the effect of the albedo feedback using the adjoint sensitivity expression

$$\delta T = \int_0^\tau T^*(-S\delta\alpha)(1/4C)dt \; . \qquad \text{(C.14)}$$

The problem with this expression is that $\delta\alpha$ depends on temperature, but which temperature? Strictly speaking, we should use the new time-dependent temperature recalculated with the feedback, but the whole point of using the adjoint method is to avoid this recalculation. Therefore, it is tempting to approximate the recalculated temperature by the unperturbed temperature T. Cacuci and Hall (1984) have shown that this approximation leads to an estimate of feedback effects correct to first order in the strength of the feedback. Consequently they have called this estimate the *sensitivity to feedback*. Subsequently, Hall (1986) has suggested estimating the actual effect of feedback from the sensitivity to feedback by summing a geometrical progression. This approach gives a formula of the form

$$\text{estimated result with feedback} = \frac{\text{result without feedback}}{1 - \text{feedback ratio}}$$

where

$$\text{feedback ratio} = \frac{\text{sensitivity to feedback}}{\text{result without feedback}} \; .$$

Table C.10 shows the success of this approach in estimating the effect of albedo and relative humidity feedbacks in a RCM.

When feedback processes in different models are compared, one looks for differences between the effects of a feedback process in the different models. The efficiency of the adjoint method is likely to make the comparison much more informative. When the adjoint functions have been calculated, the computing required to estimate the effect of the feedback is negligible. Therefore, a wide variety of feedbacks can be investigated.

C.6 EXPRESSING UNCERTAINTIES

A parameter in a model with an uncertainty of $X\%$ and a relative sensitivity of Y causes an uncertainty of $XY\%$ in the result. At first sight, this statement appears to be too naive to deal with the many different sources of uncertainty in climate models (e.g., uncertainties arising from making physical assumptions or even entirely neglecting physical processes). However, most sources of uncertainty can be expressed and quantified by introducing new parameters that are designed to represent such uncertainties. Then sensitivity analysis can quantify the effect of these uncertainties on the results. This section illustrates how this approach works in practice.

C.6.1 Sources of Uncertainty

The energy balance equation used in Section C.4 illustrates most of the important ways in which uncertainties can arise. Recall that this equation applies the Stefan-Boltzmann law and solar energy balance to a sphere with albedo α and uniform absolute temperature T:

$$4\sigma T^4 = S(1-\alpha) \; . \qquad \text{(C.15)}$$

We can expect the estimated value of T to depart from the observed global temperature because of the following:

1. Validity of physical assumptions: Does the Earth radiate like a black body with uniform temperature?
2. Completeness: Are all factors contributing to the greenhouse warming included?
3. Data uncertainties: What value should be used for the albedo?

More complex models raise other issues, such as accuracy of numerical solutions, errors in computer programming, and statistical significance of results.

The rest of this section illustrates a quantitative approach for dealing with the sources of uncertainty listed above.

C.6.1.1 Validity of Physical Assumptions

Many of the assumptions made in simple climate models are demonstrably untrue. For example, the temperature of the Earth is not uniform as assumed in this simple energy balance equation and in RCMs. However, such assumptions still may be acceptable provided that they lead to results that are essentially correct. Thus, the important issue is not only how true an assumption is, but also how sensitive the results are to departures from the truth.

By way of illustration, we return to the energy balance equation. When the temperature T is not uniform, this model is represented by the equation

$$4\sigma\langle T^4\rangle = S(1-\alpha) \; , \qquad \text{(C.16)}$$

where $\langle\ \rangle$ denotes a global average. The temperature we want to evaluate is $\langle T\rangle$, so we write the spatially dependent temperature T as the sum of $\langle T\rangle$ and a local deviation ΔT, that is, $T = \langle T\rangle + \Delta T$. Substituting this expression into Equation (C.16) gives

$$4\sigma\left(\langle T\rangle^4 + 4\langle T\rangle^3\langle\Delta T\rangle + 6\langle T\rangle^2\langle\Delta T^2\rangle + \ldots\right) = S(1-\alpha) \; . \qquad \text{(C.17)}$$

Because $\langle\Delta T\rangle$ is zero, this equation can be written

$$4\sigma\langle T\rangle^4 \simeq \frac{S(1-\alpha)}{(1+6\langle\Delta T^2\rangle/\langle T\rangle^2)} \; . \qquad \text{(C.18)}$$

Thus, the equation for the average nonuniform temperature is the same as the original equation for the uniform temperature, except there is an extra factor $[1/(1+6\langle\Delta T^2\rangle/\langle T\rangle^2)]$.

Equation (C.18) illustrates the two issues that arise when a physical assumption is made. The term $\langle\Delta T^2\rangle/\langle T\rangle^2$ is the fractional variance of the temperature, signifying how valid the assumption of uniform temperature is. However, to determine whether the assumption is acceptable we need to know how sensitive the model is to the temperature being nonuniform; that is, how sensitive it is to the fractional variance term. If we assume that $\Delta T \simeq 20$ K and $T \sim 270$ K, then the term $6\langle\Delta T^2\rangle/\langle T\rangle^2 \simeq 3\%$. Sensitivity analysis shows that this 3% effect is enough to change the temperature by about 2 K.

C.6.1.2 Completeness

Limited understanding of the wide range of atmospheric processes and the practical limitations of available computers combine to limit the completeness of all computer models. While the physical laws governing some of these processes can be reasonably well represented, the interactions and complexities of other important processes (e.g., cloud-radiation feedbacks) are very complex and only poorly understood. Even for those processes for which detailed representations have been developed, computer limitations force approximations in order to represent large areas with only a few variables and at a relatively few grid points. As a consequence, some processes may be neglected or inadequately treated in climate models; all models are incomplete in this sense. Others may also completely omit important processes.

Sensitivity analysis can help to understand the importance of these limitations by indicating the

potential importance of the various physical processes, even if they are neglected in the model. For example, we can estimate the potential radiative effects of an atmosphere in the energy balance model without resorting to the use of a significantly more complex model. The atmosphere can be thought of as a blanket that is transparent to solar radiation but which transmits only a fraction τ_{IR} of the infrared radiation (τ_{IR} is called the transmission function). In the energy balance model the infrared radiation corresponds to the term $4\sigma T^4$. A fraction $(1 - \tau_{IR})$ of this radiation is absorbed by the atmosphere, and half of this radiation, that is, $4\sigma T^4(1 - \tau_{IR})/2$, is reradiated back to the ground, tending to augment the solar radiation. Thus, the equation of energy balance at the ground becomes

$$4\sigma T^4 = S(1 - \alpha) + 4\sigma T^4(1 - \tau_{IR})/2 \,. \qquad \text{(C.19)}$$

Rearranging Equation (C.19) gives

$$4\sigma T^4 = S(1 - \alpha)2/(1 + \tau_{IR}) \,. \qquad \text{(C.20)}$$

This equation is the same as for the original model with no atmosphere, except there is an extra factor $2/(1 + \tau_{IR})$.

The transmission function τ_{IR} for an atmosphere with a water vapor mixing ratio of 10^{-4} and a CO_2 concentration of 320 parts per million by volume (ppm) is about 0.5 (Katayama 1972). Thus, the factor $2/(1 + \tau_{IR})$ is about 1.3. Sensitivity analysis of the original model shows that this factor increases the temperature by about 20°C.

C.6.1.3 Parameter Uncertainties

The effort to express uncertainties in model parameters ranges from straightforward (but laborious) to difficult. For example, the value of the albedo in the energy balance equation might best be obtained from the average of satellite measurements weighted by incident solar radiation. Thus, obtaining a value for the uncertainty would involve a detailed analysis of all of these measurements. However, sensitivity analysis shows that even an uncertainty of 10% in albedo would only change the temperature by about 3 °C. So, although the value of the albedo is important, uncertainties of 10% in the albedo are much less important to the surface temperature than the uncertainties arising from neglecting the infrared radiative properties of the atmosphere.

Much of the data in more complex climate models, however, consist of parameters used to represent the average effect of very complex processes over large, but non-uniform, areas. For example, momentum transfer between the ground and atmosphere must usually be represented by simplified empirical relationships and cannot be computed by summing the effect over each individual obstacle in a region. Expressing parameter uncertainties in these types of relationships, and then determining the impact of these uncertainties on results, helps to establish the adequacy and importance of these parametric or empirical representations.

C.6.2 Qualitative versus Quantitative Expressions of Uncertainties

Climate modelers do not settle for qualitative arguments that project a CO_2 warming, but instead use arguments based on quantitative, that is, mathematical, models. On the other hand, there is sometimes an acceptance of qualitative statements about the uncertainties in climate models (e.g., "In view of the uncertainties in our knowledge of cloud parameters ... it is premature to draw conclusions regarding the influence of clouds ..." [National Research Council 1982]). But with uncertainties emerging as one of the major issues in the CO_2 problem, perhaps it is time to encourage the use of mathematical methods of expressing uncertainty.

The previous section suggested that expressing some aspects of the sources of uncertainty mathematically is possible even in a model that makes gross approximations. A major limitation to use of uncertainty techniques in past CO_2 assessments (e.g., National Research Council 1979, 1982; Tucker 1981) has been that, without efficient methods of sensitivity analysis, it is impractical to estimate these effects. Instead, overall estimates of uncertainty have had to be based on a comparison of the results of different models, despite the danger that all the models could be equally wrong.

One aspect of achieving supportable and quantitative uncertainty analysis lies in developing practical methods of estimating sensitivities. Quantitative estimates of uncertainty can provide a basis for formulating an estimate of the overall uncertainty of

models and can help indicate priorities for model development. However, if an optimum path to model improvement is to be found, these uncertainty estimates must be used in conjunction with informed judgments based on overall model behavior in comparison to observations and on past knowledge of climate change.

C.6.3 Identifying Areas in Most Urgent Need of Research

There are many different ways that climate models could be improved. Observations of the contemporary climate could be used to reduce process uncertainties, improved ocean models could be used to reduce parameterization of oceanic processes, or greater resolution could be used to reduce aggregation error. Both modeling and computing resources are limited, however, so it is important to make improvements in the areas in which they would have the greatest potential for reducing uncertainty.

For example, in GCMs both the formation of clouds and the transfer of heat from the ground to the atmosphere are represented parametrically. But which of these processes introduces most uncertainty into the heat budget of the atmosphere? To find out, all of the radiative terms that depend on cloud cover can be flagged by introducing a coefficient, with nominal value of unity, that multiplies the cloud cover. Similarly, all the terms involving heat transfer from the ground can be multiplied by a different coefficient, also with nominal value of unity. Variations in these two different coefficients can then represent uncertainties. For example, a modeler could estimate that the uncertainty in cloud cover is 30%, while the heat transfer is correct to 10%. Sensitivity analysis of the two coefficients will then show which of these uncertainties has the greatest impact, indicating which process is in most urgent need of research.

C.7 SUMMARY AND RESEARCH RECOMMENDATIONS

Providing a supportable indication of the reliability of climate model projections is an essential but difficult task. Climate change is neither an easily observed nor adequately understood phenomenon, so the sensitivity of climate models to future perturbations is difficult to validate experimentally. But preparations for the consequences of climate change, or attempts to stave it off, are likely to require large investments and may flounder without compelling justification that the projected climate change is real.

Validation against observation would provide one of the most convincing indications of the reliability of climate model projections. Consequently, there is considerable research in the reconstruction of past climates and in the detection of CO_2-induced climate change. Most would agree, however, that the effects of climatic forcings analogous to those expected in the next century have never been observed. Therefore, not only must our ideas about future climates rely on the results of climate models, but also validation of these models must rely at least in part on a theoretical analysis of uncertainties.

To date, the most prevalent method of estimating uncertainties in the projections of climate models has been to base estimates of uncertainty on the magnitude of the disagreement among different models. However, estimates of uncertainty based on this method are likely to be misleading because models all make some of the same assumptions, and the models' results can have more in common with each other than they do with reality. The basic recommendation here is to estimate uncertainties by first identifying and quantifying sources of uncertainty and then by using sensitivity analysis to estimate the consequential uncertainty in the results. Model intercomparison still has an important role because it is essential to reconcile the disagreements between different models before we can trust them, but it is uncertainty analysis that provides the basis for a meaningful model intercomparison (by accounting for disagreements), not the other way around.

It has been shown that a wide variety of sources of uncertainty can be expressed mathematically (for example, uncertainties arising from assumptions, parameterization, omission of physical processes, and imprecise data). The simplest method for estimating the effects of such uncertainties in a model is to make a change in the model representative of the uncertainty, and to recalculate the results. This method is effective if there are just one or two

sources of uncertainty. However, in practice there are hundreds of sources of uncertainty, and it is prohibitively expensive to perform recalculations for all of them. Therefore, there is strong motivation to find more economical methods of sensitivity analysis than simple recalculation.

Several conventional methods of sensitivity analysis exist that avoid prohibitively expensive recalculations. We can determine the combined effects of differences between models by simply comparing their results, but it is difficult to sort out which model differences are causing which disagreements. We can reduce the expense of recalculation by using simpler models or shorter runs, but the resultant sensitivities may not be applicable to the state-of-the-art calculations.

The adjoint method has been developed for climate models to overcome the shortcomings of conventional methods of sensitivity analysis. The advantage of the adjoint method is that it calculates sensitivities with great efficiency even for the most complex models, and it provides physical insight for the values of the sensitivities. The disadvantage of the adjoint method is that it requires considerable effort to implement (about 4 man-years for the Oregon State University GCM, although subsequent models would require less than this level of effort).

Ultimately, our understanding of the climate is based on what we observe and measure, but this understanding owes a great deal to the use of mathematical models. The basic recommendation is to urge climate modelers to analyze the results of these models much more thoroughly, to the point that they understand both the climate changes being produced and the effects of the various approximations and assumptions in the models, and then to report these findings in their papers. This appendix has focused on methods aimed at promoting this kind of analysis.

A specific procedure for understanding some of the uncertainties in climate models is to express sources of uncertainty mathematically, then to develop methods of sensitivity analysis to quantify the effects of these uncertainties, and finally to sort out the largest effects to focus on as part of future research. The goal of this procedure is to develop a model in which all of the sources of uncertainty can be quantified and in which the effects of the uncertainties are acceptably small. So far there have been few attempts to express sources of uncertainty in climate models mathematically, because without efficient methods of sensitivity analysis there is little point in doing so. However, the adjoint method of sensitivity analysis has recently been applied successfully to 10-day simulations using a GCM with prescribed sea surface temperatures. The successful application of this method to longer simulations with more realistic ocean models would provide the first rigorous and systematic application of uncertainty analysis to the CO_2-climate problem.

The most frequent criticism of uncertainty analysis is that it can never take into account a process that has been entirely omitted from a model. Although true, this criticism misses the point of uncertainity analysis. If used intelligently in conjunction with informed judgment and physical understanding, uncertainty analysis can focus research on precisely those areas where the omission of a process is likely to be important.

REFERENCES

Aleksandrov, V. V., Arkhipov, P. L., Parkhomenko, V. P., and Stenchikov, G. L. 1983. "The Global Joint Ocean-Atmosphere Model and Its Sensitivity to the CO_2 Variation." *Izv. Akad. Nauk. SSSR, Riz. Atmos. Okena 19*:451–458.

Augustsson, T., and Ramanathan, V. 1977. "A Radiative-Convective Model Study of the CO_2 Climate Problem." *Journal of the Atmospheric Sciences 34*:448–451.

Cacuci, D. G., and Hall, M. C. G. 1984. "Efficient Estimation of Feedback Effects with Application to Climate Models." *Journal of the Atmospheric Sciences 41*:2063–2068.

Gates, W. L., Cook, K. H., and Schlesinger, M. E. 1981. "Preliminary Analysis of Experiments on the Climatic Effects of Increasing CO_2 with an Atmospheric General Circulation Model and a Climatological Ocean." *Journal of Geophysical Research 86*:6385–6393.

Ghan, S. J., Lingaas, J. W., Schlesinger, M. E., Mobley, R. L., and Gates, W. L. 1982. "A Documentation of the OSU Two-Level Atmospheric General Circulation Model" (Report No. 35). Climatic Research Institute, Oregon State University, Corvallis, Oregon.

Hall, M. C. G. 1986. "Feedback in the Climate: Accuracy of First Order Estimates." *Journal of the Atmospheric Sciences 43*:397–398.

Hall, M. C. G., Cacuci, D. G., and Schlesinger, M. E. 1982. "Sensitivity Analysis of a Radiative-Convective Model by the Adjoint Method." *Journal of the Atmospheric Sciences 39*:2038–2050.

Hansen, J. E. 1979. "Results Presented in Carbon Dioxide and Climate: A Scientific Assessment" (Report of an Ad Hoc Study Group on Carbon Dioxide and Climate). Climate Research Board, National Academy of Sciences, Washington, D.C.

Hansen, J. E., Johnson, D., Lacis, A., Lebedeff, S., Lee, P., Rind, D., and Russell, G. 1981. "Climate Impact of Increasing Atmospheric Carbon Dioxide." *Science 213*:957–966.

Hansen, J. E., Lacis, A., Rind, D., Russell, G., Stone, P., Fung, I., Rudy, T., and Lerner, J. 1984. "Climate Sensitivity: Analysis of Feedback Mechanisms." In J. E. Hansen and T. Takahashi (eds.), *Climate Processes and Climate Sensitivity*. American Geophysical Union, Washington, D.C.

Hansen, J. E., Russell, G., Rind, D., Stone, P., Lacis, A., Lebedeff, S., Ruedy, R., and Travis, L. 1983. "Efficient Three-Dimensional Global Models for Climate Studies: Models I and II." *Monthly Weather Review 111*:609–662.

Hunt, B. G., and Wells, N. C. 1979. "An Assessment of the Possible Future Climatic Impact of Carbon Dioxide Increases Based on a Coupled One-Dimensional Atmospheric-Oceanic Model." *Journal of Geophysical Research 84*:787–791.

Idso, S. B. 1980. "The Climatological Significance of a Doubling of Earth's Atmospheric Carbon Dioxide Concentration." *Science 207*:1462–1463.

Kandel, R. S. 1981. "Surface Temperature Sensitivity to Increased Atmospheric CO_2. *Nature 293*:634–636.

Katayama, A. 1972. "A Simplified Scheme for Computing Radiative Transfer in the Troposphere" (Technical Report No. 6). Department of Meteorology, University of California, Los Angeles, California.

Korzoun, V., et al. 1977. *World Water Balance and Water Resources of the Earth Including Atlas, Explanatory Notes and Monograph*. USSR Committee for the International Hydrological Decade. Published by the UNESCO Press, Paris, France.

Luther, F. M. 1982. "Radiative Effects of a CO_2 Increase: Results of a Model Comparison." *Proceedings of the Carbon Dioxide Research Conference: Carbon Dioxide, Science and Consensus* (CONF-820970). U.S. Department of Energy, Washington, D.C. Available from NTIS, Springfield, Virginia.

MacCracken, M. C., and Luther, F. M. (eds.) 1985. *Detecting the Climatic Effects of Increasing Carbon Dioxide* (DOE/ER-0235). U.S. Department of Energy, Washington, D.C. Available from NTIS, Springfield, Virginia.

MacDonald, G. F., Abarbanel, H., Carruthers, P., Chamberlain, J., Foley, H., Munk, W., Nierenberg, W., Rothaus, O., Ruderman, M., Vesecky, J., and Zachariasin, F. 1979. "The Long Term Impact of Atmospheric Carbon Dioxide on Climate" (JASON Technical Report JRS-78-07). SRI International, Arlington, Virginia.

Manabe, S. 1971. "Estimates of Future Change of Climate Due to the Increase of Carbon Dioxide Concentration in the Air." 249–264. In W. H. Mathews, W. W. Kellogg and G. D. Robinson (eds.), *Man's Impact on Climate*. The MIT Press, Cambridge, Massachusetts, 249–264.

Manabe, S., and Stouffer, R. J. 1980. "Sensitivity of a Global Climate Model to an Increase of CO_2 Concentration in the Atmosphere." *Journal of Geophysical Research 85*:5529-5554.

Manabe, S., and Stouffer, R. J. 1979. "A CO_2-Climate Sensitivity Study With a Mathematical Model of the Global Climate." *Nature 282*:491–493.

Manabe, S., and Wetherald, R. T. 1967. "Thermal Equilibrium of the Atmosphere With a Given Distribution of Relative Humidity." *Journal of the Atmospheric Sciences 24*:241–259.

Manabe, S., and Wetherald, R. T. 1975. "The Effects of Doubling the CO_2 Concentration on the Climate of a General Circulation Model." *Journal of the Atmospheric Sciences 32*:3–15.

Manabe, S., and Wetherald, R. T. 1980. "On the Distribution of Climate Change Resulting from an Increase in CO_2 Content of the Atmosphere." *Journal of the Atmospheric Sciences 37*:99–118.

Marable, J. H., Weisbin, C. R., and deSaussure, G. 1980. "Uncertainty in the Breeding Ratio of a Large Liquid-Metal Fast Breeder Reactor: Theory and Results." *Nuclear Science and Engineering 75*:30.

Mitchell, J. .F. B. 1983. "The Seasonal Response of a General Circulation Model to Changes in CO_2 and Sea Temperature." *Quarterly Journal of the Royal Meteorological Society 109*:113–152.

Möller, F. 1963. "On the Influence of Changes in CO_2 Concentration in Air on the Radiative Balance of the Earth's Surface and on the Climate." *Journal of Geophysical Research 68*:3877–3886.

National Research Council. 1979. *Carbon Dioxide and Climate: A Scientific Assessment*. National Academy Press, Washington, D.C.

National Research Council. 1982. *Carbon Dioxide and Climate: A Second Assessment*. National Academy Press, Washington, D.C.

Newell, R. E., and Dopplick, T. G. 1979. "Questions Concerning the Possible Influence of Anthropogenic CO_2 on Atmospheric Temperature." *Journal of Applied Meteorology 18*:822–825.

Pitcher, E. J., Malone, R. C., Ramanathan, V., Blackmon, M. L., Puri, K., and Bourke, W. 1983. "January and July Simulations with a Spectral General Circulation Model." *Journal of the Atmospheric Sciences 40*:580–604.

Potter, G. L. 1978. "Preliminary Zonal Model Analysis of the Climatic Change Resulting From Increased Atmospheric Carbon Dioxide" (UCRL-81575). Lawrence Livermore National Laboratory Report, Livermore, California. Available from NTIS, Springfield, Virginia.

Potter, G. L. 1980. "Zonal Model Calculation of the Climatic Effect of Increased CO_2." In J. J. Singh and A. Deepak (eds.), *Environmental and Climatic Impact of Coal Utilization*. Academic Press, New York, New York.

Ramanathan, V. 1981. "The Role of Ocean-Atmosphere Interactions in the CO_2 Climate Problem." *Journal of the Atmospheric Sciences 38:*918–930.

Ramanathan, V. 1975. "A Study of the Sensitivity of Radiative-Convective Models." In *Proceedings of the Second Conference on Atmospheric Radiation.* American Meteorological Society, Boston, Massachusetts.

Ramanathan, V., Lian, M. S., and Cess, R. D. 1979. "Increased Atmospheric CO_2: Zonal and Seasonal Estimates of the Effect on the Radiation Energy Balance and Surface Temperature." *Journal of Geophysical Research 84:*4949–4958.

Rasool, S. I., and Schneider, S. H. 1971. "Atmospheric Carbon Dioxide and Aerosols: Effects of Large Increases on Global Climate." *Science 173:*138–141.

Robinson, M., and Bauer, R. 1981. *Oceanographic Monthly Summary 1* (2): 2–3 National Weather Service, Washington, D.C.

Rowntree, P. R., and Walker, J. 1978. "The Effects of Doubling the CO_2 Concentration on Radiative-Convective Equilibrium." In J. Williams (ed.), *Carbon Dioxide, Climate and Society.* IIASA/WMO Workshop, 21–24 February 1978, Laxenburg, Austria, Pergamon Press, Oxford, United Kingdom.

Schlesinger, M. E. 1976. "A Numerical Simulation of the General Circulation of Atmospheric Ozone" (Ph. D. dissertation). University of California, Los Angeles.

Schlesinger, M. E. 1983. "A Review of Climate Model Simulations of CO_2-Induced Climatic Change" (Report No. 41). Climatic Research Institute, Oregon State University, Corvallis, Oregon.

Schlesinger, M. E., and Gates, W. L. 1979. "Numerical Simulation of the January and July Global Climate with the OSU Two-Level Atmospheric General Circulation Model" (Report No. 9). Climatic Research Institute, Oregon State University, Corvallis, Oregon.

Schlesinger, M. E., and Mitchell, J. F. B. 1985. "Model Projections of the Equilibrium Climatic Response to Increased Carbon Dioxide." In M. C. MacCracken and F. M. Luther (eds.), *Projecting the Climatic Effects of Increasing Carbon Dioxide* (DOE/ER-0237). U.S. Department of Energy, Washington, D.C. Available from NTIS, Springfield, Virginia.

Schneider, S. H. 1975. "On the Carbon-Dioxide-Climate Confusion." *Journal of the Atmospheric Sciences 32:*2060–2066.

Schneider, S. H., and Mass, C. 1975. "Volcanic Dust, Sunspots, and Temperature Trends." *Science 190:*741–746.

Sellers, W. D. 1973. "A New Global Climatic Model." *Journal of Applied Meteorology 12:*241–254.

Sellers, W. D. 1974. "A Reassessment of the Effect of CO_2 Variations on a Simple Global Climate Model." *Journal of Applied Meteorology 13:*831–833.

Temkin, R. L., and Snell, F. M. 1976. "An Annual Zonally-Averaged Hemispherical Climate Model With Diffuse Cloudiness Feedback." *Journal of the Atmospheric Sciences 33:*1671–1685.

Tucker, G. B. 1981. *The CO_2-Climate Connection: A Global Problem from an Australian Perspective.* Australian Academy of Sciences, Canberra, Australia.

Walsh, J., and Johnson, C. 1979. "An Analysis of Arctic Sea Ice Fluctuations," *Journal of Physical Oceanography 9:*580–591.

Washington, W. M., and Meehl, G. A. 1983. "General Circulation Model Experiments on the Climatic Effects Due to a Doubling and Quadrupling of Carbon Dioxide Concentration." *Journal of Geophysical Research 88:*6600–6610.

Weare, B. C., and Snell, F. .M. 1974. "A Diffuse Thin Cloud Structure as a Feedback Mechanism in Global Climatic Modeling." *Journal of the Atmospheric Sciences 31:*1725–1734.

Weisbin, C. R., Peelle, R. W., and Loebl, A. S. 1981. "An Approach to Evaluating Energy-Economy Models." *Energy 6:*999–1027.

Wetherald, R. T. and Manabe, S. 1981. "Influence of Seasonal Variation Upon the Sensitivity of a Model Climate." *Journal of Geophysical Research 86:*1194–1204.

GLOSSARY

ACRIM	Active-cavity radiometer
AER	Atmospheric and Enviromental Research, Inc.
AGCM	Atmospheric general circulation model
BADJ	Baroclinic adjustment
BAE	Bulk aerodynamic exchange
BD	Box diffusion
B.P.	Before the present era
CAENEX	Complex Atmospheric Energetics Experiment
CCM	Community climate model
CFC	Chlorofluorocarbons
ClC	Chlorocarbons
CLIMAP	Climate: Long-Range Investigation, Mapping, and Prediction
CLR	Clear, no clouds
CMA	Chemical Manufacturers Association
COHMAP	Cooperative Holocene Mapping Project
DJF	December-January-February
DOE	U.S. Department of Energy
EBM	Energy balance model
EGCM	Eddy-resolving ocean general circulation model
EPA	U.S. Environmental Protection Agency
ERE	Equivalent radiative exchange
FAH	Fixed absolute humidity
FAL	Fixed (surface) albedo
FCA	Fixed cloud altitude
FCC	Fixed cloud cover
FCP	Fixed cloud pressure
FCT	Fixed cloud temperature
FLR	Fixed lapse rate
FOD	Fixed optical depth
FRH	Fixed relative humidity
GAARS	Global Atmospheric Aerosol and Radiation Study
GCM	General circulation model
GEOSECS	Geochemical Ocean Sections
GFDL	Geophysical Fluid Dynamics Laboratory
GISS	Goddard Institute for Space Studies
GLA	Goddard Laboratory for Atmospheres
IAMAP	International Association of Meteorology and Atmospheric Physics
IAT	Ice albedo-temperature feedback
ICRCCM	Intercomparison of Radiation Codes used in Climate Models
IGY	International Geophysical Year (1957-1958)
IPCM	Intercomparison of Parameterizations in Climate Models Project

IR	Infrared
IRIS	Infrared interferometer spectrometer
ISCCP	International Satellite Cloud Climatology Project
ITCZ	Intertropical convergence zone
IWP	Ice water path (through a cloud)
JJA	June-July-August
LBL	Line-by-line
LLNL	Lawrence Livermore National Laboratory
LWC	Liquid water content
LWP	Liquid water path (through a cloud)
MALR	Moist adiabatic lapse rate
MAM	March-April-May
MONEX	Monsoon Experiment
NASA	U.S. National Aeronautics and Space Administration
NBM	Narrow band model
NCAR	National Center for Atmospheric Research
NOAA	U.S. National Oceanographic and Atmospheric Administration
NRC	National Research Council
NTP	Normal temperature and pressure
OGCM	Oceanic general circulation model
OSU	Oregon State University
PAL	Predicted albedo
PC	Penetrative convection
PCL	Predicted clouds
PD	Purely diffusive
PEBM	Planetary energy balance model
RCM	Radiative-convective model
RH	Relative humidity
SEBM	Surface energy balance model
SM1(A)	Spelman and Manabe modeling experiment 1
SM2(A)	Spelman and Manabe modeling experiment 2
SM3(A)	Spelman and Manabe modeling experiment 3
SMM	Solar Maximum Mission
SOA	State of the Art Report
SST	Sea surface temperature
STP	Standard temperature and pressure
TASU	Time alternating space uncentered
UD	Upwelling diffusion
UKMO	United Kingdom Meteorological Office
UV	Ultraviolet
VCC	Variable cloud cover
VOD	Variable optical depth
VRH	Variable relative humidity
WBM	Wide band model
WMO	World Meteorological Organization
WOCE	World Ocean Circulation Experiment
WP	Cloud water path

CITATION INDEX*

* Authors cited by name in the text are listed in this index. Where a coauthor's name is subsumed under an et al. in the text, no entry for that coauthor appears in this index. Complete references appear at the end of each chapter.

SUBJECT INDEX

*U.S. GOVERNMENT PRINTING OFFICE: 1986-491-177:30137

Manabe, S., and Wetherald, R. T. 1980. "On the Distribution of Climate Change Resulting from an Increase in CO_2 Content of the Atmosphere." *Journal of the Atmospheric Sciences 37*:99–118.

National Research Council (NRC). 1979. *Carbon Dioxide and Climate: A Scientific Assessment.* National Academy Press, Washington, D.C.

National Research Council (NRC). 1982. *Carbon Dioxide and Climate: A Second Assessment.* National Academy Press, Washington, D.C.

National Research Council (NRC). 1983. *Changing Climate.* (Board on Atmospheric Sciences and Climate). National Academy Press, Washington, D.C.

Newell, R. E., and Dopplick, T. G. 1979. "Questions Concerning the Possible Influence of Anthropogenic CO_2 on Atmospheric Temperature." *Journal of Applied Meteorology 18*:822–825.

Newell, R. E., and Dopplick, T. G. 1981. "Reply to R. G. Watts' 'Discussion of Questions Concerning the Possible Influence of Anthropogenic CO_2 on Atmospheric Temperature.' " *Journal of Applied Meteorology 20*:114–117.

Potter, G. L., and Cess, R. D. 1984. "Background Tropospheric Aerosols: Incorporation within a Statistical-Dynamical Climate Model." *Journal of Geophysical Research 89*:9521–9526.

Ramanathan, V. 1981. "The Role of Ocean-Atmosphere Interactions in the CO_2 Climate Problem." *Journal of the Atmospheric Sciences 38*:918–930.

Ramanathan, V., Lian, M. S., and Cess, R. D. 1979. "Increased Atmospheric CO_2: Zonal and Seasonal Estimates of the Effect on the Radiation Energy Balance and Surface Temperature." *Journal of Geophysical Research 84*:4949–4958.

Schneider, S. H., Kellogg, W. W., and Ramanathan, V. 1980. "Carbon Dioxide and Climate." *Science 210*:6.

Watts, R. G. 1980. "Discussion of 'Questions Concerning the Possible Influence of Anthropogenic CO_2 on Atmospheric Temperature.' " *Journal of Applied Meteorology 19*:494–495.

Watts, R. G. 1982. "Further Discussion of 'Questions Concerning the Possible Influence of Anthropogenic CO_2 on Atmospheric Temperature.' " *Journal of Applied Meteorology 21*:243–247.

Webster, P. J. 1984. "The Carbon Dioxide/Climate Controversy: Some Personal Comments on Two Recent Publications." *Climatic Change 6*:377–390.